ETHYLENE BIOLOGY AND BEYOND: NOVEL INSIGHTS IN THE ETHYLENE PATHWAY AND ITS INTERACTIONS

EDITED BY: Dominique Van Der Straeten, Angelos K. Kanellis, Caren Chang, Mondher Bouzayen, Panagiotis Kalaitzis, Jin-Song Zhang and Autar Krishen Mattoo

PUBLISHED IN: Frontiers in Plant Science

frontiers Research Topics

ISSN 1664-8714
ISBN 978-2-88963-678-5
DOI 10.3389/978-2-88963-678-5

About Frontiers

Frontiers is more than just an open-access publisher of scholarly articles: it is a pioneering approach to the world of academia, radically improving the way scholarly research is managed. The grand vision of Frontiers is a world where all people have an equal opportunity to seek, share and generate knowledge. Frontiers provides immediate and permanent online open access to all its publications, but this alone is not enough to realize our grand goals.

Frontiers Journal Series

The Frontiers Journal Series is a multi-tier and interdisciplinary set of open-access, online journals, promising a paradigm shift from the current review, selection and dissemination processes in academic publishing. All Frontiers journals are driven by researchers for researchers; therefore, they constitute a service to the scholarly community. At the same time, the Frontiers Journal Series operates on a revolutionary invention, the tiered publishing system, initially addressing specific communities of scholars, and gradually climbing up to broader public understanding, thus serving the interests of the lay society, too.

Dedication to Quality

Each Frontiers article is a landmark of the highest quality, thanks to genuinely collaborative interactions between authors and review editors, who include some of the world's best academicians. Research must be certified by peers before entering a stream of knowledge that may eventually reach the public - and shape society; therefore, Frontiers only applies the most rigorous and unbiased reviews.
Frontiers revolutionizes research publishing by freely delivering the most outstanding research, evaluated with no bias from both the academic and social point of view. By applying the most advanced information technologies, Frontiers is catapulting scholarly publishing into a new generation.

What are Frontiers Research Topics?

Frontiers Research Topics are very popular trademarks of the Frontiers Journals Series: they are collections of at least ten articles, all centered on a particular subject. With their unique mix of varied contributions from Original Research to Review Articles, Frontiers Research Topics unify the most influential researchers, the latest key findings and historical advances in a hot research area! Find out more on how to host your own Frontiers Research Topic or contribute to one as an author by contacting the Frontiers Editorial Office: researchtopics@frontiersin.org

ETHYLENE BIOLOGY AND BEYOND: NOVEL INSIGHTS IN THE ETHYLENE PATHWAY AND ITS INTERACTIONS

Topic Editors:
Dominique Van Der Straeten, Ghent University, Belgium
Angelos K. Kanellis, Aristotle University of Thessaloniki, Greece
Caren Chang, University of Maryland, College Park, United States
Mondher Bouzayen, National Polytechnic Institute of Toulouse, France
Panagiotis Kalaitzis, Mediterranean Agronomic Institute of Chania, Greece
Jin-Song Zhang, Institute of Genetics and Developmental Biology (CAS), China
Autar Krishen Mattoo, Agricultural Research Service (USDA), United States

Citation: Van Der Straeten, D., Kanellis, A. K., Chang, C., Bouzayen, M., Kalaitzis, P., Zhang, J.-S., Mattoo, A. K., eds. (2020). Ethylene Biology and Beyond: Novel Insights in the Ethylene Pathway and its Interactions. Lausanne: Frontiers Media SA. doi: 10.3389/978-2-88963-678-5

Table of Contents

frontiers in Plant Science

EDITORIAL
published: 12 March 2020
doi: 10.3389/fpls.2020.00248

Editorial: Ethylene Biology and Beyond: Novel Insights in the Ethylene Pathway and Its Interactions

Dominique Van Der Straeten[1]*, *Angelos Kanellis*[2], *Panagiotis Kalaitzis*[3], *Mondher Bouzayen*[4], *Caren Chang*[5], *Autar Mattoo*[6] and *Jin-Song Zhang*[7]

[1] Laboratory of Functional Plant Biology, Department of Biology, Ghent University, Ghent, Belgium, [2] Laboratory of Pharmacognosy, Department of Pharmaceutical Sciences, Aristotle University of Thessaloniki, Thessaloniki, Greece, [3] Department of Horticultural Genetics and Biotechnology, Mediterranean Agronomic Institute of Chania, Chania, Greece, [4] INRA Génomique et Biotechnologie des Fruits (GBF), Toulouse, France, [5] Department of Cell Biology and Molecular Genetics, University of Maryland, College Park, MD, United States, [6] Beltsville Agricultural Research Center, Agricultural Research Service (USDA), Beltsville, MD, United States, [7] Institute of Genetics and Developmental Biology, Chinese Academy of Sciences (CAS), Beijing, China

Keywords: ethylene, ACC (1-aminocyclopropane-1-carboxylic acid), stress, ACC synthase (ACS), ACC oxidase (ACO), gold standard

Editorial on the Research Topic

Ethylene Biology and Beyond: Novel Insights in the Ethylene Pathway and Its Interactions

This Research Topic presents selected contributions to **Ethylene 2018**, the **XI International Symposium on the Plant Hormone Ethylene**, held in Chania, Greece, on 2nd−6th June 2018, covering exciting new discoveries in the ethylene field.

This issue brings novel insights in ethylene signaling in bacteria, algae, and lower plants as well as evidence supporting a specific role for the ethylene precursor 1-aminocyclopropane-1-carboxylic acid (ACC) in plants.

Ethylene receptors were initially thought to be specific to plants. Interestingly, ethylene receptor homologs have been found in cyanobacteria. It was previously shown that in Synechocystis sp. an ethylene receptor regulates phototaxis and biofilm formation. In this issue, the same group (Allen et al.) demonstrates that another cyanobacterium, the filamentous species Geitlerinema sp. which possesses two ethylene receptor homologs, similarly displays ethylene-dependent alterations in phototaxis, suggesting that such signaling could be prevalent in cyanobacteria. Both species are highly sensitive to ethylene although their ethylene binding characteristics resemble that of plants, thus suggesting signal amplification in cyanobacteria.

In higher plants, subfamily-I of the Arabidopsis receptors (ETR1 and ERS1) and their interactions with downstream players have been extensively studied, while information on subfamily-II (ETR2, ERS2, and EIN4) remains sparse. Here, Berleth et al. demonstrate that ETR2 displays comparable affinities for CTR1 and EIN2 to that previously reported for ETR1, suggesting similar protein-protein interaction-mediated signal transfer for both subfamilies. In addition, the authors show enhanced stability of type-II receptor homomers and type-II:type-I heteromers as compared to type-I homomers, emphasizing the importance of type-II receptors.

Wang and Qiao present a mini-review on the transcriptional regulation of the ethylene response in Arabidopsis. Ethylene signaling involves numerous regulatory steps leading to a diversity of responses in plant growth and development. This review discusses our current understanding of the transcriptional regulation as a major control point in ethylene signaling, focusing on recent insights into the role of chromatin modification in repressing transcription.

OPEN ACCESS

Edited and reviewed by:
Gerrit T. S. Beemster, University of Antwerp, Belgium

***Correspondence:**
Dominique Van Der Straeten
dominique.vanderstraeten@ugent.be

Specialty section:
This article was submitted to Plant Physiology, a section of the journal Frontiers in Plant Science

Received: *21 January 2020*
Accepted: *18 February 2020*
Published: *12 March 2020*

Citation:
Van Der Straeten D, Kanellis A, Kalaitzis P, Bouzayen M, Chang C, Mattoo A and Zhang J-S (2020) Editorial: Ethylene Biology and Beyond: Novel Insights in the Ethylene Pathway and Its Interactions. Front. Plant Sci. 11:248. doi: 10.3389/fpls.2020.00248

Dolgikh et al. summarize recent advances on the molecular mechanisms that underlie EIN3/EIL1-directed ethylene signaling in Arabidopsis, and focus on the role of EIN3/EIL in tuning transcriptional regulation of ethylene response in time and space. Furthermore, they consider the role of EIN3/EIL1-independent regulation of ethylene signaling.

Qin et al. review hormonal crosstalk of ethylene in primary root growth of Arabidopsis and rice. Based on the proposed model, ethylene restricts primary root growth by governing auxin biosynthesis, transport, and signaling through EIN3/EIL1, ERF1, and HB52 interactions in Arabidopsis. ABA and CKs constrain primary root growth by controlling the posttranscriptional regulation of ACS resulting in stimulated ethylene synthesis. GA and ethylene antagonistically regulate stability of DELLA proteins, which act as growth repressors. Low levels of BRs hinder ethylene synthesis by BZR1 and BES1 suppressed ACS gene expression, while high levels of BRs increase ACS stability. Through a different mechanism, ethylene restricts primary root growth in rice, by augmenting auxin and ABA biosynthesis. Understanding light-dependent differences in ethylene synthesis and signaling is essential to expand our insight into the roles of ethylene in growth and development across the plant life cycle.

Harkey et al. performed a meta-analysis of multiple transcriptomic datasets to uncover responses to ethylene that are both light-dependent and light-independent. A set of 139 transcripts with robust and consistent responses to elevated ethylene across root-specific datasets was identified. This "gold standard" group of ethylene-regulated transcripts includes numerous genes encoding proteins that function in ethylene signaling and synthesis. The study further reveals a number of previously uncharacterized factors that may contribute to ethylene response phenotypes.

Plants synthesize ethylene in a two-step reaction starting with the conversion of S-adenosyl-L-methionine (SAM) to 1-aminocyclopropane-1-carboxylic acid (ACC). Vanderstraeten et al. demonstrated that ACC affects early vegetative development independently of ethylene signaling. Using ethylene biosynthesis and signaling inhibitors, as well as mutants, ACC-specific ethylene-independent growth responses in both dark- and light-grown Arabidopsis seedlings were revealed. Hence, researchers employing ACC as an ethylene precursor should be mindful of putative ACC effects confounding ethylene responses in vegetative growth. The exact mechanism underlying the ACC response remains to be identified.

While ACC may play an ethylene-independent role in plant growth and development, the three-membered ring amino-acid is probably also of paramount importance in the balanced co-existence of plants and beneficial micro-organisms around them, surmounting attacks of pathogens.

Though the genome of the pathogenic fungus *Fusarium graminearum*, which infects wheat, seems to lack genes encoding ethylene biosynthetic enzymes, Svoboda et al. identified two ACC deaminase genes, one of which encodes an active ACC deaminase. Considering that ethylene insensitive wheat exhibited higher resistance to *Fusarium* and reduced mycotoxin content, *Fusarium* knockouts of both genes were generated. No differences in the fungal infection and mycotoxin content were detected indicating that ethylene might not affect full *Fusarium* virulence.

Nonaka et al. used ACC deaminase in a Super-Agrobacterium strain to enhance transformation efficiencies of recalcitrant species. Super-Agrobacterium was updated to version 4 by introducing both an ACC deaminase and GABA transaminase gene, encoding enzymes that degrade ACC and GABA, respectively. The use of this modified strain resulted in substantial reduction of the amount of time and labor required for transformations, hence providing a more powerful tool for plant genetic engineering and functional analysis.

While most studies have focused on the conversion of SAM to ACC by ACC synthases, there has been increasing interest in the subsequent step, carried out by ACC oxidases (ACOs). Houben and Van de Poel provide a comprehensive and historical perspective on our understanding of the ACO enzyme, including its discovery, activity, evolution, expression, regulation and potential biotechnological applications.

A thorough analysis of players in ethylene signaling enabled identification of key regulators in fruit development and ripening. Not unexpectedly, translational regulation of ethylene biosynthesis and signaling appears to be fundamental in the control of ethylene effects, besides transcriptional regulation.

Mitalo et al. show that many aspects of kiwifruit ripening can be triggered by ethylene treatment or by low temperature, with the exception of aroma volatile production, a major ripening feature contributing to fruit quality, that is lacking in cold-triggered ripening. The data indicate that the production of aroma compounds is strongly ethylene-dependent and support the notion that in kiwifruit ethylene and low temperature-induced ripening may involve two different regulatory mechanisms.

Chen et al. used a modification of parallel reaction monitoring, a targeted mass spectrometry proteomic method, to study ETR receptor abundance in tomato fruit. Focusing on single peptides of rare proteins, they compared the abundance of ETRs in WT and in the NR mutant. Pearson correlations between mRNA and protein profiles were used as indicators to discriminate the two genotypes and reveal changes over fruit development. It is proposed as an approach to study ETR subfunctionalization across the plant kingdom in development as well as in plant-microorganism interactions.

Regarding the role of ethylene in pigmentation, Khunmuang et al. demonstrate that ethylene-mediated petal color fading in cut Vanda "Sansai Blue" flowers results from degradation of anthocyanidins, cyaniding, and delphinidin, and is not related to the levels of flavonols, such as kaempferol. The endogenous anthocyanin degradation process stimulated by ethylene appears related to increased peroxidase activity but was independent of flower senescence. Espley et al. investigated the incidence of internal browning flesh disorder (IBFD) in high anthocyanin red apples (Malus x domestica). The study, using the highly pigmented "Royal Gala" apple cultivar over-expressing MYB10, revealed that the anthocyanin-related transcription factor is associated with the undesirable fruit disorder. The MYB10 transgenic fruit had a high incidence of IBFD compared to wild type. Interestingly, MYB10-expressor apple had higher

expression of ethylene-related genes ACS, ACO, and ERF. Prematurely induced ethylene can advance fruit maturity and, as shown by these authors, may lead to adverse effects on storage of high-anthocyanin fruits.

Hormonal pathways are not functioning as independent routes, but rather contribute to an information web, connecting internal signaling to transduction pathways of external cues. Ethylene is involved in such an intricate network which fine-tunes development from cell and organ specification to senescence and abscission, but also incorporates external signals enabling plasticity in an ever changing environment, and controlling reactions to adverse conditions, such as those encountered as a result of global climate change.

External factors such as wind, hale or snow, and/or growth on uneven terrain, induces tension wood formation in order to reorient and uplift the stem toward its original growth position. Tension wood is characterized by the presence of gelatinous, cellulose-rich (G-)fibers with its microfibrils oriented parallel to the fiber cell axis. Seyfferth et al. demonstrated that ethylene regulates transcriptional responses related to the amount of G-fiber formation and their properties, including chemistry and cellulose microfibril angle, in hybrid aspen. The quantitative and qualitative changes in G-fibers are likely to contribute to uplifting of stems.

Given the importance of ethylene in agricultural applications and the need for sustainable crop production, on the field as well as in post-harvest control of fruits and vegetables, recent research has also focused on improved control of ethylene release and sensitivity, as well as on long-term storage conditions of crop products.

AUTHOR CONTRIBUTIONS

All authors listed have made a substantial, direct and intellectual contribution to the work, and approved it for publication.

Conflict of Interest: The authors declare that the research was conducted in the absence of any commercial or financial relationships that could be construed as a potential conflict of interest.

frontiers in Plant Science

REVIEW
published: 29 May 2019
doi: 10.3389/fpls.2019.00695

1-Aminocyclopropane-1-Carboxylic Acid Oxidase (ACO): The Enzyme That Makes the Plant Hormone Ethylene

*Maarten Houben and Bram Van de Poel**

Molecular Plant Hormone Physiology Laboratory, Division of Crop Biotechnics, Department of Biosystems, KU Leuven, Leuven, Belgium

The volatile plant hormone ethylene regulates many plant developmental processes and stress responses. It is therefore crucial that plants can precisely control their ethylene production levels in space and time. The ethylene biosynthesis pathway consists of two dedicated steps. In a first reaction, S-adenosyl-L-methionine (SAM) is converted into 1-aminocyclopropane-1-carboxylic acid (ACC) by ACC-synthase (ACS). In a second reaction, ACC is converted into ethylene by ACC-oxidase (ACO). Initially, it was postulated that ACS is the rate-limiting enzyme of this pathway, directing many studies to unravel the regulation of ACS protein activity, and stability. However, an increasing amount of evidence has been gathered over the years, which shows that ACO is the rate-limiting step in ethylene production during certain dedicated processes. This implies that also the ACO protein family is subjected to a stringent regulation. In this review, we give an overview about the state-of-the-art regarding ACO evolution, functionality and regulation, with an emphasis on the transcriptional, post-transcriptional, and post-translational control. We also highlight the importance of ACO being a prime target for genetic engineering and precision breeding, in order to control plant ethylene production levels.

Keywords: ethylene biosynthesis, 1-aminocyclopropane-1-carboxylate oxidase, transcriptional and post-translation regulation, phylogeny, physiology

OPEN ACCESS

Edited by:
Caren Chang,
University of Maryland, College Park, United States

Reviewed by:
Gyeong Mee Yoon,
Purdue University, United States
Donald Grierson,
University of Nottingham, United Kingdom

***Correspondence:**
Bram Van de Poel
Bram.vandepoel@kuleuven.be

Specialty section:
This article was submitted to Plant Physiology, a section of the journal Frontiers in Plant Science

Received: *08 April 2019*
Accepted: *09 May 2019*
Published: *29 May 2019*

Citation:
Houben M and Van de Poel B (2019) 1-Aminocyclopropane-1-Carboxylic Acid Oxidase (ACO): The Enzyme That Makes the Plant Hormone Ethylene. Front. Plant Sci. 10:695. doi: 10.3389/fpls.2019.00695

INTRODUCTION ON ETHYLENE BIOSYNTHESIS

Ethylene was the first gaseous hormone to be discovered in plants. It is an important regulator of many developmental and physiological processes such as seed dormancy, germination, vegetative growth, flowering, climacteric fruit ripening, and senescence. Additionally, ethylene was shown to play an important role in the plant's defense against biotic and abiotic stress factors (Lin et al., 2009; Van de Poel et al., 2015; Wen, 2015).

The general precursor of the ethylene biosynthesis pathway is the amino acid methionine (**Figure 1**; Lieberman et al., 1966). In a first, but general reaction, methionine is converted into S-adenosyl-L-methionine (SAM) by SAM synthetase using ATP (Adams and Yang, 1977). The subsequent reaction steps are unique to the ethylene biosynthesis pathway. First, SAM is converted into 1-aminocyclopropane-1-carboxylic acid (ACC) and 5′-methylthioadenosine (MTA) by ACC-synthase (ACS) (Murr and Yang, 1975; Adams and Yang, 1979; Boller et al., 1979). ACS is a member

of the pyridoxal-5′-phosphate (PLP) dependent aminotransferases, which use PLP as a co-factor (Boller et al., 1979). The side product MTA is recycled back to methionine by the Yang cycle to avoid a depletion of methionine during high rates of ethylene production (Murr and Yang, 1975). More details on the different steps of the Yang cycle are presented in Bürstenbinder et al. (2010) and Pommerrenig et al. (2011). In a second step, ethylene is released from ACC by ACC-oxidase (ACO) (Hamilton et al., 1990; Ververidis and John, 1991), a reaction that requires molecular oxygen (Burg and Burg, 1965). Alternatively, ACC can be converted to malonyl-ACC (MACC; Amrhein et al., 1981), γ-glutamyl-ACC (GACC; Martin and Saftner, 1995), and jasmonyl-ACC (JA-ACC; Staswick and Tiryaki, 2004). An in-depth review on the derivatization of ACC is given by Van de Poel and Van Der Straeten (2014).

THE DISCOVERY OF ACO AND ITS REACTION MECHANISM

For a long time it remained extremely difficult to purify ACO (formerly named the Ethylene Forming Enzyme, EFE) and determine its *in vitro* activity, mainly because it was thought that ACO was a membrane bound protein that lost its activity upon homogenization (Kende, 1989). Some residual or partial *in vitro* ACO activity was retained in membrane preparations of pea (Guy and Kende, 1984; Porter et al., 1986), bean (Guy and Kende, 1984; Mayne and Kende, 1986), Sprenger's asparagus (Porter et al., 1986) and kiwi fruit (Mitchell et al., 1988), which was only a fraction (5–0.5%) of the total *in vivo* ethylene production capacity. A breakthrough was made when the clone pTOM13 was characterized to code for a putative *ACO* gene of tomato (Hamilton et al., 1990). The elucidation of the protein sequence of this first ACO allowed Ververidis and John to find sequence similarity with a flavonone 3-hydroxylase of snapdragon (*Antirrhinum majus*). This homology made them realize that both iron and ascorbic acid could be essential for ACO enzyme activity. This insight made Ververidis and John (1991) the first to successfully extract and quantify *in vitro* ACO activity from melon fruit tissue.

Iron, in the form of Fe(II), is an essential metal cofactor, which is required for ACO enzyme activity (Bouzayen et al., 1991). Iron participates by coordinating the binding of the amino group of ACC to H177 and the carboxylate group of ACC to D179, which are two critical ACO residues in the reaction center (Zhang et al., 2004; Tierney et al., 2005; Brisson et al., 2012). The ascorbate cofactor is used as a reductant to catalyze the opening of the ACC-ring (Zhang et al., 2004; Murphy et al., 2014). The ACO reaction mechanism also uses molecular oxygen and bicarbonate as activators in order to catalyze the conversion of ACC into ethylene (Adams and Yang, 1981; Peiser et al., 1984). During this reaction, an unstable intermediate cyanoformate ion [$(NCCO_2)^-$] is formed, which rapidly decomposes in CO_2 and CN^- (Murphy et al., 2014). The reactive cyanide ion (CN^-) is subsequently detoxified into β-cyanoalanine (Peiser et al., 1984; Dilley et al., 2013; Murphy et al., 2014).

ACC-oxidase is a member of the 2-oxoglutarate-dependent dioxygenase (2OGD) superfamily of non-heme iron-containing proteins (Kawai et al., 2014). The 2OGD superfamily is one of the largest enzyme families in plants, with most of its members being active in oxygenation and hydroxylation reactions (Kawai et al., 2014). Nonetheless, 2OGD enzymes can have more diverse roles and participate for example in demethylations, desaturations, ring closure, ring cleavage, epimerization, rearrangement, halogenation, and demethylenation reactions in plants (Farrow and Facchini, 2014). Characteristic for all 2OGDs is the double-stranded β-helix (DSBH) core fold, which contains a typical 2-His-1-carboxylate motif required for iron binding, also encountered in ACO. This motif consists of two His residues and the carboxylate group from an Asp or a Glu residue, and is responsible for the ligation of Fe(II) in the enzyme catalytic site, and thus critical for ACC binding (Aik et al., 2015; Martinez and Hausinger, 2015; Murphy et al., 2014).

Despite the fact that 2OGD enzymes are typically localized in the cytosol (Kawai et al., 2014), the exact subcellular localization of ACO remains a matter of debate. Some studies have suggested that ACO is localized at the plasma membrane (Rombaldi et al., 1994; Ramassamy et al., 1998), as originally postulated (Kende, 1989). However, other studies have shown that ACO is localized in the cytosol (Peck et al., 1992; Reinhardt et al., 1994; Chung et al., 2002; Hudgins et al., 2006), matching the general localization of 2OGD enzymes. Other studies have measured ACO activity both for membrane/apoplast and intracellular preparations (Bouzayen et al., 1990). All these studies used immunolocalization or activity assays in combination with (sub)cellular fractionations, and perhaps these techniques did not provide sufficient resolution to elucidate the exact ACO localization. A recent study tagged a safflower (*Carthamus tinctorius*) ACO with a GFP (green fluorescent protein) and performed an ectopic localization in onion epidermis cells. Their results showed that *Ct*ACO1 localizes in the cytosol (potentially linked with membranes) and in the nucleus, but their images lacked markers for these organelles (Tu et al., 2019). All studies combined are not conclusive about the exact ACO localization, and thus the actual subcellular site of ethylene production.

ACO PHYLOGENY AND RESIDUE ANALYSIS

The plant 2OGD superfamily can be categorized into three subclasses (DOXA, DOXB, and DOXC) based on amino acid sequence similarity (Kawai et al., 2014). ACO is a part of the DOXC subclass, the largest and most diverse group, containing over 400 different 2OGDs, mainly linked to the specialized metabolism (Kawai et al., 2014). Kawai et al. (2014) further subcategorized the DOXC subclass and classified ACO as part of the DOXC53 subclade. This subclade has 2OGD members, which are typically retrieved in all angiosperms. ACO is a unique member of the plant 2OGD superfamily, because it uses ascorbate as a catalyst instead of 2-oxoglutarate (Kawai et al., 2014).

A small phylogenetic study using a limited amount of ACO sequences from tomato (*Solanum lycopersicum*), potato

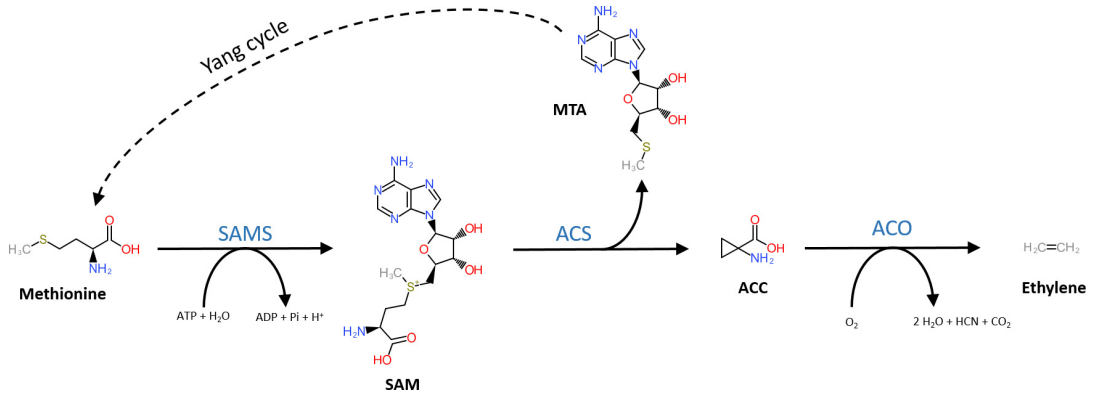

FIGURE 1 | Structural representation of the ethylene biosynthesis pathway. Methionine is converted into SAM by SAM synthetase (SAMS) requiring ATP. Next, SAM is converted into methylthioadenosine (MTA) and 1-aminocyclopropane-1-carboxylic acid (ACC) by ACC-synthase (ACS). MTA is recycled back to methionine by the Yang-cycle (several reactions depicted by the dotted line). In the final step, ACC-oxidase (ACO) catalyzes the release of ethylene from ACC using molecular oxygen.

(*Solanum tuberosum*), bonnet pepper (*Capsicum chinense*), petunia (*Petunia hybrida*), and tobacco (*Nicotiana tabacum*) classified the ACO protein family in three distinct phylogenetic groups (Jafari et al., 2013). A more detailed phylogenetic analysis of putative ACOs from mosses, lycophytes, gymnosperms, monocots, and dicots showed that ACO got more diversified after the monocot-dicot split (Clouse and Carraro, 2014). They also observed that there are three main clusters of ACOs and that monocot and dicot ACOs diverged together from a common pre-gymnosperm ancestor (Clouse and Carraro, 2014).

Because not many ACOs have been shown to be functional ACO enzymes that can convert ACC into ethylene, it remains questionable if putative ACOs used in phylogenetic analyses are in fact functional ACOs. Trivial protein sequence similarity searches may lead to false or incorrect ACO annotations in genome and protein databases. In fact, there are only a few studies that have purified recombinant ACOs for functional characterization. This was done for tomato (*Sl*ACO1-3; Solyc07g049530, Solyc12g005940, Solyc07g049550; Bidonde et al., 1998), petunia (PhACO1; Zhang et al., 2004), apple (*Md*ACO1; MDP0000195885; Dilley et al., 2013), and Arabidopsis (*At*ACO2; AT1G62380; Sun et al., 2017). The study of Clouse and Carraro (2014) used annotated, but functionally unverified, ACO protein sequences as queries to identify novel ACO sequences in other species, without performing reciprocal BLAST searches. This approach resulted in the identification of false ACOs, leading to an overestimation of the size of the ACO protein family in certain species (e.g., 13 ACO members for *Arabidopsis thaliana* instead of 5). Therefore, we have performed a novel sequence similarity search using only the tomato ACO1 (Solyc07g049530) as search query, because this protein has been shown to be a true ACO with a confirmed activity (Bidonde et al., 1998). BLASTp jobs were done for 21 species using the Phytozome (v12.1.) database and Gymno plaza 1.0 (Proost et al., 2014), and top hits were only retained after a positive reciprocal BLAST search. **Table 1** lists all the putative ACOs for some agriculturally important crops and Arabidopsis, while **Supplementary Table 1** lists all the ACOs for the other plant species used in our phylogenetic analysis. We were able to identify 5 ACO members for Arabidopsis, 7 for tomato, 7 for apple, 9 for rice, and 13 for maize (**Table 1**). All putative ACO sequences were used to build a phylogenetic tree (see **Supplementary Figure 1**), which clearly shows a cluster of "ancient" ACOs within the clade of non-seed land plants and algae. This ancient clade most likely originated from an evolutionary distant algal 2OGD that gradually diverged into a functioning ACO during seed plant evolution. A more detailed phylogenetic tree of a selected amount of agriculturally important angiosperms shows 3 clusters of ACOs (**Figure 2**). Therefore, we suggest dividing the ACO family in three types: Type I, Type II, and Type III ACO. These three clusters are also observed in the larger phylogenetic tree of **Supplementary Figure 1**. Our analysis also shows that the gymnosperm ACOs group within the Type III ACO cluster of angiosperms, and that monocot and dicot ACOs diverged separately for each individual type. Our phylogenetic analysis indicates that the 3 types of ACOs diverged in parallel from a shared non-seed plant ancestral ACO or 2ODG.

A detailed residue analysis of the ACO alignment of Arabidopsis, tomato and apple presented in **Figure 3** further confirms the existence of 3 types of ACO. The important 2-His-1-carboxylate Fe(II) binding motif is conserved in all ACOs. Shaw et al. (1996) provided some first experimental insight that this motif is composed of the H177-D179-H234 triad in *Md*ACO1 and that it is essential for ACO activity. This was confirmed in other studies in apple (Kadyrzhanova et al., 1999; Yoo et al., 2006) and for a petunia (Zhang et al., 2004) and tomato ACO (Brisson et al., 2012) (see also **Supplementary Table 2**).

Furthermore, a thorough mutagenesis study of *Md*ACO1, identified other important residues essential for ACO activity: C28, T157, K158, R175, Q188, K199, K230, R244, S246, K292, E294, E297, R299, F300, and E301 (Dilley et al., 2013). Some residues (R175, R299, and K158) have been proposed to coordinate bicarbonate binding (Zhang et al., 2004; Brisson et al., 2012; Dilley et al., 2013), while other residues (K292, K158, and F300) are proposed binding sites for ascorbate

TABLE 1 | List of ACO sequences used for construction of the maximal likelihood phylogenetic tree of *Arabidopsis thaliana, Solanum lycopersicum, Malus domestica, Oryza sativa,* and *Zea mays*.

Species	Gene	GeneID	Type	Protein (aa)	Source
Arabidopsis thaliana	*AtACO1*	AT2G19590.1	2	311	Vandenbussche et al., 2003
	AtACO2	AT1G62380.1	1	321	Raz and Ecker, 1999
	AtACO3	AT1G12010.1	1	321	Vandenbussche et al., 2003
	AtACO4	AT1G05010.1	1	324	Gómez-Lim et al., 1993
	AtACO5	AT1G77330.1	3	308	Vandenbussche et al., 2003
Apple	*MdACO1*	MDP0000195885	1	314	Dong et al., 1992
(*Malus domestica*)	*MdACO2*	MDP0000200737	1	330	Binnie and McManus, 2009
	MdACO3	MDP0000725984	1	323	Binnie and McManus, 2009
	MdACO4	MDP0000251295	1	322	
	MdACO5	MDP0000453114	1	323	
	MdACO6	MDP0000025650	3	298	
	MdACO7	MDP0000200896	2	348	
Rice	*OsACO1*	LOC_Os09g27820.1	1	323	Chae et al., 2000
(*Oryza sativa*)	*OsACO2*	LOC_Os09g27750.1	1	323	Chae et al., 2000
	OsACO3α	LOC_Os02g53180.1	1	345	Chae et al., 2000
	OsACO3β	LOC_Os02g53180.2	1	322	Chae et al., 2000
	OsACO3γ	LOC_Os02g53180.3	1	284	Chae et al., 2000
	OsACO6	LOC_Os06g37590.1	2	294	
	OsACO7	LOC_Os01g39860.1	2	313	Iwai et al., 2006
	OsACO4	LOC_Os11g08380.1	3	310	Iwai et al., 2006
	OsACO5	LOC_Os05g05680.1	3	309	Iwai et al., 2006
Tomato	*SlACO1*	Solyc07g049530.2.1	1	316	Hamilton et al., 1991
(*Solanum lycopersicum*)	*SlACO2*	Solyc12g005940.1.1	1	317	Holdsworth et al., 1987
	SlACO3	Solyc07g049550.2.1	1	317	(Bidonde et al., 1998)
	SlACO4	Solyc02g081190.2.1	1	321	Nakatsuka et al., 1998
	SlACO5	Solyc07g026650.2.1	2	302	Sell and Hehl, 2005
	SlACO6	Solyc02g036350.2.1	1	320	
	SlACO7	Solyc06g060070.2.1	3	315	
Maize	*ZmACO20*	Zm00008a017510_T01	1	453	Gallie and Young, 2004
(*Zea mays*)	*ZmACO35*	Zm00008a023130_T01	1	304	Gallie and Young, 2004
	ZmACO2	Zm00008a028217_T01	1	327	
	ZmACO8	Zm00008a009058_T01	2	239	
	ZmACO9	Zm00008a021339_T01	2	235	
	ZmACO1	Zm00008a024831_T01	2	283	
	ZmACO10	Zm00008a031986_T01	2	319	
	ZmACO11	Zm00008a008130_T01	3	326	
	ZmACO6	Zm00008a018191_T01	3	314	
	ZmACO31	Zm00008a037498_T01	3	315	Gallie and Young, 2004
	ZmACO4	Zm00008a037500_T01	3	316	
	ZmACO7	Zm00008a037501_T01	3	296	
	ZmACO15	Zm00008a037502_T01	3	315	Gallie and Young, 2004

Sequences were retrieved from Phytozome (v12.1) and top hits were only retained after a positive reciprocal BLAST search. Numbering of the different ACOs was done according to previously published work (if available), otherwise a new numbering is proposed. Putative splice variants of the same gene are represented by α, β, and γ.

(Dilley et al., 2013). Besides these six amino acids, two additional residues (R244 and S246; highly conserved and part of the so-called RXS motif) complete the ACC/bicarbonate/ascorbate binding site of ACO (Kadyrzhanova et al., 1999; Seo et al., 2004; Zhang et al., 2004; Brisson et al., 2012; Dilley et al., 2013). Interestingly, the three ACO types can be classified based on the intermediate residue present in the conserved RXS-motif. This motif consists of R-M-S for type I ACOs, R-L/I-S for type II ACOs, and R-R-S for type III ACOs. All the residues considered important for ACO activity according to Dilley et al. (2013), are conserved in the three types of ACO, except for E294, E297, and E301. E294 is not well conserved in the three ACO types, while E297 is replaced by glycine only in the type II ACOs and E301 is not conserved in type III ACOs. It remains to be investigated whether or not the 3 types of ACOs actually have differences in functionality related to for example enzyme activity and/or protein stability.

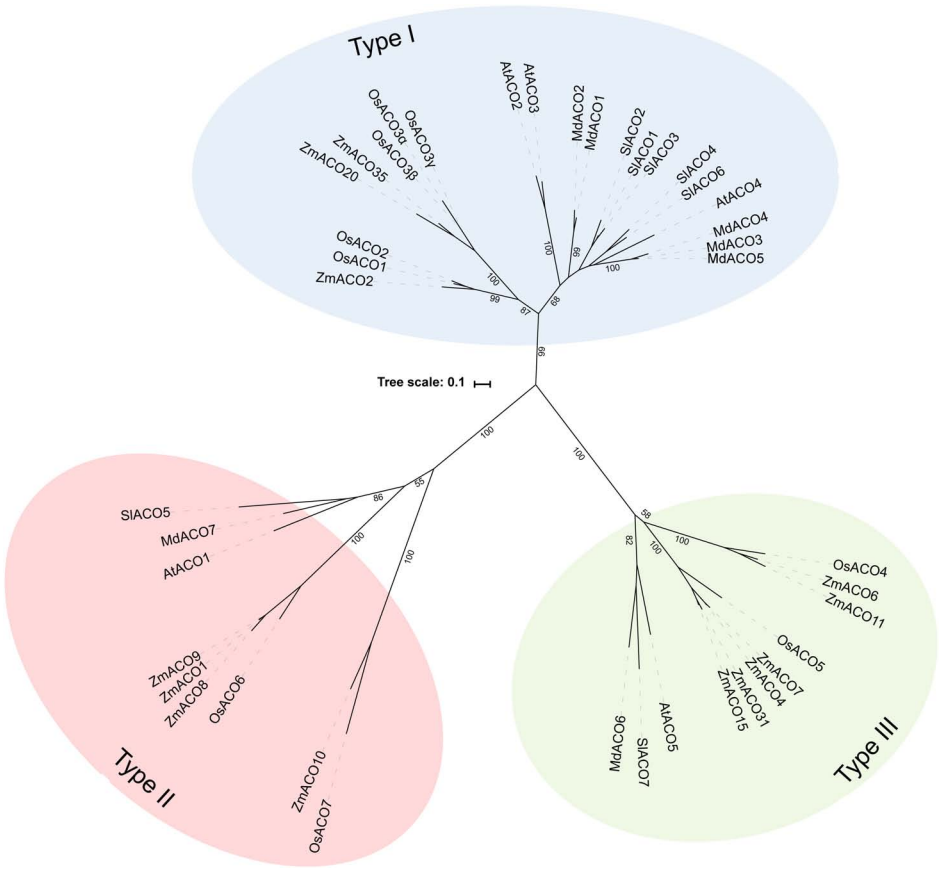

FIGURE 2 | Maximal likelihood phylogenetic tree for ACO protein sequences of *Arabidopsis thaliana* (AT), Tomato (*Solanum lycopersicum*; Solyc), Apple (*Malus domestica*; MDP), Rice (*Oryza sativa*; Os), and Maize (*Zea mays*; Zm) retrieved from Phytozome (v12.1). Protein sequences were aligned in Geneious (v10.2.2) using the MUSCLE alignment plugin. The phylogenetic tree was build using RAxML (v8.2.11) for best-scoring maximum likelihood tree with rapid bootstrapping (1000 bootstrap replicates). Bootstrap values for the main branches are depicted on the tree. Type I ACO is shown in blue, Type II ACO is shown in red, and Type III ACO is shown in green.

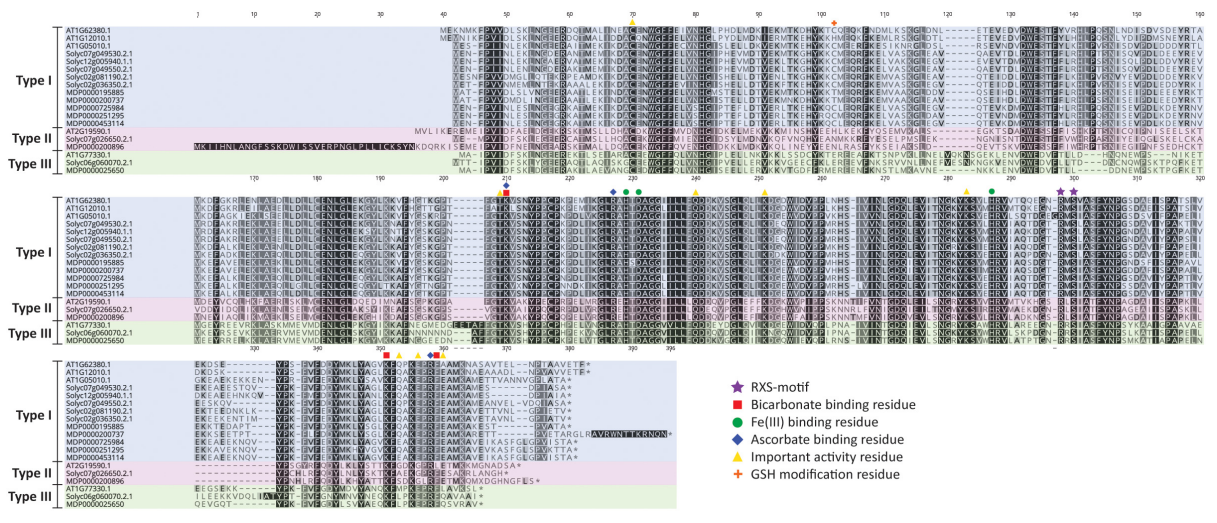

FIGURE 3 | ACO protein sequence alignment of *Arabidopsis thaliana, Solanum lycopersicum*, and *Malus domestica*. Protein sequences were aligned in Geneious (v10.2.2) using the MUSCLE alignment plugin. Important residues are marked according to the legend shown. Type I ACO is shown in blue, Type II ACO is shown in red, and Type III ACO is shown in green.

THE REGULATION OF ACO

ACC-oxidase is expressed to a variable degree in all vegetative and reproductive tissues, which led to the belief that ACO proteins are always present and ready to produce ethylene. Furthermore, treating plant tissue with ACC typically results in a rapid production of ethylene. Therefore, it has been proposed that not ACO, but ACS is the rate-limiting enzyme in ethylene biosynthesis (Adams and Yang, 1979). This hypothesis has been readily absorbed by the community, leading to an abundance of studies focusing on unraveling the regulation and function of ACS in relation to its prime role in ethylene production (Argueso et al., 2007; Booker and DeLong, 2015; Yoon, 2015). However, there is an increasing amount of evidence demonstrating the importance of ACO, and not ACS, in controlling ethylene production in plants. For example ACO is the rate limiting step during flooding of tomato (English et al., 1995) and *Rumex palustris* (Vriezen et al., 1999). ACO activity, and not the availability of ACC, has been shown to be crucial during the formation of tension wood in poplar trees (Andersson-Gunneras et al., 2003; Love et al., 2009). Ethylene induced cotton fiber cell elongation has also been linked to a strong upregulation of its respective *ACO* genes (Shi et al., 2006). ACO has also been shown to be rate limiting during the post-climacteric ripening of tomato fruit (Van de Poel et al., 2012; Grierson, 2014; Van de Poel et al., 2014a,b). Even more recently, a key role for ACO during the sex determination of cucumber flowers was discovered (Chen et al., 2016). These studies indicate that ACO can sometimes be rate limiting and thus controls ethylene production, indicative of a stringent regulatory mechanism that controls ACO expression, stability and/or activity.

Transcriptional Regulation of ACO

Despite the fact that *ACO* expression has been observed to be temporally and spatially regulated (e.g., during tomato flower and fruit development; Barry et al., 1996; Blume and Grierson, 1997; Nakatsuka et al., 1998; Van de Poel et al., 2012), only a few transcription factors have been identified that are known to control *ACO* expression (see **Table 2**). In tomato, *Sl*HB-1, a homeodomain-leucine zipper (HD-Zip) class-I transcription factor was shown to interact with the tomato *ACO1* (Solyc07g049530) promoter using gel retardation assays (Lin et al., 2008). Furthermore, experiments using virus-induced gene silencing showed that a repression of *HB-1* expression resulted in a decrease in *ACO1* transcript levels (Lin et al., 2008). Additionally, Lin et al. (2008) predicted that HB-1 could also target other ripening-related genes such as *ACO2* (Solyc12g005940), *PG1*, *RIN*, and *NOR* (Lin et al., 2008). Martel et al. (2011) reported that the master ripening regulator RIN could interact with the promoter of *HB-1*, placing HB-1 downstream of RIN during tomato fruit ripening. Later it was shown that RIN itself can interact directly with the *CArG* box in the promoter region of *ACO4* (Solyc02g081190) (Li et al., 2017). Besides HB-1 and RIN, different NAC transcription factors have also been observed to play an important role in the control of ethylene biosynthesis in tomato. Specifically, SNAC4 and SNAC9 have been shown to influence tomato fruit ripening by interacting with the promoters of *ACS2, ACS4*, and *ACO1* (Kou et al., 2016). Silencing *SNAC4* and *SNAC9* dramatically reduces the expression of these genes, inhibiting fruit ripening. Furthermore, silencing of *ERF2*, *ACS4*, and *ACO1* also reduces the expression of both *SNAC4* and *SNAC9*, which suggests the existence of a tightly controlled feedback mechanism (Kou et al., 2016).

Ethylene response factors (ERFs) have been shown to be an integral part of the ethylene signaling and response pathway. ERFs are transcription factors that can bind with *cis*-acting elements such as GCC-box motifs and dehydration-responsive elements (DREs) (Ohme-Takagi and Hideaki, 1995; Müller and Munné-Bosch, 2015). Zhang et al. (2009) showed that the tomato *ERF2* (and a homolog allele *TERF2*) was able to interact with the DRE in the promoter of *SlACO3* to activate transcription. They observed a significant increase in ethylene production of the *ERF2/TERF2* overexpression lines and a decrease in the *ERF2/TERF2* antisense-lines compared to the wild type, suggesting that these ERFs are positive regulators of *ACO3* expression in tomato (Zhang et al., 2009).

In banana (*Musa acuminata*), the transcription factor ERF11 was shown to interact directly with the GCC-box motif in the promoter region of *ACO1* and repress *ACO1* expression (Han et al., 2016). Han et al. (2016) also demonstrated that ERF11 can physically interact with the histone deacetylase HDA1, which in turn reinforces the ERF11-induced repression of *ACO1*. Furthermore, the MADS-box transcription factor MADS7 was also shown to interact directly with the promoter of *ACO1* in banana using a yeast one-hybrid (Y1H) system and a transient GUS-reporter activation assay in tobacco (Liu et al., 2015). *MADS7* is only expressed in banana fruit and its expression is stimulated by ethylene and inhibited by 1-MCP. Ectopic overexpression of *MaMADS7* in tomato fruit resulted in a 10-fold increase of *SlACO1* expression compared to wild-type fruit, and resulted in an enhanced ethylene production level (Liu et al., 2015).

Another transcription factor that controls *ACO* expression was also identified in melon fruit (*Cucumis melo*). Huang et al. (2010) reported that EIN3-like proteins EIL1 and EIL2 induce the expression of *ACO1* by interacting with different *cis*-acting elements of the *ACO1* promoter. It was hypothesized that both EIL proteins are targeted for proteolysis by EBF1/EBF2 (similar as in Arabidopsis) in the absence of ethylene, however, upon ethylene release they are stabilized and elevate the biosynthesis of ethylene by inducing the transcription of *ACO1* and thus promote ripening (Huang et al., 2010).

In cucumber (*Cucumis sativus*), the transcription factor WIP1 can regulate flower sex determination by directly binding the promoter of *ACO2* and inhibiting its expression (Chen et al., 2016). Evidence was provided using a dual luciferase activation assay in tobacco, Y1H, ChIP-qPCR, and EMSA to validate the interaction between WIP1 and the *ACO2* promoter (Chen et al., 2016). Chen et al. (2016) also demonstrated that the melon (*Cucumis melo*) homolog of WIP1 can interact with the promoter of *CmACO3*, and similarly as in cucumber, negatively influence *CmACO3* expression.

In *Arabidopsis thaliana*, the NAC transcription factor Speedy Hyponastic Growth (SHYG) was shown to interact with the

TABLE 2 | Functionally confirmed transcription factors that control *ACO* expression in *Solanum lycopersicum, Musa acuminata, Arabidopsis thaliana, Cucumis melo,* and *Cucumis sativus*.

Species	ACO target	Transcription factor	Source
Tomato (*Solanum lycopersicum*)	*ACO1*	HB-1	Lin et al., 2008
	ACO4	RIN	Li et al., 2017
	ACO1	NAC (SNAC9)	Kou et al., 2016
	ACO3	ERF2 and TERF2	Zhang et al., 2009
Banana (*Musa acuminata*)	*ACO1*	ERF11	Han et al., 2016
	ACO1	MADS7	Liu et al., 2015
Arabidopsis thaliana	*ACO5*	SHYG	Rauf et al., 2013
Melon (*Cucumis melo*)	*ACO1*	EIL1 and EIL2	Huang et al., 2010
	ACO3	WIP1	Chen et al., 2016
Cucumber (*Cucumis sativus*)	*ACO2*	WIP1	Chen et al., 2016

promoter region of *ACO5* (AT77330; Rauf et al., 2013). When *SHYG* was overexpressed using an inducible promoter, the expression of *ACO5* was shown to be strongly induced (Rauf et al., 2013).

Differential *ACO* Expression Profiles

In order to get a better insight in the differential expression of the *ACO* gene family, we have summarized the tissue-specific and developmental expression profiles for Arabidopsis and tomato using the eFP browser (http://bar.utoronto.ca/efp/cgi-bin/efpWeb.cgi; Waese et al., 2017) and the Tomato Expression Atlas (http://tea.solgenomics.net/), respectively.

Differential ACO expression in Arabidopsis thaliana

Figure 4 demonstrates that the *Arabidopsis thaliana ACO* genes show a distinct tissue-specific expression pattern. *ACO1* (AT2G19590; Type II) is upregulated during the torpedo and walking-stick stage of embryogenesis, is highly expressed in imbibed seeds and upregulated during the first stages of germination, mainly in the radicle. Furthermore, *ACO1* is also strongly expressed in the roots, where it might be involved in lateral root formation (Park et al., 2018). *ACO2* (AT1G62380; Type I) was shown to be involved in germination, where it participates in ethylene production to control endosperm cap weakening and endosperm rupture (Linkies et al., 2009; Linkies and Leubner-Metzger, 2012). *ACO2* is mostly expressed in the emerging seedling hypocotyl, where it is involved in the formation of the apical hook (Raz and Ecker, 1999). *ACO2* is also highly expressed in the phloem and companion cells of the roots (not shown in **Figure 4**; Brady et al., 2007). *ACO2* is also upregulated during flower opening and specifically during anther, stamen and petal development (van Es et al., 2018). *ACO3* (AT1G12010; Type I) is highly expressed during embryogenesis and during further seed maturation. Furthermore, *ACO3* is expressed in the root, more precisely in the phloem and companion cells (Brady et al., 2007). *ACO4* (AT1G05010; Type I) is mostly expressed in vegetative tissue such as the cotyledons, the rosette, cauline leaves, sepals, and the petiole of senescing leaves. *ACO5* (AT177330; Type III), is mainly expressed in the root (of both seedlings and adult plants), especially in the root apex and the root cap (Brady et al., 2007).

Differential ACO expression during tomato fruit development and climacteric ripening

Figure 5 summarizes the differential and tissue-specific expression of the seven *ACOs* during tomato fruit development and climacteric ripening, based on the Tomato Expression Atlas (TEA). *ACO1* (Solyc07g049530; Type I) is already expressed shortly after anthesis, and expression levels increase moderately throughout fruit development (system I). At the onset of ripening (system II), *ACO1* expression increases strongly and correlates well with the autocatalytic rise in ethylene production (Blume and Grierson, 1997; Nakatsuka et al., 1998; Alexander and Grierson, 2002; Van de Poel et al., 2012). *ACO1* expression appears to be strongest in the pericarp, septa and columella of orange to red fruit, matching the tissue-specific ACO *in vitro* activity reported by Van de Poel et al. (2014b). *ACO2* (Solyc12g005940; Type I) is expressed at anthesis, however, expression drops to a basal level during further fruit development and ripening (Van de Poel et al., 2012). Expression of *ACO3* (Solyc07g049550; Type I) is high during anthesis, but readily drops during initial fruit development. At the onset of ripening, *ACO3* expression strongly increases again. These observations are contradictory to the qPCR data observed by Van de Poel et al. (2012), who showed that *ACO3* expression declines after the breaker stage. *ACO4* (Solyc02g081190; Type I) expression is high during initial fruit development (mainly pericarp tissue) and declines thereafter to a basal expression level. However, there is a temporal increase in *ACO4* expression during the breaker stage, mainly in the columella and placenta tissue. Nakatsuka et al. (1998) showed that *ACO4* expression increases during fruit ripening, but perhaps the use of degenerate primers in the Nakatsuka study could not discriminate between *ACO4* and another *ACO* homolog. *ACO5* (Solyc07g026650; Type II) expression increases slightly after anthesis and remains at a similar level during further fruit development and ripening. However, qPCR analysis by Van de Poel et al. (2012) indicated that *ACO5* follows an expression pattern similar to that of *ACO3*. *ACO6* (Solyc02g036350; Type I) is strongly expressed at anthesis, followed by a low expression during fruit development and a

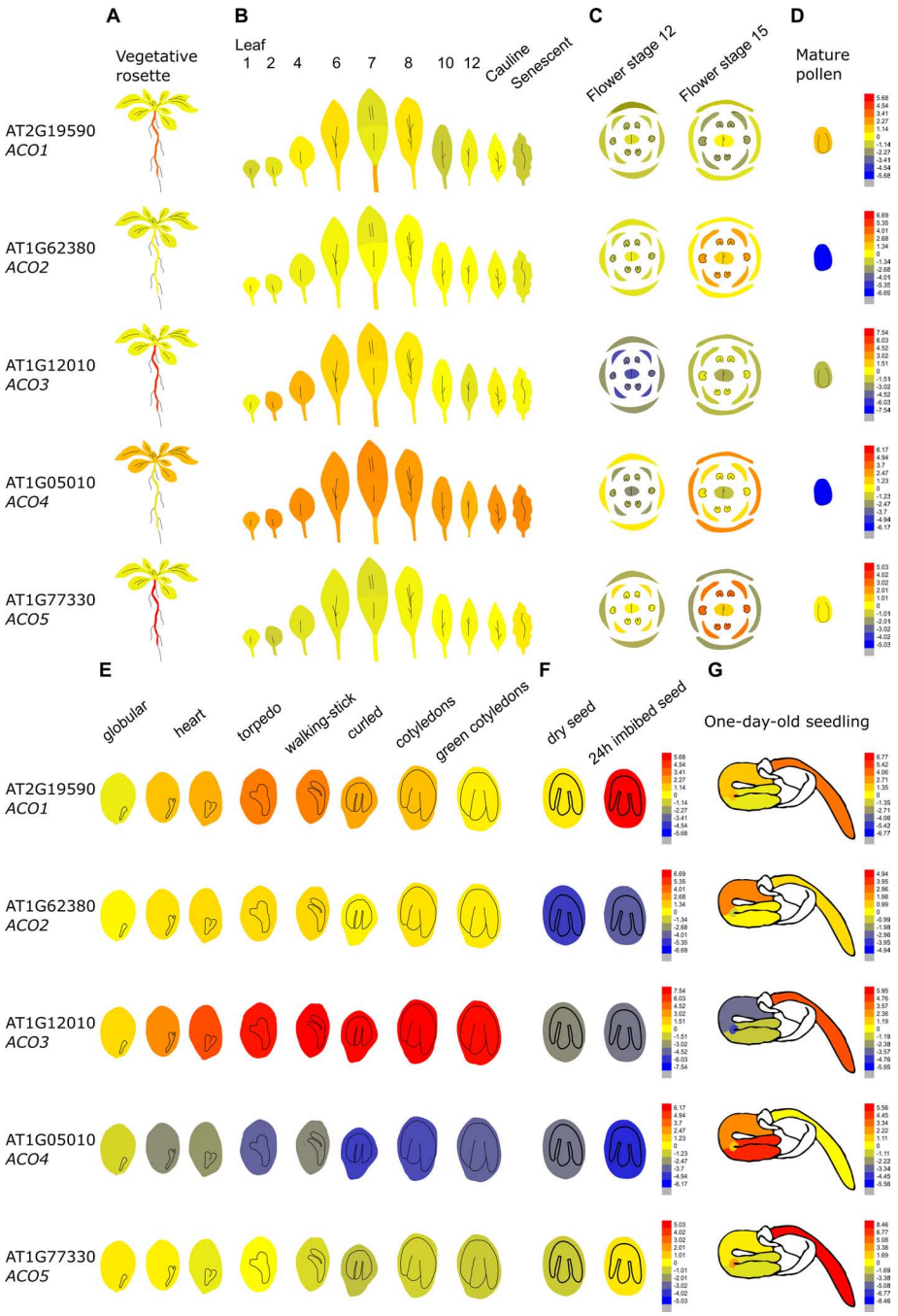

FIGURE 4 | Tissue-specific and developmental expression profiles of the five Arabidopsis ACOs. Data is adapted from the eFP browser. The color scale depicts a Log2 fold expression range (Waese et al., 2017). **(A)** Expression in the vegetative rosette and the root, **(B)** the different leaves, **(C)** the different flowering organs, **(D)** mature pollen, **(E)** the different stages of embryogenesis, **(F)** the dry and imbibed seed, and **(G)** a 1-day-old seedling (Nakabayashi et al., 2005; Schmid et al., 2005; Klepikova et al., 2016).

temporal high expression during the breaker stage, followed by a gradual decline during further ripening. *ACO6* expression is strongest in the pericarp tissue, which is also the tissue that showed the highest *in vivo* ethylene production (Van de Poel et al., 2014b). *ACO7* (Solyc06g060070; Type III) is only basally expressed during fruit development and ripening. The *ACO6* and *ACO7* genes have not yet been characterized during tomato fruit development and ripening.

Post-transcriptional Regulation of ACO

MicroRNAs (miRNAs) are often involved in the post-transcriptional regulation of diverse processes in plant growth

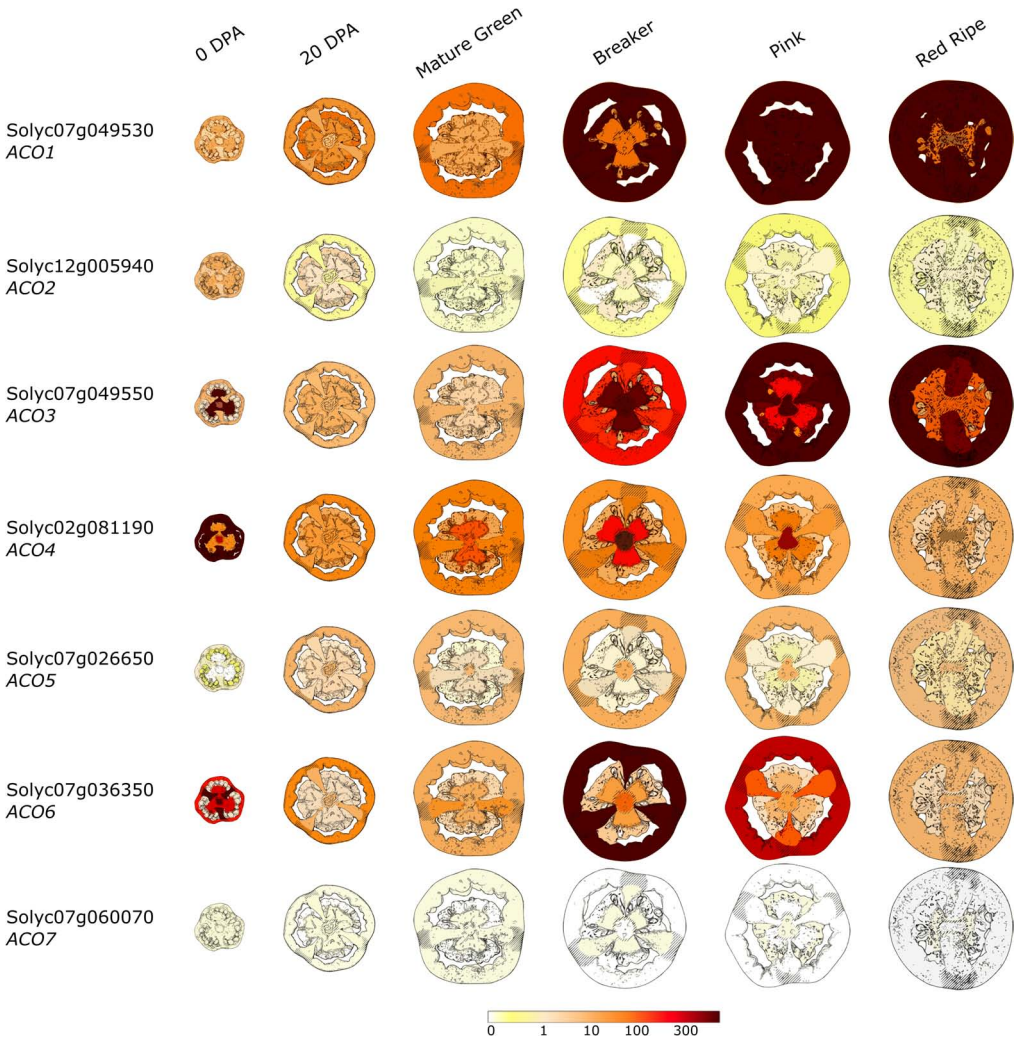

FIGURE 5 | Tissue-specific and developmental expression profiles of the seven tomato ACOs during fruit development and ripening. Data is adapted from the Tomato Expression Atlas (TEA). The color scale depicts the reads per million mapped reads (RPM). Days post anthesis (DPA).

and development. MiRNAs constitute a class of regulatory, small, non-coding RNA molecules of 20 to 24 nucleotides long, which can intervene in gene expression by cleaving mRNA transcripts in a sequence specific way (Liu et al., 2017, 2018; Yu et al., 2017). MiR396b was identified as a cold-responsive miRNA in the cold hardy citrus variety *Ponciferus trifoliata* (Zhang et al., 2014). When the precursor of this miRNA (MIR396b) was overexpressed in lemon (*Citrus lemon*), it led to an increase in cold tolerance. Interestingly, overexpression of this miRNA reduced the expression of *ACO* compared to the wild type lemon. Zhang et al. (2016) showed that miR396b directs the cleavage of *ACO* transcripts, consequently inhibiting ethylene biosynthesis.

Recently, a second miRNA was identified, which affects the expression of *ACO* (Wang et al., 2018). In tomato, *miR1917* directs the cleavage of a specific *CTR4* splice variant in tomato leading to an altered ethylene response. Overexpression of *miR1917* significantly enhanced the expression of *ACS2*, *ACS4*, *ACO1* (Solyc07g049530) and *ACO3* (Solyc07g049550), leading to specific ethylene response phenotypes such as the triple response in etiolated seedlings, an increase in epinastic curvature of leaf petioles, an increased pedicel abscission rate and an accelerated fruit ripening (Wang et al., 2018).

Post-translational Regulation of ACO

An *in vitro* phosphorylation assay using protein extracts of pre- and post-climacteric apple fruit and an ectopically expressed His-tagged *Md*ACO1 (MDP0000195885) hinted for the first time that ACO protein-protein interactions could exist (Dilley et al., 1995). It was observed that apple ACO1 could interact with unidentified proteins and resulted in the phosphorylation of these associated proteins (and possibly also ACO1 itself) in both pre-and post-climacteric samples (Dilley et al., 1995). Later Dilley et al. also speculated about a possible cysteine protease activity of ACO, unrelated to its role in catalyzing the conversion of ACC to ethylene. This hypothesis was based on sequence similarity between ACO

and a tomato cysteine protease (Matarasso et al., 2005), and the strongly conserved C28 as a key residue in the active site of this protease (Dilley et al., 2013). Using *in silico* predictions based on sequence similarity, other motifs for ACO protein-protein interactions, serine/threonine kinases, tyrosine kinases, and glycosylation were identified (Aitken, 1999; Dilley et al., 2013). Despite these predictions, only a few post-translational modifications of ACO have currently been experimentally observed.

Arabidopsis ACO2 (AT1g62380) was identified as a target in a broad proteomics screen that characterized stress-induced protein *S*-glutathionylation, suggesting that ACO2 is post-translationally modified by glutathionylation (Dixon et al., 2005). This was later confirmed in a dedicated S-glutathione pull-down assay with ACO2, where C63 was identified as the target residue for glutathionylation (Datta et al., 2015).The relevance of this post-translational glutathionylation and its involvement in ethylene production remains unknown.

Another thiol-residue modification of ACO was discovered in a large cysteine S-sulfhydration screen in Arabidopsis, which showed that ACO4 can get sulfhydrated (Aroca et al., 2015). This S-modification of ACO was recently confirmed in tomato by Jia et al. (2018), who demonstrated that H_2S production increases in stomata upon a prolonged ethylene treatment, and that this leads to the S-sulfhydration of C60 (equivalent to C63 of *At*ACO2) of *Sl*ACO1 (Solyc07g049530) and *Sl*ACO2 (Solyc12g005940). This ACO sulfhydration resulted in a significant drop in ACO activity and consequently ethylene production, unmasking a direct crosstalk between ethylene and H_2S production. It was argued that this sulfhydration was necessary to protect the plant from the detrimental effects of prolonged ethylene production and exposure (e.g., during senescence and programmed cell death) (Jia et al., 2018). At the moment, it remains unclear if this cysteine glutathionylation and/or sulfhydration leads to a different ACO activity or whether it is involved in protein interaction and/or protein stability. In general, post-translational modifications of the thiol-groups of cysteine residues by S-glutathionylation or S-sulfhydration are involved in the protection of proteins from irreversible oxidation or redox changes (Gao et al., 2009; Datta et al., 2015) or modulate protein-protein interactions (Aroca et al., 2015). The exact function of ACO S-glutathionylation and S-sulfhydration remains to be further investigated.

In petunia, Tan et al. (2014) identified GRL2 (Green-like 2) as a novel interacting partner of ACO1 in a yeast two-hybrid screen using GRL2 as bait and a cDNA library of petals and leaves as prey. They also observed that the suppression of *GRL2* expression resulted in an increased ethylene production of flowers, leading to an accelerated flower senescence. Therefore, GRL2 is proposed to serve as a negative regulator of ethylene production that can directly influence the activity of ACO1 (Tan et al., 2014).

TABLE 3 | Overview of ACO-directed transgenic applications in different agricultural crops.

Crop	Target gene	Approach	References
Apple (*Malus domestica*)	*ACO1 + ACS 8-like*	Antisense RNA	Dandekar et al., 2004
Broccoli (*Brassica oleracea*)	*ACO*	Antisense RNA	Henzi et al., 1999
	ACO2	Antisense RNA	Gapper et al., 2005
Carnation (*Dianthus caryophyllus*)	*ACO*	Antisense RNA	Savin et al., 1995
Lemon (*Citrus lemon*)	MIR396b	Overexpression	Zhang et al., 2016
Kiwi (*Actinidia chinensis*)	*ACO1-4 + ACO6*	RNAi	Atkinson et al., 2011
Melon (*Cucumis melo*)	*ACO1*	Antisense RNA	Ayub et al., 1996; Bauchot et al., 1998; Ben-Amor et al., 1999
	ACO	Antisense RNA	Guis et al., 1997
	ACO	Antisense RNA	Silva et al., 2004
	ACO1	Antisense RNA	Nuñez-Palenius et al., 2006
Papaya (*Carica papaya*)	*ACO1*	Cosuppression	López-Gómez et al., 2009
	ACO1 + ACO2	RNAi	Sekeli et al., 2014
Poplar	*ACO1*	Overexpression	Love et al., 2009
Pear (*Pyrus communis*)	*ACO1*	Sense/antisense RNA	Gao et al., 2007
Petunia	*ACO + ACS*	Antisense RNA	Huang et al., 2007
	GRL2	VIGS	Tan et al., 2014
Safflower (*Carthamus tinctorius*)	*ACO1*	Overexpression	Tu et al., 2019
Tobacco (*Nicotiana tabacum*)	*ACO*	Sense/antisense RNA	Knoester et al., 1997
Tomato (*Solanum lycopersicum*)	*ACO1*	Antisense RNA	Hamilton et al., 1990; Picton et al., 1993
	ACO1	Antisense RNA	English et al., 1995
	ACO	Antisense RNA	Batra et al., 2010
	ACO	RNAi	Xiong et al., 2005
	HD1	VIGS	Lin et al., 2008
Torenia (*Torenia fournieri*)	*ACO*	Sense/antisense RNA	Aida et al., 1998

ACO BIOTECHNOLOGY AND APPLICATIONS

Because ethylene plays a crucial role in many plant processes, including climacteric fruit ripening and senescence, excessive ethylene can lead to unwanted decay of plant-based food. Therefore, ethylene biosynthesis or signaling genes have been frequently targeted in biotechnological and transgenic approaches in order to increase the shelf life of plant-based food. Because ACO catalyzes the final step in the ethylene biosynthesis pathway, it is therefore an ideal candidate to target (instead of for example ACS or ethylene signaling components), because there are fewer risk of intervening in other pathways (e.g., ACC metabolism). **Table 3** presents an exhaustive list, although probably not exclusive, of several transgenic applications controlling ethylene production at the level of ACO for important agricultural crops.

One of the most rewarding applications of ACO-directed biotechnology in plants is the reduction of ethylene production during ripening and postharvest storage of climacteric fruit. *ACO* has been targeted using various antisense RNAi techniques to downregulate its expression and consequently decrease ethylene production, resulting in control over fruit ripening and postharvest storage. **Table 3** shows that this approach was successfully implemented for a wide variety of fruits: apple, lemon, kiwi, melon, papaya, pear, and tomato (Hamilton et al., 1990; Picton et al., 1993; English et al., 1995; Ayub et al., 1996; Guis et al., 1997; Bauchot et al., 1998; Ben-Amor et al., 1999; Dandekar et al., 2004; Silva et al., 2004; Xiong et al., 2005; Nuñez-Palenius et al., 2006; Gao et al., 2007; Lin et al., 2008; López-Gómez et al., 2009; Batra et al., 2010; Atkinson et al., 2011; Sekeli et al., 2014; Zhang et al., 2016). In all these studies, fruit ripening was delayed and shelf-life was prolonged. A similar approach has also been used to prolong the shelf life of vegetative tissue of vegetables, such as for example broccoli (Henzi et al., 1999; Gapper et al., 2005).

Transgenic approaches that silence *ACO* expression are also beneficial in floriculture. It has been shown that a reduced *ACO* expression resulted in a delay in flower senescence and flower abscission in petunia, carnation, and torenia (Savin et al., 1995; Aida et al., 1998; Huang et al., 2007; Tan et al., 2014). Besides controlling fruit ripening or flower senescence, *ACO*s have also been targeted in other ethylene-related processes. For example, tomato plants transformed with an *ACO1* antisense construct showed delayed leaf senescence (John et al., 1995) and less epinasty during soil flooding (English et al., 1995). A mutation in cucumber *ACO2* resulted in a mutant that only bears male flowers, suggesting that *ACO2* plays an important role in sex determination in cucumber flowers (Chen et al., 2016).

Besides silencing *ACO* expression and reducing ethylene production, it can sometimes be desirable to boost ethylene production, and then an *ACO* overexpression construct is most suitable. In safflower, *ACO1* overexpression was shown to stimulate the flavonoid biosynthesis pathway, which could be interesting for oilseed production (Tu et al., 2019). Overexpression of *ACO1* in poplar (*Populus tremula* × *tremuloides*) caused a stimulation of cambial cell division, which in turn resulted in an increased xylem development and an inhibition of elongation growth, which are desirable traits for the wood industry (Love et al., 2009). Altogether, these transgenic examples show the potential of controlling ethylene production levels by targeting the *ACO* gene family. Perhaps new breeding technologies such as CRISPR/Cas9-mediated mutations in the *ACO* promotor or coding sequence could also lead to novel strategies to control ethylene production in plants.

DATA AVAILABILITY

No datasets were generated or analyzed for this study.

AUTHOR CONTRIBUTIONS

Both authors have made a substantial, direct and intellectual contribution to the work, and approved it for publication.

FUNDING

This work was supported by the University of Leuven (STGBF/16/005 and C14/18/056) and the Research Foundation Flanders (SB/1S18717N, G092419N, and G0G0219N).

SUPPLEMENTARY MATERIAL

The Supplementary Material for this article can be found online at: https://www.frontiersin.org/articles/10.3389/fpls.2019.00695/full#supplementary-material

REFERENCES

Adams, D. O., and Yang, S. F. (1977). Methionine metabolism in apple tissue: implication of s-adenosylmethionine as an intermediate in the conversion of methionine to ethylene. *Plant Physiol.* 60, 892–896. doi: 10.1104/pp.60.6.892

Adams, D. O., and Yang, S. F. (1979). Ethylene biosynthesis: Identification of 1-aminocyclopropane-1-carboxylic acid as an intermediate in the conversion of methionine to ethylene. *Proc. Natl. Acad. Sci. U.S.A.* 76, 170–174. doi: 10.1073/pnas.76.1.170

Adams, D. O., and Yang, S. F. (1981). Ethylene the gaseous plant hormone: mechanism and regulation of biosynthesis. *Trends Biochem. Sci.* 6, 161–164. doi: 10.1016/0968-0004(81)90059-90051

Aida, R., Yoshida, T., Ichimura, K., Goto, R., and Shibata, M. (1998). Extension of flower longevity in transgenic torenia plants incorporating ACC oxidase transgene. *Plant Sci.* 138, 91–101. doi: 10.1016/S0168-9452(98)00139-133

Aik, W. S., Chowdhury, R., Clifton, I. J., Hopkinson, R. J., Leissing, T., McDonough, M. A., et al. (2015). Introduction to structural studies on 2-oxoglutarate-dependent oxygenases and related enzymes. *RSC Metallobiol.* 2015, 59–94. doi: 10.1039/9781782621959-00059

Aitken, A. (1999). Protein consensus sequence motifs. *Mol. Biotechnol.* 12, 241–254. doi: 10.1385/mb:12:3:241

Alexander, L., and Grierson, D. (2002). Ethylene biosynthesis and action in tomato: a model for climacteric fruit ripening. *J. Exp. Bot.* 53, 2039–2055. doi: 10.1093/jxb/erf072

Amrhein, N., Schneebeck, D., Skorupka, H., Tophof, S., and Stöckigt, J. (1981). Identification of a major metabolite of the ethylene precursor 1-aminocyclopropane-1-carboxylic acid in higher plants. *Naturwissenschaften* 68, 619–620. doi: 10.1007/BF00398617

Andersson-Gunneras, S., Hellgren, J. M., Bjorklund, S., Regan, S., Moritz, T., and Sundberg, B. (2003). Asymmetric expression of a poplar ACC oxidase controls ethylene production during gravitational induction of tension wood. *Plant J.* 34, 339–349. doi: 10.1046/j.1365-313X.2003.01727.x

Argueso, C. T., Hansen, M., and Kieber, J. J. (2007). Regulation of ethylene biosynthesis. *J. Plant Growth Regul.* 26, 92–105. doi: 10.1007/s00344-007-0013-5

Aroca, Á, Serna, A., Gotor, C., and Romero, L. C. (2015). S -Sulfhydration: a cysteine posttranslational modification in plant systems. *Plant Physiol.* 168, 334–342. doi: 10.1104/pp.15.00009

Atkinson, R. G., Gunaseelan, K., Wang, M. Y., Luo, L., Wang, T., Norling, C. L., et al. (2011). Dissecting the role of climacteric ethylene in kiwifruit (Actinidia chinensis) ripening using a 1-aminocyclopropane-1-carboxylic acid oxidase knockdown line. *J. Exp. Bot.* 62, 3821–3835. doi: 10.1093/jxb/err063

Ayub, R., Guis, M., Amor, M., Ben Gillot, L., Roustan, J.-P., Latché, A., et al. (1996). Expression of ACC oxidase antisense gene inhibits ripening of cantaloupe melon fruits. *Nat. Biotechnol.* 14, 862–866. doi: 10.1038/nbt0796-862

Barry, C. S., Blume, B., Bouzayen, M., Cooper, W., Hamilton, A. J., and Grierson, D. (1996). Differential expression of the 1-aminocyclopropane-1-carboxylate oxidase gene family of tomato. *Plant J.* 9, 525–535. doi: 10.1046/j.1365-313X.1996.09040525.x

Batra, A., Sane, V. A., Trivedi, P. K., Sane, A. P., and Nath, P. (2010). Suppression of ACC oxidase expression in tomato using heterologous gene from banana prolongs shelf-life both on vine and post-harvest. *Curr. Sci.* 99, 1243–1250.

Bauchot, A. D., Mottram, D. S., Dodson, A. T., and John, P. (1998). Effect of aminocyclopropane-1-carboxylic acid oxidase antisense gene on the formation of volatile esters in cantaloupe charentais melon (*Cv. Védrandais*). *J. Agric. Food Chem.* 46, 4787–4792. doi: 10.1021/jf980692z

Ben-Amor, M., Flores, B., Latché, A., Bouzayen, M., Pech, J. C., and Romojaro, F. (1999). Inhibition of ethylene biosynthesis by antisense ACC oxidase RNA prevents chilling injury in *Charentais cantaloupe* melons. *Plant. Cell Environ.* 22, 1579–1586. doi: 10.1046/j.1365-3040.1999.00509.x

Bidonde, S., Ferrer, M. A., Zegzouti, H., Ramassamy, S., Latche, A., Pech, J.-C., et al. (1998). Expression and characterization of three tomato 1-aminocyclopropane-1-carboxylate oxidase cDNAs in yeast. *Eur. J. Biochem.* 253, 20–26. doi: 10.1046/j.1432-1327.1998.2530020.x

Binnie, J. E., and McManus, M. T. (2009). Characterization of the 1-aminocyclopropane-1-carboxylic acid (ACC) oxidase multigene family of *Malus* domestica borkh. *Phytochemistry* 70, 348–360. doi: 10.1016/j.phytochem.2009.01.002

Blume, B., and Grierson, D. (1997). Expression of ACC oxidase promoter-GUS fusions in tomato and Nicotiana plumbaginifolia regulated by developmental and environmental stimuli. *Plant J.* 12, 731–746. doi: 10.1046/j.1365-313X.1997.12040731.x

Boller, T., Herner, R. C., and Kende, H. (1979). Assay for and enzymatic formation of an ethylene precursor, 1-aminocyclopropane-1-carboxylic acid. *Planta* 145, 293–303. doi: 10.1007/BF00454455

Booker, M. A., and DeLong, A. (2015). Producing the ethylene signal: regulation and diversification of ethylene biosynthetic enzymes. *Plant Physiol.* 169, 42–50. doi: 10.1104/pp.15.00672

Bouzayen, M., Felix, G., Latché, A., Pech, J.-C., and Boller, T. (1991). Iron: an essential cofactor for the conversion of 1-aminocyclopropane-1-carboxylic acid to ethylene. *Planta* 184, 244–247. doi: 10.1007/BF00197953

Bouzayen, M., Latché, A., and Pech, J.-C. (1990). Subcellular localization of the sites of conversion of 1-aminocyclopropane-1-carboxylic acid into ethylene in plant cells. *Planta* 180, 175–180. doi: 10.1007/BF00193992

Brady, S. M., Mace, D., Ohler, U., and Benfey, P. N. (2007). A high-resolution root spatiotemporal map reveals spatiotemporal map reveals dominant expression patterns dominant expression patterns. *Science* 318, 801–806. doi: 10.1126/science.1146265

Brisson, L., El Bakkali-Taheri, N., Giorgi, M., Fadel, A., Kaizer, J., Réglier, M., et al. (2012). 1-Aminocyclopropane-1-carboxylic acid oxidase: insight into cofactor binding from experimental and theoretical studies. *J. Biol. Inorg. Chem.* 17, 939–949. doi: 10.1007/s00775-012-0910-3

Burg, S. P., and Burg, E. A. (1965). Ethylene action and the ripening of fruits. *Science* 148, 1190–1196. doi: 10.1126/science.148.3674.1190

Bürstenbinder, K., Waduwara, I., Schoor, S., Moffatt, B. A., Wirtz, M., Minocha, S. C., et al. (2010). Inhibition of 5′-methylthioadenosine metabolism in the Yang cycle alters polyamine levels, and impairs seedling growth and reproduction in Arabidopsis. *Plant J.* 62, 977–988. doi: 10.1111/j.1365-313X.2010.04211.x

Chae, H. S., Cho, Y. G., Park, M. Y., Lee, M. C., Eun, M. Y., Kang, B. G., et al. (2000). Hormonal cross-talk between auxin and ethylene differentially regulates the expression of two members of the 1-aminocyclopropane-1-carboxylate oxidase gene family in rice (*Oryza sativa* L.). *Plant Cell Physiol.* 41, 354–362. doi: 10.1093/pcp/41.3.354

Chen, H., Sun, J., Li, S., Cui, Q., Zhang, H., Xin, F., et al. (2016). An ACC oxidase gene essential for cucumber carpel development. *Mol. Plant* 9, 1315–1327. doi: 10.1016/j.molp.2016.06.018

Chung, M.-C., Chou, S.-J., Kuang, L.-Y., Charng, Y., and Yang, S. F. (2002). Subcellular localization of 1-aminocyclopropane-1-carboxylic acid oxidase in apple fruit. *Plant Cell Physiol.* 43, 549–554. doi: 10.1093/pcp/pcf067

Clouse, R. M., and Carraro, N. (2014). A novel phylogeny and morphological reconstruction of the PIN genes and first phylogeny of the ACC-oxidases (ACOs). *Front. Plant Sci.* 5:296. doi: 10.3389/fpls.2014.00296

Dandekar, A. M., Teo, G., Defilippi, B. G., Uratsu, S. L., Passey, A. J., Kader, A. A., et al. (2004). Effect of down-regulation of ethylene biosynthesis on fruit flavor complex in apple fruit. *Transgenic Res.* 13, 373–384. doi: 10.1023/B:TRAG.0000040037.90435.45

Datta, R., Kumar, D., Sultana, A., Hazra, S., Bhattacharyya, D., and Chattopadhyay, S. (2015). Glutathione regulates ACC synthase transcription via WRKY33 and ACC oxidase by modulating mRNA stability to induce ethylene synthesis during stress. *Plant Physiol.* 169, 2963–2981. doi: 10.1104/pp.15.01543

Dilley, D. R., Kuai, J., Wilson, I. D., Pekker, Y., Zhu, Y., Burmeister, D. M., et al. (1995). Molecular biological investigations of ACC oxidase and its expression attending apple fruit ripening. *Acta Hortic* 379, 25–40. doi: 10.17660/ActaHortic.1995.379.1

Dilley, D. R., Wang, Z., Kadirjan-Kalbach, D. K., Ververidis, F., Beaudry, R., and Padmanabhan, K. (2013). 1-Aminocyclopropane-1-carboxylic acid oxidase reaction mechanism and putative post-translational activities of the ACCO protein. *AoB Plants* 5, 1–23. doi: 10.1093/aobpla/plt031

Dixon, D. P., Skipsey, M., Grundy, N. M., and Edwards, R. (2005). Stress-induced protein S-glutathionylation in *Arabidopsis*. *Plant Physiol.* 138, 2233–2244. doi: 10.1104/pp.104.058917

Dong, J. G., Olson, D., Silverstone, A., and Yang, S. F. (1992). Sequence of a cDNA coding for a 1-aminocyclopropane-1-carboxylate oxidase homolog from apple fruit. *Plant Physiol.* 98, 1530–1531. doi: 10.1104/pp.98.4.1530

English, P. J., Lycett, G. W., Roberts, J. A., and Jackson, M. B. (1995). Increased 1-aminocyclopropane-1-carboxylic acid oxidase activity in shoots of flooded tomato plants raises ethylene production to physiologically active levels. *Plant Physiol.* 109, 1435–1440. doi: 10.1104/pp.109.4.1435

Farrow, S. C., and Facchini, P. J. (2014). Functional diversity of 2-oxoglutarate/Fe(II)-dependent dioxygenases in plant metabolism. *Front. Plant Sci.* 5:524. doi: 10.3389/fpls.2014.00524

Gallie, D. R., and Young, T. E. (2004). The ethylene biosynthetic and perception machinery is differentially expressed during endosperm and embryo development in maize. *Mol. Genet. Genomics* 271, 267–281. doi: 10.1007/s00438-004-0977-9

Gao, M., Matsuta, N., Murayama, H., Toyomasu, T., Mitsuhashi, W., Dandekar, A. M., et al. (2007). Gene expression and ethylene production in transgenic pear (Pyrus communis cv. 'La France') with sense or antisense cDNA encoding ACC oxidase. *Plant Sci.* 173, 32–42. doi: 10.1016/j.plantsci.2007.03.014

Gao, X.-H., Bedhomme, M., Veyel, D., Zaffagnini, M., and Lemaire, S. D. (2009). Methods for analysis of protein glutathionylation and their application to photosynthetic organisms. *Mol. Plant* 2, 218–235. doi: 10.1093/mp/ssn072

Gapper, N. E., Coupe, S. A., McKenzie, M. J., Scott, R. W., Christey, M. C., Lill, R. E., et al. (2005). Senescence-associated down-regulation of 1-aminocyclopropane-1-carboxylate (ACC) oxidase delays harvest-induced senescence in broccoli. *Funct. Plant Biol.* 32:891. doi: 10.1071/FP05076

Gómez-Lim, M. A., Valdés-López, V., Cruz-Hernandez, A., and Saucedo-Arias, L. J. (1993). Isolation and characterization of a gene involved in ethylene biosynthesis from Arabidopsis thaliana. *Gene* 134, 217–221. doi: 10.1016/0378-1119(93)90096-L

Grierson, D. (2014). "Ethylene Biosynthesis," in *Fruit Ripening Physiology, Signalling and Genomics*, eds P. Nath, M. Bouzayen, A. K. Mattoo, and J. C. Pech (Oxfordshire: CAB International), 178–192.

Guis, M., Bouquin, T., Zegzouti, H., Ayub, R., Ben Amor, M., Lasserre, E., et al. (1997). "Differential Expression of ACC Oxidase Genes in Melon and Physiological Characterization of Fruit Expressing an Antisense ACC Oxidase Gene," in *Biology and Biotechnology of the Plant Hormone Ethylene*, eds A. K. Kanellis, C. Chang, H. Kende, and D. Grierson (Dordrecht: Springer), 327–337. doi: 10.1007/978-94-011-5546-5_40

Guy, M., and Kende, H. (1984). Conversion of 1-aminocyclopropane-1-carboxylic acid to ethylene by isolated vacuoles of Pisum sativum L. *Planta* 160, 281–287. doi: 10.1007/BF00402867

Hamilton, A. J., Bouzayen, M., and Grierson, D. (1991). Identification of a tomato gene for the ethylene-forming enzyme by expression in yeast. *Proc. Natl. Acad. Sci. U.S.A.* 88, 7434–7437. doi: 10.1073/pnas.88.16.7434

Hamilton, A. J., Lycett, G. W., and Grierson, D. (1990). Antisense gene that inhibits synthesis of the hormone ethylene in transgenic plants. *Nature* 346, 284–287. doi: 10.1038/346284a0

Han, Y., Kuang, J., Chen, J., Liu, X., Xiao, Y., Fu, C., et al. (2016). Banana transcription factor MaERF11 recruits histone deacetylase MaHDA1 and represses the expression of MaACO1 and expansins during fruit ripening. *Plant Physiol.* 171:00301.2016. doi: 10.1104/pp.16.00301

Henzi, M. X., McNeil, D. L., Christey, M. C., and Lill, R. E. (1999). A tomato antisense 1-aminocyclopropane-1-carboxylic acid oxidase gene causes reduced ethylene production in transgenic broccoli. *Funct. Plant Biol.* 26:179. doi: 10.1071/PP98083

Holdsworth, M. J., Schuch, W., and Grierson, D. (1987). Nucleotide sequence of an ethylene-related gene from tomato. *Nucleic Acids Res.* 15:10600. doi: 10.1093/nar/15.24.10600

Huang, L.-C., Lai, U.-L., Yang, S.-F., Chu, M.-J., Kuo, C.-I., Tsai, M.-F., et al. (2007). Delayed flower senescence of *Petunia hybrida* plants transformed with antisense broccoli ACC synthase and ACC oxidase genes. *Postharvest Biol. Technol.* 46, 47–53. doi: 10.1016/j.postharvbio.2007.03.015

Huang, S., Sawaki, T., Takahashi, A., Mizuno, S., Takezawa, K., Matsumura, A., et al. (2010). Melon EIN3-like transcription factors (CmEIL1 and CmEIL2) are positive regulators of an ethylene- and ripening-induced 1-aminocyclopropane-1-carboxylic acid oxidase gene (CM-ACO1). *Plant Sci.* 178, 251–257. doi: 10.1016/j.plantsci.2010.01.005

Hudgins, J. W., Ralph, S. G., Franceschi, V. R., and Bohlmann, J. (2006). Ethylene in induced conifer defense: cDNA cloning, protein expression, and cellular and subcellular localization of 1-aminocyclopropane-1-carboxylate oxidase in resin duct and phenolic parenchyma cells. *Planta* 224, 865–877. doi: 10.1007/s00425-006-0274-4

Iwai, T., Miyasaka, A., Seo, S., and Ohashi, Y. (2006). Contribution of ethylene biosynthesis for resistance to blast fungus infection in young rice plants. *Plant Physiol.* 142, 1202–1215. doi: 10.1104/pp.106.085258

Jafari, Z., Haddad, R., Hosseini, R., and Garoosi, G. (2013). Cloning, identification and expression analysis of ACC oxidase gene involved in ethylene production pathway. *Mol. Biol. Rep.* 40, 1341–1350. doi: 10.1007/s11033-012-2178-7

Jia, H., Chen, S., Liu, D., Liesche, J., Shi, C., Wang, J., et al. (2018). Ethylene-induced hydrogen sulfide negatively regulates ethylene biosynthesis by persulfidation of ACO in tomato under osmotic stress. *Front. Plant Sci.* 9:1517. doi: 10.3389/fpls.2018.01517

John, I., Drake, R., Farrell, A., Cooper, W., Lee, P., Horton, P., et al. (1995). Delayed leaf senescence in ethylene-deficient ACC-oxidase antisense tomato plants: molecular and physiological analysis. *Plant J.* 7, 483–490. doi: 10.1046/j.1365-313X.1995.7030483.x

Kadyrzhanova, D., McCully, T. J., Warner, T., Vlachonasios, K., Wang, Z., and Dilley, D. R. (1999). "Analysis of ACC Oxidase Activity by Site-Directed Mutagenesis of Conserved Amino Acid Residues," in *Biology and Biotechnology of the Plant Hormone Ethylene II*, eds A. K. Kanellis, et al. (Dordrecht: Springer), 7–12. doi: 10.1007/978-94-011-4453-7_2

Kawai, Y., Ono, E., and Mizutani, M. (2014). Evolution and diversity of the 2-oxoglutarate-dependent dioxygenase superfamily in plants. *Plant J.* 78, 328–343. doi: 10.1111/tpj.12479

Kende, H. (1989). Enzymes of ethylene biosynthesis. *Plant Physiol.* 91, 1–4. doi: 10.1104/pp.91.1.1

Klepikova, A. V., Kasianov, A. S., Gerasimov, E. S., Logacheva, M. D., and Penin, A. A. (2016). A high resolution map of the *Arabidopsis thaliana* developmental transcriptome based on RNA-seq profiling. *Plant J.* 88, 1058–1070. doi: 10.1111/tpj.13312

Knoester, M., Linthorst, H. J. M., Bol, J. F., and van Loon, L. (1997). Modulation of stress-inducible ethylene biosynthesis by sense and antisense gene expression in tobacco. *Plant Sci.* 126, 173–183. doi: 10.1016/S0168-9452(97)00097-6

Kou, X., Liu, C., Han, L., Wang, S., and Xue, Z. (2016). NAC transcription factors play an important role in ethylene biosynthesis, reception and signaling of tomato fruit ripening. *Mol. Genet. Genom.* 291, 1205–1217. doi: 10.1007/s00438-016-1177-0

Li, L., Wang, X., Zhang, X., Guo, M., and Liu, T. (2017). Unraveling the target genes of RIN transcription factor during tomato fruit ripening and softening. *J. Sci. Food Agric.* 97, 991–1000. doi: 10.1002/jsfa.7825

Lieberman, M., Kunishi, A., Mapson, L. W., and Wardale, D. A. (1966). Stimulation of ethylene production in apple tissue slices by methionine. *Plant Physiol.* 41, 376–382. doi: 10.1104/pp.41.3.376

Lin, Z., Hong, Y., Yin, M., Li, C., Zhang, K., and Grierson, D. (2008). A tomato HD-Zip homeobox protein. LeHB-1, plays an important role in floral organogenesis and ripening. *Plant J.* 55, 301–310. doi: 10.1111/j.1365-313X.2008.03505.x

Lin, Z., Zhong, S., and Grierson, D. (2009). Recent advances in ethylene research. *J. Exp. Bot.* 60, 3311–3336. doi: 10.1093/jxb/erp204

Linkies, A., and Leubner-Metzger, G. (2012). Beyond gibberellins and abscisic acid: how ethylene and jasmonates control seed germination. *Plant Cell Rep.* 31, 253–270. doi: 10.1007/s00299-011-1180-1

Linkies, A., Muller, K., Morris, K., Tureckova, V., Wenk, M., Cadman, C. S. C., et al. (2009). Ethylene interacts with abscisic acid to regulate endosperm rupture during germination: a comparative approach using lepidium sativum and *Arabidopsis thaliana*. *Plant Cell* 21, 3803–3822. doi: 10.1105/tpc.109.070201

Liu, H., Yu, H., Tang, G., and Huang, T. (2018). Small but powerful: function of microRNAs in plant development. *Plant Cell Rep.* 37, 515–528. doi: 10.1007/s00299-017-2246-5

Liu, J., Liu, L., Li, Y., Jia, C., Zhang, J., Miao, H., et al. (2015). Role for the banana AGAMOUS-like gene MaMADS7 in regulation of fruit ripening and quality. *Physiol. Plant.* 155, 217–231. doi: 10.1111/ppl.12348

Liu, W., Meng, J., Cui, J., and Luan, Y. (2017). Characterization and function of MicroRNA*s in Plants. *Front. Plant Sci.* 8:2200. doi: 10.3389/fpls.2017.02200

López-Gómez, R., Cabrera-Ponce, J. L., Saucedo-Arias, L. J., Carreto-Montoya, L., Villanueva-Arce, R., Díaz-Perez, J. C., et al. (2009). Ripening in papaya fruit is altered by ACC oxidase cosuppression. *Transgenic Res.* 18, 89–97. doi: 10.1007/s11248-008-9197-0

Love, J., Bjorklund, S., Vahala, J., Hertzberg, M., Kangasjarvi, J., and Sundberg, B. (2009). Ethylene is an endogenous stimulator of cell division in the cambial meristem of Populus. *Proc. Natl. Acad. Sci. U.S.A.* 106, 5984–5989. doi: 10.1073/pnas.0811660106

Martel, C., Vrebalov, J., Tafelmeyer, P., and Giovannoni, J. J. (2011). The tomato MADS-box transcription factor ripening inhibitor interacts with promoters involved in numerous ripening processes in a colorless nonripening-dependent manner. *Plant Physiol.* 157, 1568–1579. doi: 10.1104/pp.111.181107

Martin, M. N., and Saftner, R. A. (1995). Purification and characterization of 1-aminocyclopropane-1-carboxylic acid n-malonyltransferase from tomato fruit. *Plant Physiol.* 108, 1241–1249. doi: 10.1104/pp.108.3.1241

Martinez, S., and Hausinger, R. P. (2015). Catalytic mechanisms of Fe(II)- and 2-Oxoglutarate-dependent oxygenases. *J. Biol. Chem.* 290, 20702–20711. doi: 10.1074/jbc.R115.648691

Matarasso, N., Schuster, S., and Avni, A. (2005). A Novel Plant cysteine protease has a dual function as a regulator of 1-aminocyclopropane-1-carboxylic acid

synthase gene expression. *Plant Cell* 17, 1205–1216. doi: 10.1105/tpc.105.030775

Mayne, R. G., and Kende, H. (1986). Ethylene biosynthesis in isolated vacuoles of Vicia faba L. - requirement for membrane integrity. *Planta* 167, 159–165. doi: 10.1007/BF00391410

Mitchell, T., Porter, A. J. R., and John, P. (1988). Authentic activity of the ethylene-forming enzyme observed in membranes obtained from kiwifruit (Actinidia deliciosa). *New Phytol.* 109, 313–319. doi: 10.1111/j.1469-8137.1988.tb04200.x

Müller, M., and Munné-Bosch, S. (2015). Ethylene response factors: a key regulatory hub in hormone and stress signaling. *Plant Physiol.* 169, 32–41. doi: 10.1104/pp.15.00677

Murphy, L. J., Werner-zwanziger, U., Moilanen, J., Tuononen, H. M., and Clyburne, J. A. C. (2014). A simple complex on the verge elusive cyanoformate ion. *Science* 75, 75–79. doi: 10.1126/science.1250808

Murr, D. P., and Yang, S. F. (1975). Conversion of 5'-methylthioadenosine to methionine by apple tissue. *Phytochemistry* 14, 1291–1292. doi: 10.1016/S0031-9422(00)98613-8

Nakatsuka, A., Murachi, S., Okunishi, H., Shiomi, S., Nakano, R., Kubo, Y., et al. (1998). Differential expression and internal feedback regulation of 1-aminocyclopropane-1-carboxylate synthase, 1-aminocyclopropane-1-carboxylate oxidase, and ethylene receptor genes in tomato fruit during development and ripening. *Plant Physiol.* 118, 1295–1305. doi: 10.1104/pp.118.4.1295

Nakabayashi, K., Okamoto, M., Koshiba, T., Kamiya, Y., and Nambara, E. (2005). Genome-wide profiling of stored mRNA in *Arabidopsis thaliana* seed germination: epigenetic and genetic regulation of transcription in seed. *Plant J.* 41, 697–709. doi: 10.1111/j.1365-313X.2005.02337.x

Nuñez-Palenius, H. G., Cantliffe, D. J., Huber, D. J., Ciardi, J., and Klee, H. J. (2006). Transformation of a muskmelon 'Galia' hybrid parental line (Cucumis melo L. var. reticulatus Ser.) with an antisense ACC oxidase gene. *Plant Cell Rep.* 25, 198–205. doi: 10.1007/s00299-005-0042-0

Ohme-Takagi, M., and Hideaki, S. (1995). Ethylene-inducible DNA binding proteins that interact with an ethylene-responsive element. *Plant Cell* 7, 173–182. doi: 10.1105/tpc.7.2.173

Park, C. H., Roh, J., Youn, J., Son, S., Park, J. H., Kim, S. Y., et al. (2018). *Arabidopsis* ACC oxidase 1 coordinated by multiple signals mediates ethylene biosynthesis and is involved in root development. *Mol. Cells* 41, 923–932. doi: 10.14348/molcells.2018.0092

Peck, S. C., Reinhardt, D., Olson, D. C., Boller, T., and Kende, H. (1992). Localization of the ethylene-forming enzyme from tomatoes, 1-aminocyclopropane-1-carboxylate oxidase, in transgenic yeast. *J. Plant Physiol.* 140, 681–686. doi: 10.1016/S0176-1617(11)81023-0

Peiser, G. D., Wang, T.-T., Hoffman, N. E., Yang, S. F., Liu, H., and Walsh, C. T. (1984). Formation of cyanide from carbon 1 of 1-aminocyclopropane-1-carboxylic acid during its conversion to ethylene. *Proc. Natl. Acad. Sci. U.S.A.* 81, 3059–3063. doi: 10.1073/pnas.81.10.3059

Picton, S., Barton, S. L., Bouzayen, M., Hamilton, A. J., and Grierson, D. (1993). Altered fruit ripening and leaf senescence in tomatoes expressing an antisense ethylene-forming enzyme transgene. *Plant J.* 3, 469–481. doi: 10.1111/j.1365-313X.1993.tb00167.x

Pommerrenig, B., Feussner, K., Zierer, W., Rabinovych, V., Klebl, F., Feussner, I., et al. (2011). Phloem-specific expression of yang cycle genes and identification of novel yang cycle enzymes in plantago and *Arabidopsis*. *Plant Cell* 23, 1904–1919. doi: 10.1105/tpc.110.079657

Porter, A. J. R., Borlakoglu, J. T., and John, P. (1986). Activity of the ethylene-forming enzyme in relation to plant cell structure and organization. *J. Plant Physiol.* 125, 207–216. doi: 10.1016/S0176-1617(86)80143-2

Proost, S., Bel, M., Van Vaneechoutte, D., Van de Peer, Y., Mueller-roeber, B., and Vandepoele, K. (2014). PLAZA 3.0: an access point for plant comparative genomics. *Nucleic Acids Res.* 43, 974–981. doi: 10.1093/nar/gku986

Ramassamy, S., Olmos, E., Bouzayen, M., Pech, J., and Latché, A. (1998). 1-aminocyclopropane-1-carboxylate oxidase of apple fruit is periplasmic. *J. Exp. Bot.* 49, 1909–1915. doi: 10.1093/jexbot/49.329.1909

Rauf, M., Arif, M., Fisahn, J., Xue, G.-P., Balazadeh, S., and Mueller-Roeber, B. (2013). NAC transcription factor speedy hyponastic growth regulates flooding-induced leaf movement in *Arabidopsis*. *Plant Cell* 25, 4941–4955. doi: 10.1105/tpc.113.117861

Raz, V., and Ecker, J. R. (1999). Regulation of differential growth in the apical hook of Arabidopsis. *Development* 126, 3661–3668.

Reinhardt, D., Kende, H., and Boiler, T. (1994). Subcellular localization of 1-aminocyclopropane-1-carboxylate oxidase in tomato cells. *Planta* 195, 142–146. doi: 10.1007/BF00206302

Rombaldi, C., Lelièvre, J.-M., Latché, A., Petitprez, M., Bouzayen, M., and Pech, J.-C. (1994). Immunocytolocalization of 1-aminocyclopropane-1-carboxylic acid oxidase in tomato and apple fruit. *Planta* 192, 453–460. doi: 10.1007/BF00203582

Savin, K. W., Baudinette, S. C., Graham, M. W., Michael, M. Z., Nugent, G. D., Lu, C.-Y., et al. (1995). Antisense ACC Oxidase RNA delays carnation petal senescence. *HortScience* 30, 970–972. doi: 10.21273/HORTSCI.30.5.970

Schmid, M., Davison, T. S., Henz, S. R., Pape, U. J., Demar, M., Vingron, M., et al. (2005). A gene expression map of *Arabidopsis thaliana* development. *Nat. Genet.* 37, 501–506. doi: 10.1038/ng1543

Sekeli, R., Abdullah, J., Namasivayam, P., Muda, P., Bakar, U., Yeong, W., et al. (2014). RNA interference of 1-aminocyclopropane-1-carboxylic acid oxidase (aco1 and aco2) genes expression prolongs the shelf life of eksotika (*Carica papaya* L.) papaya fruit. *Molecules* 19, 8350–8362. doi: 10.3390/molecules19068350

Sell, S., and Hehl, R. (2005). A fifth member of the tomato 1-aminocyclopropane-1-carboxylic acid (ACC) oxidase gene family harbours a leucine zipper and is anaerobically induced. *J. DNA Seq. Mapp.* 16, 80–82. doi: 10.1080/10425170500050817

Seo, Y. S., Yoo, A., Jung, J., Sung, S.-K., Yang, D. R., Kim, W. T., et al. (2004). The active site and substrate-binding mode of 1-aminocyclopropane-1-carboxylate oxidase determined by site-directed mutagenesis and comparative modelling studies. *Biochem. J.* 380, 339–346. doi: 10.1042/bj20031762

Shaw, J., Chou, Y., Chang, R., and Yang, S. F. (1996). Characterization of the ferrous ion binding sites of apple 1-aminocyclopropane-1-carboxylate oxidase by site-directed Mutagenesis. *Biochem. Biophys. Res. Commun.* 700, 697–700. doi: 10.1006/bbrc.1996.1237

Shi, Y.-H., Zhu, S.-W., Mao, X.-Z., Feng, J.-X., Qin, Y.-M., Zhang, L., et al. (2006). Transcriptome profiling. molecular biological, and physiological studies reveal a major role for ethylene in cotton fiber cell elongation. *Plant Cell* 18, 651–664. doi: 10.1105/tpc.105.040303

Silva, J. A., Da Costa, T. S., Lucchetta, L., Marini, L. J., Zanuzo, M. R., Nora, L., et al. (2004). Characterization of ripening behavior in transgenic melons expressing an antisense 1-aminocyclopropane-1-carboxylate (ACC) oxidase gene from apple. *Postharvest Biol. Technol.* 32, 263–268. doi: 10.1016/j.postharvbio.2004.01.002

Staswick, P. E., and Tiryaki, I. (2004). The oxylipin signal jasmonic acid is activated by an enzyme that conjugates it to isoleucine in *Arabidopsis*. *Plant Cell* 16, 2117–2127. doi: 10.1105/tpc.104.023549

Sun, X., Li, Y., He, W., Ji, C., Xia, P., Wang, Y., et al. (2017). Pyrazinamide and derivatives block ethylene biosynthesis by inhibiting ACC oxidase. *Nat. Commun.* 8:15758. doi: 10.1038/ncomms15758

Tan, Y., Liu, J., Huang, F., Guan, J., Zhong, S., Tang, N., et al. (2014). PhGRL2 protein, interacting with PhACO1, is involved in flower senescence in the petunia. *Mol. Plant* 7, 1384–1387. doi: 10.1093/mp/ssu024

Tierney, D. L., Rocklin, A. M., Lipscomb, J. D., Que, L., and Hoffman, B. M. (2005). ENDOR studies of the ligation and structure of the non-heme iron site in ACC oxidase. *J. Am. Chem. Soc.* 127, 7005–7013. doi: 10.1021/ja0500862

Tu, Y., He, B., Gao, S., Guo, D., Jia, X., Dong, X., et al. (2019). CtACO1 overexpression resulted in the alteration of the flavonoids profile of safflower. *Molecules* 24:1128. doi: 10.3390/molecules24061128

Van de Poel, B., Bulens, I., Hertog, M. L. A. T. M., Nicolai, B. M., and Geeraerd, A. H. (2014a). A transcriptomics-based kinetic model for ethylene biosynthesis in tomato (Solanum lycopersicum) fruit: development, validation and exploration of novel regulatory mechanisms. *New Phytol.* 202, 952–963. doi: 10.1111/nph.12685

Van de Poel, B., Vandenzavel, N., Smet, C., Nicolay, T., Bulens, I., Mellidou, I., et al. (2014b). Tissue specific analysis reveals a differential organization and regulation of both ethylene biosynthesis and E8 during climacteric ripening of tomato. *BMC Plant Biol.* 14:11. doi: 10.1186/1471-2229-14-11

Van de Poel, B., Bulens, I., Markoula, A., Hertog, M. L. A. T. M., Dreesen, R., Wirtz, M., et al. (2012). Targeted systems biology profiling of tomato fruit reveals coordination of the Yang cycle and a distinct regulation of ethylene

biosynthesis during postclimacteric ripening. *Plant Physiol.* 160, 1498–1514. doi: 10.1104/pp.112.206086

Van de Poel, B., Smet, D., and Van Der Straeten, D. (2015). Ethylene and hormonal cross talk in vegetative growth and development. *Plant Physiol.* 169, 61–72. doi: 10.1104/pp.15.00724

Van de Poel, B., and Van Der Straeten, D. (2014). 1-aminocyclopropane-1-carboxylic acid (ACC) in plants: more than just the precursor of ethylene! *Front. Plant Sci.* 5:640. doi: 10.3389/fpls.2014.00640

van Es, S. W., Silveira, S. R., Rocha, D. I., Bimbo, A., Martinelli, A. P., Dornelas, M. C., et al. (2018). Novel functions of the *Arabidopsis* transcription factor TCP5 in petal development and ethylene biosynthesis. *Plant J.* 94, 867–879. doi: 10.1111/tpj.13904

Vandenbussche, F., Vriezen, W. H., Smalle, J., Laarhoven, L. J. J., Harren, F. J. M., and Van Der Straeten, D. (2003). Ethylene and auxin control the *Arabidopsis* response to decreased light intensity. *Plant Physiol.* 133, 517–527. doi: 10.1104/pp.103.022665

Ververidis, P., and John, P. (1991). Complete recovery in vitro of ethylene-forming activity. *Phytochemistry* 30, 725–727. doi: 10.1016/0031-9422(91)85241-q

Vriezen, W. H., Hulzink, R., Mariani, C., and Voesenek, L. A. (1999). 1-aminocyclopropane-1-carboxylate oxidase activity limits ethylene biosynthesis in Rumex palustris during submergence. *Plant Physiol.* 121, 189–196. doi: 10.1104/pp.121.1.189

Waese, J., Fan, J., Pasha, A., Yu, H., Fucile, G., Shi, R., et al. (2017). ePlant: visualizing and exploring multiple levels of data for hypothesis generation in plant biology. *Plant Cell* 29, 1806–1821. doi: 10.1105/tpc.17.00073

Wang, Y., Zou, W., Xiao, Y., Cheng, L., Liu, Y., Gao, S., et al. (2018). MicroRNA1917 targets CTR4 splice variants to regulate ethylene responses in tomato. *J. Exp. Bot.* 69, 1011–1025. doi: 10.1093/jxb/erx469

Wen, C.-K. (ed.) (2015). *Ethylene in Plants*. Dordrecht: Springer. doi: 10.1007/978-94-017-9484-8

Xiong, A.-S., Yao, Q.-H., Peng, R.-H., Li, X., Han, P.-L., and Fan, H.-Q. (2005). Different effects on ACC oxidase gene silencing triggered by RNA interference in transgenic tomato. *Plant Cell Rep.* 23, 639–646. doi: 10.1007/s00299-004-0887-7

Yoo, A., Seo, Y. S., Jung, J. W., Sung, S. K., Kim, W. T., Lee, W., et al. (2006). Lys296 and Arg299 residues in the C-terminus of MD-ACO1 are essential for a 1-aminocyclopropane-1-carboxylate oxidase enzyme activity. *J. Struct. Biol.* 156, 407–420. doi: 10.1016/j.jsb.2006.08.012

Yoon, G. M. (2015). New insights into the protein turnover regulation in ethylene biosynthesis. *Mol. Cells* 38, 597–603. doi: 10.14348/molcells.2015.0152

Yu, Y., Jia, T., and Chen, X. (2017). The 'how' and 'where' of plant microRNAs. *New Phytol.* 216, 1002–1017. doi: 10.1111/nph.14834

Zhang, X., Wang, W., Wang, M., Zhang, H.-Y., and Liu, J.-H. (2016). The miR396b of *Poncirus trifoliata* functions in cold tolerance by regulating acc oxidase gene expression and modulating ethylene–polyamine homeostasis. *Plant Cell Physiol.* 57, 1865–1878. doi: 10.1093/pcp/pcw108

Zhang, X.-N., Li, X., and Liu, J.-H. (2014). Identification of conserved and novel cold-responsive microRNAs in trifoliate orange (*Poncirus trifoliata* (L.) Raf.) Using High-Throughput Sequencing. *Plant Mol. Biol. Rep.* 32, 328–341. doi: 10.1007/s11105-013-0649-1

Zhang, Z., Ren, J.-S., Clifton, I. J., and Schofield, C. J. (2004). Crystal structure and mechanistic implications of 1-aminocyclopropane-1-carboxylic acid oxidase—the ethylene-forming enzyme. *Chem. Biol.* 11, 1383–1394. doi: 10.1016/j.chembiol.2004.08.012

Zhang, Z., Zhang, H., Quan, R., Wang, X.-C., and Huang, R. (2009). Transcriptional regulation of the ethylene response factor LeERF2 in the expression of ethylene biosynthesis genes controls ethylene production in tomato and tobacco. *Plant Physiol.* 150, 365–377. doi: 10.1104/pp.109.135830

Conflict of Interest Statement: The authors declare that the research was conducted in the absence of any commercial or financial relationships that could be construed as a potential conflict of interest.

frontiers in Plant Science

ORIGINAL RESEARCH
published: 07 June 2019
doi: 10.3389/fpls.2019.00726

Molecular Analysis of Protein-Protein Interactions in the Ethylene Pathway in the Different Ethylene Receptor Subfamilies

*Mareike Berleth[1], Niklas Berleth[2], Alexander Minges[1], Sebastian Hänsch[3], Rebecca Corinna Burkart[4], Björn Stork[2], Yvonne Stahl[4], Stefanie Weidtkamp-Peters[3], Rüdiger Simon[4] and Georg Groth[1]**

[1]Institute of Biochemical Plant Physiology, Heinrich Heine University, Düsseldorf, Germany, [2]Institute of Molecular Medicine I, Heinrich Heine University, Düsseldorf, Germany, [3]Center for Advanced Imaging, Heinrich Heine University, Düsseldorf, Germany, [4]Institute for Developmental Genetics, Heinrich Heine University, Düsseldorf, Germany

Signal perception and transmission of the plant hormone ethylene are mediated by a family of receptor histidine kinases located at the Golgi-ER network. Similar to bacterial and other plant receptor kinases, these receptors work as dimers or higher molecular weight oligomers at the membrane. Sequence analysis and functional studies of different isoforms suggest that the ethylene receptor family is classified into two subfamilies. In *Arabidopsis*, the type-I subfamily has two members (ETR1 and ERS1) and the type-II subfamily has three members (ETR2, ERS2, and EIN4). Whereas subfamily-I of the *Arabidopsis* receptors and their interactions with downstream elements in the ethylene pathway has been extensively studied in the past; related information on subfamily-II is sparse. In order to dissect the role of type-II receptors in the ethylene pathway and to decode processes associated with this receptor subfamily on a quantitative molecular level, we have applied biochemical and spectroscopic studies on purified recombinant receptors and downstream elements of the ethylene pathway. To this end, we have expressed purified ETR2 as a prototype of the type-II subfamily, ETR1 for the type-I subfamily and downstream ethylene pathway proteins CTR1 and EIN2. Functional folding of the purified receptors was demonstrated by CD spectroscopy and autokinase assays. Quantitative analysis of protein-protein interactions (PPIs) by microscale thermophoresis (MST) revealed that ETR2 has similar affinities for CTR1 and EIN2 as previously reported for the subfamily-I prototype ETR1 suggesting similar roles in PPI-mediated signal transfer for both subfamilies. We also used *in planta* fluorescence studies on transiently expressed proteins in *Nicotiana benthamiana* leaf cells to analyze homo- and heteromer formation of receptors. These studies show that type-II receptors as well as the type-I receptors form homo- and heteromeric complexes at these conditions. Notably, type-II receptor homomers and type-II:type-I heteromers are more stable than type-I homomers as indicated by their lower dissociation constants obtained in microscale thermophoresis studies. The enhanced stability of type-II complexes emphasizes the important role of type-II receptors in the ethylene pathway.

Keywords: ethylene receptor subfamilies, signaling, protein-protein interaction, microscale thermophoresis, fluorescence lifetime imaging microscopy

OPEN ACCESS

Edited by:
Dominique Van Der Straeten, Ghent University, Belgium

Reviewed by:
Derek Gingerich, University of Wisconsin–Eau Claire, United States
Chi-Kuang Wen, Shanghai Institutes for Biological Sciences (CAS), China

****Correspondence:***
Georg Groth
georg.groth@hhu.de;
georg.groth@uni-duesseldorf.de

Specialty section:
This article was submitted to Plant Physiology, a section of the journal Frontiers in Plant Science

Received: *25 March 2019*
Accepted: *16 May 2019*
Published: *07 June 2019*

Citation:
Berleth M, Berleth N, Minges A, Hänsch S, Burkart RC, Stork B, Stahl Y, Weidtkamp-Peters S, Simon R and Groth G (2019) Molecular Analysis of Protein-Protein Interactions in the Ethylene Pathway in the Different Ethylene Receptor Subfamilies. Front. Plant Sci. 10:726. doi: 10.3389/fpls.2019.00726

INTRODUCTION

The gaseous plant hormone ethylene is decisive for many growth and developmental processes in plants, including fruit ripening, senescence, and the control of biotic and abiotic stress responses, such as pathogen defense and wounding (Kieber and Ecker, 1993; O'Donnell et al., 1996; Penninckx et al., 1998; Bleecker and Kende, 2000). Most of the current knowledge about ethylene biosynthesis and signal transduction has been obtained by genetic, physiological, and biochemical studies in the model plant *Arabidopsis thaliana*. Based on these studies, a family of mainly endoplasmic reticulum (ER)-membrane bound receptors was identified to catalyze the first step in all ethylene-regulated phenomena. These receptors in which their functional state form homo- or heterodimers at the ER membrane act as negative regulators of the ethylene-signaling pathway, following an inverse-agonist model in which ethylene-binding switches off the downstream signal transmission (Bleecker et al., 1988; Hua et al., 1995; Hua and Meyerowitz, 1998; Chen et al., 2002).

Sequence analysis and functional studies disclosed that the receptor family is classified into two subfamilies. In *Arabidopsis*, isoforms ETR1 and ERS1 form subfamily-I, whereas subfamily-II contains receptor isoforms ETR2, ERS2, and EIN4 (Hua et al., 1995, 1998; Sakai et al., 1998). Common to all isoforms is a modular structure known from bacterial sensor histidine kinases. In this case, the main elements are a transmembrane (TM) domain with an ethylene binding site at the amino (N)-terminus facing the ER lumen and a large cytosolic domain comprising of a GAF domain followed by a histidine kinase (HK) domain. Genetic and biochemical studies showed that the GAF domain contributes to the formation of the active dimer and that autophosphorylation activity of the kinase domain is inhibited upon ethylene binding. In addition to the GAF and HK domain receptor isoforms, ETR1, ETR2, and EIN4 carry a response regulator domain (RD) at their carboxy (C)-terminus (Chang et al., 1993; Chen et al., 2002; Voet van Vormizeele and Groth, 2008). Despite their similar overall structure, the individual isoforms contain major differences in these modules. For instance, type-II receptors have an additional fourth transmembrane helix. The function of this additional element is still not clear, although it might function as a targeting signal (Chen et al., 2007). In addition, essential residues for histidine kinase activity are missing in this subfamily. However, *in vitro* Ser/Thr kinase activity was demonstrated for these isoforms albeit autokinase activity seems to play only a minor role in ethylene signaling (Wang et al., 2003; Moussatche and Klee, 2004).

Despite these structural dissimilarities, the general function of the different receptor isoforms and response to the plant hormone is highly redundant. Nonetheless, functional specificity among different isoforms has been described, although the underlying molecular mechanisms are still not fully understood (Binder et al., 2006; Wuriyanghan et al., 2009). But even with the exact signal output of the receptors unknown, previous studies have clearly shown that complex formation of receptors with the Raf-like kinase CONSTITUTIVE TRIPLE RESPONSE 1 (CTR1) and the integral membrane protein ETHYLENE INSENSITIVE 2 (EIN2) is an integral part of the ethylene signaling network in the response to the plant hormone. In this process, CTR1 was shown to phosphorylate EIN2 and that interaction of CTR1 with the receptors is critical for CTR1 kinase activity. The presence of ethylene leads to inactivation of the receptors, thereby inactivating CTR1 in turn resulting in dephosphorylation of EIN2. As a consequence, the C-terminal part of EIN2 ($EIN2^{479\text{-}1294}$) is cleaved off by a so far unknown mechanism and translocates to the nucleus. Here, it directly or indirectly stabilizes transcription factors EIN3/EIL1, which activate the transcription of ethylene response genes (Gao et al., 2003; Ju et al., 2012; Qiao et al., 2012; Wen et al., 2012). Remarkably, another mechanism affecting plant ethylene response was shown for the cleaved off EIN2 C-terminus as this digest inhibits the translation of *EBF1/2* mRNA in the cytosol thereby preventing EBF1/2-dependent degradation of the EIN3 master transcription factor (An et al., 2010).

In the past, various approaches analyzing the interaction of type-I receptors and downstream signaling components have been developed. For instance, in our lab, interaction of the type-I receptor ETR1 with $EIN2^{479\text{-}1294}$ was demonstrated by *in vivo* FRET-studies and quantified by *in vitro* tryptophan fluorescence quench analysis (Bisson et al., 2009). Moreover, recent studies in our lab highlighted that the conserved nuclear localization signal (NLS) sequence of EIN2 significantly contributes to the EIN2-receptor interaction and in the form of a synthetic octapeptide (NOP1) delays fruit ripening and flower senescence (Bisson et al., 2016; Kessenbrock et al., 2017; Milić et al., 2018; Hoppen et al., 2019). In contrast, related information on ethylene receptor subfamily-II is still sparse.

In the work presented here, we performed quantitative biochemical and spectroscopic studies on purified receptor preparations and downstream elements in order to elucidate the protein-protein interaction (PPI) landscape of both receptor subfamilies. To this end, we established expression and purification for the *Arabidopsis* ETR2 as a prototype of the type-II subfamily. Our studies indicate similar roles in PPI-mediated signal transduction for both receptor subfamilies. To that, we visualized homo- and heteromer formation of type-I and type-II receptors by *in planta* fluorescence lifetime analysis (FRET-FLIM) and anisotropy and quantified these interactions by microscale thermophoresis (MST) on purified recombinant proteins. In the end, our study demonstrates the enhanced stability of type-II receptor complexes compared to complexes consisting of type-I isoforms only stressing an important role of type-II receptors for ethylene signal transduction.

MATERIALS AND METHODS

Production of Recombinant *Arabidopsis* Proteins for *in vitro* Interaction Studies

Codon optimized cDNA encoding full-length AtETR2 (UniProt ID: Q0WPQ2) was purchased from GenScript USA according to the published sequence (NCBI ID: NM_113216.3). The cDNA

sequence was flanked by a 5′ *SmaI* recognition site and 3′ *XhoI* recognition site. Expression vector pGEX-4T-1 (GE Healthcare Life Sciences) and synthetic DNA were digested with *SmaI* and *XhoI* and ligated. In the resulting plasmid pGEX-4T-1_AtETR2, the region coding for a thrombin cleavage site was changed to a region coding for a tobacco etch virus (TEV) protease cleavage site (ENLYFQG). To this end, a PCR-based approach with 5′-phosphorylated primers was used (Follo and Isidoro, 2008). Furthermore, a 10 × -His-tag was C-terminally fused to ETR2 to facilitate protein purification. The construct was cloned in two successive PCR reactions (Follo and Isidoro, 2008). The resulting plasmid was verified by sequencing and termed pGEX-4T-1_TEV_ETR2_H_{10}. The DNA fragment encoding for the transmembrane domain of ETR1 (aa 1-157) was cloned into expression vector pET16b (Novagen), and base pairs coding for cysteines at positions 4 and 6 in the protein were changed to encode serine. The resulting plasmid was termed ETR1-TM^{C4SC6S}. Full-length cDNA sequence encoding for AtCTR1 (UniProt ID: Q05609) was purchased from GenScript USA according to the published sequence (NCBI ID: NM_120454.4). The DNA fragment was cloned into expression vector pET30a (Novagen) by using SLIC, and the coding region for CTR1 was extended by a cyan fluorescent protein termed mCerulean (Li and Elledge, 2007; Rizzo et al., 2007). The resulting plasmid was verified by sequencing and termed pET30a_AtCTR1_mCerulean. Primer sequences used for cloning are listed in **Supplementary Table S1**.

Molecular Cloning of AtERS1 and AtERS2 Fusions for *in planta* Interaction Studies

Expression vectors encoding for receptor proteins AtERS1 (UniProt ID: Q38846) and AtERS2 (UniProt ID: P93825) carrying a C-terminal RFP-label were kindly provided by Klaus Harter (Grefen et al., 2008). TOPO-AtERS1 and TOPO-AtERS2 entry clones were prepared by using pENTR Directional TOPO Cloning Kit (Thermo Fisher Scientific) following the manufacturer's instructions. For transient expression in *Nicotiana benthamiana,* expression vectors encoding ERS1 and ERS2 were prepared *via* Gateway LR-reaction (Thermo Fisher Scientific) using C-terminal mVenus- and mCherry-tagged destination vectors pABindmVenus and pABindmCherry, which are based on vector pMDC7 (Curtis and Grossniklaus, 2003). Expression vector pABindmVmC-ERS2 was cloned using pABindFRET as backbone by Gibson Assembly with amplification of four fragments thereby substituting fluorescent protein (FP) GFP by mVenus (Kremers et al., 2006; Gibson et al., 2009; Bleckmann et al., 2010). The resulting expression vector encodes ERS2 and contains a C-terminal mVenus-mCherry fusion protein. **Supplementary Table S1** gives an overview of primers used for cloning.

Transient Expression of AtERS1 and AtERS2 in *N. benthamiana*

Agrobacterium tumefaciens strain GV3101 pMP90 was transformed with expression vectors (pABindm Venus-ERS2, pABindmCherry-ERS2, pABindmCherry-ERS1, pABindmCherry-BTI2, pABindmVmC-ERS2) as well as vector pER-Rb encoding for an ER-marker protein tagged to mCherry (Koncz and Schell, 1986; Nelson et al., 2007). To reduce gene silencing *in planta*, expression vectors were co-transfected with silencing suppressor p19 (Qu and Morris, 2002). Cells were cultured in 2YT medium [1.6% (w/v) peptone, 1% (w/v) yeast extract, and 0.5% (w/v) NaCl], precipitated, and resuspended in AS medium [5% (w/v) sucrose, 5 mM $MgSO_4$, 5 mM glucose, 0.01% (v/v) Silwet L77, 450 µM acetosyringone]. *A. tumefaciens* cells containing mVenus- and mCherry-tagged expression vectors were mixed at 1:1 ratio to an optical density at 600 nm (OD_{600}) of 0.2 and infiltrated in 4-week-old *N. benthamiana* leaves. Transient gene expression was induced 72 –96 h after infiltration by 20 µM β-estradiol and 0.1% (v/v) Tween 20, and protein expression was analyzed from 16 to 25 h.

Expression of Recombinant *Arabidopsis* Receptor AtETR2 and Protein Kinase AtCTR1 in *Escherichia coli*

The expression vector encoding for recombinant AtETR2 was transformed into chemically competent *E. coli* C43 (DE3) (Lucigen Corporation) cells. Transformants were precultured in 2YT medium containing 100 µg/ml ampicillin at 30°C for 16 h. Preculture was diluted to an OD_{600} of 0.1 in 500 ml terrific broth (TB) medium (12 g/L peptone, 24 g/L yeast extract, 5 g/L glycerol, 1.8 g/L KH_2PO_4, 19.8 g/L K_2HPO_4) containing 100 µg/ml ampicillin and 2% ethanol (v/v). Cells were incubated at 30°C with shaking at 180 rpm. At OD_{600} = 0.4 temperature was reduced to 16°C. The bacteria were grown to OD_{600} = 0.6 and heterologous protein expression was induced with 0.5 mM isopropyl β-d-1-thiogalactopyranoside (IPTG). Cells were further grown for 4 h, harvested by centrifugation, flash-frozen in liquid nitrogen, and stored at −20°C. AtCTR1 was expressed in *E. coli* BL21 (DE3) cells. Plasmid pRARE (Novagen) was co-transformed carrying the genes for essential tRNAs encoded by rarely used codons in *E. coli*. Cells were grown at 30°C in 500 ml 2YT medium containing 25 µg/ml kanamycin and 2% ethanol (v/v). Cells were grown to an OD_{600} = 0.4, and temperature was reduced to 16°C. Protein expression was induced at OD_{600} = 0.6 by addition of 0.2 mM IPTG. Cells were further incubated for 20 h at 16°C, harvested by centrifugation, flash-frozen in liquid nitrogen, and stored at −20°C. Protein expression of recombinant proteins was analyzed by SDS-PAGE followed by immunoblotting (Laemmli, 1970; Towbin et al., 1979).

Purification of Recombinant AtETR2 and AtCTR1

Protein purification steps were performed on ice or at 4°C, if not stated otherwise. Resulting AtETR2 cell pellet was resuspended in PBS lysis buffer [PBS pH 8.0, 10% (w/v) glycerol, 1 mM DTT, 0.002% (w/v) phenylmethylsulfonyl fluoride (PMSF) and 10 mg/L DNaseI (PanReac AppliChem), 5 ml PBS lysis buffer per 1 g cells]. Cells were broken with Constants Cell Disruption System (Constant Systems) at 2.4 kbar and 5°C. Cell lysate was centrifuged for 30 min at 14,000 × *g* to

remove cell debris and inclusion bodies. The supernatant was centrifuged again for 30 min at 40,000 × *g*. The resulting membrane pellet was resuspended in PBS lysis buffer and isolation of cell membranes were achieved by centrifugation at 34,000 × *g* for 30 min. Membrane pellets were flash-frozen in liquid nitrogen and stored at −80°C. For protein solubilization, membranes were resuspended in buffer S [50 mM Tris/HCl pH 7.8, 200 mM NaCl, 1.2% (w/v) FosCholine-16, 2.5 mM DTT, 0.002% (w/v) PMSF] and stirred at 700 rpm for 1 h. Membrane fragments were removed by ultracentrifugation at 230,000 × *g* for 30 min. The resulting supernatant was loaded to a 5 ml Ni-NTA HisTrap FF column (GE Healthcare Life Sciences), equilibrated in buffer R [50 mM Tris/HCl pH 7.8, 200 mM NaCl, 2.5 mM DTT, 0.015% (w/v) FosCholine-16]. The column was washed with 10 column volumes (CV) of buffer R, followed by 20 CV buffer R-ATP (buffer R with additional 50 mM KCl, 20 mM $MgCl_2$, 10 mM ATP). The column was washed again with 10 CV buffer R, followed by 10 CV buffer R containing 50 mM imidazole. Finally, the receptor AtETR2 was eluted with 250 mM imidazole. To purify His-tagged protein kinase AtCTR1, resulting cell pellet was resuspended in lysis buffer C [50 mM HEPES/NaOH pH 7.6, 300 mM NaCl, 5% (w/v) glycerol, 5 ml lysis buffer C per 1 g cells]. About 10 mg/L DNaseI and 1 × EDTA-free cOmplete Protease Inhibitor Cocktail (Roche) were added to cells prior to cell disruption. Cells were disrupted by passing through a pre-cooled French pressure cell at 12,000 psi (1 psi = 6.9 kPa). The cell lysate was ultracentrifuged at 230,000 × *g* for 60 min. The resulting supernatant was loaded onto a 5 ml Ni-NTA HisTrap HP column (GE Healthcare Life Sciences), equilibrated in buffer C-P [buffer C with 0.002% (w/v) PMSF]. The column was washed with 10 CV of buffer C-P, followed by 20 CV buffer C-ATP [buffer C with additional 50 mM KCl, 20 mM $MgCl_2$, 10 mM ATP, 0.002% (w/v) PMSF]. The column was washed with 10 CV buffer C-P containing 50 mM imidazole and 100 mM imidazole, respectively. AtCTR1 was eluted with 500 mM imidazole in buffer C-P. Purified proteins were concentrated in a 50 kDa Amicon Ultra-15 concentrator (EDM Millipore). Buffer was changed by a desalting step on a PD-10 or PD MiniTrap G-25 column (GE Healthcare Life Sciences) depending on subsequent applications.

Circular Dichroism Spectroscopy of Recombinant *Arabidopsis* Receptor Proteins

AtETR1 and AtETR2 were expressed and purified as described in this article (**Figure 1, Supplementary Figure S1A**) and in Milić et al., 2018. Purified receptors were characterized by circular dichroism (CD) spectroscopy. For the far-UV spectra, purified *Arabidopsis* receptors were measured at a final concentration of 0.2 mg/ml in CD buffer (10 mM K_2HPO_4/KH_2PO_4 pH 8.0). Therefore, buffer was exchanged to CD buffer using a PD MiniTrap G-25 column (GE Healthcare Life Sciences) and protein samples were ultracentrifuged at 230,000 × *g* for 30 min. Protein and FosCholine-16 concentrations were determined by a Direct Detect infrared spectrometer (EMD Millipore). In blank samples, FosCholine-16 concentrations were adjusted to correspond to the final detergent concentration in the protein samples. For a detailed protocol for protein preparation, see Kessenbrock and Groth, 2017. CD spectra were recorded by a Jasco J715 spectropolarimeter (Jasco GmbH) using a cylindrical quartz cuvette with 1-mm-path-length (Hellma Analytics). Each protein spectrum was measured from 260 to 180 nm at room temperature and represents an average of 10 continuous scans recorded with a bandwidth of 1 nm at 50 nm/min. Secondary structure content of the purified receptors was calculated using reference protein set SMP50 in programs CDSSTR and CONTINLL from the CDpro software package (see **Figure 2, Supplementary Figures S1E,F**; Provencher and Glöckner, 1981; Johnson, 1999; Sreerama and Woody, 2000).

In vitro Autokinase Activity Assay of *Arabidopsis* Receptor Proteins

Autokinase activity of AtETR1 and AtETR2 was assessed by an *in vitro* kinase assay. To this end, full-length receptors were expressed and purified as previously described either with (**Figure 3**) or without the additional ATP purification step (see **Supplementary Figures S1B–D**). Purified proteins (1 mg) were incubated in kinase assay reaction buffer [50 mM Tris/HCl, pH 7.5, 0.1 mM EGTA, 0.1 mM DTT, 10 mM $Mg(CH_3COO)_2$] supplemented with 0.1 mM [γ-^{32}P]ATP (Hartmann Analytic) for 30 min at 37°C. Protein denaturation was obtained by the addition of 40 mM DTT and 2% (w/v) SDS for 30 min at 60°C prior to *in vitro* phosphorylation. The kinase reactions were stopped by the addition of SDS sample buffer, and the samples were subjected to SDS-PAGE. After Coomassie staining, the gel was dried and autoradiography was performed for 6 days.

Fluorescent Labeling for Microscale Thermophoresis Studies

Protein-protein interactions were analyzed by microscale thermophoresis (MST) (Duhr and Braun, 2006; Jerabek-Willemsen et al., 2011). Therefore, recombinant proteins were labeled with Alexa Fluor 488 succinimidyl-ester (Thermo Fisher Scientific). For this purpose, buffer of purified and concentrated AtETR2 and AtCTR1 samples were exchanged on a desalting PD-10 column. Samples were concentrated again resulting in 500-µl protein sample of AtCTR1 in labeling buffer L (50 mM K_2HPO_4/KH_2PO_4 pH 8.0, 300 mM NaCl) and AtETR2 in buffer L-R [buffer L with 0.015% (w/v) FosCholine-16]. Recombinant AtEIN2$^{479\text{-}1294}$ was expressed and purified as previously described (Bisson et al., 2016) and buffer was exchanged to labeling buffer L-E [buffer L with 6% (w/v) glycerol, 10 mM EGTA]. Expression, purification, and labeling of AtETR1 were performed as described in Milić et al., 2018. Alexa Fluor 488 succinimidyl-ester was applied to each protein in 2.5-fold excess and incubated while mixing slightly for 30 min in the dark at ambient temperature. Buffer of labeled proteins was exchanged for AtETR2 to MST buffer 1 [50 mM HEPES/NaOH pH 7.8, 300 mM NaCl, 5% (w/v) glycerol, 0.015% (w/v) FosCholine-16], for AtETR1 to MST buffer 2 [50 mM Tris/HCl pH 7.8, 300 mM

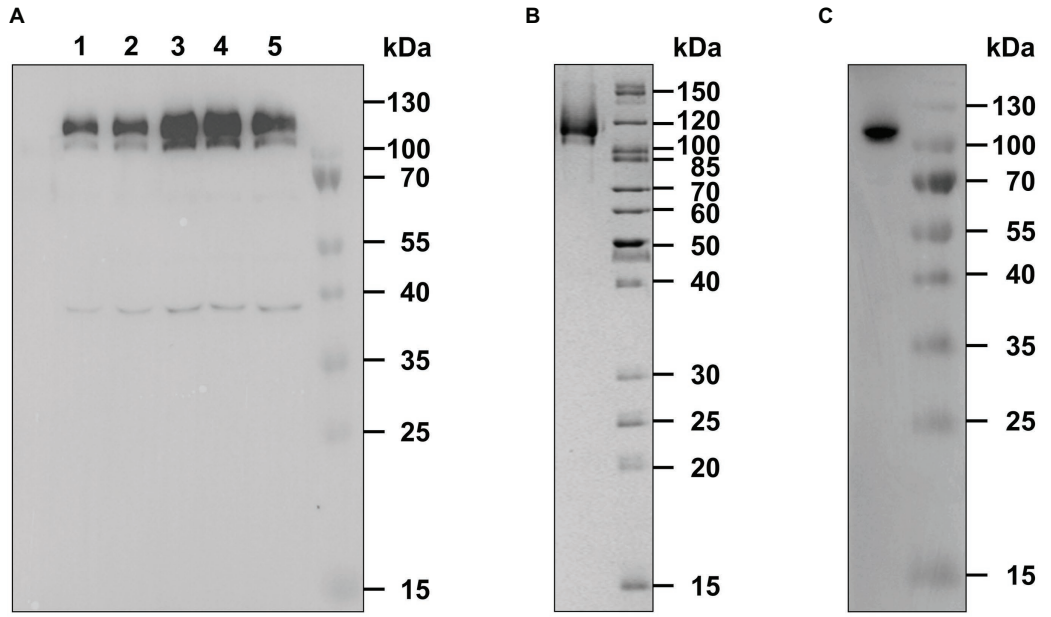

FIGURE 1 | Expression and purification of recombinant AtETR2. **(A)** *E. coli* C43(DE) strain was used for heterologous expression of *Arabidopsis thaliana* receptor ETR2. Expression was analyzed by SDS-PAGE and immunoblotting. Protein expression was monitored 1 (lane 1) to 5 h (lane 5) after induction with IPTG and detected by an anti-His antibody. AtETR2 migrates on SDS gels with an apparent molecular mass of 120 kDa. **(B)** His-tagged AtETR2 was purified by IMAC, separated by SDS-PAGE and visualized by colloidal Coomassie staining and **(C)** immunoblotting using an anti-His antibody.

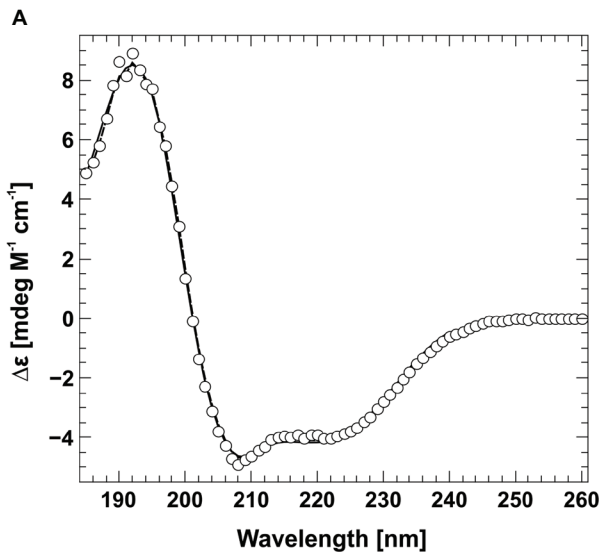

B

Algorithm	α-helix [%]	β-sheet [%]	β-turn [%]	Coil [%]
CONTINLL	48	9	18	25
CDSSTR	50	10	18	22

FIGURE 2 | Circular dichroism spectra of AtETR2. **(A)** The far-UV spectra of AtETR2 was calculated and adjusted to molar extinction (Δε) considering molecular weight and protein concentration of AtETR2. **(B)** Secondary structure content was calculated by CONTINLL (solid line) and CDSSTR (dashed line) from the CDpro software package.

NaCl, 5% (w/v) glycerol, 0.015% (w/v) FosCholine-16], and for AtCTR1 and AtEIN2$^{479\text{-}1294}$ to MST buffer 3 [50 mM Tris/HCl pH 7.8, 300 mM NaCl, 5% (w/v) glycerol]. The protein samples were centrifuged at 230,000 × *g*, for 30 min, and at 4°C. Protein samples solutions were adjusted to a final glycerol concentration of 20% (w/v), flash-frozen in liquid nitrogen, and stored at −80°C.

Quantitative Interaction Studies by Microscale Thermophoresis

Protein-protein interactions were analyzed by microscale thermophoresis. Therefore, the receptors AtETR1 and AtETR2 as well as soluble proteins AtEIN2$^{479\text{-}1294}$ and AtCTR1 were purified and labeled as previously described. Experiments were performed on a Monolith NT.115 Blue/Green (NanoTemper Technologies) in three independent replicates, whereas for negative controls, measurements were done in duplicates. If not stated otherwise, measurements were performed in standard glass capillaries (NanoTemper Technologies). For binding studies of AtEIN2$^{479\text{-}1294}$ (in MST buffer 3) to AtETR2 (in MST buffer 1), proteins were used as follows: 20 nM of labeled AtETR2, 2 μM as the highest, and 0.98 nM as the lowest AtEIN2$^{479\text{-}1294}$ concentration. Measurements were performed at 20% MST power. As a negative control, AtEIN2$^{479\text{-}1294}$ was heated to 95°C for 5 min, diluted in MST buffer 3 and mixed with 40 mM DTT and 4% (v/v) SDS. Measurements were carried out as described before. Furthermore, interaction of AtETR2 to AtEIN2$^{479\text{-}1294}$ was analyzed using 75 nM labeled AtEIN2$^{479\text{-}1294}$ and measured with 4 μM as the highest and 1.95 nM as the lowest AtETR2 concentration. Protein samples were incubated

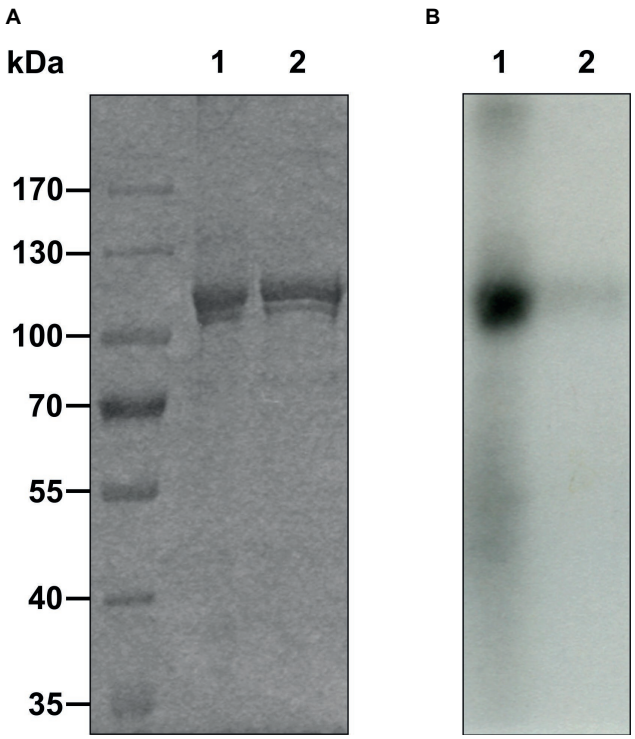

FIGURE 3 | Autophosphorylation of purified AtETR2 was performed with 0.1 mM [γ-^{32}P]ATP and magnesium as cofactor. Proteins were detected by **(A)** Coomassie staining. **(B)** Incorporation of ^{32}P was measured by autoradiography for 6 days. Experiments were performed using AtETR2 solubilized and purified without ATP purification step (1) or chemically and thermally denatured AtETR2 (2).

at ambient temperature and measured at 60% MST power. For quantification of receptor AtETR2 and AtETR1 binding to CTR1 (in MST buffer 3), receptors AtETR2 and AtETR1 (in MST buffer 2) were measured with 4 μM as highest and 0.98 nM as lowest receptor concentration. AtETR1 was mixed in a 1:1 volume ratio with labeled AtCTR1 (50 nM final concentration) and measured at 60% MST power. For AtETR2 binding to AtCTR1, labeled AtCTR1 was used in a final concentration of 20 nM. The protein mixture was incubated for 10 min at ambient temperature, transferred into premium glass capillaries, and measured at 60% MST power. As a negative control, the protein mixture was incubated directly after the 10 min incubation step with 4% (v/v) SDS and 80 mM DTT for 5 min in the dark at RT, resulting in the same protein concentrations as before mentioned. For quantification of receptor-receptor interactions, labeled receptors were used at a final concentration of 40 nM. Labeled receptors were mixed in a 1:1 ratio with non-labeled AtETR1, AtETR2 (4 μM as the highest and 0.49 nM as the lowest receptor concentration) or ETR1-TM^{C4SC6S} (MST buffer 2, 16 μM as the highest and 0.98 nM as the lowest concentration), thereby adjusting the detergent concentration to 0.0075% (w/v) FosCholine-16. Sample mixtures containing AtETR2 (labeled as well as non-labeled) were initially incubated for 10 min at RT and transferred into premium glass capillaries. All receptor-receptor binding studies were performed at 60% MST power. As negative controls, denaturation buffer (4% (v/v) SDS, 40 mM DTT in MST buffer 1 or 2, respectively) was added to the receptors. Samples were incubated for 5 min at RT in the dark and MST measurements were carried out as described for the native receptor proteins. All dissociation constants (K_d) were calculated to a binding model assuming a 1:1 stoichiometry per binding partner.

Confocal Fluorescence Microscopy

N. benthamiana epidermis cells were imaged for protein expression and protein localization using a LSM 780 laser-scanning confocal microscope (Carl Zeiss GmbH) using a C-Apochromat 40×/1.2 W Corr M27 objective with a zoom factor of 4. The pinhole was set to 1 Airy Unit (AU). The following settings were used: 488/561 beam splitter with 488 nm excitation for mVenus and 561 nm excitation for mCherry. Fluorescence was detected between 508–552 nm for mVenus and 570–624 nm for mCherry by a GaAsP detector. In combination with FM4-64 the detection wavelength of mVenus was between 490 and 552 nm. FM4-64 was detected between 562 and 626 nm. The laser strength was adjusted between 2 and 9% for mVenus, with a gain of 700–900, whereas for mCherry, a laser strength between 1 and 6% with a gain of 750–980 was used. Staining of plasma membrane was carried out using 10 μM FM4-64 which was infiltrated 20 min before image acquisition. Images were recorded and processed using Fiji software (Schindelin et al., 2012).

Fluorescence Lifetime Imaging Microscopy in *N. benthamiana* Leaves

Fluorescence lifetime imaging microscopy (FLIM) was performed using a LSM 780 confocal laser-scanning microscope additionally equipped with a single-photon counting device enabling picosecond time resolution (PicoQuant Hydra Harp 400). mVenus fluorescence was excited at 485 nm with a rate of 32 MHz with a linearly polarized pulsed diode laser (LDH-D-C-485, PicoQuant). The pinhole was set to 1 Airy Unit (AU). Excitation power was adjusted to 1 μW at the objective C-Apochromat (40×/1.2 W Corr M27) prior to measurements. mCherry was excited at 561 nm by a continuous wave laser with a laser strength of 0.1%. Emitted light of mVenus was separated into its parallel and perpendicular polarization. mVenus fluorescence was detected by Tau-SPADs (PicoQuant) in a narrow range of its emission spectrum (band-pass filter: 534/30, AHF). mCherry fluorescence detection was set by the band-pass filter (HC 607/70, AHF). Images were acquired with 256 × 256 pixel, zoom factor 4, 12.61 μs pixel dwell time, and a resolution of 210 nm/pixel. A series of 80 frames were merged into one image and further analyzed using SymphoTime64 (PicoQuant).

Fluorescence Lifetime and Anisotropy Analysis

The fluorescence lifetime of mVenus was analyzed using the software tool SymPhoTime 64, version 2.3 (PicoQuant, Berlin, Germany). Due to low excitation power to prevent photobleaching during image acquisition and the small pixel size to gain spatial

resolution, the number of photons per pixel was still low after merging of frames. An individual ROI for every dataset was generated ensuring that only pixels with a minimum number of 100 photons contributed to the decay histogram. In the donor-only case, a mono-exponential fit model, including background contribution and shifting of the instrument response function, was sufficient to describe the decay histogram of mVenus fluorescence and extract the fluorescence lifetime. In the case of FRET an additional exponent was used to describe the decay and a mean fluorescence lifetime was extracted from the resulting fit.

The steady-state anisotropy r is given by $r = \frac{I_{par} - GI_{per}}{I_{par} + 2GI_{per}}$. I_{par} and I_{per} are the average fluorescence count rates per pixel with the emission parallel (I_{par}) and perpendicular (I_{per}) to the excitation polarization direction (Gauthier et al., 2001; Sarkar et al., 2009). Orientation sensitivity differences of the detection system were corrected by determining the *G*-factor by calibration measurements using Rhodamine110. Data were statistically evaluated with GraphPad Prism using Student's *t*-test with Welch correction and Mann-Whitney test, respectively.

RESULTS

Heterologous Expression and Purification of *A. thaliana* Type-II Receptor ETR2

Previous studies have revealed the direct interaction of *A. thaliana* receptor ETR1 (AtETR1) with the C-terminus of EIN2 (aa 479-1294) *in planta.* These *in vivo* results were supported by tryptophan fluorescence quench studies on purified proteins which disclosed that receptors interact with the EIN2 downstream ethylene signaling protein with high affinity. Along the same lines, *in planta* FRET studies have demonstrated the interaction of type-II receptors and EIN2 (Bisson et al., 2009; Bisson and Groth, 2010). However, these studies did not reveal binding mode and binding affinities of the EIN2 C-terminus with type-II receptors. To clarify whether type-II and type-I receptors interact with EIN2 in a similar way and affinity as the type-I receptor subfamily, we heterologously expressed and purified ethylene receptor ETR2 from *A. thaliana* (AtETR2) as prototype of the type-II subfamily. To this end, AtETR2 expression plasmid pGEX-4T-1_TEV_ETR2_H_{10} was transformed into *E. coli* strain C43 (DE3) which has been successfully used for expression of AtETR1 (Voet van Vormizeele and Groth, 2008). Bacterial cells harboring the AtETR2 expression plasmid show an increased expression of a protein band with an apparent molecular weight of 120 kDa up to 4 h after induction, whereas 5 h after induction the corresponding protein band appear faded suggesting degradation of the over-expressed receptor by bacterial proteases (**Figure 1A**, line 5). On the basis of the expression studies showing maximum protein production 4 h after induction, cells were harvested 4 h post-induction and solubilized from the host membranes by the detergent FosCholine-16. Solubilized AtETR2 receptors were purified by metal-chelate affinity chromatography on Ni-NTA agarose (GE Healthcare). High purity of the resulting receptor preparations is indicated by the single band observed on the SDS protein gel (**Figure 1B**). Identity of the purified protein band with AtETR2 was confirmed by immunoblotting with an anti-His Tag antibody (**Figure 1C**).

Analysis of Secondary Structure and Functional Folding of AtETR2

The folding and secondary structure of AtETR2 was analyzed by circular dichroism (CD) spectroscopy. The CD spectra has two minima at 208 and 221 nm and an isosbestic point at 201 nm (**Figure 2**), indicating a predominately α-helical structure of the purified AtETR2. Secondary structure content was quantified by CONTINLL and CDSSTR—two different algorithms for secondary structure assignment—at 48–50% α-helix and 9–10% β–sheet demonstrating that the recombinant protein adopts a well-folded structure and is likely to reflect a native confirmation of the *Arabidopsis* type-II ethylene receptor ETR2. Additionally, AtETR2 functionality was probed by an *in vitro* radiolabeling autokinase assay. For that, AtETR2 was purified without ATP pre-incubation. Purified protein preparations were then incubated with [γ-^{32}P]ATP. Autoradiography of the SDS gel loaded with samples from the kinase assay revealed incorporation of ^{32}P for those samples incubated in the presence of magnesium—an essential cofactor for histidine kinase activity—but not for those containing chemically denatured AtETR2 (**Figure 3**). These results further confirm functional folding of purified AtETR2. Notably, the purified type-II receptor shows somewhat reduced kinase activity in the presence of manganese (**Supplementary Figure S1D**), which is in line with results of previous studies using the ETR2ΔGAF mutant (Moussatche and Klee, 2004). To allow for comparison to the type-I receptor subfamily in terms of protein affinities and protein activities, similar buffer and detergent conditions were applied for purification of AtETR1. The corresponding autokinase assay (**Supplementary Figure S1B**) supports that both receptor subfamilies show similar phosphorylation activities at these conditions and once again emphasizes the purification of the full-length receptors in a functional, catalytically active state.

Microscale Interaction Studies of AtETR2 and Downstream Signaling Components AtEIN2$^{479-1294}$ and CTR1

Protein-protein interactions of purified receptors with downstream ethylene signaling components EIN2 and CTR1 were monitored and quantified by microscale thermophoresis (MST). This biophysical technique is based on the motion of molecules in a temperature gradient and strongly depends on the charge, hydration-shell and size of the moving molecules. At least one of these qualities typically changes upon complex formation. Hence, thermophoresis provides a sensitive and reliable method to analyze and to quantify protein-protein interactions (Duhr and Braun, 2006; Wienken et al., 2010; Jerabek-Willemsen et al., 2011). For a start, we applied this technique to quantify the interaction of the soluble EIN2 C-terminus (AtEIN2$^{479-1294}$) with the type-II receptor prototype AtETR2. Both recombinant proteins were purified as previously described (see **Figure 1A, Supplementary Figure S2B**;

Bisson et al., 2016). Addition of EIN2$^{479\text{-}1294}$ to labeled AtETR2 shows clear changes of thermophoresis and thermophoretic signals obtained with increasing EIN2$^{479\text{-}1294}$ concentrations follow a clear binding curve. From this binding curve, an apparent dissociation constant (K_d) of 161(30) nM was obtained which is indicative of a tight and highly specific interaction of AtEIN2$^{479\text{-}1294}$ with the AtETR2 receptor. Similarly, clear changes of the thermophoretic signal were observed upon addition of AtETR2 to labeled EIN2$^{479\text{-}1294}$. The corresponding binding curve shows an apparent K_d of 147(15) nM. Any potential effect of the fluorescence probe Alexa Fluor 488 which is positioned at different sites in the two complementary titration set-ups on the interaction, integrity or stability of any of the two binding partner can be ruled out as both binding studies show almost the same low nanomolar K_d value (**Figure 4**). The tight and highly specific interaction of AtETR2-AtEIN2$^{479\text{-}1294}$ is further supported in titration studies using denatured AtEIN2$^{479\text{-}1294}$ as negative control. Here, no interaction between both binding partners was detectable. Like EIN2 the Raf-like protein kinase CTR1 is another signaling element downstream of the *Arabidopsis* ethylene receptor family. Recombinant AtCTR1 required for *in vitro* binding studies with receptors AtETR1 and AtETR2 respectively, was purified according to the methods section (see **Supplementary Figure S2A**). As described before for EIN2, protein-protein interactions of receptor proteins and AtCTR1 were analyzed by MST. To this end, AtCTR1 was labeled with the fluorescent dye Alexa 488 and was mixed with increasing concentrations of AtETR1 or AtETR2 until saturation. Binding of receptors to AtCTR1 detected as changes in thermophoresis correspond to dissociation constants (K_d) of 169(15) nM for the AtCTR1-AtETR1 interaction and of 165(20) nM for the AtCTR1-AtETR2 complex. Again, these numbers indicate a tight and highly specific interaction. Furthermore, it should be noted that both receptor subfamilies show similar affinities for AtCTR1 (**Figure 5**).

In vitro Quantification of Type-I-Type-II Receptor Interactions

To analyze the mode of receptor-receptor interactions and to quantify binding affinities, we studied protein-protein interactions within receptor subfamilies by microscale thermophoresis. To this end, we analyzed homomeric and heteromeric receptor complexes of AtETR1 and AtETR2. For that, either AtETR1 or AtETR2 was labeled with Alexa Fluor 488, and thermophoresis was recorded after the addition of the corresponding binding partner. Binding affinity and dissociation constants indicate strong binding for both receptor subfamily homomers, AtETR1-AtETR1 and AtETR2-AtETR2 (**Figure 6A**). However, a three-fold higher affinity of the type-II AtETR2-AtETR2 homomer [K_d of 96(9) nM] was detected in comparison to the type-I AtETR1-AtETR1 homomer [K_d of 326(18) nM]. In addition, our binding studies revealed that type-I and type-II receptors can also form tight heteromeric complexes with binding constants of 177(18) nM (AtETR1-AtETR2) and 217(14) nM (AtETR2-AtETR1), respectively (**Figure 6B, Supplementary Figures S3A,B**). Notably, type-II:type-I heteromeric complexes seem to be more stable than type-I homomers. No interactions were detected in the related binding studies when chemically denatured receptors were used (**Figure 6A**). Previous studies suggested that dimer and higher complex formations in the ethylene receptor family are substantially mediated by their GAF-domains (Grefen et al., 2008; Mayerhofer et al., 2015). However, the role of the receptor

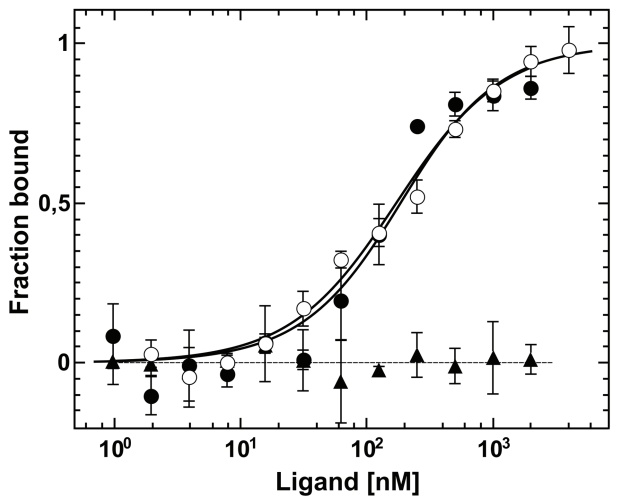

FIGURE 4 | Interaction studies of *Arabidopsis* ETR2 and EIN2 by MST. Dissociation constants of the interactions were obtained from the related binding curves. Titration of unlabeled AtEIN2$^{479\text{-}1294}$ to AtETR2 (●) is described by a dissociation constant (K_d) of 161(30) nM. Chemically and thermally denatured AtEIN2$^{479\text{-}1294}$ shows no binding event to AtETR2 (▲). Binding of unlabeled AtETR2 to AtEIN2$^{479\text{-}129}$ is represented by a K_d value of 147(15) nM (○). All data represent the mean (SD) of three independent measurements (●, ○) and duplicates (▲), respectively.

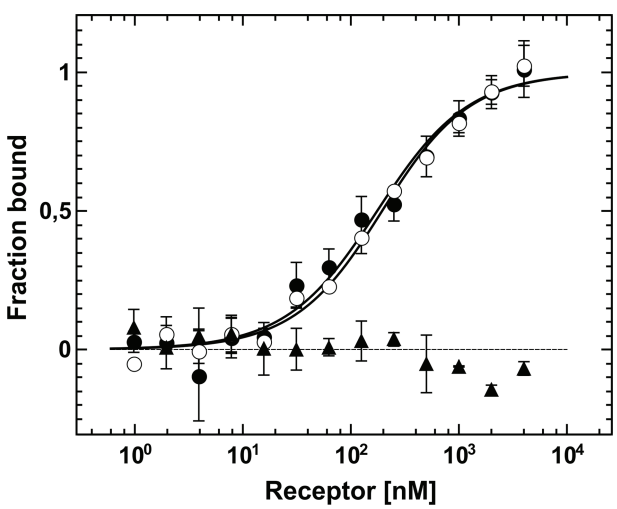

FIGURE 5 | MST based protein-protein interaction assay between AtCTR1 and receptor proteins AtETR1 and AtETR2. Binding of AtETR1 to fluorescently labeled AtCTR1 measured by MST resulted in a K_d value of 169(15) nM (○). For AtCTR1-AtETR2 complex formation a K_d value of 165(20) nM was obtained (●). As negative control, titration of chemically denatured AtCTR1 with AtETR2 is shown. Here, no binding event was observed (▲). Data are given as the mean (SD) of independent triplicates (●, ○) and duplicates (▲), respectively.

A

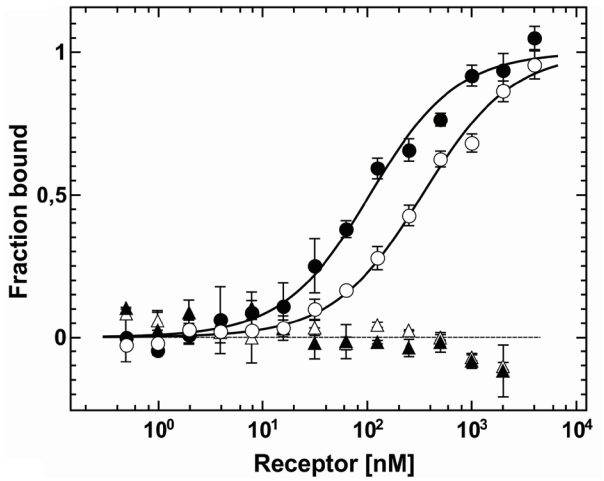

B

	Dissociation constant in [nM]	
	$ETR1_{Alexa488}$	$ETR2_{Alexa488}$
ETR1	326 ± 18	217 ± 14
ETR2	177 ± 18	96 ± 9
$ETR1\text{-}TM^{C4SC6S}$	491 ± 20	145 ± 9

FIGURE 6 | Quantification of receptor-receptor interactions by microscale thermophoresis. **(A)** For the homomeric AtETR1-AtETR1 complex formation a K_d value of 326(18) nM (○) was obtained. As negative control chemically denatured AtETR1 was used showing no binding event (△). From the binding curve of the homomeric AtETR2-AtETR2 complex a K_d value of 96(18) nM (●) was calculated. Chemically denatured AtETR2 indicates no interaction of the binding partners (▲). All data represent the mean (SD) of independent triplicates (○, ●) and duplicates (△, ▲). **(B)** Summary of the dissociation constants K_d for receptor-receptor interactions obtained by MST, also see **Supplementary Figure S3**. All data represent the mean (SD) of three independent measurements.

transmembrane-domain in complex formation was not resolved in these studies. To address this issue, we analyzed the interaction between the isolated AtETR1 transmembrane domain (ETR1-TM) and full-length receptors AtETR1 and AtETR2 *via* MST. To eliminate any stabilizing effect by disulfide bond formation (Schaller et al., 1995), cysteines in ETR1-TM were substituted to serines (C4SC6S). In the related titration experiments, tight binding of $ETR1\text{-}TM^{C4SC6S}$ to both receptor subfamily representatives (AtETR1 and AtETR2) was observed. In line with previously observed heteromeric interactions of full-length receptors, the affinity for AtETR2 was higher than for AtETR1 (**Figure 6B, Supplementary Figures S3C,D**). Taken together, the binding studies with the isolated transmembrane domain ($AtETR1\text{-}TM^{C4SC6S}$) as well as with full-length receptors emphasize that both receptor subtypes interact in homomeric and heteromeric complexes in a selective and specific manner. Moreover, the higher stability of type-II receptor homo- and heteromers highlights the importance of this subfamily to form receptor dimers or higher order oligomers in ethylene signaling.

In planta Detection of Receptor-Receptor Interactions *via* FRET-FLIM Microscopy

To analyze ethylene type-II:type-I receptor complex formations *in vivo*, we performed fluorescence lifetime imaging microscopy (FLIM). FLIM is used in plant cells to study molecular interactions and detects fluorescence resonance energy transfer (FRET) between two fluorescent-tagged proteins in close proximity (Gadella et al., 1993; Valeur, 2001; Stahl et al., 2013; Long et al., 2017). By further analysis of the donor anisotropy, this method allows the discrimination between hetero-FRET (FRET between two different donor and acceptor fluorophores) and homo-FRET (energy migration between identical fluorophores and thus identical receptors). Therefore, monomeric versions of the fluorescent proteins Venus and Cherry fused to the C-terminus of the *Arabidopsis* ethylene receptors were chosen as FRET pair (Shaner et al., 2004; Kremers et al., 2006). Tobacco epidermal leaf cells were (co-)transformed with the relevant receptor(s), and expression was induced by the addition of β-estradiol. The fluorescence lifetime measurements were performed in combination with an inducible expression system which allows the discrimination of autofluorescence and prevents overexpression artifacts (Suhling et al., 2015). To verify localization at the ER membrane in the tobacco leaf cells, we probed the intracellular localization of full-length type-II receptor AtERS2 by confocal microscopy. As a result, we observed a strictly separated localization of the PM-localized dye FM4-64 and AtERS2-mVenus, whereas a colocalization of AtERS2-mVenus with a mCherry-labeled ER-marker protein was detected (**Figures 7A,B**; Nelson et al., 2007). Additionally, we detected colocalization of AtERS2 and other *Arabidopsis* ethylene receptors which are a necessary condition for subsequent analysis of receptor-receptor interactions (**Figures 7C–F**). Type-I and type-II receptors AtERS1 and AtERS2, the ER-bound receptor Reticulon-like protein B2 (AtBTI2) as a negative control, and a tandem construct with both FPs fused to AtERS2 as a positive control were used to pinpoint *in vivo* interaction of the two receptor subfamilies. For each receptor combination, fluorescence lifetime (τ) and anisotropy (r) of the donor fluorophore mVenus were measured. Fluorescence lifetime of a fluorophore represents the average time a fluorophore remains in the fluorescent state after excitation by a pulsed laser. For heteromeric interactions, the mVenus fluorescence is quenched by FRET between mVenus and mCherry fluorophores, thereby shortening the mVenus fluorescence lifetime (Gadella et al., 1993, 1994), whereas fluorescence anisotropy represents the rotational freedom of a fluorophore. This rotation is reduced by fusion of the fluorophore to a protein, increasing the anisotropy value r. Occurrence of hetero-FRET additionally increases the anisotropy due to a direct interaction of donor and acceptor fluorophore, again limiting rotation of the donor fluorophore. Whereas in case of homo-FRET, energy can migrate radiation free from one excited mVenus fluorophore to another mVenus in close proximity but with slightly different dipole orientation. This leads to a reduced overall mVenus anisotropy due to a depolarization of the overall mVenus signal and thus decreases the observed value r for the steady state anisotropy. Thus, the measurement of anisotropy enables a direct discrimination

between homo- and heteromeric interactions (Gauthier et al., 2001; Bader et al., 2011). In our studies, we measured lifetimes for each AtERS2-mVenus combination by FLIM. As shown in **Figure 8A** cotransfections of AtERS2 with either type-I receptor AtERS1 (2.56 ns) or type-II receptor AtERS2 (2.59 ns) resulted in a significant reduction of the AtERS2-mVenus (2.90 ns) fluorescence lifetime (see **Supplementary Table S2**). In the context of the also observed lifetime reduction of the positive control (AtERS2-mVenus-mCherry) and the unchanged lifetime

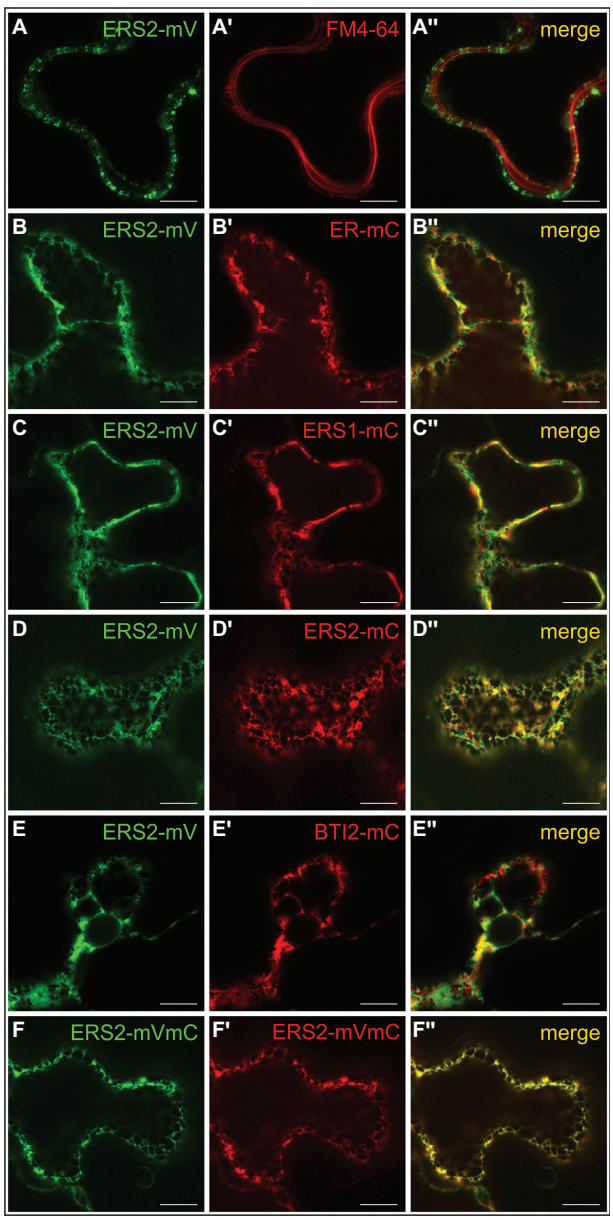

FIGURE 7 | Intracellular localization of AtERS1 and AtERS2 transiently expressed in *N. benthamiana* epidermis cells. Confocal laser scanning microscopy images of mVenus (mV) and mCherry (mC)-tagged receptor proteins. **(A–A″)** AtERS2 does not colocalize with the PM dye FM4-64 and is instead found **(B–B″)** at the ER, where colocalization with the ER-mCherry marker protein is detected. AtERS2-mVenus colocalizes with **(C–C″)** AtERS1-mCherry, **(D–D″)** AtERS2-mCherry and **(E–E″)** BTI2-mCherry at the ER. **(F–F″)** AtERS2 tagged to mVenus and mCherry is also detected at the ER. Bars = 10 µm.

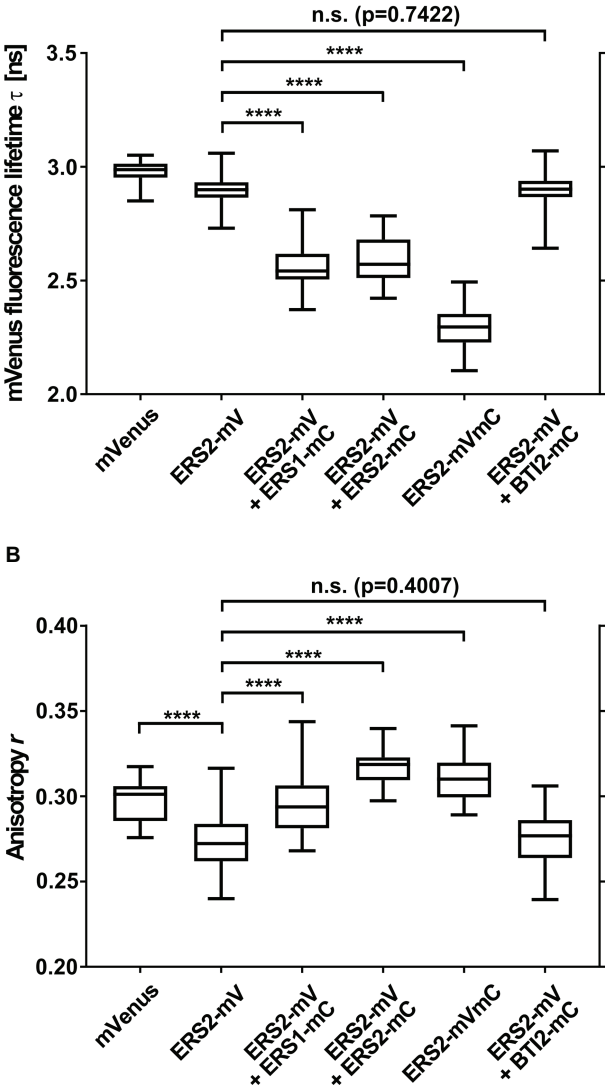

FIGURE 8 | Homo- and heteromeric interaction pattern of ethylene receptors. Depicted are **(A)** fluorescence lifetime (τ) and **(B)** anisotropy (*r*) of AtERS2-mVenus coexpressed with mCherry-tagged receptor proteins in *N. benthamiana* leaf epidermal cells. *N. benthamiana* leaf cells were transfected with the indicated proteins, protein expression was induced by β-estradiol and samples were analyzed by confocal microscopy within 16–25 h. Fluorescence lifetime and anisotropy were calculated of free fluorophore mVenus ($n = 34$), donor-only AtERS2-mVenus ($n = 113$) and coexpression of AtERS2-mVenus with either AtERS1-mCherry ($n = 68$) or AtERS2-mCherry ($n = 18$). Coexpression of AtERS2-mVenus with BTI2-mCherry ($n = 62$) was used as negative control, whereas expression of AtERS2-mVenus-mCherry ($n = 50$) was used as positive control. Distribution of mVenus fluorescence lifetime (τ) and anisotropy (*r*) are depicted as box plot: median, first and third quartiles, minimum and maximum, error bars indicate minimum and maximum of distribution. Statistical analysis was performed using Mann-Whitney test (**A**, AtERS2-mVenus + AtBTI2-mCherry) and Welch's *t*-test (all other), $^{****}p < 0.0001$, mV = mVenus, mC = mCherry. See also **Supplementary Tables S2,S3** for data.

of the negative control (AtERS2-mVenus:AtBTI2-mCherry), these data indicate heteromeric interactions of the type-I receptor AtERS1 with type-II AtERS2 as well as homomeric interactions of AtERS2 protomers. Formation of AtERS2 homomers is further supported by the observed changes in fluorophore anisotropy (see **Figure 8B**). In our experiments, we observed a decreased anisotropy ($r = 0.27$) for AtERS2-mVenus compared to free mVenus ($r = 0.30$, see **Supplementary Table S3**). Moreover, formation of type-II homomers can also be inferred from measurements of AtERS2 with AtERS1. Here, the anisotropy of AtERS2 ($r = 0.29$) is increased compared to the mVenus donor only sample, but decreased compared to the free mVenus fluorophore. In accordance to these results, no significant changes were observed for the negative control compared to the AtERS2-mVenus donor. These data are indicative for homo-FRET interactions between AtERS2-mVenus itself only. In summary, our *in planta* fluorescence studies demonstrate homomeric as well as heteromeric interactions of the type-II receptor AtERS2 *in vivo*. Furthermore, we were able to show that at these conditions homo-FRET interactions of AtERS2 take place as well in the presence as in the absence of type-I receptor AtERS1.

DISCUSSION

Previous studies on *Arabidopsis* revealed that the ethylene signal perception and transduction is mediated by five receptors localized at the ER membrane (Hua and Meyerowitz, 1998; Grefen et al., 2008). Furthermore, genetic studies identified CTR1 and EIN2 as critical regulators mediating ethylene signaling and identified both proteins as direct interaction partner of the ethylene receptor family (Kieber et al., 1993; Alonso et al., 1999; Huang et al., 2003). However, previous protein-protein interaction studies mainly focused on the prototype type-I receptor AtETR1, whereas related information on subfamily-II receptors is still sparse. Although a direct interaction of ethylene type-II receptors with either CTR1 or EIN2 has been demonstrated by yeast two-hybrid assays and *in planta* FRET studies (Cancel and Larsen, 2002; Bisson and Groth, 2010), detailed information about these interactions is still missing. To elucidate type-II receptor interactions with their downstream signaling targets in more detail, we have established a purification protocol for the *Arabidopsis* full-length type-II receptor ETR2. The protocol is based on the expression of AtETR2 in *E. coli* strain C43 (DE3), which has been successfully applied for the expression of type-I receptor AtETR1 and several other membrane proteins in the past (Miroux and Walker, 1996; Voet van Vormizeele and Groth, 2008). In this case, solubilization of AtETR2 was obtained by the zwitterionic detergent FosCholine-16 and a purification protocol similar to AtETR1 (Classen and Groth, 2012; Milić et al., 2018) was applied. Functional folding of the purified recombinant AtETR2 was verified by CD spectroscopy (see **Figure 2**). Secondary structure calculations based on CD measurements on the purified receptor determined an α–helical content of 48–50% and a β–sheet content of 9–10% which correspond well to sequence based secondary structure predictions by SOPMA (α–helical: 48% and a β–sheet: 14%) (Geourjon and Deléage, 1995; Sreerama and Woody, 2000; Kessenbrock and Groth, 2017).

Previous studies revealed that the ethylene receptors function as negative regulators and are in their active state in the absence of ethylene (Hua and Meyerowitz, 1998). *In vitro* phosphorylation assays demonstrated that receptors in their active state show autokinase activity of various degrees depending on the divalent cation used. Along these lines, our studies on purified full-length AtETR2 substantiate that the recombinant type-II receptor has higher autokinase activity in the presence of magnesium than in the presence of manganese, which is in accordance with previous studies on truncated AtETR2 lacking the transmembrane domain (Moussatche and Klee, 2004). On the other hand, almost no measurable phosphorylation activity was found for chemically denatured AtETR2 (see **Figure 3, Supplementary Figures S1C**,**D**). Taken together, our structural and functional studies on the purified AtETR2 attest that the recombinant type-II receptor used in our *in vitro* binding studies was isolated in a functional and active state. Stable complex formation of type-II receptor AtETR2 with AtEIN2 has been previously identified by *in vivo* FRET studies. Nevertheless only the AtETR1-AtEIN2 interaction was further characterized in detail by *in vitro* tryptophan quenching studies due to the lack of a purified functional type-II receptor isoform at that time (Bisson et al., 2009; Bisson and Groth, 2010). Here, we unravel a tight and highly specific complex formation of AtETR2 with the soluble cytosolic domain of EIN2 ($AtEIN2^{479\text{-}1294}$, see **Figure 4**) which reinforces the previously mentioned *in planta* FRET studies (Bisson and Groth, 2010). Noteworthy, our studies disclose similar binding affinities and binding modes for AtETR1 and AtETR2 with $AtEIN2^{479\text{-}1294}$ which substantiate similar roles of the different isoforms in PPI-based signal transfer to their downstream target. Still, the observed similar complex stability is quite surprising considering the low sequence identity of only 39% of both isoforms as well as the pronounced differences of both receptor subfamilies in their kinase activity and transmembrane architecture. However, these differences in the receptor isoforms may only come into effect at specific signaling conditions as previously shown for AtETR1 where receptor phosphorylation or binding of an ethylene agonist were shown to modulate complex stability with EIN2 (Bisson and Groth, 2010).

Genetic and biochemical studies indicate that apart from EIN2 the Raf-like kinase CTR1 also interacts with all members of the ethylene receptor family to mediate ethylene signaling at the ER membrane (Cancel and Larsen, 2002; Gao et al., 2003). Consequently, we also analyzed the interaction of the different receptor subfamilies with CTR1 in this study. As for EIN2, we found similar affinities of the CTR1 kinase with full-length receptors AtETR1 and AtETR2 representing prototypes of both subfamilies. These results differ from previous studies using yeast two-hybrid screening and pull-down assays which propose a preferred interaction of AtCTR1 with AtETR1 (Clark et al., 1998; Cancel and Larsen, 2002), although these studies did not provide clear quantitative analysis. Moreover, pull-down assays were performed with truncated receptor constructs which also affect complex stability with the CTR1 kinase.

Taken together, our binding studies determine that both receptor subtypes have similar binding affinities and binding modes with their downstream targets AtEIN2$^{479\text{-}1294}$ and AtCTR1 emphasizing similar roles of both receptor subfamilies in PPI-based signal transduction. Bearing in mind that both, CTR1 and EIN2, have been localized to the ER these results correlate well with the idea of ER-borne signaling complexes consisting of various combinations of receptor subtypes, EIN2 and CTR1 (Gao et al., 2003; Bisson et al., 2009; Bisson and Groth, 2010).

For further analysis of receptor complex formation and the role for ethylene signaling *in planta*, we used fluorescence microscopy of transiently expressed receptor proteins in *N. benthamiana* leaf cells. In their native background *Arabidopsis* receptors are localized at the ER membrane. In order to demonstrate that this localization is not affected at overexpressed conditions in the *N. benthamiana* system, we first determined subcellular localization of transiently expressed full-length type-II receptor AtERS2 by confocal microscopy. In our experiments, AtERS2 shows clear separation from the plasma membrane as evidenced by staining with FM4-64. On the other hand, clear colocalization with an ER-marker protein, with ethylene receptor AtERS1 or ER-bound *Arabidopsis* receptor Reticulon-like protein B2 (AtBTI2, Nziengui et al., 2007) was observed indicative of a proper localization of AtERS2 at the ER membrane in the *N. benthamiana* system. In subsequent *in planta* interaction studies, we analyzed fluorescence lifetime and anisotropy of a type-II receptor construct (AtERS2-mVenus) in combination with the type-I receptor isoform AtETR1. While changes in fluorescence lifetime refer to a direct interaction of different fluorophores (hetero-FRET), changes in anisotropy provide additional information about FRET processes between identical fluorophores (homo-FRET). Here, direct excitation of a fluorophore (mVenus) by another identical fluorophore in close proximity leads to a decreased anisotropy due to a depolarization effect. Hence, by analyzing fluorescence lifetime and anisotropy the homo- and hetero-FRET state of a donor fluorophore can be discriminated and thereby homo- and heteromeric interaction of the tagged protein (Gauthier et al., 2001; Bader et al., 2011). The results obtained in our FLIM experiments clarify that type-II receptor AtERS2 forms uniform homomeric complexes, but also heteromeric complexes with type-I receptor AtERS1 *in planta*. Thereby, the *in planta* interaction studies confirm our *in vitro* analysis which also attests homomeric complex formation of AtETR1 and AtETR2 but also tight heteromeric interaction of both receptor subfamilies. Previous studies proposed that the additional N-terminal α-helix in type-II receptors might serve as signal sequence (Chen et al., 2007). The tight affinity of type-II receptor homomeric and heteromeric complexes observed in our *in vitro* binding studies now suggests that the additional helix of type-II receptor may serve an increased complex stability. In principle, the tight affinity of type-II receptor complexes could also be related to sequence variation in individual helix segments. However, sequence alignment of both subtypes (**Supplementary Figure S4**) reveals that transmembrane helices of AtETR1 and AtETR2 are highly conserved (66% identical residues). In total, only five residues (G59/I88, A67/M96, L73/G102, A90/F119 and M104/T133 with the ETR1 residue and position given first) show low conservation. But even these residues have not experienced drastic changes in terms of physicochemical properties. Moreover, in a regular α-helix they do not align on the same surface. Consequently, a single of these minor changes then would have to account for the observed large differences in complex stability which is highly unlikely.

Heretofore, interactions of the ethylene receptor family were mainly attributed to the receptor GAF-domain (Xie et al., 2006; Grefen et al., 2008). However, we should bear in mind that the TM domain was not expressed in these studies. The quantitative binding studies presented in this work demonstrate for the first time that the isolated TM domain substantially contributes to receptor complex formation and probably plays a major role in mediating receptor-receptor interactions. Furthermore, previous studies demonstrated that receptors are stabilized by covalent cysteine crosslinks, although their impact on complex formation was not addressed (Schaller et al., 1995; Schaller and Bleecker, 1995). To address this point, we mutated the two cysteines near the amino terminus of AtETR1 (positions 4 and 6) to serine in order to prevent disulfide bond formation in the TM domain of the receptor. The tight and highly specific binding of the purified ETR1-TM^{C4SC6S} mutant to either AtETR1 or AtETR2 together with previous genetic studies of Xie et al. (2006) suggest that disulfide linkage is not essential for AtETR1 signaling.

In summary, our studies demonstrate that the type-II receptor AtETR2 binds AtEIN2 and AtCTR1 with similar affinities as type-I receptor AtETR1 indicating a similar role of both receptor subfamilies in PPI-based signal transfer, although they may still differ in other signal output mechanism mediated by post-translational modification such as phosphorylation or ubiquitination (Moussatche and Klee, 2004; O'Malley et al., 2005; Chen et al., 2007; Kevany et al., 2007). Specifically, the similar affinity of both subfamilies for their downstream targets may explain functional redundancy of the ethylene receptor family, i.e., the common function of all members to repress the constitutive ethylene response, although individual receptors can adopt specific functions that are not replaceable by other isoforms (Liu and Wen, 2012). Moreover, the similar affinity of both subfamilies for CTR1 and EIN2 may indicate that both target the same site in the receptors. However, a sequence alignment of the CTR1 N-terminus and the EIN2 C-terminus, which have been identified in previous studies to mediate binding to the receptors, reveals no particular sequence element to support this idea. Still, we have to bear in mind that, in the end, the 3D structure of a protein determines the interaction. Hence, structures of receptor complexes with CTR1 and/or EIN2 will ultimately unravel the binding site and signal transfer mechanism for both downstream signaling proteins.

Noteworthy, both receptor isoforms efficiently and specially bind to representatives of each subfamily, although interaction with type-II receptor protomers is slightly preferred probably due to a stabilizing effect of the additional TM helix in these receptors. These mixed dimers or higher molecular weight oligomers may reflect functional synergism of the different receptor subtypes to control scope, scale, and pace of ethylene responses.

The preferred association of ETR1 with type-II receptors determined in our *in vitro* binding studies is fully in line with previous co-purification experiments of ETR1 with tagged versions of ERS1, ETR2, ERS2, and EIN4 from *Arabidopsis* membrane extracts (Gao et al., 2008) underscoring the biological significance of quantitative studies on purified individual components of the signaling pathway. To further dissect the functional role of the receptor heteromeric complexes for ethylene signaling, *in planta* studies on chimeric receptors consisting of different subdomains from the two subfamilies in different ethylene *loss-of-function* backgrounds may prove promising.

DATA AVAILABILITY

The datasets generated for this study are available on request to the corresponding author.

AUTHOR CONTRIBUTIONS

GG conceived the project, planned, designed, and supervised the research. MB and NB planned and performed experiments with the assistance of SW-P, SH, and RCB. AM assisted with statistical analysis. MB, GG, NB, AM, SW-P, and SH analyzed data. MB, NB, and GG wrote the manuscript. SW-P and AM critical edited the manuscript. SH, SW-P, BS, YS, and RS provided expertise and feedback.

FUNDING

This work was funded by the Deutsche Forschungsgemeinschaft (DFG, German Research Foundation)—Projektnummer 267205415—SFB 1208 (project B06 to GG, B04 to RS and project Z02 to SW-P) and GR1616/10-1 to GG and STA12/12 1-1 to YS.

ACKNOWLEDGMENTS

The authors thank the staff from the botanical garden of the university for cultivation and supply of *N. benthamiana* plants. We gratefully acknowledge technical support in vector cloning of Patricia Bartschies, Kerstin Förster, and Lena Müller.

SUPPLEMENTARY MATERIAL

The Supplementary Material file for this article can be found online at: https://www.frontiersin.org/articles/10.3389/fpls.2019.00726/full#supplementary-material

REFERENCES

Alonso, J. M., Hirayama, T., Roman, G., Nourizadeh, S., and Ecker, J. R. (1999). EIN2, a bifunctional transducer of ethylene and stress responses in *Arabidopsis*. *Science* 284, 2148–2152. doi: 10.1126/science.284.5423.2148

An, F., Zhao, Q., Ji, Y., Li, W., Jiang, Z., Yu, X., et al. (2010). Ethylene-induced stabilization of ETHYLENE INSENSITIVE3 and EIN3-LIKE1 is mediated by proteasomal degradation of EIN3 binding F-box 1 and 2 that requires EIN2 in *Arabidopsis*. *Plant Cell* 22, 2384–2401. doi: 10.1105/tpc.110.076588

Bader, A. N., Hoetzl, S., Hofman, E. G., Voortman, J., Van Bergen En Henegouwen, P. M. P., Van Meer, G., et al. (2011). Homo-FRET imaging as a tool to quantify protein and lipid clustering. *ChemPhysChem* 12, 475–483. doi: 10.1002/cphc.201000801

Binder, B. M., O'Malley, R. C., Wang, W., Zutz, T. C., and Bleecker, A. B. (2006). Ethylene stimulates nutations that are dependent on the ETR1 receptor. *Plant Physiol.* 142, 1690–1700. doi: 10.1104/pp.106.087858

Bisson, M. M. A., Bleckmann, A., Allekotte, S., and Groth, G. (2009). EIN2, the central regulator of ethylene signalling, is localized at the ER membrane where it interacts with the ethylene receptor ETR1. *Biochem. J.* 424, 1–6. doi: 10.1042/BJ20091102

Bisson, M. M. A., and Groth, G. (2010). New insight in ethylene signaling: autokinase activity of ETR1 modulates the interaction of receptors and EIN2. *Mol. Plant* 3, 882–889. doi: 10.1093/mp/ssq036

Bisson, M. M. A., Kessenbrock, M., Müller, L., Hofmann, A., Schmitz, F., Cristescu, S. M., et al. (2016). Peptides interfering with protein-protein interactions in the ethylene signaling pathway delay tomato fruit ripening. *Sci. Rep.* 6, 1–11. doi: 10.1038/srep30634

Bleckmann, A., Weidtkamp-Peters, S., Seidel, C. A. M., and Simon, R., (2010). Stem cell signaling in *Arabidopsis* requires CRN to localize CLV2 to the plasma membrane. *Plant Physiol.* 152, 166–176. doi: 10.1104/pp.109.149930

Bleecker, A. B., Estelle, M. A., Somerville, C., and Kende, H. (1988). Insensitivity to ethylene conferred by a dominant mutation in *Arabidopsis thaliana*. *Science* 241, 1086–1089. doi: 10.1126/science.241.4869.1086

Bleecker, A. B., and Kende, H. (2000). Ethylene: a gaseous signal molecule in plants. *Annu. Rev. Cell Dev. Biol.* 16, 1–18. doi: 10.1146/annurev.cellbio.16.1.1

Cancel, J. D., and Larsen, P. B. (2002). Loss-of-function mutations in the ethylene receptor ETR1 cause enhanced sensitivity and exaggerated response to ethylene in *Arabidopsis*. *Plant Physiol.* 129, 1557–1567. doi: 10.1104/pp.003780

Chang, C., Kwok, S. F., Bleecker, A. B., and Meyerowitz, E. M. (1993). *Arabidopsis* ethylene-response gene ETR1: similarity of product to two-component regulators. *Science* 262, 539–544. doi: 10.1126/science.8211181

Chen, Y. F., Randlett, M. D., Findell, J. L., and Schaller, G. E. (2002). Localization of the ethylene receptor ETR1 to the endoplasmic reticulum of *Arabidopsis*. *J. Biol. Chem.* 277, 19861–19866. doi: 10.1074/jbc.M201286200

Chen, Y. F., Shakeel, S. N., Bowers, J., Zhao, X. C., Etheridge, N., and Schaller, G. E. (2007). Ligand-induced degradation of the ethylene receptor ETR2 through a proteasome-dependent pathway in *Arabidopsis*. *J. Biol. Chem.* 282, 24752–24758. doi: 10.1074/jbc.M704419200

Clark, K. L., Larsen, P. B., Wang, X., and Chang, C. (1998). Association of the *Arabidopsis* CTR1 Raf-like kinase with the ETR1 and ERS ethylene receptors. *Proc. Natl. Acad. Sci. USA* 95, 5401–5406. doi: 10.1073/pnas.95.9.5401

Classen, E., and Groth, G. (2012). Cloning, expression and purification of orthologous membrane proteins: a general protocol for preparation of the histidine sensor kinase ETR1 from different species. *Mol. Membr. Biol.* 29, 26–35. doi: 10.3109/09687688.2012.667576

Curtis, M. D., and Grossniklaus, U. (2003). A gateway cloning vector set for high-throughput functional analysis of genes *in planta*. *Plant Physiol.* 133, 462–469. doi: 10.1104/pp.103.027979

Duhr, S., and Braun, D. (2006). Why molecules move along a temperature gradient. *Proc. Natl. Acad. Sci. USA* 103, 19678–19682. doi: 10.1073/pnas.0603873103

Follo, C., and Isidoro, C. (2008). A fast and simple method for simultaneous mixed site-specific mutagenesis of a wide coding sequence. *Biotechnol. Appl. Biochem.* 49, 175–183. doi: 10.1042/BA20070045

Gadella, T. W. J., Clegg, R. M., and Jovint, T. M. (1994). Fluorescence lifetime imaging microscopy: pixel-by-pixel analysis of phase-modulation data.

Bioimaging 2, 139–159. doi: 10.1002/1361-6374(199409)2:3<139::AID-BIO4>3.0.CO;2-T

Gadella, T. W. J., Jovin, T. M., and Clegg, R. M. (1993). Fluorescence lifetime imaging microscopy (FLIM): spatial resolution of microstructures on the nanosecond time scale. *Biophys. Chem.* 48, 221–239. doi: 10.1016/0301-4622(93)85012-7

Gao, Z., Chen, Y. F., Randlett, M. D., Zhao, X. C., Findell, J. L., Kieber, J. J., et al. (2003). Localization of the Raf-like kinase CTR1 to the endoplasmic reticulum of *Arabidopsis* through participation in ethylene receptor signaling complexes. *J. Biol. Chem.* 278, 34725–34732. doi: 10.1074/jbc.M305548200

Gao, Z., Wen, C. K., Binder, B. M., Chen, Y. F., Chang, J., Chiang, Y. H., et al. (2008). Heteromeric interactions among ethylene receptors mediate signaling in *Arabidopsis*. *J. Biol. Chem.* 283, 23801–23810. doi: 10.1074/jbc.M800641200

Gauthier, I., Tramier, M., Durieux, C., Coppey, J., Pansu, R. B., Nicolas, J. C., et al. (2001). Homo-FRET microscopy in living cells to measure monomer-dimer transition of GFP-tagged proteins. *Biophys. J.* 80, 3000–3008. doi: 10.1016/S0006-3495(01)76265-0

Geourjon, C., and Deléage, G. (1995). SOPMA: significant improvement in protein secondary structure prediction by c prediction from alignments and joint prediction. *Bioinformatics* 11, 681–684. doi: 10.1093/bioinformatics/11.6.681

Gibson, D. G., Young, L., Chuang, R. Y., Venter, J. C., Hutchison, C. A., and Smith, H. O. (2009). Enzymatic assembly of DNA molecules up to several hundred kilobases. *Nat. Methods* 6, 343–345. doi: 10.1038/nmeth.1318

Grefen, C., Städele, K., Růžička, K., Obrdlik, P., Harter, K., and Horák, J. (2008). Subcellular localization and *in vivo* interactions of the *Arabidopsis thaliana* ethylene receptor family members. *Mol. Plant* 1, 308–320. doi: 10.1093/mp/ssm015

Hoppen, C., Müller, L., Albrecht, A. C., and Groth, G. (2019). The NOP-1 peptide derived from the central regulator of ethylene signaling EIN2 delays floral senescence in cut flowers. *Sci. Rep.* 9, 1–8. doi: 10.1038/s41598-018-37571-x

Hua, J., Chang, C., Sun, Q., and Meyerowitz, E. M. (1995). Ethylene insensitivity conferred by *Arabidopsis* ERS gene. *Science* 269, 1712–1714. doi: 10.1126/science.7569898

Hua, J., and Meyerowitz, E. M. (1998). Ethylene responses are negatively regulated by a receptor gene family in *Arabidopsis thaliana*. *Cell* 94, 261–271. doi: 10.1016/S0092-8674(00)81425-7

Hua, J., Sakai, H., Nourizadeh, S., Chen, Q. G., Bleecker, A. B., Ecker, J. R., et al. (1998). EIN4 and ERS2 are members of the putative ethylene receptor gene family in *Arabidopsis*. *Plant Cell* 10, 1321–1332. doi: 10.1105/tpc.10.8.1321

Huang, Y., Li, H., Hutchison, C. E., Laskey, J., and Kieber, J. J. (2003). Biochemical and functional analysis of CTR1, a protein kinase that negatively regulates ethylene signaling in *Arabidopsis*. *Plant J.* 33, 221–233. doi: 10.1046/j.1365-313X.2003.01620.x

Jerabek-Willemsen, M., Wienken, C. J., Braun, D., Baaske, P., and Duhr, S. (2011). Molecular interaction studies using microscale thermophoresis. *Assay Drug Dev. Technol.* 9, 342–353. doi: 10.1089/adt.2011.0380

Johnson, W. C. (1999). Analyzing protein circular dichroism spectra for accurate secondary structures. *Proteins* 35, 307–312. doi: 10.1002/(SICI)1097-0134(19990515)35:3<307::AID-PROT4>3.0.CO;2-3

Ju, C., Yoon, G. M., Shemansky, J. M., Lin, D. Y., Ying, Z. I., Chang, J., et al. (2012). CTR1 phosphorylates the central regulator EIN2 to control ethylene hormone signaling from the ER membrane to the nucleus in *Arabidopsis*. *Proc. Natl. Acad. Sci. USA* 109, 19486–19491. doi: 10.1073/pnas.1214848109

Kessenbrock, M., and Groth, G. (2017). Circular dichroism and fluorescence spectroscopy to study protein structure and protein–protein interactions in ethylene signaling. *Methods Mol. Biol.* 1573, 141–159. doi: 10.1007/978-1-4939-6854-1

Kessenbrock, M., Klein, S. M., Müller, L., Hunsche, M., Noga, G., and Groth, G. (2017). Novel protein-protein inhibitor based approach to control plant ethylene responses: synthetic peptides for ripening control. *Front. Plant Sci.* 8:1528. doi: 10.3389/fpls.2017.01528

Kevany, B. M., Tieman, D. M., Taylor, M. G., Cin, V. D., and Klee, H. J. (2007). Ethylene receptor degradation controls the timing of ripening in tomato fruit. *Plant J.* 51, 458–467. doi: 10.1111/j.1365-313X.2007.03170.x

Kieber, J. J., and Ecker, J. R. (1993). Ethylene gas: it's not just for ripening any more! *Trends Genet.* 9, 356–362. doi: 10.1016/0168-9525(93)90041-F

Kieber, J. J., Rothenberg, M., Roman, G., Feldmann, K. A., and Ecker, J. R. (1993). CTR1, a negative regulator of the ethylene response pathway in *Arabidopsis*, encodes a member of the raf family of protein kinases. *Cell* 72, 427–441. doi: 10.1016/0092-8674(93)90119-B

Koncz, C., and Schell, J. (1986). The promoter of TL-DNA gene 5 controls the tissue-specific expression of chimeric genes carried by a novel type of agrobacterium binary vector. *Mol. Gen. Genet.* 204, 383–396. doi: 10.1007/BF00331014

Kremers, G. J., Goedhart, J., Van Munster, E. B., and Gadella, T. W. J. (2006). Cyan and yellow super fluorescent proteins with improved brightness, protein folding, and FRET förster radius. *Biochemistry* 45, 6570–6580. doi: 10.1021/bi0516273

Laemmli, U. K. (1970). Cleavage of structural proteins during the assembly of the head of bacteriophage T4. *Nature* 227, 680–685. doi: 10.1038/227680a0

Li, M. Z., and Elledge, S. J. (2007). Harnessing homologous recombination *in vitro* to generate recombinant DNA *via* SLIC. *Nat. Methods* 4, 251–256. doi: 10.1038/nmeth1010

Liu, Q., and Wen, C. K. (2012). Cooperative ethylene receptor signaling. *Plant Signal. Behav.* 7, 1009–1013. doi: 10.4161/psb.20937

Long, Y., Stahl, Y., Weidtkamp-Peters, S., Postma, M., Zhou, W., Goedhart, J., et al. (2017). *In vivo* FRET-FLIM reveals cell-type-specific protein interactions in *Arabidopsis* roots. *Nature* 548, 97–102. doi: 10.1038/nature23317

Mayerhofer, H., Panneerselvam, S., Kaljunen, H., Tuukkanen, A., Mertens, H. D. T., and Mueller-Dieckmann, J. (2015). Structural model of the cytosolic domain of the plant ethylene receptor 1 (ETR1). *J. Biol. Chem.* 290, 2644–2658. doi: 10.1074/jbc.M114.587667

Milić, D., Dick, M., Mulnaes, D., Pfleger, C., Kinnen, A., Gohlke, H., et al. (2018). Recognition motif and mechanism of ripening inhibitory peptides in plant hormone receptor ETR1. *Sci. Rep.* 8, 1–12. doi: 10.1038/s41598-018-21952-3

Miroux, B., and Walker, J. E. (1996). Over-production of proteins in Escherichia coli: mutant hosts that allow synthesis of some membrane proteins and globular proteins at high levels. *J. Mol. Biol.* 260, 289–298. doi: 10.1006/jmbi.1996.0399

Moussatche, P., and Klee, H. J. (2004). Autophosphorylation activity of the *Arabidopsis* ethylene receptor multigene family. *J. Biol. Chem.* 279, 48734–48741. doi: 10.1074/jbc.M403100200

Nelson, B. K., Cai, X., and Nebenführ, A. (2007). A multicolored set of *in vivo* organelle markers for co-localization studies in *Arabidopsis* and other plants. *Plant J.* 51, 1126–1136. doi: 10.1111/j.1365-313X.2007.03212.x

Nziengui, H., Bouhidel, K., Pillon, D., Der, C., Marty, F., and Schoefs, B. (2007). Reticulon-like proteins in *Arabidopsis thaliana*: structural organization and ER localization. *FEBS Lett.* 581, 3356–3362. doi: 10.1016/j.febslet.2007.06.032

O'Donnell, P. J., Calvert, C., Atzorn, R., Wasternack, C., Leyser, H. M. O., and Bowles, D. J. (1996). Ethylene as a signal mediating the wound response of tomato plants. *Science*. 274, 1914–1917. doi: 10.1126/science.274.5294.1914

O'Malley, R. C., Rodriguez, F. I., Esch, J. J., Binder, B. M., O'Donnell, P. J., Klee, H. J., et al. (2005). Ethylene-binding activity, gene expression levels, and receptor system output for ethylene receptor family members from *Arabidopsis* and tomato. *Plant J.* 41, 651–659. doi: 10.1111/j.1365-313X.2004.02331.x

Penninckx, I. A. M. A., Thomma, B. P. H. J., Buchala, A., Métraux, J.-P., and Broekaert, W. F. (1998). Concomitant activation of jasmonate and ethylene response pathways is required for induction of a plant defensin gene in *Arabidopsis*. *Plant Cell* 10, 2103–2113. doi: 10.1105/tpc.10.12.2103

Provencher, S. W., and Glöckner, J. (1981). Estimation of globular protein secondary structure from circular dichroism. *Biochemistry* 20, 33–37. doi: 10.1021/bi00504a006

Qiao, H., Shen, Z., Huang, S. C., Schmitz, R. J., Urich, M. A., Briggs, S. P., et al. (2012). Processing and subcellular trafficking of ER-tethered EIN2 control response to ethylene gas. *Science* 338, 390–393. doi: 10.1126/science.1225974

Qu, F., and Morris, T. J. (2002). Efficient infection of *Nicotiana benthamiana* by tomato bushy stunt virus is facilitated by the coat protein and maintained by p19 through suppression of gene silencing. *Mol. Plant-Microbe Interact.* 15, 193–202. doi: 10.1094/MPMI.2002.15.3.193

Rizzo, M. A., Springer, G., Segawa, K., Zipfel, W. R., and Piston, D. W. (2007). Optimization of pairings and detection conditions for measurement of FRET

between cyan and yellow fluorescent proteins. *Microsc. Microanal.* 12, 238–254. doi: 10.1017/s1431927606060235

Sakai, H., Hua, J., Chen, Q. G., Chang, C., Medrano, L., Bleecker, A. B., et al. (1998). ETR2 is an ETR1-like gene involved in ethylene signaling in *Arabidopsis*. *Proc. Natl. Acad. Sci. USA* 95, 5812–5817. doi: 10.1073/pnas.95.10.5812

Sarkar, P., Koushik, S. V., Vogel, S. S., Gryczynski, I., and Gryczynski, Z. (2009). Photophysical properties of cerulean and Venus fluorescent proteins. *J. Biomed. Opt.* 12, 1–25. doi: 10.1117/1.3156842

Schaller, G. E., and Bleecker, A. B. (1995). Ethylene-binding sites generated in yeast expressing the *Arabidopsis* ETR1 gene. *Science* 270, 1809–1811. doi: 10.1126/science.270.5243.1809

Schaller, G. E., Ladd, A. N., Lanahan, M. B., Spanbauer, J. M., and Bleecker, A. B. (1995). The ethylene response mediator ETR1 from *Arabidopsis* forms a disulfide-linked dimer. *J. Biol. Chem.* 270, 12526–12530. doi: 10.1074/jbc.270.21.12526

Schindelin, J., Arganda-Carreras, I., Frise, E., Kaynig, V., Longair, M., Pietzsch, T., et al. (2012). Fiji: An open-source platform for biological-image analysis. *Nat. Methods* 9, 676–682. doi: 10.1038/nmeth.2019

Shaner, N. C., Campbell, R. E., Steinbach, P. A., Giepmans, B. N. G., Palmer, A. E., and Tsien, R. Y. (2004). Improved monomeric red, orange and yellow fluorescent proteins derived from Discosoma sp. red fluorescent protein. *Nat. Biotechnol.* 22, 1567–1572. doi: 10.1038/nbt1037

Sreerama, N., and Woody, R. W. (2000). Estimation of protein secondary structure from circular dichroism spectra: comparison of CONTIN, SELCON, and CDSSTR methods with an expanded reference set. *Anal. Biochem.* 287, 252–260. doi: 10.1006/abio.2000.4880

Stahl, Y., Grabowski, S., Bleckmann, A., Kühnemuth, R., Weidtkamp-Peters, S., Pinto, K. G., et al. (2013). Moderation of *Arabidopsis* root stemness by CLAVATA1 and ARABIDOPSIS CRINKLY4 receptor kinase complexes. *Curr. Biol.* 23, 362–371. doi: 10.1016/j.cub.2013.01.045

Suhling, K., Hirvonen, L. M., Levitt, J. A., Chung, P. H., Tregidgo, C., Le Marois, A., et al. (2015). Fluorescence lifetime imaging (FLIM): basic concepts and some recent developments. *Med. Photonics* 27, 3–40. doi: 10.1016/j.medpho.2014.12.001

Towbin, H., Staehelin, T., and Gordon, J. (1979). Electrophoretic transfer of proteins from polyacrylamide gels to nitrocellulose sheets: procedure and some applications. *Proc. Natl. Acad. Sci. USA* 76, 4350–4354. doi: 10.1002/bies.950190612

Valeur, B. (2001). *Molecular fluorescence principles and applications*. (Weinheim: Wiley-VCH).

Voet van Vormizeele, J., and Groth, G. (2008). Ethylene controls autophosphorylation of the histidine kinase domain in ethylene receptor ETR1. *Mol. Plant* 1, 380–387. doi: 10.1093/mp/ssn004

Wang, W., Hall, A. E., O'Malley, R., and Bleecker, A. B. (2003). Canonical histidine kinase activity of the transmitter domain of the ETR1 ethylene receptor from *Arabidopsis* is not required for signal transmission. *Proc. Natl. Acad. Sci. USA* 100, 352–357. doi: 10.1073/pnas.0237085100

Wen, X., Zhang, C., Ji, Y., Zhao, Q., He, W., An, F., et al. (2012). Activation of ethylene signaling is mediated by nuclear translocation of the cleaved EIN2 carboxyl terminus. *Cell Res.* 22, 1613–1616. doi: 10.1038/cr.2012.145

Wienken, C. J., Baaske, P., Rothbauer, U., Braun, D., and Duhr, S. (2010). Protein-binding assays in biological liquids using microscale thermophoresis. *Nat. Commun.* 1, 1–7. doi: 10.1038/ncomms1093

Wuriyanghan, H., Zhang, B., Cao, W., Ma, B., Lei, G., Liu, Y., et al. (2009). The ethylene receptor ETR2 delays floral transition and affects starch accumulation in Rice. *Plant Cell* 21, 1473–1494. doi: 10.1105/tpc.108.065391

Xie, F., Liu, Q., and Wen, C.-K. (2006). Receptor signal output mediated by the ETR1 N terminus is primarily subfamily I receptor dependent. *Plant Physiol.* 142, 492–508. doi: 10.1104/pp.106.082628

Conflict of Interest Statement: The authors declare that the research was conducted in the absence of any commercial or financial relationships that could be construed as a potential conflict of interest.

frontiers in Plant Science

MINI REVIEW
published: 18 June 2019
doi: 10.3389/fpls.2019.00790

New Insights in Transcriptional Regulation of the Ethylene Response in *Arabidopsis*

Likai Wang[1,2] *and Hong Qiao*[1,2]*

[1] *Institute for Cellular and Molecular Biology, The University of Texas at Austin, Austin, TX, United States,* [2] *Department of Molecular Biosciences, The University of Texas at Austin, Austin, TX, United States*

As any living organisms, plants must respond to a wide variety of environmental stimuli. Plant hormones regulate almost all aspects of plant growth and development. Among all the plant hormones, ethylene is the only gaseous plant hormone that plays pleiotropic roles in plant growth, plant development and stress responses. Transcription regulation is one main mechanism by which a cell orchestrates gene activity. This control allows the cell or organism to respond to a variety of intra- and extracellular signals and thus mount a response. Here we review the progress of transcription regulation in the ethylene response.

Keywords: ethylene, transcription regulation, *Arabidopsis*, histone, hormone

OPEN ACCESS

Edited by:
Caren Chang,
University of Maryland, United States

Reviewed by:
Gyeong Mee Yoon,
Purdue University, United States
Jose M. Alonso,
North Carolina State University, United States

***Correspondence:**
Hong Qiao
hqiao@austin.utexas.edu

Specialty section:
This article was submitted to Plant Physiology, a section of the journal Frontiers in Plant Science

Received: *25 March 2019*
Accepted: *31 May 2019*
Published: *18 June 2019*

Citation:
Wang L and Qiao H (2019) New Insights in Transcriptional Regulation of the Ethylene Response in Arabidopsis. Front. Plant Sci. 10:790. doi: 10.3389/fpls.2019.00790

TRANSCRIPTIONAL REGULATION IN THE ETHYLENE RESPONSE

Like all living organisms, plants must respond to a wide variety of environmental stimuli. Plant hormones, produced in response to environmental stimuli, regulate almost all aspects of plant growth and development. Ethylene is a gaseous plant hormone that plays pleiotropic roles in plant growth, plant development, and stress responses. Histone acetylation, which is modulated through ethylene-mediated signaling, regulates dynamic changes in chromatin structure that result in transcriptional regulation in responses to ethylene.

Ethylene is perceived by a family of receptors bound to the endoplasmic reticulum (ER) membrane (Chang et al., 1993; Bleecker et al., 1998; Hua and Meyerowitz, 1998; Hua et al., 1998; Sakai et al., 1998). Each receptor binds ethylene via a copper cofactor that is provided by the copper transporter *RESPONSIVE-TO-ANTAGONIST 1* (RAN1)(Hirayama et al., 1999). In the absence of ethylene, ethylene receptor ETHYLENE RECEPTOR 1 (ETR1) interacts with CONSTITUTIVE TRIPLE RESPONSE 1 (CTR1), a downstream negative regulator of ethylene signaling (Chang et al., 1993; Kieber et al., 1993; Gao et al., 2003; Shakeel et al., 2015). CTR1 is a protein kinase that phosphorylates ETHYLENE INSENSITIVE 2 (EIN2), a key positive regulator of ethylene signaling (Alonso et al., 1999; Ju et al., 2012), preventing the ethylene response. In addition, in the absence of ethylene, EIN2 protein levels are regulated by EIN2 TARGETING PROTEIN 1 and 2 (ETP1/2) via ubiquitin/proteasome-mediated degradation (Qiao et al., 2009).

In the presence of ethylene both ethylene receptors and CTR1 are inactivated, and the C-terminal end of EIN2 is dephosphorylated and cleaved by unknown mechanisms. The cleaved C-terminal end of EIN2 translocates to the nucleus (Qiao et al., 2012; Wen et al., 2012; Ju et al., 2015) where it facilitates the acetylation of histone 3 at K14 and K23 (H3K14 and H3K23, respectively) to regulate ETHYLENE INSENSITIVE 3 (EIN3) and ETHYLENE INSENSITIVE 3

LIKE1 (EIL1) – dependent transcriptional regulation (Zhang et al., 2016). The cleaved EIN2 C-terminal end also translocates into the P-body through associating with 3′UTRs of EIN3 BINDING F-BOX1 (EBF1) and EBF2, further repressing their translation (Guo and Ecker, 2003). EBF1 and EBF2 in turn stabilize EIN3 and EIL1, resulting in activation of EIN3- and EIL1-dependent transcription and the activation of an ethylene response (Li et al., 2015; Merchante et al., 2015).

Both genetic and molecular studies have demonstrated that EIN3 and EIL1 are positive regulators that are necessary and sufficient for the ethylene response (Chao et al., 1997; Guo and Ecker, 2003; Chang et al., 2013). The *EIN3* gene encodes a nuclear-localized protein that is essential to the response to ethylene (Chao et al., 1997). In the absence of EIN3, plants are partially insensitive to ethylene both at the morphological and molecular levels (Chao et al., 1997; Guo and Ecker, 2003). The EIN3 binding motif was identified after analysis of the promoters of the genes that are highly up-regulated by ethylene and followed by validation using an electrophoresis mobility shift assay (EMSA) (Ohme-Takagi and Shinshi, 1990; Eyal et al., 1993; Meller et al., 1993; Sessa et al., 1995; Shinshi et al., 1995; Sato et al., 1996; Solano et al., 1998). Using the EMSA assay, EIN3 was shown to form a homodimer in the presence of DNA *in vitro* (Solano et al., 1998). However, whether the homodimer is formed *in vivo* and whether the homodimer is required for EIN3 to function in the ethylene signaling are unknown. A number of transcription factors are known to form homodimers or heterodimers, which have different specificities and affinities for certain DNA motifs (Funnell and Crossley, 2012). Finding out whether the dimerization is necessary for EIN3′s function *in vivo* will be an interesting question in the transcriptional regulation of the ethylene response.

To explore the transcription regulation in response to ethylene, Chang et al characterized the dynamic ethylene transcriptional response by identifying targets of EIN3, the master regulator of the ethylene signaling pathway, using chromatin immunoprecipitation sequencing and transcript sequencing during a time course of ethylene treatment (Chang et al., 2013). They found that the number of genes bound by EIN3 does not change significantly in response to ethylene. The amount of EIN3 bound increases upon ethylene treatment, and the expression of most of EIN3-bound genes is up regulated by ethylene, which is consistent with a role of EIN3 as a transcriptional activator. Chang et al. also analyzed the sequences of EIN3-bound regions identified by ChIP-seq (Ohme-Takagi and Shinshi, 1990; Eyal et al., 1993; Meller et al., 1993; Sessa et al., 1995; Shinshi et al., 1995; Sato et al., 1996; Solano et al., 1998). A motif similar to that previously identified in the promoter regions of ethylene up-regulated genes was present in EIN3-bound regions (Ohme-Takagi and Shinshi, 1990; Eyal et al., 1993; Meller et al., 1993; Sessa et al., 1995; Shinshi et al., 1995; Sato et al., 1996; Solano et al., 1998). Intriguingly, Chang et al. also found that ethylene-induced transcription occurs in temporal waves that were regulated by EIN3 with the potentially distinct layers of transcriptional control (Chang et al., 2013). EIN3 binding was found to modulate a multitude of downstream transcriptional cascades, including a major feedback regulatory circuitry of the ethylene signaling pathway, as well as most of the hormone-mediated growth response pathways, which indicates that network-level feedback regulation results in overall system control and homeostasis (Chang et al., 2013). This type of study can be applied to identify novel components in signaling pathways (Rosenfeld et al., 2002; Amit et al., 2007; Tsang et al., 2007; Avraham and Yarden, 2011; Feng et al., 2011; Yosef and Regev, 2011).

Although the transcriptional activation has been the main focus in the ethylene response, transcriptome analysis in Chang's study clearly showed that nearly 50% of ethylene-altered genes are down regulated and that a subset of ethylene-repressed genes are bound by EIN3 (Chang et al., 2013). Notably, most of the genes are down regulated by ethylene within 1 h of treatment. This result strongly suggests that transcriptional repression plays a critical role in early ethylene response. Interestingly, a recent study from the Qiao lab showed that transcriptional repression dose plays important roles in ethylene response. We identified two histone deacetylases (HDACs) SIRTUIN 1 and 2 (SRT1 and SRT2) that regulate ethylene-repressed genes (Zhang et al., 2018). Notably the study found that SRT2 binds the target promoter regions to inhibit acetylation of histone 3 at K9 (H3K9Ac), repressing gene expression in response to ethylene (**Figure 1**).

Transcriptional repression by chromatin modification is one of the principal mechanisms employed by eukaryotic active repressors (Thiel et al., 2004; Kagale and Rozwadowski, 2011). The importance of HDACs in transcriptional repression during plant growth and development has been well established (Song et al., 2005; Li et al., 2017). For example, in *Arabidopsis*, the EAR motif containing class II ETHYLENE RESPONSIVE ELEMENT BINDING FACTORS (ERFs), such as ERF3 and ERF4, which are known to function as active repressors *in vitro* and *in vivo*, have been shown to physically interact with AtSAP18, which in turn interacts and forms a repression complex with AtHDA19 (Fujimoto et al., 2000; Ohta et al., 2001; McGrath et al., 2005; Song and Galbraith, 2006). AtERF7, another EAR motif-containing class II ERF protein, is also known to recruit AtHDA19 via a physical interaction with AtSIN3 (Song et al., 2005). *In planta*, coexpression of AtERF3, AtSAP18, and AtHDA19 or AtERF7, AtSIN3, and AtHDA19 results in greater transcriptional repression of reporter genes as compared to when these proteins are expressed alone suggesting a role for AtSAP18, AtSIN3, and AtHDA19 in ERF-mediated transcriptional repression possibly via histone deacetylation (Song et al., 2005; Song and Galbraith, 2006). Yet, whether EAR containing proteins are also required for SRT1 and SRT2 mediated transcriptional repression in response to ethylene is unknown (Zhang et al., 2018). It also remains unclear whether the ethylene response has a molecular mechanism of transcriptional repression similar to that induced by other plant hormones. Exploring the molecular mechanism of transcriptional

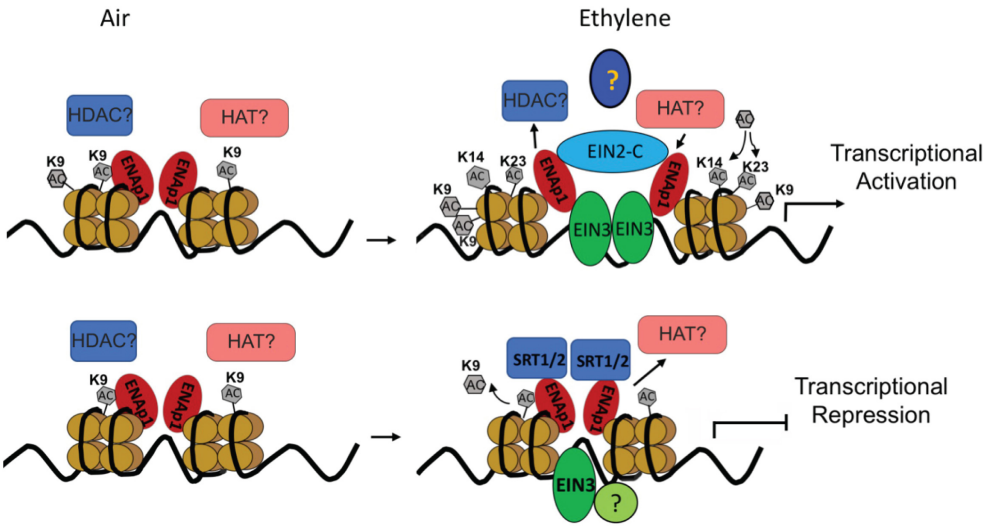

FIGURE 1 | Diagram to illustrate the transcription regulation in ethylene response. Upper panel: in the absence of ethylene, no ethylene regulated transcription regulation; In the presence of ethylene, accumulated EIN3 interacts with ENAP1 and EIN2 c-terminus, which elevates histone acetylation of H3K14Ac and H3K23Ac through an interaction with unidentified histone acetyltransferases to activate EIN3 dependent transcriptional activation. Lower panel: In the absence of ethylene, ethylene down-regulated genes are transcribed; In the presence of ethylene, histone deacetylase SRT1 and SRT2 are recruited to target genes to keep a low level of H3K9Ac, resulting in the targets for transcriptional repression.

repression will provide more insight into ethylene signaling and ethylene response.

HISTONE ACETYLATION IN ETHYLENE-MEDIATED TRANSCRIPTIONAL REGULATION

In eukaryotes, the binding of transcription factors is mainly determined by chromatin structure, namely the state of the genome's packaging with specific structural proteins, mainly histones. Chromatin undergoes different dynamics structure changes, further influences transcription factor binding. Among all the regulations, histone acetylation results in a switch between repressive and permissive chromatin. In general, acetylation neutralizes the positive charges of lysine residues and decreases the interaction between histone and DNA, leading to a more relaxed chromatin structure, which is associated with transcriptional activation. In contrast, deacetylation induces a compact chromatin structure, which is associated with transcriptional repression (Fletcher and Hansen, 1996; Steger and Workman, 1996; Luger and Richmond, 1998).

A Number of studies have shown a tight link between histone acetylation and plant hormone responses (Zhu, 2010). In the studies of ethylene signaling, authors found that GENERAL CONTROL NON-REPRESSED PROTEIN 5 (GCN5), which belongs to a family of histone acetyl transferases (HATs), promotes transcriptional activation (Brownell and Allis, 1996; Grant et al., 1997; Bian et al., 2011; Weake and Workman, 2012; Ryu et al., 2014). The *Arabidopsis gcn5* mutant shows hypersensitivity to ethylene treatment. In the *gcn5* mutant, the histone acetylation at H3K9 and H3K14 in the promoter regions of ethylene response genes is elevated, and the elevation is associated with the up-regulation of gene expression (Poulios and Vlachonasios, 2016). In *Arabidopsis*, the HAC family, which are the homologs of CREB-binding protein (CBP) and p300, the mammalian family of HAT domain containing transcriptional coactivators, play pleotropic roles in plant growth and development (Pandey et al., 2002; Li et al., 2014). The *hac1hac5* double mutant was found to have a constitutive triple response phenotype (Pandey et al., 2002; Li et al., 2014). It was expected that gene expression would be down regulated in the *hac1hac5* double mutant due to the reduction of histone acetylation levels; however, similar to that in *gcn5* mutant, the downstream ethylene responsive genes are elevated in *hac1hac5* double mutant (Li et al., 2014), suggesting an indirect regulation of ethylene responsive genes by HAC1 and HAC5.

Expression of two HDACs, *HAD6* and *HDA19*, are specifically elevated by ethylene treatment. The expression of ethylene responsive gene *ERF1* is anti-correlated with the levels of histone H3 acetylation in *35S:HDA19* transgenic plants, showing that HDA19 indirectly influences *ERF1* gene expression (Zhou et al., 2005). It is possible that HDA19 induces ERF1 expression by preventing binding of an unknown transcription repressor that regulates ERF1 expression (Zhou et al., 2005). JAZ proteins recruit HDA6 to deacetylate histones and obstruct the chromatin binding of EIN3/EIL1, therefore repressing EIN3/EIL1-dependent transcription and inhibiting jasmonic acid-mediated signaling (Zhu et al., 2011). This provides evidence that histone acetylation regulates EIN3 target genes.

H3K14Ac and H3K23Ac, but not H3K9Ac, H3K18Ac, or H3K27Ac, are elevated by ethylene treatment at the molecular level (Zhang et al., 2016; Yoon et al., 2017). Interestingly, even though the levels of H3K9Ac are not regulated by ethylene, the

levels of H3K9Ac in the promoters of ethylene up-regulated genes are higher than that in those ethylene down-regulated genes both with and without ethylene treatments (Zhang et al., 2016; Yoon et al., 2017). Presumably, H3K9Ac is a pre-existing mark that labels genes regulated by ethylene, whereas the elevation of H3K14Ac and H3K23Ac is positively associated with gene activation. Most importantly, the ethylene-induced change of histone acetylation is EIN2 dependent. However, EIN2 is not a histone or a DNA binding protein, and the biochemical function of EIN2-C remains unknown. Yeast two-hybrid screening and ChIP-re-ChIP suggests that EIN2-C is associated with histones at least in part through EIN2 NUCLEAR ASSOCIATED PROTEIN 1 (ENAP1), which has histone binding activity (**Figure 1**; Zhang et al., 2017). It is possible that EIN2-C is a scaffolding protein that is important for the formation of HAT-containing protein complexes in response to ethylene. Identification of HAT or HDAC that functions in cooperation with EIN2-C would validate this assumption. In contrast to transcriptional activation, histone acetylation of H3K9Ac was found to be involved in the transcriptional repression, and the regulation is partially mediated by histone deacetylase SRT1 and SRT2 (**Figure 1**).

Taken together, currently available data suggest that in the absence of ethylene ENAP1 binds to histones to keep chromatin in a relaxed state poised for a rapid response to ethylene (**Figure 1**). In the presence of ethylene, EIN2-C is translocated to the nucleus where it interacts with ENAP1 and potentially HATs resulting in histone acetylation. This causes an uncompacting of chromatin, resulting in more EIN3 binding to target genes and ultimately transcription activation (**Figure 1**). It is not known how the histone acetylation targets are determined in the presence of ethylene. Zhang et al. showed that EIN3 is partially required for the ethylene-induced elevation of H3K14Ac and H3K23Ac (Pandey et al., 2002), suggesting that EIN3 might mark histone acetylation targets. Multi-protein assemblies have been shown to determine the substrate specificities and targeting of integral HAT subunits. The molecular mechanism of how EIN3, ENAP1, and EIN2-C coordinate to integrate the histone acetylation and transcription regulation remains to be elucidated. Beside histone acetylation regulation in transcriptional activation, histone acetylation has been shown to be involved in transcriptional repression in ethylene response. As mentioned above, SRT1 and SRT2 mediate transcriptional repression that requires a low level of H3K9Ac (Yosef and Regev, 2011). How the H3K9Ac levels are determined in the desired targets in the first place is an interesting and important question that needs to be addressed.

CONCLUDING REMARKS AND FUTURE PERSPECTIVES

Plants must respond accurately and quickly to hormones, and this necessitates a flexible and rapid way to control gene expression. The acetylation of histone tails by HATs neutralizes positive charges on these proteins that would otherwise interact with negatively charged DNA, facilitating nucleosome unwrapping for rapid transcription activation. How plants utilize a limited number of HATs and HDACs to specifically regulate responses to different hormones is largely unknown. Presumably, the specificity relies on the partners of HATs and HDACs. Identification of the HAT- and HDAC-containing complexes upon ethylene treatment will reveal details of the molecular mechanisms that underlie the ethylene response. Recent studies have clearly shown that different tissues respond to plant hormones differently (Garg et al., 2012; Pattison et al., 2015; Raines et al., 2016). Most available data on histone acetylation induced by plant hormones come from analyses of the whole plant. Studies of histone acetylation in individual tissues and in different cell types will provide more detailed insight into how histone acetylation controls responses to plant hormones. Transcription factor binding in eukaryotes is highly dependent on the context of binding sites on chromatin, but little is known about how EIN3 determines histone acetylation sites in target genes. A more complete understanding of the molecular mechanism of determination of transcriptional activation and transcriptional repression during the ethylene response will facilitate development of methods to improve crop production.

AUTHOR CONTRIBUTIONS

Both authors listed have made a substantial, direct and intellectual contribution to the work, and approved it for publication.

FUNDING

This work was supported by a grant from the National Institutes of Health (NIH) (R01GM115879-01) to HQ.

ACKNOWLEDGMENTS

We thank the members of the Qiao laboratory for critical reading of this manuscript.

REFERENCES

Alonso, J. M., Hirayama, T., Roman, G., Nourizadeh, S., and Ecker, J. R. (1999). EIN2, a bifunctional transducer of ethylene and stress responses in Arabidopsis. *Science* 284, 2148–2152. doi: 10.1126/science.284.5423.2148

Amit, I., Citri, A., Shay, T., Lu, Y., Katz, M., Zhang, F., et al. (2007). A module of negative feedback regulators defines growth factor signaling. *Nat. Genet.* 39, 503–512. doi: 10.1038/ng1987

Avraham, R., and Yarden, Y. (2011). Feedback regulation of EGFR signalling: decision making by early and delayed loops. *Nat. Rev. Mol. Cell Biol.* 12, 104–117. doi: 10.1038/nrm3048

Bian, C., Xu, C., Ruan, J., Lee, K. K., Burke, T. L., Tempel, W., et al. (2011). Sgf29 binds histone H3K4me2/3 and is required for SAGA complex recruitment and histone H3 acetylation. *EMBO J.* 30, 2829–2842. doi: 10.1038/emboj.2011.193

Bleecker, A. B., Esch, J. J., Hall, A. E., Rodriguez, F. I., and Binder, B. M. (1998). The ethylene-receptor family from Arabidopsis: structure and function. *Philos. Trans. R. Soc. Lond. B. Biol. Sci.* 353, 1405–1412. doi: 10.1098/rstb.1998.0295

Brownell, J. E., and Allis, C. D. (1996). Special HATs for special occasions: linking histone acetylation to chromatin assembly and gene activation. *Curr. Opin. Genet. Dev.* 6, 176–184. doi: 10.1016/s0959-437x(96)80048-7

Chang, C., Kwok, S. F., Bleecker, A. B., and Meyerowitz, E. M. (1993). Arabidopsis ethylene-response gene ETR1: similarity of product to two-component regulators. *Science* 262, 539–544. doi: 10.1126/science.8211181

Chang, K. N., Zhong, S., Weirauch, M. T., Hon, G., Pelizzola, M., Li, H., et al. (2013). Temporal transcriptional response to ethylene gas drives growth hormone cross-regulation in Arabidopsis. *eLife* 2:e00675. doi: 10.7554/eLife.00675

Chao, Q. M., Rothenberg, M., Solano, R., Roman, G., Terzaghi, W., Ecker, J. R., et al. (1997). Activation of the ethylene gas response pathway in Arabidopsis by the nuclear protein ETHYLENE-INSENSITIVE3 and related proteins. *Cell* 89, 1133–1144. doi: 10.1016/s0092-8674(00)80300-1

Eyal, Y., Meller, Y., Lev-Yadun, S., and Fluhr, R. (1993). A basic-type PR-1 promoter directs ethylene responsiveness, vascular and abscission zone-specific expression. *Plant J.* 4, 225–234. doi: 10.1046/j.1365-313x.1993.04020225.x

Feng, Z., Lin, M., and Wu, R. (2011). The regulation of aging and longevity: a new and complex role of p53. *Genes Cancer* 2, 443–452. doi: 10.1177/1947601911410223

Fletcher, T. M., and Hansen, J. C. (1996). The nucleosomal array: structure/function relationships. *Crit. Rev. Eukaryot. Gene Expr.* 6, 149–188. doi: 10.1615/critreveukargeneexpr.v6.i2-3.40

Fujimoto, S. Y., Ohta, M., Usui, A., Shinshi, H., and Ohme-Takagi, M. (2000). Arabidopsis ethylene-responsive element binding factors act as transcriptional activators or repressors of GCC box-mediated gene expression. *Plant Cell* 12, 393–404. doi: 10.1105/tpc.12.3.393

Funnell, A. P., and Crossley, M. (2012). Homo- and heterodimerization in transcriptional regulation. *Adv. Exp. Med. Biol.* 747, 105–121. doi: 10.1007/978-1-4614-3229-6_7

Gao, Z., Chen, Y. F., Randlett, M. D., Zhao, X. C., Findell, J. L., Kieber, J. J., et al. (2003). Localization of the Raf-like kinase CTR1 to the endoplasmic reticulum of Arabidopsis through participation in ethylene receptor signaling complexes. *J. Biol. Chem.* 278, 34725–34732. doi: 10.1074/jbc.M305548200

Garg, R., Tyagi, A. K., and Jain, M. (2012). Microarray analysis reveals overlapping and specific transcriptional responses to different plant hormones in rice. *Plant Signal. Behav.* 7, 951–956. doi: 10.4161/psb.20910

Grant, P. A., Duggan, L., Côté, J., Roberts, S. M., Brownell, J. E., Candau, R., et al. (1997). Yeast Gcn5 functions in two multisubunit complexes to acetylate nucleosomal histones: characterization of an Ada complex and the SAGA (Spt/Ada) complex. *Genes Dev.* 11, 1640–1650. doi: 10.1101/gad.11.13.1640

Guo, H. W., and Ecker, J. R. (2003). Plant responses to ethylene gas are mediated by SCF (EBF1/EBF2)-dependent proteolysis of EIN3 transcription factor. *Cell* 115, 667–677. doi: 10.1016/s0092-8674(03)00969-3

Hirayama, T., Kieber, J. J., Hirayama, N., Kogan, M., Guzman, P., Nourizadeh, S., et al. (1999). RESPONSIVE-TO-ANTAGONIST1, a Menkes/Wilson disease-related copper transporter, is required for ethylene signaling in Arabidopsis. *Cell* 97, 383–393. doi: 10.1016/s0092-8674(00)80747-3

Hua, J., and Meyerowitz, E. M. (1998). Ethylene responses are negatively regulated by a receptor gene family in Arabidopsis thaliana. *Cell* 94, 261–271. doi: 10.1016/s0092-8674(00)81425-7

Hua, J., Sakai, H., Nourizadeh, S., Chen, Q. G., Bleecker, A. B., Ecker, J. R., et al. (1998). EIN4 and ERS2 are members of the putative ethylene receptor gene family in Arabidopsis. *Plant Cell* 10, 1321–1332. doi: 10.1105/tpc.10.8.1321

Ju, C., Van de Poel, B., Cooper, E. D., Thierer, J. H., Gibbons, T. R., Delwiche, C. F., et al. (2015). Conservation of ethylene as a plant hormone over 450 million years of evolution. *Nat. Plants* 1:14004. doi: 10.1038/nplants.2014.4

Ju, C. L., Yoon, G. M., Shemansky, J. M., Lin, D. Y., Ying, Z. I., Chang, J., et al. (2012). CTR1 phosphorylates the central regulator EIN2 to control ethylene hormone signaling from the ER membrane to the nucleus in Arabidopsis. *Proc. Natl. Acad. Sci. U.S.A.* 109, 19486–19491. doi: 10.1073/pnas.1214848109

Kagale, S., and Rozwadowski, K. (2011). EAR motif-mediated transcriptional repression in plants: an underlying mechanism for epigenetic regulation of gene expression. *Epigenetics* 6, 141–146. doi: 10.4161/epi.6.2.13627

Kieber, J. J., Rothenberg, M., Roman, G., Feldmann, K. A., and Ecker, J. R. (1993). Ctr1, a negative regulator of the ethylene response pathway in arabidopsis, encodes a member of the Raf family of protein-kinases. *Cell* 72, 427–441. doi: 10.1016/0092-8674(93)90119-b

Li, C., Xu, J., Li, J., Li, Q., and Yang, H. (2014). Involvement of Arabidopsis HAC family genes in pleiotropic developmental processes. *Plant Signal. Behav.* 9:e28173. doi: 10.4161/psb.28173

Li, W., Lacey, R. F., Ye, Y., Lu, J., Yeh, K. C., Xiao, Y., et al. (2017). Triplin, a small molecule, reveals copper ion transport in ethylene signaling from ATX1 to RAN1. *PLoS Genet.* 13:e1006703. doi: 10.1371/journal.pgen.1006703

Li, W. Y., Ma, M., Feng, Y., Li, H., Wang, Y., Ma, Y., et al. (2015). EIN2-directed translational regulation of ethylene signaling in arabidopsis. *Cell* 163, 670–683. doi: 10.1016/j.cell.2015.09.037

Luger, K., and Richmond, T. J. (1998). The histone tails of the nucleosome. *Curr. Opin. Genet. Dev.* 8, 140–146.

McGrath, K., Dombrecht, B., Manners, J. M., Schenk, P. M., Edgar, C. I., Maclean, D. J. C., et al. (2005). Repressor- and activator-type ethylene response factors functioning in jasmonate signaling and disease resistance identified via a genome-wide screen of Arabidopsis transcription factor gene expression. *Plant Physiol.* 139, 949–959. doi: 10.1104/pp.105.068544

Meller, Y., Sessa, G., Eyal, Y., and Fluhr, R. (1993). DNA-protein interactions on a cis-DNA element essential for ethylene regulation. *Plant Mol. Biol.* 23, 453–463. doi: 10.1007/bf00019294

Merchante, C., Brumos, J., Yun, J., Hu, Q., Spencer, K. R., Enríquez, P., et al. (2015). Gene-specific translation regulation mediated by the hormone-signaling molecule EIN2. *Cell* 163, 684–697. doi: 10.1016/j.cell.2015.09.036

Ohme-Takagi, M., and Shinshi, H. (1990). Structure and expression of a tobacco beta-1,3-glucanase gene. *Plant Mol. Biol.* 15, 941–946. doi: 10.1007/bf00039434

Ohta, M., Matsui, K., Hiratsu, K., Shinshi, H., and Ohme-Takagi, M. (2001). Repression domains of class II ERF transcriptional repressors share an essential motif for active repression. *Plant Cell* 13, 1959–1968. doi: 10.1105/tpc.13.8.1959

Pandey, R., Müller, A., Napoli, C. A., Selinger, D. A., Pikaard, C. S., Richards, E. J., et al. (2002). Analysis of histone acetyltransferase and histone deacetylase families of Arabidopsis thaliana suggests functional diversification of chromatin modification among multicellular eukaryotes. *Nucleic Acids Res.* 30, 5036–5055. doi: 10.1093/nar/gkf660

Pattison, R. J., Csukasi, F., Zheng, Y., Fei, Z., van der Knaap, E., Catalá, C., et al. (2015). Comprehensive tissue-specific transcriptome analysis reveals distinct regulatory programs during early tomato fruit development. *Plant Physiol.* 168, 1684–1701. doi: 10.1104/pp.15.00287

Poulios, S., and Vlachonasios, K. E. (2016). Synergistic action of histone acetyltransferase GCN5 and receptor CLAVATA1 negatively affects ethylene responses in Arabidopsis thaliana. *J. Exp. Bot.* 67, 905–918. doi: 10.1093/jxb/erv503

Qiao, H., Chang, K. N., Yazaki, J., and Ecker, J. R. (2009). Interplay between ethylene, ETP1/ETP2 F-box proteins, and degradation of EIN2 triggers ethylene responses in Arabidopsis. *Genes Dev.* 23, 512–521. doi: 10.1101/gad.1765709

Qiao, H., Shen, Z., Huang, S. S., Schmitz, R. J., Urich, M. A., Briggs, S. P., et al. (2012). Processing and subcellular trafficking of ER-Tethered EIN2 control response to ethylene gas. *Science* 338, 390–393. doi: 10.1126/science.1225974

Raines, T., Blakley, I. C., Tsai, Y. C., Worthen, J. M., Franco-Zorrilla, J. M., Solano, R., et al. (2016). Characterization of the cytokinin-responsive transcriptome in rice. *BMC Plant Biol.* 16:260. doi: 10.1186/s12870-016-0932-z

Rosenfeld, N., Elowitz, M. B., and Alon, U. (2002). Negative autoregulation speeds the response times of transcription networks. *J. Mol. Biol.* 323, 785–793. doi: 10.1016/s0022-2836(02)00994-4

Ryu, H., Cho, H., Bae, W., and Hwang, I. (2014). Control of early seedling development by BES1/TPL/HDA19-mediated epigenetic regulation of ABI3. *Nat. Commun.* 5:4138. doi: 10.1038/ncomms5138

Sakai, H., Hua, J., Chen, Q. G., Chang, C., Medrano, L. J., Bleecker, A. B., et al. (1998). ETR2 is an ETR1-like gene involved in ethylene signaling in Arabidopsis. *Proc. Natl. Acad. Sci. U.S.A.* 95, 5812–5817. doi: 10.1073/pnas.95.10.5812

Sato, F., Kitajima, S., Koyama, T., and Yamada, Y. (1996). Ethylene-induced gene expression of osmotin-like protein, a neutral isoform of tobacco PR-5,

is mediated by the AGCCGCC cis-sequence. *Plant Cell Physiol.* 37, 249–255. doi: 10.1093/oxfordjournals.pcp.a028939

Sessa, G., Meller, Y., and Fluhr, R. (1995). A GCC element and a G-box motif participate in ethylene-induced expression of the PRB-1b gene. *Plant Mol. Biol.* 28, 145–153. doi: 10.1007/bf00042046

Shakeel, S. N., Gao, Z., Amir, M., Chen, Y. F., Rai, M. I., Haq, N. U., et al. (2015). Ethylene regulates levels of ethylene receptor/CTR1 signaling complexes in Arabidopsis thaliana. *J. Biol. Chem.* 290, 12415–12424. doi: 10.1074/jbc.M115.652503

Shinshi, H., Usami, S., and Ohme-Takagi, M. (1995). Identification of an ethylene-responsive region in the promoter of a tobacco class I chitinase gene. *Plant Mol. Biol.* 27, 923–932. doi: 10.1007/bf00037020

Solano, R., Stepanova, A., Chao, Q., and Ecker, J. R. (1998). Nuclear events in ethylene signaling: a transcriptional cascade mediated by ethylene-insensitive3 and ethylene-response-factor1. *Genes Dev.* 12, 3703–3714. doi: 10.1101/gad.12.23.3703

Song, C. P., Agarwal, M., Ohta, M., Guo, Y., Halfter, U., Wang, P., et al. (2005). Role of an Arabidopsis AP2/EREBP-type transcriptional repressor in abscisic acid and drought stress responses. *Plant Cell* 17, 2384–2396. doi: 10.1105/tpc.105.033043

Song, C. P., and Galbraith, D. W. (2006). AtSAP18, an orthologue of human SAP18, is involved in the regulation of salt stress and mediates transcriptional repression in Arabidopsis. *Plant Mol. Biol.* 60, 241–257. doi: 10.1007/s11103-005-3880-3889

Steger, D. J., and Workman, J. L. (1996). Remodeling chromatin structures for transcription: what happens to the histones? *Bioessays* 18, 875–884. doi: 10.1002/bies.950181106

Thiel, G., Lietz, M., and Hohl, M. (2004). How mammalian transcriptional repressors work. *Eur. J. Biochem.* 271, 2855–2862. doi: 10.1111/j.1432-1033.2004.04174.x

Tsang, J., Zhu, J., and van Oudenaarden, A. (2007). MicroRNA-mediated feedback and feedforward loops are recurrent network motifs in mammals. *Mol. Cell.* 26, 753–767. doi: 10.1016/j.molcel.2007.05.018

Weake, V. M., and Workman, J. L. (2012). SAGA function in tissue-specific gene expression. *Trends Cell Biol.* 22, 177–184. doi: 10.1016/j.tcb.2011.11.005

Wen, X., Zhang, C., Ji, Y., Zhao, Q., He, W., An, F., et al. (2012). Activation of ethylene signaling is mediated by nuclear translocation of the cleaved EIN2 carboxyl terminus. *Cell Res.* 22, 1613–1616. doi: 10.1038/cr.2012.145

Yoon, K. J., Ringeling, F. R., Vissers, C., Jacob, F., Pokrass, M., Jimenez-Cyrus, D., et al. (2017). Temporal control of mammalian cortical neurogenesis by m(6) a methylation. *Cell* 171, 877–889.e817. doi: 10.1016/j.cell.2017.09.003

Yosef, N., and Regev, A. (2011). Impulse control: temporal dynamics in gene transcription. *Cell* 144, 886–896. doi: 10.1016/j.cell.2011.02.015

Zhang, F., Qi, B., Wang, L., Zhao, B., Rode, S., Riggan, N. D., et al. (2016). EIN2-dependent regulation of acetylation of histone H3K14 and non-canonical histone H3K23 in ethylene signalling. *Nat. Commun.* 7:13018. doi: 10.1038/ncomms13018

Zhang, F., Wang, L., Ko, E. E., Shao, K., and Qiao, H. (2018). Histone deacetylases SRT1 and SRT2 interact with ENAP1 to mediate ethylene-induced transcriptional repression. *Plant Cell* 30, 153–166. doi: 10.1105/tpc.17.00671

Zhang, F., Wang, L., Qi, B., Zhao, B., Ko, E. E., Riggan, N. D., et al. (2017). EIN2 mediates direct regulation of histone acetylation in the ethylene response. *Proc. Natl. Acad. Sci. U.S.A.* 114, 10274–10279. doi: 10.1073/pnas.1707937114

Zhou, C., Zhang, L., Duan, J., Miki, B., and Wu, K. (2005). Histone deacetylase19 is involved in jasmonic acid and ethylene signaling of pathogen response in arabidopsis. *Plant Cell* 17, 1196–1204. doi: 10.1105/tpc.104.028514

Zhu, Y. X. (2010). The epigenetic involvement in plant hormone signaling. *Chin. Sci. Bull.* 55, 2198–2203. doi: 10.1007/s11434-010-3193-2

Zhu, Z. Q., An, F., Feng, Y., Li, P., Xue, L., Jiang, Z., et al. (2011). Derepression of ethylene-stabilized transcription factors (EIN3/EIL1) mediates jasmonate and ethylene signaling synergy in Arabidopsis. *Proc. Natl. Acad. Sci. U.S.A.* 108, 12539–12544. doi: 10.1073/pnas.1103959108

Conflict of Interest Statement: The authors declare that the research was conducted in the absence of any commercial or financial relationships that could be construed as a potential conflict of interest.

frontiers in Plant Science

ORIGINAL RESEARCH
published: 05 July 2019
doi: 10.3389/fpls.2019.00888

Low Temperature Storage Stimulates Fruit Softening and Sugar Accumulation Without Ethylene and Aroma Volatile Production in Kiwifruit

Oscar W. Mitalo[1], Sumire Tokiwa[1], Yuki Kondo[1], Takumi Otsuki[1], Ivan Galis[1,2], Katsuhiko Suezawa[3], Ikuo Kataoka[3], Anh T. Doan[1], Ryohei Nakano[1†], Koichiro Ushijima[1] and Yasutaka Kubo[1]*

[1] Graduate School of Environmental and Life Science, Okayama University, Okayama, Japan, [2] Institute of Plant Science and Resources, Okayama University, Kurashiki, Japan, [3] Faculty of Agriculture, Kagawa University, Miki, Japan

OPEN ACCESS

Edited by:
Mondher Bouzayen, National Polytechnic Institute of Toulouse, France

Reviewed by:
María Serrano, Universidad Miguel Hernández de Elche, Spain
M. Teresa Sanchez-Ballesta, Instituto de Ciencia y Tecnología de Alimentos y Nutrición (ICTAN), Spain

***Correspondence:**
Yasutaka Kubo
ykubo@okayama-u.ac.jp

†Present address:
Ryohei Nakano, Graduate School of Agriculture, Kyoto University, Kyoto, Japan

Specialty section:
This article was submitted to Plant Physiology, a section of the journal Frontiers in Plant Science

Received: *15 February 2019*
Accepted: *21 June 2019*
Published: *05 July 2019*

Citation:
Mitalo OW, Tokiwa S, Kondo Y, Otsuki T, Galis I, Suezawa K, Kataoka I, Doan AT, Nakano R, Ushijima K and Kubo Y (2019) Low Temperature Storage Stimulates Fruit Softening and Sugar Accumulation Without Ethylene and Aroma Volatile Production in Kiwifruit. Front. Plant Sci. 10:888. doi: 10.3389/fpls.2019.00888

Fruit ripening in response to propylene (an ethylene analog), 1-methylcyclopropene (1-MCP, an ethylene action inhibitor), and low temperature (5°C) treatments was characterized in "Kosui" kiwifruit (*Actinidia rufa* × *A. chinensis*). Propylene treatment induced ethylene production, with increased expression levels of *1-aminocyclopropane-1-carboxylic acid* (*ACC*) *synthase 1* (*AcACS1*) and *ACC oxidase 2* (*AcACO2*), and rapid fruit softening together with increased expression levels of *polygalacturonase* (*AcPG*) and *expansin 1* (*AcEXP1*) within 5 days (d). Fruit soluble solids concentration (SSC) and contents of sucrose, glucose, and fructose together with the expression levels of β-*amylase 1* (*Acβ-AMY1*), *Acβ-AMY2*, and *invertase* (*AcINV3-1*) increased rapidly after 5 d exposure to propylene. Furthermore, propylene exposure for 5 d was sufficient to induce the production of key aroma volatile compounds, ethyl- and methyl butanoate, accompanied with increased expression levels of *alcohol acyl transferase* (*AcAAT*). Application of 1-MCP at the start of the experiment, followed by continuous exposure to propylene, significantly delayed fruit softening, changes in SSC and sugars, and strongly suppressed the production of ethylene, aroma volatiles, and expression of associated genes. During storage, fruit softening, SSC and sugar increase, and increased expression of genes associated with cell wall modification and carbohydrate metabolism were registered without detectable ethylene production; however, these changes occurred faster at 5°C compared to 22°C. Interestingly, ethyl and methyl butanoate as well as *AcAAT* expression were undetectable in kiwifruit during storage, while they were rescued by post-storage propylene exposure, indicating that the production of aroma volatile compounds is strongly ethylene-dependent. Transcript levels of a NAC-related transcription factor (TF), *AcNAC3*, increased in response to both propylene and low temperature treatments, while *AcNAC5* was exclusively up-regulated by propylene. By contrast, transcript levels of a MADS-box TF, *AcMADS2*, exclusively increased in response to low temperature. The above findings indicate that kiwifruit ripening is inducible by either ethylene or low temperature signals. However, fruit ripened by low temperature were deficient in ethylene-dependent

aroma volatiles, suggesting that ethylene signaling is non-functional during low temperature-modulated ripening in kiwifruit. These data provide further evidence that ethylene-dependent and low temperature-modulated ripening in kiwifruit involve different regulatory mechanisms.

Keywords: ethylene, ethyl butanoate, low temperature, methyl butanoate, softening, sugars

INTRODUCTION

The plant hormone ethylene regulates a wide range of plant growth and developmental processes, including fleshy fruit ripening (Lashbrook et al., 1998; Giovannoni, 2004). During ripening, fleshy fruit undergo various physiological, biochemical, and structural changes including softening, starch degradation to sugars, pigment accumulation, and production of aroma volatiles (Klee and Giovannoni, 2011; Osorio et al., 2013). The onset of fruit ripening in climacteric fruit such as tomatoes, apples, and peaches is accompanied by a marked increase in ethylene production (Xu et al., 2012), which is regulated at the transcriptional level via the differential expression of genes encoding two key enzymes: 1-aminocyclopropane-1-carboxylic acid (ACC) synthase (ACS) and ACC oxidase (ACO) (Wang et al., 2002; Cherian et al., 2014).

Kiwifruit (*Actinidia* spp.) are categorized as climacteric, since fruit ripening is largely driven by ethylene-regulated changes in gene expression (Antunes, 2007; Yin et al., 2008). Exogenous ethylene or propylene treatment initiates rapid fruit softening through the induction of several cell wall modification-associated genes such as *polygalacturonase* (*AcPG*) and *expansin 1* (*AcEXP1*) (Wang et al., 2000; Atkinson et al., 2011; Mworia et al., 2012). In addition, kiwifruit respond to exogenous ethylene/propylene by increasing their soluble solids concentration (SSC), which is associated with the induction of various starch degradation-related genes such as β-*amylase* (*Acβ-AMY*) (Nardozza et al., 2013; McAtee et al., 2015; Hu et al., 2016). Ripe kiwifruit produce a composite of aroma volatiles, consisting of mainly aldehydes and esters (Marsh et al., 2006). Characteristic kiwifruit esters have been identified as ethyl butanoate and methyl butanoate (Zhang et al., 2009), and their regulation by ethylene has been previously described (Atkinson et al., 2011; Günther et al., 2011, 2015). Ethylene-induced ripening changes in kiwifruit are usually followed by a sharp increase in ethylene production caused by the up-regulation of key biosynthetic genes *AcACS1* and *AcACO2* (Pratt and Reid, 1974; Mworia et al., 2010; Atkinson et al., 2011; McAtee et al., 2015).

Kiwifruit exhibit a peculiar ripening behavior, as substantial softening in healthy intact fruit occurs during low temperature storage in the absence of any detectable ethylene (Antunes, 2007; Yin et al., 2009). Arpaia et al. (1987) demonstrated that kiwifruit are sensitive to extremely low ethylene concentrations (as low as 0.01 $\mu L L^{-1}$). Consequently, the substantial softening during storage at <1.5°C in air (presumed to contain 0.001 $\mu L L^{-1}$ ethylene) is believed to be controlled by basal levels of system I ethylene that is present in most fruit and plant tissues (Kim et al., 1999; Pranamornkith et al., 2012; Jabbar and East, 2016). However, to date, there is no direct evidence linking system I ethylene to kiwifruit ripening during low temperature storage, and thus, the regulatory mechanisms associated with this phenomenon remain less well understood.

Over the past few years, this study group has been dedicated to elucidating the molecular mechanisms underpinning low temperature-modulated fruit ripening in kiwifruit. A preliminary study by Mworia et al. (2012) demonstrated that healthy intact "Sanuki Gold" kiwifruit softened; accumulated *AcPG*, *Pectate lyase* (*AcPL*), and *AcEXP1* mRNAs; and decreased their titratable acidity (TA) during storage at 4°C, but not at 25°C, despite the lack of any detectable increase in ethylene production. These changes were not suppressed by frequent application of 1-methylcyclopropene (1-MCP) to keep fruit insensitive to ethylene, indicating that they occur outside the sphere of ethylene influence. Similar results were reported using different kiwifruit cultivars (Asiche et al., 2017; Mitalo et al., 2018, 2019), confirming that low temperature-modulated ripening is common to all kiwifruit cultivars. Follow-up transcriptomic studies revealed that a distinct set of ripening-associated genes in kiwifruit were uniquely regulated by low temperature, independent of ethylene (Asiche et al., 2018). Despite these findings, low temperature-modulated ripening in kiwifruit remains a poorly understood phenomenon. There is a growing need to conduct more focused studies to examine the similarities and differences in the molecular regulation of ethylene-induced and low temperature-modulated ripening in kiwifruit.

Using gas chromatography–mass spectrometry (GC–MS) to analyze the volatiles and soluble sugar contents of "Kosui" kiwifruit, an interspecific hybrid between *Actinidia rufa* and *A. chinensis*, this study sought to investigate the impact of low temperature (5°C) on sugar and aroma volatile profiles relative to ethylene effect. Changes in sugar composition and aroma volatile production in response to propylene, 1-MCP, and during storage at 5 and 22°C were compared, and their concomitant gene expression patterns are reported. Our results indicate that the production of aroma volatiles is strongly ethylene-dependent and is absent during cold storage, providing evidence that ethylene signaling is non-functional during low temperature-modulated ripening.

MATERIALS AND METHODS

Plant Material and Treatments

"Kosui" kiwifruit grown under standard cultural practices were harvested from a commercial orchard in Takamatsu, Japan at a physiological maturity stage [170 days (d) after full bloom (DAFB), firmness: 73.02 ± 3.39 N, SSC: 7.79 ± 0.18%,

TA: 2.20 ± 0.03%]. After harvesting, careful sorting was conducted to exclude fruit with physical injuries, disease symptoms, and those producing ethylene. Fruit were then divided into five sets, corresponding to the various treatments.

Ethylene-Dependent Ripening

Three sets of 30 fruit each were used in this experiment. The first set was held in gas-tight plastic containers that were continuously treated with 5000 μLL^{-1} propylene, a well-known ethylene analog (McMurchie et al., 1972; Mworia et al., 2010; Asiche et al., 2016). Propylene treatment was done to induce ethylene signaling, and to allow for determination of endogenous ethylene produced by the fruit. The second set was initially exposed to 2 μLL^{-1} 1-MCP for 12 h followed by continuous exposure to 5000 μLL^{-1} propylene. 1-MCP was released by dissolving SmartFresh^{TM} powder (AgroFresh, PA, United States) in water. The third set contained non-treated fruit as a control. All treatments were carried out at 22°C for up to 9 d. Soda lime was placed in plastic containers during propylene and 1-MCP treatments to reduce CO_2 accumulation.

Low Temperature-Modulated Ripening

Two sets of 300 fruit each were stored either at 5 or 22°C in air for up to 49 d. During storage, fruit were individually wrapped in perforated polythene bags to reduce water loss, before placing them (∼10 cm apart) in plastic trays. Ethylene production pattern of each fruit was monitored at weekly intervals throughout the storage period. To avoid ethylene accumulation in the storage chambers, fruit that produced detectable ethylene (<10%) were excluded based on previous observations that ethylene production correlated with the appearance of disease symptoms (Asiche et al., 2018). At the end of the storage period, fruit at 5°C were further divided into two groups before being transferred to 22°C for up to 14 d; one group was continuously treated with propylene as described above, while the other group was left untreated. Similarly, fruit at 22°C were divided into two groups; one group was continuously treated with propylene and the other one was left untreated.

Evaluation of Changes in Ethylene Production, Firmness, SSC, and TA

To determine ethylene production, individual fruit were incubated in a 440-mL container for up to 1 h. Ethylene production rate was measured by withdrawing 1 mL of headspace gas and injecting it into a gas chromatograph (Model GC4 CMPF, Shimadzu, Kyoto, Japan), equipped with a flame ionization detector (set at 200°C) and an activated alumina column (set at 80°C) (Mworia et al., 2012). This procedure has a minimum ethylene detection capacity of 0.01 $nLg^{-1}\ h^{-1}$. Fruit firmness was measured at two equatorial regions of peeled fruit using a penetrometer (model SMT-T-50, Toyo Baldwin, Tokyo, Japan) fitted with an 8-mm plunger. Data were recorded as Newtons (N) and firmness was expressed as a mean of five independent biological replications. SSC and TA were determined using fruit juice as described elsewhere (Asiche et al., 2018; Mitalo et al., 2019).

Collection of Aroma Volatiles

Aroma volatile compounds were collected according to the procedure by Sobhy et al. (2017), with slight modifications. Intact fruit were placed into sealed 1360-mL containers equipped with two ports; one for the air inlet and another port for the outlet. Dried air, purified by passing through a charcoal filter, was introduced to sweep through the headspace at approximately 0.75 L min^{-1}. The air was then pulled out through the outlet port fitted with a custom-made 10-cm glass trap (5 mm inner diameter), filled with Porapak Q (200 mg, Supelco Analytical, Bellefonte, PA, United States) held in place by two plugs of silanized glass wool. Porapak Q traps were conditioned before use by flushing with 2 mL methanol (Sigma–Aldrich Co., United States), followed by 2 mL dichloromethane (DCM, Wako Pure Chemical Industries, Japan), dried, and then placed overnight in an oven at 60°C for complete drying. To exclude the effect of background volatiles in air, empty containers having no fruit were included in the collection setup. Aroma volatiles were collected over 24 h periods. After each collection period, volatile compounds were eluted from Porapak Q traps with 1 mL DCM after adding 400 ng tetralin (1,2,3,4-tetrahydronaphthalene; Nacalai Tesque, Japan) on the top of each column. Tetralin was used as an internal standard. The samples were stored in 1.5 mL glass vials at −20°C until further analysis.

Extraction and Derivatization of Soluble Sugars

Soluble sugars were obtained and derivatized as described by Wang et al. (2010). Briefly, the samples (0.1 g) were ground in liquid nitrogen and extracted in 1.4 mL of 100% methanol with ribitol (12 μg) added as an internal standard. After fractionating the non-polar metabolites into chloroform, 150 μL of the polar phase was transferred into a 1.5 mL micro-centrifuge tube to measure the metabolites (soluble sugars). These were dried under vacuum without heating, flushed with nitrogen gas, and then derivatized sequentially with methoxyamine hydrochloride and *N*-methyl-*N*-trimethylsilyl-trifluoroacetamide (Lisec et al., 2006). The samples were stored at −20°C until further analysis.

GC–MS Conditions and Chemical Analysis

Volatile eluates and metabolites were analyzed using an Agilent 240 GC–MS ion trap system coupled with Agilent 7891A GC fitted with the HP-5MS column (5% phenyl methyl silox, 30 m length × 0.25 mm inner diameter × 0.25 μm film thickness) (Agilent Technologies, Santa Clara, CA, United States). One microliter of each eluted sample was injected in split mode (1:30) into the injector port of the GC instrument held at 230°C via an Agilent 7693A auto-sampler. Helium (1 mL/min) was used as carrier gas, and MS ionization was achieved by electron impact (EI) at emission current 30 μAmps for volatiles (10 μAmps for metabolites) in the ion trap held at 200°C (transfer line was 260°C). For headspace volatile analyses, the GC oven temperature was programmed at 40°C

for 3 min, and then increased at 5°C min^{-1} to 180°C, followed by 20°C min^{-1} ramp to 300°C, where it was held for an additional 5 min before returning to initial conditions. For metabolite samples, GC temperature program was 5 min at 60°C, followed by 5°C min^{-1} to 300°C, 5 min hold period, and return to initial temperature and equilibration. MS data were collected in full scan mode in mass range *m/z* 40–300 for volatiles (*m/z* 40–750 for metabolites), and analyzed by Agilent Workstation Version 7.0.2 software. Aroma volatiles and metabolites were identified by comparing their fragmentation patterns with those from the NIST 2011 Mass Spectral Library and Software (National Institute of Standards and Technology, United States). Co-injection with authentic standards was undertaken to confirm tentative identifications where possible. Quantifications were based on standard curves generated for each target compound and internal standards.

RNA Extraction

Total RNA was extracted from ∼3 g of outer pericarp tissue (three biological replications) using a method for polysaccharide-rich tissues (Ikoma et al., 1996), with slight modifications. DNase I (Nippon Gene, Tokyo) treatment followed by clean-up using FavorPrep after Tri-Reagent RNA Clean-up Kit (Favorgen Biotech Co., Pingtung, Taiwan) were carried out to remove genomic DNA contamination from the extracted RNA.

Quantitative Real-Time PCR (RT-qPCR)

The method used was similar to that reported in our previous study (Asiche et al., 2018). Briefly, first strand cDNA was synthesized from 2.4 μg of RNA using RevTra Ace reverse transcriptase (Toyobo, Osaka, Japan), and random hexamer primer according to the manufacturer's instructions. Gene-specific primers (**Supplementary Table 1**) for RT-qPCR analysis were designed using Primer3 software (version 0.4.0[1]). Gene expression of three biological replications was examined on a MyiQ Single-Color Reverse Transcriptase-Quantitative PCR Detection System (Bio-Rad, Hercules, CA, United States) using TB Green™ Premix Ex Taq™ II (Tli RNaseH Plus) (TaKaRa, Shiga, Japan) according to the manufacturer's instructions. *AcActin* was used as the housekeeping gene. The specificity of all primers was verified by melting curve analysis. Relative gene expression was calculated using the $2^{-\Delta\Delta Ct}$ method with samples at harvest (0 d) calibrated as 1.

Statistical Analysis

Data obtained in this study were subjected to statistical analyses using R software (version 3.4.0, R Project). ANOVA followed by *post hoc* Tukey's tests ($p \leq 0.05$) were used to detect differences in fruit ripening characteristics and gene expression levels among the different treatments.

[1]http://bioinfo.ut.ee/primer3-0.4.0/

RESULTS

Induction of Ethylene Biosynthesis in Postharvest Kiwifruit

At harvest, kiwifruit used in this study did not produce any detectable ethylene levels. To understand the molecular mechanisms responsible for ethylene production during postharvest handling, we determined the effects of propylene and 1-MCP treatments, as well as storage temperature (**Figure 1**).

As expected, endogenous climacteric ethylene production was detected in propylene-treated fruit at a level of 0.23 nLg^{-1} h^{-1} after 5 d, increasing to 0.63 nLg^{-1} h^{-1} after 9 d (**Figure 1A**). No endogenous ethylene production was measured in fruit pre-treated with 1-MCP, nor in the control fruit, throughout the experimental period. The expression of ethylene biosynthetic genes, *AcACS1* and *AcACO2*, significantly increased in propylene-treated fruit after 5 and 9 d by 123–176- and 143–179-fold, respectively (**Figures 1B,C**). *AcACS1* expression showed no measurable changes in fruit pre-treated with 1-MCP, while *AcACO2* expression was significantly reduced to <60-fold. During storage, no endogenous ethylene production was measured in healthy intact fruit either at 5 or 22°C throughout the experimental period (**Figure 1D**). There were no transcriptional changes observed in *AcACS1* (**Figure 1E**), while *AcACO2* showed a considerable expression increase (65-fold) in fruit at 5°C after 49 d (**Figure 1F**). These observations indicate that production of climacteric ethylene in kiwifruit requires ethylene signaling (triggered by propylene), and is largely dependent upon the transcriptional regulation of *AcACS1*.

Kiwifruit Softening Is Inducible by Either Ethylene or Low Temperature

Following propylene treatment, kiwifruit firmness rapidly decreased from 73 to 10 N within 2 d, and to <3 N after 5 d (**Figure 2A**). Fruit pre-treated with 1-MCP showed only a slight decrease in firmness, to 50 N after 9 d. The cell wall modification-associated genes, *AcPG* and *AcEXP1*, showed a marked increase in expression (>1000- and 71-fold, respectively) during propylene treatment after 5 and 9 d (**Figures 2B,C**). The induction of both genes by propylene was significantly reduced by 1-MCP pre-treatment. Control fruit showed no significant changes in firmness, and the expression of both *AcPG* and *AcEXP1* was maintained at minimal levels throughout the experimental period.

The firmness of fruit stored at 5°C showed a substantial decrease from 73 to 24 N after 21 d, and to 3 N after 49 d (**Figure 2D**). At 22°C, fruit firmness showed only a slight decrease to 45 N after 21 d with no further changes thereafter. Both *AcPG* and *AcEXP1* expression showed sustained increases in fruit at 5°C, whereas their expression in fruit at 22°C were maintained at low levels throughout the storage period (**Figures 2E,F**).

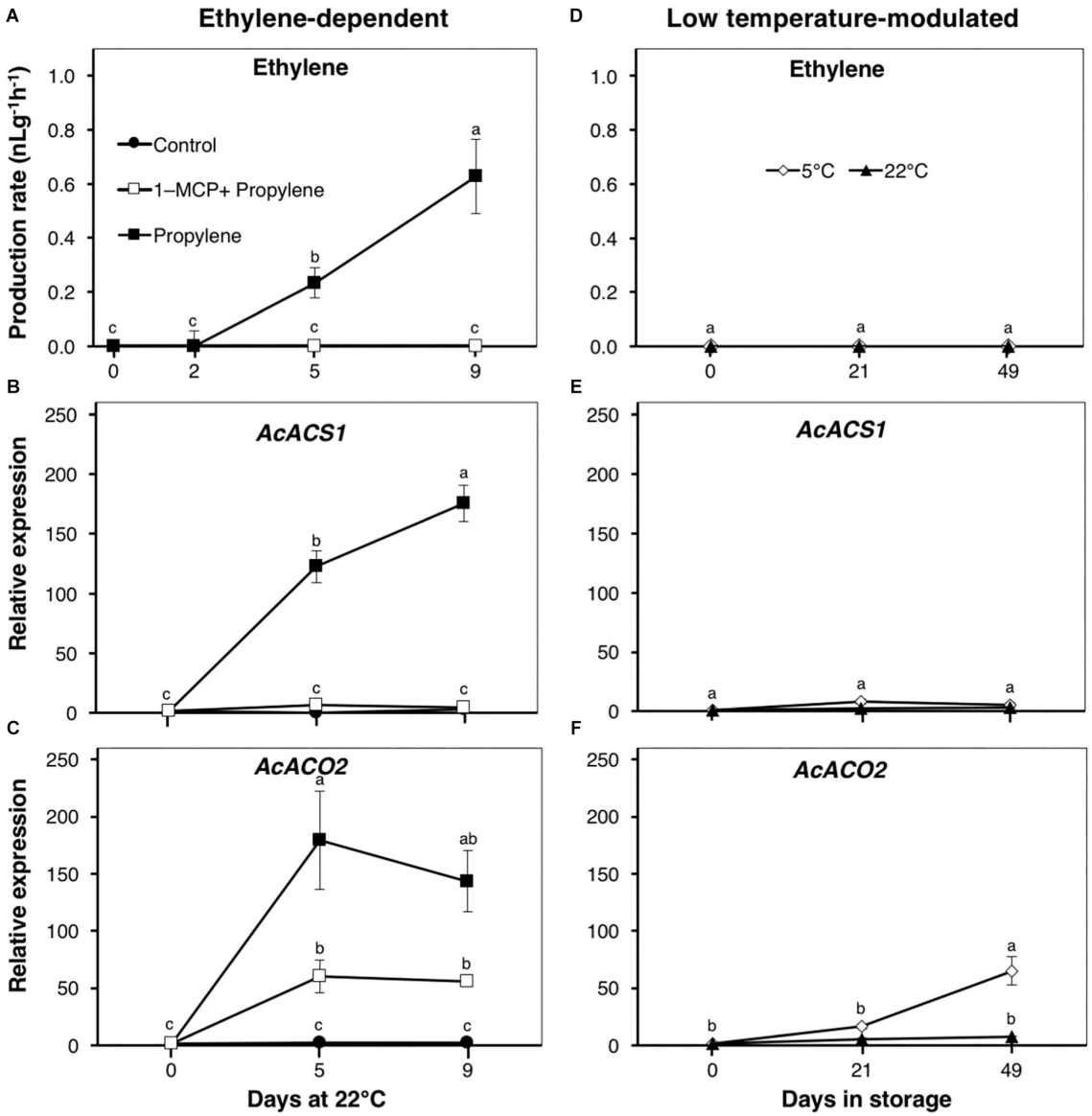

FIGURE 1 | Ethylene production and expression patterns of ethylene biosynthetic genes in kiwifruit. **(A)** Ethylene production pattern during ethylene-dependent ripening. Control: non-treated; propylene: continuously treated with propylene (5000 μLL^{-1}, 22°C) for up to 9 d; 1-MCP+Propylene: a single exposure to 1-methylcyclopropene (1-MCP, 2 μLL^{-1}) for 12 h immediately after harvest, followed by continuous propylene treatment for up to 9 d. **(D)** Ethylene production during low temperature-modulated ripening. Kiwifruit immediately after harvest were separately stored at either 5 or 22°C in ethylene-free air for up to 49 d. Relative transcript levels of ethylene biosynthetic genes, *1-aminocyclopropane-1-carboxylate* (*ACC*) *synthase 1* (*AcACS1*, Achn364251) and *ACC oxidase 2* (*AcACO2*, Achn326461), were determined against at-harvest (0 d) samples by RT-qPCR using kiwifruit *actin* (EF063572) as an endogenous control **(B,C,E,F)**. Data are mean (±SE) of at least three independent biological replications. Error bars not shown are smaller than the symbol used. Different letters indicate significant differences in ANOVA (Tukey's test, $p < 0.05$).

Changes in the Composition of Major Soluble Sugars

The SSC of propylene-treated fruit increased rapidly from 7.8% to a maximum 16.5% after 5 d (**Figure 3A**). This increase was significantly delayed by 1-MCP pre-treatment, with fruit showing little change for the first 5 d; a substantial increase to 13.2% was observed after 9 d. There was a rapid increase in sucrose content of propylene-treated fruit, from 0.7 to 33.1 mg gFW^{-1} after 5 d, also followed by a sudden decrease to 8.9 mg gFW^{-1} after 9 d (**Figure 3B**). Both glucose and fructose contents showed a sustained increase in propylene-treated fruit to 40 and 36 mg gFW^{-1}, respectively, after 9 d (**Figures 3C,D**). The increase in sucrose, glucose, and fructose contents by propylene treatment was significantly delayed by 1-MCP pre-treatment, although the fruit eventually attained almost similar contents at the end of the experimental period. No measurable changes in

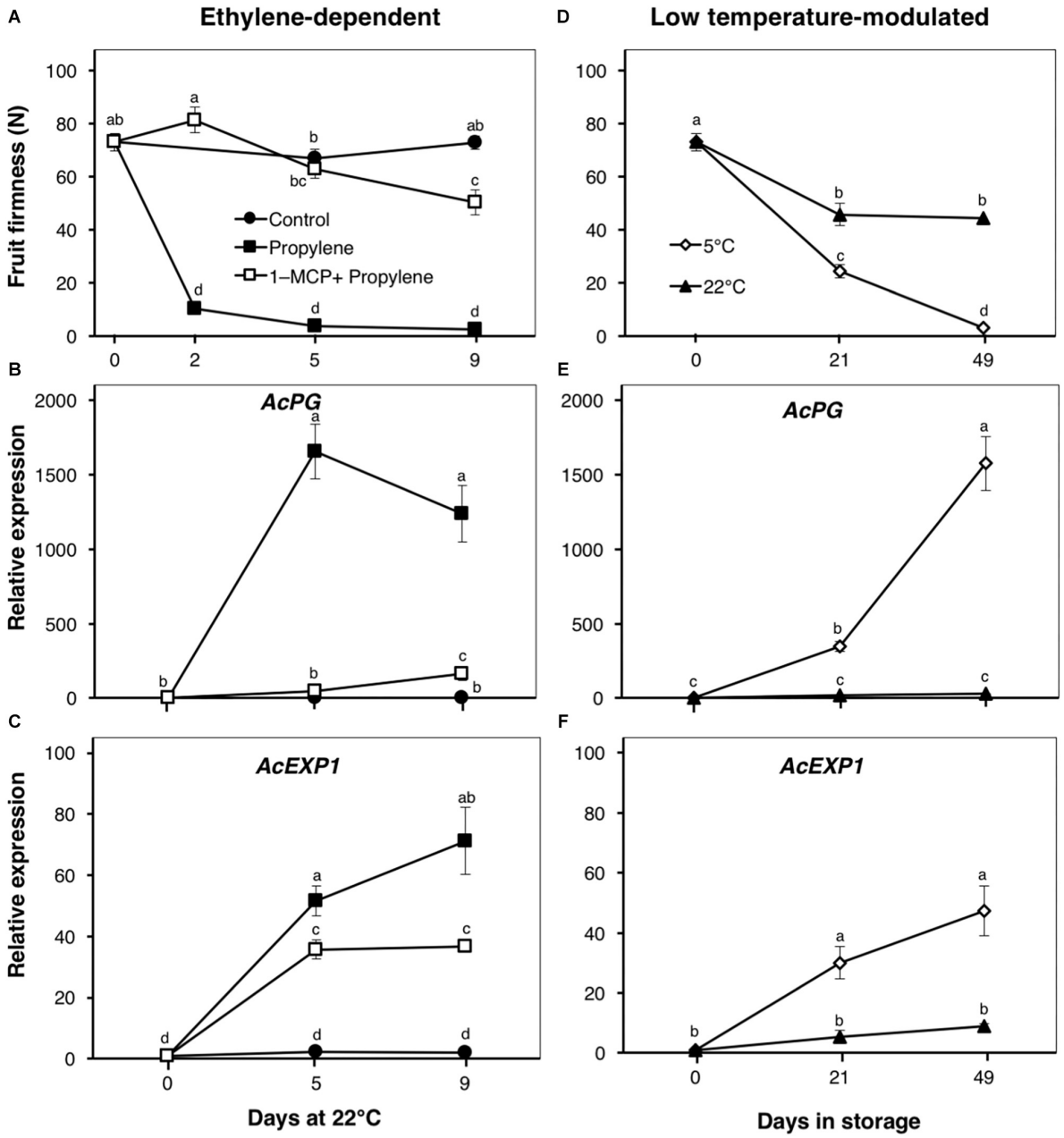

FIGURE 2 | Fruit softening and expression patterns of genes encoding cell wall modifying enzymes in kiwifruit. **(A)** Ethylene-dependent softening in kiwifruit. Control: non-treated; propylene: continuously treated with propylene (5000 μLL^{-1}, 22°C) for up to 9 d; 1-MCP+Propylene: a single exposure to 1-MCP (2 μLL^{-1}) for 12 h immediately after harvest, followed by continuous propylene treatment for up to 9 d. **(D)** Low temperature-modulated softening in kiwifruit. Kiwifruit immediately after harvest were separately stored at either 5 or 22°C in ethylene-free air for up to 49 d. Relative transcript levels of kiwifruit *polygalacturonase* (*AcPG*, Achn051381) and *expansin 1* (*AcEXP1*, Achn336951) were determined against at-harvest (0 d) samples by RT-qPCR using kiwifruit *actin* (EF063572) as an endogenous control **(B,C,E,F)**. Data are mean (±SE) of at least three independent biological replications. Error bars not shown are smaller than the symbol used. Different letters indicate significant differences in ANOVA (Tukey's test, $p < 0.05$).

SSC, as well as the contents of sucrose, glucose, and fructose, were observed in non-treated fruit. During storage, SSC and the contents of glucose and fructose exhibited a sustained increase with no significant differences between fruit at 5 and 22°C (**Figures 3E,G,H**), while the sucrose content rose sharply in fruit at 5°C to a maximum 20.4 mg gFW^{-1} after 21 d followed by a decrease to 7.2 mg gFW^{-1} after 49 d (**Figure 3F**). The sucrose content steadily increased in fruit at 22°C to 33.5 mg gFW^{-1} after 49 d.

Since the content of soluble sugars was significantly affected by propylene and storage, we examined the expression patterns of genes associated with starch degradation (*Ac*β*-AMY1* and

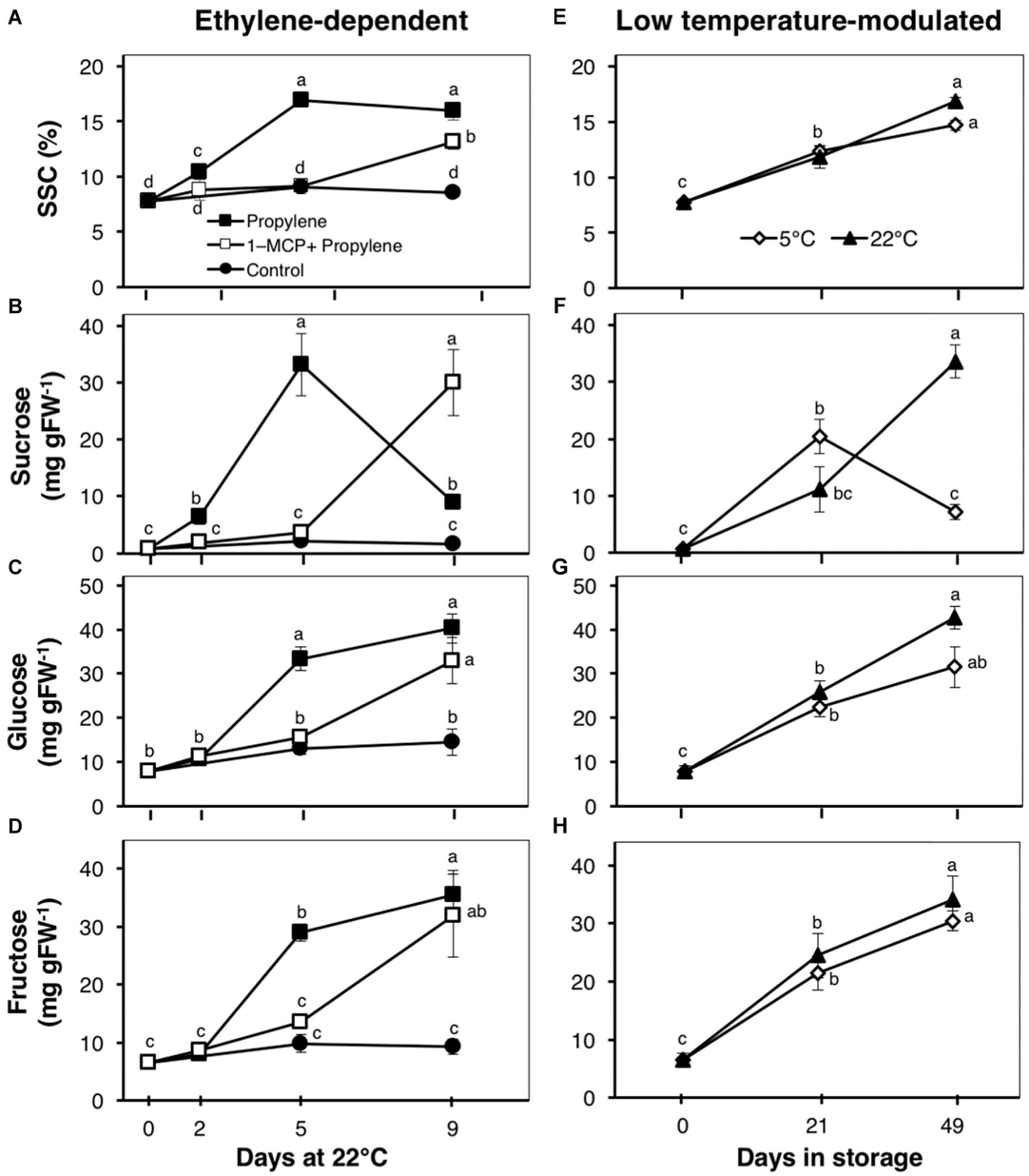

FIGURE 3 | Total soluble solids concentration (SSC) and composition of major sugars in kiwifruit. **(A–D)** Changes in SSC and concentration of sucrose, glucose, and fructose during ethylene-dependent ripening. Control: non-treated; propylene: continuously treated with propylene (5000 μLL^{-1}, 22°C) for up to 9 d; 1-MCP+Propylene: a single exposure to 1-MCP (2 μLL^{-1}) for 12 h immediately after harvest, followed by continuous propylene treatment for up to 9 d. **(E–H)** Changes in SSC and concentration of sucrose, glucose, and fructose during low temperature-modulated ripening. Kiwifruit immediately after harvest were stored at either 5 or 22°C. Data are mean (±SE) of five independent biological replications. Error bars not shown are smaller than the symbol used. Different letters indicate significant differences in ANOVA (Tukey's test, $p < 0.05$).

*Ac*β-*AMY2*) and sucrose metabolism (*AcINV3-1*) (**Figure 4**). *Ac*β-*AMY1* and *Ac*β-*AMY2* both showed an increase in expression in propylene-treated fruit as the soluble sugars increased, while they were significantly suppressed in fruit pre-treated with 1-MCP (**Figures 4A,B**). During storage, there was a small increase in *Ac*β-*AMY1* expression in fruit at 5°C after 49 d, whereas no significant expression changes were observed in fruit at 22°C (**Figure 4D**). On the other hand, *Ac*β-*AMY2* expression increased in fruit at both 5 and 22°C, to a maximum (five to sevenfold) after 21 d, and later decreased after 49 d (**Figure 4E**). *AcINV3-1* showed only a small expression increase (twofold) in propylene-treated fruit after 5 d, while no significant changes were observed in fruit pre-treated with 1-MCP (**Figure 4C**). However, *AcINV3-1* expression significantly increased (by fivefold after 21 d, and fourfold after 49 d) during storage of fruit at 5°C; no

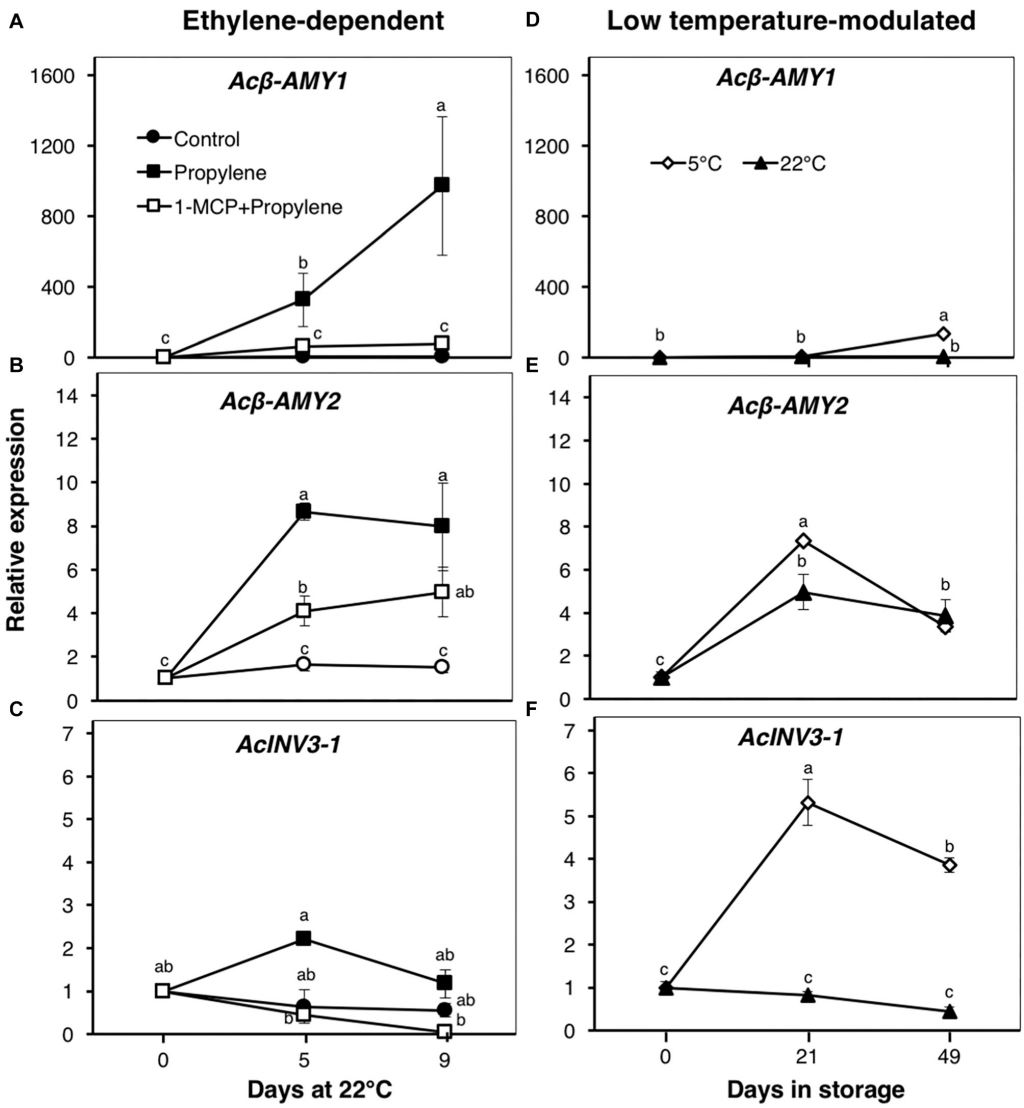

FIGURE 4 | Expression patterns of genes encoding starch degradation and sucrose metabolism enzymes in kiwifruit. Relative transcript levels of β-*amylase 1* (*Acβ-AMY1*, Achn141771 and *Acβ-AMY2*, Achn212571) **(A,B,D,E)** and *invertase 3-1* (*AcINV3-1*, Achn319711) **(C,F)** were determined against at-harvest (0 d) samples by RT-qPCR using kiwifruit *actin* (EF063572) as an endogenous control. Data are mean (±SE) of three independent biological replications. Error bars not shown are smaller than the symbol used. Different letters indicate significant differences in ANOVA (Tukey's test, $p < 0.05$).

measurable changes in expression were recorded in fruit at 22°C (**Figure 4F**).

Aroma Volatile Production Is Strongly Ethylene-Dependent, and Is Undetectable During Low Temperature-Modulated Fruit Ripening

Fruit aroma volatiles were identified and quantified by GC–MS during ethylene-dependent ripening, after 49 d storage at either 5 or 22°C, and during 14 d shelf life (at 22°C) (**Figure 5**). The major volatiles detected were esters; particularly ethyl butanoate and methyl butanoate (**Supplementary Figures 1**, **2**), which are considered to form part of the characteristic ripe fruit flavor for kiwifruit (Zhang et al., 2009; Atkinson et al., 2011). Propylene-treated fruit produced large amounts of ethyl butanoate at a rate of 4.2 ngg^{-1} h^{-1} after 5 d, and 20.9 ngg^{-1} h^{-1} after 9 d (**Figure 5A**). Similarly, methyl butanoate was detected at a rate of 0.2 ngg^{-1} h^{-1} in propylene-treated fruit after 5 d; no further increase was observed thereafter (**Figure 5B**). No measurable increase in the production of both esters was observed in fruit pre-treated with 1-MCP, as well as in control fruit. During storage, ethyl butanoate and methyl butanoate levels were undetectable in fruit at either 5 or 22°C, while they only increased during post-storage treatment with propylene (**Figures 5C,D**), consistent with endogenous ethylene production (**Supplementary Figure 3**).

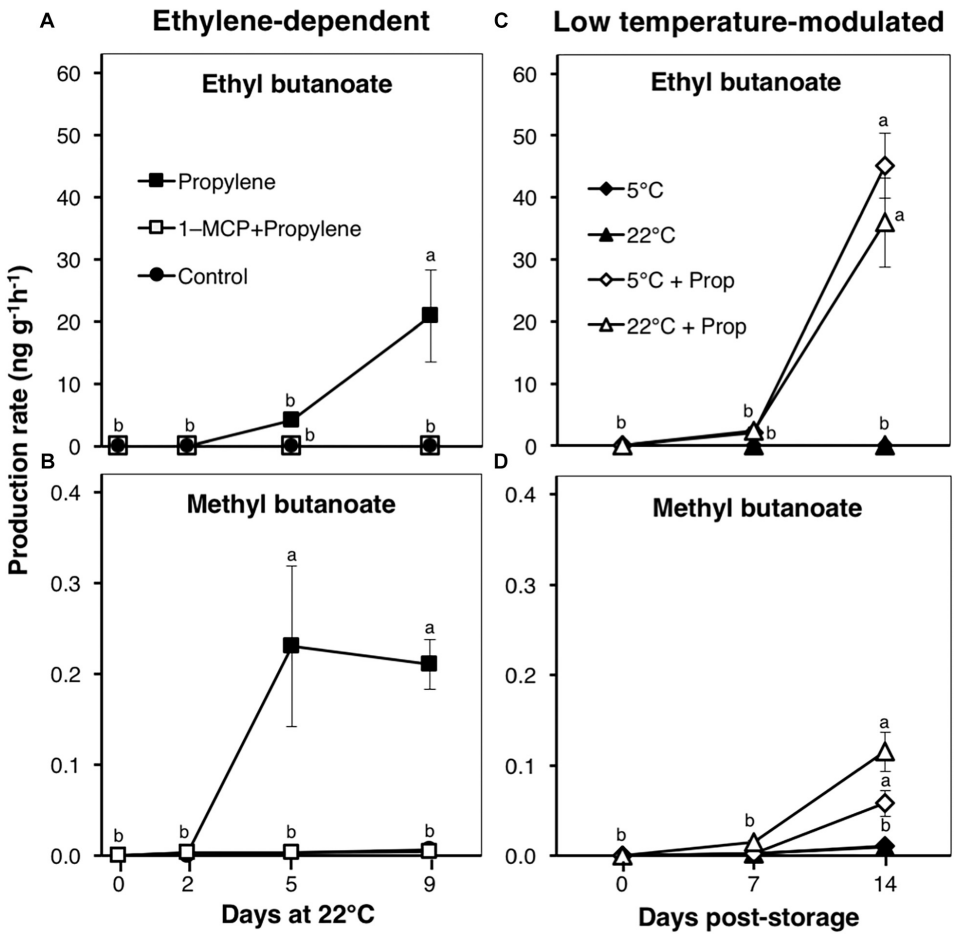

FIGURE 5 | Aroma volatile production patterns in kiwifruit. **(A,B)** Changes in production rates of ethyl- and methyl butanoate during ethylene-dependent ripening. Control: non-treated; propylene: continuously treated with propylene (5000 μLL^{-1}, 22°C) for up to 9 d; 1-MCP+Propylene: a single exposure to 1-MCP (μLL^{-1}) for 12 h immediately after harvest, followed by continuous propylene treatment for up to 9 d. **(C,D)** Ethyl- and methyl butanoate production rates in kiwifruit after storage at either 5 or 22°C. After 49 d storage, fruit were transferred to 22°C with or without propylene-treatment. Data are mean (±SE) of three independent biological replications containing at least three fruit each. Error bars not shown are smaller than the symbol used. Different letters indicate significant differences in ANOVA (Tukey's test, $p < 0.05$).

We also examined the expression of *AcAAT*, which encodes an alcohol acyl transferase associated with ester production during fruit ripening (Souleyre et al., 2005; Günther et al., 2011). *AcAAT* showed a dramatic increase in expression in propylene-treated fruit after 5 d (∼2000-fold) and 9 d (∼11,000-fold), while no significant changes were observed in fruit pre-treated with 1-MCP (**Figure 6A**). By contrast, *AcAAT* showed no significant changes in expression during storage at either 5 or 22°C, whereas it was massively up-regulated (>10,000-fold) 7 d after post-storage treatment with propylene (**Figure 6B**).

Expression Analysis of Fruit Ripening-Associated Transcription Factors

As various TFs including MADS-box and NAC domains have been shown to be key regulators of fruit ripening in kiwifruit and other fruit species (Fujisawa et al., 2013; McAtee et al., 2015; Nieuwenhuizen et al., 2015), we determined the expression of three TF-encoding genes (**Figure 7**). *AcNAC3* was considerably up-regulated (121- and 309-fold after 5 and 9 d, respectively) in propylene-treated fruit (**Figure 7A**). Its expression was significantly suppressed (64-fold) in fruit pre-treated with 1-MCP, while only a small increase (18-fold) was observed in the control fruit. During storage, *AcNAC3* was also remarkably up-regulated (>200-fold) in fruit at 5°C both after 21 and 49 d, as well as after 7 d post-storage propylene treatment; only a small expression increase (<40-fold) was observed in fruit at 22°C (**Figure 7D**). A second NAC-related gene, *AcNAC5*, showed an expression increase (53-fold) 9 d after propylene-treatment, while it was significantly inhibited (14-fold) by 1-MCP pre-treatment (**Figure 7B**). During storage, *AcNAC5* showed no significant change in expression in fruit at either 5 or 22°C, except in post-storage propylene-treated fruit where it was up-regulated (45-fold) after 7 d (**Figure 7E**). *AcMADS2* showed a completely different expression pattern, as it showed no specific response to

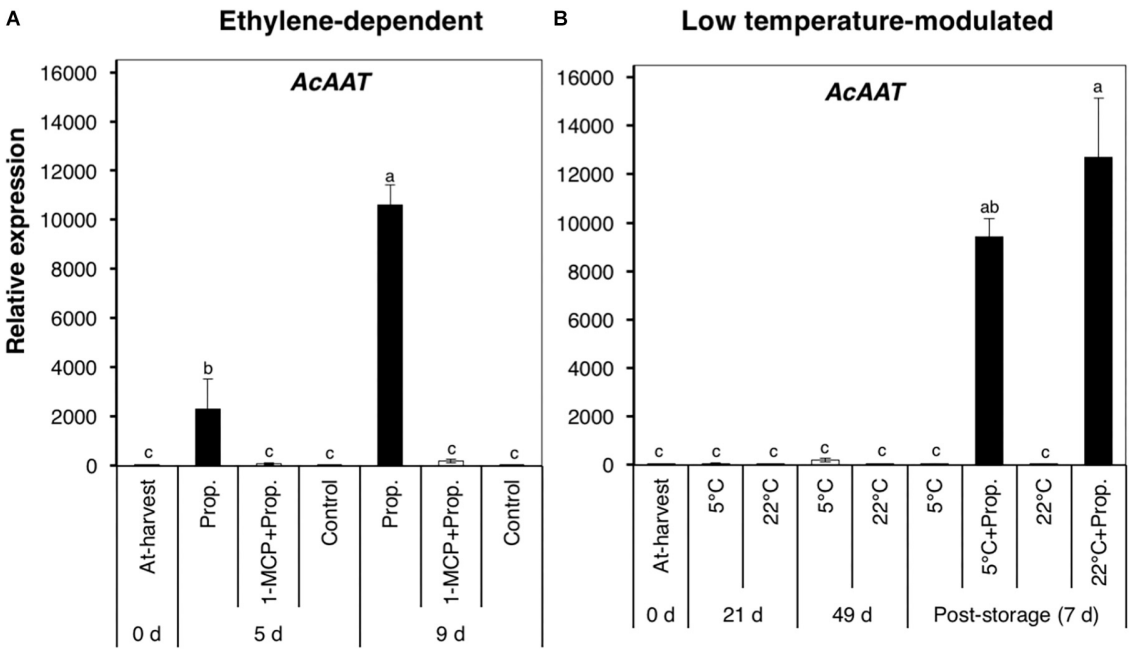

FIGURE 6 | Expression pattern of an alcohol acyl transferase-encoding gene in kiwifruit during ethylene-dependent **(A)** and low temperature-modulated ripening **(B)**. Relative transcript levels of *AcAAT* (KJ626345) were determined against at-harvest (0 d) samples by RT-qPCR using kiwifruit *actin* (EF063572) as an endogenous control. Data are mean (±SE) of three independent biological replications. Error bars not shown are smaller than the symbol used. Different letters indicate significant differences in ANOVA (Tukey's test, $p < 0.05$).

propylene treatment (**Figure 7C**), while it was up-regulated in fruit at 5°C after 21 d (17-fold) and 49 d (33-fold) (**Figure 7F**). There was no significant change in expression of *AcMADS2* in fruit stored at 22°C. It is also worth noting that *AcMADS2* expression in fruit at 5°C substantially dropped after transfer of the fruit to 22°C.

DISCUSSION

The ripening behavior of kiwifruit has elicited great interest, as substantial fruit softening during cold storage essentially occurs in the absence of any detectable ethylene; exogenous or endogenous (Antunes, 2007; Yin et al., 2009). In the present work, our results using "Kosui" kiwifruit are consistent with previous research; fruit softening and the expression of cell wall modification-associated genes were induced during storage at 5°C (**Figure 2**), despite the lack of any measurable increase in ethylene production (**Figure 1**). It has been suggested that fruit softening during low temperature storage is brought about by basal levels of system I ethylene (Kim et al., 1999), based on the high sensitivity of kiwifruit to ethylene (Pranamornkith et al., 2012; Jabbar and East, 2016). However, the present work strongly suggests that ethylene signaling is non-functional during low temperature-modulated ripening in kiwifruit.

In climacteric fruit, the ethylene biosynthetic pathway is well known to be subject to positive feedback regulation (Kende, 1993). In tomato (Barry et al., 2000), pear (Hiwasa et al., 2003), and banana (Inaba et al., 2007), exposure of fruit to exogenous ethylene/propylene triggers a sharp increase in ethylene production with increased expression of ethylene biosynthetic genes. In kiwifruit, the up-regulation of ethylene biosynthetic genes, *AcACS1* and *AcACO2*, by propylene exposure, coupled with their significant inhibition by 1-MCP (**Figures 1B,C**), strongly indicate that ethylene biosynthesis is under the influence of ethylene signaling. These observations agree with previous reports suggesting that ethylene biosynthesis during kiwifruit ripening is regulated by a positive feedback mechanism (Whittaker et al., 1997; Mworia et al., 2010). The expression pattern of *AcACS1* suggests that it is strongly ethylene-dependent, as 1-MCP pre-treatment absolutely inhibited its induction by propylene (**Figure 1B**). Of great importance is the fact that there was no measurable increase in *AcACS1* expression throughout storage of fruit at either 5 or 22°C (**Figure 1E**), which would account for the undetectable ethylene production (**Figure 1D**). Therefore, lack of ethylene-dependent *AcACS1* expression, together with undetectable ethylene production during kiwifruit storage, strongly advocate for the idea that ethylene signaling is non-existent. The increase in *AcACO2* expression after 49 d at 5°C (**Figure 1F**) is insignificant, since it has been shown using tomato that ACS regulates the rate-limiting step in ethylene biosynthesis (Yip et al., 1992; Wang et al., 2002).

It has been shown in previous studies that during fruit ripening, the production of aroma volatiles (especially esters) is regulated by the ethylene signaling pathway. Aroma volatile production was strongly inhibited in ethylene-suppressed kiwifruit (Atkinson et al., 2011), melon (Pech et al., 2008), and apple (Defilippi et al., 2004; Schaffer et al., 2007) lines.

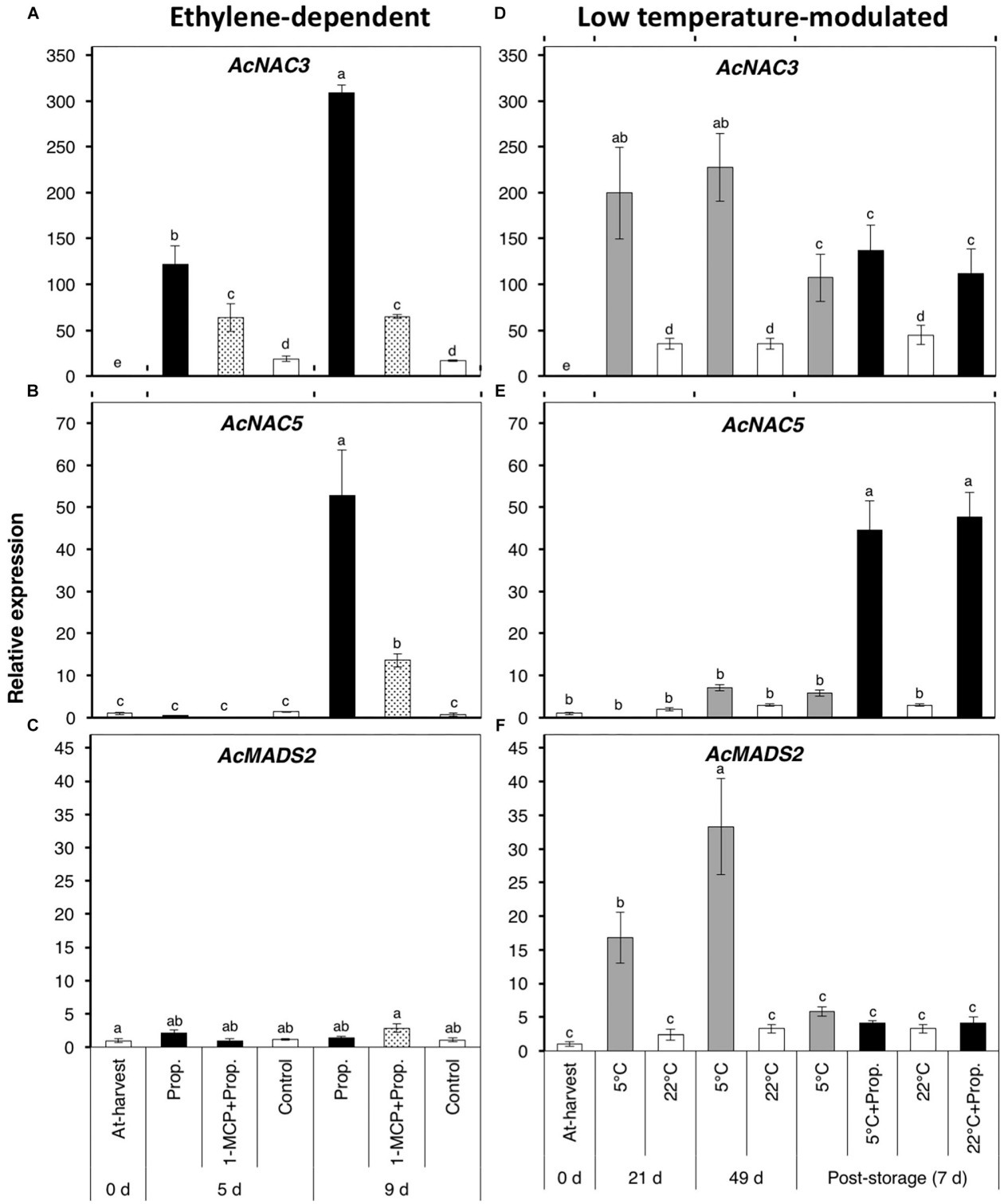

FIGURE 7 | Expression patterns of genes encoding ripening-associated transcription factors (TFs) in kiwifruit during ethylene-dependent and low temperature-modulated ripening. Relative transcript levels of *AcNAC3* (Achn134171) **(A,D)**, *AcNAC5* (Achn169421) **(B,E)**, and *AcMADS2* (Achn235371) **(C,F)** were determined against at-harvest (0 d) samples by RT-qPCR using kiwifruit *actin* (EF063572) as an endogenous control. Data are mean (±SE) of three independent biological replications. Error bars not shown are smaller than the symbol used. Different letters indicate significant differences in ANOVA (Tukey's test, $p < 0.05$).

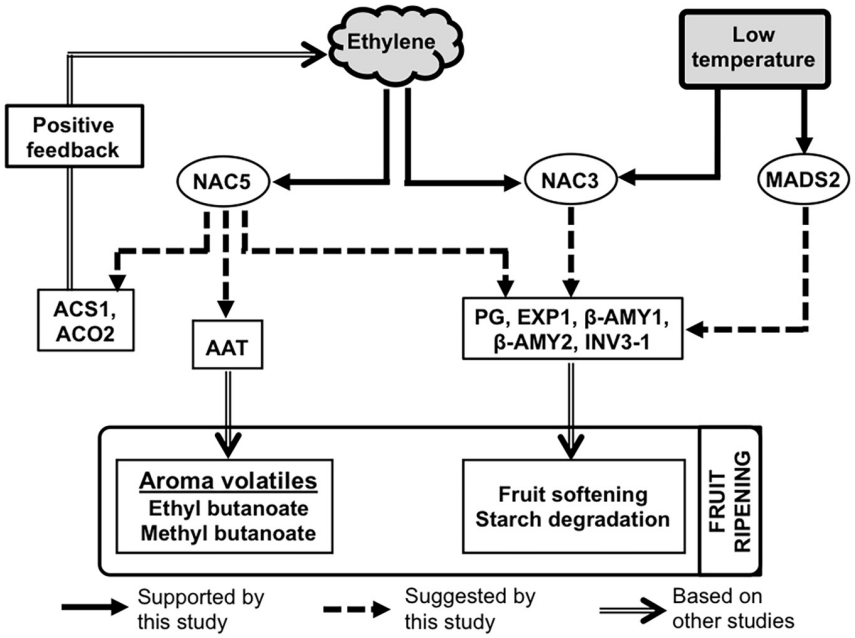

FIGURE 8 | A possible molecular model for the distinct roles of ethylene and low temperature in fruit ripening regulation in kiwifruit. Ethylene signaling recruits a set of specific TFs such as NAC5, as well as shared TFs such as NAC3 which possibly regulate the expression of several genes related with aroma volatile production (*AcAAT*), fruit softening (*AcPG* and *AcEXP1*), and starch degradation (*Ac*β*-AMY1*, *Ac*β*-AMY2*, *AcINV3-1*). Similarly, a low temperature signal recruits specific TFs including MADS2 and shared TFs such as NAC3 that regulate several ripening-related genes, except those associated with aroma volatile emission.

Additionally, transgenic lines treated with exogenous ethylene produced increasing concentrations of aroma volatile compounds (Schaffer et al., 2007; Atkinson et al., 2011). Another study by Defilippi et al. (2005) further demonstrated that the expression of *MdAAT*, together with the activity of the associated enzyme, is a rate-limiting step in ester biosynthesis in apple fruit, and both are regulated by ethylene. In the present work, propylene treatment induced the expression of *AcAAT*, together with the production of ethyl butanoate and methyl butanoate in kiwifruit (**Figures 5**, **6**), and their complete suppression by 1-MCP confirmed that they are strongly regulated by the ethylene pathway. It is interesting that the production of these aroma volatiles, as well as the induction of *AcAAT* expression, was not observed in fruit during storage at either 5 or 22°C, further arguing for the lack of ethylene signaling during low temperature-modulated ripening.

Fruit SSC and the concentrations of sucrose, glucose, and fructose increased in response to propylene, as well as during storage at both 5 and 22°C (**Figure 3**). These changes coincided with increased expression of *Ac*β*-AMY1* and *Ac*β*-AMY2* (**Figures 4A,B,D,E**), which have been previously linked to starch degradation and sugar accumulation in kiwifruit (Nardozza et al., 2013; McAtee et al., 2015; Hu et al., 2016). The above observations suggest that changes in soluble sugars might involve regulatory mechanisms that are independent of both ethylene and low temperature. This is consistent with previous research using different kiwifruit cultivars (Arpaia et al., 1987; Boquete et al., 2004; Mworia et al., 2012; Asiche et al., 2018). However, *Ac*β*-AMY1* appears to have a stronger response to ethylene since its expression during storage is relatively low (**Figures 4A,D**). Previous studies in tomatoes (Gao et al., 2007), melons (Pech et al., 2008), and apples (Defilippi et al., 2004) have also demonstrated that there is an ethylene-independent component in starch metabolism and sugar accumulation during fruit ripening. Nevertheless, the expression pattern of *AcINV3-1* suggests that it is more aligned to low temperature response than to ethylene, since its expression increased markedly in fruit at 5°C, but only slightly in response to propylene (**Figures 4C,F**).

The distinction between ethylene-induced and low temperature-modulated ripening has been difficult to accomplish due to the existence of genes that respond to both stimuli, such as *AcPG* and *AcEXP1* (**Figure 2**). The expression of *AcNAC3* was also up-regulated by both propylene and low temperature (**Figures 7A,D**), suggesting its potential role in the regulation of both ethylene-induced and low temperature-modulated ripening. However, its induction during low temperature storage is likely to be independent of ethylene, since it was previously shown that inhibiting ethylene signaling by 1-MCP failed to suppress its upregulation at 5°C (Asiche et al., 2018). NAC-related TFs are involved in regulation of several ripening-associated genes. In tomato, SlNAC4 was shown to regulate fruit ripening and carotenoid accumulation (Zhu et al., 2014), while in banana, several NAC TFs are induced during fruit ripening and are known to physically interact with ethylene insensitive 3 (EIN3)-like (EIL), a major component in the ethylene signaling pathway (Shan et al., 2012). In the present study, the observation that *AcNAC5* was exclusively induced by propylene and not by low temperature (**Figures 7B,E**) challenges the notion that ethylene

signaling is functional during low temperature-modulated fruit ripening. *AcNAC5* expression correlates well with aroma volatile production patterns, suggesting its potential role in regulation of *AcAAT* and aroma volatile biosynthesis during ethylene-dependent ripening in kiwifruit. By contrast, *AcMADS2* expression was substantially induced at 5°C whereas propylene treatment failed to affect its transcript levels (**Figures 7C,F**), suggesting its potential role in regulation of fruit ripening during cold storage. Our previous studies have also demonstrated the exclusive induction of *AcMADS2* by low temperature in different kiwifruit cultivars (Mitalo et al., 2018, 2019), confirming its alignment to regulatory mechanisms associated with low temperature response. However, since aroma volatiles were undetectable in fruit ripened by low temperature (**Figures 5C,D**), it appears that *AcMADS2* does not have the capacity to bind or activate *AcAAT* or other aroma-related genes which essentially belong to the ethylene pathway.

In summary, the present work has demonstrated that kiwifruit ripening is inducible independently by either ethylene or low temperature signals (**Figure 8**). Fruit ripened by either stimulus can attain similar quality characteristics in terms of firmness and soluble sugar levels. However, production of aroma volatiles (especially esters: ethyl butanoate and methyl butanoate) and the expression of *AcAAT* appear to be strongly dependent on the ethylene signal. These ethylene-dependent components show negligible changes during low temperature-modulated fruit ripening, providing evidence for the absence of ethylene signaling during cold storage. A distinct group of TFs such as those encoded by *AcNAC5* are exclusively induced by ethylene, suggesting their involvement in regulating ethylene-induced ripening, while a second group encoded by genes such as *AcMADS2* are exclusively aligned to low temperature response. Therefore, it appears that ethylene-induced and low temperature-modulated ripening in kiwifruit involve distinct regulatory mechanisms.

DATA AVAILABILITY

All datasets (generated/analyzed) for this study are included in the manuscript and/or the **Supplementary Files**.

AUTHOR CONTRIBUTIONS

OM, ST, and YKu conceived and designed the study. OM, ST, YKo, TO, and AD performed most of the experiments with close supervision from YKu, IG, RN, and KU. IG did the GC–MS analysis. KS and IK provided technical assistance. OM wrote the first draft of the manuscript. YKu and IG substantially improved the first draft of the manuscript. All the authors have read and approved the submitted version.

FUNDING

This work was supported in part by a Grant-in-Aid for Scientific Research (grant nos. 24380023, 25660027, and 16H04873 to YKu) from the Japan Society for the Promotion of Science, Japan and also partially by the Joint Usage/Research Center, Institute of Plant Science and Resources, Okayama University.

SUPPLEMENTARY MATERIAL

The Supplementary Material for this article can be found online at: https://www.frontiersin.org/articles/10.3389/fpls.2019.00888/full#supplementary-material

REFERENCES

Antunes, M. D. (2007). The role of ethylene in kiwifruit ripening and senescence. *Stewart Postharvest Rev.* 3:1. doi: 10.2212/spr.2007.2.9

Arpaia, M. L., Labavitch, J. M., Greve, C., and Kader, A. A. (1987). Changes in the cell wall components of kiwifruit during storage in air or controlled atmosphere. *J. Am. Soc. Hortic. Sci.* 112, 474–481.

Asiche, W. O., Mitalo, O. W., Kasahara, Y., Tosa, Y., Mworia, E. G., Owino, W. O., et al. (2018). Comparative transcriptome analysis reveals distinct ethylene-independent regulation of ripening in response to low temperature in kiwifruit. *BMC Plant Biol.* 18:47. doi: 10.1186/s12870-018-1264-y

Asiche, W. O., Mitalo, O. W., Kasahara, Y., Tosa, Y., Mworia, E. G., Ushijima, K., et al. (2017). Effect of storage temperature on fruit ripening in three kiwifruit cultivars. *Hortic. J.* 86, 403–410. doi: 10.2503/hortj.okd-028

Asiche, W. O., Mworia, E. G., Oda, C., Mitalo, O. W., Owino, W. O., Ushijima, K., et al. (2016). Extension of shelf-life by limited duration of propylene and 1-MCP treatments in three kiwifruit cultivars. *Hortic. J.* 85, 76–85. doi: 10.2503/hortj.mi-066

Atkinson, R. G., Gunaseelan, K., Wang, M. Y., Luo, L., Wang, T., Norling, C. L., et al. (2011). Dissecting the role of climacteric ethylene in kiwifruit (*Actinidia chinensis*) ripening using a 1-aminocyclopropane-1-carboxylic acid oxidase knockdown line. *J. Exp. Bot.* 62, 3821–3835. doi: 10.1093/jxb/err063

Barry, C. S., Llop-Tous, M. I., and Grierson, D. (2000). The regulation of 1-aminocyclopropane-1-carboxylic acid synthase gene expression during the transition from system-1 to system-2 ethylene synthesis in tomato. *Plant Physiol.* 123, 979–986. doi: 10.1104/pp.123.3.979

Boquete, E. J., Trinchero, G. D., Fraschina, A. A., Vilella, F., and Sozzi, G. O. (2004). Ripening of 'Hayward' kiwifruit treated with 1-methylcyclopropene after cold storage. *Postharvest Biol. Technol.* 32, 57–65. doi: 10.1016/j.postharvbio.2003.09.013

Cherian, S., Figueroa, C. R., and Nair, H. (2014). 'Movers and shakers' in the regulation of fruit ripening: a cross-dissection of climacteric versus non-climacteric fruit. *J. Exp. Bot.* 65, 4705–4722. doi: 10.1093/jxb/eru280

Defilippi, B. G., Dandekar, A. M., and Kader, A. A. (2004). Impact of suppression of ethylene action or biosynthesis on flavor metabolites in apple (*Malus domestica* Borkh) fruits. *J. Agric. Food Chem.* 52, 5694–5701. doi: 10.1021/jf049504x

Defilippi, B. G., Kader, A. A., and Dandekar, A. M. (2005). Apple aroma: alcohol acyltransferase, a rate limiting step for ester biosynthesis, is regulated by ethylene. *Plant Sci.* 168, 1199–1210. doi: 10.1016/j.plantsci.2004.12.018

Fujisawa, M., Nakano, T., Shima, Y., and Ito, Y. (2013). A large-scale identification of direct targets of the tomato MADS box transcription factor RIPENING INHIBITOR reveals the regulation of fruit ripening. *Plant Cell* 25, 371–386. doi: 10.1105/tpc.112.108118

Gao, H. Y., Zhu, B. Z., Zhu, H. L., Zhang, Y. L., Xie, Y. H., Li, Y. C., et al. (2007). Effect of suppression of ethylene biosynthesis on flavor products in

tomato fruits. *Russ. J. Plant Physiol.* 54, 80–88. doi: 10.1134/s1021443707010128

Giovannoni, J. J. (2004). Genetic regulation of fruit development and ripening. *Plant Cell* 16, S170–S180.

Günther, C. S., Chervin, C., Marsh, K. B., Newcomb, R. D., and Souleyre, E. J. (2011). Characterization of two alcohol acyltransferases from kiwifruit (*Actinidia* spp.) reveals distinct substrate preferences. *Phytochemistry* 72, 700–710. doi: 10.1016/j.phytochem.2011.02.026

Günther, C. S., Marsh, K. B., Winz, R. A., Harker, R. F., Wohlers, M. W., White, A., et al. (2015). The impact of cold storage and ethylene on volatile ester production and aroma perception in 'Hort16A' kiwifruit. *Food Chem.* 169, 5–12. doi: 10.1016/j.foodchem.2014.07.070

Hiwasa, K., Kinugasa, Y., Amano, S., Hashimoto, A., Nakano, R., Inaba, A., et al. (2003). Ethylene is required for both the initiation and progression of softening in pear (*Pyrus communis* L.) fruit. *J. Exp. Bot.* 54, 771–779. doi: 10.1093/jxb/erg073

Hu, X., Kuang, S., Zhang, A. D., Zhang, W. S., Chen, M. J., Yin, X. R., et al. (2016). Characterization of starch degradation related genes in postharvest kiwifruit. *Int. J. Mol. Sci.* 17:2112. doi: 10.3390/ijms17122112

Ikoma, Y., Yano, M., Ogawa, K., Yoshioka, T., Xu, Z. C., Hisada, S., et al. (1996). Isolation and evaluation of RNA from polysaccharide-rich tissues in fruit for quality by cDNA library construction and RT-PCR. *J. Japan Soc. Hortic. Sci.* 64, 809–814. doi: 10.2503/jjshs.64.809

Inaba, A., Liu, X., Yokotani, N., Yamane, M., Lu, W. J., Nakano, R., et al. (2007). Differential feedback regulation of ethylene biosynthesis in pulp and peel tissues of banana fruit. *J. Exp. Bot.* 58, 1047–1057. doi: 10.1093/jxb/erl265

Jabbar, A., and East, A. R. (2016). Quantifying the ethylene induced softening and low temperature breakdown of 'Hayward' kiwifruit in storage. *Postharvest Biol. Technol.* 113, 87–94. doi: 10.1016/j.postharvbio.2015.11.002

Kende, H. (1993). Ethylene biosynthesis. *Ann. Rev. Plant Biol.* 44, 283–307.

Kim, H. O., Hewett, E. W., and Lallu, N. (1999). The role of ethylene in kiwifruit softening. *Acta Hortic.* 498, 255–262. doi: 10.17660/ActaHortic.1999.498.29

Klee, H. J., and Giovannoni, J. J. (2011). Genetics and control of tomato fruit ripening and quality attributes. *Ann. Rev. Genet.* 45, 41–59. doi: 10.1146/annurev-genet-110410-132507

Lashbrook, C. C., Tieman, D. M., and Klee, H. J. (1998). Differential regulation of the tomato *ETR* gene family throughout plant development. *Plant J.* 15, 243–252. doi: 10.1046/j.1365-313x.1998.00202.x

Lisec, J., Schauer, N., Kopka, J., Willmitzer, L., and Fernie, A. R. (2006). Gas chromatography mass spectrometry-based metabolite profiling in plants. *Nat. Protoc.* 1, 387–396. doi: 10.1038/nprot.2006.59

Marsh, K. B., Friel, E. N., Gunson, A., Lund, C., and MacRae, E. (2006). Perception of flavor in standardized fruit pulps with additions of acids or sugars. *Food Qual. Pref.* 17, 376–386. doi: 10.1016/j.foodqual.2005.04.011

McAtee, P. A., Richardson, A. C., Nieuwenhuizen, N. J., Gunaseelan, K., Hoong, L., Chen, X., et al. (2015). The hybrid non-ethylene and ethylene ripening response in kiwifruit (*Actinidia chinensis*) is associated with differential regulation of MADS-box transcription factors. *BMC Plant Biol.* 15:304. doi: 10.1186/s12870-015-0697-9

McMurchie, E. J., McGlasson, W. B., and Eaks, I. L. (1972). Treatment of fruit with propylene gives information about the biogenesis of ethylene. *Nature* 237, 235–236. doi: 10.1038/237235a0

Mitalo, O. W., Asiche, W. O., Kasahara, Y., Tosa, Y., Owino, W. O., Mworia, E. G., et al. (2018). Characterization of ripening-related genes involved in ethylene-independent low temperature-modulated ripening in 'rainbow red' kiwifruit during storage and on-vine. *Hortic. J.* 87, 421–429. doi: 10.2503/hortj.okd-035

Mitalo, O. W., Asiche, W. O., Kasahara, Y., Tosa, Y., Tokiwa, S., Ushijima, K., et al. (2019). Comparative analysis of fruit ripening and associated genes in two kiwifruit cultivars ('Sanuki Gold' and 'Hayward') at various storage temperatures. *Postharvest Biol. Technol.* 147, 20–28. doi: 10.1016/j.postharvbio.2018.08.017

Mworia, E. G., Yoshikawa, T., Salikon, N., Oda, C., Asiche, W. O., Yokotani, N., et al. (2012). Low-temperature-modulated fruit ripening is independent of ethylene in 'Sanuki Gold' kiwifruit. *J. Exp. Bot.* 63, 963–971. doi: 10.1093/jxb/err324

Mworia, E. G., Yoshikawa, T., Yokotani, N., Fukuda, T., Suezawa, K., Ushijima, K., et al. (2010). Characterization of ethylene biosynthesis and its regulation during fruit ripening in kiwifruit, *Actinidia chinensis* 'Sanuki Gold'. *Postharvest Biol. Technol.* 55, 108–113. doi: 10.1016/j.postharvbio.2009.08.007

Nardozza, S., Boldingh, H. L., Osorio, S., Höhne, M., Wohlers, M., Gleave, A. P., et al. (2013). Metabolic analysis of kiwifruit (*Actinidia deliciosa*) berries from extreme genotypes reveals hallmarks for fruit starch metabolism. *J. Exp. Bot.* 64, 5049–5063. doi: 10.1093/jxb/ert293

Nieuwenhuizen, N. J., Chen, X., Wang, M. Y., Matich, A. J., Perez, R. L., Allan, A. C., et al. (2015). Natural variation in monoterpene synthesis in kiwifruit: transcriptional regulation of terpene synthases by NAC and EIN3-like transcription factors. *Plant Physiol.* 167, 1243–1258. doi: 10.1104/pp.114.254367

Osorio, S., Scossa, F., and Fernie, A. (2013). Molecular regulation of fruit ripening. *Front. Plant Sci.* 4:198. doi: 10.3389/fpls.2013.00198

Pech, J. C., Bouzayen, M., and Latché, A. (2008). Climacteric fruit ripening: ethylene-dependent and independent regulation of ripening pathways in melon fruit. *Plant Sci.* 175, 114–120. doi: 10.1016/j.plantsci.2008.01.003

Pranamornkith, T., East, A., and Heyes, J. (2012). Influence of exogenous ethylene during refrigerated storage on storability and quality of *Actinidia chinensis* (cv. Hort16A). *Postharvest Biol. Technol.* 64, 1–8. doi: 10.1016/j.postharvbio.2011.09.011

Pratt, H. K., and Reid, M. S. (1974). Chinese gooseberry: seasonal patterns in fruit growth and maturation, ripening, respiration and the role of ethylene. *J. Sci. Food Agric.* 25, 747–757. doi: 10.1002/jsfa.2740250702

Schaffer, R. J., Friel, E. N., Souleyre, E. J., Bolitho, K., Thodey, K., Ledger, S., et al. (2007). A genomics approach reveals that aroma production in apple is controlled by ethylene predominantly at the final step in each biosynthetic pathway. *Plant Physiol.* 144, 1899–1912. doi: 10.1104/pp.106.093765

Shan, W., Kuang, J. F., Chen, L., Xie, H., Peng, H. H., Xiao, Y. Y., et al. (2012). Molecular characterization of banana NAC transcription factors and their interactions with ethylene signaling component EIL during fruit ripening. *J. Exp. Bot.* 63, 5171–5187. doi: 10.1093/jxb/ers178

Sobhy, I. S., Miyake, A., Shinya, T., and Galis, I. (2017). Oral secretions affect HIPVs induced by generalist (*Mythimna loreyi*) and specialist (*Parnara guttata*) herbivores in rice. *J. Chem. Ecol.* 43, 929–943. doi: 10.1007/s10886-017-0882-4

Souleyre, E. J., Greenwood, D. R., Friel, E. N., Karunairetnam, S., and Newcomb, R. D. (2005). An alcohol acyl transferase from apple (cv. Royal Gala), MpAAT1, produces esters involved in apple fruit flavor. *FEBS J.* 272, 3132–3144. doi: 10.1111/j.1742-4658.2005.04732.x

Wang, H., Ma, F., and Cheng, L. (2010). Metabolism of organic acids, nitrogen and amino acids in chlorotic leaves of 'Honeycrisp' apple (*Malus domestica* Borkh) with excessive accumulation of carbohydrates. *Planta* 232, 511–522. doi: 10.1007/s00425-010-1194-x

Wang, K. L. C., Li, H., and Ecker, J. R. (2002). Ethylene biosynthesis and signaling networks. *Plant Cell* 14, S131–S151.

Wang, Z. Y., MacRae, E. A., Wright, M. A., Bolitho, K. M., Ross, G. S., and Atkinson, R. G. (2000). *Polygalacturonase* gene expression in kiwifruit: relationship to fruit softening and ethylene production. *Plant Mol. Biol.* 42, 317–328.

Whittaker, D. J., Smith, G. S., and Gardner, R. C. (1997). Expression of ethylene biosynthetic genes in *Actinidia chinensis* fruit. *Plant Mol. Biol.* 34, 45–55.

Xu, F., Yuan, S., Zhang, D. W., Lv, X., and Lin, H. H. (2012). The role of alternative oxidase in tomato fruit ripening and its regulatory interaction with ethylene. *J. Exp. Bot.* 63, 5705–5716. doi: 10.1093/jxb/ers226

Yin, X. R., Allan, A. C., Zhang, B., Wu, R. M., Burdon, J., Wang, P., et al. (2009). Ethylene-related genes show a differential response to low temperature during 'Hayward' kiwifruit ripening. *Postharvest Biol. Technol.* 52, 9–15. doi: 10.1016/j.postharvbio.2008.09.016

Yin, X. R., Chen, K. S., Allan, A. C., Wu, R. M., Zhang, B., Lallu, N., et al. (2008). Ethylene-induced modulation of genes associated with the ethylene signaling pathway in ripening kiwifruit. *J. Exp. Bot.* 59, 2097–2108. doi: 10.1093/jxb/ern067

Yip, W. K., Moore, T., and Yang, S. F. (1992). Differential accumulation of transcripts for four tomato 1-aminocyclopropane-1-carboxylate synthase

homologs under various conditions. *Proc. Nat. Acad. Sci. U.S.A.* 89, 2475–2479. doi: 10.1073/pnas.89.6.2475

Zhang, B., Yin, X. R., Li, X., Yang, S. L., Ferguson, I. B., and Chen, K. S. (2009). Lipoxygenase gene expression in ripening kiwifruit in relation to ethylene and aroma production. *J. Agric. Food Chem.* 57, 2875–2881. doi: 10.1021/jf900 0378

Zhu, M., Chen, G., Zhou, S., Tu, Y., Wang, Y., Dong, T., et al. (2014). A new tomato NAC (N AM/A TAF1/2/C UC2) transcription factor, SlNAC4, functions as a positive regulator of fruit ripening and carotenoid accumulation. *Plant Cell Physiol.* 55, 119–135. doi: 10.1093/pcp/pct162

Conflict of Interest Statement: The authors declare that the research was conducted in the absence of any commercial or financial relationships that could be construed as a potential conflict of interest.

frontiers in Plant Science

MINI REVIEW
published: 10 July 2019
doi: 10.3389/fpls.2019.00874

The Coordination of Ethylene and Other Hormones in Primary Root Development

Hua Qin[1,2], *Lina He*[3] *and Rongfeng Huang*[1,2]*

[1]Biotechnology Research Institute, Chinese Academy of Agricultural Sciences, Beijing, China, [2]National Key Facility of Crop Gene Resources and Genetic Improvement, Beijing, China, [3]College of Biological Sciences and Biotechnology, Beijing Forestry University, Beijing, China

The primary root is the basic component of root systems, initiates during embryogenesis and develops shortly after germination, and plays a key role in early seedling growth and survival. The phytohormone ethylene shows significant inhibition of the growth of primary roots. Recent findings have revealed that the inhibition of ethylene in primary root elongation is mediated *via* interactions with phytohormones, such as auxin, abscisic acid, gibberellin, cytokinins, jasmonic acid, and brassinosteroids. Considering that *Arabidopsis* and rice are the model plants of dicots and monocots, as well as the fact that hormonal crosstalk in primary root growth has been extensively investigated in *Arabidopsis* and rice, a better understanding of the mechanisms in *Arabidopsis* and rice will increase potential applications in other species. Therefore, we focus our interest on the emerging studies in the research of ethylene and hormone crosstalk in primary root development in *Arabidopsis* and rice.

Keywords: ethylene, hormones, primary root, elongation, crosstalk

OPEN ACCESS

Edited by:
Angelos K. Kanellis, Aristotle University of Thessaloniki, Greece

Reviewed by:
Maren Müller, University of Barcelona, Spain
Anna N. Stepanova, North Carolina State University, United States

***Correspondence:**
Rongfeng Huang
rfhuang@caas.cn

Specialty section:
This article was submitted to Plant Physiology, a section of the journal Frontiers in Plant Science

Received: *08 March 2019*
Accepted: *19 June 2019*
Published: *10 July 2019*

Citation:
Qin H, He L and Huang R (2019) The Coordination of Ethylene and Other Hormones in Primary Root Development. Front. Plant Sci. 10:874. doi: 10.3389/fpls.2019.00874

INTRODUCTION

As an underground organ of plants, the root system plays a vital role in the absorption and translocation of water and nutrients. The root system generally consists of two principal root types: the primary root and secondary roots. Primary root is formed embryonically. It is the basic component of the root system that absorbs mineral nutrients and provides mechanical support for shoot growth in young seedlings (Zheng et al., 2016). The growth of primary roots is maintained by two basal developmental processes: cell proliferation in the root apical meristem (RAM) and cell elongation in the elongation zone. Phytohormones are central regulators of plant root growth and development. Multiple phytohormones, including ethylene, auxin, abscisic acid (ABA), gibberellin (GA), cytokinin (CK), jasmonic acid (JA), strigolactone (SL), and brassinosteroid (BR), have been shown to play vital roles in the regulation of primary root growth (Li et al., 2015; Pacifici et al., 2015; Hu et al., 2017; Qin and Huang, 2018).

Ethylene is a gaseous plant hormone that is synthesized from S-adenosylmethionine (SAM), which is converted to 1-aminocyclopropane-1-carboxylate (ACC) by ACC synthase (ACS). ACC is then converted to ethylene by ACC oxidase (ACO; Yang and Hoffman, 1984). Ethylene is perceived by a family of membrane-bound receptors (Hua et al., 1998; Hua and Meyerowitz, 1998). These receptors then inhibit the function of the Ser/Thr kinase CONSTITUTIVE TRIPLE RESPONSE1 (CTR1; Kieber et al., 1993), leading to the dephosphorylation and C-terminal

cleavage of ETHYLENE INSENSITIVE2 (EIN2; Alonso et al., 1999; Ju et al., 2012; Qiao et al., 2012; Wen et al., 2012; Salehin and Estelle, 2015). The split EIN2 C-terminus translocates into the nucleus where it enables activation of the master transcriptional regulators EIN3 and EIN3-LIKE1 (EIL1), resulting in the induction of ethylene-triggered transcriptional response (Chao et al., 1997). In *Arabidopsis*, EIN2 is regulated by proteasomal degradation through EIN2 TARGETING PROTEIN1/2 (ETP1/2), whereas Maohuzi3 (MHZ3) protects OsEIN2 from proteasome-mediated degradation in rice (**Figure 1**; Qiao et al., 2009; Ma et al., 2017). Mutants with enhanced ethylene biosynthesis or signaling exhibit short primary roots (Kieber et al., 1993; Vogel et al., 1998; Woeste et al., 1999). By contrast, loss-of-function mutations of ethylene signaling components such as *ein2*, *ein3*, and *eil1* or treatment of seedlings with ethylene inhibitors such as the biosynthesis inhibitors 2-aminoethoxyvinylglycin (AVG; Ruzicka et al., 2007) and pyrazinamide (PZA; Sun et al., 2017), as well as the perception inhibitor silver nitrate ($AgNO_3$; Ruzicka et al., 2007) and 1-methylcyclopropene (1-MCP; Serek et al., 1995) lead to increased primary root length and reduced ethylene response (Chao et al., 1997; Alonso et al., 1999; Ma et al., 2013; Yang et al., 2015).

An increasing number of investigations have revealed that ethylene affects primary root growth *via* two successive processes: cell proliferation and cell elongation (Ruzicka et al., 2007; Street et al., 2015). Cell proliferation occurs at the RAM, which is composed of a quiescent center (QC), surrounding stem cells, and a group of mitotically active cells. The QC plays important roles in maintaining stem cell populations within the root meristem (Ortega-Martinez et al., 2007; Heyman et al., 2013). Accumulating evidence has revealed that ethylene induces irregular transverse cell divisions in the QC (Ortega-Martinez et al., 2007; Ni et al., 2014). Furthermore, ethylene inhibition of cell proliferation at the RAM is mainly achieved by restricting epidermal cell expansion (Street et al., 2015; Vaseva et al., 2018). Moreover, ethylene also inhibits the elongation of cells in the elongation zone. Ethylene stimulates auxin biosynthesis and basipetal auxin transport toward the elongation zone, where it activates a local auxin response leading to inhibition of cell elongation (Ruzicka et al., 2007). In summary, ethylene inhibits primary root growth by regulating cell proliferation in the RAM and cell elongation in the elongation zone.

In addition to ethylene, other plant hormones are also involved in regulating primary root growth, and accumulating data have shown that plant hormones interact with each other to regulate primary root growth (Thole et al., 2014; Pacifici et al., 2015; Van de Poel et al., 2015; Harkey et al., 2018). As a model plant of dicots and monocots, the results obtained in *Arabidopsis* and rice can be instructive for other species.

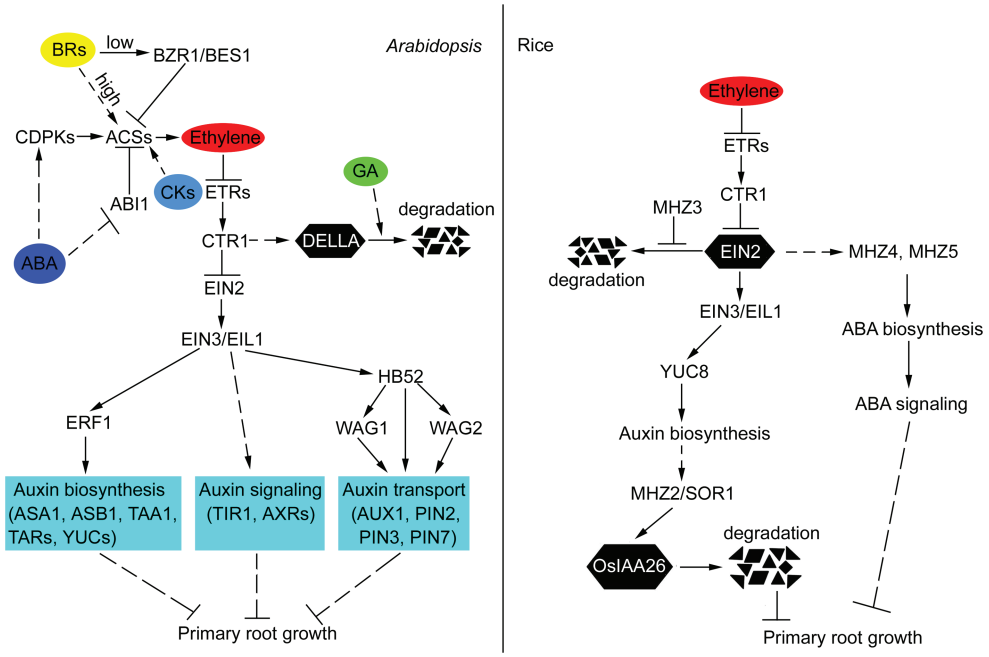

FIGURE 1 | Crosstalk of ethylene and other hormones in the primary root growth of *Arabidopsis* and rice. In *Arabidopsis*, ethylene inhibits primary root growth by regulating auxin biosynthesis, transport, and signaling. EIN3/EIL1, ERF1, and HB52 function as crosstalk nodes between ethylene and auxin in this process. ABA promotes ethylene biosynthesis by affecting the posttranscriptional regulation of ACS. GA and ethylene antagonistically regulate the stability of DELLA proteins, which act as growth repressors. CKs induce ethylene biosynthesis by stabilizing ACS stability. Low concentrations of BRs inhibit ethylene biosynthesis by activating BZR1 and BES1 to repress the expression of *ACSs*. High levels of BRs induce ethylene biosynthesis through increasing the stability of ACSs. In rice, ethylene restricts primary root growth by increasing auxin and ABA biosynthesis. Auxin accumulation promotes SOR1-mediated degradation of OsIAA26, thus repressing normal root growth. MHZ3 stabilizes OsEIN2 to facilitate ethylene signal transduction. The solid lines indicate direct interactions, and the dashed lines indicate indirect interactions. The arrows indicate stimulatory effects, whereas the T sharp symbol indicates inhibitory effects.

In this current review, we summarize the current studies on the crosstalk of ethylene with other phytohormones during primary root development in *Arabidopsis* and rice, including auxin, ABA, GA, CKs, BRs, and JA, which contributes to better understanding of the role of ethylene in primary root development.

Interaction of Ethylene and Auxin in Primary Root Growth

As an omnipotent regulator of root development, auxin inhibits the primary root elongation, and this effect is most probably mediated in crosstalk with ethylene (Hu et al., 2017; Qin and Huang, 2018). Auxin and ethylene act synergistically in the regulation of primary root elongation (Ruzicka et al., 2007; Swarup et al., 2007; Qin et al., 2017; Zemlyanskaya et al., 2018), and this regulation is mainly through the modulation of cell proliferation in the RAM and cell elongation in the elongation zone (Ruzicka et al., 2007; Street et al., 2015). The transcription of auxin biosynthesis and transport genes is regulated by ethylene, and the treatment of ethylene promotes auxin accumulation in the root tip, as revealed by indole-3-acetic acid (IAA) measurements and *DR5* reporter expression (Stepanova et al., 2005; Ruzicka et al., 2007; Qin et al., 2017; Mendez-Bravo et al., 2019). Moreover, disrupting auxin biosynthesis by L-kynurenine or yucasin [5-(4-chlorophenyl)-4H-1,2,4-triazole-3-thiol] impairs the ethylene effect on primary root growth (He et al., 2011; Qin et al., 2017). *Via* analysis of mutants that showed reduced sensitivity to ethylene in the primary roots, a set of *weak ethylene insensitive* (*wei*) mutants was isolated, such as *wei2/anthranilate synthase α1* (*asa1*), *wei7/anthranilate synthase β1* (*asb1*), and *wei8*/tryptophan aminotransferase of arabidopsis1 (taa1; Stepanova et al., 2005, 2008). *WEI2/ASA1* and *WEI7/ASB1* encode α and β subunits of anthranilate synthase, respectively, which is a rate-limiting enzyme involved in the biosynthesis of the auxin precursor tryptophan (Trp; Stepanova et al., 2005). *WEI8/TAA1* encodes key enzymes involved in the indole-3-pyruvic acid (IPyA) pathway, which is the most important pathway for producing auxin in plants (Stepanova et al., 2008; Mashiguchi et al., 2011). In addition to the defects of auxin biosynthesis, mutations affecting auxin transport, perception, or signaling also result in reduced sensitivity to ethylene (Hu et al., 2017; Merchante and Stepanova, 2017; Qin and Huang, 2018). Ethylene is one of the important players that regulate the auxin flow (Luschnig et al., 1998; Ruzicka et al., 2007; Stepanova et al., 2007; Swarup et al., 2007). Abnormal levels of ethylene can result in an imbalance in the auxin gradient, which in turn leads to a higher auxin content, and ultimately result in the inhibition of cell elongation and primary root growth. Mutations in influx carriers of the AUXIN1 (AUX1) family or efflux carriers of the PIN-FORMED (PIN) family lead to ethylene-resistance root phenotype (Luschnig et al., 1998; Ruzicka et al., 2007; Stepanova et al., 2007; Swarup et al., 2007). Loss of function of *AUXIN RESISTANT2* (*AXR2*) and *AXR3*, which are involved in the auxin signaling pathway, results in reduced ethylene sensitivity in primary root (Stepanova et al., 2007; Swarup et al., 2007). Mutants of auxin receptor *transport inhibitor response1* (*tir1*) show an ethylene-insensitive primary root growth (**Figure 1**; Alonso et al., 2003).

With an established method for screening ethylene-response mutants in rice, several mutants with defective ethylene response in primary root were identified (Ma et al., 2013). Among these mutants, some auxin biosynthesis- and signaling-related mutants, such as *maohuzi2* (*mhz2/sor1*) and *rice ethylene-insensitive7* (*rein7/yuc8*; **Figure 1**), have been identified (Qin et al., 2017; Chen et al., 2018). MHZ2, a RING finger E3 ubiquitin ligase, regulates ethylene response in primary roots by interacting with OsIAA26, an atypical Aux/IAA protein involved in the auxin signaling pathway (Chen et al., 2018). *REIN7* encodes an orthologue of *YUCCA8* (*YUC8*) and loss of *REIN7* function results in reduced auxin biosynthesis and ethylene insensitivity in primary roots (Qin et al., 2017). These studies suggest that ethylene-triggered inhibition of primary root elongation requires auxin biosynthesis, transport, and signaling, and the underlying mechanism is conserved in different species.

Emerging studies have shown that several transcription factors are involved in ethylene signaling or ethylene response, such as EIN3, the canonical transcription factor involved in the ethylene signaling pathway, regulating auxin biosynthesis by activating *YUC* transcripts (Liu et al., 2016; Qin et al., 2017). ETHYLENE RESPONSE FACTOR1 (ERF1), a direct target of EIN3, is responsive to ethylene and directly activates *ASA1*. ASA1 encodes a rate-limiting enzyme in Trp biosynthesis where auxin is derived. The activation of *ASA1* promotes auxin biosynthesis, results in the increased auxin accumulation, and thus inhibits primary root elongation (Solano et al., 1998; Mao et al., 2016). HOMEOBOX PROTEIN52 (HB52), which acts downstream of EIN3, binds to the promoters of *PIN2*, *WAVY ROOT GROWTH1* (*WAG1*), and *WAG2* to increase their expression. WAG1 and WAG2 phosphorylate PIN2, thus modulating auxin transport (**Figure 1**; Miao et al., 2018). These transcription factors act as nodes in the crosstalk between ethylene and auxin in primary root growth, implying that ethylene regulates primary root growth by modulating auxin biosynthesis, transport, and signaling.

Coordination of Ethylene and Abscisic Acid in Primary Root Growth

ABA regulates many aspects of plant growth and development, including primary root elongation (Luo et al., 2014; Li et al., 2017; Sun et al., 2018). Studies have shown that ABA has biphasic effects on primary root growth, depending on its concentration, environmental conditions, developmental context, genotypes, and plant species. Typically, low concentrations of ABA stimulate primary root growth, whereas high concentrations inhibit it (Rowe et al., 2016; Li et al., 2017).

Increasing numbers of studies in *Arabidopsis* have suggested that ABA inhibits primary root growth mainly acting on cortical cells in the elongation zone, and this process requires the ethylene signaling pathway (Beaudoin et al., 2000; Ghassemian et al., 2000; Dietrich et al., 2017). The ethylene signaling mutant *ethylene response1* (*etr1-1*) and *ein2* showed resistance to ABA-inhibited primary root growth, whereas the

ABA-resistant mutant *ABA-insensitive1* (*abi1-1*) and the ABA-deficient mutant *aba2* exhibited a normal ethylene response in the roots (Beaudoin et al., 2000; Ghassemian et al., 2000; Thole et al., 2014). Moreover, disruption of ABA biosynthesis or signaling in the *ein2*, *ein3,* or *ctr1* mutant background by introducing the *aba2* or *abi1* mutation did not alter the ethylene response phenotypes of the respective ethylene mutants (Beaudoin et al., 2000; Cheng et al., 2009). The above results suggest that ABA-inhibited primary root growth requires a functional ethylene signaling pathway but that ethylene-inhibited root growth is ABA-independent. Recent studies have indicated that ABA inhibits primary root growth by increasing ethylene biosynthesis (Luo et al., 2014). ABA activates two calcium-dependent protein kinases, CPK4 and CPK11, which phosphorylate the C-terminus of ACS6 and increase the stability of ACS6 in ethylene biosynthesis, thus promoting the biosynthesis of ethylene (**Figure 1**). Disruption of ethylene biosynthesis by AVG relieves the inhibitory effect of ABA on primary root growth (Luo et al., 2014; Li et al., 2017). In addition, a protein phosphatase type 2C, ABI1, a negative regulator of ABA signaling, negatively regulates ethylene biosynthesis by counteracting the phosphorylation of ACS2/ACS6 mediated by MITOGENACTIVATED PROTEIN KINASE 6 (MAPK6; **Figure 1**; Ludwikow et al., 2014). Together, these results suggest that ABA treatment induces ethylene biosynthesis, thus leading to the inhibition of primary root growth, and that ABA responses require normal ethylene signaling.

ABA and ethylene crosstalk in rice have been revealed by two ethylene-response mutants: *mhz4* and *mhz5* (Ma et al., 2014; Yin et al., 2015). MHZ4 is a homologue of *Arabidopsis* ABA4, which is involved in ABA biosynthesis. *MHZ5* encodes a carotenoid isomerase, which is essential for ABA biosynthesis in etiolated rice shoots and roots. Mutations in *MHZ4* and *MHZ5* reduce the ethylene response in roots but enhance the ethylene response in the coleoptiles of etiolated seedlings. Overexpression of *MHZ4/5* results in enhanced ethylene sensitivity in roots and reduced ethylene sensitivity in coleoptiles. Genetic studies have revealed that the MHZ4/5-mediated ABA pathway in rice acts downstream of ethylene signaling to inhibit root growth (**Figure 1**), which is different from that in *Arabidopsis*, where ABA inhibits root growth through promoting ethylene biosynthesis, suggesting that different mechanisms have evolved in these two species. In addition, the MHZ4/5-mediated ABA pathway in rice acts upstream of ethylene signaling to control coleoptile growth (Ma et al., 2014; Yin et al., 2015), suggesting that the interaction between ethylene and ABA is distinctive in different tissues.

Integration of Ethylene and Gibberellins in Primary Root Growth

GAs also play an important role in primary root growth. Mutation in GA biosynthesis genes or disruption of GA biosynthesis by paclobutrazol, an inhibitor of GA biosynthesis, substantially reduces the rate of cell proliferation in the *Arabidopsis* root meristem (Achard et al., 2009; Ubeda-Tomas et al., 2009; Lee et al., 2012). GAs have been proposed to promote root growth in *Arabidopsis* by increasing the elongation of both dividing and post-mitotic endodermal cells, thereby indirectly controlling the division and elongation of other types of root cells and the overall root meristem size (Ubeda-Tomas et al., 2009).

GAs are perceived in the cell through a simple pathway that is regulated by a family of proteins known as DELLA proteins, a subfamily of the GRAS family of putative transcriptional regulators (Richards et al., 2001; Daviere and Achard, 2013). In *Arabidopsis*, the DELLA family comprises GA-INSENSITIVE (GAI), REPRESSOR OF GA (RGA), RGA-LIKE1 (RGL1), RGL2, and RGL3 (Peng et al., 1997; Silverstone et al., 1998). GAs promote the degradation of DELLA proteins. However, ethylene treatment delays the GA-induced diminishing of green fluorescent protein (GFP)-RGA fusion constructs from root cell nuclei *via* a CTR1-dependent signaling pathway (**Figure 1**). Moreover, mutations in GAI and RGA reduce the sensitivity to ethylene in primary root growth, and exogenous GA treatment substantially releases the inhibition by ethylene of primary root growth (Achard et al., 2003), suggesting that ethylene and GA act antagonistically in primary root growth.

In rice, GA participates in the modulation of cell elongation and proliferation in the root meristem, GA deficiency leads to short primary roots (Li et al., 2015), and exogenous applications of GA can increase primary root growth and ethylene production (Lee and Yoon, 2018). *Via* an analysis of the ethylene-responsive genes in the roots of *mhz7/osein2* and *mhz6/oseil1* compared with the wild type by RNA sequencing, some genes are involved in GA biosynthesis and the catabolic pathway has been identified (Yang et al., 2015). Considering that ethylene inhibits primary root growth, while GA promotes it, ethylene may reduce endogenous GA contents by the transcriptional regulation of GA biosynthesis and catabolic genes in primary roots.

Interactions Between Ethylene, Cytokinins, Jasmonic Acid, and Brassinosteroids in Primary Root Growth

CKs are widely considered to inhibit primary root growth in *Arabidopsis* (Cary et al., 1995; Riefler et al., 2006; Ioio et al., 2012). Accumulating studies showed that CKs regulate primary root growth by interacting with ethylene, and this interaction mainly occurs in cell proliferation in the RAM (Street et al., 2015; Van de Poel et al., 2015; Liu et al., 2017). In *Arabidopsis*, treatment of etiolated seedlings with CKs produces a phenotype similar to ethylene (Cary et al., 1995), suggesting that CKs and ethylene may act synergistically to regulate specific growth and developmental processes. Further research shows that CK treatment increases the stability of the ethylene biosynthesis protein ACS5, leading to increased ethylene production (**Figure 1**; Chae et al., 2003; Hansen et al., 2009). Proteome analysis in *Arabidopsis* roots reveals that CKs upregulate the majority of proteins in the ethylene biosynthesis pathway (Zdarska et al., 2013). These results suggest that CKs inhibit primary root growth through enhancing ethylene biosynthesis. However, Kushwah et al. (2011) reported that CKs can induce primary root elongation, and this response is mediated by the ethylene signaling pathway through the ethylene receptor

ETHYLENE RESISTANT1 (ETR1) and its downstream signaling element EIN2, suggesting that the ethylene signaling pathway is required for CK-induced primary root growth response. In rice, recent research suggests that exogenous CKs upregulate the transcription of ethylene biosynthesis genes in primary roots, resulting in increased ethylene biosynthesis and inhibition of primary root growth (Zou et al., 2018).

The function of JA in plant resilience to many environmental challenges has been well studied, and its role in root growth has also been reported (Wasternack and Hause, 2013; Huang et al., 2017; Guo et al., 2018). Exogenous application of JA inhibits various aspects of seedling growth, including primary root growth (Wasternack and Hause, 2013; Huang et al., 2017). In response to the JA signal, the F-box protein CORONATINE INSENSITIVE1 (COI1) recruits JASMONATE ZIM-domain (JAZ) repressors for ubiquitination and degradation, thereby relieving the repression of transcription factors and enabling the expression of JA-responsive genes and JA responses (Thines et al., 2007; Katsir et al., 2008; Fernandez-Calvo et al., 2011; Qi et al., 2015). Complicated modes of interaction between JA and ethylene have been investigated in different processes. JA enhances aluminum-induced primary root growth inhibition, and this process is controlled by ethylene. Aluminum-induced upregulation of pCOI1:COI1-VENUS in the root apex transition zone was significantly repressed in the *ein3eil1* double mutant, suggesting that JA acts downstream of ethylene in aluminum-induced primary root growth inhibition (Yang et al., 2017). In addition, JA and ethylene act synergistically to regulate root hair development, through direct interaction of JASMONATE ZIM-DOMAIN (JAZ) proteins, which are degraded after JA treatment, with EIN3/EIL1 to attenuate its transcriptional activity (Zhu et al., 2006, 2011). The above studies suggest that different mechanisms are present in different tissues, and additional studies are needed to elucidate the involvement of JA-ethylene crosstalk in primary root growth.

BRs, a class of plant-specific steroid hormones, play important roles in regulating primary root growth. Low concentrations of BRs can induce root growth, while high concentrations inhibit root growth (Clouse et al., 1996; Mussig et al., 2003; Lv et al., 2018). Mutations in BR biosynthesis or signaling pathway exhibit reduced cell proliferation in the RAM and decreased cell length in the mature zone, thus leading to shortened roots (Li et al., 1996; Mussig et al., 2003; Lv et al., 2018). BRs, perceived by the BRASSINOSTEROID INSENSITIVE1 (BRI1) receptor, activate the transcription factors BRI1-EMS-SUPPRESSOR1 (BES1) and BRASSINOSTEROID RESISTANT1 (BZR1), which in turn induce the BR response (Yin et al., 2002; Yu et al., 2011; Oh et al., 2012). Several studies have shown that BRs regulate primary root growth through modulating ethylene biosynthesis, namely, low levels of BRs inhibit ethylene biosynthesis by activating BZR1 and BES1 to repress the expression of *ACSs* (Lv et al., 2018). Although high levels of BRs induce ethylene biosynthesis by increasing the stability of ACSs (**Figure 1**), these dual effects on ethylene lead to biphasic effects of BRs on primary root growth (Lim et al., 2002; Hansen et al., 2009; Lv et al., 2018).

CONCLUSIONS AND PERSPECTIVES

During the past few years, multiple studies have provided molecular connections between ethylene and primary root growth. In this review, we integrated recent data showing the molecular details of the interactions between ethylene and other plant hormones in the regulation of primary root development (**Figure 1**). In particular, ethylene regulates primary root growth through modulating auxin biosynthesis, transport, and signaling, and this regulatory mechanism is conserved in *Arabidopsis* and rice. ABA and CKs inhibit primary root growth in *Arabidopsis* by affecting the posttranscriptional regulation of ACS, which results in increased ethylene synthesis. However, in rice, ethylene inhibition of primary root growth requires ABA function, and this mode of ethylene-ABA interaction is fundamentally different from that in *Arabidopsis*, suggesting that different mechanisms exist in different species. GA and ethylene antagonistically regulate the stability of DELLA proteins, which act as growth repressors. BRs have biphasic effects on primary root growth, namely, low concentrations of BRs inhibit ethylene biosynthesis by activating BZR1 and BES1 to repress the expression of *ACSs*, whereas high levels of BRs induce ethylene biosynthesis through increasing the stability of ACSs. Based on the above results, a general interaction model where ethylene plays a central role is presented (**Figure 1**). Thus, this review provides an overview on the crosstalk of ethylene and other hormones in primary root growth, increasing our understanding of the regulation of ethylene in primary root growth.

Primary root growth begins during embryo development and is easily affected by adverse soil conditions. Plant hormones act as all-encompassing regulators of normal root growth and mediate root morphological responses to abiotic stresses (De Smet et al., 2015). Further investigations should focus on how plants perceive external changes and translate cues into adaptive responses by modulating endogenous hormone crosstalk dynamics. Moreover, there is a complex regulatory network among phytohormones, and different regulatory mechanisms exist in different tissues, at different developmental stages, and in different species (Luo et al., 2014; Ma et al., 2014; Yin et al., 2015; Abts et al., 2017). Thus, researchers should try to understand hormone crosstalk in a multidimensional space, and the development of effective hormone detection methods and computational models will greatly promote research on hormone crosstalk.

With the advancement of technology, high-throughput technology provides an opportunity to track complex regulatory pathways during primary root growth for detecting the molecular mechanisms that govern hormone crosstalk and the nodes of interactions between different hormone pathways (Hung and Weng, 2017). However, caution and further validation are required when using those data. In addition, it is also interesting to clarify the regulatory network of ethylene and other hormones in multiple cell types. Single-cell transcriptome sequencing can provide us with an overview of ethylene and other hormone actions in specific cells (Ziegenhain et al., 2017;

Denyer et al., 2019), and cell type-specific promoters allow us to study the function of a desired protein in particular cell types and to reveal the main sites of ethylene and other hormone actions (Vaseva et al., 2016).

AUTHOR CONTRIBUTIONS

All the authors discussed and created the review's outline. HQ wrote the manuscript. RH edited the manuscript.

FUNDING

This work was funded by the National Natural Science Foundation of China grant numbers 31801445 and 31871551, the Major Special Foundation of Transgenic Plants in China grant number 2018ZX0800913B, the China Postdoctoral Science Foundation grant numbers 2017M620964 and 2018T110161, the Fundamental Research Funds for Central Non-profit Scientific Institution grant number 1610392019004, and the Innovation Project of Chinese Academy of Agricultural Sciences.

REFERENCES

Abts, W., Vandenbussche, B., De Proft, M. P., and Van de Poel, B. (2017). The role of auxin-ethylene crosstalk in orchestrating primary root elongation in sugar beet. *Front. Plant Sci.* 8:444. doi: 10.3389/fpls.2017.00444

Achard, P., Gusti, A., Cheminant, S., Alioua, M., Dhondt, S., Coppens, F., et al. (2009). Gibberellin signaling controls cell proliferation rate in *Arabidopsis*. *Curr. Biol.* 19, 1188–1193. doi: 10.1016/j.cub.2009.05.059

Achard, P., Vriezen, W. H., Van Der Straeten, D., and Harberd, N. P. (2003). Ethylene regulates *Arabidopsis* development *via* the modulation of DELLA protein growth repressor function. *Plant Cell* 15, 2816–2825. doi: 10.1105/tpc.015685

Alonso, J. M., Hirayama, T., Roman, G., Nourizadeh, S., and Ecker, J. R. (1999). EIN2, a bifunctional transducer of ethylene and stress responses in *Arabidopsis*. *Science* 284, 2148–2152.

Alonso, J. M., Stepanova, A. N., Solano, R., Wisman, E., Ferrari, S., Ausubel, F. M., et al. (2003). Five components of the ethylene-response pathway identified in a screen for weak ethyleneinsensitive mutants in *Arabidopsis*. *Proc. Natl. Acad. Sci. USA* 100, 2992–2997. doi: 10.1073/pnas.0438070100

Beaudoin, N., Serizet, C., Gosti, F., and Giraudat, J. (2000). Interactions between abscisic acid and ethylene signaling cascades. *Plant Cell* 12, 1103–1115. doi: 10.1105/tpc.12.7.1103

Cary, A. J., Liu, W. N., and Howell, S. H. (1995). Cytokinin action is coupled to ethylene in its effects on the inhibition of root and hypocotyl elongation in *Arabidopsis thaliana* seedlings. *Plant Physiol.* 107, 1075–1082. doi: 10.1104/pp.107.4.1075

Chae, H. S., Faure, F., and Kieber, J. J. (2003). The eto1, eto2, and eto3 mutations and cytokinin treatment increase ethylene biosynthesis in *Arabidopsis* by increasing the stability of ACS protein. *Plant Cell* 15, 545–559. doi: 10.1105/tpc.006882

Chao, Q. M., Rothenberg, M., Solano, R., Roman, G., Terzaghi, W., and Ecker, J. R. (1997). Activation of the ethylene gas response pathway in *Arabidopsis* by the nuclear protein ETHYLENE-INSENSITIVE3 and related proteins. *Cell* 89, 1133–1144. doi: 10.1016/S0092-8674(00)80300-1

Chen, H., Ma, B., Zhou, Y., He, S. J., Tang, S. Y., Lu, X., et al. (2018). E3 ubiquitin ligase SOR1 regulates ethylene response in rice root by modulating stability of aux/IAA protein. *Proc. Natl. Acad. Sci. USA* 115, 4513–4518. doi: 10.1073/pnas.1719387115

Cheng, W. H., Chiang, M. H., Hwang, S. G., and Lin, P. C. (2009). Antagonism between abscisic acid and ethylene in *Arabidopsis* acts in parallel with the reciprocal regulation of their metabolism and signaling pathways. *Plant Mol. Biol.* 71, 61–80. doi: 10.1007/s11103-009-9509-7

Clouse, S. D., Langford, M., and McMorris, T. C. (1996). A brassinosteroid-insensitive mutant in *Arabidopsis thaliana* exhibits multiple defects in growth and development. *Plant Physiol.* 111, 671–678. doi: 10.1104/pp.111.3.671

Daviere, J. M., and Achard, P. (2013). Gibberellin signaling in plants. *Development* 140, 1147–1151. doi: 10.1242/dev.087650

De Smet, S., Cuypers, A., Vangronsveld, J., and Remans, T. (2015). Gene networks involved in hormonal control of root development in *Arabidopsis thaliana*: a framework for studying its disturbance by metal stress. *Int. J. Mol. Sci.* 16, 19195–19224. doi: 10.3390/ijms160819195

Denyer, T., Ma, X. L., Klesen, S., Scacchi, E., Nieselt, K., and Timmermans, M. C. P. (2019). Spatiotemporal developmental trajectories in the *Arabidopsis* root revealed using high-throughput single-cell RNA sequencing. *Dev. Cell* 48, 840–852. doi: 10.1016/j.devcel.2019.02.022

Dietrich, D., Pang, L., Kobayashi, A., Fozard, J. A., Boudolf, V., Bhosale, R., et al. (2017). Root hydrotropism is controlled via a cortex-specific growth mechanism. *Nat. Plants* 3, 17057. doi: 10.1038/nplants.2017.57

Fernandez-Calvo, P., Chini, A., Fernandez-Barbero, G., Chico, J. M., Gimenez-Ibanez, S., Geerinck, J., et al. (2011). The *Arabidopsis* bHLH transcription factors MYC3 and MYC4 are targets of JAZ repressors and act additively with MYC2 in the activation of jasmonate responses. *Plant Cell* 23, 701–715. doi: 10.1105/tpc.110.080788

Ghassemian, M., Nambara, E., Cutler, S., Kawaide, H., Kamiya, Y., and McCourt, P. (2000). Regulation of abscisic acid signaling by the ethylene response pathway in arabidopsis. *Plant Cell* 12, 1117–1126. doi: 10.1105/tpc.12.7.1117

Guo, Q., Yoshida, Y., Major, I. T., Wang, K., Sugimoto, K., Kapali, G., et al. (2018). JAZ repressors of metabolic defense promote growth and reproductive fitness in *Arabidopsis*. *Proc. Natl. Acad. Sci. USA* 115, E10768–E10777. doi: 10.1073/pnas.1811828115

Hansen, M., Chae, H. S., and Kieber, J. J. (2009). Regulation of ACS protein stability by cytokinin and brassinosteroid. *Plant J.* 57, 606–614. doi: 10.1111/j.1365-313X.2008.03711.x

Harkey, A. F., Watkins, J. M., Olex, A. L., Dinapoli, K. T., Lewis, D. R., Fetrow, J. S., et al. (2018). Identification of transcriptional and receptor networks that control root responses to ethylene. *Plant Physiol.* 176, 2095–2118. doi: 10.1104/pp.17.00907

He, W. R., Brumos, J., Li, H. J., Ji, Y. S., Ke, M., Gong, X. Q., et al. (2011). A small-molecule screen identifies L-kynurenine as a competitive inhibitor of TAA1/TAR activity in ethylene-directed auxin biosynthesis and root growth in *Arabidopsis*. *Plant Cell* 23, 3944–3960. doi: 10.1105/tpc.111.089029

Heyman, J., Cools, T., Vandenbussche, F., Heyndrickx, K. S., Van Leene, J., Vercauteren, I., et al. (2013). ERF115 controls root quiescent center cell division and stem cell replenishment. *Science* 342, 860–863. doi: 10.1126/science.1240667

Hu, Y., Vandenbussche, F., and Van Der Straeten, D. (2017). Regulation of seedling growth by ethylene and the ethylene-auxin crosstalk. *Planta* 245, 467–489. doi: 10.1007/s00425-017-2651-6

Hua, J., and Meyerowitz, E. M. (1998). Ethylene responses are negatively regulated by a receptor gene family in *Arabidopsis thaliana*. *Cell* 94, 261–271. doi: 10.1016/S0092-8674(00)81425-7

Hua, J., Sakai, H., Nourizadeh, S., Chen, Q. G., Bleecker, A. B., Ecker, J. R., et al. (1998). EIN4 and ERS2 are members of the putative ethylene receptor gene family in *Arabidopsis*. *Plant Cell* 10, 1321–1332. doi: 10.1105/tpc.10.8.1321

Huang, H., Liu, B., Liu, L., and Song, S. (2017). Jasmonate action in plant growth and development. *J. Exp. Bot.* 68, 1349–1359. doi: 10.1093/jxb/erw495

Hung, J. H., and Weng, Z. (2017). Analysis of microarray and RNA-seq expression profiling data. *Cold Spring Harb. Protoc.* 2017, 191–196. doi: 10.1101/pdb.top093104

Ioio, R. D., Galinha, C., Fletcher, A. G., Grigg, S. P., Molnar, A., Willemsen, V., et al. (2012). A PHABULOSA/cytokinin feedback loop controls root growth in *Arabidopsis*. *Curr. Biol.* 22, 1699–1704. doi: 10.1016/j.cub.2012.07.005

Ju, C., Yoon, G. M., Shemansky, J. M., Lin, D. Y., Ying, Z. I., Chang, J., et al. (2012). CTR1 phosphorylates the central regulator EIN2 to control ethylene hormone signaling from the ER membrane to the nucleus in *Arabidopsis*. *Proc. Natl. Acad. Sci. USA* 109, 19486–19491. doi: 10.1073/pnas.1214848109

Katsir, L., Schilmiller, A. L., Staswick, P. E., He, S. Y., and Howe, G. A. (2008). COI1 is a critical component of a receptor for jasmonate and the bacterial virulence factor coronatine. *Proc. Natl. Acad. Sci. USA* 105, 7100–7105. doi: 10.1073/pnas.0802332105

Kieber, J. J., Rothenberg, M., Roman, G., Feldmann, K. A., and Ecker, J. R. (1993). CTR1, a negative regulator of the ethylene response pathway in *Arabidopsis*, encodes a member of the raf family of protein kinases. *Cell* 72, 427–441. doi: 10.1016/0092-8674(93)90119-B

Kushwah, S., Jones, A. M., and Laxmi, A. (2011). Cytokinin interplay with ethylene, auxin, and glucose signaling controls *Arabidopsis* seedling root directional growth. *Plant Physiol.* 156, 1851–1866. doi: 10.1104/pp.111.175794

Lee, L. Y., Hou, X., Fang, L., Fan, S., Kumar, P. P., and Yu, H. (2012). STUNTED mediates the control of cell proliferation by GA in *Arabidopsis*. *Development* 139, 1568–1576. doi: 10.1242/dev.079426

Lee, H. Y., and Yoon, G. M. (2018). Regulation of ethylene biosynthesis by phytohormones in etiolated rice (*Oryza sativa* L.) seedlings. *Mol. Cell* 41, 311–319. doi: 10.14348/molcells.2018.2224

Li, X., Chen, L., Forde, B. G., and Davies, W. J. (2017). The biphasic root growth response to abscisic acid in *Arabidopsis* involves interaction with ethylene and auxin signalling pathways. *Front. Plant Sci.* 8:1493. doi: 10.3389/fpls.2017.01493

Li, J., Nagpal, P., Vitart, V., McMorris, T. C., and Chory, J. (1996). A role for brassinosteroids in light-dependent development of *Arabidopsis*. *Science* 272, 398–401. doi: 10.1126/science.272.5260.398

Li, J. T., Zhao, Y., Chu, H. W., Wang, L. K., Fu, Y. R., Liu, P., et al. (2015). SHOEBOX modulates root meristem size in rice through dose-dependent effects of gibberellins on cell elongation and proliferation. *PLoS Genet.* 11:e1005464. doi: 10.1371/journal.pgen.1005464

Lim, S. H., Chang, S. C., Lee, J. S., Kim, S. K., and Kim, S. Y. (2002). Brassinosteroids affect ethylene production in the primary roots of maize (*Zea mays* L.). *J. Plant Biol.* 45, 148–153. doi: 10.1007/BF03030307

Liu, G. C., Gao, S., Tian, H. Y., Wu, W. W., Robert, H. S., and Ding, Z. J. (2016). Local transcriptional control of YUCCA regulates auxin promoted root-growth inhibition in response to aluminium stress in *Arabidopsis*. *PLoS Genet.* 12:e1006360. doi: 10.1371/journal.pgen.1006360

Liu, J. L., Moore, S., Chen, C. L., and Lindsey, K. (2017). Crosstalk complexities between auxin, cytokinin, and ethylene in *Arabidopsis* root development: from experiments to systems modeling, and back again. *Mol. Plant* 10, 1480–1496. doi: 10.1016/j.molp.2017.11.002

Ludwikow, A., Ciesla, A., Kasprowicz-Maluski, A., Mitula, F., Tajdel, M., Galganski, L., et al. (2014). *Arabidopsis* protein phosphatase 2C ABI1 interacts with type I ACC synthases and is involved in the regulation of ozone-induced ethylene biosynthesis. *Mol. Plant* 7, 960–976. doi: 10.1093/mp/ssu025

Luo, X., Chen, Z., Gao, J., and Gong, Z. (2014). Abscisic acid inhibits root growth in *Arabidopsis* through ethylene biosynthesis. *Plant J.* 79, 44–55. doi: 10.1111/tpj.12534

Luschnig, C., Gaxiola, R. A., Grisafi, P., and Fink, G. R. (1998). EIR1, a root-specific protein involved in auxin transport, is required for gravitropism in *Arabidopsis thaliana*. *Genes Dev.* 12, 2175–2187. doi: 10.1101/gad.12.14.2175

Lv, B., Tian, H., Zhang, F., Liu, J., Lu, S., Bai, M., et al. (2018). Brassinosteroids regulate root growth by controlling reactive oxygen species homeostasis and dual effect on ethylene synthesis in *Arabidopsis*. *PLoS Genet.* 14:e1007144. doi: 10.1371/journal.pgen.1007144

Ma, B., He, S. J., Duan, K. X., Yin, C. C., Chen, H., Yang, C., et al. (2013). Identification of rice ethylene-response mutants and characterization of MHZ7/OsEIN2 in distinct ethylene response and yield trait regulation. *Mol. Plant* 6, 1830–1848. doi: 10.1093/mp/sst087

Ma, B., Yin, C. C., He, S. J., Lu, X., Zhang, W. K., Lu, T. G., et al. (2014). Ethylene-induced inhibition of root growth requires abscisic acid function in rice (*Oryza sativa* L.) seedlings. *PLoS Genet.* 10:e1004701. doi: 10.1371/journal.pgen.1004701

Ma, B., Zhou, Y., Chen, H., He, S. J., Huang, Y. H., Zhao, J., et al. (2017). Membrane protein MHZ3 stabilizes OsEIN2 in rice by interacting with its Nramp-like domain. *Proc. Natl. Acad. Sci. USA* 115, 2520–2525. doi: 10.1073/pnas.1718377115

Mao, J. L., Miao, Z. Q., Wang, Z., Yu, L. H., Cai, X. T., and Xiang, C. B. (2016). *Arabidopsis* ERF1 mediates cross-talk between ethylene and auxin biosynthesis during primary root elongation by regulating ASA1expression. *PLoS Genet.* 12:e1005760. doi: 10.1371/journal.pgen.1005760

Mashiguchi, K., Tanaka, K., Sakai, T., Sugawara, S., Kawaide, H., Natsume, M., et al. (2011). The main auxin biosynthesis pathway in *Arabidopsis*. *Proc. Natl. Acad. Sci. USA* 108, 18512–18517. doi: 10.1073/pnas.1108434108

Mendez-Bravo, A., Ruiz-Herrera, L. F., Cruz-Ramirez, A., Guzman, P., Martinez-Trujillo, M., Ortiz-Castro, R., et al. (2019). CONSTITUTIVE TRIPLE RESPONSE1 and PIN2 act in a coordinate manner to support the indeterminate root growth and meristem cell proliferating activity in *Arabidopsis* seedlings. *Plant Sci.* 280, 175–186. doi: 10.1016/j.plantsci.2018.11.019

Merchante, C., and Stepanova, A. N. (2017). The triple response assay and its use to characterize ethylene mutants in *Arabidopsis*. *Methods Mol. Biol.* 1573, 163–209. doi: 10.1007/978-1-4939-6854-1_13

Miao, Z. Q., Zhao, P. X., Mao, J. L., Yu, L. H., Yuan, Y., Tang, H., et al. (2018). HOMEOBOX PROTEIN52 mediates the crosstalk between ethylene and auxin signaling during primary root elongation by modulating auxin transport-related gene expression. *Plant Cell* 30, 2761–2778. doi: 10.1105/tpc.18.00584

Mussig, C., Shin, G. H., and Altmann, T. (2003). Brassinosteroids promote root growth in *Arabidopsis*. *Plant Physiol.* 133, 1261–1271. doi: 10.1104/pp.103.028662

Ni, J., Shen, Y., Zhang, Y., and Wu, P. (2014). Definition and stabilisation of the quiescent Centre in rice roots. *Plant Biol.* 16, 1014–1019. doi: 10.1111/plb.12138

Oh, E., Zhu, J. Y., and Wang, Z. Y. (2012). Interaction between BZR1 and PIF4 integrates brassinosteroid and environmental responses. *Nat. Cell Biol.* 14, 802–864. doi: 10.1038/ncb2545

Ortega-Martinez, O., Pernas, M., Carol, R. J., and Dolan, L. (2007). Ethylene modulates stem cell division in the *Arabidopsis thaliana* root. *Science* 317, 507–510. doi: 10.1126/science.1143409

Pacifici, E., Polverari, L., and Sabatini, S. (2015). Plant hormone cross-talk: the pivot of root growth. *J. Exp. Bot.* 66, 1113–1121. doi: 10.1093/jxb/eru534

Peng, J. R., Carol, P., Richards, D. E., King, K. E., Cowling, R. J., Murphy, G. P., et al. (1997). The *Arabidopsis* GAI gene defines a signaling pathway that negatively regulates gibberellin responses. *Genes Dev.* 11, 3194–3205. doi: 10.1101/gad.11.23.3194

Qi, T., Huang, H., Song, S., and Xie, D. (2015). Regulation of jasmonate-mediated stamen development and seed production by a bHLH-MYB complex in *Arabidopsis*. *Plant Cell* 27, 1620–1633. doi: 10.1105/tpc.15.00116

Qiao, H., Chang, K. N., Yazaki, J., and Ecker, J. R. (2009). Interplay between ethylene, ETP1/ETP2 F-box proteins, and degradation of EIN2 triggers ethylene responses in *Arabidopsis*. *Genes Dev.* 23, 512–521. doi: 10.1101/gad.1765709

Qiao, H., Shen, Z., Huang, S. S., Schmitz, R. J., Urich, M. A., Briggs, S. P., et al. (2012). Processing and subcellular trafficking of ER-tethered EIN2 control response to ethylene gas. *Science* 338, 390–393. doi: 10.1126/science.1225974

Qin, H., and Huang, R. (2018). Auxin controlled by ethylene steers root development. *Int. J. Mol. Sci.* 19:3656. doi: 10.3390/ijms19113656

Qin, H., Zhang, Z., Wang, J., Chen, X., Wei, P., and Huang, R. (2017). The activation of OsEIL1 on YUC8 transcription and auxin biosynthesis is required for ethylene-inhibited root elongation in rice early seedling development. *PLoS Genet.* 13:e1006955. doi: 10.1371/journal.pgen.1006955

Richards, D. E., King, K. E., Ait-ali, T., and Harberd, N. P. (2001). How gibberellin regulates plant growth and development: a molecular genetic analysis of gibberellin signaling. *Annu. Rev. Plant Physiol.* 52, 67–88. doi: 10.1146/annurev.arplant.52.1.67

Riefler, M., Novak, O., Strnad, M., and Schmülling, T. (2006). *Arabidopsis* cytokinin receptor mutants reveal functions in shoot growth, leaf senescence, seed size, germination, root development, and cytokinin metabolism. *Plant Cell* 18, 40–54. doi: 10.1105/tpc.105.037796

Rowe, J. H., Topping, J. F., Liu, J. L., and Lindsey, K. (2016). Abscisic acid regulates root growth under osmotic stress conditions *via* an interacting hormonal network with cytokinin, ethylene and auxin. *New Phytol.* 211, 225–239. doi: 10.1111/nph.13882

Ruzicka, K., Ljung, K., Vanneste, S., Podhorska, R., Beeckman, T., Friml, J., et al. (2007). Ethylene regulates root growth through effects on auxin biosynthesis and transport-dependent auxin distribution. *Plant Cell* 19, 2197–2212. doi: 10.1105/tpc.107.052126

Salehin, M., and Estelle, M. (2015). Ethylene prunes translation. *Cell* 163, 543–544. doi: 10.1016/j.cell.2015.10.032

Serek, M., Tamari, G., Sisler, E. C., and Borochov, A. (1995). Inhibition of ethylene-induced cellular senescence symptoms by 1-methylcyclopropene, a new inhibitor of ethylene action. *Physiol. Plant.* 94, 229–232. doi: 10.1111/j.1399-3054.1995.tb05305.x

Silverstone, A. L., Ciampaglio, C. N., and Sun, T. (1998). The *Arabidopsis* RGA gene encodes a transcriptional regulator repressing the gibberellin signal transduction pathway. *Plant Cell* 10, 155–169. doi: 10.1105/tpc.10.2.155

Solano, R., Stepanova, A., Chao, Q., and Ecker, J. R. (1998). Nuclear events in ethylene signaling: a transcriptional cascade mediated by ETHYLENE-INSENSITIVE3 and ETHYLENE-RESPONSE-FACTOR1. *Genes Dev.* 12, 3703–3714. doi: 10.1101/gad.12.23.3703

Stepanova, A. N., Hoyt, J. M., Hamilton, A. A., and Alonso, J. M. (2005). A link between ethylene and auxin uncovered by the characterization of two root-specific ethylene-insensitive mutants in *Arabidopsis*. *Plant Cell* 17, 2230–2242. doi: 10.1105/tpc.105.033365

Stepanova, A. N., Robertson-Hoyt, J., Yun, J., Benavente, L. M., Xie, D. Y., DoleZal, K., et al. (2008). TAA1-mediated auxin biosynthesis is essential for hormone crosstalk and plant development. *Cell* 133, 177–191. doi: 10.1016/j.cell.2008.01.047

Stepanova, A. N., Yun, J., Likhacheva, A. V., and Alonso, J. M. (2007). Multilevel interactions between ethylene and auxin in *Arabidopsis* roots. *Plant Cell* 19, 2169–2185. doi: 10.1105/tpc.107.052068

Street, I. H., Aman, S., Zubo, Y., Ramzan, A., Wang, X., Shakeel, S. N., et al. (2015). Ethylene inhibits cell proliferation of the *Arabidopsis* root meristem. *Plant Physiol.* 169, 338–350. doi: 10.1104/pp.15.00415

Sun, X., Li, Y., He, W., Ji, C., Xia, P., Wang, Y., et al. (2017). Pyrazinamide and derivatives block ethylene biosynthesis by inhibiting ACC oxidase. *Nat. Commun.* 8:15758. doi: 10.1038/ncomms15758

Sun, L. R., Wang, Y. B., He, S. B., and Hao, F. S. (2018). Mechanisms for abscisic acid inhibition of primary root growth. *Plant Signal. Behav.* 13:e1500069. doi: 10.1080/15592324.2018.1500069

Swarup, R., Perry, P., Hagenbeek, D., Van Der Straeten, D., Beemster, G. T., Sandberg, G., et al. (2007). Ethylene upregulates auxin biosynthesis in *Arabidopsis* seedlings to enhance inhibition of root cell elongation. *Plant Cell* 19, 2186–2196. doi: 10.1105/tpc.107.052100

Thines, B., Katsir, L., Melotto, M., Niu, Y., Mandaokar, A., Liu, G., et al. (2007). JAZ repressor proteins are targets of the SCF(COI1) complex during jasmonate signalling. *Nature* 448, 661–665. doi: 10.1038/nature05960

Thole, J. M., Beisner, E. R., Liu, J., Venkova, S. V., and Strader, L. C. (2014). Abscisic acid regulates root elongation through the activities of auxin and ethylene in *Arabidopsis thaliana*. *G3 – Genes Genom. Genet.* 4, 1259–1274. doi: 10.1534/g3.114.011080

Ubeda-Tomas, S., Federici, F., Casimiro, I., Beemster, G. T., Bhalerao, R., Swarup, R., et al. (2009). Gibberellin signaling in the endodermis controls *Arabidopsis* root meristem size. *Curr. Biol.* 19, 1194–1199. doi: 10.1016/j.cub.2009.06.023

Van de Poel, B., Smet, D., and Van Der Straeten, D. (2015). Ethylene and hormonal cross talk in vegetative growth and development. *Plant Physiol.* 169, 61–72. doi: 10.1104/pp.15.00724

Vaseva, I. I., Qudeimat, E., Potuschak, T., Du, Y., Genschik, P., Vandenbussche, F., et al. (2018). The plant hormone ethylene restricts *Arabidopsis* growth *via* the epidermis. *Proc. Natl. Acad. Sci. USA* 115, E4130–E4139. doi: 10.1073/pnas.1717649115

Vaseva, I. I., Vandenbussche, F., Simon, D., Vissenberg, K., and Van Der Straeten, D. (2016). Cell type specificity of plant hormonal signals: case studies and reflections on ethylene. *Russ. J. Plant Physiol.* 63, 577–586. doi: 10.1134/S1021443716050149

Vogel, J. P., Woeste, K. E., Theologis, A., and Kieber, J. J. (1998). Recessive and dominant mutations in the ethylene biosynthetic gene ACS5 of *Arabidopsis* confer cytokinin insensitivity and ethylene overproduction, respectively. *Proc. Natl. Acad. Sci. USA* 95, 4766–4771. doi: 10.1073/pnas.95.8.4766

Wasternack, C., and Hause, B. (2013). Jasmonates: biosynthesis, perception, signal transduction and action in plant stress response, growth and development. An update to the 2007 review in annals of botany. *Ann. Bot.* 111, 1021–1058. doi: 10.1093/aob/mct067

Wen, X., Zhang, C. L., Ji, Y. S., Zhao, Q., He, W. R., An, F. Y., et al. (2012). Activation of ethylene signaling is mediated by nuclear translocation of the cleaved EIN2 carboxyl terminus. *Cell Res.* 22, 1613–1616. doi: 10.1038/cr.2012.145

Woeste, K. E., Ye, C., and Kieber, J. J. (1999). Two *Arabidopsis* mutants that overproduce ethylene are affected in the posttranscriptional regulation of 1-aminocyclopropane-1-carboxylic acid synthase. *Plant Physiol.* 119, 521–529. doi: 10.1104/pp.119.2.521

Yang, Z. B., He, C. M., Ma, Y. Q., Herde, M., and Ding, Z. J. (2017). Jasmonic acid enhances Al-induced root growth inhibition. *Plant Physiol.* 173, 1420–1433. doi: 10.1104/pp.16.01756

Yang, S. F., and Hoffman, N. E. (1984). Ethylene biosynthesis and its regulation in higher-plants. *Annu. Rev. Plant Physiol.* 35, 155–189. doi: 10.1146/annurev.pp.35.060184.001103

Yang, C., Ma, B., He, S. J., Xiong, Q., Duan, K. X., Yin, C. C., et al. (2015). MAOHUZI6/ETHYLENE INSENSITIVE3-LIKE1 and ETHYLENE INSENSITIVE3-LIKE2 regulate ethylene response of roots and coleoptiles and negatively affect salt tolerance in rice. *Plant Physiol.* 169, 148–165. doi: 10.1104/pp.15.00353

Yin, C. C., Ma, B., Collinge, D. P., Pogson, B. J., He, S. J., Xiong, Q., et al. (2015). Ethylene responses in rice roots and coleoptiles are differentially regulated by a carotenoid isomerase-mediated abscisic acid pathway. *Plant Cell* 27, 1061–1081. doi: 10.1105/tpc.15.00080

Yin, Y., Wang, Z. Y., Mora-Garcia, S., Li, J., Yoshida, S., Asami, T., et al. (2002). BES1 accumulates in the nucleus in response to brassinosteroids to regulate gene expression and promote stem elongation. *Cell* 109, 181–191. doi: 10.1016/S0092-8674(02)00721-3

Yu, X., Li, L., Zola, J., Aluru, M., Ye, H., Foudree, A., et al. (2011). A brassinosteroid transcriptional network revealed by genome-wide identification of BESI target genes in *Arabidopsis thaliana*. *Plant J.* 65, 634–646. doi: 10.1111/j.1365-313X.2010.04449.x

Zdarska, M., Zatloukalova, P., Benitez, M., Sedo, O., Potesil, D., Novak, O., et al. (2013). Proteome analysis in *Arabidopsis* reveals shoot- and root-specific targets of cytokinin action and differential regulation of hormonal homeostasis. *Plant Physiol.* 161, 918–930. doi: 10.1104/pp.112.202853

Zemlyanskaya, E. V., Omelyanchuk, N. A., Ubogoeva, E. V., and Mironova, V. V. (2018). Deciphering auxin-ethylene crosstalk at a systems level. *Int. J. Mol. Sci.* 19:E4060. doi: 10.3390/ijms19124060

Zheng, H., Pan, X., Deng, Y., Wu, H., Liu, P., and Li, X. (2016). AtOPR3 specifically inhibits primary root growth in *Arabidopsis* under phosphate deficiency. *Sci. Rep.* 6:24778. doi: 10.1038/srep24778

Zhu, Z., An, F., Feng, Y., Li, P., Xue, L., Mu, A., et al. (2011). Derepression of ethylene-stabilized transcription factors (EIN3/EIL1) mediates jasmonate and ethylene signaling synergy in *Arabidopsis*. *Proc. Natl. Acad. Sci. USA* 108, 12539–12544. doi: 10.1073/pnas.1103959108

Zhu, C. H., Gan, L. J., Shen, Z. G., and Xia, K. (2006). Interactions between jasmonates and ethylene in the regulation of root hair development in *Arabidopsis*. *J. Exp. Bot.* 57, 1299–1308. doi: 10.1093/jxb/erj103

Ziegenhain, C., Vieth, B., Parekh, S., Reinius, B., Guillaumet-Adkins, A., Smets, M., et al. (2017). Comparative analysis of single-cell RNA sequencing methods. *Mol. Cell* 65, 631–643. doi: 10.1016/j.molcel.2017.01.023

Zou, X., Shao, J., Wang, Q., Chen, P., Zhu, Y., and Yin, C. (2018). Supraoptimal cytokinin content inhibits rice seminal root growth by reducing root meristem size and cell length *via* increased ethylene content. *Int. J. Mol. Sci.* 19:E4051. doi: 10.3390/ijms19124051

Conflict of Interest Statement: The authors declare that the research was conducted in the absence of any commercial or financial relationships that could be construed as a potential conflict of interest.

frontiers in Plant Science

ORIGINAL RESEARCH
published: 30 July 2019
doi: 10.3389/fpls.2019.00950

Cyanobacteria Respond to Low Levels of Ethylene

Cidney J. Allen[1], Randy F. Lacey[1†], Alixandri B. Binder Bickford[2], C. Payton Beshears[1], Christopher J. Gilmartin[3] and Brad M. Binder[1]*

[1] Department of Biochemistry & Cellular and Molecular Biology, The University of Tennessee, Knoxville, Knoxville, TN, United States, [2] West High School, Knoxville, TN, United States, [3] Farragut High School, Knoxville, TN, United States

Ethylene is a gas that has long been known to act as a plant hormone. We recently showed that a cyanobacterium, *Synechocystis* sp. PCC 6803 (Synechocystis) contains an ethylene receptor (SynEtr1) that regulates cell surface and extracellular components leading to altered phototaxis and biofilm formation. To determine whether other cyanobacteria respond to ethylene, we examined the effects of exogenous ethylene on phototaxis of the filamentous cyanobacterium, *Geitlerinema* sp. PCC 7105 (Geitlerinema). A search of the Geitlerinema genome suggests that two genes encode proteins that contain an ethylene binding domain and Geitlerinema cells have previously been shown to bind ethylene. We call these genes *GeiEtr1* and *GeiEtr2* and show that in air both are expressed. Treatment with ethylene decreases the abundance of *GeiEtr1* transcripts. Treatment of Geitlerinema with 1000 nL L^{-1} ethylene affected the phototaxis response to white light as well as monochromatic red light, but not blue or green light. This is in contrast to Synechocystis where we previously found ethylene affected phototaxis to all three colors. We also demonstrate that application of ethylene down to 8 nL L^{-1} stimulates phototaxis of both cyanobacteria as well as biofilm formation of Synechocystis. We formerly demonstrated that the transcript levels of *slr1214* and *CsiR1* in Synechocystis are reduced by treatment with 1000 nL L^{-1} ethylene. Here we show that application of ethylene down to 1 nL L^{-1} causes a reduction in *CsiR1* abundance. This is below the threshold for most ethylene responses documented in plants. By contrast, *slr1214* is unaffected by this low level of ethylene and only shows a reduction in transcript abundance at the highest ethylene level used. Thus, cyanobacteria are very sensitive to ethylene. However, the dose-binding characteristics of ethylene binding to Geitlerinema and Synechocystis cells as well as to the ethylene binding domain of SynEtr1 heterologously expressed in yeast, are similar to what has been reported for plants and exogenously expressed ethylene receptors from plants. These data are consistent with a model where signal amplification is occurring at the level of the receptors.

Keywords: cyanobacteria, ethylene receptor, ethylene binding, Synechocystis, Geitlerinema, phototaxis, biofilm

OPEN ACCESS

Edited by:
Caren Chang,
University of Maryland, College Park, United States

Reviewed by:
Annegret Wilde,
University of Freiburg, Germany
Shangwei Zhong,
Peking University, China

****Correspondence:***
Brad M. Binder
bbinder@utk.edu

†Present address:
Randy F. Lacey,
Department of Microbiology and Biochemistry, School of Biological Sciences, Victoria University of Wellington, Wellington, NZ, United States

Specialty section:
This article was submitted to Plant Physiology, a section of the journal Frontiers in Plant Science

Received: *25 March 2019*
Accepted: *08 July 2019*
Published: *30 July 2019*

Citation:
Allen CJ, Lacey RF, Binder Bickford AB, Beshears CP, Gilmartin CJ and Binder BM (2019) Cyanobacteria Respond to Low Levels of Ethylene. Front. Plant Sci. 10:950. doi: 10.3389/fpls.2019.00950

INTRODUCTION

Ethylene is an important plant hormone that affects plant growth, development, and responses to many stresses (Mattoo and Suttle, 1991; Abeles et al., 1992). Ethylene receptors in plants have been studied for many decades and much is known about how they bind ethylene and signal to downstream signaling proteins (Merchante et al., 2013; Lacey and Binder, 2014; Bakshi et al., 2015).

These receptors, as well as several other plant hormone receptors, have homology to bacterial two-component receptors that signal via a histidine autophosphorylation followed by phosphotransfer to downstream targets (Chang et al., 1993; Schaller et al., 2011; Kabbara et al., 2018). Several research groups have proposed that plants acquired these two-component-like receptors from the cyanobacterium that gave rise to chloroplasts where the free-living cyanobacterium became an endosymbiont and most of the bacterial genome was acquired by the host cell (Kehoe and Grossman, 1996; Martin et al., 2002; Mount and Chang, 2002; Timmis et al., 2004; Schaller et al., 2011). In support of this, some cyanobacteria contain predicted ethylene binding proteins and several cyanobacteria species have been documented to bind ethylene (Rodriguez et al., 1999; Mount and Chang, 2002; Wang et al., 2006).

Many microorganisms respond to ethylene (Abeles et al., 1992; Bakshi and Binder, 2018). However, it was only recently that a non-plant species, *Synechocystis* sp. PCC 6803 (hereafter referred to as Synechocystis), was documented to contain a functional ethylene receptor (Lacey and Binder, 2016). In this unicellular cyanobacterium, the receptor is encoded by the *slr1212* gene locus and has been variously referred to as *Ethylene response 1* (*SynEtr1*) (Kaneko et al., 1996; Ulijasz et al., 2009; Lacey and Binder, 2016), *His-kinase44* (*Hik44*) (Los et al., 2008), *Positive phototaxisA* (Narikawa et al., 2011) (*PixA*), and *UV intensity response Sensor* (*UirS*) (Song et al., 2011; Ramakrishnan and Tabor, 2016). It is the only gene in the Synechocystis genome predicted to encode a protein with an ethylene binding domain. The protein contains a functional ethylene binding domain at the N-terminus followed by a phytochrome-like domain known as a cyanobacteriochrome, and a his-kinase domain at the C-terminus (Yoshihara et al., 2004; Ikeuchi and Ishizuka, 2008; Ulijasz et al., 2009; Narikawa et al., 2011; Song et al., 2011; Lacey and Binder, 2016; Ramakrishnan and Tabor, 2016). Thus, this is a receptor for both light and ethylene. Various studies have also delineated components of the signaling pathway downstream of the receptor (Narikawa et al., 2011; Song et al., 2011; Lacey and Binder, 2016; Ramakrishnan and Tabor, 2016). From these studies a model for light signal transduction from SynEtr1 has developed (Ramakrishnan and Tabor, 2016) where UV-A light stimulates histidine autophosphorylation followed by phosphotransfer to a conserved aspartate on the slr1213 response regulator protein. The phosphorylated slr1213 enhances the transcription of a small, non-coding RNA called *CsiR1* and *slr1214* which encodes a second response regulator protein. In contrast to UV-A light, application of 1000 nL L^{-1} ethylene reduces the transcript abundance of *CsiR1* and *slr1214* (Lacey et al., 2018), but it is not known whether or not this occurs via regulation of SynEtr1 histidine kinase activity. Ethylene also causes changes in the cell surface of Synechocystis cells leading to enhanced biofilm formation, more directed motility of single cells in response to directional light, and faster phototaxis when the cells aggregate (Lacey and Binder, 2016; Kuchmina et al., 2017; Lacey et al., 2018).

Many additional putative ethylene receptors have been identified in a wide array of bacteria and several non-plant eukaryotes (Mount and Chang, 2002; Wang et al., 2006; Lacey and Binder, 2016; Hérivaux et al., 2017; Kabbara et al., 2018), but it remains to be determined whether or not other cyanobacteria respond to ethylene. With this in mind we studied ethylene responses in *Geitlerinema* sp. PCC 7105. This was originally named *Oscillatoria* sp. PCC 7105 (Rippka et al., 1979) and is referred to as Geitlerinema in this paper. This is a filamentous cyanobacterium that binds ethylene and is predicted to contain two ethylene receptors (Wang et al., 2006; Lacey and Binder, 2016). Here we document that ethylene alters phototaxis behavior of Geitlerinema and Synechocystis at low concentrations. These concentrations are below the threshold for most, but not all ethylene responses in plants. However, ethylene dose-binding experiments on Geitlerinema, Synechocystis, and the heterologously expressed ethylene binding domain of SynEtr1 indicate that the affinity of ethylene to the cyanobacterial receptors is similar to what has been reported in plants. Thus, we predict that signal amplification occurs at the level of the receptors.

MATERIALS AND METHODS

Strains and Growth Conditions

Geitlerinema PCC 7105 cells were from the laboratory of Anthony Bleecker and were originally obtained from the American Type Culture Collection (stock ATCC29120). *Synechocystis* PCC 6803 cells were obtained from the Pasteur Institute. Liquid cultures of both were maintained in BG-11 medium (Rippka et al., 1979).

Phototaxis Assays

Phototaxis assays were conducted at 20–21°C in flow-through chambers with continuous gas flow with either ethylene-free air or air with ethylene at the concentrations indicated in each figure. All assays were replicated at least three times.

Phototaxis assays for Synechocystis were conducted for 4 days (d) as previously described using directional white light at a fluence rate of 30 μmol m^{-2} s^{-1} (Lacey and Binder, 2016). These assays were quantified by measuring the maximum distance moved by cells from the leading edge of the colony at the start of the assay. For phototaxis assays on Geitlerinema, cells were placed on 0.4% (v/v) agar BG-11 plates and allowed to grow several days under white fluorescent lights. Efforts were made to start with similar quantities of cells. However, the filamentous nature of this species made it difficult to start with identical numbers of cells. A similar problem has been noted by others studying another filamentous cyanobacteria, *Nostoc punctiforme* (Campbell et al., 2015). The plates were then wrapped with aluminum foil except for a 13 × 13 mm square above the location next to the cells. This area was illuminated from above with white fluorescent lights (42 μmol m^{-2} s^{-1}) for 5–7 days to allow cells to move into the illuminated area and grow. At this time, we used one of two methods to examine phototaxis. In some assays, we used methods modified from Biddanda et al. (2015) and illustrated

in **Supplementary Figure 1A**. In this method, the first opening above the cells was blocked, a second opening made 25 mm away, and illumination provided from above. Unless otherwise specified, cells were then allowed to respond to light for 2–5 d in response to 42 μmol m^{-2} s^{-1} of white, or 16 μmol m^{-2} s^{-1} of blue (λ_{max} = 462 nm), green (λ_{max} = 528 nm), or red (λ_{max} = 672 nm) light. In other assays, the Geitlerinema cells were exposed to directional white light using methods modified from Campbell et al. (2015). In this method, each petri dish was masked with black paper except for a 5 mm slit at one edge of the plate. The cells were then exposed for 24 h to directional white light through the slit at a fluence rate of 30 μmol m^{-2} s^{-1}. The distance moved toward the light was then quantified by measuring the maximum distance moved by cells from the leading edge of the colony at the start of the assay. For these experiments, white lighting was provided by an LED light panel and monochromatic lighting provided by LED arrays from Quantum Devices Inc. (Barneveld, WI, United States). For both species, images were acquired with a flatbed scanner. In control experiments to examine the effect of these wavelengths of light on growth, we allowed filaments to become established on the BG-11 agar under white light for 1 d, and then exposed the entire plate to either white, red, green, or blue light at the same levels of illumination as used in phototaxis assays. We then scanned the plates 2 d later and used ImageJ to determine the optical density of the colonies.

For polychromatic light experiments, cells were placed on 0.4% (v/v) agar BG-11 plates and exposed to polychromatic light from above the cells for 4 d (**Supplementary Figure 1B**). Polychromatic light was provided by white light from a slide projector focused onto a prism and images were acquired with a Canon EOS Rebel Xsi.

Biofilm Assays

Biofilm formation by Synechocystis cells was assayed with modifications to the methods of Agostoni et al. (2016). For this, cells were grown in BG-11 liquid culture to a density of OD_{750} = 0.5 and 15 mL placed into a 250 mL flask. Samples were then incubated in flow through chambers with ethylene-free air or various dosages of ethylene for 5 d under white light (30 μmol m^{-2} s^{-1}) provided by an LED panel. Non-adhered cells were removed by aspiration and 0.5% (w/v) crystal violet added for 2 min to stain the cells that remain attached. The stain was removed and the cells washed three times with 15 mL of phosphate-buffered saline. The cells were then resuspended in 10 mL of 95% (v/v) ethanol for 30 min, and the OD_{588} measured. All assays were replicated at least three times.

RNA Isolation, Complementary DNA Synthesis, and Quantitative Real-Time Reverse Transcriptase (qRT)-PCR

For Synechocystis, cells were exposed to phototaxis conditions for 1 d in ethylene-free air at which time they were either kept in ethylene-free air or treated with ethylene at concentrations ranging from 1 to 1000 nL L^{-1} for 4 h using methods previously described (Lacey et al., 2018). Briefly, ethylene was injected into sealed chambers to yield the designated concentration. Cells were harvested off the agar 4 h later for RNA isolation and further processing. For Geitlerinema, cells were maintained in non-directional light and exposed to ethylene-free air or 1000 nL L^{-1} ethylene for 4 h after which the cells were harvested with forceps. To make harvesting of cells easier, cells were kept in Petri dishes filled with 30 mL BG-11 media. For both species, RNA isolation, complementary DNA synthesis, and qRT-PCR were carried out as previously described (Lacey and Binder, 2016). Primers used for *SynEtr1*, *CsiR1*, *slr1213*, and *slr1214* from Synechocystis have previously been described (Lacey et al., 2018). Synechocystis data were normalized to the *tryptophan synthase gene* (*TrpA*) gene (Zhang et al., 2008) and then to levels of each gene transcript in air-treated controls.

In Geitlerinema, we first determined which housekeeping gene to use. For this, we analyzed the RNA abundance of candidate genes in air- and ethylene-treated cells using qRT-PCR. This was normalized to total RNA (**Supplementary Figure 2**). From this we determined that the abundance of these transcripts was not significantly altered by application of 1000 nL L^{-1} ethylene. We chose a gene (gene locus WP_026097408) annotated as a *tRNA pseudouridine synthase* (*TruB*) as our housekeeping gene because its levels were very similar in air versus ethylene. Thus, we normalized the RNA abundance of *GeiEtr1* and *GeiEtr2* to the abundance of *TruB* and then to air-treated controls. Primers for qPCR were 5′-ATGTGGGAAACTGTCAAAACTTTATTTT-3′ (forward) and 5′-CCGAAGCCTGCTGGGTAA-3′ (reverse) for *GeiEtr1*, 5′-ATGTGGACCGCTCTCGAATCGCTCC-3′ (forward) and 5′-CCCGAACGAAATCCATGACTGCTGA-3′ (reverse) for *GeiEtr2*, and 5′-ATGGCGGGCTTTCTGAACCTGG-3′ (forward) and 5′-CCGAAAATGGTGTTTGATCGC-3′ for *TruB*.

Quantitative PCR was performed as described in Lacey and Binder (2016). All data represent the average ± SEM from three technical replicates done on three biological replicates.

Ethylene Binding Assays

Ethylene binding assays were conducted on Geitlerinema and Synechocystis cells as previously described for bacteria (Wang et al., 2006) and on the ethylene binding domain of SynEtr1 fused to glutathione-*S*-transferase (SynEtr1[1-130]GST) expressed in *Pichia pastoris* as described by Lacey and Binder (2016). In control samples, specific ethylene binding at 1000 nL L^{-1} ethylene to Synechocystis cells lacking SynEtr1 (ΔSynEtr1) and *P. pastoris* with empty vector (pPICZ) was determined. The ΔSynEtr1 Synechocystis have been previously described (Lacey and Binder, 2016). Assays were conducted using $^{14}C_2H_4$ custom synthesized by ViTrax (Placentia, CA, United States). Briefly, experiments were conducted on 0.8 (wet weight) of bacteria cells placed on Whatman No. 1 paper filters or 1 g (wet weight) *P. pastoris* cells placed on glass filters. Samples were then treated with either $^{14}C_2H_4$ at the indicated concentrations to determine total binding or $^{14}C_2H_4$ plus 1000-fold excess $^{12}C_2H_4$ to determine non-specific background

binding. Specific binding was calculated by subtracting non-specific binding from total binding. All experiments were done in triplicate.

RESULTS

Geitlerinema Has Two Putative Ethylene Receptors

The sequenced Geitlerinema genome contains two genes predicted to encode proteins with an ethylene-binding domain (see the **Supplementary Data** for full DNA and amino acid sequences). We are calling them Geitlerinema *Ethylene response1* (*GeiEtr1*) and *GeiEtr2* following the nomenclature for the first ethylene receptor discovered, *AtETR1* from *Arabidopsis thaliana*. *GeiEtr1* is at DNA coordinates 3597293–3599260 and is predicted to encode a protein 655 amino acids long, whereas *GeiEtr2* is at DNA coordinates 3147733–3150810 and is predicted to encode a 1025 amino acid long protein. An examination of the genome neighborhoods of these two genes (**Supplementary Figure 3**) reveals one gene grouped with *GeiEtr1* predicted to encode a lycopene cyclase and two genes grouped with *GeiEtr2* where one is predicted to encode a protein with a diguanylate cyclase domain and the other annotated as a starch phosphorylase.

The predicted ethylene binding domain of GeiEtr1 shares 43% homology and GeiEtr2 41% homology with the binding domain of the canonical ethylene receptor, AtETR1. An alignment of the ethylene domains from GeiEtr1 and GeiEtr2 with the ethylene receptor from Synechocystis and the five receptors from *A. thaliana* (AtETR1, AtETR2), Ethylene Response Sensor1 (AtERS1), AtERS2, and Ethylene Insensitive4 (AtEIN4) reveals that both proteins from Geitlerinema have retained many amino acids in common with functional ethylene receptors. Seven amino acid residues are required for ethylene binding to AtETR1 (Rodriguez et al., 1999; Wang et al., 2006). All seven of these amino acids are conserved in GeiEtr1 and GeiEtr2 suggesting that they too can bind ethylene (**Figure 1A**). Consistent with previous research (Hua et al., 1998), this alignment also shows that the subfamily 1 receptors from *A. thaliana*, AtETR1 and AtERS1, have a short N-terminus extension (approximately 19 amino acids) ahead of the ethylene binding domain, whereas there is a longer hydrophobic stretch of amino acids (approximately 50 amino acids) in the subfamily 2 receptors, AtERS2, AtETR2, and AtEIN4. The proteins from cyanobacteria have an N-terminal stretch intermediate in length (approximately 30 amino acids) between the subfamily 1 and 2 receptors. It is also interesting to note that whereas the plant receptors have two cysteines near the N-terminus that form disulfide bonds to form stable homodimers (Schaller et al., 1995; Hall et al., 2000), the cyanobacteria proteins only have one cysteine in this region of the protein that may fulfill the same function. An unrooted cladogram based on the amino acid sequences of the ethylene binding domains of these seven proteins shows that the ethylene receptors from plants fall into two subfamilies with the bacterial receptors forming a distinct third subfamily (**Figure 1B**), consistent with a previous analysis (Wang et al., 2006). The predicted domain structure of GeiEtr1 is similar to AtERS1 and AtERS2 where there is a N-terminal ethylene binding domain followed by a GAF (for cGMP-specific phosphodiesterase, adenyl cyclases, and FhlA) domain and a C-terminal kinase domain, but no receiver domain (**Figure 1C**). By contrast, GeiEtr2 has additional domains with a PAS (for Per-Arnt-Sim) and PAC domain between the ethylene binding and GAF domains as well as a C-terminal receiver domain. The arrangement of PAS, PAC, and GAF domains in GeiEtr2 is reminiscent of the domain arrangement of SynEtr1 that functions as a photoreceptor.

We were curious to know if either receptor is expressed and whether or not ethylene affected the transcript abundance of either gene. To answer these questions we extracted RNA from samples kept in air versus 1000 nL L^{-1} ethylene for 4 h. We chose this dosage of ethylene because it is commonly used in plant research and has been shown to affect the physiology and growth of Synechocystis (Lacey and Binder, 2016; Henry et al., 2017) and causes wide-spread changes in the transcriptome of Synechocystis (Lacey et al., 2018). Also, we have previously found that 1000 nL L^{-1} ethylene alters transcript abundance of various genes in Synechocystis cells within 4 h (Lacey et al., 2018). From this analysis we observed that both *GeiEtr1* and *GeiEtr2* are expressed in air. Upon application of ethylene, *GeiEtr1* abundance decreased, but the abundance of *GeiEtr2* showed no statistically significant change (**Figure 1D**).

Ethylene Alters Phototaxis of Geitlerinema

We have previously shown that ethylene accelerates phototaxis of Synechocystis toward white light (Lacey and Binder, 2016). We therefore examined the effect of ethylene on phototaxis of Geitlerinema. Because this is a filamentous cyanobacterium, we adapted the methods of Biddanda et al. (2015) to conduct these assays where the bacteria were exposed to an area of illumination at a distance from their starting location (**Supplementary Figure 1A**). In air, cells displayed phototaxis movement in response to white light where most, but not all cells, moved to the new position of illumination after 5 d (**Supplementary Figure 4**). Given this result we conducted phototaxis assays toward white light for 5 d to determine whether application of ethylene increased or decreased movement. Interestingly, the application of 1000 nL L^{-1} ethylene altered the response to white light so that the cells formed a ring outside the area of illumination (**Figure 2A**). To determine if this ring of cells is due to higher light sensitivity causing the cells to avoid the area with the highest light levels, we conducted these assays at a 10-fold dimmer light intensity. At this dimmer light level, the cells move into the entire area of illumination so that no ring of cells is present (**Supplementary Figure 5**) suggesting that ethylene sensitizes Geitlerinema to higher light intensities.

We have also previously demonstrated that ethylene accelerates phototaxis of Synechocystis toward monochromatic light including red, green, and blue light (Lacey and Binder, 2016). Therefore, we examined phototaxis of Geitlerinema cells in response to these colors of light. In

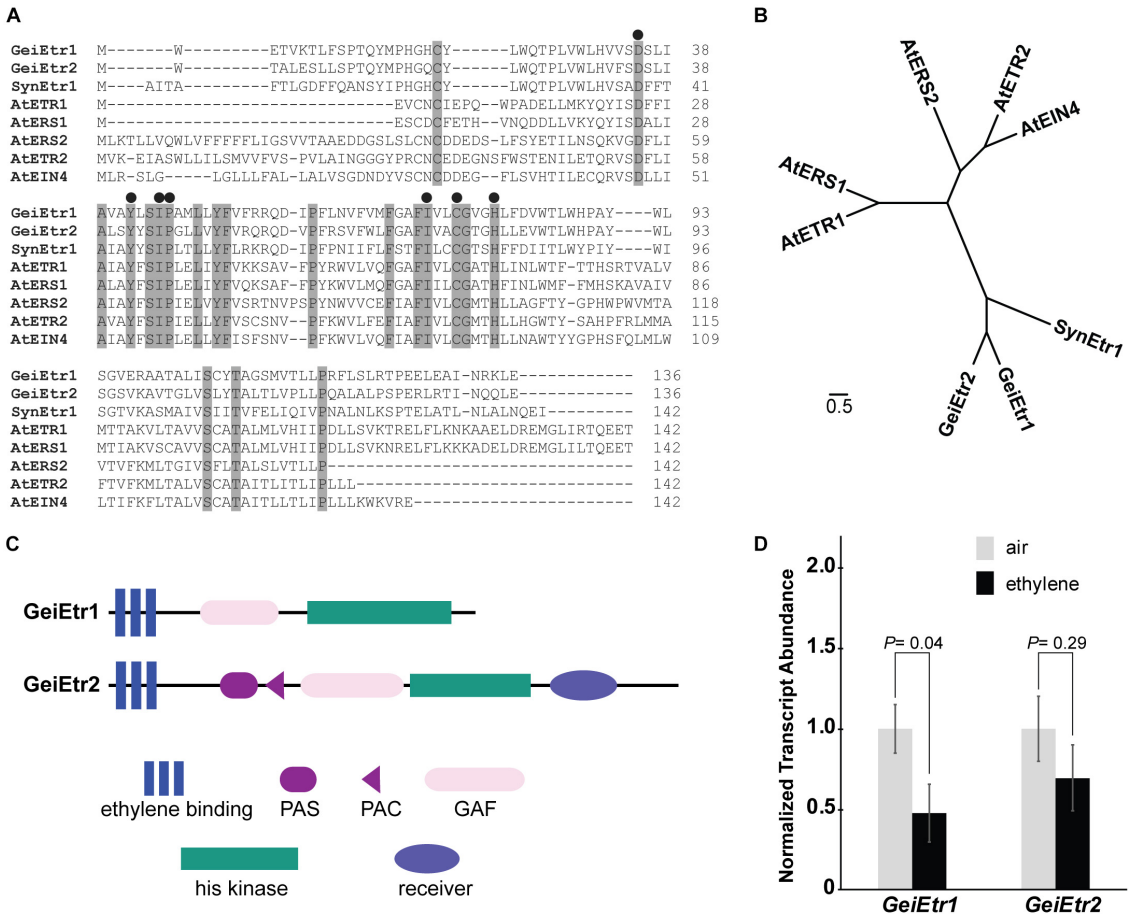

FIGURE 1 | Geitlerinema has two putative ethylene receptors. A BLAST search of the *Geitlerinema* PCC 7105 genome reveals that it has two genes, *GeiEtr1* and *GeiEtr2*, that are predicted to encode proteins with an ethylene binding domain. **(A)** Alignment of the predicted amino acid sequences of the ethylene-binding domains of GeiEtr1 and GeiEtr2 with the ethylene-binding domains of the receptors from *Synechocystis* sp. PCC 6803 (Syn) and *Arabidopsis thaliana* (At). Shaded residues are conserved in all eight sequences. Black circles above the sequences mark amino acids required for ethylene binding to AtETR1. **(B)** Unrooted tree based on the amino acid sequences of the ethylene binding domains from panel **A**. The cladogram was generated using Clustal Omega with default settings and visualized using FigTree version 1.4.2. **(C)** Predicted domain structures of GeiEtr1 and GeiEtr2. Domain predictions were made using the Simple Modular Architecture Research Tool (SMART) http://smart.embl-heidelberg.de/ (Schultz et al., 1998; Letunic et al., 2012). **(D)** Transcript abundance of *GeiEtr1* and *GeiEtr2* in air versus 1000 nL L^{-1} ethylene were determined using qRT-PCR. Data were normalized to the levels of *TruB* and then to the level of each gene in air and represent the average ± SEM. *P*-values were determined using Student's *t*-test.

air, phototaxis occurred faster in response to red and green light compared to white light (**Supplementary Figure 4**). By contrast, the cells did not phototaxis in response to blue light and appeared to show unbiased movement with few cells accumulating in the area of illumination. This is consistent with results using Synechocystis where blue light normally does not cause phototaxis and has been found to promote growth and inhibit motility (Wilde et al., 2002; Chau et al., 2017). We also examined the effects of these different light qualities on cell growth and found that growth occurred in white, red, and green light at similar rates but growth did not occur in blue light (**Supplementary Figure 6**). This suggests that the larger number of cells in the new area of illumination in red and green light is not simply caused by more growth compared to white light.

Because red and green light cause faster phototaxis compared to white light, we shortened the assay time-frame from 5 to 2 d in order to determine whether ethylene stimulates or inhibits phototaxis. Under these conditions, 1000 nL L^{-1} ethylene altered the phototaxis pattern in response to red light where the cells aggregated at the edge of the area of illumination (**Figure 2A**). By contrast, ethylene caused no measurable change in phototaxis in response to either green or blue light. This is in contrast to our observations with Synechocystis where 1000 nL L^{-1} ethylene caused a measurable increase in phototaxis toward both (Lacey and Binder, 2016).

Cyanobacteria integrate various light inputs including wavelength information (Chau et al., 2017). We were therefore curious to examine the response of Geitlerinema cells to polychromatic light. In air, the cells moved into the light spectrum between orange and blue (**Figure 2B**). By contrast, in the presence of 1000 nL L^{-1} ethylene the cells moved into a wider range of wavelengths of light that included red light. Together,

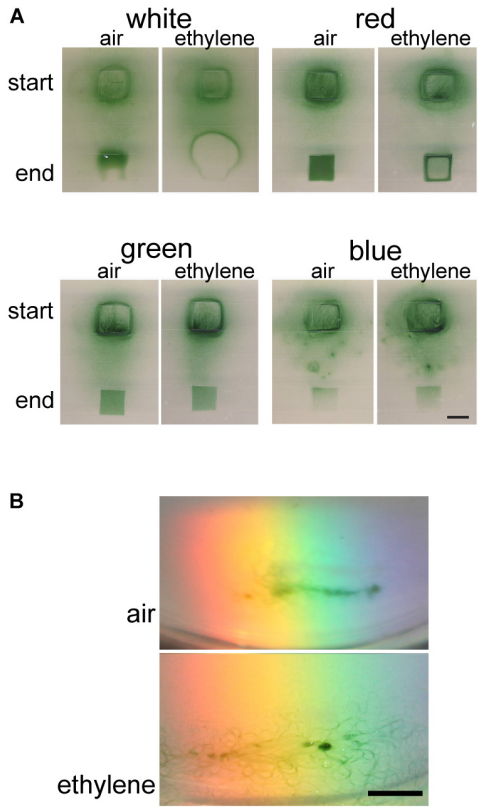

FIGURE 2 | Ethylene alters phototaxis of Geitlerinema. Cells were placed on soft agar and exposed to light as described in the section "Materials and Methods." Phototaxis in air versus 1000 nL L^{-1} exogenous ethylene was examined. **(A)** Phototaxis responses to 42 μmol m^{-2} s^{-1} of white light for 5 d compared to 16 μmol m^{-2} s^{-1} of red light for 2 d, green light for 2 d, or blue light for 5 d are shown. The position where the colony of cells started and end position of lighting is indicated. Scale bar = 1 cm. **(B)** Response of cells to polychromatic light for 5 d. Scale bar = 0.5 cm.

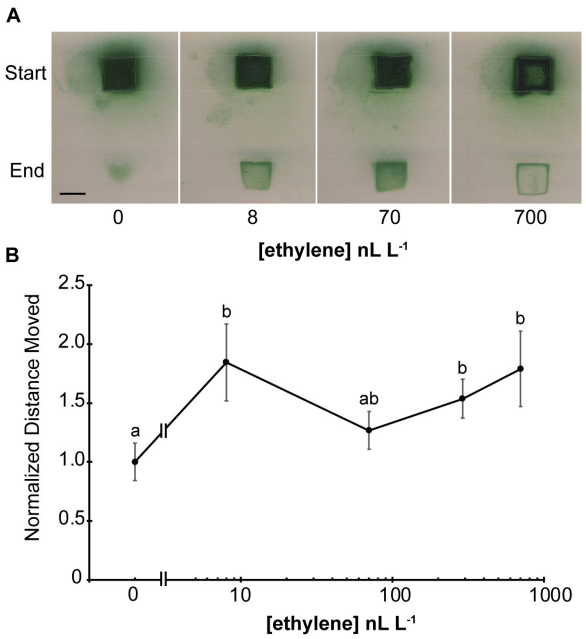

FIGURE 3 | Geitlerinema responds to low levels of exogenous ethylene. **(A)** Cells were placed on soft agar and exposed to white light from above using a protocol modified from Biddanda et al. (2015) as described in the section "Materials and Methods." The position where the colony of cells started and end position after 5 d of lighting are indicated. Scale bar = 1 cm. **(B)** Phototaxis assays were conducted by exposing cells to directional light for 24 h using a protocol modified from Campbell et al. (2015) as described in the section "Materials and Methods." The maximum distance moved from the initial colony position was measured and normalized to distance moved in air. Data represent the average ± SEM from five replicates. Statistical analysis was done with ANOVA and the different letters indicate significant differences ($P < 0.05$). In both panels, cells were kept in flow-through chambers maintained at the indicated concentration of exogenous ethylene.

these results indicate that ethylene affects the phototaxis response of Geitlerinema cells to different wavelengths of light.

Low Levels of Exogenous Ethylene Affect Geitlerinema

Plants respond to a wide range of ethylene concentrations and even show transient growth inhibition at very low concentrations (0.2 nL L^{-1}) of exogenous ethylene (Chen and Bleecker, 1995; Binder et al., 2004). We therefore wished to know the threshold concentration of ethylene that affects phototaxis of Geitlerinema. To examine this we conducted phototaxis assays in response to white light for 5 d in the presence of different concentrations of ethylene or ethylene-free air (**Figure 3A** and **Supplementary Figure 7**). Under these conditions, even the lowest concentration used, 8 nL L^{-1}, resulted in faster phototaxis since more filaments of cells moved into the illuminated area of the plate than were observed in ethylene-free air. Increasing the ethylene levels to 70 nL L^{-1} caused more phototaxis. By contrast, treatment with 700 nL L^{-1} ethylene caused the cells to form a distinct band around the edge of the illuminated area reminiscent to the ring that formed farther from the light with 1000 nL L^{-1} (**Figure 2**).

To gain a better understanding about what appears to be enhanced phototaxis at low levels of ethylene, we also conducted phototaxis experiments where the cells were exposed to directional white light. In air, cells moved from the original colony in all directions relative to the light, but the largest distance moved was toward the light source (**Supplementary Figure 8**). Application of ethylene at the lowest dose used (8 nL L^{-1}) significantly increased the distance moved by cells toward directional white light and the response seems to be saturated by this level of ethylene (**Figure 3B** and **Supplementary Figure 8**). These data support the idea that low ethylene levels increase phototaxis in this cyanobacterium.

Low Levels of Exogenous Ethylene Affect Synechocystis

Because low levels of exogenous ethylene affect Geitlerinema, we tested whether or not low levels of ethylene also affect the physiology of Synechocystis. For this we measured phototaxis and biofilm formation, both of which are increased by application

of 1000 nL L^{-1} ethylene (Lacey and Binder, 2016). Application of ethylene at the lowest dose used (8 nL L^{-1}) significantly increased the distance moved by cells in response to directional white light (**Figure 4A**). There is a slight increase in phototaxis at 70 nL L^{-1} but the response seems to be largely saturated with 8 nL L^{-1} applied ethylene. A similar dose–response curve was observed with biofilm formation except that saturation of the response at 8 nL L^{-1} is more clearly seen (**Figure 4B**). As a comparison, the threshold ethylene concentration typically observed for responses in plants is above 10 nL L^{-1} with saturation of responses occurring in a concentration range of 1–100 μL L^{-1} ethylene depending on the response being measured and the species studied (Chadwick and Burg, 1970; Lyon, 1970; Burdett, 1972; Goeschl and Kays, 1975; De Munk and Duineveld, 1986; Beaudry and Kays, 1988; Chen and Bleecker, 1995).

These assays were conducted using flow-through chambers to maintain constant O_2 and CO_2 concentrations over the long time period (4 d) of the assays. A limitation of this method is that it is difficult to reliably deliver lower ethylene concentrations. Previously, we showed that application of 1000 nL L^{-1} ethylene causes a rapid (within 30 min) decrease in the transcript levels of *CsiR1* and *slr1214* (Lacey et al., 2018). This allowed us to conduct shorter term experiments where ethylene was simply injected into a sealed chamber with phototaxing cells. We compared the transcript levels of *SynEtr1*, *slr1213*, *CsiR1*, and *slr1214* after 4 h treatments with varying dosages of exogenous ethylene. Results from this showed that ethylene at dosages between 1 and 1000 nL L^{-1} had no significant effect on the transcript abundance of either *SynEtr1* or *slr1213* (**Figure 4C**). By contrast, *CsiR1* transcript abundance was altered by application of as low as 1 nL L^{-1} ethylene and increasing levels of ethylene resulted in a concomitant decrease in the levels of *CsiR1* transcript. By contrast, lower dosages of exogenous ethylene had no effect on *slr1214* transcript. However, treatment with 1000 nL L^{-1} ethylene resulted in a decrease in *slr1214*. These results with 1000 nL L^{-1} ethylene are consistent with our prior results examining these four transcripts (Lacey et al., 2018). Together, these data indicate that Synechocystis responds to ethylene at levels as low as 1 nL L^{-1}.

Ethylene Dose-Binding to Geitlerinema, Synechocystis, and SynEtr1[1-130]GST

The ethylene dose-dependency of binding to AtETR1 parallels the dose-dependency for long-term growth inhibition of dark-grown *A. thaliana* seedlings in response to ethylene (Chen and Bleecker, 1995; Schaller and Bleecker, 1995). This suggests that this response is related to the binding affinity to the receptors. We were curious to know if a similar relationship between ethylene binding and responses in Synechocystis and Geitlerinema existed. If true, we predicted that ethylene dose-binding characteristics should saturate at around 10–100 nL L^{-1} ethylene. To test this, we conducted ethylene dose-binding experiments across a range of ethylene concentrations on Geitlerinema and Synechocystis cells, and SynEtr1[1-130]GST expressed in *P. pastoris* (**Figure 5**). In all three cases, ethylene binding continued to increase as ethylene levels were increased up to 1000 nL L^{-1}, demonstrating that ethylene-binding activity does not saturate at 100 nL L^{-1}. At 1000 nL L^{-1}, there was no specific ethylene-binding activity detected in Δ*SynEtr1* Synechocystis cells with *SynEtr1* deleted or in *P. pastoris* cells that were expressing empty vector, consistent with what has previously been reported (Rodriguez et al., 1999; McDaniel and Binder, 2012). Ethylene binding did not reach obvious saturation in the range of concentrations we tested so we estimated the K_d-values with curve fitting. We fitted the data with GraphPad Prism (Ver. 7.04) using default settings for one binding site and measuring specific binding. This yielded sigmoidal curves with estimated K_d-values of 335 ± 227 nL L^{-1} for Geitlerinema, 248 ± 16 nL L^{-1} for Synechocystis, and 127 ± 12 nL L^{-1} for SynEtr1[1-130]GST. These values are in the same range as what has been observed in many plants (Sisler, 1979; Goren and Sisler, 1986; Sisler et al., 1986; Smith et al., 1987; Blankenship and Sisler, 1989, 1993; Sanders et al., 1990) and somewhat higher than what has been reported for *A. thaliana* plants (Sanders et al., 1991) and exogenously expressed AtETR1 (Schaller and Bleecker, 1995). This suggests that the sensitivity of ethylene responses in these cells is not explained simply by the binding affinity of ethylene to the receptors.

DISCUSSION

We have previously shown that the cyanobacterium Synechocystis contains a functional ethylene receptor that regulates cell physiology including phototaxis and biofilm formation and that many other bacteria may contain functional ethylene receptors (Rodriguez et al., 1999; Wang et al., 2006; Lacey and Binder, 2016). In this study we provide evidence supporting the idea that another cyanobacterium, Geitlerinema, responds to ethylene and contains two ethylene receptor isoforms. Application of ethylene to Geitlerinema alters phototaxis indicating a conservation of function for ethylene signaling in both Geitlerinema and Synechocystis. At low ethylene concentrations, ethylene stimulates phototaxis toward white light for both species. It is unclear if this is occurring because of faster movement of individual cells/filaments or movement that is more directed toward the light or both. Using single-cell tracking assays, Kuchmina et al. (2017) demonstrated that higher concentrations of endogenously produced ethylene do not affect the speed of cells, but rather cause movement that is more directed toward the illumination (Kuchmina et al., 2017). It is unknown if this also applies to Synechocystis cells once they aggregate as used in our assays or to Geitlerinema filaments. At higher concentrations, ethylene appeared to sensitize Geitlerinema to the light so that the cells tended to avoid higher levels of illumination. No such sensitization caused by ethylene has been observed in Synechocystis. Like Synechocystis (Lacey and Binder, 2016), ethylene alters phototaxis of Geitlerinema in response to white light and monochromatic red light. However, unlike our prior results studying Synechocystis, ethylene does not have a measurable effect on phototaxis of Geitlerinema in response to monochromatic blue or green light. Interestingly, ethylene affected responses to polychromatic light where Geitlerinema cells phototaxed into a wider range

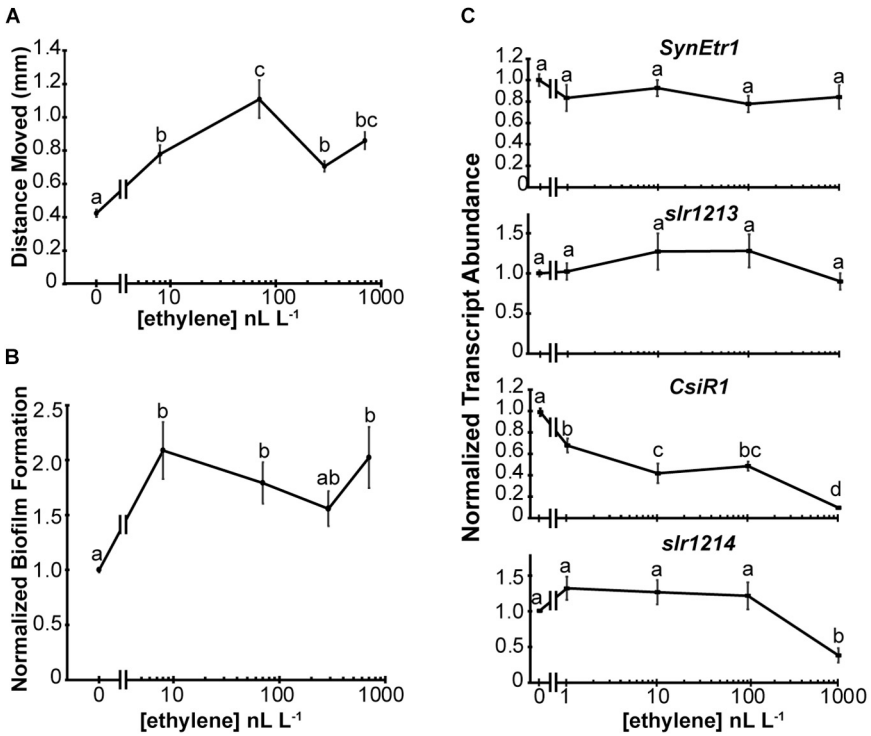

FIGURE 4 | Synechocystis responds to low levels of exogenous ethylene. The effects of various dosages of exogenous ethylene on Synechocystis were measured. **(A)** Phototaxis assays were conducted and the maximum distance moved from the initial colony position measured. **(B)** Biofilm formation was quantified by measuring the staining of attached cells using Crystal Violet. Data are normalized to staining of cells in the absence of ethylene. In panels **(A,B)**, cells were kept in flow-through chambers maintained at 0, 8, 70, 290, or 700 nL L^{-1} exogenous ethylene for 4 d and data are the average ± SEM. **(C)** The gene transcript abundance of *SynEtr1*, *slr1213*, *CsiR1*, and *slr1214* was measured using qRT-PCR from RNA extracted from cells maintained at 0, 1, 10, 100, or 1000 nL L^{-1} exogenous ethylene for 4 h in sealed chambers under phototaxis conditions. Data were normalized to the transcript levels of the *TrpA* reference gene and normalized to cells kept in ethylene-free air. Data represent the average ± SEM from three biological replicates with three technical replicates each. In all panels, statistical analyses were done with ANOVA and the different letters indicate significant differences ($P < 0.05$).

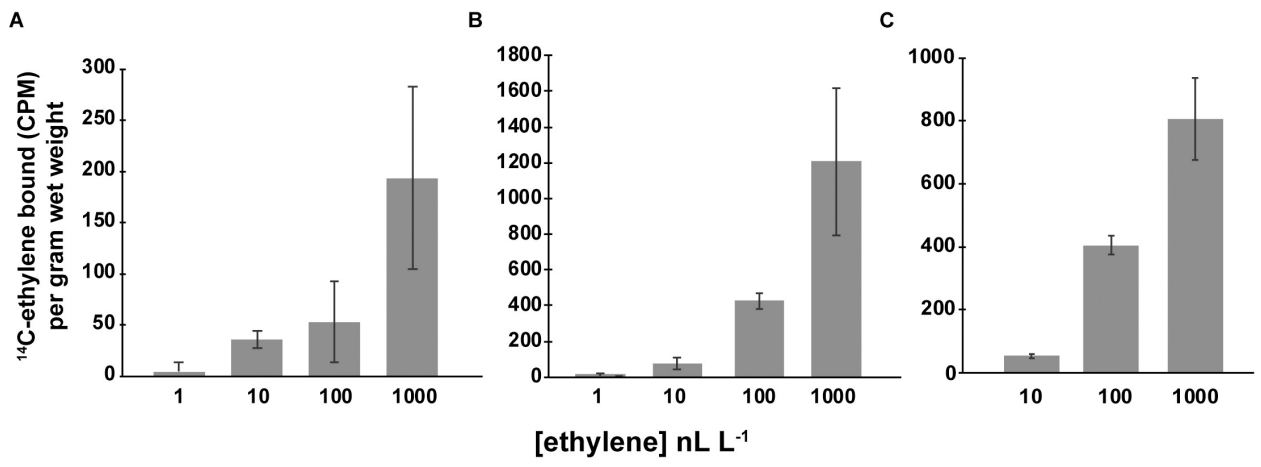

FIGURE 5 | Specific ethylene binding. Ethylene-binding assays were conducted as detailed in the section "Materials and Methods" on **(A)** Geitlerinema cells, **(B)** Synechocystis cells, and **(C)** *P. pastoris* cells expressing the ethylene binding domain of SynEtr1 (SynEtr1[1-130]GST). Assays were carried out at the indicated ethylene concentrations of ^{14}C-ethylene to determine total binding. Non-specific binding was determined using the same concentrations of ^{14}C-ethylene in the presence of 1000-fold excess non-radioactive ethylene. Specific binding was then calculated by subtracting non-specific binding activity from total binding activity. Data are the average specific binding ± SD.

of wavelengths of light in the presence of ethylene versus in ethylene-free air. This shows that ethylene can affect wavelength integration by these cells.

A model for signal transduction from SynEtr1 in Synechocystis has developed (Ramakrishnan and Tabor, 2016) where UV-A light stimulates histidine autophosphorylation of SynEtr1 followed by phosphotransfer to a conserved aspartate on slr1213. The phosphorylated slr1213 enhances the transcription of *CsiR1* and *slr1214* which contain a common transcription start site and appears to be co-transcribed in response to UV-A light (Ramakrishnan and Tabor, 2016). In contrast to UV-A light, application of 1000 nL L^{-1} ethylene reduces the transcript abundance of *CsiR1* and *slr1214* (Lacey et al., 2018). It is currently unknown whether or not ethylene signaling from SynEtr1 also affects histidine kinase activity to regulate *CsiR1* and *slr1214* levels. However, application of ethylene reveals that the regulation of *CsiR1* and *slr1214* is not entirely overlapping. First, we previously showed that application of 1000 nL L^{-1} ethylene caused a rapid and prolonged down regulation of *CsiR1*, whereas this treatment caused a rapid and transient down-regulation of *slr1214* (Lacey et al., 2018). In this study we provide further evidence for more complex regulation where low levels of ethylene decrease *CsiR1* levels, but it requires a much higher level of ethylene to reduce the abundance of *slr1214*. We currently do not know the basis for these differences in regulation but it is possible that the transcript stabilities of these genes are regulated differently.

In Synechocystis, the ethylene dose–responses for phototaxis and biofilm formation show an inverse correlation with the dose–response for *CsiR1* abundance suggesting that *CsiR1* plays an important inhibitory role for these two responses. However, its function in Synechocystis and the mechanisms by which it affects Synechocystis physiology are poorly studied. One possibility is that *CsiR1* is functioning in transcriptional or post-transcriptional regulation in Synechocystis (Georg et al., 2009; Hernández-Prieto et al., 2012). In Synechocystis, both biofilm formation and motility are dependent on type IV pili (Bhaya et al., 1999, 2000; Yoshihara et al., 2001; Burriesci and Bhaya, 2008; Schuergers et al., 2015). The RNA chaperone Hfq affects Synechocystis motility and type IV pilus function (Dienst et al., 2008; Schuergers et al., 2014) suggesting that *CsiR1* may also affect motility and biofilm formation by altering type IV pili, perhaps by altering expression of certain pilin proteins. However, it is likely that regulation by ethylene is more complex than simply regulating *CsiR1* since removing slr1214 eliminates physiological responses to ethylene (Lacey and Binder, 2016).

We have previously studied the effects of ethylene on Synechocystis using 300 and 1000 nL L^{-1} exogenous ethylene (Lacey and Binder, 2016; Henry et al., 2017; Lacey et al., 2018). This is a common concentration range to use in plants, but in aqueous environments, ethylene levels are often reported to be lower than this (Abeles et al., 1992). We therefore examined the physiological responses of Synechocystis and Geitlerinema to a range of ethylene concentrations and found that both species physiologically respond to levels of ethylene as low as 8 nL L^{-1}. We quantified the effects of ethylene on increasing biofilm formation and phototaxis in Synechocystis and discovered that both responses saturate at between 8 and 70 nL L^{-1}. This suggests that both responses occur over a narrow dynamic range of ethylene concentrations, although we cannot rule out that these cells have physiological responses that occur at ethylene concentrations lower than used in this study. By comparison, plants have a wide dynamic range over several orders of magnitude of ethylene concentration. For instance, the growth of dark-grown *A. thaliana* seedlings is inhibited in a dose-dependent manner over a range of ethylene concentrations between 10 and 1000 nL L^{-1} (Chen and Bleecker, 1995). It is interesting to note that induction of chitinase-B also has dose-dependent induction over two orders of magnitude ethylene concentration. However, whereas growth inhibition saturates at 1000 nL L^{-1}, chitinase-B induction saturates at a 10-fold higher concentration (Chen and Bleecker, 1995). It is therefore of note that the reduction of *CsiR1* transcript abundance in Synechocystis occurs in a dose-dependent manner over a wide range of ethylene concentrations between 1 and 1000 nL L^{-1}. This raises the possibility that there may be other physiological responses in Synechocystis occurring in different ranges of ethylene concentration from biofilm formation and phototaxis. It is also interesting that *CsiR1* transcript abundance was reduced by application of as low as 1 nL L^{-1} ethylene. This low level of ethylene is below the threshold for most responses reported in plants (Abeles et al., 1992). Exceptions are that stimulation of *Ricinodendron rautanenii* seed germination has been observed with 1 nL L^{-1} treatments (Keegan et al., 1989) and transient growth inhibition responses occur in dark grown *A. thaliana* seedlings down to 0.2 nL L^{-1} ethylene (Binder et al., 2004).

The long-term growth inhibition response of dark-grown *A. thaliana* to ethylene has a dose-dependency that parallels the dose-dependency of ethylene binding to AtETR1 (Chen and Bleecker, 1995; Schaller and Bleecker, 1995). This led us to predict that ethylene binding to Geitlerinema and Synechocystis cells, as well as heterologously expressed SynEtr1, would saturate at between 8 and 100 nL L^{-1} ethylene. However, our results indicate that this is not the case. Thus, unlike the long-term growth inhibition response of dark-grown *A. thaliana* seedlings to ethylene, there is no obvious correlation between the amount of ethylene bound and physiological responses in these two species of cyanobacteria. It is interesting to note that the dose-dependency of ethylene binding to Synechocystis and SynEtr1[1-130]GST parallels the decrease in *CsiR1* transcript caused by ethylene. The K_d for ethylene binding to AtETR1 heterologously expressed in yeast is reported at 36 nL L^{-1} (Schaller and Bleecker, 1995) yet *A. thaliana* seedlings are able to respond to ethylene concentrations approximately 300-fold below this level with a transient growth inhibition response (Binder et al., 2004). Our results indicate there may be a similar discrepancy between ethylene binding and ethylene responses where Synechocystis responds to 1 nL L^{-1} ethylene yet the estimated binding affinity is over 100-fold higher. These observations suggest that signal amplification is occurring. In bacterial chemotaxis receptors, such amplification occurs because of physical clustering of the receptors. In this model, binding of ligand to one receptor causes conformational changes in surrounding, ligand-free receptors

through physical interactions (Briegel and Jensen, 2017; Bi and Sourjik, 2018). Thus, it is possible that amplification of ethylene signaling in these cyanobacteria, as well as in plants, is occurring at the level of the receptors. However, it remains to be determined whether a similar clustering of ethylene receptors and amplification of signal is occurring in either plants or cyanobacteria.

The ecophysiological role of ethylene for cyanobacteria remains unanswered but it is likely that cyanobacteria encounter ethylene in the environment produced by other organisms or produced abiotically from sunlight photochemically converting dissolved organics to ethylene (Swinnerton and Linnenborn, 1967; Wilson et al., 1970; Swinnerton and Lamontagne, 1974; Ratte et al., 1993, 1998). It is known that ethylene diffuses in water and ethylene levels vary in aqueous environments depending on environmental conditions resulting in ethylene concentrations in the range where we observe responses (Swinnerton and Lamontagne, 1974; Plass et al., 1992; Ratte et al., 1993, 1998). Thus, ethylene may be acting as a signal for cells to move into light conditions that optimize photosynthesis or reduce light stress or it may be a signal to establish a symbiotic relationship with another organisms. Our results showing that ethylene causes Geitlerinema cells to avoid high light supports the idea that it is a stress signal. However, these are not mutually exclusive ideas and ethylene may be regulating a variety of functions.

In summary, we have shown that two cyanobacteria species respond to low levels of ethylene. Our results support the hypothesis that ethylene perception evolved prior to green plants and is likely to be wide-spread in cyanobacteria species. Given the diversity of putative receptors in various microbes and the presence of multiple receptor isoforms in certain species (Mount and Chang, 2002; Wang et al., 2006; Lacey and Binder, 2016; Hérivaux et al., 2017; Kabbara et al., 2018; Papon and Binder, 2019), it is likely that the mechanisms of ethylene signaling and responses controlled by ethylene are diverse.

DATA AVAILABILITY

All datasets for this study are included in the manuscript and/or the **Supplementary Files**.

AUTHOR CONTRIBUTIONS

RL, CA, and BB designed the experiments. BB wrote the manuscript with the help of RL. All authors performed the experiments.

FUNDING

This work was supported by funds from the University of Tennessee Program for Excellence & Equity in Research (PEER) (to CA). Research funding was provided by grants from the US National Science Foundation (IOS-1254423 and MCB-1517032 to BB).

ACKNOWLEDGMENTS

The authors thank M. B. Stalans, J. B. Case, A. J. Schafer, J. Shreck, T. Payne, A. Patterson, J. Mondal, E. E. Helmbrecht, and B. D. Bruce for technical assistance and advice.

SUPPLEMENTARY MATERIAL

The Supplementary Material for this article can be found online at: https://www.frontiersin.org/articles/10.3389/fpls.2019.00950/full#supplementary-material

REFERENCES

Abeles, F. B., Morgan, P. W., and Saltveit, M. E. (1992). *In Ethylene in Plant Biology*. San Diego, Academic Press.

Agostoni, M., Waters, C. M., and Montgomery, B. L. (2016). Regulation of biofilm formation and cellular buoyancy through modulating intracellular cyclic di-GMP levels in engineered cyanobacteria. *Biotech. Bioeng.* 113, 311–319. doi: 10.1002/bit.25712

Bakshi, A., and Binder, B. M. (2018). "CHAPTER 8 Plant Ethylene Sensing and Signalling,"in *Gas Sensing in Cells*, ed. S. Aono, (London: The Royal Society of Chemistry), 253–291 doi: 10.1039/9781788012836-00253

Bakshi, A., Shemansky, J., Chang, C., and Binder, B. (2015). History of research on the plant hormone ethylene. *J Plant Growth Regul.* 34, 1–19.

Beaudry, R., and Kays, S. J. (1988). Effect of ethylene source on abscission of pepper plant organs. *HortScience* 23, 742–744.

Bhaya, D., Bianco, N. R., Bryant, D., and Grossman, A. (2000). Type IV pilus biogenesis and motility in the cyanobacterium *Synechocystis* sp. *PCC*6803. Mol Micro 37, 941–951. doi: 10.1046/j.1365-2958.2000.02068.x

Bhaya, D., Watanabe, N., Ogawa, T., and Grossman, A. R. (1999). The role of an alternative sigma factor in motility and pilus formation in the cyanobacterium *Synechocystis* sp. *strain PCC*6803. *Proc. Natl. Acad. Sci. U.S.A.* 96, 3188–3193. doi: 10.1073/pnas.96.6.3188

Bi, S., and Sourjik, V. (2018). Stimulus sensing and signal processing in bacterial chemotaxis. *Curr. Opin. Microbiol.* 45, 22–29. doi: 10.1016/j.mib.2018.02.002

Biddanda, B., McMillan, A., Long, S., Snider, M., and Weinke, A. (2015). Seeking sunlight: rapid phototactic motility of filamentous mat-forming cyanobacteria optimize photosynthesis and enhance carbon burial in Lake Huron's submerged sinkholes. *Front. Microbiol.* 6:930. doi: 10.3389/fmicb.2015.00930.

Binder, B. M., Mortimore, L. A., Stepanova, A. N., Ecker, J. R., and Bleecker, A. B. (2004). Short-term growth responses to ethylene in *Arabidopsis* seedlings are EIN3/EIL1 independent. *Plant Physiol.* 136, 2921–2927. doi: 10.1104/pp.104.050393

Blankenship, S. M., and Sisler, E. C. (1989). Ethylene binding changes in apple and morning glory during ripening and senescence. *J. Plant Growth Reg.* 8, 37–44. doi: 10.1007/bf02024924

Blankenship, S. M., and Sisler, E. C. (1993). Ethylene binding site affinity in ripening apples. *J. Am. Soc. Hort Sci.* 118, 609–612. doi: 10.21273/jashs.118.5.609

Briegel, A., and Jensen, G. (2017). Progress and potential of electron cryotomography as illustrated by its application to bacterial chemoreceptor arrays. *Ann. Rev. Biophys.* 46, 1–21. doi: 10.1146/annurev-biophys-070816-033555

Burdett, A. N. (1972). Ethylene synthesis in lettuce seeds: its physiological significance. *Plant Physiol.* 50, 719–722. doi: 10.1104/pp.50.6.719

Burriesci, M., and Bhaya, D. (2008). Tracking phototactic responses and modeling motility of *Synechocystis* sp. *strain PCC*6803. *J. Photochem. Photobiol.* 91, 77–86. doi: 10.1016/j.jphotobiol.2008.01.012

Campbell, E. L., Hagen, K. D., Chen, R., Risser, D. D., Ferreira, D. P., Meeks, J. C., et al. (2015). Genetic analysis reveals the identity of the photoreceptor for

phototaxis in hormogonium filaments of < span class = "named-content genus-species" id = "named-content-1" > Nostoc punctiforme < /span >. *J. Bact.* 197, 782–791. doi: 10.1128/jb.02374-14

Chadwick, A., and Burg, S. P. (1970). Regulation of root growth by auxin-ethylene interaction. *Plant Physiol.* 45, 192–200. doi: 10.1104/pp.45.2.192

Chang, C., Kwok, S. F., Bleecker, A. B., and Meyerowitz, E. M. (1993). Arabidopsis ethylene-response gene ETR1: similarity of product to two-component regulators. *Science* 262, 539–544. doi: 10.1126/science.8211181

Chau, R. M. W., Bhaya, D., and Huang, K. C. (2017). Emergent phototactic responses of cyanobacteria under complex light regimes. *mBio* 8:e02330-16.

Chen, Q. H. G., and Bleecker, A. B. (1995). Analysis of ethylene signal-transduction kinetics associated with seedling-growth response and chitinase induction in wild-type and mutant *Arabidopsis*. *Plant Physiol.* 108, 597–607. doi: 10.1104/pp.108.2.597

De Munk, W. J., and Duineveld, T. L. J. (1986). The role of ethylene in the flowering response of bulbous plants. *Biol. Plantarum* 28, 85–90. doi: 10.1007/bf02885198

Dienst, D., Dühring, U., Mollenkopf, H., Vogel, J., Golecki, J., Hess, W. R.,et al. (2008). The cyanobacterial homologue of the RNA chaperone Hfq is essential for motility of *Synechocystis* sp PCC 6803. *Microbiology* 154, 3134–3143. doi: 10.1099/mic.0.2008/020222-0

Georg, J., Voß, B., Scholz, I., Mitschke, J., Wilde, A., Hess, W. R., et al. (2009). Evidence for a major role of antisense RNAs in cyanobacterial gene regulation. *Mol. Sys. Biol.* 5:305. doi: 10.1038/msb.2009.63

Goeschl, J. D., and Kays, S. J. (1975). Concentration dependencies of some effects of ethylene on etiolated pea, peanut, bean, and cotton seedlings. *Plant Physiol.* 55, 670–677. doi: 10.1104/pp.55.4.670

Goren, R., and Sisler, E. C. (1986). Ethylene-binding characteristics in phaseolus, citrus, and ligustrum plants. *Plant Growth Regul.* 4, 43–54. doi: 10.1007/bf00025348

Hall, A. E., Findell, J. L., Schaller, G. E., Sisler, E. C., and Bleecker, A. B. (2000). Ethylene perception by the ERS1 protein in *Arabidopsis*. *Plant Physiol.* 123, 1449–1457.

Henry, M. L., Charton, M., Alignan, M., Maury, P., Luniov, A., Pelletier, I., et al. (2017). Ethylene stimulates growth and affects fatty acid content of *Synechocystis* sp. *PCC* 6803. *Algal Res.* 2, 234–239. doi: 10.1016/j.algal.2017.07.032

Hérivaux, A., Dugé de Bernonville, T., Roux, C., Clastre, M., Courdavault, V., Gastebois, A., et al. (2017). The identification of phytohormone receptor homologs in early diverging fungi suggests a role for plant sensing in land colonization by fungi. *mBio* 8:e01739-16.

Hernández-Prieto, M. A., Schön, V., Georg, J., Barreira, L., Varela, J., Hess, W. R., et al. (2012). Iron deprivation in *Synechocystis*: inference of pathways, non-coding RNAs, and regulatory elements from comprehensive expression profiling. *G3* 2, 1475–1495. doi: 10.1534/g3.112.003863

Hua, J., Sakai, H., Nourizadeh, S., Chen, Q. H. G., Bleecker, A. B., Ecker, J. R., et al. (1998). EIN4 and ERS2 are members of the putative ethylene receptor gene family in *Arabidopsis*. *Plant Cell* 10, 1321–1332. doi: 10.1105/tpc.10.8.1321

Ikeuchi, M., and Ishizuka, T. (2008). Cyanobacteriochromes: a new superfamily of tetrapyrrole-binding photoreceptors in cyanobacteria. *Photochem. Photobiol. Sci.* 7, 1159–1167. doi: 10.1039/b802660m

Kabbara, S., Hérivaux, A., Dugé de Bernonville, T., Courdavault, V., Clastre, M., Gastebois, A., et al. (2018). Diversity and evolution of sensor histidine kinases in eukaryotes. *Genome Biol. Evol.* 11, 86–108. doi: 10.1093/gbe/evy213

Kaneko, T., Sato, S., Kotani, H., Tanaka, A., Asamizu, E., Nakamura, Y., et al. (1996). Sequence analysis of the genome of the unicellular cyanobacterium *Synechocystis* sp. *strain* PCC6803. II. Sequence determination of the entire genome and assignment of potential protein-coding regions. DNA Res. 3, 109–136. doi: 10.1093/dnares/3.3.109

Keegan, A. B., Kelly, K. M., and Staden, J. V. (1989). Ethylene involvement in dormancy release of *Ricinodendron* rautanenii seeds. *Ann. Bot* 63, 229–234. doi: 10.1093/oxfordjournals.aob.a087737

Kehoe, D. M., and Grossman, A. R. (1996). Similarity of a chromatic adaptation sensor to phytochrome and ethylene receptors. *Science* 273, 1409–1412. doi: 10.1126/science.273.5280.1409

Kuchmina, E., Klähn, S., Jakob, A., Bigott, W., Enke, H., Dühring, U., et al. (2017). Ethylene production in Synechocystis sp. PCC 6803 promotes phototactic movement. *Microbiology* 163, 1937–1945. doi: 10.1099/mic.0.000564

Lacey, R. F., Allen, C. J., Bakshi, A., and Binder, B. M. (2018). Ethylene causes transcriptomic changes in *Synechocystis* during phototaxis. *Plant Direct* 2, 1–16. doi: 10.1002/pld3.48

Lacey, R. F., and Binder, B. M. (2014). How plants sense ethylene gas — the ethylene receptors. *J. Inorg. Biochem.* 133, 58–62. doi: 10.1016/j.jinorgbio.2014.01.006

Lacey, R. F., and Binder, B. M. (2016). Ethylene regulates the physiology of the cyanobacterium *Synechocystis* sp. PCC 6803 via an ethylene receptor. *Plant Physiol.* 171, 2798–2809. doi: 10.1104/pp.16.00602

Letunic, I., Doerks, T., and Bork, P. (2012). SMART 7: recent updates to the protein domain annotation resource. *Nuc. Acids Res.* 40, D302–D305. doi: 10.1093/nar/gkr931

Los, D. A., Suzuki, I., Zinchenko, V. V., and Murata, N. (2008). "Stress responses in syenechocystis: regulated genes and regulatory systems,"in *The Cyanobacteria: Molecular Biology, Genomics and Evolution* eds A Herrero, E Flores, (Norfolk: Caister Academic Press), 117–157.

Lyon, C. J. (1970). Ethylene inhibition of auxin transport by gravity in leaves. *Plant Physiol.* 45, 644–646. doi: 10.1104/pp.45.5.644

Martin, W., Rujan, T., Richly, E., Hansen, A., Cornelsen, S., Lins, T., et al. (2002). Evolutionary analysis of *Arabidopsis*, cyanobacterial, and chloroplast genomes reveals plastid phylogeny and thousands of cyanobacterial genes in the nucleus. *Proc. Natl. Acad. Sci. U.S.A.* 99, 12246–12251. doi: 10.1073/pnas.182432999

Mattoo, A. K., and Suttle, J. C. (1991). *In The Plant Hormone Ethylene*. Boca Raton, FL: CRC Press.

McDaniel, B., and Binder, B. M. (2012). ETHYLENE RECEPTOR1 (ETR1) is sufficient and has the predominant role in mediating inhibition of ethylene responses by silver in *Arabidopsis thaliana*. *J. Biol. Chem.* 287, 26094–26103. doi: 10.1074/jbc.m112.383034

Merchante, C., Alonso, J. M., and Stepanova, A. N. (2013). Ethylene signaling: simple ligand, complex regulation. *Curr. Opin Plant Biol.* 16, 554–560. doi: 10.1016/j.pbi.2013.08.001

Mount, S. M., and Chang, C. (2002). Evidence for a plastid origin of plant ehylene rceptor genes. *Plant Physiol.* 130, 10–14. doi: 10.1104/pp.005397

Narikawa, R., Suzuki, F., Yoshihara, S., Higashi, K., Watanabe, A., Ikeuchi, M., et al. (2011). Novel photosensory two-component system (PixA-NixB-NixC) involved in the regulation of positive and negative phototaxis of cyanobacterium *Synechocystis* sp. PCC 6803. *Plant Cell Physiol.* 52, 2114–2224. doi: 10.1093/pcp/pcr155

Papon, N., and Binder, B. M. (2019). An evolutionary perspective on ethylene sensing in microorganisms. *Trends Microbiol.* 27, 193–196. doi: 10.1016/j.tim.2018.12.002

Plass, C., Koppmann, R., and Rudolph, J. (1992). Light hydrocarbons in the surface water of the mid-atlantic. *J. Atmos. Chem.* 15, 235–251. doi: 10.1007/bf00115396

Ramakrishnan, P., and Tabor, J. J. (2016). Repurposing *Synechocystis* PCC6803 UirS–UirR as a UV-Violet/Green photoreversible transcriptional regulatory tool in E. *coli*. *ACS Synth. Biol.* 5, 733–740. doi: 10.1021/acssynbio.6b00068

Ratte, M., Bujok, O., Spitzy, A., and Rudolph, J. (1998). Photochemical alkene formation in seawater from dissolved organic carbon: results from laboratory experiments. *J. Geophys. Res.* 103, 5707–5717. doi: 10.1029/97jd03473

Ratte, M., Plass-Dülmer, C., Koppmann, R., Rudolph, J., and Denga, J. (1993). Production mechanism of C2-C4 hydrocarbons in seawater: field measurements and experiments. *Global Bichem. Cycles* 7, 369–378. doi: 10.1029/93gb00054

Rippka, R., Deruelles, J., Waterbury, J. B., Herdman, M., and Stainier, R. Y. (1979). Generic assignments, strain histories and properties of pure cultures of cyanobacteria. *Microbiology* 111, 1–61. doi: 10.1099/00221287-111-1-1

Rodriguez, F. I., Esch, J. J., Hall, A. E., Binder, B. M., Schaller, G. E., Bleecker, A. B., et al. (1999). A copper cofactor for the ethylene receptor ETR1 from *Arabidopsis*. *Science* 283, 996–998. doi: 10.1126/science.283.5404.996

Sanders, I. O., Harpham, N. V. J., Raskin, I., Smith, A. R., and Hall, M. A. (1991). Ethylene binding in wild type and mutant *Arabidopsis thaliana* (L.) *Heynh*. *Ann. Bot.* 68, 97–103. doi: 10.1093/oxfordjournals.aob.a088242

Sanders, I. O., Ishizawa, K., Smith, A. R., and Hall, M. A. (1990). Ethylene binding and action in rice seedlings. *Plant Cell Physiol.* 31, 1091–1099.

Schaller, G. E., and Bleecker, A. B. (1995). Ethylene-binding sites generated in yeast expressing the *Arabidopsis* ETR1 gene. *Science* 270, 1809–1811. doi: 10.1126/science.270.5243.1809

Schaller, G. E., Ladd, A. N., Lanahan, M. B., Spanbauer, J. M., and Bleecker, A. B. (1995). The ethylene response mediator ETR1 from *Arabidopsis* forms a disulfide-linked dimer. *J. Biol. Chem.* 270, 12526–12530. doi: 10.1074/jbc.270.21.12526

Schaller, G. E., Shiu, S-H., and Armitage, J. P. (2011). Two-component systems and their co-option for eukaryotic signal transduction. *Curr. Biol.* 21, R320–R330. doi: 10.1016/j.cub.2011.02.045

Schuergers, N., Nürnberg, D. J., Wallner, T., Mullineaux, C. W., and Wilde, A. (2015). PilB localisation correlates with the direction of twitching motility in the cyanobacterium *Synechocystis* sp. PCC 6803. *Microbiology* 161, 960–966. doi: 10.1099/mic.0.000064

Schuergers, N., Ruppert, U., Watanabe, S., Nürnberg, D. J., Lochnit, G., Dienst, D., et al. (2014). Binding of the RNA chaperone Hfq to the type IV pilus base is crucial for its function in *Synechocystis* sp. PCC 6803. *Mol. Microbiol.* 92, 840–852. doi: 10.1111/mmi.12595

Schultz, J., Milpetz, F., Bork, P., and Ponting, C. P. (1998). SMART, a simple modular architecture research tool: identification of signaling domains. *Proc. Natl. Acad. Sci. U.S.A.* 95, 5857–5864. doi: 10.1073/pnas.95.11.5857

Sisler, E. C. (1979). Measurement of ethylene binding in plant tissue. *Plant Physiol.* 64, 538–542. doi: 10.1104/pp.64.4.538

Sisler, E. C., Reid, M.S., and Yang, S. F. (1986). Effect of antagonists of ethylene action on binding of ethylene in cut carnations. *Plant Growth Reg.* 4, 213–218. doi: 10.1007/bf00028164

Smith, A. R., Robertson, D., Sanders, I. O., Williams, R. A. N., and Hall, M. A. (1987) Ethylene binding sites. In *Plant Hormone Receptors* ed D Klambt (Berlin: Springer-Verlag), 229–238. doi: 10.1007/978-3-642-72779-5_20

Song, J-Y., Cho, H. S., Cho, J-I., Jeon, J-S., Lagarias, J. C., Park, Y-I., et al. (2011). Near-UV cyanobacteriochrome signaling system elicits negative phototaxis in the cyanobacterium *Synechocystis* sp. PCC 6803. *Proc. Natl. Acad. Sci. U.S.A.* 108, 10780–10785. doi: 10.1073/pnas.1104242108

Swinnerton, J. W., and Lamontagne, R. A. (1974). Oceanic distribution of low-molecular-weight hydrocarbons. *Environ. Sci. Tech.* 8, 657–663. doi: 10.1021/es60092a006

Swinnerton, J. W, and Linnenborn, V. J. (1967). Gaseous hydrocarbons in sea water: determination. *Science* 156, 1119–1120. doi: 10.1126/science.156.3778.1119

Timmis, J. N., Ayliffe, M. A., Huang, C. Y., and Martin, W. (2004). Endosymbiotic gene transfer: organelle genomes forge eukaryotic chromosomes. *Nat. Rev. Genet.* 5, 123–135. doi: 10.1038/nrg1271

Ulijasz, A. T., Cornilescu, G., von Stetten, D., Cornilescu, C., Velazquez Escobar, F., Zhang, J., et al. (2009). Cyanochromes are blue/green light photoreversible photoreceptors defined by a stable double cysteine linkage to a phycoviolobilin-type chromophore. *J. Biol. Chem.* 284, 29757–29772. doi: 10.1074/jbc.M109.038513

Wang, W., Esch, J. E., Shiu, S. H., Agula, H., Binder, B. M., Chang, C., et al. (2006). Identification of important regions for ethylene binding and signaling in the transmembrane domain of the ETR1 ethylene receptor of *Arabidopsis*. *Plant Cell* 18, 3429–3442. doi: 10.1105/tpc.106.044537

Wilde, A., Fiedler, B., and Börner, T. (2002). The cyanobacterial phytochrome Cph2 inhibits phototaxis towards blue light. *Mol. Micro.* 44, 981–988. doi: 10.1046/j.1365-2958.2002.02923.x

Wilson, D. F., Swinnerton, J. W., and Lamontagne, R. A. (1970). Production of carbon monoxide and gaseous hydrocarbons in seawater: relation to dissolved organic carbon. *Science* 18, 1577–1579. doi: 10.1126/science.168.3939.1577

Yoshihara, S., Geng, X., Okamoto, S., Yura, K., Murata, T., Go, M., et al. (2001). Mutational analysis of genes involved in pilus structure, motility and transformation competency in the unicellular motile cyanobacterium *Synechocystis* sp. PCC6803. *Plant Cell Physiol.* 42, 63–73. doi: 10.1093/pcp/pce007

Yoshihara, S., Katayama, M., Geng, X., and Ikeuchi, M. (2004). Cyanobacterial phytochrome-like pixja holoprotein shows novel reversible photoconversion between blue- and green-absorbing forms. *Plant Cell Physiol.* 45, 1729–1737. doi: 10.1093/pcp/pch214

Zhang, Z., Pendse, N., Phillips, K., Cotner, J., and Khodursky, A. (2008). Gene expression patterns of sulfur starvation in *Synechocystis* sp. PCC 6803. *BMC Genomics* 9:344. doi: 10.1186/1471-2164-9-344

Conflict of Interest Statement: The authors declare that the research was conducted in the absence of any commercial or financial relationships that could be construed as a potential conflict of interest.

frontiers in Plant Science

ORIGINAL RESEARCH
published: 09 August 2019
doi: 10.3389/fpls.2019.01004

Ethylene Induces a Rapid Degradation of Petal Anthocyanins in Cut *Vanda* 'Sansai Blue' Orchid Flowers

Sudarat Khunmuang[1,2], Sirichai Kanlayanarat[1,2], Chalermchai Wongs-Aree[1,2], Shimon Meir[3], Sonia Philosoph-Hadas[3], Michal Oren-Shamir[4], Rinat Ovadia[4] and Mantana Buanong[1,2]*

[1]Division of Postharvest Technology, School of Bioresources and Technology, King Mongkut's University of Technology Thonburi (Bangkhuntien) Thakam, Bangkok, Thailand, [2]Postharvest Technology Innovation Center, Office of the Higher Education Commission, Bangkok, Thailand, [3]Department of Postharvest Science, Agricultural Research Organization (ARO), The Volcani Center, Rishon LeZion, Israel, [4]Department of Ornamental Plants and Agricultural Biotechnology, Agricultural Research Organization (ARO), The Volcani Center, Rishon LeZion, Israel

Ethylene plays a major role in the regulation of flower senescence, including in the ethylene-sensitive *Vanda* 'Sansai Blue' orchid flowers. This cut flower is popular in Thailand due to its light blue big size florets possessing a beautiful shape pattern. In the present study, we further examined the rapid ethylene-induced process of active anthocyanin degradation in cut *Vanda* 'Sansai Blue' flowers, which occurred much before detection of other typical senescence-related symptoms. For this purpose, the cut inflorescences were exposed to air (control), 1 or 10 μl L^{-1} ethylene for 24 h, or to 0.2 μl L^{-1} 1-methylcyclopropene (1-MCP) for 6 h followed by 10 μl L^{-1} ethylene for 24 h at 21°C, and the effects of these treatments on various parameters were assayed. While the fading-induced effect of ethylene was not concentration-dependent in this range, the ethylene treatment significantly reduced the flower vase life in a concentration-dependent manner, further confirming the separation of the bleaching process from senescence. Exposure of the inflorescences to 1-MCP pre-treatment followed by 10 μl L^{-1} ethylene, recovered both inflorescence color and anthocyanin content to control levels. Quantification of total anthocyanin content, performed by HPLC analysis on the basis of cyanidin-3-glocuside equivalents, showed that ethylene reduced and 1-MCP recovered the anthocyanins profile in non-hydrolyzed anthocyanin samples of *Vanda* 'Sansai Blue' florets, assayed at half bloom and bloom developmental stages. The results showed that the ethylene-induced color fading, observed immediately after treatment, resulted from a significant reduction in the levels of the two main anthocyanidins, cyanidin and delphinidin, as well as of other anthocyanidins present in low abundance, but not from changes in the levels of flavonols, such as kaempferol. This anthocyanin degradation process seems to operate *via* ethylene-increased peroxidase activity, detected at the bud stage. Taken together, our results suggest that the ethylene-induced rapid color bleaching in petals of cut *Vanda* 'Sansai Blue' flowers is an outcome of *in-planta* anthocyanin degradation, partially mediated by increased peroxidase activity, and proceeds independently of the flower senescence process.

Keywords: anthocyanidins, color fading, cyaniding, delphinidin, ethylene sensitivity, peroxidase activity, senescence symptoms, cut *Vanda* orchid flowers

OPEN ACCESS

Edited by:
Autar Krishen Mattoo, United States Department of Agriculture, United States

Reviewed by:
Antonio Ferrante, University of Milan, Italy
Kazuo Ichimura, Institute of Vegetable and Floriculture Science, NARO, Japan

***Correspondence:**
Sonia Philosoph-Hadas
vtsoniap@volcani.agri.gov.il

Specialty section:
This article was submitted to Plant Physiology, a section of the journal Frontiers in Plant Science

Received: *09 April 2019*
Accepted: *18 July 2019*
Published: *09 August 2019*

Citation:
Khunmuang S, Kanlayanarat S, Wongs-Aree C, Meir S, Philosoph-Hadas S, Oren-Shamir M, Ovadia R and Buanong M (2019) Ethylene Induces a Rapid Degradation of Petal Anthocyanins in Cut Vanda 'Sansai Blue' Orchid Flowers. Front. Plant Sci. 10:1004. doi: 10.3389/fpls.2019.01004

INTRODUCTION

The plant hormone ethylene (Bleecker and Kende, 2000) plays a vital role in the regulation of flower senescence, manifested in a range of symptoms including wilting, discoloration, bud degeneration, and abscission (Reid and Wu, 1992), which also occur in senescing orchid flower species (Goh et al., 1985; Woltering and Van Doorn, 1988). The responses to ethylene vary widely between species (Reid and Wu, 1992), although they are often consistent within families or subfamilies (Van Doorn, 2001). The *Orchidaceae* is classified as one of the ethylene-sensitive flower families, with a variable sensitivity to ethylene among the species and cultivars (Akamine, 1963; Burg and Dijkman, 1967; Goh et al., 1985; Woltering and Van Doorn, 1988). *Cattleya, Paphiopedilum*, *Dendrobium*, *Phalaenopsis*, and *Cymbidium* orchids were found to be highly sensitive to ethylene, which caused color fading and wilting of sepal tips, as well as bud and flower abscission (Woltering and Van Doorn, 1988; Porat et al., 1995; Ketsa and Rugkong, 2000). Additionally, *Cymbidium* orchids showed a dramatic response to exogenous ethylene, including induction of anthocyanin formation in female reproductive parts (Goh et al., 1985). Thus, the variation in postharvest life can partly be ascribed to differences in endogenous ethylene biosynthesis, as well as to differences in sensitivity to endogenous and exogenous ethylene (Goh et al., 1985; Woltering and Van Doorn, 1988).

1-Methylcyclopropene (1-MCP), an effective blocker of ethylene perception, is considered to bind to the ethylene receptor irreversibly, resulting in the inhibition of ethylene action (Serek et al., 1994; Sisler et al., 1996). 1-MCP prevents damage from exogenous ethylene in numerous potted plants and cut flower species (Serek et al., 1994, 2006; Serek and Sisler, 2001). Application of 1-MCP suppressed 1-aminocyclopropane-1-carboxylic acid oxidase (ACO) activity and ethylene production in *Cattleya alliance* orchids (Yamane et al., 2004). 1-MCP also delayed senescence in *Cymbidium* flowers with damaged pollinia, thereby extending their vase life, protected the flowers from the deleterious effects of exogenous ethylene, and prevented premature flower senescence generated by the damaged pollinia (Heyes and Johnston, 1998).

The *Vanda* 'Sansai Blue' orchid is a hybrid of *V. Crimson Glory* × *V. coerulea*, with big beautiful light blue florets, and a vase life of about 11–12 days (Khunmuang et al., 2016, 2018). The main senescence symptoms were flower wilting, epinasty, petal discoloration, and abscission. Our previous study showed that exposure of three *Vanda* cultivars, 'Patchara Delight', 'Pure Wax', and 'Sansai Blue' to 10 μl L^{-1} exogenous ethylene for 24 h significantly reduced by about 50% their vase life (Khunmuang et al., 2019). Ethylene treatment resulted in partial reduction of the anthocyanin content of 'Patchara Delight' after 2 days of vase life, mainly in the full bloom developmental stage, but had no effect on the coloration of 'Pure Wax' except in the bud stage. The flowers of 'Sansai Blue' showed a fast discoloration that occurred much before the wilting and other senescence symptoms (Khunmuang et al., 2019).

While regulation of anthocyanin biosynthesis at the physiological and molecular levels in flowers has been well studied and documented (Bradley et al., 1998; Weiss, 2000; Quattrocchio et al., 2006; Albert et al., 2009, 2010; Davies et al., 2012; Schwinn et al., 2014), the process of anthocyanin degradation was hardly investigated (Vaknin et al., 2005; Oren-Shamir, 2009). Recent studies reported that vacuolar peroxidases, belonging to the class III peroxidase, were responsible for the *in-planta* degradation of anthocyanins in *Brunfelsia calycina* flowers and in ripening grape berries grown in high temperatures (Zipor et al., 2014; Movahed et al., 2016; Lecourieux et al., 2017; Pastore et al., 2017). Therefore, it was of interest to further investigate in the present study, the rapid color fading in response of cut *Vanda* 'Sansai Blue' flowers to exogenous ethylene, focusing on the mechanism of anthocyanin breakdown process.

MATERIALS AND METHODS

Plant Materials and Treatments

Inflorescences of *Vanda* 'Sansai Blue' orchid were obtained from a commercial farm in Kanchanaburi province, Thailand. Orchid inflorescences bearing 5–8 open florets and 2–4 buds were selected for the experiment, and transported to King Mongkut's University of Technology Thonburi (KMUTT), Bangkhuntien campus, Bangkok within 1.5 h. Upon arrival to the laboratory, flower stems were re-cut under water to a 20-cm length from the stem end to the lower first flower.

For application of ethylene, inflorescences in vases with distilled water were exposed either to air as control, or to 1 or 10 μl L^{-1} ethylene for 24 h, in a 43-L glass chamber. The 1-MCP and ethylene treatment was applied by exposing the inflorescences to 0.2 μl L^{-1} 1-MCP (0.14% w:w; Ethylbloc®, FloraLife, Walterboro, SC, USA) for 6 h, followed by exposure to 10 μl L^{-1} ethylene for 24 h, in a 43-L glass chamber. All treatments were performed in a controlled environment room, maintained at 21 ± 2°C, 70–80% RH, under cool-white fluorescence light for 12 h day^{-1}. After treatments, flowers in vases with distilled water were incubated in the observation room throughout the experimental period.

Individual florets from five different developmental stages (tight bud; colored bud; half bloom; bloom; and full bloom) were detached from the inflorescences immediately or 2 days after treatments, photographed for their visual appearance, and assayed for their anthocyanin content as indicated below.

Evaluation of Inflorescence Vase Life Longevity

The number of senescing florets in the orchid inflorescences was recorded during the experiment. The vase life was terminated when more than 30% of the florets in an inflorescence lost quality due to petal necrosis, wilting (expressed in loss of turgidity – "sleepiness"), and/or abscission.

Determination of Anthocyanin Content by Spectrophotometer

Total anthocyanin was extracted and quantified as previously described (Rodriguez-Saona and Wrolstad, 2005). Samples (about 0.1 g) of fresh petals of florets at different developmental stages were grounded under liquid nitrogen to a fine powder, mixed with 10 ml of 0.01% HCl in methanol, and the extracts were incubated overnight in darkness at 4°C. Absorbance of these extracts was monitored at 530 nm using a spectrophotometer (UV-1800 Shimadzu). Anthocyanin content in the samples was expressed as OD530 mg FW^{-1}.

Extraction and Purification of Anthocyanin Samples for HPLC

Vanda floret petal samples (approximately 5 g FW) were homogenized in 20 ml of acidified methanol (containing 0.01% HCl), and incubated overnight in darkness at 4°C. The samples were filtered through Whatman no. 1 filter papers. The supernatant was removed, the pellet was re-extracted in 20 ml of acidified methanol, and the extracts were combined. The combined supernatants were dried at 40°C under vacuum (Buchi Evaporator; Vacuum controller V-800: Rotavapor R-205: Heating Bath B-490: Vac®V-500: Recirculating chiller B-740). The samples were evaporated until droplet, and the volume of the anthocyanin extract was adjusted to 0.5 ml with acidified water (containing 0.01% HCl).

The anthocyanin extraction-purification method was performed according to Rodriguez-Saona and Wrolstad (2005), with slight modifications. The anthocyanins were purified using a C18 cartridge (Water Sep-Pak®). The C18 cartridge was activated by flushing twice with methanol, followed by flushing three times with acidified water. The anthocyanins extract (dissolved in acidified water) was loaded into the activated cartridge, and then washed twice with acidified water to remove sugars, acids, and water soluble compounds, followed by washing with ethyl acetate for elimination of procyanidins. Finally, anthocyanins were eluted by acidified methanol. The purified anthocyanins were concentrated by evaporation at 40°C under vacuum, using a rotary evaporator.

HPLC Analysis and Composition of Total Anthocyanin

The non-hydrolyzed anthocyanin extracts were analyzed by HPLC (Shimadzu; DGU-20AS Degasser: LC-20AT Liquid Chromatograph: SPD-M20A Photo Diode Array Detector: SIL-20A Auto Sampler: C18 Inertsil® ODS-3; 4.6 mm × 250 mm, 5 µm column). The mobile phase consisted of solvent A (4% phosphoric acid in water) and solvent B (100% acetonitrile). Elution was performed in a linear gradient at the following ratios of solvent A and solvent B – 95:5, 77:23, 77:23, and 95:5 during 1, 25, 29, and 29.01 min, respectively, at a flow rate of 0.7 ml min^{-1} for 40 min. Chromatograms were obtained by LC solution program. Purified anthocyanins were dissolved in 4% phosphoric acid prior to HPLC purification. Anthocyanins were identified by comparing the retention time (RT) and spectral patterns of standard compounds. The content of the main three non-hydrolyzed anthocyanins at RT of 27.6, 33.8, and 36.0 min, were calculated and expressed as cyanidin-3-glucoside equivalents, after running a standard curve in HPLC under the same conditions. The contents were calculated according to the following equation: $Y = 5586.6X - 34{,}050$ (Y = peak area; X = ng cyanidin-3-glucoside).

For determination of anthocyanidins composition, another sample of purified anthocyanins (1.5–10 mg DW, lyophilized) was hydrolyzed by boiling in 2 N HCl for 1 h, and separated as described by Dela et al. (2003). Hydrolyzed anthocyanin samples were analyzed by HPLC (Shimadzu, Japan) equipped with an LC-10AT, an SCL-10A, and an SPD-M10AVP photodiode array detector. Separation was performed on a RP-C18 column (201TP54, Grace Vydac) at 27°C with the following solutions: (A) H_2O, pH 2.3 and (B) H_2O:MeCN:HOAc (107:50:40), pH 2.3. The solutions were applied as a linear gradient from a ratio of 4:1 (A:B) to 3:7 over 45 min, and held at a ratio of 3:7 for an additional 10 min at a flow rate of 0.5 ml min^{-1}. Anthocyanidins and flavonols were identified by comparing both the RT and the absorption spectrum from 250 to 650 nm to those of standard purified anthocyanidins and flavonols (obtained from Apin Chemicals, UK; Polyphenols, Norway; Sigma Aldrich, USA).

Extraction and Determination of Peroxidase Activity

Peroxidase (POD) activity of *Vanda* florets was determined as previously described (Gerailoo and Ghasemnezhad, 2011), with some modifications. Enzyme extraction for POD activity was prepared by homogenization of 2 g of floret petal samples in 20 ml extraction buffer composed of 50 mM phosphate buffer, pH 7, and 1% PVPP (w/v). The samples were centrifuged for 30 min at 12,000× *g*, and the supernatant was used to determine enzyme activity. POD activity was assayed by measuring spectrophotometrically the formation of guaiacol in l ml reaction mixture composed of 450 µl guaiacol 25 mM, 450 µl H_2O_2 225 mM, and 1 ml crude enzyme. The formation of tetraguaiacol was measured at 470 nm, and the activity was expressed as units per mg protein. Protein concentrations were measured as described by Bradford (1976).

Statistical Analysis

Experiments were arranged in a completely randomized design (CRD), with 6–8 replicate stems for each treatment. Data were analyzed using ANOVA, and differences among means were compared using Tukey Test.

RESULTS

Exposure of cut *Vanda* 'Sansai Blue' inflorescences to two ethylene concentrations for 24 h resulted in a dramatic bleaching of the florets at development stages B (colored bud) and C (half bloom) already during the 24 h of ethylene treatment (**Figure 1A**). On the other hand, in the more developed stages, D (bloom) and E (full bloom), the decrease in petal pigmentation

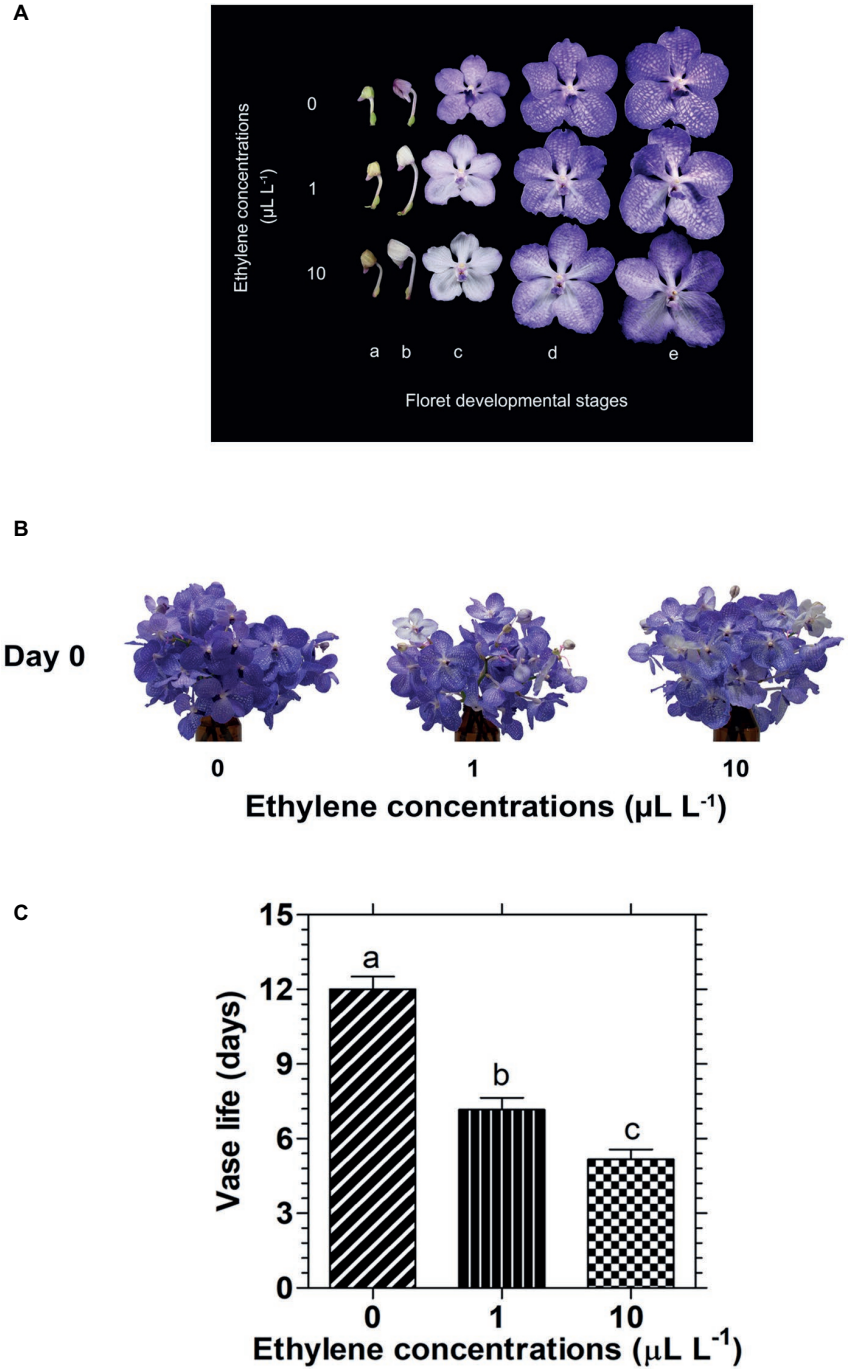

FIGURE 1 | Effect of exposure of cut *Vanda* 'Sansai Blue' flowers to different ethylene concentrations on the visual appearance of florets at various developmental stages **(A)**, on the visual appearance of cut inflorescences photographed immediately after removal from the ethylene environment (day 0) **(B)**, and on their vase life longevity **(C)**. The inflorescences were exposed to 0 (control), 1, or 10 μl L^{-1} ethylene for 24 h at 21 ± 2°C, and then placed in the observation room. The different floret developmental stages were defined as follows: a, tight bud; b, colored bud; c, half bloom; d, bloom; e, full bloom. The results in graph **(C)** represent means ± SE of 6–8 inflorescence replicates per treatment. Different letters indicate significant differences at $p < 0.01$.

was less noticeable at the end of the ethylene exposure (**Figure 1A**). Indeed, the appearance of a bunch of inflorescences held in the vase after their removal from the atmosphere of both ethylene concentrations, showed a faded color compared to control, but they were still blueish because most florets were in stages D and E (**Figure 1B**). It should be noted that the fast bleaching of the florets at developmental stages B and C (**Figure 1A**), and the visual color appearance of the whole inflorescences at day 0 (**Figure 1B**) were similar for the two ethylene concentrations. By contrast, the significant reduction

in their vase life longevity following exposure to ethylene was concentration-dependent (**Figure 1C**). Thus, exposure of the inflorescences to 1 or 10 μl L^{-1} ethylene significantly shortened their vase life to 7.2 and 5.2 days, respectively, as compared to control flowers which lasted for 12 days of vase life (**Figure 1C**).

In order to further examine the effect of ethylene on flower pigmentation during vase life, the inflorescences were exposed to 10 μl L^{-1} ethylene or to 0.2 μl L^{-1} 1-MCP followed by 10 μl L^{-1} ethylene. The results depicted in **Figure 2** demonstrate that the color intensity of the ethylene-treated flowers dramatically decreased on days 4 and 8, and this effect was completely inhibited by the 1-MCP pretreatment, which recovered the color appearance to that of control flowers at these time points (**Figure 2**).

A similar pattern of changes in response to these treatments was obtained in the anthocyanin content of florets, analyzed during 2 days of vase life after treatment. Thus, ethylene treatment significantly reduced the anthocyanin content of florets at the developmental stages of colored bud (**Figure 3A**) and half bloom (**Figure 3B**) on day 0, while the ethylene-induced reduction was less significant for florets at bloom stage (**Figure 3C**). On the other hand, on day 2, the reduction in anthocyanin content was significant for all three developmental stages (**Figure 3**). 1-MCP pretreatment abolished completely the ethylene effect on the anthocyanin content in all floret development stages at both time points, and recovered the anthocyanin levels to those of control florets (**Figure 3**).

More than eight anthocyanin peaks were observed in the chromatogram of *Vanda* 'Sansai Blue' florets at bloom stage following the HPLC analysis of non-hydrolyzed samples (**Figure 4A**). Two major anthocyanins were separated at RT of 27.6 and 33.8 min, and six less abundant anthocyanins appeared at RT of 19.5, 22.5, 25.0, 30.4, 36.0, and 38.9 min. The content of all these anthocyanins (peak height and area) remained similar in control florets at bloom stage after 2 days of vase life (**Figure 4D**). A drastic decrease of all anthocyanins could be observed in the ethylene-treated flowers, when flowers were removed from the ethylene atmosphere (day 0) (**Figure 4B**), and the small remaining residues of anthocyanin peaks further decreased to almost nullified levels on day 2 (**Figure 4E**). 1-MCP pretreatment prevented completely and very efficiently the ethylene-enhanced effect on the anthocyanin degradation

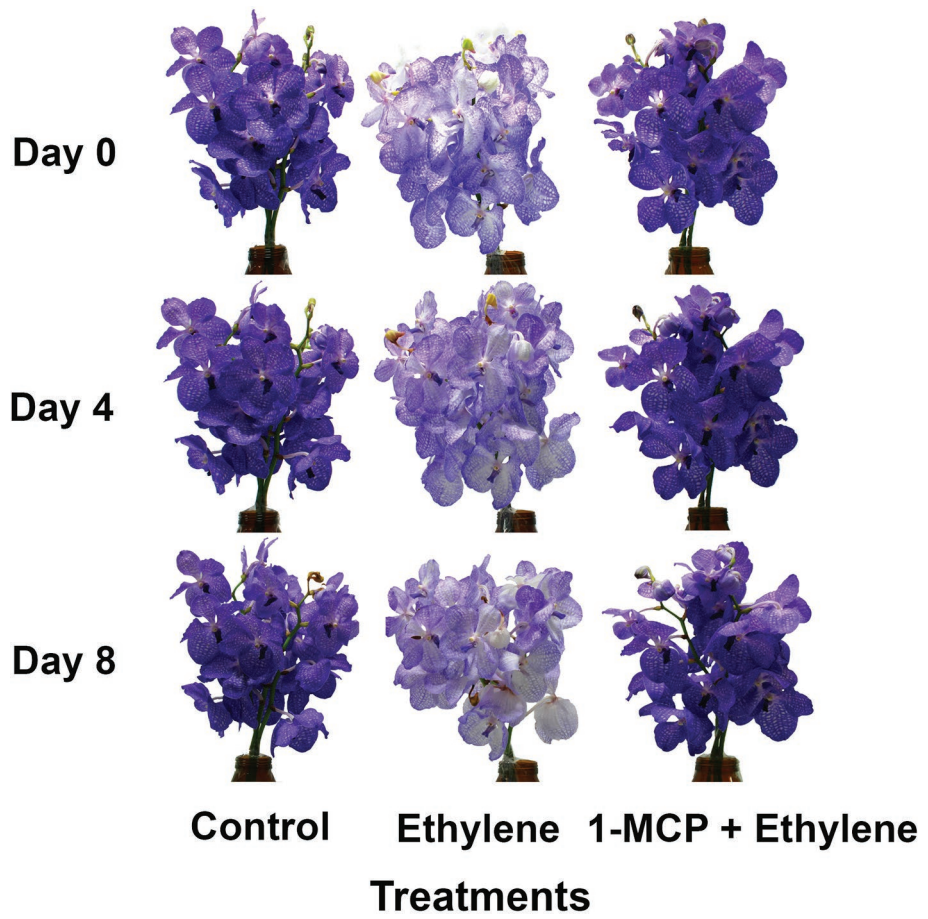

FIGURE 2 | Effect of ethylene and 1-MCP pre-treatments on the visual appearance of inflorescences during vase life of cut *Vanda* 'Sansai Blue' flowers after treatment application. The inflorescences were exposed to air (control), 10 μl L^{-1} ethylene for 24 h, or to 0.2 μl L^{-1} 1-MCP for 6 h followed by 10 μl L^{-1} ethylene for 24 h at 21 ± 2°C, and then placed in the observation room.

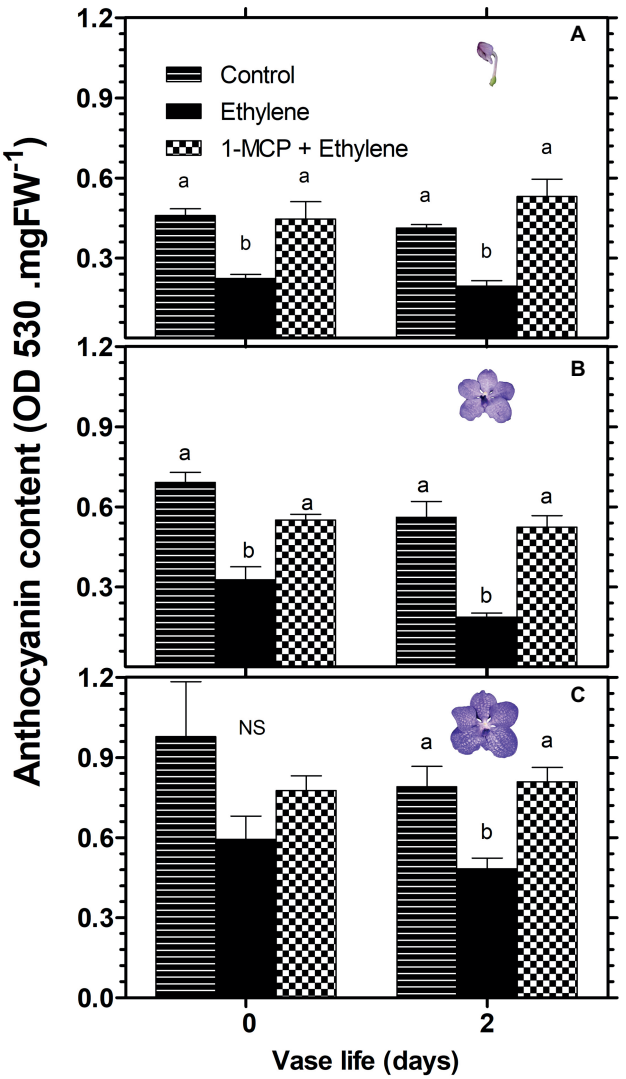

FIGURE 3 | Effect of ethylene and 1-MCP pre-treatments on changes in anthocyanin content of cut *Vanda* 'Sansai Blue' flowers at different developmental stages of colored bud **(A)**, half bloom **(B)**, and bloom **(C)**, during 2 days of vase life after treatments. Ethylene and 1-MCP pre-treatments were applied as detailed in **Figure 2**, and florets at the indicated developmental stages were sampled and assayed spectrophotometrically for anthocyanin content. The results represent means ± SE of four floret replicates per treatment. Different letters indicate significant differences among treatments at the different time points, at $p < 0.05$ for day 0, or at $p < 0.01$ for day 2 (graph **A**); at $p < 0.01$ (graphs **B,C**); NS, not significant.

both on day 0 (**Figure 4C**), and on day 2 (**Figure 4F**). Thus, the 1-MCP pretreatment recovered the anthocyanin levels to those of control untreated flowers (**Figures 4A,D**).

Similar results were obtained also for florets analyzed at the half bloom stage, in which the anthocyanins were nullified already on day 0 (data not shown). A quantitative data for the HPLC analysis described above is presented in **Figure 5** for total anthocyanins (the sum of peak area of all anthocyanins), expressed as cyanidin-3-glucoside equivalents. The data show that the ethylene treatment nullified the content of total anthocyanins during the ethylene exposure of florets at half bloom stage (**Figure 5A**), while at the bloom stage there was a continuous degradation of anthocyanins in response to ethylene between day 0 and day 2 (**Figure 5B**). 1-MCP pretreatment prevented the ethylene-induced anthocyanin degradation, and the levels of anthocyanins at half bloom stage even increased over control levels (**Figure 5A**), suggesting that anthocyanins were also synthesized during this period.

Analysis of hydrolyzed anthocyanin samples revealed that most of the anthocyanin pigments in *Vanda* 'Sansai Blue' flowers were based on delphinidin and cyanidin backbones (**Figure 6**). The results confirmed the previous findings, and show that ethylene reduced all anthocyanidins during the treatment at bloom stage florets (**Figure 6B**). Kaempferol was found to be the dominant flavonol in *Vanda* 'Sansai Blue' flowers (**Figure 7**), but unlike the anthocyanidins, the flavonols were not affected by the ethylene treatment (**Figure 7B**).

Anthocyanin degradation was reported to be mediated by enzymatic activity of the class III peroxidase (POX) (Zipor et al., 2014; Movahed et al., 2016; Lecourieux et al., 2017; Pastore et al., 2017). Therefore, in an attempt to investigate the mechanism of anthocyanin degradation in cut *Vanda* 'Sansai Blue' flowers, we have examined the effect of ethylene treatment on total peroxidase (POD) activity at different developmental stages (**Figure 8**). The results show a significant ethylene-induced increase in POD activity on day 2 in the colored bud stage (**Figure 8A**). 1-MCP pretreatment resulted in the lower POD activity, generally at all developmental stages, and it inhibited completely the ethylene-induced increase in POD activity (**Figure 8**). These results suggest that the ethylene-induced anthocyanin degradation in the cut *Vanda* 'Sansai Blue' flowers seems to be mediated by increased POD activity.

DISCUSSION

Ethylene Induces Color Fading in *Vanda* Flowers Independently of Senescence

The effect of exogenous ethylene treatment on cut *Vanda* 'Sansai Blue' flowers was very dramatic and rapid, and was already pronounced during the 24 h of exposure to the ethylene atmosphere (**Figures 1A,B**). In the younger flower developmental stages of colored buds and half bloom, the florets became almost completely white, while in the more advanced developmental stages, the bleaching was only partial during the ethylene treatment (**Figure 1B**), and the pigment degradation continued to take place throughout vase life (**Figure 2**). Both ethylene concentrations of 1 and 10 μl L^{-1} induced the same degree of color fading (**Figures 1A,B, 2**), indicating that the fading-induced effect of ethylene was not concentration-dependent in this range. On the other hand, the effect of ethylene treatment on flower senescence, expressed in a significant reduction of vase life due to floret wilting, was dependent on ethylene concentrations (**Figure 1C**). This suggests that the two processes of the rapid ethylene-induced anthocyanin degradation and the ethylene-induced senescence,

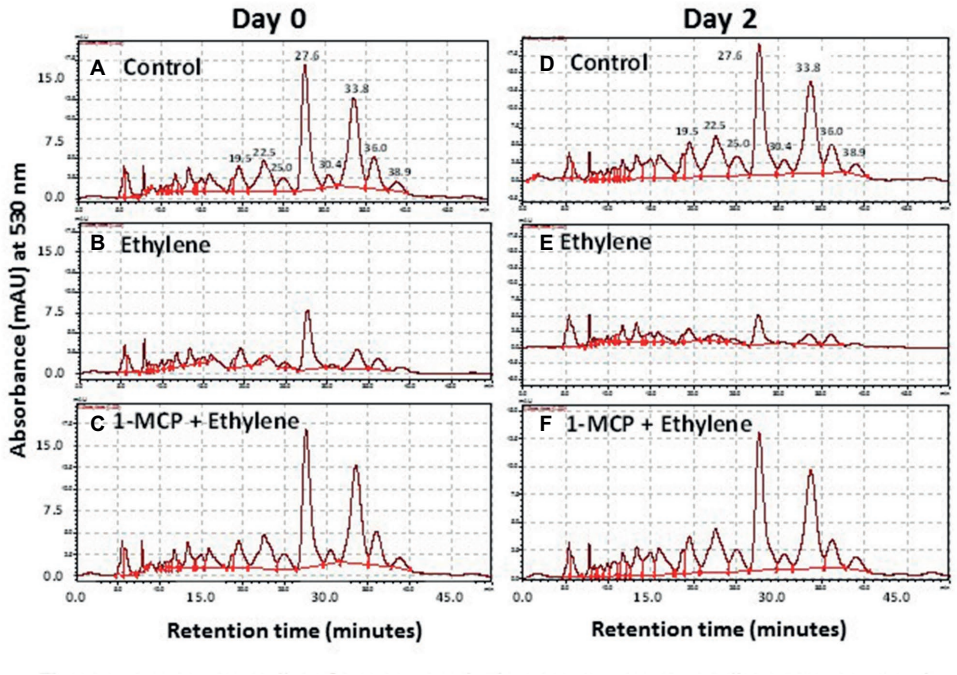

FIGURE 4 | Representative chromatograms of non-hydrolyzed anthocyanins, extracted from *Vanda* cv. 'Sansai Blue' florets, showing changes in the content of the two main anthocyanin peaks in response to ethylene and 1-MCP pre-treatments, immediately **(A–C)** and 2 days **(D–F)** after treatments. Anthocyanins were extracted from control **(A,D)**, ethylene-treated **(B,E)** or 1-MCP, and ethylene-treated **(C,F)** florets at the bloom developmental stage (see **Figure 1A**). Ethylene and 1-MCP pre-treatments were applied as detailed in **Figure 2**.

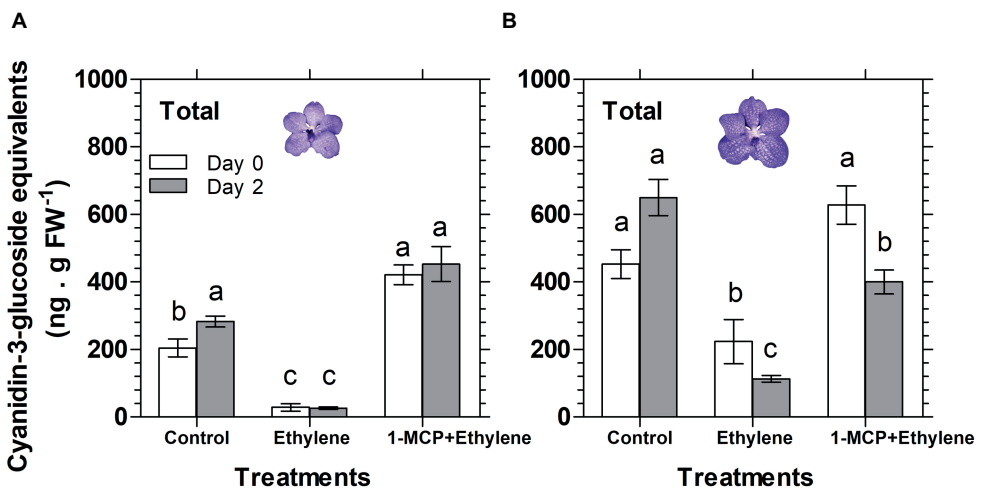

FIGURE 5 | Effect of ethylene and 1-MCP pre-treatments on changes, detected 2 days after treatments, in the content of total anthocyanins extracted from florets at half bloom **(A)** or bloom **(B)** developmental stages, based on the chromatogram peak areas of non-hydrolyzed samples of *Vanda* 'Sansai Blue' florets. Ethylene and 1-MCP pre-treatments were applied as detailed in **Figure 2**, and the anthocyanin level was calculated as cyanidin-3-glucoside equivalents. The results represent means ± SE of three floret replicates per treatment, and different letters indicate significant differences among treatments at the different time points, at $p < 0.01$.

proceed as separate processes at a different timing in cut *Vanda* 'Sansai Blue' flowers.

This conclusion is further supported by the following additional observations: (1) the wilting of the florets occurred first in the florets at the more advanced developmental stages, which are located at the bottom of the inflorescence, and proceeded upward. However, the upper florets that became completely bleached were still turgid and continued to bloom and grow until the end of the experiment (**Figure 2**). The decrease in water uptake in the ethylene-treated flowers

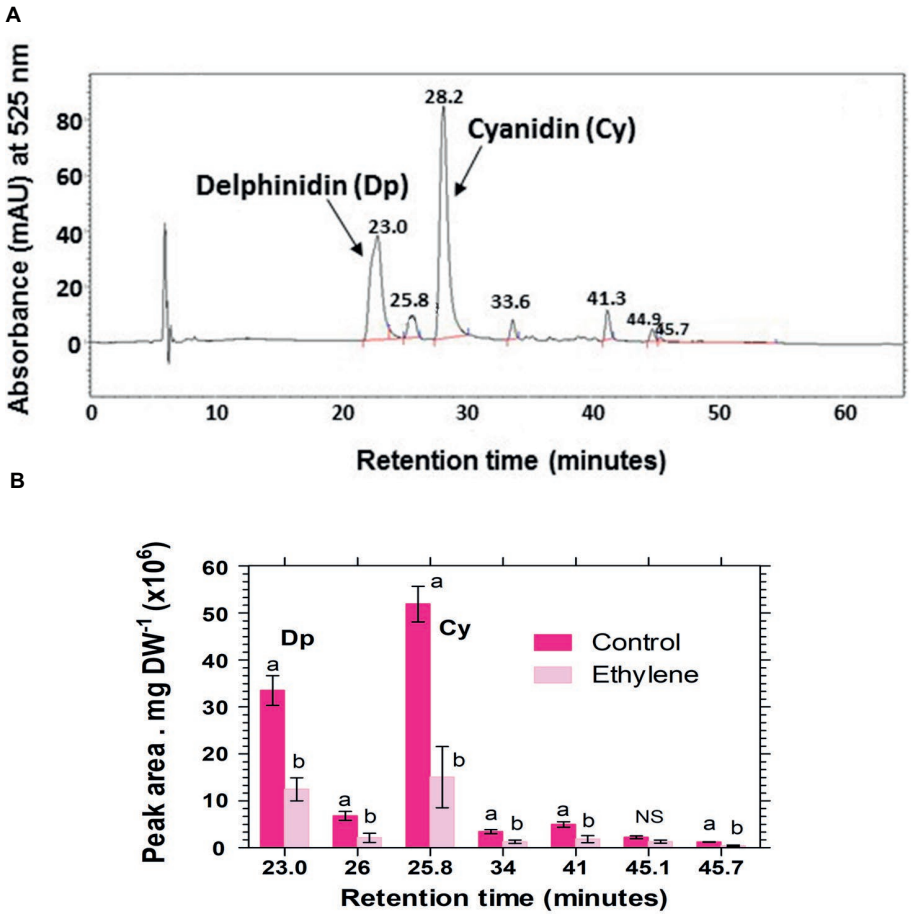

FIGURE 6 | A typical chromatogram profile of anthocyanidins detected in control hydrolyzed samples of *Vanda* 'Sansai Blue' florets **(A)**, and effect of ethylene treatment on the levels of these anthocyanidins, detected 2 days after treatment **(B)**. The inflorescences were exposed either to air (control) or to 10 µl L^{-1} ethylene for 24 h at 21 ± 2°C. Anthocyanins were extracted from florets at the bloom developmental stage (see **Figure 1A**), 2 days after treatment, hydrolyzed, purified and chromatographed. The results in graph **(B)** represent means ± SE of three floret replicates per treatment, and different letters indicate significant differences among treatments at the different time points, at $p < 0.01$ (for 21.44, 25.57, 45.7 min RT), or at $p < 0.05$ (for 37.43, 28.4, 34.37 min RT); NS, not significant. Dp, Delphinidin; Cy, Cyanidin.

was the reason for the enhanced decrease of the inflorescences FW, but the first wilted florets at the bottom of the inflorescence could be observed only when their FW decreased to about 93% of the initial value (Khunmuang et al., 2016, 2018). (2) The ethylene-induced bleaching of cut *Vanda* 'Sansai Blue' flowers was not accompanied by wilting symptoms or any other well-documented senescence parameters, such as ion leakage, protein degradation, and increased amino acid content (Mayak, 1987; Van Doorn, 2001; Van Doorn and Woltering, 2008; Rogers, 2013; Dar et al., 2014), during more than 7 days after treatment (Khunmuang et al., 2019). The presented results further suggest that the rapid ethylene-induced anthocyanin degradation of cut *Vanda* 'Sansai Blue' flowers proceeds as a separate process, independently from the well-characterized senescence-associated processes.

A similar fast ethylene-induced color fading was reported long ago in *Vanda* flowers, but in an indirect manner in response to pollination or emasculation, which induced high levels of endogenous ethylene production (Akamine, 1963; Burg and Dijkman, 1967; Goh et al., 1985). Thus, emasculation of *Vanda* 'Rose Marie' resulted in increased ethylene evolution, which started after a 10-h lag period, and fading became evident after additional 8–12 h (Burg and Dijkman, 1967). A similar time course of ethylene evolution and fading was reported for *Vanda* 'Miss Agnes Joaquim' flowers after their emasculation, in which ethylene production was correlated with the degree of color fading (Akamine, 1963). In *Vanda* 'Petamboerant' flowers, endogenous ethylene production rates increased in control flowers after 75 h, while pollination or emasculation enhanced the process by inducing ethylene production within 1 or 28 h, respectively (Burg and Dijkman, 1967). Consequently, the lower petals of pollinated or emasculated *Vanda* 'Petamboeran' flowers started to fade after 8–10 or 35 h, respectively, as compared to petals of control flowers which faded after about 80 h (Burg and Dijkman, 1967). Also in other orchid flowers of *Phalaenopsis* (Porat et al., 1995) and *Dendrobium* 'Pompadour' (Ketsa and Rugkong, 2000), pollination induced endogenous ethylene production, which enhanced their senescence.

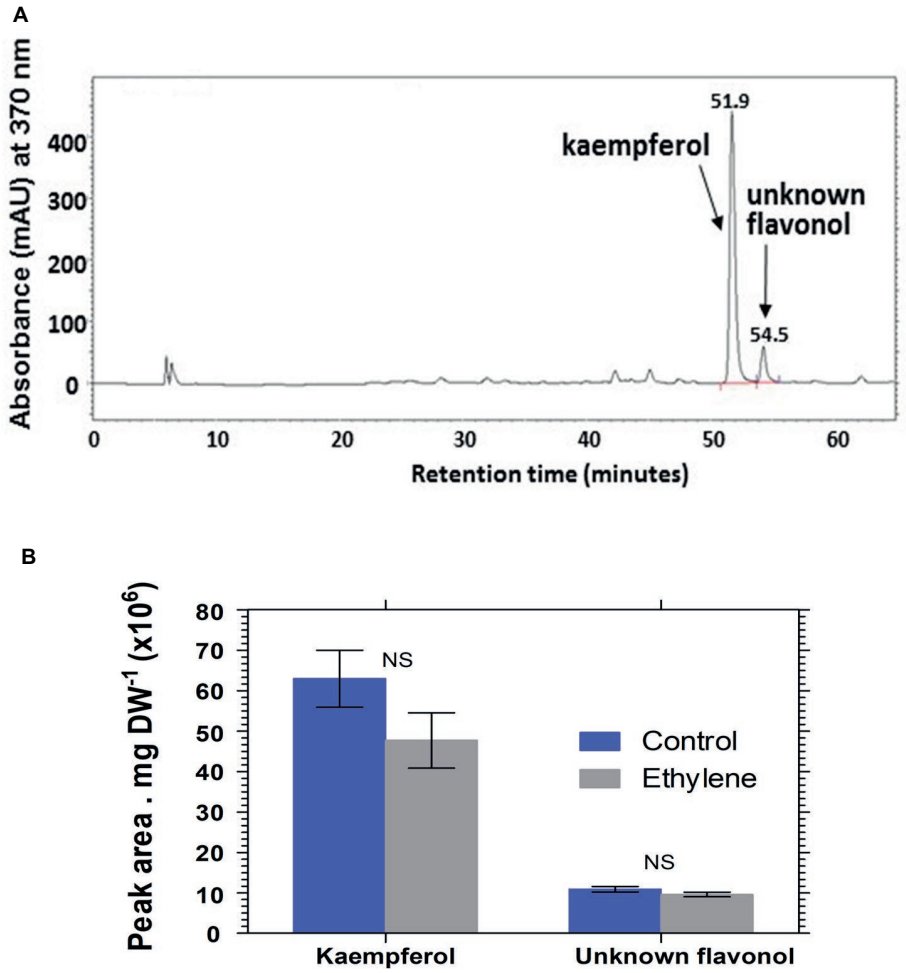

FIGURE 7 | A typical chromatogram profile of flavonols detected in control hydrolyzed samples of *Vanda* 'Sansai Blue' florets **(A)**, and effect of ethylene treatment on the levels of these flavonols detected 2 days after treatment **(B)**. The inflorescences were exposed either to air (control) or to 10 µl L^{-1} ethylene for 24 h at 21 ± 2°C. Flavonols were extracted from florets at the bloom developmental stage (see **Figure 1A**), 2 days after treatment, hydrolyzed, purified, and chromatographed. The results in graph **(B)** represent means ± SE of three floret replicates per treatment. NS, not significant.

A more direct effect of exogenous ethylene was reported recently, describing pulsing of cut *Vanda* 'Sansai Blue' flowers with the ethylene-releasing compound, ethephon. This treatment resulted in reduced water uptake and vase life longevity, and this effect was prevented by 1-MCP pretreatment, but the effect on color bleaching was less visible (Khunmuang et al., 2016). This discrepancy between the treatments could be ascribed to the fact that the ethylene released by ethephon pulsing affected more the stems, and less directly the florets at the younger developmental stages. In other orchid flowers, application of 10 µl L^{-1} ethephon by dipping for 5 min decreased significantly the water uptake of cut *Dendrobium* 'Planty Fushia' flowers, and reduced their vase life. Termination of vase life was due to senescence and abscission of the open florets at the bottom of the inflorescences, and prevention of opening of the florets at the bud stages that were abscised (Mohammadpour et al., 2015). These ethephon effects on cut *Dendrobium* "Planty Fushia" flowers were completely inhibited by 1-MCP pretreatment. Application of 0.25–2 µl L^{-1} 1-MCP to cut *Dendrobium* 'Burana Jade' flowers was even more effective in maintaining the FW as compared to control flowers (Yoodee and Obsuwan, 2013). This indicates that 1-MCP is effective also in inhibition of endogenous ethylene.

Anthocyanin Degradation Is Responsible for the Rapid Color Fading

The visible bleaching of the cut *Vanda* 'Sansai Blue' flowers (**Figures 1A,B, 2**) was due to anthocyanin pigment degradation induced by the ethylene treatments (**Figure 3**). The reduction in anthocyanin content in florets at half bloom and bloom stages in response to ethylene was quantitatively quite similar during the ethylene treatment (**Figure 3**). The light blueish color (**Figure 1B**) on day 0 and during vase life (**Figure 2**) observed in the ethylene-treated flowers reflected the pigment residues in the florets at more advanced developmental stages. The initial content of the anthocyanins in the more advanced

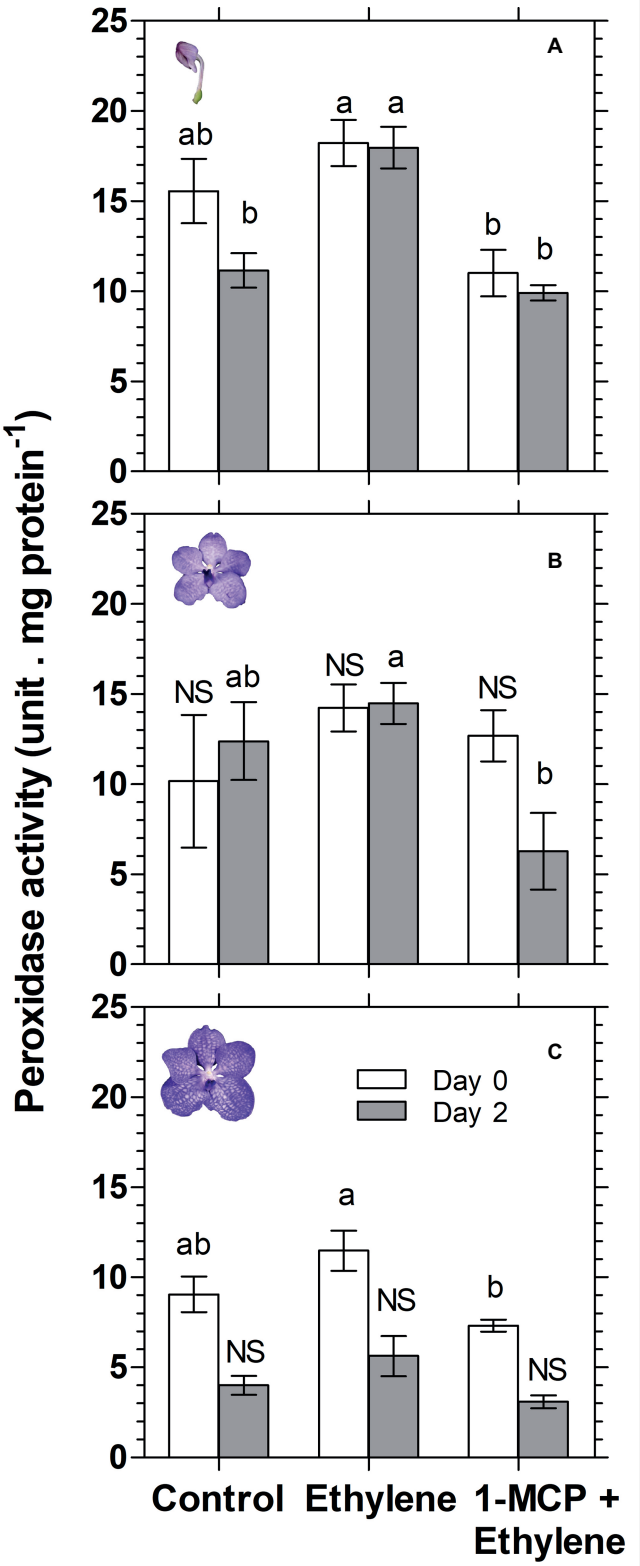

FIGURE 8 | Effect of ethylene and 1-MCP pre-treatments on changes in total peroxidase (POD) activity of *Vanda* 'Sansai Blue' cut flowers assayed at different developmental stages of colored bud **(A)**, half bloom **(B)**, and

(*Continued*)

FIGURE 8 | bloom **(C)**, during 2 days of vase life after treatments. Ethylene and 1-MCP pre-treatments were applied as detailed in **Figure 2**, and florets at the indicated developmental stages were sampled and assayed for POD activity. The results represent means ± SE of four floret replicates per treatment. Different letters indicate significant differences among treatments at the different time points, at $p < 0.05$ for day 0, or at $p < 0.01$ for day 2 (graph **A**); at $p < 0.01$ (graph **B**); at $p < 0.05$ for day 0 (graph **C**); NS, not significant.

developmental stages (**Figure 3C**) was much higher than in the early developmental stages (**Figure 3A**), and the anthocyanins continued to decrease in the ethylene-treated flowers (**Figures 2, 3**). The higher anthocyanin contents in the more developed floret stages (**Figure 3C**) indicate that anthocyanins continued to be synthesized in the flowers until reaching the full bloom stage. 1-MCP pretreatment completely inhibited the ethylene-induced floret bleaching (**Figure 2**), and anthocyanin degradation (**Figures 3–5**). Indeed, the visual appearance on day 8 of inflorescences pretreated with 1-MCP shows that their color was more pronounced than that of the control untreated flowers (**Figure 2**), but on the other hand, more florets with "sleepiness" symptoms at the bottom were detected (Khunmuang et al., 2019).

The results presented in **Figure 3** clearly demonstrate that anthocyanin content increases with development (zero time in each stage), but this process takes time (about 10 days from bud to a fully open flower). On the other hand, during the initial 2 days of vase life, anthocyanin levels did not change in the control samples of each developmental stage, but they were reduced significantly in the ethylene-treated samples, and this reduction was inhibited by 1-MCP. These results clearly show that the decreased anthocyanin levels resulted from the ethylene-induced degradation rather than from inhibition of anthocyanin biosynthesis.

Our previous study showed that while the effect of ethylene treatment in reducing the vase life longevity was similar in three cut *Vanda* cultivars, the effect of ethylene on flower color bleaching and anthocyanin content varied among the cultivars and floret stages (Khunmuang et al., 2019). The anthocyanin content of *Vanda* 'Pure Wax' flowers was almost unaffected by ethylene, except at the bud stage, while in cut *Vanda* 'Patchara Delight' flowers it was partially reduced after 2 days of vase life, mainly in the full bloom developmental stage. This suggests that the three *Vanda* cultivars differ in their sensitivity to ethylene, which is expressed at different developmental stages, and the *Vanda* 'Sansai Blue' flowers are unique among the three cultivars in their high sensitivity to ethylene manifested in the rapid color fading.

Variation in ethylene sensitivity may be related to differences in the concentration and affinity of the ethylene receptors and/or to the activity of downstream components in the signal transduction pathway, which activates gene transcription and translation (Bleecker and Kende, 2000). It was previously suggested that *Vanda* 'Sansai Blue' flowers are sensitive to ethylene but the flower itself produced very low amount of ethylene (Goh et al., 1985; Khunmuang et al., 2016, 2018).

Ethylene Induces Degradation of Anthocyanins *in planta*

More than eight anthocyanins were observed in *Vanda* 'Sansai Blue' flowers analyzed at the bloom stage by HPLC of unhydrolyzed samples, and all of them were fast degraded by ethylene treatment (**Figure 4**). Pigment accumulation, anthocyanin structure and the expression of floral anthocyanin genes were analyzed in anthocyanin-based colored florets of a pale-mauve *Vanda* hybrid (*V. teres* × *V. hookeriana*) (Junka et al., 2011). The anthocyanins gradually accumulated during all the developmental stages of the florets. Based on HPLC and LC-ESI-MSn analyses, the anthocyanins in the pale-mauve hybrid were composed of only five types of cyanidin derivatives, which were diversely conjugated with some hexose sugars and organic acids, such as ferrulic, sinapic, and malonic acids (Junka et al., 2011). On the other hand, more than 11 anthocyanins were observed in the violet-blue and red-purple flowers of the *Vanda* hybrid cultivars, from which eight major acylated anthocyanins were isolated (Tatsuzawa et al., 2004). Four of those pigments were based on cyanidin 3,7,3′-triglucoside, and the other four pigments were based on delphinidin 3,7,3′-triglucoside as their deacylanthocyanins. The distribution of these pigments was investigated in the flowers of four species and 13 hybrids by the analytical process of HPLC. Unfortunately, the *Vanda* 'Sansai Blue' was not included in this survey, but our anthocyanins hydrolyzed extract analysis revealed that most anthocyanidins in this cultivar are based on both delphinidin and cyanidin as well (**Figure 6**). The acylated anthocyanins of cyanidin and delphinidin contribute to make the blue flower color in the *Vanda* cultivars, as well as the presence of delphinidin glycosides (Tatsuzawa et al., 2004). This is generally true according to previous studies of orchids, which indicated that the bluing effect was dependent on the numbers of hydroxycinnamic acids (Lu et al., 1992; Honda and Saito, 2002).

The main flavonols that were found in *Vanda* 'Sansai Blue' florets were kaempherol and another unknown flavonol, which were not affected by the ethylene treatment (**Figure 7**). It seems, therefore, that they are not involved in the ethylene-induced color fading. Based on these results, it is clear that the ethylene-induced bleaching of *Vanda* 'Sansai Blue' flowers occurring *in planta* is ascribed only to the degradation of anthocyanins and not of flavonols.

Ethylene-Induced Anthocyanin Degradation Is Mediated by Peroxidase

Anthocyanin degradation has been detected *in vivo* in some systems such as the loss of red pigmentation in maturing leaves of *Photinia* spp. (Oren-Shamir and Nissim-Levi, 1999). The enzymatic degradation hypothesis was strongly supported by the investigation on *B. calycina* Benth., in which active anthocyanin degradation by oxidation was reported *in planta* (Vaknin et al., 2005; Oren-Shamir, 2009; Zipor et al., 2014). This loss of color from dark purple to white was dependent on anthocyanin degradation, and *de novo* synthesis of mRNAs and proteins during the different stages of development, well before flower senescence has started (Vaknin et al., 2005), similar to the results reported in the present study for *Vanda* 'Sansai Blue' flowers. A candidate peroxidase was partially purified and characterized, its intracellular localization was determined for *B. calycina* flowers (Zipor et al., 2014), and the transcript sequence of this peroxidase was fully identified. A basic peroxidase, BcPrx01, was responsible for the *in planta* degradation of anthocyanins in *B. calycina* flowers. BcPrx01 had the ability to degrade complex anthocyanins, it co-localized with these pigments in the vacuoles of petals, and both the mRNA and protein levels of BcPrx01 were greatly induced in parallel to the degradation of anthocyanins (Zipor et al., 2014). Recent studies confirmed the degradation of anthocyanins *in planta* by peroxidases, which exhibited higher activity at elevated temperatures (Movahed et al., 2016; Lecourieux et al., 2017; Pastore et al., 2017). Overexpression of the grapevine peroxidase gene (*Vvi-Prx31*) decreased anthocyanin contents in *Petunia hybrida* petals under heat stress condition, suggesting that a high temperature can stimulate peroxidase activity and anthocyanin degradation in ripening grape berries (Movahed et al., 2016). BcPrx01 and Vvi-Prx3 are vacuolar peroxidases, belonging to the class III peroxidase family (POX), and are able to catalyze the reduction of toxic H_2O_2 that reaches the vacuoles by oxidizing a variety of secondary metabolites (Hiraga et al., 2001).

Class III plant peroxidases (POXs) are plant-specific oxidoreductase, which participate in lignification, suberization, auxin catabolism, wound healing, and defense against pathogen infection (Hiraga et al., 2001). Studies have provided information on the regulatory mechanisms of wound- and pathogen-induced expression of some *POX* genes. These studies suggest that *POX* genes are induced *via* different signal transduction pathways from those of other known defense-related genes (Ishige et al., 1993; Ito et al., 1994). Furthermore, high temperature (35°C) increased ethylene production and concentration of H_2O_2, and the activity of POX in plum fruit (Niu et al., 2017). It seems, therefore, that ethylene is an enhancer of peroxidase activity. It is important to emphasize that in the present study, total peroxidase (POD) was assayed, rather than the specific class III peroxidase (POX). This may explain the insignificant effects of ethylene on peroxidase activity obtained on day 0 at all assayed developmental stages (**Figure 8**). Nevertheless, we could demonstrate that ethylene treatment significantly increased total POD activity on day 2 at the bud developmental stage, and this effect was inhibited completely by 1-MCP pretreatment (**Figure 8A**). These results are consistent with the results of anthocyanin content at the bud stage (**Figure 3A**). This may indicate that POD activity is highly affected by ethylene at the bud stage, relative to the other developmental stages. Since the anthocyanins accumulate in the vacuole, it is necessary that the vacuolar peroxidase (POX) will degrade them. Our results indicate that at the bud stage, the activity of POX in the POD extract is relatively high, and therefore the results for the ethylene effects at this stage were significant (**Figure 8A**). Alternatively, since the anthocyanins are synthesized in the cytoplasm at the bud stage, it is still possible that they are degraded by the cytoplasmic peroxidase in response to ethylene, before reaching the vacuole. Additionally, the insignificant effects of ethylene on POD activity obtained at the other developmental

stages (**Figures 8B,C**), may indicate that another unknown mechanism is possibly involved in this process, which needs a further study.

Taken together, our results suggest that the ethylene-induced anthocyanins degradation in cut *Vanda* 'Sansai Blue' flowers seems to be mediated by increased POD activity *in-planta*. This effect, which is fast and independent of the flower senescence process, is mainly expressed at the bud developmental stage, in which the anthocyanin degradation was most prominent.

DATA AVAILABILITY

All datasets generated for this study are included in the manuscript and/or the supplementary files.

AUTHOR CONTRIBUTIONS

SKh, MB, SM, SP-H, CW-A, and SKa were responsible for the conception, design of the experiments, and interpretation of data. SKh performed the laboratory experiments and the HPLC analyses. MO-S and RO were responsible for the anthocyanin analyses and determination. SKh, MB, SM, and SP-H were involved in drafting the work. SP-H and SM were responsible for the writing, editing, and final approval of the version to be published. All authors revised and approved the final version.

FUNDING

The research was supported by the Royal Golden Jubilee (RGJ) Ph.D. Program (Grant No. PHD/0120/2553), the Thailand Research Fund (TRF).

ACKNOWLEDGMENTS

We would like to thank the Postharvest Technology Innovation Center, Office of the Higher Education Commission, Bangkok, Thailand, for the laboratory facilities.

REFERENCES

Akamine, E. A. (1963). Ethylene production in fading *Vanda* orchid blossoms. *Science* 14, 12–17.

Albert, N. W., Arathoon, S., Collette, V. E., Schwinn, K. E., Jameson, P. E., Lewis, D. H., et al. (2010). Activation of anthocyanin synthesis in *Cymbidium* orchids: variability between known regulators. *Plant Cell Tissue Organ Cult.* 100, 355–360. doi: 10.1007/s11240-009-9649-0

Albert, N. W., Lewis, D. H., Zhang, H., Irving, L. J., Jameson, P. E., and Davies, K. M. (2009). Light-induced vegetative anthocyanin pigmentation in *Petunia*. *J. Exp. Bot.* 60, 2191–2202. doi: 10.1093/jxb/erp097

Bleecker, A. B., and Kende, H. (2000). Ethylene: a gaseous signal molecule in plants. *Ann. Rev. Cell Develop. Biol.* 16, 1–18. doi: 10.1146/annurev.cellbio.16.1.1

Bradford, M. M. (1976). A rapid and sensitive method for the quantitation of microgram quantities of protein utilizing the principle of protein-dye binding. *Anal. Biochem.* 72, 248–254. doi: 10.1016/0003-2697(76)90527-3

Bradley, J. M., Davies, K. M., Deroles, S. C., Bloor, S. J., and Lewis, D. H. (1998). The maize *Lc* regulatory gene up-regulates the flavonoid biosynthetic pathway of *Petunia*. *Plant J.* 13, 381–392. doi: 10.1046/j.1365-313X.1998.00031.x

Burg, S. P., and Dijkman, M. J. (1967). Ethylene and auxin participation in pollen induced fading of *Vanda* orchid blossoms. *Plant Physiol.* 42, 1648–1650. doi: 10.1104/pp.42.11.1648

Dar, R. A., Tahir, I., and Ahmad, S. S. (2014). Physiological and biochemical changes associated with flower development and senescence in *Dianthus chinensis*. *Indian J. Plant Physiol.* 19, 215–221. doi: 10.1007/s40502-014-0104-9

Davies, K. M., Albert, N. W., and Schwinn, K. E. (2012). From landing lights to mimicry: the molecular regulation of flower coloration and mechanisms for pigmentation patterning. *Funct. Plant Biol.* 39, 619–638. doi: 10.1071/FP12195

Dela, G., Or, E., Ovadia, R., Nissim-Levi, A., Weiss, D., and Oren-Shamir, M. (2003). Changes in anthocyanin concentration and composition in 'jaguar' rose flowers due to transient high-temperature conditions. *Plant Sci.* 164, 333–340. doi: 10.1016/S0168-9452(02)00417-X

Gerailoo, S., and Ghasemnezhad, M. (2011). Effect of salicylic acid on antioxidant enzyme activity and petal senescence in 'Yellow Island' cut rose flowers. *J. Fruit Ornamental Plant Res.* 19, 183–193. doi: 10.1007/978-94-007-6428-6_15

Goh, C. J., Halevy, A. H., and Kofranek, A. M. (1985). Ethylene evolution and sensitivity in cut orchid flowers. *Sci. Hortic.* 26, 57–67. doi: 10.1016/0304-4238(85)90102-5

Heyes, J. A., and Johnston, J. W. (1998). 1-Methylcyclopropene extends *Cymbidium* orchid vase life and prevents damaged pollinia from accelerating senescence. *New Zealand J. Crop Hortic. Sci.* 26, 319–324. doi: 10.1080/01140671.1998.9514070

Hiraga, S., Sasaki, K., Ito, H., Ohashi, Y., and Matsui, H. (2001). A large family of class III plant peroxidases. *Plant Cell Physiol.* 42, 462–468. doi: 10.1093/pcp/pce061

Honda, T., and Saito, N. (2002). Recent progress in the chemistry of polyacylated anthocyanins as flower color pigments. *Heterocycles* 56, 633–692. doi: 10.3987/REV-01-SR(K)2

Ishige, F., Mori, H., Yamazaki, K., and Imaseki, H. (1993). Identification of a primary leaves basic clycoprotein induced by ethylene in Azuki bean as a cationic peroxidase. *Plant Physiol.* 101, 193–199. doi: 10.1104/pp.101.1.193

Ito, H., Kimizuka, F., Ohbayashi, A., Matsui, H., Honma, M., Shinmyo, A., et al. (1994). Molecular cloning and characterization of two complementary DNAs encoding putative peroxidases from rice (*Oryza sativa* L.) shoots. *Plant Cell Rep.* 13, 361–366. doi: 10.1007/BF00234138

Junka, N., Kanlayanarat, S., Buanong, M., Wongchaochant, S., and Wongs-Aree, C. (2011). Analysis of anthocyanins and the expression patterns of genes involved in biosynthesis in two *Vanda* hybrids. *Int. J. Agric. Biol.* 13, 873–880.

Ketsa, S., and Rugkong, A. (2000). Ethylene production, senescence and ethylene sensitivity in *Dendrobium* 'pompadour' flowers following pollination. *J. Hortic. Sci. Biotechnol.* 75, 149–153. doi: 10.1080/14620316.2000.11511214

Khunmuang, S., Kanlayanarat, S., Wongchaochant, S., Wongs-Aree, C., Meir, S., Philosoph-Hadas, S., et al. (2018). Development of means for delaying senescence and prolonging the vase life of cut flowers of *Vanda* orchid cv. 'Sansai blue'. *Acta Hortic.* 1213, 581–586. doi: 10.17660/ActaHortic.2018.1213.88

Khunmuang, S., Kanlayanarat, S., Wongs-Aree, C., Meir, S., Philosoph-Hadas, S., and Buanong, M. (2016). Effect of ethephon and 1-MCP treatment on the vase life of cut 'Sansai blue' *Vanda*. *Acta Hortic.* 1131, 119–125. doi: 10.17660/ActaHortic.2016.1131.16

Khunmuang, S., Kanlayanarat, S., Wongs-Aree, C., Meir, S., Philosoph-Hadas, S., and Buanong, M. (2019). Variability in the response to ethylene of three cultivars of cut *Vanda* orchid flowers. *Acta Hortic.* (in press).

Lecourieux, F., Kappel, C., Pieri, P., Charon, J., Pillet, J., Hilbert, G., et al. (2017). Dissecting the biochemical and transcriptomic effects of a locally applied heat treatment on developing cabernet sauvignon grape berries. *Front. Plant Sci.* 8:53. doi: 10.3389/fpls.2017.00053

Lu, T. S., Saito, N., Yokoi, M., Shigihara, A., and Honda, T. (1992). Acylated pelargonidin glycosides in the red-purple flowers of *Pharbitis nil*. *Phytochemistry* 31, 289–295. doi: 10.1016/0031-9422(91)83056-Q

Mayak, S. (1987). Senescence of cut flowers. *HortScience* 22, 863–865.

Mohammadpour, R., Buanong, M., Jitareerat, P., Wongs-Aree, C., and Uthairatanakij, A. (2015). Response of *Dendrobium* 'Planty Fushia' to ethylene and ethylene inhibitor. *Acta Hortic.* 1078, 99–106. doi: 10.17660/ActaHortic.2015.1078.13

Movahed, N., Pastore, C., Cellini, A., Allegro, G., Valentini, G., Zenoni, S., et al. (2016). The grapevine *VviPrx31* peroxidase as a candidate gene involved in anthocyanin degradation in ripening berries under high temperature. *J. Plant Res.* 129, 513–526. doi: 10.1007/s10265-016-0786-3

Niu, J., Zhang, G., Zhang, W., Goltsev, V., Sun, S., Wang, J., et al. (2017). Anthocyanin concentration depends on the counterbalance between its synthesis and degradation in plum fruit at high temperature. *Sci. Rep.* 7:7684. doi: 10.1038/s41598-017-07896-0

Oren-Shamir, M. (2009). Does anthocyanin degradation play a significant role in determining pigment concentration in plants? *Plant Sci.* 177, 310–316. doi: 10.1016/j.plantsci.2009.06.015

Oren-Shamir, M., and Nissim-Levi, A. (1999). Temperature and gibberellin effects on growth and anthocyanin pigmentation in *Photinia* leaves. *J. Hortic. Sci. Biotechnol.* 74, 355–360.

Pastore, C., Dal Santo, S., Zenoni, S., Movahed, N., Allegro, G., Valentini, G., et al. (2017). Whole plant temperature manipulation affects flavonoid metabolism and the transcriptome of grapevine berries. *Front. Plant Sci.* 8:929. doi: 10.3389/fpls.2017.00929

Porat, R., Halevy, A. H., Serek, M., and Borochov, A. (1995). An increase in ethylene sensitivity following pollination is the initial event triggering an increase in ethylene production and enhanced senescence of *Phalaenopsis* orchid flowers. *Physiol. Plant.* 93, 778–784. doi: 10.1111/j.1399-3054.1995.tb05131.x

Quattrocchio, F., Verweij, W., Kroon, A., Spelt, C., Mol, J., and Koes, R. (2006). PH4 of *Petunia* is an R2R3 MYB protein that activates vacuolar acidification through interactions with basic-helix-loop-helix transcription factors of the anthocyanin pathway. *Plant Cell* 18, 1274–1291. doi: 10.1105/tpc.105.034041

Reid, M. S., and Wu, M. J. (1992). Ethylene and flower senescence. *Plant Growth Regul.* 11, 37–43. doi: 10.1007/BF00024431

Rodriguez-Saona, L. E., and Wrolstad, R. E. (2005). "Extraction, isolation, and purification of anthocyanins" in *Handbook of food analytical chemistry (Vol 2): Pigments, colorants, flavors, texture, and bioactive food components*. eds. R. E. Wrolstad, T. F. Acree, E. A. Decker, M. H. Penner, D. S. Reid, S. J. Schwartz et al. (New Jersey: John Wiley & Sons Inc.), 7–17.

Rogers, H. J. (2013). From models to ornamentals: how is flower senescence regulated? *Plant Mol. Biol.* 82, 563–574. doi: 10.1007/s11103-012-9968-0

Schwinn, K. E., Boase, M. R., Bradley, J. M., Lewis, D. H., Deroles, S. C., Martin, C. R., et al. (2014). MYB and bHLH transcription factor transgenes increase anthocyanin pigmentation in *Petunia* and lisianthus plants, and the *Petunia* phenotypes are strongly enhanced under field conditions. *Front. Plant Sci.* 5:603. doi: 10.3389/fpls.2014.00603

Serek, M., Reid, M. S., and Sisler, E. C. (1994). A volatile ethylene inhibitor improves the postharvest life of potted roses. *J. Amer. Soc. Hort. Sci.* 119, 572–577.

Serek, M., and Sisler, E. C. (2001). Efficacy of inhibitor of ethylene binding in improvement of the postharvest characteristics of potted flowering plants. *Postharvest Biol. Technol.* 23, 161–166. doi: 10.1016/S0925-5214(01)00109-0

Serek, M., Woltering, E. J., Sisler, E. C., Frello, S., and Sriskandarajah, S. (2006). Controlling ethylene responses in flowers at the receptor level. *Biotechnol. Adv.* 24, 368–381. doi: 10.1016/j.biotechadv.2006.01.007

Sisler, E. C., Dupille, E., and Serek, M. (1996). Effect of 1-methylcyclopropene and methylene-cyclopropane on ethylene binding and ethylene action on cut carnations. *Plant Growth Regul.* 18, 79–86. doi: 10.1007/BF00028491

Tatsuzawa, F., Saito, N., Seki, H., Yokoi, M., Yukawa, T., Shinoda, K., et al. (2004). Acylated anthocyanins in the flowers of *Vanda* (Orchidaceae). *Biochem. Syst. Ecol.* 32, 651–664. doi: 10.1016/j.bse.2004.02.004

Vaknin, H., Bar-Akiva, A., Ovadia, R., Nissim-Levi, A., Forer, I., Weiss, D., et al. (2005). Active anthocyanin degradation in *Brunfelsia calycina* (yesterday–today–tomorrow) flowers. *Planta* 222, 19–26. doi: 10.1007/s00425-005-1509-5

Van Doorn, W. G. (2001). Categories of petal senescence and abscission: a re-evaluation. *Ann. Bot.* 87, 447–456. doi: 10.1006/anbo.2000.1357

Van Doorn, W. G., and Woltering, E. J. (2008). Physiology and molecular biology of petal senescence. *J. Exp. Bot.* 59, 453–480. doi: 10.1093/jxb/erm356

Weiss, D. (2000). Regulation of flower pigmentation and growth: multiple signaling pathways control anthocyanin synthesis in expanding petals. *Physiol. Plant.* 110, 152–157. doi: 10.1034/j.1399-3054.2000.110202.x

Woltering, E. J., and Van Doorn, W. G. (1988). Role of ethylene in senescence of petals - morphological and taxonomical relationships. *J. Exp. Bot.* 39, 1605–1616. doi: 10.1093/jxb/39.11.1605

Yamane, K., Yamaki, Y., and Fujishige, N. (2004). Effect of exogenous ethylene and 1-MCP on ACC oxidase activity, ethylene production and vase life in *Cattleya Aliliances. J. Japan. Soc. Hort. Sci.* 73, 128–133. doi: 10.2503/jjshs.73.128

Yoodee, Y., and Obsuwan, K. (2013). Effects of 1-MCP on postharvest life of cut *Dendrobium* 'Burana Jade' inflorescences. *Acta Hortic.* 970, 261–265. doi: 10.17660/ActaHortic.2013.970.31

Zipor, G., Duarte, P., Carqueijeiro, I., Shahar, L., Ovadia, R., Teper-Bamnolker, P., et al. (2014). *In planta* anthocyanin degradation by a vacuolar class III peroxidase in *Brunfelsia calycina* flowers. *New Phytol.* 205, 653–665. doi: 10.1111/nph.13038

Conflict of Interest Statement: The authors declare that the research was conducted in the absence of any commercial or financial relationships that could be construed as a potential conflict of interest.

frontiers in Plant Science

REVIEW
published: 26 August 2019
doi: 10.3389/fpls.2019.01030

Shaping Ethylene Response: The Role of EIN3/EIL1 Transcription Factors

Vladislav A. Dolgikh[1,2], *Evgeniya M. Pukhovaya*[1,2] *and Elena V. Zemlyanskaya*[1,2]*

[1] Institute of Cytology and Genetics, Siberian Branch of Russian Academy of Sciences, Novosibirsk, Russia, [2] Department of Natural Sciences, Novosibirsk State University, Novosibirsk, Russia

OPEN ACCESS

Edited by:
Jin-Song Zhang, Institute of Genetics and Developmental Biology (CAS), China

Reviewed by:
Xing Wen, Southern University of Science and Technology, China
Hong Qiao, University of Texas at Austin, United States
Shangwei Zhong, Peking University, China

***Correspondence:**
Elena V. Zemlyanskaya
ezemlyanskaya@bionet.nsc.ru

Specialty section:
This article was submitted to Plant Physiology, a section of the journal Frontiers in Plant Science

Received: *30 April 2019*
Accepted: *23 July 2019*
Published: *26 August 2019*

Citation:
Dolgikh VA, Pukhovaya EM and Zemlyanskaya EV (2019) Shaping Ethylene Response: The Role of EIN3/EIL1 Transcription Factors. Front. Plant Sci. 10:1030. doi: 10.3389/fpls.2019.01030

EIN3/EIL1 transcription factors are the key regulators of ethylene signaling that sustain a variety of plant responses to ethylene. Since ethylene regulates multiple aspects of plant development and stress responses, its signaling outcome needs proper modulation depending on the spatiotemporal and environmental conditions. In this review, we summarize recent advances on the molecular mechanisms that underlie EIN3/EIL1-directed ethylene signaling in Arabidopsis. We focus on the role of EIN3/EIL1 in tuning transcriptional regulation of ethylene response in time and space. Besides, we consider the role of EIN3/EIL1-independent regulation of ethylene signaling.

Keywords: ETHYLENE-INSENSITIVE3, ETHYLENE-INSENSITIVE3-LIKE, epigenetic regulation, protein–protein interactions, cross-talk

KEY COMPONENTS OF ETHYLENE SIGNALING PATHWAY

Plant hormone ethylene coordinates numerous developmental processes (including germination, soil emergence, seedling growth, fruit ripening, senescence, abscission, etc.), as well as diverse biotic and abiotic stress responses (Abeles et al., 2012). Ethylene has also been shown to induce typical morphological changes in dark-grown seedlings (inhibition of hypocotyl and root elongation, radial swelling of hypocotyl, and exaggeration of apical hook) known as "the triple response" (Ecker, 1995). Ethylene is produced from *L*-methionine, which is consequently converted to *S*-adenosyl-*L*-methionine (by SAM-synthetases), 1-aminocyclopropane-1-carboxylic acid (ACC) (by ACC synthases), and ethylene (by ACC oxidases) (reviewed in Booker and DeLong, 2015). Ethylene is perceived by a family of receptors (ETHYLENE RESPONSE 1, ETR1; ETHYLENE RESPONSE SENSOR 1, ERS1; ETR2, ETHYLENE INSENSITIVE 4, EIN4; and ERS2 in Arabidopsis) localized in the endoplasmic reticulum (ER) membrane (reviewed in Lacey and Binder, 2014). Upon binding, ethylene inactivates them and thereby blocks the serine–threonine protein kinase CONSTITUTIVE TRIPLE RESPONSE 1 (CTR1) activity promoting the cleavage of ER-anchored EIN2 protein (reviewed in Chang, 2016; Hu et al., 2017). EIN2 C-terminal domain (EIN2-C) released upon cleavage indirectly triggers EIN3 and EIN3-Like (EIL) transcription factors (TFs) that are considered the key transcriptional regulators of ethylene response (**Figure 1**). Noteworthy, these TFs function as a hub that integrates and processes different cues to "shape" ethylene response in accordance with spatiotemporal and environmental conditions. Below, we will focus on the nuclear events that conduct EIN3/EIL activation and set their functional output.

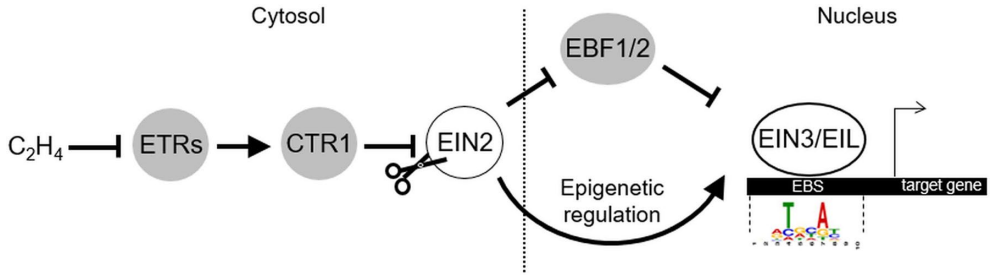

FIGURE 1 | The key components of ethylene signaling pathway. Gray and white circles depict negative and positive regulators of ethylene signaling, correspondingly. Position frequency matrix for Arabidopsis EIN3 binding motif (Chang et al., 2013) was retrieved from CIS-BP database (Weirauch et al., 2014) and visualized using Tomtom tool (http://meme-suite.org/tools/tomtom; Gupta et al. 2007). The model is based on the findings reported previously (Chang, 2016; Hu et al., 2017). The explanations are in the text. EBS, EIN3 binding site.

ACTIVATION OF EIN3 AND ITS HOMOLOGS IN RESPONSE TO ETHYLENE

EIL is a small family of plant-specific proteins. There are six genes encoding the members of this family in *Arabidopsis thaliana* genome (*EIN3*, *EIL1-5*) (Chao et al., 1997; Guo and Ecker, 2004). They harbor a conservative N-terminal DNA-binding domain with a unique fold structure (Song et al., 2015). EIN3, EIL1, and EIL2 represent functionally homologous proteins involved in the regulation of ethylene-responsive genes (Chao et al., 1997; Solano et al., 1998; Alonso et al., 2003; An et al., 2010). The most closely related EIN3 and EIL1 are considered the major regulators since *ein3 eil1* double mutants show complete ethylene insensitivity in terms of the triple response, pathogen resistance, and the ability to fully suppress *ctr1* mutation (reviewed in Guo and Ecker, 2004; Cho and Yoo, 2015). Two paralogs differentially regulate ethylene response in the seedlings (EIN3) and in adult leaves and stems (EIL1) (An et al., 2010). Yet, a minor, *EIL2* role in the regulation of ethylene response is supported by its capability to complement *ein3* mutation when overexpressed (Chao et al., 1997). In **Figure 2**, we visualized tissue-specific expression levels of *EIL* genes based on publicly available data on transcriptome profiling in different Arabidopsis tissues retrieved from ThaleMine v1.10.4 (https://apps.araport.org/thalemine/; Krishnakumar et al., 2017). Unlike *EIN3* and *EIL1*, *EIL2* transcripts level is low throughout plant tissues; moderate *EIL2* expression is restricted to root apical meristem and pollen (**Figure 2**). Therefore, EIL2 function could be limited to specific spatiotemporal conditions. EIL3/SLIM1 does not function in ethylene pathway but regulates sulfur deficiency response; no defined roles of EIL4 and EIL5 have been reported to date (reviewed in Guo and Ecker, 2004; Wawrzyńska and Sirko, 2014).

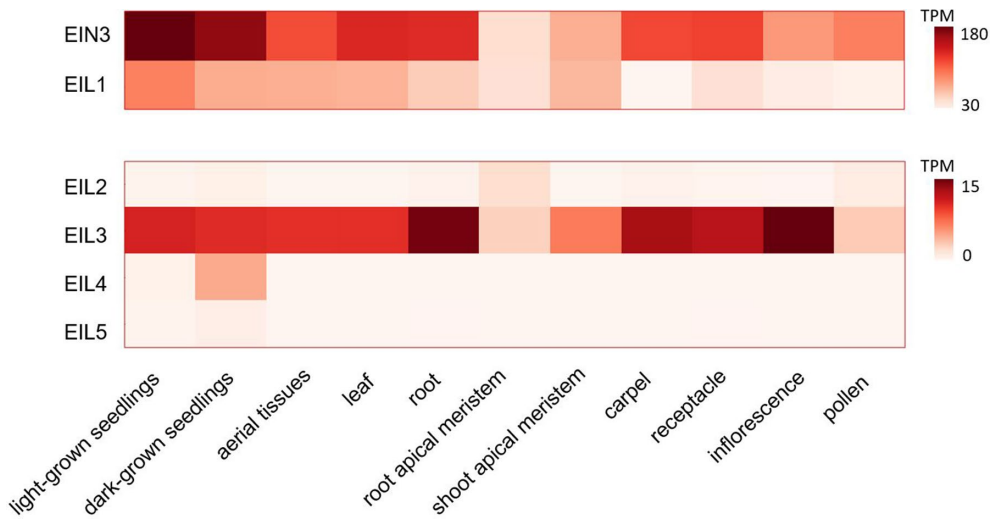

FIGURE 2 | Tissue specificity of *EIL* genes expression. Publicly available datasets on transcriptome profiling of different Arabidopsis tissues (light- and dark-grown seedlings (Rühl et al., 2012; Oh et al., 2014), aerial tissues (Sani et al., 2013), leaf (Wollmann et al., 2012), root (Li et al., 2013), root and shoot apical meristems (Kang et al., 2014; Nozue et al., 2015), carpel (Martínez-Fernández et al., 2014), receptacle (Niederhuth et al., 2013), inflorescence (Gan et al., 2011), pollen (Loraine et al., 2013) were used for visualization. The corresponding expression levels were retrieved from ThaleMine v1.10.4 (https://apps.araport.org/thalemine/; Krishnakumar et al., 2017). TPM, transcripts per million.

EIN3 and EIL1 activation in response to ethylene is the target for complex regulation. EIN3 and EIL1 are short-living proteins that undergo ubiquitination and proteasomal degradation driven by ubiquitin-ligases EIN3 BINDING F-BOX1 (EBF1) and EBF2 (**Figures 1** and **3A**) (Gagne et al., 2004; An et al., 2010). Stabilization of EIN3/EIL1 upon ethylene release plays a pivotal role in triggering ethylene-directed gene expression. Ethylene dampens EBF1/2 levels *via* i) translational repression of *EBF1/2* mRNA in the cytosol promoted by EIN2-C (Li et al., 2015; Merchante et al., 2015), and ii) EIN2-dependent proteasomal degradation of EBF1/2 proteins (An et al., 2010) (**Figure 1**). Stabilized EIN3/EIL1 accumulate in the nucleus.

EIN3/EIL1 are predominantly transcriptional activators (Chang et al., 2013; reviewed in Cho and Yoo, 2015). In Arabidopsis, EIN3, EIL1, and EIL2 specifically bind a short DNA sequence referred to as EIN3 binding site (EBS) in gene promoters (**Figure 1**) (Solano et al., 1998; Chang et al., 2013; Song et al., 2015; O'Malley et al., 2016). EIN3 binds its target loci as a homodimer, and the dimerization is DNA independent (Solano et al., 1998; Song et al., 2015). Accordingly, EIN3 demonstrates higher binding affinity to the inverted repeats of EBS compared to the monomeric site in the *in vitro* experiments (Song et al., 2015). EIN3 binding to the targets is facilitated by elevated levels of H3K14 and non-canonical H3K23 histone acetylation both promoted by a EIN2-C-scaffolded histone acetylation complex, which is triggered upon EIN2-C interaction with a histone binding protein EIN2 NUCLEAR ASSOCIATED PROTEIN 1 (ENAP1) (Zhang et al., 2016; Zhang et al., 2017; reviewed in Wang and Qiao, 2019) (**Figure 3**). Since neither EIN2-C nor ENAP1 possess histone acetyltransferase domains, they might recruit other proteins to promote histone modifications. EIN3 is capable of interacting with ENAP1, too, and it is thought to contribute to ethylene-induced elevation of H3K14 and H3K23 acetylation as well (Zhang et al., 2016).

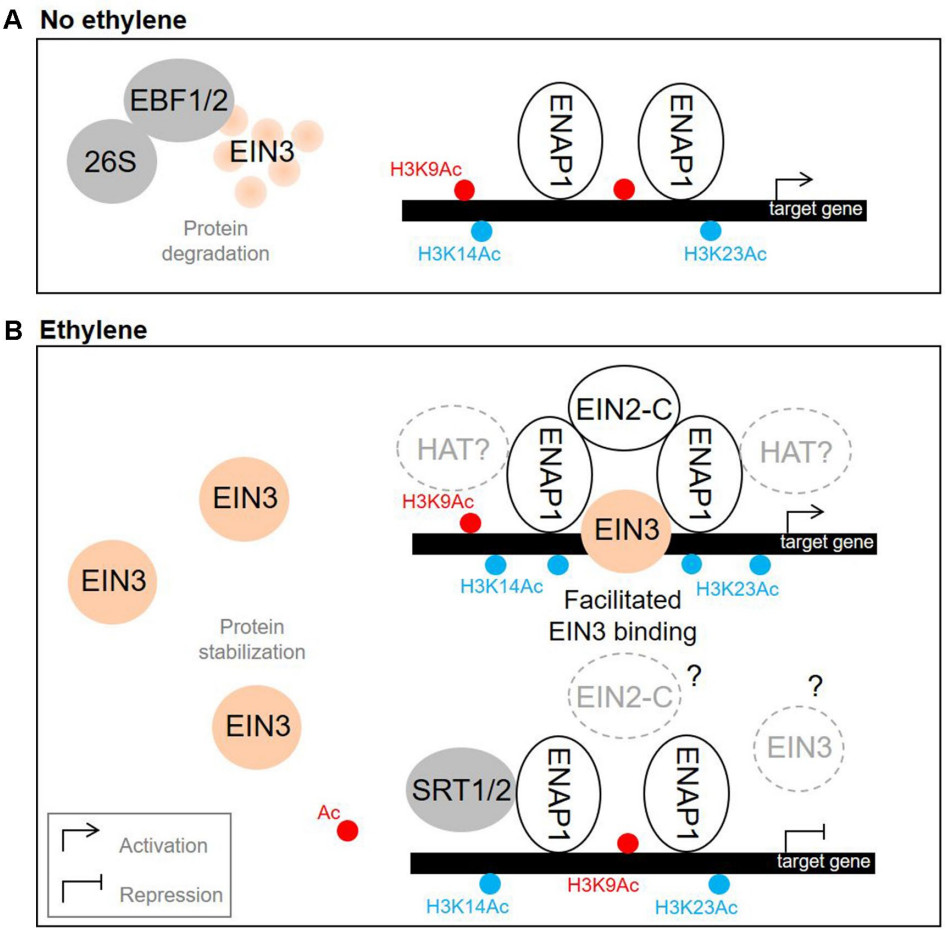

FIGURE 3 | Nuclear events that promote ethylene response. **(A)** Without ethylene, EIN3 undergoes EBF1/2-driven degradation. **(B)** Upon ethylene treatment, EIN3 is stabilized. On one hand, EIN2 C-terminal domain interacts with ENAP1, which results in elevation of H3K14Ac and H3K23Ac levels, facilitated EIN3 binding to the target promoters and activation of gene expression. On the other hand, SRT1 and SRT2 histone deacetylases mediate ethylene-directed transcriptional repression by downregulating the levels of H3K9 acetylation. The models are based on the findings reported previously (Gagne et al., 2004; Li et al., 2015; Merchante et al., 2015; Zhang et al., 2016; Zhang et al., 2017; Zhang et al., 2018a). Gray and white solid circles depict negative and positive regulators of ethylene signaling, correspondingly. EIN3 is depicted in orange, H3K9Ac—in red, H3K14Ac and H3K23Ac—in blue. Dashed circles denote putative regulators (with a question mark inside) and putative regulations (with a question mark outside). HAT, histone acetyltransferase; 26S, 26S proteasome.

Along with well-known EIN3/EIL1-promoted gene transcriptional activation, ethylene downregulates a considerable set of genes (Chang et al., 2013; Harkey et al., 2018). In a recent work, Zhang et al. (2018a) demonstrated that histone deacetylases SRT1 and SRT2 mediate transcriptional repression in response to ethylene by downregulating the levels of H3K9 acetylation (at least for a particular set of ethylene-repressed genes) (**Figure 3**). Both deacetylases interact with ENAP1, and the function of *SRT2* is *EIN2*- and *EIN3/EIL1*-dependent. The mechanism used to distinguish between the activator and repressor pathways as well as the role of EIN3/EIL1 in SRT1/2-mediated gene repression are still unclear and need further investigations.

EIN3/EIL1-REGULATED TRANSCRIPTIONAL NETWORKS

Upon DNA binding, EIN3/EIL1 modulate multiple transcriptional cascades. Ethylene-sensitive EIN3 target genes encoding TFs include *ERF1*, involved in a range of ethylene responses (Solano et al., 1998), *PIF3*, *RSL4*, *ESE1*, and *CBF1/2/3*, the regulators of de-etiolation, root hair development, salt and cold stress responses, correspondingly (Zhang et al., 2011; Shi et al., 2012; Zhong et al., 2012; Feng et al., 2017). To supplement this list, numerous TF-encoding genes comprising representatives of AP2/ERF, WRKY, NAC, and other families were retrieved from whole-genome data on EIN3 binding and ethylene-induced transcriptomes (Chang et al., 2013). Besides, EIN3 directly regulates expression of chlorophyll biosynthesis genes *PORA/B* (Zhong et al., 2009), the pigment-binding proteins *LHC* essential for photosynthesis initiation (Liu et al., 2017), the immune receptor *FLS2* (Boutrot et al., 2010), and the apical hook formation regulator *HLS1* (Lehman et al., 1996; Shen et al., 2016). EIN3/EIL1 affect the pathways of many hormones (Chang et al., 2013), including direct regulation of hormones biosynthesis (e.g., salicylic acid biosynthesis gene *SID2*, Chen et al., 2009), and signaling (e.g., type-A negative regulators of cytokinin signaling *ARR5/7/15*, Shi et al., 2012). To maintain a homeostasis, EIN3 activates a feedback regulatory circuit by inducing transcription of *EBF2* (Konishi and Yanagisawa, 2008) and probably some other negative regulators of ethylene signaling (Chang et al., 2013).

To provide a proper phenotypic outcome upon ethylene release, these transcriptional cascades and the downstream growth control pathways should be tightly coordinated, which is supported by data on the dynamic changes of ethylene-induced transcriptomes in etiolated Arabidopsis seedlings where four distinct transcriptional waves are segregated (Chang et al., 2013). The observed transcription kinetics may be due to distinct mechanisms of transcriptional control, or the heterogeneity of the ethylene response in different tissues (Chang et al., 2013). Transcriptome profiling of Arabidopsis mutants identified large groups of EIN3/EIL1-regulated genes that were co-regulated by the other TFs such as RHD6 (root hair development) and PIFs (light signaling) (Feng et al., 2017; Shi et al., 2018), which implies co-regulation of EIN3/EIL1-triggered transcription by certain developmental and environmental cues. In the following sections, we illustrate that EIN3/EIL1 proteins represent crucial targets for tuning the downstream transcriptional cascades in time and space.

TUNING TRANSCRIPTIONAL REGULATION OF ETHYLENE RESPONSE

Epigenetic Regulation of Spatiotemporal Expression of EIN3/EIL1 Target Genes

Climacteric fleshy fruits (the ones that demonstrate a respiratory burst at the beginning of ripening) use ethylene as a ripening signal (McMurchie et al., 1972). Mature fruit produces ethylene in an autocatalytic manner (system II) unlike immature fruit and vegetative tissues where self-inhibitory ethylene production (system I) is implemented. Autocatalytic regulation suggests a positive feedback loop controlling ethylene synthesis. Presumably, the corresponding regulatory circuit includes EIN3 triggered transcriptional cascade that finally activates ethylene biosynthesis genes (*ACSes* and *ACOs*) (Vandenbussche et al., 2012; Lü et al., 2018). To prevent uncontrolled ethylene production, this circuit should be under a tight spatiotemporal regulation.

Epigenetic modifications often promote spatiotemporal regulation of plant hormone responses (reviewed in Yamamuro et al., 2016). In Arabidopsis, a repressive mark H3K27me3 regulates expression of a large number of genes (Lafos et al., 2011). A systematic analysis of epigenome and transcriptome data suggests that climacteric fruits use removal of H3K27me3 to trigger autocatalytic system II ethylene production specifically in the mature fruit (Lü et al., 2018). Accordingly, EIN3 targeted promoters—a part of transcriptional feedback circuit controlling climacteric fruit ripening (*RIN* in tomato, *NAC* in peach and banana)—are associated with the repressive histone mark H3K27me3 in leaf and immature fruit. They become demethylated and therefore accessible only in the ripening fruit tissues. Presumably, this epigenetic mechanism prevents autocatalytic ethylene production in vegetative and immature fruit tissues.

Recently, using a systematic analysis of publicly available ChIP-Seq data on EIN3 binding in Arabidopsis, we have demonstrated that EIN3 direct targets are enriched in a chromatin state 4 according to the classification of Sequeira-Mendes et al. (2014), which is associated with H3K27me3 repressive mark (Zemlyanskaya et al., 2017b). Therefore, H3K27me3-associated epigenetic silencing might be a more general mechanism providing spatiotemporal specificity of ethylene response *via* restriction of EIN3 function.

Modulation of EIN3/EIL1 Protein Stability

Regulation of EIN3/EIL1 levels *via* the control of the protein stability by EBF1/2 is a pivotal mechanism of EIN3/EIL1 adjustment in ethylene signaling. Simultaneously, it can be affected by environmental factors resulting in a modulation of transcriptional response to ethylene. Plants germinating in the darkness assume a light-regulated developmental program known as skotomorphogenesis, which phenotypically results in rapid hypocotyl elongation, small closed chlorotic cotyledons, and apical hook formation (McNellis and Deng, 1995).

EIN3/EIL1 and their target genes (e.g., *HLS1*, *ERF1*, *PIF3*, *PORA/B*) play essential roles in these processes. They contribute in chlorosis and increased apical hook curvature of buried seedlings, induce shortening and thickening of hypocotyl to enhance lifting capacity of the seedling, and finally promote seedlings greening upon light irradiation (Zhong et al., 2009; Zhong et al., 2012; Zhong et al., 2014; Shen et al., 2016).

In the seedlings growing through the soil, EIN3/EIL1 are stabilized by both light signaling and ethylene, which accumulates in response to mechanical pressure. In the former case, E3 ubiquitin ligase CONSTITUTIVE PHOTOMORPHOGENIC 1 (COP1), a central repressor of light signaling, directly targets EBF1/2 for ubiquitination and degradation (Shi et al., 2016a). As seedlings grow toward the surface, light intensity gradually increases. As a result, COP1 activity, which is negatively regulated by photoreceptors (Podolec and Ulm, 2018), gradually decreases attenuating ethylene response.

When the seedling reaches the soil surface, light triggers a dramatic developmental transition known as de-etiolation that leads to immediate termination of ethylene responses. Light-activated photoreceptor phytochrome B (phyB) directly interacts with both EIN3 and EBF1/2 proteins, thereby stimulating robust EIN3 degradation, rapidly turning off ethylene signaling (Shi et al., 2016b; Luo and Shi, 2019).

Repression of EIN3/EIL1 Transcriptional Activity

In this section, we consider the cross-talk of ethylene signaling pathway with jasmonic acid (JA) and gibberellins (GA) based on an inhibition of EIN3/EIL1 transcriptional activity due to their physical interactions with repressor proteins (**Table 1**). These protein–protein interactions (PPI) rather prevent EIN3/EIL1 binding to DNA than cause changes in protein stability (Zhu et al., 2011; An et al., 2012; Zhang et al., 2014). JA and ethylene synergistically regulate certain aspects of plant development (such as root hair development and inhibition of root growth) and tolerance to necrotrophic fungi. The transcriptional repressors JASMONATE ZIM-DOMAIN (JAZ) are the master regulators that interact with MYC2, MYC3, and MYC4 TFs and negatively control JA signaling (reviewed in Wasternack and Song, 2017). JAZ proteins interact with EIN3/EIL1 and enhance EIN3/EIL1 binding to HDA6, an RPD-type histone deacetylase (Zhu et al., 2011; Zhu and Lee, 2015). The resulting complex inhibits EIN3/EIL1-mediated transcription. Upon JA treatment, JAZ degrades, attenuating HDA6-EIN3/EIL1 association and therefore activating EIN3/EIL1. Therefore, pathogenesis-related genes *ERF1* and *ORA59*, directly regulated by EIN3/EIL1, as well as their downstream target *PDF1.2*, are upregulated in response to JA.

At the same time, MYC2, MYC3, and MYC4 transcriptional regulators of JA signaling interact with EIN3/EIL1, inhibiting their function (Song et al., 2014; Zhang et al., 2014). Thus, *ERF1*, *ORA59*, and *PDF1.2* genes are upregulated in *myc2* mutants. This inhibitory mechanism underlies ethylene-JA antagonism. Particularly, JA-directed abolishment of ethylene-promoted apical hook formation proceeds *via* MYC2-mediated attenuation of *HOOKLESS1* (*HLS1*) expression, which is the key regulator of hook development and a direct EIN3/EIL1 target (Lehman et al., 1996; An et al., 2012; Song et al., 2014; Zhang et al., 2014). Additionally, MYC2 targets *EBF1*, inducing its expression and therefore promoting EIN3/EIL1 degradation (Zhang et al., 2014). Noteworthy, the inhibitory effect in the EIN3–MYC2 complex is reciprocal: the interaction suppresses MYC2 activity as well and thereby ethylene attenuates JA-regulated plant defense response against insect attack (Song et al., 2014). Similarly, EIN3 plays an inhibitory role in sulfur deficiency response, forming heterodimers with EIL3/SLIM1 TF and preventing its target gene recognition by EIL3/SLIM1 (Wawrzyńska and Sirko, 2016).

Just as in the case of JA-ethylene synergy, GA enhances apical hook curvature at least partially *via* a release of EIN3/EIL1 from repressor proteins. DELLA proteins are the main transcriptional repressors of GA responses (Sun and Gubler, 2004). Two members of this family (RGA and GAI) are capable of associating with EIN3/EIL1 DNA-binding domain and inhibiting EIN3/EIL1 function (An et al., 2012). In response to GAs, DELLA proteins rapidly degrade, thereby de-repressing EIN3/EIL1-mediated transcription of at least the *HLS1* gene.

EIN3/EIL1 Cooperate With Other TFs in an Interdependent Manner

EIN3/EIL1's capability to function cooperatively with the transcriptional regulators of the other signaling pathways provides another possibility to shape spatiotemporal patterns of ethylene response. This cooperation implies the cross-talk of TFs bound to DNA that goes along with the physical interaction of these TFs (**Table 1**). In buried seedlings, the chloroplasts' development is arrested at the etioplast stage, characterized by an immature arrangement of the inner membranes and pigment molecules (Solymosi and Schoefs, 2010; Jarvis and López-Juez, 2013). EIN3 and PHYTOCHROME INTERACTING FACTOR3 (PIF3), a darkness-stabilized transcriptional regulator of light signaling, form an interdependent module that represses chloroplast development in buried seedlings (Liu et al., 2017). Namely, EIN3 and PIF3 directly interact and bind the promoters of *LIGHT HARVESTING COMPLEX* (*LHC*) genes in a cooperative manner to synergistically suppress their expression. Upon light exposure, the levels of EIN3 and PIF3 decrease, and activation of *LHC* expression triggers chloroplast differentiation.

Interestingly, another TF from PIF family, PIF4, interacts with EIN3 as well (Yazaki et al., 2016), and both TFs target *HLS1*, the key regulator of apical hook development (An et al., 2012; Zhang et al., 2018b). However, EIN3 and PIF4 activate *HLS1* transcription independently (Zhang et al., 2018b).

Cooperative regulation also guides ethylene functioning in root hair development. EIN3 promotes root hair elongation by directly activating *RHD6-LIKE4* (*RSL4*) gene (Feng et al., 2017). Besides, EIN3 physically interacts with ROOT HAIR DEFECTIVE6 (RHD6), a major regulator of root hair development that targets *RSL4* as well (Yi et al., 2010; Feng et al., 2017). Both EIN3 and RHD6 co-activate *RSL4* more efficiently than either of them alone (Feng et al., 2017). The role of EIN3–RHD6 cooperative action is most likely not limited to *RSL4* regulation, but rather covers a quite extensive set of genes and contributes to ethylene-promoted

root hair initiation as well (Feng et al., 2017). Similarly, in papaya, EIN3 homolog CpEIN3a interacts with CpNAC2, and both TFs directly activate the transcription of carotenoid biosynthesis-related genes *CpPDS4* and *CpCHY-b* expressed during fruit ripening (Fu et al., 2017). Both TFs possess a combinatory effect on the regulation of their targets.

Besides, EIN3/EIL1 are capable of binding gene promoters and affecting gene expression indirectly *via* physical interactions with other TFs and modulation of their activity (**Table 1**). Increase of auxin biosynthesis in the root tip epidermis *via* upregulation of *TRYPTOPHAN AMINOTRANSFERASE OF ARABIDOPSIS 1* (*TAA1*) plays a pivotal role in ethylene-induced inhibition of root growth (Vaseva et al., 2018). EIN3 targets *TAA1* promoter through a "piggyback" interaction with RESPONSE REGULATOR 1 (ARR1), a transcriptional regulator of cytokinin signaling, thereby enhancing ARR1 transcriptional activity (Yan et al., 2017). Similarly, EIN3/EIL1 interact with FER-LIKE FE DEFICIENCY-INDUCED TRANSCRIPTION FACTOR (FIT), a central regulator of Fe acquisition in roots, activating FIT abundance (Lingam et al., 2011). Moreover, EIN3/EIL1 bridges FIT to the transcriptional Mediator complex to recruit RNA-pol and promote the regulation of iron homeostasis (Yang et al., 2014).

EIN3/EIL1-INDEPENDENT ETHYLENE SIGNALING

There is growing evidence that despite their essential role, EIN3/EIL1 TFs are not indispensable components of ethylene response. Thus, kinetic studies distinguish two phases of ethylene-induced growth inhibition of the hypocotyl in etiolated Arabidopsis seedlings: a transient phase I (up to 2 h) and a sustained phase II (Binder et al., 2004; Chang et al., 2013). Both phases require EIN2 function, while only the second requires EIN3/EIL1 (Binder et al., 2004). Intriguingly, unlike etiolated seedlings, light-grown *ein3 eil1* double mutants do not demonstrate the total loss of long-term ethylene responses (Harkey et al., 2018). Moreover, osmotic stress-induced cell cycle arrest in leaf primordia that coincides with enhanced activation of the ethylene signal is EIN3 independent (Skirycz et al., 2011). These observations favor the existence of an alternative pathway. One possible candidate to promote such regulation is a PAM domain-containing protein EER5. It negatively regulates ethylene signaling during hypocotyl elongation in etiolated seedlings regardless of EIN3 by promoting downregulation of a gene subset upon ethylene treatment. In addition, it physically interacts with EIN2-C (Christians et al., 2008). EER5 regulates magnitude of ethylene response *via* perception of ERS1 signal (Deslauriers et al., 2015).

CONCLUDING REMARKS AND PERSPECTIVES

Ethylene response is a target for a complex regulation, in which EIN3/EIL1 TFs play a crucial role. Recent studies shed light on multiple layers of complexity in tuning EIN3/EIL1 function (including epigenetic gene silencing and modulation of EIN3/EIL1 stability and activity *via* PPIs) that facilitate the

TABLE 1 | Protein–protein interactions involved in modulation of EIN3/EIL1 function.

Protein	Organism	Pathway	Function	PPI targets	Interaction output	Reference
EIN3/EIL1 stability						
EBF1/2	*Arabidopsis thaliana*	Ethylene signaling	F-box protein	EIN3/EIL1	EIN3/EIL1 degradation	Gagne et al., 2004; An et al., 2010
COP1	*Arabidopsis thaliana*	Light signaling	E3 ubiquitin ligase	EBF1/2	EIN3/EIL1 stabilization	Shi et al., 2016a
phyB	*Arabidopsis thaliana*	Light signaling	Protein binding	EIN3/EIL1, EBF1/2	EIN3 degradation	Shi et al., 2016b
AKIN10	*Arabidopsis thaliana*	Catabolic pathways	PK	EIN3	EIN3 degradation	Kim et al., 2017
EIN3/EIL1 repression						
RGA, GAI	*Arabidopsis thaliana*	GA signaling	RP	EIN3/EIL1/2	EIN3/EIL1 repression	An et al., 2012
JAZ1	*Arabidopsis thaliana*	JA signaling	RP	EIN3/EIL1, HDA6	EIN3/EIL1 repression in complex with HDA6	Zhu et al., 2011
MYC2/3/4	*Arabidopsis thaliana*	JA signaling	TF	EIN3/EIL1	EIN3/EIL1 repression	Song et al., 2014; Zhang et al., 2014
EIL3/SLIM	*Arabidopsis thaliana*	Sulfur deficiency response	TF	EIN3	EIL3/SLIM repression	Wawrzyńska and Sirko, 2016
EIN3/EIL1 cooperation with other TFs						
RHD6	*Arabidopsis thaliana*	Root hair formation	TF	EIN3	*RSL4* co-activation	Feng et al., 2017
PIF3	*Arabidopsis thaliana*	Light signaling		EIN3	*LHC* co-repression	Liu et al., 2017
CpNAC2	*Carica papaya* L.	Carotenoid biosynthesis	TF	CpEIN3a	*CpPDS4* and *CpCHY-b* co-activation	Fu et al., 2017
FIT	*Arabidopsis thaliana*	Iron acquisition pathway	TF	EIN3/EIL1	FIT stabilization	Lingam et al., 2011
MED25	*Arabidopsis thaliana*	N/A	Mediator subunit	EIN3/EIL1	FIT activation	Yang et al., 2014
ARR1	*Arabidopsis thaliana*	Cytokinin signaling	TF	EIN3	ARR1 activation	Yan et al., 2017

PPI, protein–protein interaction; JA, jasmonic acid; GA, gibberellins; TF, transcription factor; RP, repressor protein; PK, protein kinase.

"shaping" of ethylene response according to spatiotemporal and environmental conditions. At the same time, these findings open up new perspectives for further research. Growing evidence of the important role that epigenetic landscape plays in EIN3/EIL1 functioning requires its more detailed characterization. Particularly, the contribution of distinct epigenetic modifications as well as ENAP1 patterns in modulation of EIN3/EIL1 function is of interest. In view of interdependent cooperation of EIN3/EIL1 with some TFs described recently, the detailed analysis of nucleotide context surrounding EIN3 binding sites requires more attention, and genome-wide research appears helpful both to generalize resent findings and to predict new connections. Moreover, it would be interesting to clarify the role of epigenetic regulation and PPIs in suppression of gene expression upon ethylene treatment.

Yet, despite their essential role, EIN3/EIL1 are not indispensable regulators of ethylene response. To couple the molecular events and phenotypic responses more precisely, EIL2 function in ethylene signaling and EIN3/EIL independent pathways are to be elucidated.

AUTHOR CONTRIBUTIONS

VAD and EMP performed the literature search and drafted the paper. VAD performed the analysis of the transcriptome datasets. EVZ revised and edited the manuscript. All authors read and approved the final manuscript.

FUNDING

The work was funded by the Russian Foundation for Basic Research through grant № 18-29-13040. Meta-analysis of the transcriptome datasets was done in the frame of the project supported by the Russian Foundation for Basic Research and the government of Novosibirsk region through grant № 18-44-540039.

ACKNOWLEDGMENTS

We thank Nadya Omelyanchuk for the critical reading of the manuscript and for fruitful discussions.

REFERENCES

Abeles, F. B., Morgan, P. W., and Saltveit, M. E., Jr. (2012). Ethylene in plant biology. Academic press. San Diego, CA.

Alonso, J. M., Stepanova, A. N., Solano, R., Wisman, E., Ferrari, S., Ausubel, F. M., et al. (2003). Five components of the ethylene-response pathway identified in a screen for weak ethylene-insensitive mutants in Arabidopsis. *Proc. Natl. Acad. Sci. U.S.A.* 100, 2992–1997. doi: 10.1073/pnas.0438070100

An, F., Zhao, Q., Ji, Y., Li, W., Jiang, Z., Yu, X., et al. (2010). Ethylene-induced stabilization of ETHYLENE INSENSITIVE3 and EIN3-LIKE1 is mediated by proteasomal degradation of EIN3 binding F-box 1 and 2 that requires EIN2 in Arabidopsis. *Plant Cell* 22, 2384–2401. doi: 10.1105/tpc.110.076588

An, F., Zhang, X., Zhu, Z., Ji, Y., He, W., Jiang, Z., et al. (2012). Coordinated regulation of apical hook development by gibberellins and ethylene in etiolated Arabidopsis seedlings. *Cell Res.* 22, 915–927. doi: 10.1038/cr.2012.29

Binder, B. M., Mortimore, L. A., Stepanova, A. N., Ecker, J. R., and Bleecker, A. B. (2004). Short-term growth responses to ethylene in Arabidopsis seedlings are EIN3/EIL1 independent. *Plant Physiol.* 136, 2921–2927. doi: 10.1104/pp.104.050393

Booker, M. A., and DeLong, A. (2015). Producing the ethylene signal: regulation and diversification of ethylene biosynthetic enzymes. *Plant Physiol.* 169, 42–50. doi: 10.1104/pp.15.00672

Boutrot, F., Segonzac, C., Chang, K. N., Qiao, H., Ecker, J. R., Zipfel, C., et al. (2010). Direct transcriptional control of the Arabidopsis immune receptor FLS2 by the ethylene-dependent transcription factors EIN3 and EIL1. *Proc. Natl. Acad. Sci. U.S.A.* 107, 14502–14507. doi: 10.1073/pnas.1003347107

Chang, C. (2016). Q&A: how do plants respond to ethylene and what is its importance? *BMC Biol.* 14, 7. doi: 10.1186/s12915-016-0230-0

Chang, K. N., Zhong, S., Weirauch, M. T., Hon, G., Pelizzola, M., Li, H., et al. (2013). Temporal transcriptional response to ethylene gas drives growth hormone cross-regulation in Arabidopsis. *Elife* 2, e00675. doi: 10.7554/eLife.00675

Chao, Q., Rothenberg, M., Solano, R., Roman, G., Terzaghi, W., and Ecker, J. R. (1997). Activation of the ethylene gas response pathway in Arabidopsis by the nuclear protein ETHYLENE-INSENSITIVE3 and related proteins. *Cell* 89, 1133–1144. doi: 10.1016/S0092-8674(00)80300-1

Chen, H., Xue, L., Chintamanani, S., Germain, H., Lin, H., Cui, H. et al. (2009). ETHYLENE INSENSITIVE3 and ETHYLENE INSENSITIVE3-LIKE1 repress SALICYLIC ACID INDUCTION DEFICIENT2 expression to negatively regulate plant innate immunity in Arabidopsis. *Plant Cell* 21, 2527–2540. doi: 10.1105/tpc.108.065193

Cho, Y. H., and Yoo, S. D. (2015). Novel connections and gaps in ethylene signaling from the ER membrane to the nucleus. *Front. Plant Sci.* 5, 733. doi: 10.3389/fpls.2014.00733

Christians, M. J., Robles, L. M., Zeller, S. M., and Larsen, P. B. (2008). The eer5 mutation, which affects a novel proteasome-related subunit, indicates a prominent role for the COP9 signalosome in resetting the ethylene-signaling pathway in Arabidopsis. *Plant J.* 55, 467–577. doi: 10.1111/j.1365-313X.2008.03521.x

Deslauriers, S. D., Alvarez, A. A., Lacey, R. F., Binder, B. M., and Larsen, P. B. (2015). Dominant gain-of-function mutations in transmembrane domain III of ERS1 and ETR1 suggest a novel role for this domain in regulating the magnitude of ethylene response in Arabidopsis. *New Phytol.* 208, 442–455. doi: 10.1111/nph.13466

Ecker, J. R. (1995). The ethylene signal transduction pathway in plants. *Science* 268, 667–675. doi: 10.1126/science.7732375

Feng, Y., Xu, P., Li, B., Li, P., Wen, X., An, F., et al. (2017). Ethylene promotes root hair growth through coordinated EIN3/EIL1 and RHD6/RSL1 activity in Arabidopsis. *Proc. Natl. Acad. Sci. U.S.A.* 114, 13834–13839. doi: 10.1073/pnas.1711723115

Fu, C. C., Han, Y. C., Kuang, J. F., Chen, J. Y., and Lu, W. J. (2017). Papaya CpEIN3a and CpNAC2 co-operatively regulate carotenoid biosynthesis-related genes CpPDS2/4, CpLCY-e and CpCHY-b during fruit ripening. *Plant Cell Physiol.* 58, 2155–2165. doi: 10.1093/pcp/pcx149

Gagne, J. M., Smalle, J., Gingerich, D. J., Walker, J. M., Yoo, S., Yanagisawa, S., et al. (2004). Ubiquitin-protein ligases that repress ethylene action and promote growth by directing EIN3 degradation. *Proc. Natl. Acad. Sci.* 101, 6803–6808. doi: 10.1073/pnas.0401698101

Gan, X., Stegle, O., Behr, J., Steffen, J. G., Drewe, P., and Hildebrand, K. L. (2011). Multiple reference genomes and transcriptomes for Arabidopsis thaliana. *Nature* 477, 419–423. doi: 10.1038/nature10414

Guo, H., and Ecker, J. R. (2004). The ethylene signaling pathway: new insights. *Curr. Opin. Plant Biol.* 7, 40–49. doi: 10.1016/j.pbi.2003.11.011

Gupta, S., Stamatoyannopoulos, J. A., Bailey, T. L., and Noble, W. S. (2007). Quantifying similarity between motifs. *Genome Biol.* 8, R24. doi: 10.1186/gb-2007-8-2-r24

Harkey, A. F., Watkins, J. M., Olex, A. L., DiNapoli, K. T., Lewis, D. R., Fetrow, J. S., et al. (2018). Identification of transcriptional and receptor networks that control root responses to ethylene. *Plant Physiol.* 176, 2095–2118. doi: 10.1104/pp.17.00907

Hu, Y., Vandenbussche, F., and Van Der Straeten, D. (2017). Regulation of seedling growth by ethylene and the ethylene–auxin crosstalk. *Planta* 245, 467–489. doi: 10.1007/s00425-017-2651-6

Jarvis, P., and López-Juez, E. (2013). Biogenesis and homeostasis of chloroplasts and other plastids. *Nat. Rev. Mol. Cell. Biol.* 14, 787–802. doi: 10.1038/nrm3702

Kang, J., Yu, H., Tian, C., Zhou, W., Li, C., Jiao, Y., et al. (2014). Suppression of photosynthetic gene expression in roots is required for sustained root growth under phosphate deficiency. *Plant Physiol.* 165, 1156–1170. doi: 10.1104/pp.114.238725

Kim, G. D., Cho, Y. H., and Yoo, S. D. (2017). Regulatory functions of cellular energy sensor SNF1-Related Kinase1 for leaf senescence delay through ETHYLENE-INSENSITIVE3 repression. *Sci. Rep*. 7, 3193. doi: 10.1038/s41598-017-03506-1

Konishi, M., and Yanagisawa, S. (2008). Ethylene signaling in Arabidopsis involves feedback regulation via the elaborate control of EBF2 expression by EIN3. *Plant J.* 55, 821–831. doi: 10.1111/j.1365-313X.2008.03551.x

Krishnakumar, V., Contrino, S., Cheng, C. Y., Belyaeva, I., Ferlanti, E. S., Miller, J. R., et al. (2017). ThaleMine: a warehouse for Arabidopsis data integration and discovery. *Plant Cell Physiol.* 58, e4. doi: 10.1093/pcp/pcw200

Lacey, R. F., and Binder, B. M. (2014). How plants sense ethylene gas—The ethylene receptors. *J. Inorg. Biochem.* 133, 58–62. doi: 10.1016/j.jinorgbio.2014.01.006

Lafos, M., Kroll, P., Hohenstatt, M.L., Thorpe, F.L., Clarenz, O., and Schubert, D. (2011). Dynamic regulation of H3K27 trimethylation during Arabidopsis differentiation. *PLoS Genet.* 7, e1002040. doi: 10.1371/journal.pgen.1002040

Lehman, A., Black, R., and Ecker, J. R. (1996). HOOKLESS1, an ethylene response gene, is required for differential cell elongation in the Arabidopsis hypocotyl. *Cell* 85, 183–194. doi: 10.1016/S0092-8674(00)81095-8

Li, W., Lin, W. D., Ray, P., Lan, P., and Schmidt, W. (2013). Genome-wide detection of condition-sensitive alternative splicing in Arabidopsis roots. *Plant Physiol.* 162, 1750–1763. doi: 10.1104/pp.113.217778

Li, W., Ma, M., Feng, Y., Li, H., Wang, Y., Ma, Y., et al. (2015). EIN2-directed translational regulation of ethylene signaling in Arabidopsis. *Cell* 163, 670–683. doi: 10.1016/j.cell.2015.09.037

Lingam, S., Mohrbacher, J., Brumbarova, T., Potuschak, T., Fink-Straube, C., Blondet, E., et al. (2011). Interaction between the bHLH transcription factor FIT and ETHYLENE INSENSITIVE3/ETHYLENE INSENSITIVE3-LIKE1 reveals molecular linkage between the regulation of iron acquisition and ethylene signaling in Arabidopsis. *Plant Cell*. 23, 1815–1829. doi: 10.1105/tpc.111.084715

Liu, X., Liu, R., Li, Y., Shen, X., Zhong, S., and Shi, H. (2017). EIN3 and PIF3 form an interdependent module that represses chloroplast development in buried seedlings. *Plant Cell* 29, 3051–3067. doi: 10.1105/tpc.17.00508

Loraine, A. E., McCormick, S., Estrada, A., Patel, K., and Qin, P. (2013). RNA-seq of Arabidopsis pollen uncovers novel transcription and alternative splicing. *Plant Physiol.* 162, 1092–1109. doi: 10.1104/pp.112.211441

Lü, P., Yu, S., Zhu, N., Chen, Y. R., Zhou, B., Pan, Y., et al. (2018). Genome encode analyses reveal the basis of convergent evolution of fleshy fruit ripening. *Nat. Plants* 4, 784–791. doi: 10.1038/s41477-018-0249-z

Luo, Y., and Shi, H. (2019). Direct regulation of phytohormone actions by photoreceptors. *Trends Plant Sci.* 24, 105–108. doi: 10.1016/j.tplants.2018.11.002

Martínez-Fernández, I., Sanchís, S., Marini, N., Balanzá, V., Ballester, P., Navarrete-Gómez, M., et al. (2014). The effect of NGATHA altered activity on auxin signaling pathways within the Arabidopsis gynoecium. *Front. Plant Sci.* 5, 210. doi: 10.3389/fpls.2014.00210

Merchante, C., Brumos, J., Yun, J., Hu, Q., Spencer, K. R., Enríquez, P., et al. (2015). Gene-specific translation regulation mediated by the hormone-signaling molecule EIN2. *Cell* 163, 684–697. doi: 10.1016/j.cell.2015.09.036

McMurchie, E. J., McGlasson, W. B., and Eaks., I. L. (1972). Treatment of fruit with propylene gives information about the biogenesis of ethylene. *Nature* 237, 235–236. doi: 10.1038/237235a0

McNellis, T. W., and Deng, X. W. (1995). Light control of seedling morphogenetic pattern. *Plant Cell* 7, 1749–1761. doi: 10.1105/tpc.7.11.1749

Niederhuth, C. E., Patharkar, O. R., and Walker, J. C. (2013). Transcriptional profiling of the Arabidopsis abscission mutant hae hsl2 by RNA-Seq. *BMC Genomics* 14, 37. doi: 10.1186/1471-2164-14-37

Nozue, K., Tat, A. V., Kumar Devisetty, U., Robinson, M., Mumbach, M. R., Ichihashi, Y., et al. (2015). Shade avoidance components and pathways in adult plants revealed by phenotypic profiling. *PLoS Genet*. 11, e1004953. doi: 10.1371/journal.pgen.1004953

Oh, E., Zhu, J. Y., Bai, M. Y., Arenhart, R. A., Sun, Y., and Wang, Z. Y. (2014). Cell elongation is regulated through a central circuit of interacting transcription factors in the Arabidopsis hypocotyl. *Elife* 3, e03031. doi: 10.7554/eLife.03031

O'Malley, R. C., Huang, S. C., Song, L., Lewsey, M. G., Bartlett, A., Nery, J. R., et al. (2016). Cistrome and epicistrome features shape the regulatory DNA landscape. *Cell* 165, 1280–1292. doi: 10.1016/j.cell.2016.04.038

Podolec, R., and Ulm, R. (2018). Photoreceptor-mediated regulation of the COP1/SPA E3 ubiquitin ligase. *Curr. Opin. Plant Biol.* 45 (Pt A), 18–25. doi: 10.1016/j.pbi.2018.04.018

Rühl, C., Stauffer, E., Kahles, A., Wagner, G., Drechsel, G., Rätsch, G., et al. (2012). Polypyrimidine tract binding protein homologs from Arabidopsis are key regulators of alternative splicing with implications in fundamental developmental processes. *Plant Cell* 24, 4360–4375. doi: 10.1105/tpc.112.103622

Sani, E., Herzyk, P., Perrella, G., Colot, V., and Amtmann, A. (2013). Hyperosmotic priming of Arabidopsis seedlings establishes a long-term somatic memory accompanied by specific changes of the epigenome. *Genome Biol.* 14, R59. doi: 10.1186/gb-2013-14-6-r59

Shen, X., Li, Y., Pan, Y., and Zhong, S. (2016). Activation of HLS1 by mechanical stress via ethylene-stabilized EIN3 is crucial for seedling soil emergence. *Front. Plant. Sci.* 7, 1571. doi: 10.3389/fpls.2016.01571

Shi, Y., Tian, S., Hou, L., Huang, X., Zhang, X., Guo, H., et al. (2012). Ethylene signaling negatively regulates freezing tolerance by repressing expression of CBF and type-A ARR genes in Arabidopsis. *Plant Cell*. 24, 2578–2595. doi: 10.1105/tpc.112.098640

Shi, H., Lyu, M., Luo, Y., Liu, S., Li, Y., He, H., et al. (2018). Genome-wide regulation of light-controlled seedling morphogenesis by three families of transcription factors. *Proc. Natl. Acad. Sci. U.S.A*. 115, 6482–6487. doi: 10.1073/pnas.1803861115

Shi, H., Liu, R., Xue, C., Shen, X., Wei, N., Deng, X. W., et al. (2016a). Seedlings transduce the depth and mechanical pressure of covering soil using COP1 and ethylene to regulate EBF1/EBF2 for soil emergence. *Curr. Biol.* 26, 139–149. doi: 10.1016/j.cub.2015.11.053

Shi, H., Shen, X., Liu, R., Xue, C., Wei, N., Deng, X. W., et al. (2016b). The red light receptor phytochrome B directly enhances substrate–E3 ligase interactions to attenuate ethylene responses. *Dev. Cell* 39, 597–610. doi: 10.1016/j.devcel.2016.10.020

Skirycz, A., Claeys, H., De Bodt, S., Oikawa, A., Shinoda, S., Andriankaja, M., et al. (2011). Pause-and-stop: the effects of osmotic stress on cell proliferation during early leaf development in Arabidopsis and a role for ethylene signaling in cell cycle arrest. *Plant Cell* 2011 (23), 1876–1888. doi: 10.1105/tpc.111.084160

Sequeira-Mendes, J., Aragüez, I., Peiró, R., Mendez-Giraldez, R., Zhang, X., Jacobsen, S. E., et al. (2014). The functional topography of the Arabidopsis genome is organized in a reduced number of linear motifs of chromatin states. *Plant Cell* 26, 2351–2366. doi: 10.1105/tpc.114.124578

Solano, R., Stepanova, A., Chao, Q., and Ecker, J. R. (1998). Nuclear events in ethylene signaling: a transcriptional cascade mediated by ETHYLENE-INSENSITIVE3 and ETHYLENE-RESPONSE-FACTOR1. *Genes Dev*. 12, 3703–3714. doi: 10.1101/gad.12.23.3703

Solymosi, K., and Schoefs, B. (2010). Etioplast and etio-chloroplast formation under natural conditions: the dark side of chlorophyll biosynthesis in angiosperms. *Photosynth. Res.* 105, 143–166. doi: 10.1007/s11120-010-9568-2

Song, S., Huang, H., Gao, H., Wang, J., Wu, D., Liu, X., et al. (2014). Interaction between MYC2 and ETHYLENE INSENSITIVE3 modulates antagonism between jasmonate and ethylene signaling in Arabidopsis. *Plant Cell* 26, 263–279. doi: 10.1105/tpc.113.120394

Song, J., Zhu, C., Zhang, X., Wen, X., Liu, L., Peng, J., et al. (2015). Biochemical and structural insights into the mechanism of DNA recognition by Arabidopsis ETHYLENE INSENSITIVE3. *PLoS One* 10, e0137439. doi: 10.1371/journal.pone.0137439

Sun, T. P., and Gubler, F. (2004). Molecular mechanism of gibberellin signaling in plants. *Annu. Rev. Plant Biol*. 55, 197–223. doi: 10.1146/annurev.arplant.55.031903.141753

Vandenbussche, F., Vaseva, I., Vissenberg, K., and Van Der Straeten, D. (2012). Ethylene in vegetative development: a tale with a riddle. *New Phytol*. 194, 895–909. doi: 10.1111/j.1469-8137.2012.04100.x

Vaseva, I. I., Qudeimat, E., Potuschak, T., Du, Y., Genschik, P., Vandenbussche, F., et al. (2018). The plant hormone ethylene restricts Arabidopsis growth via the epidermis. *Proc. Natl. Acad. Sci. U.S.A*. 115, E4130–E4139. doi: 10.1073/pnas.1717649115

Wang, L., and Qiao, H. (2019). New insights in transcriptional regulation of the ethylene response in Arabidopsis. *Front. Plant. Sci.* 10, 790. doi: 10.3389/fpls.2019.00790

Wasternack, C., and Song, S. (2017). Jasmonates: biosynthesis, metabolism, and signaling by proteins activating and repressing transcription. *J. Exp. Bot.* 68, 1303–1321. doi: 10.1093/jxb/erw443

Wawrzyńska, A., and Sirko, A. (2014). To control and to be controlled: understanding the Arabidopsis SLIM1 function in sulfur deficiency through comprehensive investigation of the EIL protein family. *Front. Plant. Sci.* 5, 575. doi: 10.3389/fpls.2014.00575

Wawrzyńska, A., and Sirko, A. (2016). EIN3 interferes with the sulfur deficiency signaling in Arabidopsis thaliana through direct interaction with the SLIM1 transcription factor. *Plant Sci.* 253, 50–57. doi: 10.1016/j.plantsci.2016.09.002

Wollmann, H., Holec, S., Alden, K., Clarke, N. D., Jacques, P.É., and Berger, F. (2012). Dynamic deposition of histone variant H3.3 accompanies developmental remodeling of the Arabidopsis transcriptome. *PLoS Genet.* 8, e1002658. doi: 10.1371/journal.pgen.1002658

Weirauch, M. T., Yang, A., Albu, M., Cote, A. G., Montenegro-Montero, A., Drewe, P., et al. (2014). Determination and inference of eukaryotic transcription factor sequence specificity. *Cell* 158, 1431–1443. doi: 10.1016/j.cell.2014.08.009

Yamamuro, C., Zhu, J. K., and Yang, Z. (2016). Epigenetic modifications and plant hormone action. *Mol. Plant* 9, 57–70. doi: 10.1016/j.molp.2015.10.008

Yan, Z., Liu, X., Ljung, K., Li, S., Zhao, W., Yang, F., et al. (2017). Type B response regulators act as central integrators in transcriptional control of the auxin biosynthesis enzyme TAA1. *Plant Physiol.* 175, 1438–1454. doi: 10.1104/pp.17.00878

Yang, Y., Ou, B., Zhang, J., Si, W., Gu, H., Qin, G., et al. (2014). The Arabidopsis mediator subunit MED16 regulates iron homeostasis by associating with EIN3/EIL1 through subunit MED25. *Plant J.* 77, 838–851. doi: 10.1111/tpj.12440

Yazaki, J., Galli, M., Kim, A. Y., Nito, K., Aleman, F., Chang, K. N., et al. (2016). Mapping transcription factor interactome networks using HaloTag protein arrays. *Proc. Natl. Acad. Sci. U.S.A.* 113, E4238– E4247. doi: 10.1073/pnas.1603229113

Yi, K., Menand, B., Bell, E., and Dolan, L. (2010). A basic helix-loop-helix transcription factor controls cell growth and size in root hairs. *Nat. Genet.* 42, 264–267. doi: 10.1038/ng.529

Zemlyanskaya, E. V., Levitsky, V. G., Oshchepkov, D. Y., Grosse, I., and Mironova, V. V. (2017b). The interplay of chromatin landscape and DNA-binding context suggests distinct modes of EIN3 regulation in Arabidopsis thaliana. Front. *Plant. Sci.* 7, 2044. doi: 10.3389/fpls.2016.02044

Zhang, L., Li, Z., Quan, R., Li, G., Wang, R., and Huang, R. (2011). An AP2 domain-containing gene, ESE1, targeted by the ethylene signaling component EIN3 is important for the salt response in Arabidopsis. *Plant Physiol*. 157, 854–865. doi: 10.1104/pp.111.179028

Zhang, F., Qi, B., Wang, L., Zhao, B., Rode, S., Riggan, N. D., et al. (2016). EIN2-dependent regulation of acetylation of histone H3K14 and non-canonical histone H3K23 in ethylene signalling. *Nat. Commun*. 7, 13018. doi: 10.1038/ncomms13018

Zhang, F., Wang, L., Ko, E. E., Shao, K., and Qiao, H. (2018a). Histone deacetylases SRT1 and SRT2 interact with ENAP1 to mediate ethylene-induced transcriptional repression. *Plant Cell* 30, 153–166. doi: 10.1105/tpc.17.00671

Zhang, X., Ji, Y., Xue, C., Ma, H., Xi, Y., Huang, P., et al. (2018b). Integrated regulation of apical hook development by transcriptional coupling of EIN3/EIL1 and PIFs in Arabidopsis. *Plant Cell* 30, 1971–1988. doi: 10.1105/tpc.18.00018

Zhang, F., Wang, L., Qi, B., Zhao, B., Ko, E. E., Riggan, N. D., et al. (2017). EIN2 mediates direct regulation of histone acetylation in the ethylene response. *Proc. Natl. Acad. Sci. U.S.A.* 114, 10274–10279. doi: 10.1073/pnas.1707937114

Zhang, X., Zhu, Z., An, F., Hao, D., Li, P., Song, J., et al. (2014). Jasmonate-activated MYC2 represses ETHYLENE INSENSITIVE3 activity to antagonize ethylene-promoted apical hook formation in Arabidopsis. *Plant Cell* 26, 1105–1117. doi: 10.1105/tpc.113.122002

Zhong, S., Shi, H., Xue, C., Wang, L., Xi, Y., Li, J., et al. (2012). A molecular framework of light-controlled phytohormone action in Arabidopsis. *Curr. Biol.* 22, 1530–1535. doi: 10.1016/j.cub.2012.06.039

Zhong, S., Shi, H., Xue, C., Wei, N., Guo, H., and Deng, X. W. (2014). Ethylene-orchestrated circuitry coordinates a seedling's response to soil cover and etiolated growth. *Proc. Natl. Acad. Sci. U.S.A*. 111, 3913–3920. doi: 10.1073/pnas.1402491111

Zhong, S., Zhao, M., Shi, T., Shi, H., An, F., Zhao, Q., et al. (2009). EIN3/EIL1 cooperate with PIF1 to prevent photo-oxidation and to promote greening of Arabidopsis seedlings. *Proc. Natl. Acad. Sci. U.S.A*. 106, 21431–21436. doi: 10.1073/pnas.0907670106

Zhu, Z., An, F., Feng, Y., Li, P., Xue, L., A. M., et al. (2011). Derepression of ethylene-stabilized transcription factors (EIN3/EIL1) mediates jasmonate and ethylene signaling synergy in Arabidopsis. *Proc. Natl. Acad. Sci. U.S.A*. 108, 12539–12544. doi: 10.1073/pnas.1103959108

Zhu, Z., and Lee, B. (2015). Friends or foes: new insights in jasmonate and ethylene co-actions. *Plant Cell Physiol.* 56, 414–420. doi: 10.1093/pcp/pcu171

Conflict of Interest Statement: The authors declare that the research was conducted in the absence of any commercial or financial relationships that could be construed as a potential conflict of interest.

frontiers in Plant Science

ORIGINAL RESEARCH
published: 29 August 2019
doi: 10.3389/fpls.2019.01054

Targeted Proteomics Allows Quantification of Ethylene Receptors and Reveals SlETR3 Accumulation in Never-Ripe Tomatoes

Yi Chen[1†], Valérie Rofidal[2†], Sonia Hem[2], Julie Gil[1,2], Joanna Nosarzewska[1], Nathalie Berger[2], Vincent Demolombe[2], Mondher Bouzayen[1], Beenish J. Azhar[3,4], Samina N. Shakeel[3,4], G. Eric Schaller[4], Brad M. Binder[5], Véronique Santoni[2] and Christian Chervin[1]**

[1] GBF, Université de Toulouse, INRA, Toulouse, France, [2] BPMP, CNRS, INRA, Montpellier SupAgro, Université de Montpellier, Montpellier, France, [3] Department of Biochemistry, Quaid-i-azam University, Islamabad, Pakistan, [4] Department of Biological Sciences, Dartmouth College, Hanover, NH, United States, [5] Department of Biochemistry, Cellular, and Molecular Biology, University of Tennessee, Knoxville, TN, United States

Ethylene regulates fruit ripening and several plant functions (germination, plant growth, plant-microbe interactions). Protein quantification of ethylene receptors (ETRs) is essential to study their functions, but is impaired by low resolution tools such as antibodies that are mostly nonspecific, or the lack of sensitivity of shotgun proteomic approaches. We developed a targeted proteomic method, to quantify low-abundance proteins such as ETRs, and coupled this to mRNAs analyses, in two tomato lines: Wild Type (WT) and Never-Ripe (NR) which is insensitive to ethylene because of a gain-of-function mutation in ETR3. We obtained mRNA and protein abundance profiles for each ETR over the fruit development period. Despite a limiting number of replicates, we propose Pearson correlations between mRNA and protein profiles as interesting indicators to discriminate the two genotypes: such correlations are mostly positive in the WT and are affected by the NR mutation. The influence of putative post-transcriptional and post-translational changes are discussed. In NR fruits, the observed accumulation of the mutated ETR3 protein between ripening stages (Mature Green and Breaker + 8 days) may be a cause of NR tomatoes to stay orange. The label-free quantitative proteomics analysis of membrane proteins, concomitant to Parallel Reaction Monitoring analysis, may be a resource to study changes over tomato fruit development. These results could lead to studies about ETR subfunctions and interconnections over fruit development. Variations of RNA-protein correlations may open new fields of research in ETR regulation. Finally, similar approaches may be developed to study ETRs in whole plant development and plant-microorganism interactions.

Keywords: ethylene, receptor, hormone, signaling, tomato

OPEN ACCESS

Edited by:
Dominique Van Der Straeten, Ghent University, Belgium

Reviewed by:
Chi-Kuang Wen, Shanghai Institutes for Biological Sciences (CAS), China
Maria Manuela Rigano, University of Naples Federico II, Italy

****Correspondence:***
Véronique Santoni
veronique.santoni@inra.fr
Christian Chervin
christian.chervin@ensat.fr

[†]These author share first authorship

Specialty section:
This article was submitted to Plant Physiology, a section of the journal Frontiers in Plant Science

Received: *22 March 2019*
Accepted: *29 July 2019*
Published: *29 August 2019*

Citation:
Chen Y, Rofidal V, Hem S, Gil J, Nosarzewska J, Berger N, Demolombe V, Bouzayen M, Azhar BJ, Shakeel SN, Schaller GE, Binder BM, Santoni V and Chervin C (2019) Targeted Proteomics Allows Quantification of Ethylene Receptors and Reveals SlETR3 Accumulation in Never-Ripe Tomatoes. Front. Plant Sci. 10:1054. doi: 10.3389/fpls.2019.01054

INTRODUCTION

Ethylene is a plant hormone involved in many developmental processes such as seed germination, root initiation, root hair development, flower development, sex determination, fruit ripening, senescence, and responses to biotic and abiotic stresses (Merchante et al., 2013). Recent research has shown that ethylene sensing is also found in cyanobacteria, such *Synechocystis* (Lacey and Binder, 2016) and possibly in early diverging fungi, such as *Rhizophagus* (Hérivaux et al., 2017).

Ethylene gas is perceived by specific receptors (EThylene Receptors, ETRs) localized at the endoplasmic reticulum (Chen et al., 2002). Since the initial description of the first ethylene receptor, AtETR1 from *Arabidopsis thaliana* (Chang et al., 1993), several studies combining genetics, molecular biology, and biochemistry have led to a model whereby the receptors function as negative regulators and ethylene releases this inhibition (Shakeel et al., 2013; Lacey and Binder, 2014; Ju and Chang, 2015). Thus, ETR abundance may be a critical determinant of ethylene signaling. This is supported in tomato where a study showed that the level of insensitivity to ethylene is related to the expression level of an ETR1 gain-of-function (GOF) mutant (Gallie, 2010). Additionally, other authors observed that ethylene insensitivity, due to a receptor GOF mutant, can be partially overcome with increased gene dosage of WT gene (Hall et al., 1999). In other words, the ethylene signaling may be governed by the relative amount of WT ETRs versus mutant ETRs.

A major bottleneck in understanding ETR roles is the absence of a method to quantify the protein levels of all receptor isoforms in the same sample mainly due to the absence of specific antibodies against ETRs (Chen et al., 2002; Kevany et al., 2007; Mata et al., 2018). Hence, two studies correlating receptor protein abundance using antibodies to transcript levels of each ETR isoform made conflicting observations (Kevany et al., 2007; Kamiyoshihara et al., 2012) raising the need for a better method of ETR protein detection. To reach this objective, a targeted mass spectrometry proteomic method, called parallel reaction monitoring (PRM) was recently described to study ETR receptor abundance in tomato fruit (Mata et al., 2018). We adapted this strategy, focusing on single peptides of rare proteins, to compare the abundance of ETRs in WT and in the NR mutant. In this mutant, *ETR3* harbors a Pro36Leu mutation in the ethylene-binding domain, which renders the plant ethylene insensitive to block fruit ripening as well as downregulating the mRNA levels of *ETR1* and *ETR4* at Breaker stage (Hackett et al., 2000). Additionally, these authors showed that the NR fruit changes from green to orange, but never completes ripening by turning red, due to a lack of lycopene accumulation at the end of the ripening period.

RESULTS AND DISCUSSION

Development of the PRM Analyses for the Seven Tomato ETRs

To better understand the ETRs roles in the control of important traits such as tomato fruit ripening, it is critical to have a method to quantify the levels of all receptor isoforms at different developmental stages. The tomato (*Solanum lycopersicum)* genome encodes seven ETR isoforms (SlETR1 through SlETR7). Recent advances in large-scale shotgun proteomics have led to identify a large set of proteins including SlETR3 and SlETR4 in green to red ripe tomato fruits using the ITAG 2.3 database (Feb 2013) (Szymanski et al., 2017) and SlETR1, 3 and 4, using the UniProt FASTA database (Dec 2015) in red ripe tomatoes (Mata et al., 2017). In a large-scale label-free proteomic study, we identified SlETR1, 4, 6, and 7 using the most recent ITAG 3.2 (June 2017), in pooled skin and flesh tissues of both the WT and NR genotypes of the MicroTom cultivar, in four development stages from immature green to Breaker + 8 days (**Table S2a**; **Methods S1b**). These four ETRs were identified but not quantified in all fruit development stages (**Table S2b**). Such large-scale shotgun studies can identify thousands of proteins in biological samples but may result in an under representation of low-abundance proteins such as ETRs. In contrast, targeted approaches such as the PRM performed on quadrupole-Orbitrap mass spectrometers, offers clear advantage in targeting and quantifying low-abundance analytes (Bourmaud et al., 2016).

A PRM strategy was thus developed to identify ETRs in tomato fruit over the ripening period (**Figure 1A**). Microsomal proteins were extracted from tomato fruits at four developmental stages. Proteins were fractionated through SDS-PAGE gel electrophoresis and subsequently digested by trypsin (**Figure 1A**). The success of a PRM-based targeted assay depends on choosing the most appropriate proteotypic peptides for use as specific tracers of each of the proteins of interest (Bourmaud et al., 2016). An *in silico* analysis was performed in order to discriminate between the 7 ETRs and 16 labeled proteotypic peptides (at least 2 proteotypic peptides/ETR) were synthesized (**Table S1a**) and used in a PRM approach to identify the corresponding endogenous ETRs (**Figure 1B**, **Figure S1**).

Among the 16 proteotypic ETR peptides, 15 were identified with high confidence (rdopt > 0.95), except the peptide GLHVLLTDDDDVNR that belongs to ETR5 (rdopt = 0.94) (**Table S1a**, **Figure S1**). Thus, the seven ETRs encoded by the tomato genome were identified in the two genotypes whatever the developmental stage (**Figure 2B**, **Figure S1**). To quantify the ETRs over fruit maturation, the labeled peptides were spiked into a biological matrix using seven adapted peptide concentrations to obtain calibration curves used to determine their quantification limit (**Figure S2**). All identified peptides showed linear regressions with regression coefficients above 0.90 allowing their relative quantification (**Figure S2**). The accumulation profiles of the different peptides for each ETR revealed high correlation coefficients (**Figure 2C**) except in the case of ETR5, likely due to a low protein accumulation during fruit ripening and a limited dynamic range (**Figure S2**). However, the power that reflects the reproducibility of the significance (Zhang and Wen, 2019) appears low with either ETR1 or ETR2 or ETR7 pep3, suggesting that more replicates would be necessary to make better predictions.

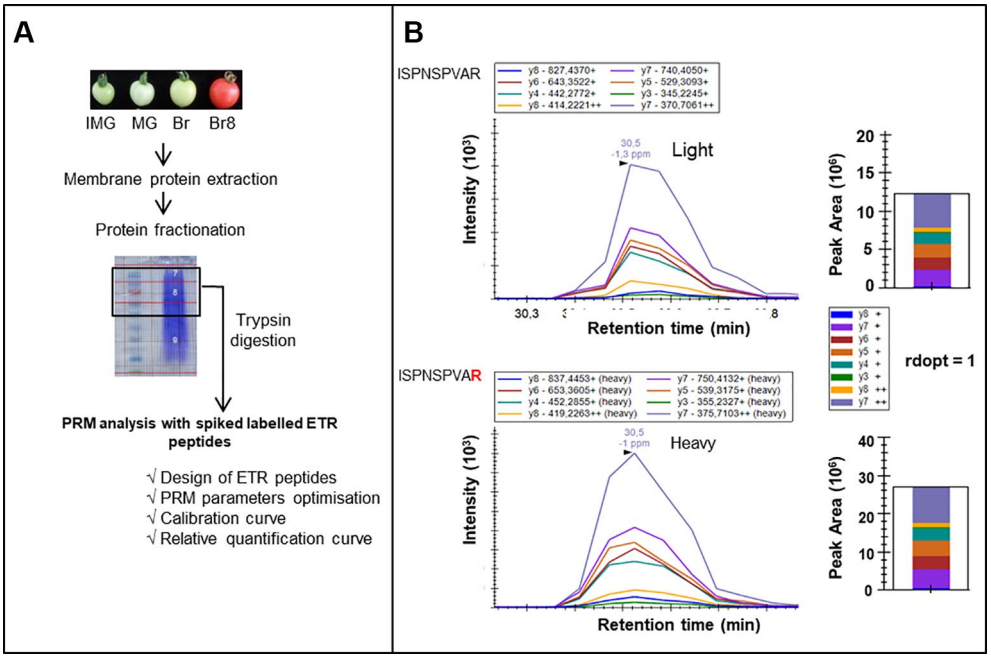

FIGURE 1 | PRM workflow for identification and relative quantification of ethylene receptors. **(A)** Tomato fruits (*Solanum lycopersicum*) from wild-type (WT) plants and NR (never ripe) mutants were collected at four developmental stages: IMG, ImMature Green; MG, Mature Green; Br, Breaker; and Br8, Breaker + 8 days. Membrane proteins were extracted and fractionated through SDS-PAGE electrophoresis. Proteins above 50 kDa were digested with trypsin, and peptides were injected in LC-MS/MS [(nano-HPLC coupled to a quadrupole Orbitrap Qexactive + (Thermo)]. A PRM analysis was optimized through i) the design of ETR peptides, ii) the optimization of PRM parameters, and iii) calibration curves with labeled peptides to identify and relatively quantify ETRs. **(B)** LC–PRM data validating the identification of ETR1. Heavy peptide (ISPNSPVAR) was spiked into IMG WT biological sample. Selected transitions were extracted for the heavy and endogenous peptides, and rdopt value was calculated using Skyline software (see *Materials and Methods*).

Changes in the Seven ETR Proteins Over Tomato Development in WT and NR Backgrounds

Using PRM, we successfully measured the relative amount of the seven ETRs in a series of ripening tomatoes (**Figure 2B**). This showed that the protein levels of ETR1, 2, 5, 6, and 7 dropped from Br to Br8 stages in WT, but this was not the case with ETR3 and ETR4 (**Figure 2B**) indicating that there is a differential regulation of ETRs. In addition, one interesting result is an accumulation of ETR3 in the NR fruit between the mature green stage (MG), and the Breaker + 8 days stage (Br8), which delimits the ripening phase (**Figure 2B**) (Hoeberichts et al., 2002). ETR3 is mutated in the NR background rendering the plant insensitive to ethylene (Wilkinson et al., 1995), and tomato fruit ripening has previously been shown to be blocked by GOF mutations in ETR1 (Okabe et al., 2012). However, since protein content was not determined in earlier studies (Wilkinson et al., 1995; Okabe et al., 2012), our study brings further understanding on how ripening may be blocked in NR fruits at the ETR protein level. Various studies indicate that ethylene acts as a negative regulator. In this model, in air without ethylene, the receptors output leads to inhibition of the ethylene signaling pathway. When ethylene is present, it alleviates this inhibition (Shakeel et al., 2013). Receptors that cannot bind ethylene, such as the mutant ETR3 receptor in the NR background, are thus incapable of turning off. Based on this, we propose that the low levels of the mutant ETR3 in the NR at the early stages of fruit ripening only leads to partial ethylene insensitivity because there is not enough mutant receptor to mask ethylene perception when the other receptor isoforms bind ethylene. In contrast, when mutant ETR3 levels increase at later stages during ripening, the increased signaling from the mutant receptor masks the perception of ethylene by the other receptors.

To evaluate whether such dynamic regulation is possible, we examined the ethylene growth inhibition kinetics of hypocotyls of two *Arabidopsis* ethylene receptor mutants, *etr1-1* and *etr2-1*. The *etr1-1* plants are ethylene insensitive, and *etr2-1* has a large reduction in ethylene sensitivity (Bleecker et al., 1988; Chang et al., 1993; Sakai et al., 1998). *ETR1* is constitutively expressed, whereas *ETR2* occurs at low levels in air and is induced by ethylene within 2 h (Binder et al., 2004a; Hua and Meyerowitz, 1998). Similarly, we observed an induction of *etr2-1* by ethylene (**Figure 3A**). We predicted that if this model of regulation is correct, *etr1-1* seedlings should show no response to ethylene. In contrast, the *etr2-1* seedlings should have a transient growth inhibition response because initially the levels of *etr2-1* are predicted to be too low to block ethylene perception, but upon induction by ethylene, the higher *etr2-1* levels should block ethylene signaling. As shown in **Figure 3B**, WT seedlings had ethylene response kinetics similar to previous studies where growth was inhibited for as long as ethylene was present (Binder et al., 2004b; Binder et al., 2006). In contrast, the *etr1-1* seedlings had no

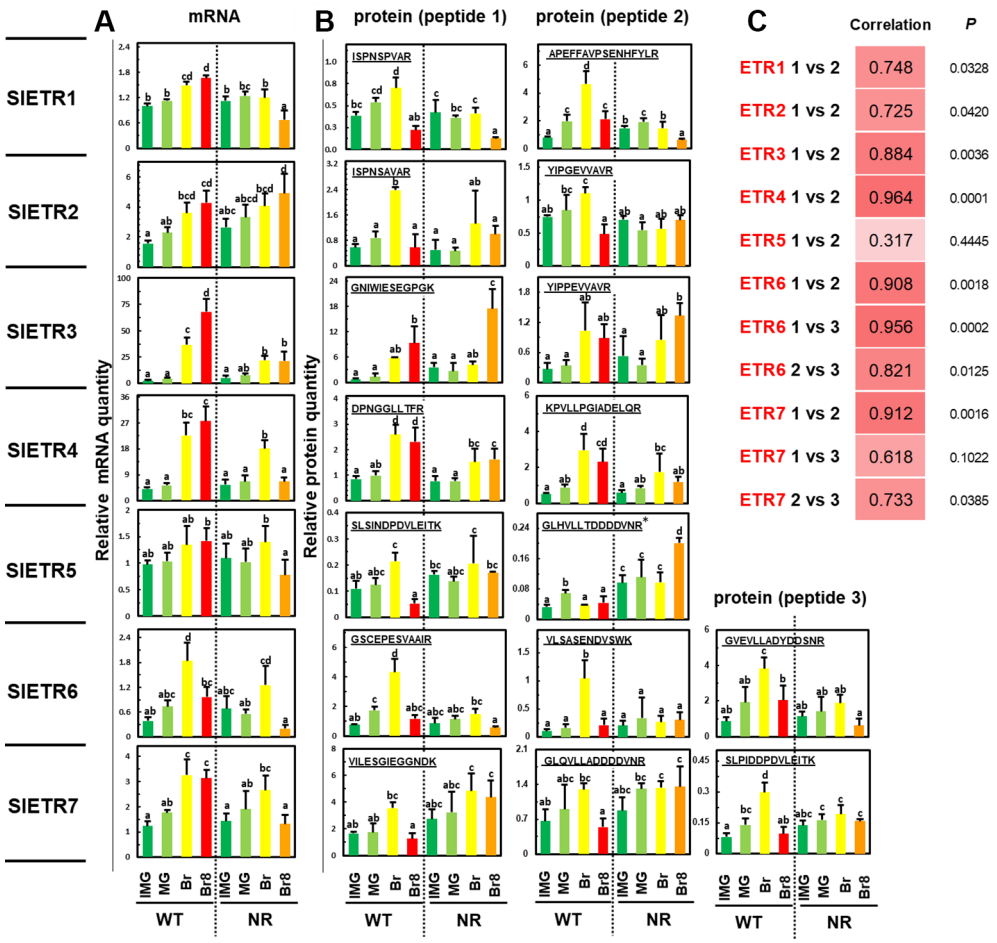

FIGURE 2 | Variations of abundance of mRNAs and proteins of the seven ETRs over fruit development in WT and NR genetic variants of *Solanum lycopersium*, cv. MicroTom. Four development stages were sampled: immature green (IMG, dark green bars), mature green (MG, light green bars), breaker (Br, yellow bars), and breaker + 8 days (Br8, red bars in WT, orange bars in NR). The results show **(A)** the quantities of RNAs relative to that of ETR1 at the IMG stage and **(B)** the relative quantity of protein based on the ratio between endogenous and spiked labeled peptide (see *Materials and Methods* for calculation details). See **Table S1** for details about peptides "1, 2, and 3" for each ETR. The results are the means of three independent biological replicates, error bars show SE, and the small letters show significant differences at 0.05 level (Fisher's LSD test). *Peptide at the bottom limit of the linear regression in dynamic range. **(C)** Pearson correlation coefficients between the profiles of the various specific peptides tested in this study. *P* is the probability of the correlation; the power values were calculated at the 0.05 risk.

measurable response to ethylene, but did have a slow decline in growth rate over time similar to what has been observed in WT seedlings in air (Binder et al., 2006). Interestingly, *etr2-1* seedlings responded transiently to the application of ethylene with an acceleration in growth rate starting at approximately 2 h after the initial application of ethylene. These results are consistent with our model that proposes that increased levels of a mutant ethylene receptor can cause ethylene insensitivity *in planta*.

The receptors form higher-order complexes much like bacterial chemoreceptors (Shakeel et al., 2013). Thus, in this model, it is possible that the increased levels of mutant receptors are blocking perception by direct interactions between mutant and non-mutant receptors. Alternatively, the increase in mutant receptor levels might be blocking access of WT receptors to downstream effectors such as CTR1. In either case, this model explains why NR fruits start to ripen, but then stop at later stages. This model is consistent with observations in *Arabidopsis* where the ethylene insensitivity of several receptor gain-of-function mutants are overcome by increasing levels of WT receptors (Hall et al., 1999).

The NR mutant fruit fails to turn red (**Figure 4A**), and this is due to a limited accumulation of lycopene (red pigment) as previously shown (Liu et al., 2012). Support for this is that using a large-scale label-free quantitative proteomic approach on the same microsomal extracts, with three biological replicates (see **Table S2**), we observed a decreased accumulation of two key enzymes for lycopene synthesis, zeta-carotene desaturase and phytoene desaturase, in the NR samples compared to WT (**Figure 4B**); ratios around 2.5 show enzymes that were 2.5-fold more present in WT than in NR. Lower accumulation of lycopene in fruits has also been observed with a GOF mutation in ETR1, but the abundance of receptor protein was not determined (Okabe et al., 2012). The label-free data available

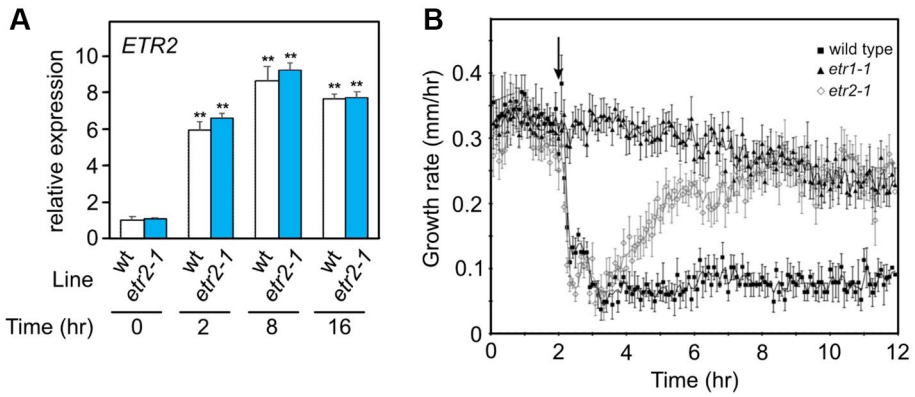

FIGURE 3 | (A) Gene expression based on qPCR for *ETR2* alleles of dark-grown WT and etr2-1 seedlings treated for the indicated times with 10 μL L^{-1} ethylene. Expression was normalized to a tubulin control and is presented as relative to the untreated WT control. Statistical analysis was performed using one-way ANOVA with *post hoc* Tukey HSD test for comparison of induction compared to the 0 time point for each genotype (** $P < 0.01$); n = 3 biological replicates. No significant difference was found between the *ETR2* allele expression levels in WT and etr2-1 at any time point (t-test, $P > 0.05$). Error bars show SE. **(B)** Effect of *etr1-1* and *etr2-1* on the short-term ethylene response in etiolated *Arabidopsis* seedlings. A kinetic analysis of hypocotyl growth was carried out on *etr1-1* and *etr2-1* mutants, by time lapse imaging. For comparison, Columbia (wt) seedling responses are included. The seedlings were grown in air for 2 *h*, at which time, 10 μL L^{-1} ethylene was added. The average ± SEM from at least six seedlings is shown.

through the ProteomeXchange database are interesting resources to mine for additional changes occurring at the membrane in the tomato fruit development.

Additionally, the NR mutation led to higher C_2H_4 production than in WT in ripening tomatoes (**Figure 4C**), which was already observed in ETR1 GOF mutant tomato (Mubarok et al., 2015). Finally, the NR mutation also resulted in higher levels of ETR5 and ETR7 at Br8 (**Figure 2B**). However, because these ETRs are WT proteins and do not harbor mutations altering their sensitivity to ethylene, their higher accumulation is predicted to cause a milder change in ethylene sensitivity, as observed by Hall et al. (1999), as opposed to accumulation of NR, which leads to ethylene insensitivity. Moreover, care should be taken as we observed relative protein values, as discussed below.

Indeed, additional experiments will be necessary to switch from peptide quantification to protein quantification, mainly because of post-translational modifications that can alter the true protein quantification. For instance, the increased abundance of the peptide GNIWIESEGPGK in NR at Br8 stage could be the consequence of *in vivo* serine dephosphorylation, inducing an apparent increase in the quantity of the non-modified peptide. This latter hypothesis would suggest that ETR3 is phosphorylated at this site and less phosphorylated in NR than in WT. It remains an open question whether or not this site is phosphorylated. Other reasons for such discrepancies between peptides are different digestion efficiencies along the protein sequence and partial adsorption of labeled peptides into vials. We obtained similar accumulation profiles for ETR3, ETR4, ETR6, and ETR7 to those reported by Mata et al. (2018) in the WT plant and small differences for ETR1, 2 and 5. Mata et al. (2018) did not test NR. However, there are important differences to note between our study and Mata's study as they used a different cultivar, very different growth conditions, and different methods for protein extraction. Despite these differences, we think both data sets will shed new light on ethylene signaling during fruit development.

Are There Positive or Negative Correlations Between the Seven ETR mRNAs and Protein Levels?

Another critical question for ETRs is to understand the relationship between the abundance of mRNA and of the corresponding proteins because prior studies revealed conflicting results about such correlations in the tomato fruit (Kevany et al., 2007; Kamiyoshihara et al., 2012). Therefore, we examined the transcript levels of each *ETR* using qRT-PCR and correlated this information with protein quantification results (**Table S3**, and **Figures 2A**, **B**). With only four points per correlation, the powers, which represent the reproducibility of the significance, are too weak to make any solid conclusion (**Table S3**). Mata et al. (2018) found positive correlations between RNAs and proteins, but the correlation was only significant for ETR3. In WT, a positive correlation was generally observed between RNA and protein levels (**Figures 2A**, **B**), and this can be verified by averaging results of pep1 and pep2, then piling up all RNA data and all protein data to generate the Pearson correlation coefficient, with a total of 28 values. The Pearson correlation is then 0.754, the *P* value is 3.5810^{-6}, and the power is 0.998. This is very global, and suppresses all possible analyses between the different stages and different ETRs, but at least, it validates the positive correlation proposed by Kamiyoshihara et al., (2012) and invalidates the negative correlation proposed by Kevany et al. (2007). In NR, when comparing RNA and protein levels globally, as described above, the Pearson correlation coefficient with a total of 28 values is then 0.586, the *P* value is 1.0410^{-3}, and the power is 0.919. Thus, NR modifies the correlation

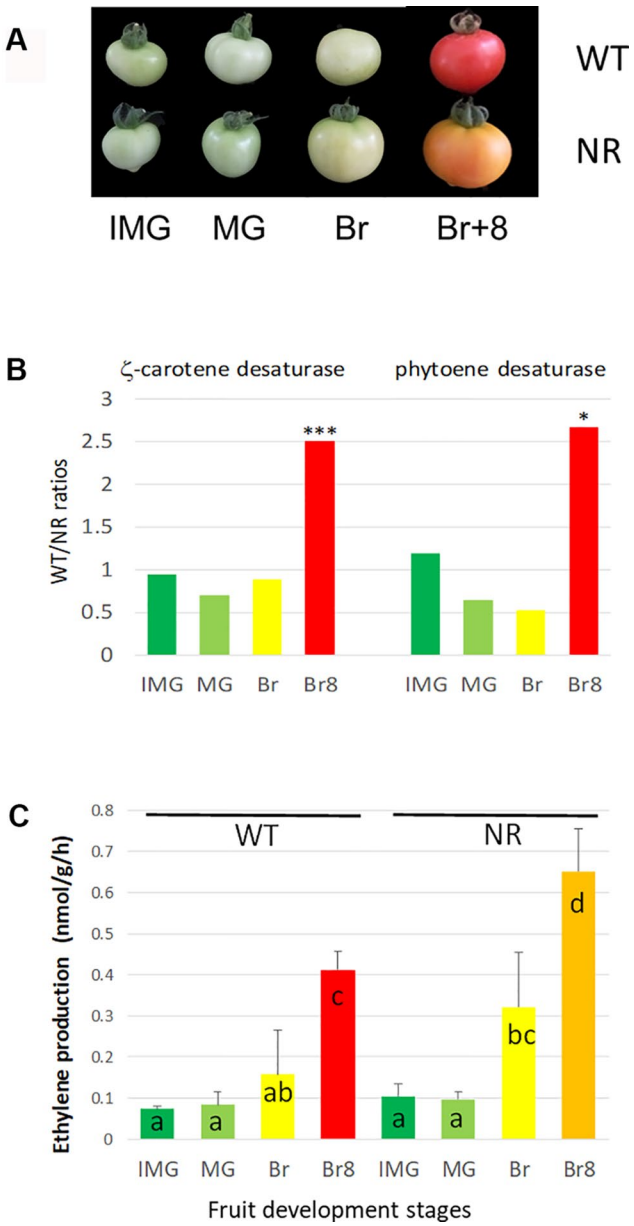

FIGURE 4 | Phenotypes and biochemical changes in WT and NR tomato cultivars. **(A)** Four development fruit stages, used in this study, in two MicroTom tomato lines, WT stands for wild type, and NR stands for never ripe. IMG stands for IMmature Green, MG stands for Mature Green, Br stands for Breaker, and Br + 8 stands for Breaker + 8 days. Both cultivars originate from LE Pereira Peres' Laboratory (Universidade de São Paulo, Brazil) and have been described previously (see *Materials and Methods*). **(B)** Ratios WT/NR of two enzymes involved in lycopene accumulation as a function of fruit development stages. Data obtained by label-free analysis on the same extracts as for PRM. The protein analysis was performed as described in **Methods S1b**, using the ITAG 3.2 annotation. The ratios were performed by means of three biological replicates (data available in **Supp. Table 2b**). * and *** stands for $P < 0.05$ and $P < 0.001$, respectively, resulting of t-test comparisons between WT and NR means at a similar stage. Carotene desaturase: Solyc01g097810, Phytoene desaturase: Solyc03g123760. **(C)** Ethylene production by developing fruits (two lines and four stages as described above). The results are the means of three independent biological replicates, error bars show SE, and the small letters show significant differences at 0.05 level (Fisher's LSD test).

compared to WT. When comparing WT to NR, at the Br8 stage, the NR mutation caused a decreased accumulation of mRNA of *ETR1*, *ETR3*, *ETR4*, *ETR6*, and *ETR7* (**Figures 2A**, **B**) suggesting some as yet unknown transcriptional controls. In *Arabidopsis*, the etr1-1 gain-of-function mutation did not cause changes in the transcript levels of the other four receptor isoforms (O'Malley et al., 2005). However, this mutation did result in higher levels of mutant etr1-1 protein compared to ETR1 levels in wild-type plants, even though transcript levels for this receptor were unchanged (Zhao et al., 2002). The mRNA variations observed of the seven ETRs matched previous observations analyzed from various RNAseq in tomatoes (Chen et al., 2018).

The NR Mutation seems to Affect the Correlation Between mRNA and Protein Levels

The NR mutation also causes several changes in the correlations between mRNA and protein abundance (**Figure 2B**), in particular, in the case of ETR1 where the Pearson coefficient changed from negative in WT (−0.17 and 0.59 for PEP1 and PEP2, respectively) to positive in NR (0.93 and 0.96 for PEP1 and PEP2, respectively) (**Table S3**). However, the weakness of power values would require a higher number of points to strengthen the correlation analysis; thus, **Table S3** is used to give trends at a glance. For the ETR4 and ETR7 receptors, mRNA levels decreased at BR8 in NR with either little to no change in protein levels (**Figures 2A**, **B**) suggesting that breakdown of these receptors is reduced in the NR mutant background. Further analysis will be required to determine the mechanism by which this occurs. For other ETRs such as ETR4 and ETR6, mRNA/protein correlation coefficients were very high and minimally affected by the NR mutation (**Table S3**); however, the power values were still too low for validating the trends.

CONCLUSIONS

We developed a PRM strategy that allowed the comparison of the abundance of ETRs in NR and WT tomato plants. Because ethylene has important roles in regulating plant development and responses to stresses, this method will be of wide use to study the roles of this phytohormone in diverse responses and plant species. However, calibration will be necessary for each peptide in each plant species. The observation that the GOF mutant ETR3 protein accumulates in orange mature fruit of the NR mutant is an example of regulation that would have remained unknown without the development of this new method. mRNA/protein correlations could also bring information about the regulation that occurs in ethylene signaling in fruit tissues, but more replicates are necessary. Given that ETRs in *Arabidopsis* show patterns of subfunctionalization (Shakeel et al., 2013), the use of PRM in tomato and other plant species will provide critical

information about ETR subfunctionalization across the plant kingdom.

MATERIALS AND METHODS

Plant Materials and Growth Conditions

Two tomato lines (*Solanum lycopersicum*) cv. Micro-tom were used, WT and NR mutant (Pro36Leu), both previously described (Carvalho et al., 2011). In addition to fruit color difference, these authors showed that NR seedlings are less sensitive to exogenous ethylene than WT seedlings, a classical response of ETR GOF mutants. Plants were grown in culture rooms with the following conditions: day/night (26°C for 18 h, 18°C for 8 h), light intensity 250 $\mu mol.m^{-2}.s^{-1}$, relative humidity at 80%. Four fruit stages were studied: IMmature Green (IMG), Mature Green (MG) fruit were harvested 20 and 38 days after flower anthesis, respectively; Breaker (Br) fruit was harvested once fruit color changed from green to yellow and red fruit (Br + 8) was harvested 8 days later (**Figure 4A**). Ethylene was analyzed using gas chromatography as previously described (Trapet et al., 2016) by incubating the fruit for 3 h. *Arabidopsis* lines (*Arabidopsis thaliana*) cv. Colombia were used, WT and *etr1-1 and etr2-1*, using growing conditions and growth monitoring described previously (Shakeel et al., 2013, and refs herein).

mRNA Purification and qPCR Analysis

For each fruit stage, the skin, together with pericarp tissues were collected and divided in three biological replicates of five fruits each, originated from different fruits, then ground to a fine powder in liquid nitrogen using a ball grinder. Total RNAs were purified from 100 mg of frozen sample with ReliaPrep™ RNA Tissue Miniprep System (Promega), according to the manufacturer's instructions. RNA was treated with DNase I (Invitrogen-AM1906), then 2 µg of RNA was treated with GoScript Reverse Transcriptase (Promega-A5003). Quantitative real-time PCR (qPCR) reactions were performed using 5 ng of cDNA per well as described before (Chervin and Deluc, 2010). EF1α, GAPDH, and actin were selected as house-keeping genes. All primers (**Table S1c**) were designed with primer-blast (https://www.ncbi.nlm.nih.gov/tools/primer-blast/). SlETR1 expression in WT at IMG stage was used as control for all genes at all stages.

Microsomal Protein Extraction

The fruit samples used for mRNA extraction were also used for protein extraction, performed at 4°C according to previous studies (Bono et al., 1995; Kamiyoshihara et al., 2012) with some modifications. Briefly, 3 g of frozen ground powder was mixed with 25 ml of extraction buffer (50 mM Tris-HCl pH 7.0, 10 mM EDTA, 0.5 M sucrose, 3% PVPP w/v, 10 mM DTT, 100 µM PMSF, cOmplete™ Protease Inhibitor Cocktail (one tablet/100 ml), 1 mM phenantrolin, 1 mM Na-orthovanadate). The slurry was filtered through glass cotton at 300*g*, for 5 min and 900*g* for10 min). Then, left-over tissue bits were removed at 3,000*g* for 15 min. The resulting supernatant was centrifuged at 48,000*g* for 60 min. The pellet was resuspended in 25 mM TrisHCl buffer pH 7.0, 250 mM sucrose, 1 mM $CaCl_2$, 1 mM $MgCl_2$, and cOmplete™ Protease Inhibitor Cocktail (one tablet/10 ml). Proteins were quantified with DC™ Protein Assay (Bio-Rad). Proteins (80 µg/lane) were fractionated using 10% precast SDS-PAGE gel electrophoresis (Biorad) after incubation at 37°C for 30 min in a loading buffer (50 mM Tris-HCl pH7.0, 10% glycerol, 4% SDS, 100 mM DTT, stained with bromophenol blue). The gels were then stained with Coomassie blue (R250, BioRad), then rinsed with acetic acid/methanol (Destain, BioRad). Each lane was cut in two bands, and bands containing proteins with a molecular weight above 50 kDa (with ETR dimers and monomers) were further analyzed by mass spectrometry.

Targeted LC-Parallel Reaction Monitoring Analyses

Protein digestion: Gel band treatments and trypsin digestion were performed as described in **Methods S1b**. Briefly, proteins in gel slices were reduced, alkylated, and digested overnight at 37°C with modified trypsin at a 1:100 enzyme/protein ratio (Promega, Madison, WI, USA). Peptides were extracted twice by the addition of 200 µL of 80% acetonitrile (ACN) and 2% formic acid (FA), and then dried in a vacuum centrifuge. Peptides were then resuspended in 20 µl FA 2%.

ETR peptide selection: To select ETR peptides to be studied in the PRM experiment, ETRs were digested *in silico* using MS digest (ProteinProspector tool, v. 5.19.1, University of California). Search criteria included digestion by trypsin, peptide mass from 500 to 4,000 Da, a minimum peptide length of six amino acids, and a uniqueness in the ITAG 3.2 database digested *in silico*. The peptides should also contain a minimal number of methionine residues because of their putative oxidation, of asparagine and glutamine residues because of their putative deamidation, of glutamic acid or glutamine as first amino acid because of the pyro-glutamination, of serine, threonine, or tyrosine residues because they can be phosphorylated. Then, the presence of proline was privileged because of its property to facilitate the MS/MS fragmentation. In addition, the proteotypic peptides previously identified in shotgun analyses (Mata et al., 2017; Szymanski et al., 2017) were preferentially selected. For the seven selected ETRs, 16 proteotypic peptides were selected. Labeled (or heavy) crude synthetic peptides were synthetized (PEPotec, ThermoFisher Scientific) with carbamidomethylation of cysteins and isotopic labeling of the last sequence amino acid (R: +10 Da ($^{13}C6$, $^{15}N4$) or K: +8 Da ($^{13}C6$, $^{15}N2$) (**Table S1a**).

Parallel Reaction Monitoring (PRM): Labeled peptides were mixed together in a hand-adjusted concentration-balanced mixture to equilibrate individual peptides signals and spiked in a biological matrix made of IMG WT sample in a similar quantity to the one used in all samples further analysed (**Figure 2** and **Figure S1**). The peptide mixture was analyzed using an UltiMate™ NCS-3500RS Ultra High Performance Liquid Chromatography system interfaced online with a nano easy ion source and a Q Exactive Plus Orbitrap mass spectrometer (ThermoFisher Scientific Inc, Waltham, MA,

USA). Peptides were first loaded onto a pre-column (Thermo Scientific PepMap 100 C18, 5 µm particle size, 100 Å pore size, 300 µm i.d. x 5 mm length) from the Ultimate 3000 autosampler with 0.05% trifluoroacetic acid for 3 min at a flow rate of 10 µL/min. Then, the column valve was switched to allow elution of peptides from the pre-column onto the analytical column (Thermo Fisher Scientific Inc, Waltham, MA, USA, C18, 2 µm particle size, 100 Å pore size, 75 µm i.d. x 50 cm length). Loading buffer (solvent A) was 0.1% formic acid (FA) and elution buffer (solvent B) was 80% ACN + 0.1% FA. The three step gradients were 4–25% of solvent B for 103 min, then 25–40% of solvent B up to 123 min, and 40–90% of solvent B from 123 to 125 min, at a flow rate of 300 nL/min. The total chromatographic run time was 150 min including a high organic wash and re-equilibration steps. Peptides were transferred to the gaseous phase with positive ion electrospray ionization at 1.7 kV. Labeled peptides were checked by High-energy Collisional Dissociation MS/MS with regard to their retention time, charge, and m/z (**Table S1a**). A schedule PRM method was developed to simultaneously target all peptides (16 light peptides and 16 heavy peptides) in the protein sample (analytical details provided in **Methods S1a**). The Q-Exactive Plus Orbitrap instrument was operated as follows: a full MS scan spectra considering a mass range of 350–2,000 m/z was acquired with a resolution of 17.500 with an automatic gain control (AGC) fixed at $3e^6$ ions and a maximum injection time set at 100 ms. Targeted MS/MS spectra were acquired with a resolution of 140.000 with an AGC fixed at $2e^5$ and with the maximum injection time set at 1,000 ms. An MS/MS spectral library was acquired using a mixture of 16 heavy labeled synthetic peptides (**Methods S1a**). After manual checking of effective co-elution of endogenous and isotopically labeled peptides and after elimination of transitions showing interference, the Rdot-product (rdotp) values were calculated with Skyline (MacLean et al., 2010) (**Figure S1**), and peptides were relatively quantified with at least four transitions (**Figure 1**, **Table S1a**, and **Figure S1**).

Calibration curve was established using stable isotope-labeled peptides spiked into WT IMG samples prior to LC–MS/MS analysis using seven different peptide concentrations adapted for each peptide (**Figure S2**). Provided that the regression coefficient was above 0.90 and the rdopt was above 0.95, the peptide was qualified to be further quantified. For each peptide, the ratios of the endogenous to labeled peak areas were compared to obtain a relative quantification according to the genotypes and the development stages, as follows: relative level of endogenous peptide = sum of all transition intensities of the endogenous/sum of all transition intensities of the labeled.

The Pearson correlations have been calculated using R code, *via* the Wessa online tool (https://www.wessa.net/rwasp_correlation.wasp). The powers of the Pearson correlations were calculated using Sigmaplot (Systat Sotware, Inc.) at the 0.05 level.

Quantitative Real-Time PCR

For qPCR of *Arabidopsis* seedlings, 4-day-old dark-grown seedlings were grown in hydrocarbon-free air as described (Hall et al., 2012) and treated with 10 µL of L-1 ethylene for the indicated times at the end of their growth cycle. Total RNA was extracted from seedlings using the E.Z.N.A. Plant RNA Kit (Omega Bio-Tek), DNase treatment was performed using TURBO DNA free kit (Invitrogen), and cDNA was synthesized using the SuperScript III First Strand cDNA Synthesis Kit (Invitrogen, USA) according to the manufacturer's instructions. Real-time PCR was performed using iTaq Universal SYBR Green Supermix (Bio-Rad) and primer sets specific for ETR2 (5′-AGAGAAACTCGGGTGCGATGT-3′ and 5′-TCACTGTCGTCGCCACCATC-3′) and b-tubulin (At5g62700) control (5′-TGGTGGAGCCTTACAACGCTACTT-3′ and 5′-TTCACAGCAAGCTTACGGAGGTCA-3t).

Time Lapse Imaging

Ethylene growth response kinetics of etiolated *Arabidopsis* seedlings were determined according to methods previously described (Binder et al., 2004a and Binder et al., 2004b) on 2-day-old, dark-grown *Arabidopsis* seedlings grown on 0.8% (w/v) agar plates with half-strength Murashige and Skoog medium at pH 5.7 (Murashige and Skoog, 1962).

DATA AVAILABILITY

The PRM data are deposited to PeptideAtlas, accessible *via* ftp://PASS01274:DB4724xpa@ftp.peptideatlas.org/, Username: PASS01274, Password: DB4724xpa; and the label-free data are deposited to ProteomeXchange with the dataset identifier PXD011412, Username: reviewer72717@ebi.ac.uk, Password: g7EGcQI4.

AUTHOR CONTRIBUTIONS

CC and VS conceived the study. YC performed tomato culture, fruit sampling, protein extraction and purification, and mRNA extraction and analyses. VR performed protein digestion and MS/MS analyses. VR and SH designed specific peptides with help by JG, JN, and NB, who performed preliminary studies. VR, SH, and VD analyzed the MS/MS data. BA performed Arabidopsis gene expression analysis under the supervision of SS and GS. BB performed Arabidopsis kinetic analysis. BA, SS, BB, and GS analyzed and interpreted Arabidopsis data. YC, BB, VR, SH, MB, VS, and CC interpreted the data and wrote the manuscript. All authors read and approved the final manuscript.

FUNDING

The authors acknowledge CSC for the PhD studentship to Y Chen, and INRA for a Starter Research grant to V Santoni and C Chervin. Part of this work was supported by the National Science Foundation Grants IOS-1456487 to GS and MCB-1517032 to GS and BB, and the International Research Support Initiative Program of Higher Education Commission of Pakistan to BA.

ACKNOWLEDGMENTS

Thanks to B Cooper (USDA, Beltsville, USA) for the initial advice about protein extraction and, later, for the critique of the results. Thanks to JJ Bono (CNRS, Toulouse, France) and HJ Klee (University of Florida, Gainesville, USA) for help to optimize the microsomal protein extraction, and to LE Pereira Peres (Universidade de São Paulo, Brazil) for the NR MicroTom cultivar. The authors acknowledge the Mass Spectrometry Proteomic Platform (MSPP) for PRM and quantitative label-free experiments. Finally, thanks to the two reviewers for their time and fruitful comments.

SUPPLEMENTARY MATERIAL

The Supplementary Material for this article can be found online at: https://www.frontiersin.org/articles/10.3389/fpls.2019.01054/full#supplementary-material.

REFERENCES

Bleecker, A. B., Estelle, M. A., Somerville, C., and Kende, H. (1988). Insensitivity to ethylene conferred by a dominant mutation in Arabidopsis thaliana. *Science* 241, 1086–1089. doi: 10.1126/science.241.4869.1086

Binder, B. M., O'Malley, R. C., Wang, W., Moore, J. M., Parks, B. M., Spalding, E. P., et al. (2004a). Arabidopsis seedling growth response and recovery to ethylene. A kinetic analysis. *Plant Phys.* 136, 2913–2920. doi: 10.1104/pp.104.050369

Binder, B. M., Mortimore, L. A., Stepanova, A. N., Ecker, J. R., and Bleecker, A. B. (2004b). Short-term growth responses to ethylene in Arabidopsis seedlings are EIN3/EIL1 independent. *Plant Phys.* 136, 2921–2927. doi: 10.1104/pp.104.050393

Binder, B. M., O'Malley, R. C., Wang, W., Zutz, T. C., and Bleecker, A. B. (2006). Ethylene stimulates nutations that are dependent on the ETR1 receptor. *Plant Phys.* 142, 1690–1700. doi: 10.1104/pp.106.087858

Bono, J. J., Riond, J., Nicolaou, K. C., Bockovich, N. J., Estevez, V. A., Cullimore, J. V., et al. (1995). Characterization of a binding site for chemically synthesized lipo-oligosaccharidic NodRm factors in particulate fractions prepared from roots. *Plant* J7, 253–260. doi: 10.1046/j.1365-313X.1995.7020253.x

Bourmaud, A., Gallien, S., and Domon, B. (2016). Parallel reaction monitoring using quadrupole-Orbitrap mass spectrometer: Principle and applications. *Proteomics* 16, 2146–2159. doi: 10.1002/pmic.201500543

Carvalho, R. F., Campos, M. L., Pino, L. E., Crestana, S. L., Zsögön, A., Lima, J. E., et al. (2011). Convergence of developmental mutants into a single tomato model system: 'Micro-Tom' as an effective toolkit for plant development research. *Plant Methods* 7, 18. doi: 10.1186/1746-4811-7-18

Chang, C., Kwok, S. F., Bleecker, A. B., and Meyerowitz, E. M. (1993). Arabidopsis ethylene-response gene ETR1: similarity of product to two-component regulators. *Science* 262, 539–544. doi: 10.1126/science.8211181

Chen, Y., Grimplet, J., David, K., Castellarin, S. D., Terol, J., Wong, D. C. J., et al. (2018). Ethylene receptors and related proteins in climacteric and non-climacteric fruits. *Plant Sci.* 276, 63–72. doi: 10.1016/j.plantsci.2018.07.012

Chen, Y.-F., Randlett, M. D., Findell, J. L., and Schaller, G. E. (2002). Localization of the ethylene receptor ETR1 to the endoplasmic reticulum of Arabidopsis. *J. Biol. Chem.* 277, 19861–19866. doi: 10.1074/jbc.M201286200

Chervin, C., and Deluc, C. (2010). Ethylene signalling receptors and transcription factors over the grape berry development: gene expression profiling. *Vitis* 49, 129–136.

Gallie, D. R. (2010). Regulated ethylene insensitivity through the inducible expression of the Arabidopsis etr1-1 mutant ethylene receptor in tomato. *Plant Phys.* 152, 1928–1939. doi: 10.1104/pp.109.151688

Hackett, R. M., Ho, C. W., Lin, Z., Foote, H. C., Fray, R. G., and Grierson, D. (2000). Antisense inhibition of the Nr gene restores normal ripening to the tomato Never-ripe mutant, consistent with the ethylene receptor-inhibition model. *Plant Phys.* 124, 1079–1086. doi: 10.1104/pp.124.3.1079

Hall, A. E., Chen, Q. G., Findell, J. L., Schaller, G. E., and Bleecker, A. B. (1999). The relationship between ethylene binding and dominant insensitivity conferred by mutant forms of the ETR1 ethylene receptor. *Plant Phys.* 121, 291–300. doi: 10.1104/pp.121.1.291

Hérivaux, A., Dugé de Bernonville, T., Roux, C., Clastre, M., Courdavault, V., Gastebois, A., et al. (2017). The identification of phytohormone receptor homologs in early diverging fungi suggests a role for plant sensing in land colonization by fungi. *mBio* 8, e01739–e01716. doi: 10.1128/mBio.01739-16

Hoeberichts, F. A., Van Der Plas, L. H. W., and Woltering, E. J. (2002). Ethylene perception is required for the expression of tomato ripening-related genes and associated physiological changes even at advanced stages of ripening. *Postharvest Biol. Technol.* 26, 125–133. doi: 10.1016/S0925-5214(02)00012-1

Hua, J., and Meyerowitz, E. M. (1998). Ethylene responses are negatively regulated by a receptor gene family in Arabidopsis thaliana. *Cell* 94, 261–271. doi: 10.1016/S0092-8674(00)81425-7

Ju, C., and Chang, C. (2015). Mechanistic insights in ethylene perception and signal transduction. *Plant Phys.* 169, 85–95. doi: 10.1104/pp.15.00845

Kamiyoshihara, Y., Tieman, D. M., Huber, D. J., and Klee, H. J. (2012). Ligand-induced alterations in the phosphorylation state of ethylene receptors in tomato fruit. *Plant Phys.* 160, 488–497. doi: 10.1104/pp.112.202820

Kevany, B. M., Tieman, D. M., Taylor, M. G., Cin, V. D., and Klee, H. J. (2007). Ethylene receptor degradation controls the timing of ripening in tomato fruit. *Plant J.* 51, 458–467. doi: 10.1111/j.1365-313X.2007.03170.x

Lacey, R. F., and Binder, B. M. (2014). How plants sense ethylene gas—the ethylene receptors. *J. Inorg. Biochem.* 133, 58–62. doi: 10.1016/j.jinorgbio.2014.01.006

Lacey, R. F., and Binder, B. M. (2016). Ethylene regulates the physiology of the Cyanobacterium synechocystis sp. PCC 6803 *via an* ethylene receptor. *Plant Phys.* 171, 2798–2809. doi: 10.1104/pp.16.00602

Liu, L., Wei, J., Zhang, M., Zhang, L., Li, C., and Wang, Q. (2012). Ethylene independent induction of lycopene biosynthesis in tomato fruits by jasmonates. *J. Exp. Bot.* 63, 5751–5761. doi: 10.1093/jxb/ers224

MacLean, B., Tomazela, D. M., Shulman, N., Chambers, M., Finney, G. L., Frewen, B., et al. (2010). Skyline: an open source document editor for creating and analyzing targeted proteomics experiments. *Bioinformatics* 26, 966–968. doi: 10.1093/bioinformatics/btq054

Mata, C. I., Fabre, B., Parsons, H. T., Hertog, M., Van Raemdonck, G., Baggerman, G., et al. (2018). Ethylene receptors, CTRs and EIN2 target protein identification and quantification through parallel reaction monitoring during tomato fruit ripening. *Front. Plant Sci.* 9, 1626. doi: 10.3389/fpls.2018.01626

Mata, C. I., Fabre, B., Hertog, MLATM, Parsons, H. T., Deery, M. J., Lilley, K. S., et al. (2017). In-depth characterization of the tomato fruit pericarp proteome. *Proteomics* 17, 1–2. doi: 10.1002/pmic.201600406

Merchante, C., Alonso, J. M., and Stepanova, A. N. (2013). Ethylene signaling: simple ligand, complex regulation. *Curr. Opin. Plant Biol.* 16, 554–560. doi: 10.1016/j.pbi.2013.08.001

Mubarok, S., Okabe, Y., Fukuda, N., Ariizumi, T., and Ezura, H. (2015). Potential Use of a weak ethylene receptor mutant, Sletr1-2, as breeding material to extend fruit Shelf life of tomato. *J. Agric. Food Chem.* 63, 7995–8007. doi: 10.1021/acs.jafc.5b02742

Murashige, T., and Skoog, F. (1962). Arevised medium for rapid growth and bioassays with tobacco tissue culture. *Physiol. Plant* 15, 473–497. doi: 10.1111/j.1399-3054.1962.tb08052.x

Okabe, Y., Asamizu, E., Ariizumi, T., Shirasawa, K., Tabata, S., and Ezura, H. (2012). Availability of Micro-Tom mutant library combined with TILLING in molecular breeding of tomato fruit shelf-life. *Breeding Sci.* 62, 202–208. doi: 10.1270/jsbbs.62.202

O'Malley, R. C., Rodriguez, F. I., Esch, J. J., Binder, B. M., O'Donnell, P., Klee, H. J., et al. (2005). Ethylene-binding activity, gene expression levels, and receptor system output for ethylene receptor family members from Arabidopsis and tomato. *Plant J.* 41, 651–659. doi: 10.1111/j.1365-313X.2004.02331.x

Sakai, H., Hua, J., Chen, Q. H. G., Chang, C., Medrano, L. J., Bleecker, A. B., et al. (1998). ETR2 is an ETR1-like gene involved in ethylene signaling in Arabidopsis. *Proc. Nat. Acad. Sci.* 95, 5812–5817. doi: 10.1073/pnas.95.10.5812

Shakeel, S. N., Wang, X., Binder, B. M., and Schaller, G. E. (2013). Mechanisms of signal transduction by ethylene: overlapping and non-overlapping signalling roles in a receptor family. *AoB Plants* 5, plt010. doi: 10.1093/aobpla/plt010

Szymanski, J., Levin, Y., Savidor, A., Breitel, D., Chappell-Maor, L., Heinig, U., et al. (2017). Label-free deep shotgun proteomics reveals protein dynamics during tomato fruit tissues development. *Plant J.* 90, 396–417. doi: 10.1111/tpj.13490

Trapet, P., Avoscan, L., Klinguer, A., Pateyron, S., Citerne, S., Chervin, C., et al. (2016). The Pseudomonas fluorescens siderophore pyoverdine weakens Arabidopsis thaliana defense in favor of growth in iron-deficient conditions. *Plant Phys.* 171, 675–693. doi: 10.1104/pp.15.01537

Wilkinson, J. Q., Lanahan, M. B., Yen, H. C., Giovannoni, J. J., and Klee, H. J. (1995). An ethylene-inducible component of signal transduction encoded by never-ripe. *Science* 270, 1807–1809. doi: 10.1126/science.270.5243.1807

Zhang, Y., and Wen, C. K. (2019). Statistics as part of scientific reasoning in plant sciences: overlooked issues and recommended solutions. *Mol. Plant* 12, 7–9. doi: 10.1016/j.molp.2018.11.001

Zhao, X., Qu, X., Mattews, D. E., and Schaller, G. E. (2002). Effect of ethylene pathway mutations upon expression of the ethylene receptor ETR1 from Arabidopsis. *Plant Phys.* 130, 1983–1991. doi: 10.1104/pp.011635.

Conflict of Interest Statement: The authors declare that the research was conducted in the absence of any commercial or financial relationships that could be construed as a potential conflict of interest.

The handling editor is currently organizing a Research Topic with one of the authors MB, and confirms the absence of any other collaboration at the time of review

frontiers in Plant Science

ORIGINAL RESEARCH
published: 10 September 2019
doi: 10.3389/fpls.2019.01072

Biochemical Characterization of the *Fusarium graminearum* Candidate ACC-Deaminases and Virulence Testing of Knockout Mutant Strains

Thomas Svoboda[1], Alexandra Parich[2], Ulrich Güldener[3], Denise Schöfbeck[2], Krisztian Twaruschek[1], Marta Václavíková[2], Roland Hellinger[2], Gerlinde Wiesenberger[1], Rainer Schuhmacher[2] and Gerhard Adam[1]*

[1] Department of Applied Genetics and Cell Biology, University of Natural Resources and Life Sciences, Vienna (BOKU), Tulln, Austria, [2] BOKU, Department for Agrobiotechnology (IFA-Tulln), Institute of Bioanalytics and Agro-Metabolomics, Tulln, Austria, [3] Department of Bioinformatics, TUM School of Life Sciences Weihenstephan, Technical University of Munich, Freising, Germany

OPEN ACCESS

Edited by:
Panagiotis Kalaitzis, Mediterranean Agronomic Institute of Chania, Greece

Reviewed by:
Luca Sella, University of Padova, Italy
Guotian Li, Huazhong Agricultural University, China

***Correspondence:**
Thomas Svoboda
thomas.svoboda@boku.ac.at

Specialty section:
This article was submitted to Plant Physiology, a section of the journal Frontiers in Plant Science

Received: 16 April 2019
Accepted: 07 August 2019
Published: 10 September 2019

Citation:
Svoboda T, Parich A, Güldener U, Schöfbeck D, Twaruschek K, Václavíková M, Hellinger R, Wiesenberger G, Schuhmacher R and Adam G (2019) Biochemical Characterization of the Fusarium graminearum Candidate ACC-Deaminases and Virulence Testing of Knockout Mutant Strains. Front. Plant Sci. 10:1072. doi: 10.3389/fpls.2019.01072

Fusarium graminearum is a plant pathogenic fungus which is able to infect wheat and other economically important cereal crop species. The role of ethylene in the interaction with host plants is unclear and controversial. We have analyzed the inventory of genes with a putative function in ethylene production or degradation of the ethylene precursor 1-aminocyclopropane carboxylic acid (ACC). *F. graminearum*, in contrast to other species, does not contain a candidate gene encoding ethylene-forming enzyme. Three genes with similarity to ACC synthases exist; heterologous expression of these did not reveal enzymatic activity. The *F. graminearum* genome contains in addition two ACC deaminase candidate genes. We have expressed both genes in *E. coli* and characterized the enzymatic properties of the affinity-purified products. One of the proteins had indeed ACC deaminase activity, with kinetic properties similar to ethylene-stress reducing enzymes of plant growth promoting bacteria. The other candidate was inactive with ACC but turned out to be a D-cysteine desulfhydrase. Since it had been reported that ethylene insensitivity in transgenic wheat increased *Fusarium* resistance and reduced the content of the mycotoxin deoxynivalenol (DON) in infected wheat, we generated single and double knockout mutants of both genes in the *F. graminearum* strain PH-1. No statistically significant effect of the gene disruptions on fungal spread or mycotoxin content was detected, indicating that the ability of the fungus to manipulate the production of the gaseous plant hormones ethylene and H_2S is dispensable for full virulence.

Keywords: *Fusarium graminearum*, ACC (1-aminocyclopropane-1-carboxylic acid), ACC synthase, ACC deaminase, ketobutyrate

INTRODUCTION

Ethylene is a gaseous plant hormone mediating developmental processes, such as fruit ripening, flower senescence, leaf abscission, as well as root elongation and has a strong influence on growth and yield of crop plants (Dubois et al., 2018). Furthermore, in a complex interplay with other plant hormones, ethylene has an important role in plant immunity (Broekaert et al., 2006; Ent and Pieterse, 2018; Li et al., 2019).

In plants, ethylene is derived from methionine *via* S-adenosyl-L-methionine. In a first dedicated and typically rate limiting step, 1-aminocyclopropane carboxylic acid (ACC) synthase converts S-adenosyl-L-methionine into the precursor ACC, from which ethylene is released by ACC oxidase. Ethylene perception and signalling were elucidated by genetic analysis of the model system *Arabidopsis thaliana*. The hormone is perceived by the copper containing receptor proteins ETR1 and related proteins (Gallie, 2015) that are present in the endoplasmic reticulum membrane. The Raf-kinase like protein CTR1 (Constitutive Triple Response 1) is associated with the ethylene receptor. In the absence of ethylene, CTR1 phosphorylates the ER-localized EIN2 protein at its cytosolic C-terminal part, which is then in the inactive state. When ethylene binds to the receptor, CTR is inhibited and EIN2 becomes dephosphorylated by phosphatases. The C-terminal domain of dephosphorylated EIN2 is then cleaved off and enters the nucleus, which ultimately leads to stabilization of the EIN3 transcription factor against proteasomal degradation (Qiao et al., 2012). EIN3 and the related EIL1 protein subsequently bind to promoters and activate the expression of multiple ethylene-responsive transcription factors (Huang et al., 2016), most importantly of the Ethylene Response Factor 1 (ERF1), which in turn induce the expression of a large number of ethylene responsive genes. With respect to plant defense, genes encoding pathogenesis-related proteins and biosynthetic genes for defense metabolites are induced by ethylene, often in a complex interplay with jasmonic acid. Ethylene and jasmonic acid signaling are considered to mediate defense against necrotrophic pathogens (Glazebrook, 2005) and hemibiotrophic pathogens switching to a necrotrophic mode after an initial biotrophic phase.

Studies with mutants that are deficient in ethylene biosynthesis or are ethylene-insensitive revealed the relevance of ethylene signaling in plant defense, but also the complexity of the interaction (Broekaert et al., 2006). For instance, Arabidopsis *ein2* mutants lost the ability to induce several pathogenesis-related (PR) genes in response to *Alternaria brassicicola* but nevertheless showed unchanged resistance, while the same mutants showed increased susceptibility to *Botrytis cinerea* (Thomma et al., 1999). In transgenic tobacco, which was engineered to become ethylene insensitive by overexpression of a dominant interfering ethylene receptor allele from Arabidopsis (*etr1-1*), breakdown of non-host resistance to several soil fungi was observed (Knoester et al., 1998), and also increased susceptibility to the pathogens *Botrytis cinerea* and *Fusarium oxysporum* (Geraats et al., 2003). Not all aspects of ethylene signaling are conserved between dicotyledonous and monocotyledonous plants (Yang et al., 2015). Nevertheless, ethylene clearly has a role, for instance in defense of rice against the fungal pathogen *Magnaporthe grisea*. Yet, in general, the outcome of virulence tests may be strongly dependent on the combination of host plant and pathogen species (Ent and Pieterse, 2018).

In contrast to the observed trend indicating a role for ethylene in mediating resistance, there are reports that ethylene signaling may also be utilized by fungal pathogens to increase host susceptibility. In the rice interaction with *Cochliobolus miyabeanus* (causing brown spot disease) treatment of plants with the ethylene releasing compound ethephon enhanced susceptibility, while plants with a silenced *OsEIN2* homolog (showing decreased expression of ethylene responsive defense genes) were more resistant (De Vleesschauwer et al., 2010). Similarly, in the interaction between *Fusarium oxysporum* f. sp. *raphani* and *Arabidopsis thaliana*, the ethylene insensitive *etr1-1* mutant was more resistant (Pantelides et al., 2013).

In line with this, the agriculturally relevant pathogen and mycotoxin producer *Fusarium graminearum*, which is in the focus of our interest, was also reported to be less virulent on transgenic wheat with silenced *EIN2* homologs, and importantly, much lower amounts of the mycotoxin DON accumulated in the infected plants. Thus, the fungus may exploit ethylene signaling to promote virulence (Chen et al., 2009). Yet, this is highly controversial. Most gene expression results comparing wheat cultivars of either high or low *Fusarium* resistance found correlations with gene expression consistent with a stronger resistance-associated ethylene-response. A stronger and more rapid response of genes involved in ethylene biosynthesis, ethylene signaling and ethylene response (Ding et al., 2011; Gottwald et al., 2012) and also higher amounts of ACC early in the infection were found in highly resistant cultivars (e.g. Wang et al., 2018). Furthermore, chemical manipulation of ethylene signaling revealed that treatment of highly resistant wheat cultivars with ethylene biosynthesis inhibitors (1-methylcyclopropene and cyclopropane-1,1-dicarboxylic acid) negatively affected resistance to initial infection and disease spread, while treatment with compounds enhancing ethylene production (ethephon and ACC) increased resistance of wheat to *F. graminearum* in highly susceptible cultivars (Foroud et al., 2018).

Several microbes are capable to synthesize ethylene and can consequently trigger ethylene dependent gene expression. In contrast, some microbes can downregulate ethylene production (reviewed in Ravanbakhsh et al., 2018). Fungi can form ethylene at unphysiologically high methionine concentrations in the medium by first transaminating methionine to 4-(methylsulfanyl)-2-oxobutanoate, better known by the synonym 2-keto-methyl-thio-butyrate (KMBA). In a second non-enzymatic reaction, KMBA is then cleaved by hydroxyl radicals (e.g. generated from H_2O_2 and Fe^{2+}) and ethylene is released [see *MetaCyc* Pathway: ethylene biosynthesis III (microbes)]. This unspecific pathway is seemingly the predominant one in the fungus *Botrytis cinerea* (Chagué et al.,

Abbreviations: DON, deoxynivalenol; D3G, deoxynivalenol-3-O-glucoside; ACC, 1-aminocyclopropane carboxylic acid; KBA, ketobutyric acid; ACS, ACC synthase; ACD, ACC deaminase; ACO, ACC oxidase; EFE, ethylene forming enzyme; KMBA, 4-methylthio-2-oxobutanoic acid; CTR, constitutive triple response; EIN, ethylene insensitive; EIL, ethylene insensitive like; PR, pathogen related; FMM, fusarium minimal media.

2002). In contrast, many bacteria, particularly plant pathogenic *Pseudomonas* species, can synthesize ethylene from oxoglutarate and arginine *via* the Ethylene Forming Enzyme (EFE). This enzyme is also present in some fungi [*MetaCyc* Pathway: ethylene biosynthesis II (microbes)], for instance in *Penicillium digitatum* (Johansson et al., 2014) which causes fruit rot in citrus. In addition, some fungi, e.g., *Penicillium citrinum* (Kakuta et al., 2001) contain ACC synthase and can synthesize ethylene using the plant pathway [*MetaCyc* Pathway: ethylene biosynthesis I (plants)]. Microbes can also have the ability to downregulate ethylene signalling by interfering with ethylene production. For instance, a bacterial type III effector protein (HopAF1 from *Pseudomonas syringae*) reduces ethylene production by targeting methionine recycling in the Yang cycle (Washington et al., 2016). Also, small molecules can be used as effectors, such as the bacterial rhizobitoxin, which directly inhibits ACC synthase (Yasuta et al., 1999; Sugawara et al., 2006). The ethylene precursor ACC, a signal molecule in plants, is transported *via* the xylem and phloem and causes ethylene production in tissue distant to its site of production (Van de Poel and Van Der Straeten, 2014). The most widely employed mechanism of plant associated bacteria (Gamalero and Glick, 2015; Nascimento et al., 2018) to downregulate ethylene production is the production of ACC deaminase enzymes, which degrade ACC into α-ketobutyric acid (KBA) and ammonia. Reduction of "stress-ethylene" *via* ACC deaminase has been found to be the mode of action of plant growth promoting rhizobacteria that improve the ability of plants to cope with different abiotic stresses, like salt stress (Singh et al., 2015; Qin et al., 2016) or heavy metal stress (Grichko et al., 2000). Expression of ACC deaminase in transgenic tomato was sufficient to enhance growth despite increased heavy metal accumulation (Grichko et al., 2000). ACC deaminases were found and characterized also in several plant associated fungi, for instance in the pathogen *Penicillium citrinum* (Jia et al., 2000), and the biocontrol strain *Trichoderma asperellum* (Viterbo et al., 2010). Such genes have been detected in many fungal genomes, and phylogenetic analysis has provided evidence for multiple independent acquisitions of bacterial ACC genes by horizontal gene transfer (Bruto et al., 2014).

Our research group is interested in virulence mechanisms of *Fusarium graminearum*. Due to the reported ability of this fungus to exploit ethylene signaling for virulence (Chen et al., 2009) and the controversial proposed roles of ethylene in Fusarium head blight resistance, we started to search for genes in *Fusarium graminearum* potentially involved in either ethylene production or downregulation of ethylene signaling, and to experimentally test candidate genes by heterologous expression and gene disruption.

MATERIALS AND METHODS

Bioinformatical Analysis

For the bioinformatic analysis of the genome annotation of *F. graminearum* (PH-1) the PEDANT genome database was used (Walter et al., 2009). The FGSG gene models are still available at http://gbrowse.boku.ac.at/cgi-bin/gb2/gbrowse/Fusarium_graminearum_PH1/and in FungiDB (https://fungidb.org/fungidb/). BLAST searches were performed at NCBI (https://blast.ncbi.nlm.nih.gov/Blast.cgi).

Cloning of *Fusarium graminearum* ACS and ACD Candidate Genes in *E. coli* DH10B

Both *ACD* candidate genes were amplified from gDNA of *F. graminearum* PH-1 using fusion PCR. All PCRs were done as follows: 2 min/95°C initial denaturation followed by 25 cycles of 30 s/95°C, 30 s at primer-dependent calculated annealing temperatures, 1 min/kb at 72°C and a single 72°C/5 min step at the end. All primers and fragment lengths are listed in **Supplementary Table 1**. The two *ACD* candidate genes were cloned in pETDuet-1. The coding region of *ACD1* (FGSG_02678) was cloned *via* BamHI/NotI, and *ACD2* (FGSG_12669) as EcoRI/NotI fragment. Plasmid pET30-UW4-651, containing an ACC deaminase from *Pseudomonas putida* was kindly provided by Prof. Glick, Waterloo, Ontario (Hontzeas et al., 2004). The BglII/HindIII fragment from this plasmid containing the ACD coding sequence was cloned into pETDuet-1 and into pACYCDuet-1 (BamHI/HindIII), a plasmid containing P15A ori (compatible with pETDuet-1) and a chloramphenicol resistance marker.

ACS1 (FGSG_05184) was amplified from genomic DNA due to the lack of introns, while *ACS2* (FGSG_07606) was amplified from cDNA which was prepared from mycelium harvested from PDA medium according to the protocol of the "RevertAid H Minus First Strand cDNA Synthesis Kit" (Thermo Scientific, Vienna, Austria). *ACS3* (FGSG_13587) was cloned from genomic DNA by fusion PCR. First the exons were amplified with the respective primers shown in **Supplementary Table 1**. Due to the overhangs which are homologous with the primer for amplification of the adjacent exon, amplification of two fused exons was achieved by fusion PCR. *ACS1* was cloned in pET-Duet1 into MCS1 *via* EcoRI/NotI while ACS2 and ACS3 were cloned using BamHI/NotI. The plasmids are listed in **Supplementary Table 4**.

Expression of *ACS* Candidate Genes in *E. coli*

After induction of transformed *E. coli* strain BL21/DE3 with 1 mM IPTG cells were harvested by centrifugation and the pellets were resuspended in 0.1 M Na-phosphate buffer pH 7.6. For cell disruption a Branson Sonifier W-250 D (Branson Ultrasonics Corporation, Danbury, CT, USA) was used with the following settings: 12 x 5 s pulse and 1 min pause. After centrifugation at 18,000 g the proteins were purified from the supernatants by affinity chromatography using a HisTrap© FF crude 1 ml column using an ÄKTA purifier (GE Healthcare, Austria). For rapid preparations His-select® spin columns (H7787, Sigma-Aldrich, Vienna, Austria) were used.

Tests of ACC Synthase Activity

The *ACS* candidate genes were expressed in *E. coli* and ACC synthase activity was tested in living cells by measuring the conversion of methionine into ACC. For this IPTG-induced cultures were supplemented with methionine to a final concentration of 100 mg/l. Samples were drawn after 0, 0.5, 1, 3 and 24 h. The cells were harvested by

centrifugation, resuspended in 0.1 M HEPES-KOH buffer pH 8.5 and disrupted by sonication as described above. The concentrations of methionine and ACC in the culture supernatant and in the soluble cell extract were measured by GC-MS.

For *in vitro* tests the proteins were purified using a rapid procedure (His-Select spin columns) according to the manufacturer's instructions. The activity of the ACC synthases was tested in presence of 50 mM HEPES-KOH buffer (pH 8.5) with 200 µM S-adenosyl-L-methionine (A7007, Sigma-Aldrich, Vienna, Austria) and 10 µM pyridoxal phosphate (P9255, Sigma-Aldrich, Vienna, Austria). Samples were taken every 30 min for 3 h and then after 16, 20, and 24 h and measured by GC-MS.

GC-MS Measurements of ACC and KBA

The standards for 1-aminocyclopropane-carboxylic acid (ACC; EMD 149101-1G) and 2-ketobutyric acid (KBA; K401, Sigma-Aldrich, Vienna, Austria) were purchased from Sigma-Aldrich. The solvents methanol LC-MS grade (Honeywell 34966) and pyridine p.A. (Merck 1.09728.0500) were obtained from Merck. The derivatisation chemicals methoxyamine hydrochloride (MOX; 226904, Sigma-Aldrich, Vienna, Austria) and N-methyl-N-trimethylsilyl trifluoroacetamide (MSTFA; 701270.201, Macherey-Nagel) were purchased from Sigma Aldrich and Macherey-Nagel, respectively. The stock solutions of ACC and KBA were prepared in 50% aqueous methanol.

The unpurified protein extracts were centrifuged for 10 min at 14,000 rpm at 4°C, 10 µL of the supernatant were transferred into micro-inserts in GC/HPLC vials and dried overnight using a centrifugal evaporator (Labconco, Kansas City, MO) at 15°C. Subsequently an automated two step derivatisation was carried out using the GC auto sampler (PAL LHX-xt, CTC Analytics, Carrboro, NC). To this end the residue was resuspended in 50 µL MOX (20 mg/ml pyridine) and agitated for 90 min at 90°C. After addition of 50 µL MSTFA the mixture was again agitated at 90°C for 60 min.

For GC-MS analysis, 1 µL of the derivate was injected into the split-/splitless injector of an Agilent 7890A gas chromatograph coupled to a 5975C inert XL MSD detector (Agilent, Waldbronn, Germany), equipped with ChemStation software (version E.02.01.1177) and operated in pulsed splitless mode at 250°C. Chromatographic separation was carried out on an HP5-ms column (30 m x 0.25 mm x 0.25 µm; Agilent Technologies, Waldbronn, Germany) at a constant flow of 1 ml/min helium. Temperature program: 50°C, 2 min hold, to 120°C (10°C/min, 5 min hold), to 150°C (5°C/min), to 325°C (70°C/min, 10 min hold). The MSD was operated with interface set to 335°C, the EI source to 230°C and the MSD quadrupole to 150°C, solvent delay 6 min, scan range of *m/z* 50–300, dwell time 100 ms. SIM mode was used for quantification of the ACC 1TMS derivate *m/z* 83 (quant ion), 130, 173; ACC 2TMS derivate *m/z* 147 (quant ion), 202, 230 and KBA 1TMS derivate *m/z* 89, 172, 188 (quant ion).

Ethylene Measurements

Ethylene (Ethylen Ecocyl 2.5) was purchased from Linde. Ethylene concentrations were determined by GC-FID (Hewlett Packard, Series 2, 5890 Series 2 plus, Agilent, Santa Clara, USA) coupled to a head space autosampler (Hewlett Packard, HP 7694, Agilent, Santa Clara, USA) using the following parameters. Headspace sampler: Oven, sample loop and transferline temperature 45°C, loop 3 ml, loop fill time 0.1 min and injection time 0.2 min; vial parameters: equilibration time 0.5 min, pressurizing time 0.2 min, GC cycle time 11 min. Chromatographic separation was carried out on a Restek Rt-QS-Bond column (30 m × 0.53 mm × 20 µm), using Helium as carrier gas (3.3 ml/min constant flow). Temperature program: 30°C, 1 min hold, to 60°C with 30°C/min, 3.5 min hold. Split injection (30:1) was used and the injector and the flame ionization detector (FID) were set to 250°C. Quantification was based on peak heights and external calibration (10 concentration levels between 0.17 µg/L and 10.65 µg/L). Calibration results were used to estimate the limit of detection (LOD = 0.67 µg/L) and limit of quantification (LOQ = 2.3 µg/L) with the ValiData software Version 3.02.48. Data were processed using MassHunter (Agilent Technologies, Qualitative Analysis B.06.00). Peak areas of the quantification ions were used for comparative quantification and the compound identity was confirmed by comparison with MS spectra of reference standards.

In Vitro Test of ACC Deaminase Candidate Genes

To follow the fate of ACC and KBA in liquid cultures of the *E. coli* BL21/DE3 strain transformed with empty vector or ACD expression vectors, a feeding experiment was performed. The empty vector control allows tracing of possible metabolization products of the target substances by *E. coli*. Expression of the target genes was induced by adding 1 mM IPTG and incubation overnight at 20°C, 140 rpm. ACC and KBA were added (0.5 mg/ml final concentration) to the IPTG-induced cultures. Samples were taken after 0, 1, 3 and 24 h and analyzed for ACC and KBA by GC-MS.

For characterization of the kinetic properties of the ACC deaminase from *Fusarium graminearum* a colorimetric assay relying on the reaction of phenylhydrazine with a ketone to phenylhydrazone was used (Penrose and Glick, 2003). The assay contained purified ACD2 (0.5 mg/ml), ACC concentrations ranging from 0.1 to 100 mM as well as 100 mM Na-phosphate buffer pH 7.6. A calibration curve was generated using KBA.

D-Cysteine Desulfhydrase Assay of ACD1 With D-Cysteine and L-Cysteine

To test ACD1 (later renamed DCS1 since the protein has D-cysteine desulfhydrase instead of ACC deaminase activity) for activity, 5 µl of the raw protein extract, which was obtained by sonification of IPTG induced cells, were tested in a total volume of 60 µl containing 0.1 M Tris–HCl pH 7.6 and 8 mM D-cysteine and incubation at 37°C for 15 min. The colorimetric assay was performed according to Penrose and Glick (2003), using pyruvic acid for calibration. ACD1 was purified by liquid chromatography *via* the His-tag using HisTrap™ columns (GE29-0510-21, Sigma

Aldrich, Vienna, Austria). Affinity purified ACD1 was tested for substrate specificity in 50 mM phosphate buffer pH 7.6 using 8 mM of the respective substrate, D-cysteine, L-cysteine, 2-aminoethyl-L-cysteine, or water as negative control. For determination of kinetic properties 0.1–30 mM D-cysteine as substrate were used. All reactions were incubated for 5 min at 30°C and stopped by the addition of 900 µl 0.56 M HCl.

ilvA Knock-Out in *E. coli* T7-Express

In order to be compatible with the T7 polymerase based expression system we knocked out *ilvA* in the expression host strain. The resulting strain is auxotrophic for isoleucine due to the loss of the ability to synthesize KBA, an intermediate of isoleucine biosynthesis. We obtained the *ilvA* mutant *E. coli* strain JW3745-2 from "The Coli Genetic Stock Center." The kanamycin resistance gene replacing the *ilvA* gene was amplified with primers 5′CGGAGATGTGGTAGTAATTC-3′ and 5′-GCCGTTTATTATGGCCGATC-3′, which bind in the neighbouring genes *ilvD* and *ilvY*. The 2085 bp fragment was purified and adjusted to a final concentration of 100 ng/µl. The strain to be transformed, *E. coli* T7-express (NEB, Frankfurt am Main, Germany), was first endowed with plasmid pKD46, which contains an arabinose inducible phage lambda *red* recombinase (Datsenko and Wanner, 2000). The PCR product (100 ng) was used for electroporation followed by selection on LB+kanamycin plates at 37°C, leading also to the loss of the temperature sensitive pKD46. Kanamycin resistant mutants unable to grow on M9 plates were tested by PCR. The resulting strain—T7 express *ilvA*::*Kan*^{R}—is available upon request. This strain was further transformed with the empty pET-DUET-1 vector or with pET-DUET-1 containing either ACD1, ACD2, or the positive control of *Pseudomonas putida* in MCSI. Expression was induced by IPTG (1 mM final concentration).

The positive control from *P. putida* (*ACDP*) was released from pET30a by BglII/HindIII cleavage and cloned into BamHI/HindIII digested pACYCDUET-1. This vector was transformed together with one of the *ACS* genes in pETDUET-1 into the generated *E. coli* T7-express lacking *ilvA*. *ACS4* of *Arabidopsis thaliana* (AT2G22810.1) in pETDUET-1 served as a positive control. Transformants were selected on LB plates containing ampicillin (100 mg/l) and chloramphenicol (25 mg/l). For the spottings, M9 was supplemented either with 3 mM methionine or 3 mM ACC.

Preparation of Knock-Out Mutants in *F. graminearum*

PEG-mediated protoplast transformation was performed as described by Twaruschek et al. (2018). For gene disruptions the split marker strategy was applied and fragments for transformation were produced as described below. The 3′ and 5′ flanking region of the candidate genes were cloned in pASB42 (see Twaruschek et al., 2018) adjacent to *hph-amdS* cassette flanked by two loxP sites (Steiger et al., 2011) using the primers listed in **Supplementary Table 2**. Screening of transformants was performed as described in (Twaruschek et al., 2018) using the primers listed in **Supplementary Table 3**. For multiplex PCR, three primers which are either located outside of the flanking region which was used for homologous recombination, or in the resistance cassette, or in the target gene to be disrupted were used. The corresponding primers in the resistance cassette were 5′AGAAGTACTCGCCGATAGTG-3′ for the 5′-flanking region, and 5′-ACACCTGCCGTGTCAGCC-3′ for the 3′-flanking region. The primers were designed in a way that the band of the wild type and the one of the knock-out strain can be easily differentiated.

For generating *acd1 acd2* double mutants, a knock-out construct with HSVtk-nptII as selection marker was generated: *ACS* flanking region containing plasmids pTS24, pTS35 and pTS45 were cut with HindIII/SalI. pTS14 and pTS58 were cut with BcuI/SfiI and pTS61 was digested BglII/BcuI (**Supplementary Table 4**). The HSVtk-nptII cassette from pKT245 was digested the same way to replace amdS-hyg (Twaruschek et al., 2018). Two independent, genotypically identical mutants (strains TS_ACD1Δ_2 and TS_ACD1Δ_13, listed in **Supplementary Table 5**) lacking *ACD1* were transformed using the split marker strategy. For screening of the double knock-out candidates, the same outer primer and the one within the gene as for the single knock-out screening were used. Due to a different resistance cassette the primers in the cassette were adapted to 5′-GTAGACCGCAAATGAGCAAC-3′ for the screening of the 5′ region, and 5′-GCCACAGCAGCCACGACA-3′ for the 3′ region. The resulting strains have the genotype *dcs1*Δ::*loxP-hyg-amdS-loxP* *acd2*Δ::*loxP-nptII-HSVtk-loxP* (**Supplementary Table 6**). Six PCR confirmed double-knockout strains were chosen for the virulence test with 10 replicates per strain. The progress of infection was observed over a time period of 16 days followed by analysis of DON and D3G after harvesting.

Test of Utilization of ACC as Sole Nitrogen Source

Fusarium Minimal Medium (FMM, for recipe see Twaruschek et al., 2018) was modified by replacing $NaNO_3$ with 3 mM ACC. Suspensions containing 10^5 spores were spotted onto the plates, which were incubated for 10 days at 20°C in the dark.

Wheat Infections

For the infection assays the cultivar Apogee (Mackintosh et al., 2006) was used. Ten microliters of a spore suspension with $4*10^4$ spores/ml was pipetted into each of four florets of two spikelets in the middle of the ear. Moistened plastic bags were used to cover the infected ears for 24 h to maintain high humidity. Plants were kept in a growth chamber (20°C with 16 h/8 h light/dark periods) and the disease progression was observed over a time period of 16 days by counting the infected spikelets every other day. For toxin analysis the ears at the endpoint of 16 days were harvested, frozen in liquid nitrogen and ground in a Retsch mill (Retsch MM400) using steel balls. For extraction 400 µl solvent (acetonitrile/water/acetic acid =

79: 20: 1) per 100 mg sample was added. The samples were extracted for 1 h at 20°C, 180 rpm, and centrifuged for 10 min at 14,000 g, and a 1:10 dilution was prepared for analysis by HPLC-MS.

Quantitative Analysis of DON and D3G

Deoxynivalenol (DON) and DON-3-O-glucoside (D3G) were determined by HPLC-MS/MS. A 1290 UHPLC system from Agilent Technologies (Waldbronn, Germany) equipped with Gemini C18 column (150 × 4.6 mm, 5 µm; Phenomenex, Aschaffenburg, Germany) was used for separation of analytes. The mobile phase eluents were composed of water and methanol (A: 80:20, v/v; B: 3:97, v/v) and contained both 5 mM ammonium acetate. The applied gradient was as follows: 0–1 min (0% B); 1–6 min (linear gradient from 0% B to 50% B); 6.1–8 min (flushing of the column with 100% B), 8–10 min (column equilibration with 0% B). The chromatographic system was maintained at 25°C and the flow rate of mobile phase was set to 800 µl/min.

Detection and quantification of both target analytes were performed on mass spectrometer QTrap 4000 (Sciex, Foster City, CA, USA), equipped with a TurboV electrospray ionization source. The system was operating in negative electrospray ionization mode (ESI-). The following source parameters were applied: curtain gas 35 psi (240 kPa), ion spray voltage (4 kV), temperature 550°C, ion source gas 1 and 2 both 50 psi (344 kPa), collision gas (nitrogen) high, and the interface heater on. The following selected reaction monitoring (SRM) transitions with a dwell time of 25 ms were used: DON (retention time 5.75 min) m/z 355.1 (declustering potential, DP, 65 V), product ions m/z 265.2 (collision energy, CE, 28 V) and m/z 59.2 (CE, 21 V); D3G (retention time 5.45 min) m/z 517.3 (DP, 56 V), product ions m/z 427.1 (CE, 25 V) and m/z 59.1 (CE, 18 V). Data were processed with Analyst 1.6.3 software from Sciex and further data processing and calculation of concentrations were performed using Microsoft Excel 2010. The limits of detection and quantification for DON and D3G were 10 and 25 ng/ml, respectively.

Cysteine Racemase Test

To check whether *F. graminearum* is able to convert L-cysteine into D-cysteine or vice versa, protein extracts were tested for racemase activity. Pre-cultures were prepared by inoculation of 10^5 spores of strain PH-1 in 100 ml FMM medium. After 3 days of incubation the mycelia were harvested using a sterile filter funnel, washed and inoculated in modified FMM ($MgSO_4$ replaced by $MgCl_2$ and supplemented with 1 mM D- or L-cysteine). The cultures were incubated at 20°C overnight followed by filtration of the mycelium. The mycelia were blotted dry, frozen in liquid nitrogen, pulverized using Retsch mill and 2 µl 50 mM Na-phosphate buffer pH 6.6 was added per milligram mycelium followed by vortexing 3 × 30 s. The protein extracts were centrifuged and the supernatant was used.

The assay contained 20 µl of the protein extract, 75 µl 50 mM phosphate buffer pH 6.6, and 25 µl D- or L-cysteine (10 mM final). The negative controls were supplemented with buffer instead of cysteine. Samples were taken after 0 and 24 h by transferring 50 µl of the samples into a tube containing 150 µl MeOH. One volume of ice-cold chloroform and four volumes of ice-cold methanol were added. The mixtures were shaken at 4°C for 15 min and precipitated proteins were pelleted by centrifugation at 12,000 g at 4°C for 10 min. The clear aqueous phase was transferred into another 1.5 ml reaction vial. The process was repeated once and the collected methanol phase was evaporated in a centrifugal vacuum evaporator. The dried residue was kept at −20°C until derivatization. Marfey's reagent (Pierce TS-48895) was used for derivatization of enantiomers to receive diastereomers. This derivatization allows chromatographic separation and detection of isobaric compounds derived from D-/ L-cysteine.

Quantification of D-, L-Cysteine Racemization Using LC-HR-MS Measurements

For quantification of D-cysteine desulfhydrase activity and to measure racemase activity an ultra-high performance liquid chromatography (UHPLC) Vanquish system coupled to a QExactive HF Orbitrap (both ThermoFisher) was applied to measure D-/L-cysteine levels. Five microliters of sample extract was injected for chromatographic separation on a Gemini NX-C18 column (150 × 3 mm ID, 5 µm, 110 Å, Phenomenex), which was protected by a pre-column and maintained at 25°C at a constant flow rate of 400 µl/min. To achieve chromatographic separation of the cysteine derivatives a gradient program with linear gradient segments was applied. Buffer A was water containing 0.1% formic acid and buffer B was acetonitrile containing 0.1% formic acid. The gradient program was as follows (% acetonitrile/ time in minutes): 10/0, 10/3, 45/56.1, 99/57, 99/62, 10/63, 10/70. UV traces were recorded at 220 and 340 nm.

The MS system was equipped with a heated electrospray ionization (HESI) source. The ESI interface was operated in fast polarity-switching mode, using 55 L/min sheath gas flow, 5 L/min auxiliary gas flow, a spray voltage of 3.5/3.0 kV respectively for the positive and negative ionization mode, S-lens level 55, capillary temperature 320°C and auxiliary gas temperature 350°C. FT-Orbitrap was operated in full scan mode acquiring profile spectra for the scan range m/z 100–1000 with a resolving power of 120,000 FWHM (at m/z 200) and automatic gain control setting of $3x10^6$ with a maximum injection time of 200 ms. The mass analyzer's mass accuracy was calibrated on a daily basis using Pierce LTQ Velos ESI ion calibration solution (ThermoFisher). A 1:1 mixture of the solution for positive and for negative ionization was prepared for calibration. The system was operated with TUNE 2.8 SP1 software and the direct control plugin for Chromeleon 7.2 SR4. Data processing was performed with XCalibur 4.0.27.19 (ThermoFisher). Quantification of area under the curve for the detected analytes was obtained with the XCalibur plug-in QuanBrowser. The retention times and m/z species used for quantification of the analytes were as follows: Marfey's reagent 23.80 min, L-cysteine 46.75 min, D-cysteine 49.90 min, D-valine 38.70 min, d8-D-valine 38.60 min, LL-cystine 47.20 min, DD-cystine 53.90 min, and DL-cystine 44.7 min. Note that Marfey's reagent reacts with both the primary amines and the free sulfhydryl groups in cysteine. The

retention time of the diastereomeric amino acid derivatives was determined using pure enantiomeric reference standards (Sigma-Aldrich, Vienna, Austria). Reference materials were prepared in 10 mM HCl and working solution for calibration were diluted in water. An internal standard calibration was applied to account for matrix effects as well as for variation of chemical derivatization with the Marfey's reagent. Due to the lack of sufficient isotopically labelled D- and L-cysteine and DD-, DL-, and LL-cystine reference standards, the representative amino acid D-valine was chosen as internal standard. Accordingly, quotient of analyte/ISTD area under the curve was calculated for all analytes. The ISTD concentration of 6.94 μM after spiking the analytes into the sample and derivatization was kept constant for all calibration standards and the biological samples. The applied concentrations for cysteine to calculate calibration function and for analyte quantification were 16, 80, 400, 2,000, and 10,000 μM. The obtained calibration function was linear for the chosen concentration range. The limit of detection was estimated in a serial dilution experiment for the analytes with greater than 2.89 μM.

RESULTS

Bioinformatical Analysis of the *F. graminearum* Genome—Presence of EFE?

The first question we addressed was whether the genome sequence of *F. graminearum* contains candidate genes that might allow the fungus to synthesize ethylene and thereby exploit ethylene signaling to increase virulence. The EFE pathway is the most efficient mechanism to produce ethylene. Therefore, we started the search for candidate genes using an EFE with biochemically confirmed activity (GenBank: EKV19239.1) as a query in a BLASTP search. As shown by Johansson et al. (2014), the associated mitochondrial import sequence was missed in the genome annotation of *Penicillium digitatum* (Marcet-Houben et al., 2012). The protein sequence in the database starts at the second in-frame ATG and is missing a number of N-terminal amino acids present in the protein sequence of the purified enzymes (see **Supplementary Figure 1**). We therefore used the modified gene model proposed by Johansson et al. (2014), which is highly similar to gene model (XP_002562422.1) from *Penicillium chrysogenum*/*P. rubens* (van den Berg et al., 2008). The BLASTP search using the N-terminally extended sequence (EKV19239.1) as query against the *F. graminearum* PH-1 genome yielded five hypothetical proteins (FGSG_00893, FGSG_00048, FGSG_03213, FGSG_08081, FGSG_02301) with sequence identities lower than 24% (low E-values below 9e-15, query covers below 75%). These low-similarity genes most likely encode members of the 2OG-Fe(II) oxygenase superfamily (pfam03171) with functions other than ethylene formation. The whole *F. graminearum* species complex (taxid:569360) contained no good candidate *EFE* gene, with the notable exception of *F. venenatum* (XP_025583657.1), having 66.39% identity with a query cover of 99%. The sequences differ to the highest extent in the putative mitochondrial import sequence, which is shorter in *Fusarium*. Interestingly, many other *Fusarium* species, particularly from the *F. oxysporum* and *F. fujikuroi* species complex had also highly similar genes, indicating that *EFE* could be present and conserved in the genus *Fusarium* (taxid:5506) after all (see **Supplementary Figure 1**). Yet, also in other *Penicillium* species, non-functional homologs highly similar to the enzymatically active *P. digitatum EFE* exist. Site-specific mutagenesis had revealed that introduction of several amino acids, which are different in the inactive enzyme from *P. chrysogenum,* into the active *Pseudomonas syringae* pv. *phaseolicola* enzyme (P32021.1, Fukuda et al., 1992), leads to loss of activity of the latter (Johansson et al., 2014). The candidate gene from *F. oxysporum* f. sp. *cepae* (RKK90967.1, as published by Armitage et al., 2018), has the highest similarity with the N-terminally extended *P. digitatum* gene (65% sequence identity over 88% of the query sequence). Using this protein sequence as query, the BLASTP results indicate that many gene models of other *Fusarium oxysporum* isolates are probably missing the C-terminal exon and therefore run into a premature stop. Closer analysis of one of these putatively truncated EFE candidates (Accession PCD42226.1) has shown that this is due to a GT → GA mutation in a donor splice site, which is then no longer recognized by automated annotation algorithms. However, studies of *Fusarium* splicing by (Zhao et al., 2013) have shown that the organism does actually use GA as a donor site, therefore the algorithm used to detect these "premature stops" might have overlooked an intron, and the truncated gene models might, in fact, not be truncated at all. **Supplementary Figure 1** shows the respective alignment, indicating that the hypothetical protein AU210_004756 from *Fusarium oxysporum* f. sp. *radicis-cucumerinum* can easily be modified to resemble the non-truncated candidates of other species. A potential exception is the unordered region (blue letters in **Supplementary Figure 1**), which was not included in the structural model of Johansson and coworkers (2014). In summary, we conclude that the *EFE* homologs seem to be widespread in different *Fusarium* species, but functional testing is necessary to find out whether the candidates are indeed encoding active enzymes or not. In contrast, *F. graminearum* and close relatives (*F. culmorum*, *F. pseudograminearum*) do not possess *EFE*.

Identification of ACC Synthase, Oxidase, and Deaminase Candidate Genes in the *F. graminearum* Genome

Using headspace GC-MS we found increased ethylene production of *F. graminearum* PH-1 on medium with 20 mM methionine added (**Supplementary Figure 2**), which suggests that the ACC synthase pathway might be active. Yet, we cannot rule out that the observed ethylene production is due to the unspecific pathway III found in a broad range of microbes.

We investigated whether *F. graminearum* possesses ACC synthase and ACC oxidase candidate genes. A BLASTP search with the sequence of the enzymatically active enzyme from *Penicillium citrinum* (BAA92149.1, described by Kakuta et al. in 2001) revealed three candidate genes: *FGSG_05184*/*FGRAMPH1_01G17303*, (named *ACS1* in this study), *FGSG_07606/FGRAMPH1_01T25199* (*ACS2*), and *FGSG_13587* (*ACS3*). These genes were already previously annotated as ACC-synthases in the Fusarium Genome Database (FGDB) by Wong et al. (2011). The alignment score

between the ACC synthase of *P. citrinum* and *Fusarium* genes is 52.3 for ACS1, 37.1 for ACS2 and 29.8 for ACS3. An alignment of these three predicted proteins with the ACC synthase of *P. citrinum* and an ACC synthase from *Triticum aestivum* (AAB18416.1), which were both confirmed to be active when expressed in *E. coli* (Subramaniam et al., 1996; Kakuta et al., 2001), is shown in **Supplementary Figure 3**. The phylogenetic tree shows that ACS3 is closely related to ACC synthase of *T. aestivum* and ACS1 is closely related to the confirmed gene of *P. citrinum*. The candidate genes have highly conserved residues involved in the catalytic activity and were therefore selected for experimental testing by heterologous expression in *E. coli*.

A BLAST search with a confirmed ACC oxidase from the basidiomycete *Agaricus bisporus* (Swiss-Prot H9ZYN5) showed that *F. graminearum* genome contains two predicted genes, *FGSG_09103* and *FGSG_11522*, with 79% and 88% query cover and 38% and 34% identical amino acids, respectively, while three other hits showed lower similarity. Both of these candidate genes are annotated as "isopenicillin N synthase and related dioxygenases," and are rather unlikely to have ACO activity, however, confirming this would require experimental testing.

While the results of Chen et al. (2009) suggest that *F. graminearum* exploits signaling for virulence by having the ability to produce ethylene, also, the opposite scenario cannot be excluded. We therefore searched for ACC deaminase candidate genes. A BLASTP search with a biochemically characterized ACC deaminase of *Trichoderma asperellum* (ACX94231.1, Viterbo et al., 2010) showed two hits in which the query cover was 99% and 98%, respectively, with 84% and 42% identical amino acids. These two genes (*FGSG_02678*/*FGRAMPH1_01T06417*, named *ACD1* and *FGSG_12669*/*FGRAMPH1_01T16927*, named *ACD2*) are also annotated as ACC deaminases also in FungiDB. The alignment of the confirmed ACC deaminase of *T. asperellum* with both candidate genes of *F. graminearum* is shown in **Supplementary Figure 4**. The phylogenetic analysis showed that *ACD2* is closer related to the confirmed ACC deaminase of *T. asperellum*.

Activity Test of *ACS* Candidate Genes

To test for ACC formation activity, we cloned all three *ACS* candidate genes into pETDuet-1. This vector allows co-expression with an ACC deaminase in an *in vivo* test (see below). *E. coli* transformants were induced to express the *Fusarium ACS* candidate genes. The protein extracts were analysed by SDS-PAGE and bands of the expected sizes were detected (see **Supplementary Figure 5**). Feeding assays were performed with induced cells, and the consumption of methionine added to the medium, as well as the potential formation of ACC in the cell pellets were measured by GC-MS. Yet, none of the transformants showed activity. Similarly, protein extracts generated from induced ACS-expressing *E. coli* were tested using S-adenosyl-L-methionine as substrate, but again, ACC formation could not be detected. Some ACC synthases have been reported to be quite unstable proteins and difficult to handle. We therefore purified the proteins with spin columns to speed up the purification process, again without success. Consequently, we tried an *in vivo* approach by complementation of an isoleucine deficiency in *E. coli via* coupled ACS/ACD activity. The test was based on the ability of an *ilvA* mutant

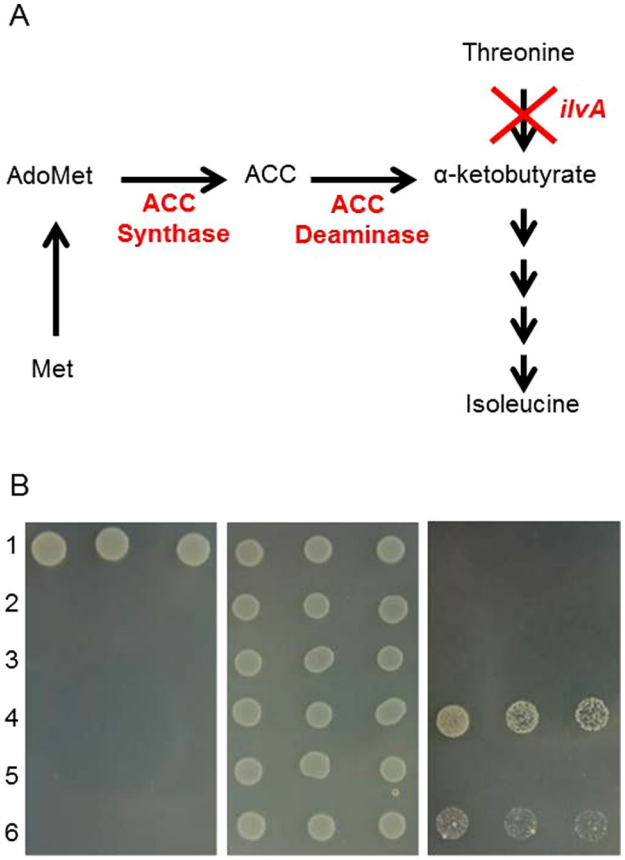

FIGURE 1 | *In vivo* testing of 1-aminocyclopropane carboxylic acid (ACC) deaminase candidate genes. **(A)** schematic of modified isoleucine biosynthesis pathway. **(B)** suppression of isoleucine auxotrophy of the Δ*ilvA* mutant strain by expression of ACC deaminase genes. The Δ*ilvA* mutant of T7 express was transformed with the constructs indicated below. Cultures of the transformants and of the parental strains were spotted in serial dilutions (1:10, 1:50, 1:100, 1:200 from left to right) onto the following media: M9 (left panel), M9 + isoleucine (middle) and M9 + 0.05 mM ACC + 1 mM IPTG + 100 mg/L ampicillin (right). 1, T7 express; 2, T7 express Δ*ilvA*; 3, Δ*ilvA* + pET-duet1; 4, Δ*ilvA* + *ACD1* from *P. putida*; 5, Δ*ilvA* + *ACD1* from *F. graminearum*; 6, Δ*ilv5* + *ACD2* from *F. graminearum*.

to grow on minimal medium (M9) without added isoleucine (Tarun et al., 1998), first due to the conversion of S-adenosylmethionine into ACC by an active ACS, and further conversion of ACC to the isoleucine precursor α-ketobutyrate by an ACC deaminase (see **Figure 1A**). For these experiments, the *Pseudomonas* ACD was cloned into pACYCDuet-1, which is compatible with pETDuet-1 and allows both proteins to be produced in one cell. We also combined the two genes in one plasmid (pETDuet-1), but no growth could be detected after co-expression, indicating a lack of ACS activity. Tests with ACC added to the medium and expression of ACD showed the functionality of the ACD part of the assay (see below).

Testing ACD Candidate Genes in the *E. coli ilvA* Knock-out Strain

The product of the ACC deaminase reaction, α-ketobutyrate, is an intermediate of isoleucine biosynthesis in *E. coli*. If ACC

is supplemented and ACD activity is present, an *ilvA* knockout strain is able to grow using the KBA formed from ACC to produce isoleucine. To allow testing of expression vectors based on the T7 RNA polymerase expression system (pET vectors), the *ilvA* mutation was introduced into the *E. coli* strain T7 Express by transferring the *ilvA*::Kan^R mutation from a strain from the *E. coli* knockout collection into the expression host (see *Materials and Methods* section). The ACD expression plasmids were introduced into the strain generated (T7 Express *ilvA*::Kan^R). Both the pETDuet-1 vector containing the *Pseudomonas putida* ACD gene serving as positive control and the *Fusarium ACD2* expression vector allowed growth of the *ilvA* mutant on minimal media supplemented with ACC, demonstrating the presence of active enzymes. In contrast, no evidence for activity of the *ACD1* encoded protein was obtained with this assay (**Figure 1B**).

Characterization of the ACC Deaminase Activity of the *ACD2* Gene Product

The pilot experiment with the modified *E. coli ilvA* strain already indicated that Acd2 has the predicted ACC deaminase activity. This was also confirmed by a colorimetric assay with permeabilized cells (see **Supplementary Figure 6**). Furthermore, a test of the crude protein extract revealed that Acd2 shows ACC deaminase activity similar to the positive control of *Pseudomonas putida,* while Acd1 did not show measurable activity. Likewise, GC-MS analysis did not reveal activity of Acd1, but clearly KBA formation was detected with Acd2. A feeding assay using ACD-expressing *E. coli* revealed that independently of the expressed gene, supplemented KBA was consumed by *E. coli* and also partly transaminated to 2-aminobutyric acid released to the medium. The activity test was repeated with the affinity purified protein (**Figure 2A**). The Acd2 protein remained constantly active over the whole assay period observed (60 min) and was used to determine the enzymatic properties (**Figure 2B**). The K_m value of Acd2 for ACC was determined to be 3.3 ± 0.7 mM and v_{max} to 1.3 ± 0.06 µmol mg^{-1} min^{-1}.

Acd1 Shows D-Cysteine Desulfhydrase Activity

It had previously been shown in an elegant work, that ACC deaminases and D-cysteine desulfhydrases from *P. putida* not only share a high sequence similarity, but can be interconverted into each other by site directed mutagenesis (Todorovic and Glick, 2008).

An alignment of both *Fusarium* candidate proteins with these *Pseudomonas* proteins is shown in **Figure 3**. The highlighted amino acids at positions 302 and 322 are specific for ACC deaminases and D-cysteine desulfhydrases. While Acd1 and the cysteine desulfhydrase from *P. putida* contain leucine and threonine, respectively, at these positions, Acd2 and the *Pseudomonas* ACC deaminase have methionine and leucine. Acd1 was therefore tested with D-cysteine as substrate. D-cysteine desulfhydrases convert D-cysteine into pyruvate, H_2S and NH_3. The formed pyruvate reacts with 2,4-dinitrophenylhydrazine, and this activity could be confirmed using the colorimetric assay. Neither L-cysteine nor S-(3-aminoethyl)-L-cysteine, which were used as alternative substrates, were consumed confirming the substrate specificity. The K_m value of Acd1 for D-cysteine was determined to be about 18 mM and v_{max} was 5.5 µmol mg^{-}1 min^{-}1. Since the ACD1/FGSG_02678 gene product shows D-cysteine desulfhydrase activity but not ACC deaminase activity we renamed the gene *DCS1*.

Due to the high specificity of the D-cysteine desulfhydrase and the presumably very low concentrations of D-cysteine *in planta*, we assumed that the fungus itself might be able to racemize L-cysteine to D-cysteine instead of obtaining the latter from the plant. To test this, a protein extract from a *Fusarium* culture, which had been pre-treated with D-cysteine, was incubated with L-cysteine for 24 h. Indeed, an increase in the D-cysteine concentration from a level below the limit of detection to around 2.5 mM was determined (data not shown, see Materials and Methods section) indicating the presence of a cysteine racemase. Yet, protein extracts of *Fusarium* cultures, which had been pre-exposed to L-cysteine first, did not show any detectable D-cysteine formation.

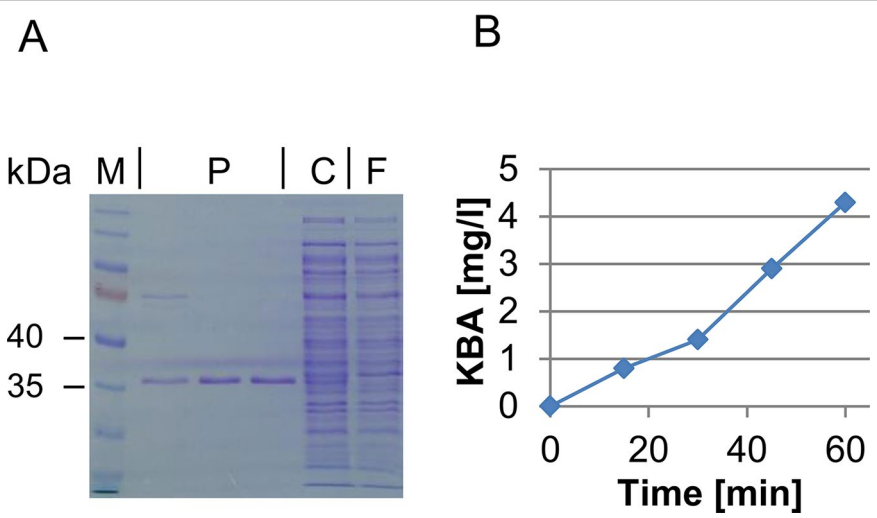

FIGURE 2 | Purification and activity test of Acd2. **(A)** SDS-PAGE showing purification of Acd2 protein. M, size marker (Page Ruler, prestained, Thermo Scientific 26616); P, fractions of affinity purified Acd2; C, crude extract; F, flow through after affinity purification. **(B)** KBA formation by purified Acd2 protein over time; KBA concentration was determined by GC-MS as described in the *Materials and Methods* section.

```
CDSH      ----MIKQQLARFNRLDL-LGQPTALEKLERLSTWLGRD--LYVKRDDL-TPLAMGGNKL      52
ACD1      --MVTLPSPFSDIDRVQLLFNRPTDIEPLSRLTESVNNNVKLWIAREDRNSGLAFAGNKV      58
ACDP      -------MNLNRFERYPLTFG-PSPITPLKRLSEHLGGKVELYAKREDCNSGLAFGGNKT      52
ACD2      MTVVTLPEPFASIPRENFLFG-ASPLQPLPRISAALGGKVNVYAKREDCNSGLAYGGNKV      59
                    :  : *  : :.  : :  * *::  :. .  ::  *:*  : ** .***

CDSH      RKLEYLAADALAQGADTLITAGALQSNHVRQTAAIAAKLGLGCVALLENPLGTDDNNYTG      112
ACD1      RKLEYVLADALAQGADTVVTTGGIQSNHMCQTSAAAARLGLKVALYPADRVASNDAEYKY      118
ACDP      RKLEYLIPEAIEQGCDTLVSIGGIQSNQTRQVAAVAAHLGMKCVLVQENWVNYSDAVYDR      112
ACD2      RKLEYLAAEAQAEGCDTLVSIGGVQSNHTRAVTAVASKLGLKAATVQEHWVDWEDPGYEK      119
          *****:  :*  :*.**::: *.:***:   .:* *::**:  .    . :  .*  *

CDSH      NGNRLLLDLFDAKVELVENLD--NADEQLQALADRLRSNGKKPYLVPIGGS-NALGALGY      169
ACD1      LGNIQANAILGAETF------P--VDTAEETVITTLKDRGQKPYSIPPGASSHPLGGLGY      170
ACDP      VGNIEMSRIMGADVRLDAAGFDIGIRPSWEKAMSDVVERGGKPFPIPAGCSEHPYGGLGF      172
ACD2      VGNIQLSRLMGGDVRLDPSTFGIEHKTTLAKLKDELKSNGQKPYYIPAGASDHPLGGLGF      179
           **     ::....                      : ..* **: :* * * :  *.**:

CDSH      VRAGLELAEQIKDTGLTFAAVVLASGSAGTHSGLALALSEAL----P--ELPVIGVTVSR      223
ACD1      ARWAFELLEQEKKIGVTFDTIALVAGSCSTLGGLLAGLKLAQKEQIPGSKKRLIGFSVLH      230
ACDP      VGFAEEVRQQEKELGFKFDYIVVCSVTGSTQAGMVVGFAADG-----R-SKNVIGVDASA      226
ACD2      ARWAFEVEAQEKELGIFFDTVIVCAVTGSTFAGMIAGFKLAQKKNGSP-ARKIIGIDASG      238
          .  . *:  * *. *. *  : : : : .* .*:  .:             :**. .

CDSH      SDE-DQRPKVQGLAERTAELLGMDLP--DAFNVELWDEYFAPRYGEPNAGTLAAVKLLAS      280
ACD1      KSKKDVEALVLKTSRTTASKIGISPNEITADDFEINTSYIGDGYGQLNDSTAEAMKKLAR      290
ACDP      KPE-QTKAQILRIARHTAELVELG-REITEEDVVLDTRFAYPEYGLPNEGTLEAIRLCGS      284
ACD2      KVQ-QTFDQVLRIAKNTAAKIGLSEDDITADDVILDPNYNAKVYGIPDETTLEAMRFGAA      297
          . : :    :   :. **  : :.       :. :   :    **  :  *  *::  .

CDSH      QEGLLLDPVYTGKAMAGLLDGIGRQRFD-EGPIIFLHTGGAPALFAYKDFL---     330
ACD1      KEGILTDPVYTGKAFTGLLDLAKTGYLN-GKNVLFLHTGGQAVLSAYPGLRE--     341
ACDP      LEGVLTDPVYEGKSMHGMIEMVRRGEFPDGSKVLYAHLGGAPALNAYSFLFRNG     338
ACD2      TEAFITDPVYEGKSLAGMMDLIKTGKIA-GGNVLYAHLGGQLALNAYSSI----     346
           *..: **** **:: *:::      :     ::: * **  .* **  :
```

FIGURE 3 | Alignment of D-cysteine desulfhydrase (CDSH) from *P. putida* (GenBank: AFY17401.1) and ACD from *P. putida* (ACDP; UniProtKB/Swiss-Prot: Q5PWZ8.1) with the predicted proteins Acd1 and Acd2 from *F. graminearum*. The highlighted amino acids are characteristic for a D-cysteine desulfhydrase (green) or for an ACC deaminase (yellow), respectively.

ACD2 and *DCS1* Knock-Out Strains Show Unaltered Virulence

We constructed *acd2*Δ and *dcs1*Δ knock-out strains using a *hph-amdS* cassette flanked by two *loxP* sites (Steiger et al., 2011). The virulence of three independent mutants lacking *DCS1* and four independent *ACD2* deletion strains (**Supplementary Figures 7A** and **B**) was tested with 15 replicates per strain. On average, a marginally lower virulence of both, the *acd2*Δ and *dcs1*Δ knock-out strains was observed, but the results did not reach the threshold of statistical significance (**Figures 4A, B**). Virulence tests were also carried out with the double-knockout strains. Neither the single (*acd2*Δ or *dcs1*Δ), nor the double knock-out (*acd2*Δ *dcs1*Δ) strains (**Supplementary Figure 7C**) showed a significantly reduced virulence, indicating that these genes are dispensable during infection (**Figure 4C**).

The main problem with *F. graminearum* is contamination of grain with the mycotoxin deoxynivalenol (DON) and the plant detoxification product DON-3-glucoside (D3G). The *Arabidopsis* DON-detoxifying glucosyltransferase UGT73C5 is rapidly and transiently induced by ACC and jasmonic acid (Poppenberger et al., 2003). We therefore determined the concentrations of DON and D3G in infected ears at the endpoint by grinding and extracting 15 infected ears individually. The average DON values of the heads infected with *acd1*Δ were lower compared to wild type treated ears. Yet, these values were not significantly different due to high fluctuations in DON content between individual samples (**Supplementary Figure 8**).

Fusarium graminearum Is Able to Use ACC as Sole Nitrogen Source

Plant growth promoting rhizobacteria (PGPR), which provide increased stress tolerance to plants, had been shown to be able to grow on media with ACC as sole nitrogen source (Penrose and Glick, 2003). We therefore tested whether also *F. graminearum* can grow on ACC. Spores of four independent *acd2*Δ knockout strains were spotted on modified FMM with ACC as sole nitrogen source together with one ectopic mutant and the wild type control (PH-1). After 1 week of incubation, the wild-type and the ectopic mutant grew well on ACC as sole nitrogen source, while

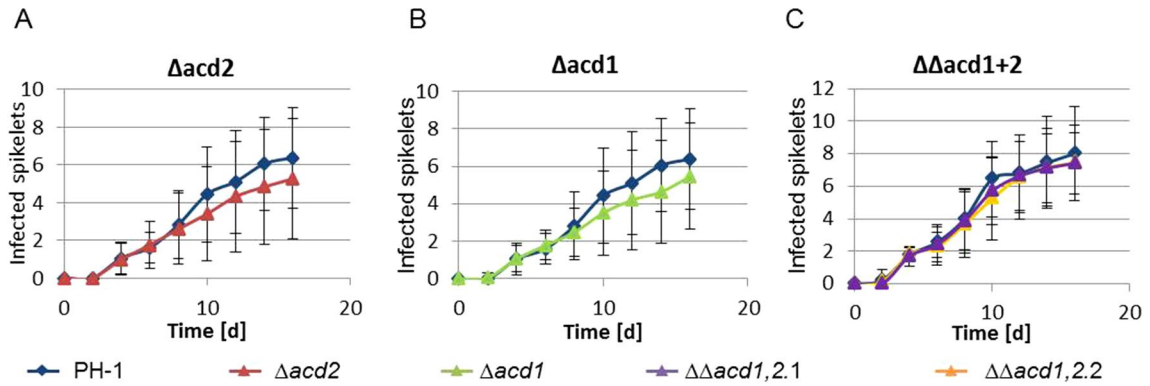

FIGURE 4 | Virulence tests of the single and double knock-out mutants. Ears of the wheat cultivar Apogee were infected with PH-1 and the indicated mutant strains. **(A)** and **(B)**: PH-1 vs. Δ*acd2* and Δ*acd1*, respectively; the mean number of infected spikelets from 15 inoculated ears are shown for each strain and time point. **(C)** PH-1 (mean number of infected spikelets from 10 inoculated ears) compared to six independent double knock-out strains (ΔΔ*acd1,2*) derived from two independent acd1 single knock-out strains. For each graph, the mean number of infected spikelets from 10 inoculated ears for each of the three independent double knock-out strains were used at each time point. t-test was performed but no statistically significant difference was evidenced.

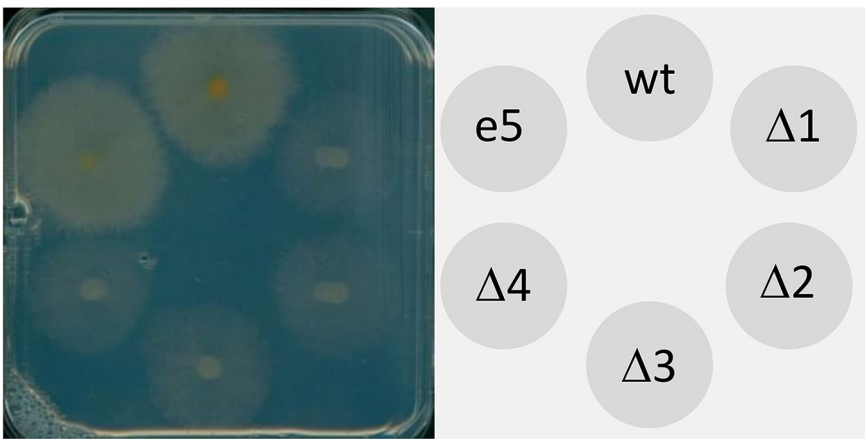

FIGURE 5 | Utilization of 1-aminocyclopropane carboxylic acid (ACC) by *Fusarium graminearum***.** Spores (10^5) of the following strains were spotted onto modified FMM with ACC as sole nitrogen source: wt, PH-1; Δ, four independent *acd2*Δ knock-out strains; e, ectopic transformant. The plate was incubated at 20°C for 10 days in the dark.

growth of the *ACD2* knockout strains was strongly retarded but not completely blocked (**Figure 5**). In contrast, all strains were equally well growing on standard FMM plates which were used as control (not shown). A possible explanation for continued growth of the mutant strains might be a partial non-enzymatic degradation of ACC in the medium.

DISCUSSION

Our bioinformatical investigation revealed that various *Fusarium* species (particularly from the *F. oxysporum* and *F. fujikuroi* complex) might possess EFE as a means to synthesize ethylene. Yet, it remains to be tested whether the candidate genes are indeed encoding enzymatically active proteins. Existing gene models have to be used with caution. For instance, in the case of *Fusarium mangiferae*, where fungal ethylene production has been implicated in malformation of mango fruits (Ansari et al., 2013), the gene model is questionable (see **Supplementary Figure 1**). A closer look at the DNA sequence of FMAN_06358 showed that the annotated intron might not be real. However, intron retention leads to a model with a frameshift, as indicated in **Supplementary Figure 1**. Questionable non-functional splice sites might be a cause for truncated *F. oxysporum* models lacking the last exon, and hence, for these species, experimental testing is warranted. Nevertheless, the focus of this study was on the cereal pathogen *F. graminearum*, and for this species, ethylene synthesis *via* the EFE pathway can be excluded.

Three candidates for ACC synthases were found in *F. graminearum*. Orthologs of these genes also exist in other *Fusarium* species. Therefore, certain *Fusarium* species apart from *F. graminearum* might potentially possess both the EFE

and the ACS pathway, a phenomenon so far only described for *Penicillium digitatum* (Chalutz and Lieberman, 1977). Activity of heterologously expressed ACC synthases in *E. coli*, e.g. of the wheat ACC gene (Subramaniam et al., 1996, shown in the alignment in **Supplementary Figure 3**), has been described. Yet, many plant ACC synthases are notoriously unstable and difficult to handle *in vitro*. Our efforts to demonstrate synthesis of ACC with S-adenosyl-methionine *in vitro* with the *E. coli*-expressed affinity-purified protein were unsuccessful with all three candidates. Likewise, upon feeding of IPTG induced *E. coli* cells with methionine, no ACC formation in cell extracts could be detected. We therefore adopted the growth-based assay originally described by Tarun et al. (1998) for use with the T7 expression system. With the functional *Pseudomonas putida* ACC deaminase as a bridge (see **Figure 1**), no growth upon expression of any of the *F. graminearum* ACS candidate genes was observed on M9 medium (data not shown). However, in an experiment using headspace GC-MS, ethylene production by *F. graminearum* on minimal media supplemented with 20 mM methionine was observed, which means the fungus either has ACC synthase activity or uses the transamination pathway *via* KMBA.

Potentially, the *Fusarium* ACC synthases may be active only in a complex with other proteins and could play a role in the synthesis of secondary metabolites containing ACC or ACC-like substances. Recently, a first bacterial ACC synthase was described (Xu et al., 2018), which is involved in synthesis of guangnanmycin. Coronatine, a well-known *Pseudomonas* metabolite interfering with defense signaling (Geng et al., 2014), contains coronamic acid, which has strong structural similarity to ACC and induces the synthesis of ethylene from methionine (Kenyon and Turner, 1992) by activating JA signaling (Uppalapati et al., 2005). An isolate of the fungus *Trichothecium crotocinigenum*, belonging to the hypocreales like *Fusarium*, is able to produce a diketopiperazine type cyclic "dipeptide" containing ACC (cyclo-(L-pipecolinylaminocyclopropane-carboxylic acid) (Long, 2014)). Also in the cotoxin II nonribosomal peptide from the plant pathogen *Bipolaris zeicola* (Ueda et al., 1992) ACC is a building block. Yet, none of the ACC synthase candidate genes is located in or near a predicted gene cluster suggestive of a role in secondary metabolite biosynthesis. Both ACC deaminase genes and two of the three ACC synthase candidates are located on the slowly evolving, conserved sub-genome (Wang et al., 2017). Only *ACS2* (FGSG_07606) is located on the fast evolving subgenome. Analysis of published transcriptomics data from Zhang et al. (2012) and Wang et al. (2017) indicates that both *ACD1* (renamed *DCS1*) and *ACD2* are preferentially expressed during infection as compared to vegetative mycelial growth (5.3-fold and 6.8-fold higher, respectively), while of the ACC synthase genes, only the first candidate *ACS1* (FGSG_05184) exhibits increased expression in planta (3.8-fold). We plan in further work to perform metabolomic analyses using the generated ACS knockout strains. While this research was going on, an alternative gene model for ACS3 has been deposited in FUNGI DB. The former ACS3, FGSG_13587 gene model was modified upon availability of more robust RNA sequencing data. The current model, FGRAMPH1_01G27057, incorporates some changes due to an updated splicing pattern and extended N- and C-termini (**Supplementary Figure 3**). Furthermore, extensive adenosine to inosine editing (Bian et al., 2019) during sexual development was found in all three ACS candidate genes (Liu et al., 2019).

Regarding ACC oxidases, we are not aware of any biochemically characterized functional enzyme from an ascomycete. There are reports that ethylene synthesis and signalling play a role in sexual development of the slime mold *Dictyostelium discoideum* and also in the basidiomycete *Agaricus bisporus* (Wood and Hammond, 1977; Zhang et al., 2016). Silencing and overexpression of a putative *ACO* gene (http://dictybase.org/gene/DDB_G0277497) from the slime mold affected ethylene production (Amagai et al., 2007). Using the *D. discoideum ACO* gene as a BLAST query against the *F. graminearum* genome yields a list of genes that is similar to the results of a query using the *A. bisporus ACO*, but with a different order. Since we could not demonstrate ACC synthase activity, we did not further investigate whether these multiple candidates have indeed ACO activity, but this is clearly a topic for further research.

The search for potential ethylene production genes was inspired by the claim by Chen et al. (2009) suggesting *F. graminearum* might exploit ethylene production to trigger increased plant susceptibility. Yet, many transcriptome studies suggest the opposite (Kazan and Gardiner, 2018). This is true also for other *Fusarium* species. For instance, upregulation of banana ethylene biosynthesis and of ethylene-responsive transcription factors were implicated in the resistance response against *Fusarium oxysporum* f. sp. *cubense* (Li et al., 2013). Consequently, we also searched for ACC deaminase candidate genes having the potential to counteract ethylene defense signaling. Only one of the two purified ACD candidate gene products, Acd2, showed activity with ACC in the classical colorimetric assay with toluene-permeabilized cells (Penrose and Glick, 2003). The *F. graminearum* Acd2 enzyme has kinetic properties very similar to previously described ACDs from plant-beneficial bacteria or pathogenic fungi. For instance, the ACC deaminases from *Pseudomonas putida* and *Penicillium citrinum* showed K_m values of 3.40 and 4.80 mM, respectively, compared to 3.31 mM for *F. graminearum* Acd2. The enzymatic activity of Acd2 did allow growth of isoleucine-deficient *E. coli* on M9-medium supplemented with ACC. Yet, the *Fusarium* Acd2 protein seems to work better at lower temperatures, e.g., 30°C, than the routine *E. coli* growth temperature of 37°C.

With an increasing number of genome sequences available, it became evident that gene products from bacteria (Ekimova et al., 2018) and from plants with high similarity to ACC deaminases exist. However, they are inactive with ACC, but have D-cysteine desulfhydrase activity (DCS). It was shown by site-directed mutagenesis that exchanging only two amino acids was sufficient to convert *Pseudomonas* ACC deaminase into an enzyme with Dcysteine desulfhydrase activity, and *vice versa* (Todorovic and Glick, 2008). We noticed that the inactive ACD1 (DCS1) candidate had the amino acids suggesting it might be a D-cysteine desulfhydrase (**Figure 3**). This was confirmed by enzymatic assays with the purified protein. The *F. graminearum* enzyme is inactive with L-cysteine. D-cysteine desulfhydrase catalyses the following reaction: D-cysteine + $H_2O \rightarrow H_2S$ + NH_3 + pyruvate. The product H_2S is, like ethylene, a gaseous

signaling molecule with an increasingly recognized importance in animals and plants (Li et al., 2016; Filipovic and Jovanovic, 2017; Ziogas et al., 2018; Corpas et al., 2019). In crosstalk with other hormones, H_2S is mediating increased resistance to abiotic stresses (Shi et al., 2015), for instance drought resistance in wheat (Li et al., 2017). In banana, hydrogen sulfide slows down senescence *via* affecting ethylene signaling (Ge et al., 2017) by downregulating the expression of both ACC synthase and ACC oxidase genes. Hydrogen sulfide can modify many proteins and change their activity by persulfidation or S-sulfhydration, where the cysteine-SH is converted into a persulfide group (-SSH) (Aroca et al., 2015). It has been recently shown that H_2S in tomato negatively regulates ethylene biosynthesis by persulfidation of ACC oxidase (Jia et al., 2018). The relevance of H_2S in plant-pathogen interaction is still largely unknown with the exception of some storage diseases (Huo et al., 2018).

F. graminearum and other species are able to produce auxin, and auxin levels are increased in *Fusarium* infected plants (Kidd et al., 2011; Wang et al., 2018). Elevated auxin levels trigger induction of ACC synthase and oxidase in various plants (Grossmann, 2000). We have unpublished evidence that, in an early stage of the interaction, auxin production is indeed a virulence factor of *F. graminearum* (Svoboda et al., in preparation). We hypothesized that ethylene might increase resistance of the plant when formed later in a necrotrophic interaction, and that the ACC deaminase candidate genes might be used by *Fusarium* to counteract ethylene formation. In this case, inactivation of ACC deaminase should reduce the virulence of mutants. To test the relevance of the ACC deaminase *ACD2* and *DCS1* (formerly *ACD1*) in plant disease development we generated single-gene knockout strains, and additionally the *acd2*Δ *dcs1*Δ double mutants. These strains were used for infection of the rapid cycling and highly *Fusarium*-susceptible wheat cultivar Apogee. No significant difference was detectable at the end-point or in the area under the disease progression curve. Furthermore, the levels of the mycotoxin DON and the plant detoxification product DON-3-O-glucoside determined at the endpoint of the infections after 16 days were highly variable. No significant difference was observed between wild type, the single *acd2*Δ and *dcs1*Δ strains, the ectopic insertion mutants or the double mutant. ACC deaminase and D-cysteine desulfhydrase are obviously dispensable for full virulence of *F. graminearum* on wheat, at least on the highly susceptible cultivar Apogee. This is in contrast to the interaction of tomato with the root-infecting pathogen *Verticillium dahliae*. In this pathosystem, host resistance to the wilt pathogen could be increased *via* expression of a bacterial ACC deaminase in tomato, which was under control of promoters limiting the expression to the site of infection (Robison et al., 2001). In line with this, it was recently reported that ACC deaminase knockout mutants of *Verticillium* were less virulent, while overexpression led to increased virulence (Tsolakidou et al., 2018). The only other evidence for a role of a fungal ACD we are aware of is the case of the plant growth promoting fungus *Trichoderma asperellum* T203. In this case, ACD was not deleted, but silenced using RNAi, the effects of which are often ephemeral. Nevertheless, the results suggested that the strain with reduced ACD activity has a decreased ability to promote root elongation of *Brassica napus* (Viterbo et al., 2010).

We tested whether *F. graminearum* can utilize ACC as a nitrogen source, which is clearly the case (**Figure 5**). Thus, instead of preventing the mobile signaling molecule ACC, generated at the infection front, from moving to other plant parts and triggering resistance, the main but marginal function of ACC deaminase could be utilization of a low-abundance nitrogen source. The enzyme has a K_m in the mM range. The highest reported (Wang et al., 2018) ACC concentration in infected ears of the highly *Fusarium* resistant cultivar Sumai3 of around 45 mg/kg could be relevant, especially assuming the local concentrations might be higher than this average. On the other hand, these <0.5 mM amounts of ACC seem to be of minor relevance, considering that reported levels of free amino acids in developing grain are in the range of 300 to 50 mM from 7 days post-anthesis to ripening (Howarth et al., 2008).

Likewise, the role of D-cysteine desulfhydrase in *Fusarium* is enigmatic. The expression of both *ACD2* and *DCS1* is higher during plant infection than in axenic cultures. A cysteine desulfhydrase gene (dcyD/yedO) also exists in *E. coli*. It is upregulated during sulfur starvation and may allow utilization of D-cysteine (if available in the environment). The only other known function of dcyD is protection against toxicity of very high levels of D-cysteine when present in minimal medium, since D-cysteine blocks threonine deaminase, the gene product of *ilvA* (Soutourina et al., 2001). Toxicity of D-cysteine is low in rich medium or when isoleucine is supplemented. Nevertheless, there are D-cysteine containing secondary metabolites that are orders of magnitude more toxic. If *Fusarium* is able to degrade them, *DCS1* might play a role to utilize the released D-cysteine. For instance, the *Aspergillus* metabolite malformin A contains two D-cysteine residues in the cyclic pentapeptide. Recently, malformin E was described to have a minimal inhibitory concentration of about 7 μM for *Fusarium solani* (Ma et al., 2016) and below 1 μM for *E. coli*. Many microbes can also produce highly toxic aminovinyl-cysteine-containing peptides that contain D-cysteine (Sit et al., 2011). This suggests a role in microbe-microbe interaction rather than in plant-pathogen interaction. Yet, the advantage seems minimal, since a *dcs1Δ* mutant is still able to grow on D-cysteine (data not shown), which is expected since the *F. graminearum* genome contains D-amino-acid oxidases.

We did not obtain evidence supporting a role of *DCS1* in plant disease. Still, utilization of a (marginal) sulfur source could be a function. The major sulfur transport forms during grain filling are glutathione and S-methyl-methionine (Bourgis et al., 1999), and both are highly abundant. While we are not aware of any reports of relevant concentrations of D-cysteine in plants, it has been described that peas possess transaminases producing D-alanine—and possibly other D-amino acids—in seedlings (Ogawa et al., 1973). It is, however, difficult to envision how a low-affinity enzyme with a K_m of ~18 mM could make a relevant contribution to the utilization of sulfur sources. On the other hand, plants also

have D-cysteine desulfhydrases (e.g. Arabidopsis AT1G48420), which may be involved in H_2S signaling. Potentially, the fungus itself may be able to synthesize D-cysteine from L-cysteine. Our preliminary experiments indicated that *F. graminearum* has racemase activity that can potentially convert L-cysteine into D-cysteine. Cysteine racemase is a rarely reported activity (Espaillat et al., 2014). Formed D-cysteine might then be used by Dcs1 to produce a volatile H_2S signal. Potentially, *F. graminearum* might be able to take up cysteine from the host and affect levels of glutathione, which is crucial for maintenance of the redox balance during infection. Glutathione (GSH) levels clearly have an impact on plant defense in general, most likely *via* affecting NPR1 and salicylic acid production (Ghanta et al., 2011; Kovacs et al., 2015) but also direct effects on ethylene production were reported (Datta et al., 2015). *Arabidopsis thaliana* transgenic plants with increased GSH content upregulated several ACS transcripts, and in addition, ACO protein levels were also increased, while in a *pad2-1* mutant with reduced GSH levels, the opposite effect was observed (Datta et al., 2015). Yet, our virulence tests do not support such a scenario. Inactivation of both ACC deaminase and D-cysteine desulfhydrase did not have a significant impact on the virulence of *F. graminearum*, at least not in the highly susceptible wheat cultivar Apogee. This outcome is not unprecedented. Other genes with a highly suggestive function were also found to be dispensable, such as genes encoding enzymes for degradation of salicylic acid (Hao et al., 2018; Qi et al., 2019; Rocheleau et al., 2019), despite clear evidence that salicylic acid plays an important role in the defense of wheat against *F. graminearum* (Makandar et al., 2006; Makandar et al., 2012). In future work we intend to investigate the role *Fusarium* ACC synthase candidate genes by generating triple knock-out mutants, to clarify the role of fungal ethylene production in the interaction with the host plant.

DATA AVAILABILITY

All datasets generated for this study are included in the manuscript and the supplementary files.

AUTHOR CONTRIBUTIONS

TS constructed plasmids. TS performed experiments. GW, RS, and GA conceived the concept. GW supervised experimental work. KT and UG did the bioinformatical analyses. DS, RH, MV, and AP performed the analytical measurements. TS, KT, GW, and GA wrote the paper and all authors amended and corrected the paper.

FUNDING

This work was funded by the Austria Science Fund (FWF), SFB Fusarium (F3702 and F3715), and the DFG (LAP3714).

SUPPLEMENTARY MATERIAL

The Supplementary Material for this article can be found online at: https://www.frontiersin.org/articles/10.3389/fpls.2019.01072/full#supplementary-material

REFERENCES

Amagai, A., Soramoto, S.-S., Saito, S.-H., and Maeda, Y. (2007). Ethylene induces zygote formation through an enhanced expression of zyg1 in Dictyostelium mucoroides. *Exp. Cell Res.* 313, 2493–2503. doi: 10.1016/j.yexcr.2007.04.012

Ansari, M. W., Shukla, A., Pant, R. C., and Tuteja, N. (2013). First evidence of ethylene production by Fusarium mangiferae associated with mango malformation. *Plant Signal. Behav.* 8, e22673. doi: 10.4161/psb.22673

Armitage, A. D., Taylor, A., Sobczyk, M. K., Baxter, L., Greenfield, B. P. J., Bates, H. J., et al. (2018). Characterisation of pathogen-specific regions and novel effector candidates in *Fusarium oxysporum* f. *sp. cepae*. *Sci. Rep.* 8, 13530. doi: 10.1038/s41598-018-30335-7

Aroca, Á., Serna, A., Gotor, C., and Romero, L. C. (2015). S-sulfhydration: a cysteine posttranslational modification in plant systems. *Plant Physiol.* 168, 334–342. doi: 10.1104/pp.15.00009

Bian, Z., Ni, Y., Xu, J.-R., and Liu, H. (2019). A-to-I mRNA editing in fungi: occurrence, function, and evolution. *Cell. Mol. Life Sci.* 76, 329–340. doi: 10.1007/s00018-018-2936-3

Bourgis, F., Roje, S., Nuccio, M. L., Fisher, D. B., Tarczynski, M. C., Li, C., et al. (1999). S-methylmethionine plays a major role in phloem sulfur transport and is synthesized by a novel type of methyltransferase. *Plant Cell* 11, 1485–1498. doi: 10.1105/tpc.11.8.1485

Broekaert, W. F., Delauré, S. L., De Bolle, M. F. C., and Cammue, B. P. A. (2006). The role of ethylene in host-pathogen interactions. *Annu. Rev. Phytopathol.* 44, 393–416. doi: 10.1146/annurev.phyto.44.070505.143440

Bruto, M., Prigent-Combaret, C., Luis, P., Moënne-Loccoz, Y., and Muller, D. (2014). Frequent, independent transfers of a catabolic gene from bacteria to contrasted filamentous eukaryotes. *Proc. Biol. Sci.* 281, 20140848. doi: 10.1098/rspb.2014.0848

Chagué, V., Elad, Y., Barakat, R., Tudzynski, P., and Sharon, A. (2002). Ethylene biosynthesis in Botrytis cinerea. *FEMS Microbiol. Ecol.* 40, 143–149. doi: 10.1111/j.1574-6941.2002.tb00946.x

Chalutz, E., and Lieberman, M. (1977). Methionine-induced ethylene production by *Penicillium digitatum*. *Plant Physiol.* 60, 402–406. doi: 10.1104/pp.60.3.402

Chen, X., Steed, A., Travella, S., Keller, B., and Nicholson, P. (2009). *Fusarium graminearum* exploits ethylene signalling to colonize dicotyledonous and monocotyledonous plants. *New Phytol.* 182, 975–983. doi: 10.1111/j.1469-8137.2009.02821.x

Corpas, F. J., González-Gordo, S., Cañas, A., and Palma, J. M. (2019). Nitric oxide (NO) and hydrogen sulfide (H2S) in plants: Which is first? *J. Exp. Bot*. doi: 10.1093/jxb/erz031

Datsenko, K. A., and Wanner, B. L. (2000). One-step inactivation of chromosomal genes in *Escherichia coli* K-12 using PCR products. *Proc. Natl. Acad. Sci. U. S. A.* 97, 6640–6645. doi: 10.1073/pnas.120163297

Datta, R., Kumar, D., Sultana, A., Hazra, S., Bhattacharyya, D., and Chattopadhyay, S. (2015). Glutathione regulates 1-aminocyclopropane-1-carboxylate synthase transcription *via* WRKY33 and 1-aminocyclopropane-1-carboxylate oxidase by modulating messenger RNA stability to induce ethylene synthesis during stress. *Plant Physiol.* 169, 2963–2981. doi: 10.1104/pp.15.01543

De Vleesschauwer, D., Yang, Y., Cruz, C. V., and Höfte, M. (2010). Abscisic acid-induced resistance against the brown spot pathogen *Cochliobolus miyabeanus* in rice involves MAP kinase-mediated repression of ethylene signaling. *Plant Physiol.* 152, 2036–2052. doi: 10.1104/pp.109.152702

Ding, L., Xu, H., Yi, H., Yang, L., Kong, Z., Zhang, L., et al. (2011). Resistance to hemi-biotrophic *F. graminearum* infection is associated with coordinated and ordered expression of diverse defense signaling pathways. *PLoS One* 6, e19008. doi: 10.1371/journal.pone.0019008

Dubois, M., Van den Broeck, L., and Inzé, D. (2018). The pivotal role of ethylene in plant growth. *Trends Plant Sci.* 23, 311–323. doi: 10.1016/j.tplants.2018.01.003

Ekimova, G. A., Fedorov, D. N., Tani, A., Doronina, N. V., and Trotsenko, Y. A. (2018). Distribution of 1-aminocyclopropane-1-carboxylate deaminase and D-cysteine desulfhydrase genes among type species of the genus Methylobacterium. *Antonie Van Leeuwenhoek* 111, 1723–1734. doi: 10.1007/s10482-018-1061-5

Ent, S.V. der, and Pieterse, C. M. J. (2018). Ethylene: multi-tasker in plant–attacker interactions, in: Annual Plant Reviews Online. *Am. Cancer Soc.* pp, 343–377. doi: 10.1002/9781119312994.apr0485

Espaillat, A., Carrasco-López, C., Bernardo-García, N., Pietrosemoli, N., Otero, L. H., Álvarez, L., et al. (2014). Structural basis for the broad specificity of a new family of amino-acid racemases. *Acta Crystallogr., D, Biol. Crystallogr.* 70, 79–90. doi: 10.1107/S1399004713024838

Filipovic, M. R., and Jovanovic, V. M. (2017). More than just an intermediate: hydrogen sulfide signalling in plants. *J. Exp. Bot.* 68, 4733–4736. doi: 10.1093/jxb/erx352

Foroud, N. A., Pordel, R., Goyal, R. K., Ryabova, D., Eranthodi, A., Chatterton, S., et al. (2018). Chemical activation of the ethylene signalling pathway promotes *Fusarium graminearum* resistance in detached wheat heads. *Phytopathology*. 109 (5), 796–803. doi: 10.1094/PHYTO-08-18-0286-R

Fukuda, H., Ogawa, T., Ishihara, K., Fujii, T., Nagahama, K., Omata, T., et al. (1992). Molecular cloning in *Escherichia coli*, expression, and nucleotide sequence of the gene for the ethylene-forming enzyme of Pseudomonas syringae pv. *phaseolicola PK2.Biochem. Biophys. Res. Commun.* 188, 826–832. doi: 10.1016/0006-291X(92)91131-9

Gallie, D. R. (2015). Ethylene receptors in plants — why so much complexity? *F1000Prime Rep.* 7, 39. doi: 10.12703/P7-39

Gamalero, E., and Glick, B. R. (2015). Bacterial modulation of plant ethylene levels. *Plant Physiol.* 169, 13–22. doi: 10.1104/pp.15.00284

Ge, Y., Hu, K.-D., Wang, S.-S., Hu, L.-Y., Chen, X.-Y., Li, Y.-H., et al. (2017). Hydrogen sulfide alleviates postharvest ripening and senescence of banana by antagonizing the effect of ethylene. *PLoS One* 12, e0180113. doi: 10.1371/journal.pone.0180113

Geng, X., Jin, L., Shimada, M., Kim, M. G., and Mackey, D. (2014). The phytotoxin coronatine is a multifunctional component of the virulence armament of *Pseudomonas syringae*. *Planta* 240, 1149–1165. doi: 10.1007/s00425-014-2151-x

Geraats, B. P. J., Bakker, P. A. H. M., Lawrence, C. B., Achuo, E. A., Höfte, M., and van Loon, L. C. (2003). Ethylene-insensitive tobacco shows differentially altered susceptibility to different pathogens. *Phytopathology* 93, 813–821. doi: 10.1094/PHYTO.2003.93.7.813

Ghanta, S., Bhattacharyya, D., and Chattopadhyay, S. (2011). Glutathione signaling acts through NPR1-dependent SA-mediated pathway to mitigate biotic stress. *Plant Signal. Behav.* 6, 607–609. doi: 10.4161/psb.6.4.15402

Glazebrook, J. (2005). Contrasting mechanisms of defense against biotrophic and necrotrophic pathogens. *Annu. Rev. Phytopathol.* 43, 205–227. doi: 10.1146/annurev.phyto.43.040204.135923

Gottwald, S., Samans, B., Lück, S., and Friedt, W. (2012). Jasmonate and ethylene dependent defence gene expression and suppression of fungal virulence factors: two essential mechanisms of Fusarium head blight resistance in wheat? *BMC Genomics* 13, 369. doi: 10.1186/1471-2164-13-369

Grichko, V. P., Filby, B., and Glick, B. R. (2000). Increased ability of transgenic plants expressing the bacterial enzyme ACC deaminase to accumulate Cd, Co, Cu, Ni, Pb, and Zn. *J. Biotechnol.* 81, 45–53. doi: 10.1016/S0168-1656(00)00270-4

Grossmann, K. (2000). Mode of action of auxin herbicides: a new ending to a long, drawn out story. *Trends Plant Sci.* 5, 506–508. doi: 10.1016/S1360-1385(00)01791-X

Hao, G., Naumann, T. A., Vaughan, M. M., McCormick, S., Usgaard, T., Kelly, A., et al. (2018). Characterization of a *Fusarium graminearum* salicylate hydroxylase. *Front. Microbiol.* 9, 3219. doi: 10.3389/fmicb.2018.03219

Hontzeas, N., Zoidakis, J., Glick, B. R., and Abu-Omar, M. M. (2004). Expression and characterization of 1-aminocyclopropane-1-carboxylate deaminase from the rhizobacterium *Pseudomonas putida* UW4: a key enzyme in bacterial plant growth promotion. *Biochim. Biophys. Acta* 1703, 11–19. doi: 10.1016/j.bbapap.2004.09.015

Howarth, J. R., Parmar, S., Jones, J., Shepherd, C. E., Corol, D.-I., Galster, A. M., et al. (2008). Co-ordinated expression of amino acid metabolism in response to N and S deficiency during wheat grain filling. *J. Exp. Bot.* 59, 3675–3689. doi: 10.1093/jxb/ern218

Huang, P.-Y., Catinot, J., and Zimmerli, L. (2016). Ethylene response factors in Arabidopsis immunity. *J. Exp. Bot.* 67, 1231–1241. doi: 10.1093/jxb/erv518

Huo, J., Huang, D., Zhang, J., Fang, H., Wang, B., Wang, C., et al. (2018). Hydrogen sulfide: a gaseous molecule in postharvest freshness. *Front. Plant Sci.* 9, 1172. doi: 10.3389/fpls.2018.01172

Jia, H., Chen, S., Liu, D., Liesche, J., Shi, C., Wang, J., et al. (2018). Ethylene-induced hydrogen sulfide negatively regulates ethylene biosynthesis by persulfidation of ACO in tomato under osmotic stress. *Front. Plant Sci.* 9, 1517. doi: 10.3389/fpls.2018.01517

Jia, Y. J., Ito, H., Matsui, H., and Honma, M. (2000). 1-aminocyclopropane-1-carboxylate (ACC) deaminase induced by ACC synthesized and accumulated in *Penicillium citrinum* intracellular spaces. *Biosci. Biotechnol. Biochem.* 64, 299–305. doi: 10.1271/bbb.64.299

Johansson, N., Persson, K. O., Larsson, C., and Norbeck, J. (2014). Comparative sequence analysis and mutagenesis of ethylene forming enzyme (EFE) 2-oxoglutarate/Fe(II)-dependent dioxygenase homologs. *BMC Biochem.* 15, 22. doi: 10.1186/1471-2091-15-22

Kakuta, Y., Igarashi, T., Murakami, T., Ito, H., Matsui, H., and Honma, M. (2001). 1-Aminocyclopropane-1-carboxylate synthase of *Penicillium citrinum*: primary structure and expression in *Escherichia coli* and *Saccharomyces cerevisiae. Biosci. Biotechnol. Biochem.* 65, 1511–1518. doi: 10.1271/bbb.65.1511

Kazan, K., and Gardiner, D. M. (2018). Transcriptomics of cereal–*Fusarium graminearum* interactions: what we have learned so far. *Mol. Plant Pathol.* 19, 764–778. doi: 10.1111/mpp.12561

Kenyon, J. S., and Turner, J. G. (1992). The stimulation of ethylene synthesis in *Nicotiana tabacum* leaves by the phytotoxin coronatine. *Plant Physiol.* 100, 219–224. doi: 10.1104/pp.100.1.219

Kidd, B. N., Kadoo, N. Y., Dombrecht, B., Tekeoglu, M., Gardiner, D. M., Thatcher, L. F., et al. (2011). Auxin signaling and transport promote susceptibility to the root-infecting fungal pathogen *Fusarium oxysporum* in Arabidopsis. *Mol. Plant Microbe Interact.* 24, 733–748. doi: 10.1094/MPMI-08-10-0194

Knoester, M., van Loon, L. C., van den Heuvel, J., Hennig, J., Bol, J. F., and Linthorst, H. J. (1998). Ethylene-insensitive tobacco lacks nonhost resistance against soil-borne fungi. *Proc. Natl. Acad. Sci. U. S. A.* 95, 1933–1937. doi: 10.1073/pnas.95.4.1933

Kovacs, I., Durner, J., and Lindermayr, C. (2015). Crosstalk between nitric oxide and glutathione is required for Nonexpressor of Pathogenesis-Related Genes 1 (NPR1)-dependent defense signaling in *Arabidopsis thaliana*. *New Phytol.* 208, 860–872. doi: 10.1111/nph.13502

Li, C., Shao, J., Wang, Y., Li, W., Guo, D., Yan, B., et al. (2013). Analysis of banana transcriptome and global gene expression profiles in banana roots in response to infection by race 1 and tropical race 4 of *Fusarium oxysporum* f. *sp. cubense. BMC Genomics* 14, 851. doi: 10.1186/1471-2164-14-851

Li, H., Li, M., Wei, X., Zhang, X., Xue, R., Zhao, Y., et al. (2017). Transcriptome analysis of drought-responsive genes regulated by hydrogen sulfide in wheat (Triticum aestivum L.) leaves. *Mol. Genet. Genomics MGG* 292, 1091–1110. doi: 10.1007/s00438-017-1330-4

Li, N., Han, X., Feng, D., Yuan, D., and Huang, L.-J. (2019). Signaling crosstalk between salicylic acid and ethylene/jasmonate in plant defense: do we understand what they are whispering? *Int. J. Mol. Sci.* 20. doi: 10.3390/ijms20030671

Li, Z.-G., Min, X., and Zhou, Z.-H. (2016). Hydrogen sulfide: a signal molecule in plant cross-adaptation. *Front. Plant Sci.* 7, 1621. doi: 10.3389/fpls.2016.01621

Liu, J., Wang, D., Su, Y., Lang, K., Duan, R., Wu, Y., et al. (2019). FairBase: a comprehensive database of fungal A-to-I RNA editing. *Database* 2019. baz018. doi: 10.1093/database/baz018

Long, S. (2014). Studies of fungal natural products and the degradation of A- and SS-trenbolone. PhD (Doctor of Philosophy) thesis, University of Iowa. doi: 10.17077/etd.1lp8ven5

Ma, Y.-M., Liang, X.-A., Zhang, H.-C., and Liu, R. (2016). Cytotoxic and antibiotic cyclic pentapeptide from an endophytic *Aspergillus tamarii* of Ficus carica. *J. Agric. Food Chem.* 64, 3789–3793. doi: 10.1021/acs.jafc.6b01051

Mackintosh, C. A., Garvin, D. F., Radmer, L. E., Heinen, S. J., and Muehlbauer, G. J. (2006). A model wheat cultivar for transformation to improve resistance to

Fusarium head blight. *Plant Cell Rep.* 25, 313–319. doi: 10.1007/s00299-005-0059-4

Makandar, R., Essig, J. S., Schapaugh, M. A., Trick, H. N., and Shah, J. (2006). Genetically engineered resistance to *Fusarium* head blight in wheat by expression of Arabidopsis NPR1. *Mol. Plant Microbe Interact.* 19, 123–129. doi: 10.1094/MPMI-19-0123

Makandar, R., Nalam, V. J., Lee, H., Trick, H. N., Dong, Y., and Shah, J. (2012). Salicylic acid regulates basal resistance to *Fusarium* head blight in wheat. *Mol. Plant Microbe Interact.* 25, 431–439. doi: 10.1094/MPMI-09-11-0232

Marcet-Houben, M., Ballester, A.-R., de la Fuente, B., Harries, E., Marcos, J. F., González-Candelas, L., et al. (2012). Genome sequence of the necrotrophic fungus *Penicillium digitatum*, the main postharvest pathogen of citrus. *BMC Genomics* 13, 646. doi: 10.1186/1471-2164-13-646

Nascimento, F. X., Rossi, M. J., and Glick, B. R. (2018). Ethylene and 1-Aminocyclopropane-1-carboxylate (ACC) in plant-bacterial interactions. *Front. Plant Sci.* 9, 114. doi: 10.3389/fpls.2018.00114

Ogawa, T., Fukuda, M., and Sasaoka, K. (1973). Occurrence of D-amino acid aminotransferase in pea seedlings. *Biochem. Biophys. Res. Commun.* 52, 998–1002. doi: 10.1016/0006-291X(73)91036-X

Pantelides, I. S., Tjamos, S. E., Pappa, S., Kargakis, M., and Paplomatas, E. J. (2013). The ethylene receptor ETR1 is required for *Fusarium oxysporum* pathogenicity. *Plant Pathol.* 62, 1302–1309. doi: 10.1111/ppa.12042

Penrose, D. M., and Glick, B. R. (2003). Methods for isolating and characterizing ACC deaminase-containing plant growth-promoting rhizobacteria. *Physiol. Plant.* 118, 10–15. doi: 10.1034/j.1399-3054.2003.00086.x

Poppenberger, B., Berthiller, F., Lucyshyn, D., Sieberer, T., Schuhmacher, R., Krska, R., et al. (2003). Detoxification of the *Fusarium* mycotoxin deoxynivalenol by a UDP-glucosyltransferase from *Arabidopsis thaliana*. *J. Biol. Chem.* 278, 47905–47914. doi: 10.1074/jbc.M307552200

Qi, P.-F., Zhang, Y.-Z., Liu, C.-H., Chen, Q., Guo, Z.-R., Wang, Y., et al. (2019). Functional analysis of FgNahG clarifies the contribution of salicylic acid to wheat (*Triticum aestivum*) resistance against *Fusarium* head blight. *Toxins* 11. doi: 10.3390/toxins11020059

Qiao, H., Shen, Z., Huang, S. C., Schmitz, R. J., Urich, M. A., Briggs, S. P., et al. (2012). Processing and subcellular trafficking of ER-tethered EIN2 control response to ethylene gas. *Science* 338, 390–393. doi: 10.1126/science.1225974

Qin, Y., Druzhinina, I. S., Pan, X., and Yuan, Z. (2016). Microbially mediated plant salt tolerance and microbiome-based solutions for saline agriculture. *Biotechnol. Adv.* 34, 1245–1259. doi: 10.1016/j.biotechadv.2016.08.005

Ravanbakhsh, M., Sasidharan, R., Voesenek, L. A. C. J., Kowalchuk, G. A., and Jousset, A. (2018). Microbial modulation of plant ethylene signaling: ecological and evolutionary consequences. *Microbiome* 6, 52. doi: 10.1186/s40168-018-0436-1

Robison, M. M., Shah, S., Tamot, B., Pauls, K. P., Moffatt, B. A., and Glick, B. R. (2001). Reduced symptoms of Verticillium wilt in transgenic tomato expressing a bacterial ACC deaminase. *Mol. Plant Pathol.* 2, 135–145. doi: 10.1046/j.1364-3703.2001.00060.x

Rocheleau, H., Al-Harthi, R., and Ouellet, T. (2019). Degradation of salicylic acid by *Fusarium graminearum*. *Fungal Biol.* 123, 77–86. doi: 10.1016/j.funbio.2018.11.002

Shi, H., Ye, T., Han, N., Bian, H., Liu, X., and Chan, Z. (2015). Hydrogen sulfide regulates abiotic stress tolerance and biotic stress resistance in Arabidopsis. *J. Integr. Plant Biol.* 57, 628–640. doi: 10.1111/jipb.12302

Singh, R. P., Shelke, G. M., Kumar, A., and Jha, P. N. (2015). Biochemistry and genetics of ACC deaminase: a weapon to stress ethylene produced in plants. *Front. Microbiol.* 6, 937. doi: 10.3389/fmicb.2015.00937

Sit, C. S., Yoganathan, S., and Vederas, J. C. (2011). Biosynthesis of aminovinyl-cysteine-containing peptides and its application in the production of potential drug candidates. *Acc. Chem. Res.* 44, 261–268. doi: 10.1021/ar1001395

Soutourina, J., Blanquet, S., and Plateau, P. (2001). Role of D-cysteine desulfhydrase in the adaptation of *Escherichia coli* to D-cysteine. *J. Biol. Chem.* 276, 40864–40872. doi: 10.1074/jbc.M102375200

Steiger, M. G., Vitikainen, M., Uskonen, P., Brunner, K., Adam, G., Pakula, T., et al. (2011). Transformation system for *Hypocrea jecorina* (*Trichoderma reesei*) that favors homologous integration and employs reusable bidirectionally selectable markers. *Appl. Environ. Microbiol.* 77, 114–121. doi: 10.1128/AEM.02100-10

Subramaniam, K., Abbo, S., and Ueng, P. P. (1996). Isolation of two differentially expressed wheat ACC synthase cDNAs and the characterization of one of their genes with root-predominant expression. *Plant Mol. Biol.* 31, 1009–1020. doi: 10.1007/BF00040719

Sugawara, M., Okazaki, S., Nukui, N., Ezura, H., Mitsui, H., and Minamisawa, K. (2006). Rhizobitoxine modulates plant-microbe interactions by ethylene inhibition. *Biotechnol. Adv.* 24, 382–388. doi: 10.1016/j.biotechadv.2006.01.004

Tarun, A. S., Lee, J. S., and Theologis, A. (1998). Random mutagenesis of 1-aminocyclopropane-1-carboxylate synthase: a key enzyme in ethylene biosynthesis. *Proc. Natl. Acad. Sci. U. S. A.* 95, 9796–9801. doi: 10.1073/pnas.95.17.9796

Thomma, B. P., Eggermont, K., Tierens, K. F., and Broekaert, W. F. (1999). Requirement of functional ethylene-insensitive 2 gene for efficient resistance of Arabidopsis to infection by *Botrytis cinerea*. *Plant Physiol.* 121, 1093–1102. doi: 10.1104/pp.121.4.1093

Todorovic, B., and Glick, B. R. (2008). The interconversion of ACC deaminase and D-cysteine desulfhydrase by directed mutagenesis. *Planta* 229, 193–205. doi: 10.1007/s00425-008-0820-3

Tsolakidou, M.-D., Pantelides, I., Tzima, A., Kang, S., Paplomatas, E., and Tsaltas, D. (2018). Disruption and overexpression of the gene encoding ACC (1-aminocyclopropane-1-carboxylic acid) deaminase in soil-borne fungal pathogen *Verticillium dahliae* revealed the role of ACC as a potential regulator of virulence and plant defense. *Mol. Plant Microbe Interact.* 32 (6), 639–653. doi: 10.1094/MPMI-07-18-0203-R

Twaruschek, K., Spörhase, P., Michlmayr, H., Wiesenberger, G., and Adam, G. (2018). New plasmids for fusarium transformation allowing positive-negative selection and efficient cre-loxP mediated marker recycling. *Front. Microbiol.* 9, 1954. doi: 10.3389/fmicb.2018.01954

Ueda, K., Xiao, J.-Z., Doke, N., and Nakatsuka, S. (1992). Structure of BZR-cotoxin II produced by *Bipolaris zeicola* race 3, the cause of leaf spot disease in corn. *Tetrahedron Lett.* 33, 5377–5380. doi: 10.1016/S0040-4039(00)79098-8

Uppalapati, S. R., Ayoubi, P., Weng, H., Palmer, D. A., Mitchell, R. E., Jones, W., et al. (2005). The phytotoxin coronatine and methyl jasmonate impact multiple phytohormone pathways in tomato. *Plant J. Cell Mol. Biol.* 42, 201–217. doi: 10.1111/j.1365-313X.2005.02366.x

Van de Poel, B., and Van Der Straeten, D. (2014). 1-aminocyclopropane-1-carboxylic acid (ACC) in plants: more than just the precursor of ethylene! *Front. Plant Sci.* 5, 640. doi: 10.3389/fpls.2014.00640

van den Berg, M. A., Albang, R., Albermann, K., Badger, J. H., Daran, J.-M., Driessen, A. J. M., et al. (2008). Genome sequencing and analysis of the filamentous fungus *Penicillium chrysogenum*. *Nat. Biotechnol.* 26, 1161–1168. doi: 10.1038/nbt.1498

Viterbo, A., Landau, U., Kim, S., Chernin, L., and Chet, I. (2010). Characterization of ACC deaminase from the biocontrol and plant growth-promoting agent *Trichoderma asperellum* T203. *FEMS Microbiol. Lett.* 305, 42–48. doi: 10.1111/j.1574-6968.2010.01910.x

Walter, M. C., Rattei, T., Arnold, R., Güldener, U., Münsterkötter, M., Nenova, K., et al. (2009). PEDANT covers all complete RefSeq genomes. *Nucleic Acids Res.* 37, 408–411. doi: 10.1093/nar/gkn749

Wang, L., Li, Q., Liu, Z., Surendra, A., Pan, Y., Li, Y., et al. (2018). Integrated transcriptome and hormone profiling highlight the role of multiple phytohormone pathways in wheat resistance against *Fusarium* head blight. *PLoS One* 13. doi: 10.1371/journal.pone.0207036

Wang, Q., Jiang, C., Wang, C., Chen, C., Xu, J.-R., and Liu, H. (2017). Characterization of the two-speed subgenomes of *Fusarium graminearum* reveals the fast-speed subgenome specialized for adaption and infection. *Front. Plant Sci.* 8, 140. doi: 10.3389/fpls.2017.00140

Washington, E. J., Mukhtar, M. S., Finkel, O. M., Wan, L., Banfield, M. J., Kieber, J. J., et al. (2016). *Pseudomonas syringae* type III effector HopAF1 suppresses plant immunity by targeting methionine recycling to block ethylene induction. *Proc. Natl. Acad. Sci. U. S. A.* 113, E3577–E3586. doi: 10.1073/pnas.1606322113

Wong, P., Walter, M., Lee, W., Mannhaupt, G., Münsterkötter, M., Mewes, H.-W., et al. (2011). FGDB: revisiting the genome annotation of the plant pathogen *Fusarium graminearum*. *Nucleic Acids Res.* 39, D637–D639. doi: 10.1093/nar/gkq1016

Wood, D. A., and Hammond, J. B. W. (1977). Ethylene production by axenic fruiting cultures of *Agaricus bisporus*. *Appl. Environ. Microbiol.* 34, 228–229.

Xu, Z., Pan, G., Zhou, H., and Shen, B. (2018). Discovery and characterization of 1-aminocyclopropane-1-carboxylic acid synthase of bacterial origin. *J. Am. Chem. Soc.* 140 (49), 16957–16961. doi: 10.1021/jacs.8b11463

Yang, C., Lu, X., Ma, B., Chen, S.-Y., and Zhang, J.-S. (2015). Ethylene signaling in rice and Arabidopsis: conserved and diverged aspects. *Mol. Plant* 8, 495–505. doi: 10.1016/j.molp.2015.01.003

Yasuta, T., Satoh, S., and Minamisawa, K. (1999). New assay for rhizobitoxine based on inhibition of 1-aminocyclopropane-1-carboxylate synthase. *Appl. Environ. Microbiol.* 65, 849–852.

Zhang, C., Huang, T., Shen, C., Wang, X., Qi, Y., Shen, J., et al. (2016). Downregulation of ethylene production increases mycelial growth and primordia formation in the button culinary-medicinal mushroom, *Agaricus bisporus* (Agaricomycetes). *Int. J. Med. Mushrooms* 18, 1131–1140. doi: 10.1615/IntJMedMushrooms.v18.i12.80

Zhang, X.-W., Jia, L.-J., Zhang, Y., Jiang, G., Li, X., Zhang, D., et al. (2012). In planta stage-specific fungal gene profiling elucidates the molecular strategies of *Fusarium graminearum* growing inside wheat coleoptiles. *Plant Cell* 24, 5159–5176. doi: 10.1105/tpc.112.105957

Zhao, C., Waalwijk, C., de Wit, P. J. G. M., Tang, D., and van der Lee, T. (2013). RNA-Seq analysis reveals new gene models and alternative splicing in the fungal pathogen *Fusarium graminearum*. *BMC Genomics* 14, 21. doi: 10.1186/1471-2164-14-21

Ziogas, V., Molassiotis, A., Fotopoulos, V., and Tanou, G. (2018). Hydrogen Sulfide: A potent tool in postharvest fruit biology and possible mechanism of action. *Front. Plant Sci.* 9, 1375. doi: 10.3389/fpls.2018.01375

Conflict of Interest Statement: The authors declare that the research was conducted in the absence of any commercial or financial relationships that could be construed as a potential conflict of interest.

frontiers in Plant Science

REVIEW
published: 12 September 2019
doi: 10.3389/fpls.2019.01094

Light Modulates Ethylene Synthesis, Signaling, and Downstream Transcriptional Networks to Control Plant Development

*Alexandria F. Harkey[1], Gyeong Mee Yoon[2], Dong Hye Seo[2], Alison DeLong[3] and Gloria K. Muday[1]**

[1] Department of Biology and Center for Molecular Signaling, Wake Forest University, Winston-Salem, NC, United States, [2] Department of Botany and Plant Pathology, Purdue University, West Lafayette, IN, United States, [3] Department of Molecular Biology, Cell Biology and Biochemistry, Brown University, Providence, RI, United States

OPEN ACCESS

Edited by:
Dominique Van Der Straeten, Ghent University, Belgium

Reviewed by:
Jan Smalle, University of Kentucky, United States
Anna N. Stepanova, North Carolina State University, United States

***Correspondence:**
Gloria K. Muday
muday@wfu.edu

Specialty section:
This article was submitted to Plant Physiology, a section of the journal Frontiers in Plant Science

Received: *02 June 2019*
Accepted: *09 August 2019*
Published: *12 September 2019*

Citation:
Harkey AF, Yoon GM, Seo DH, DeLong A and Muday GK (2019) Light Modulates Ethylene Synthesis, Signaling, and Downstream Transcriptional Networks to Control Plant Development. Front. Plant Sci. 10:1094. doi: 10.3389/fpls.2019.01094

The inhibition of hypocotyl elongation by ethylene in dark-grown seedlings was the basis of elegant screens that identified ethylene-insensitive Arabidopsis mutants, which remained tall even when treated with high concentrations of ethylene. This simple approach proved invaluable for identification and molecular characterization of major players in the ethylene signaling and response pathway, including receptors and downstream signaling proteins, as well as transcription factors that mediate the extensive transcriptional remodeling observed in response to elevated ethylene. However, the dark-adapted early developmental stage used in these experiments represents only a small segment of a plant's life cycle. After a seedling's emergence from the soil, light signaling pathways elicit a switch in developmental programming and the hormonal circuitry that controls it. Accordingly, ethylene levels and responses diverge under these different environmental conditions. In this review, we compare and contrast ethylene synthesis, perception, and response in light and dark contexts, including the molecular mechanisms linking light responses to ethylene biology. One powerful method to identify similarities and differences in these important regulatory processes is through comparison of transcriptomic datasets resulting from manipulation of ethylene levels or signaling under varying light conditions. We performed a meta-analysis of multiple transcriptomic datasets to uncover transcriptional responses to ethylene that are both light-dependent and light-independent. We identified a core set of 139 transcripts with robust and consistent responses to elevated ethylene across three root-specific datasets. This "gold standard" group of ethylene-regulated transcripts includes mRNAs encoding numerous proteins that function in ethylene signaling and synthesis, but also reveals a number of previously uncharacterized gene products that may contribute to ethylene response phenotypes. Understanding these light-dependent differences in ethylene signaling and synthesis will provide greater insight into the roles of ethylene in growth and development across the entire plant life cycle.

Keywords: ethylene, light, transcriptomic meta-analysis, ethylene response, ethylene biosynthesis, hypocotyl, root

INTRODUCTION

Plant responses to the gaseous hormone ethylene are an excellent model for studying the relationships between hormone synthesis, signaling, transcriptional changes, and development. The identification of ethylene-insensitive mutants in Arabidopsis using molecular genetics opened a new era in dissecting plant hormone signaling (Bleecker et al., 1988; Guzman and Ecker, 1990). Ethylene-insensitive mutants were identified as lacking the ethylene "triple response" in dark-grown seedlings (short, thick hypocotyl and exaggerated apical hook), remaining tall in the presence of excess ethylene (Alonso et al., 2003; Guo and Ecker, 2003; Yanagisawa et al., 2003). This approach enabled the isolation of mutations affecting the activities of core ethylene response machinery, including receptors, signaling proteins, and transcription factors. The functions of these signaling components, as well as the pathways for ethylene synthesis, have subsequently been assayed in additional tissues beyond dark-grown hypocotyls, demonstrating that many of these proteins function in all tissues and growth conditions, but also revealing branches of the ethylene signaling and synthesis pathways that have distinct roles in light-grown plants and in other developmental stages. In particular, ethylene-responsive transcriptional networks and regulatory controls of ethylene biosynthesis show profound differences between light- and dark-grown tissues. Although some of these differences have been reviewed previously (Rodrigues et al., 2014; Booker and DeLong, 2015; Yoon, 2015; Yu and Huang, 2017), recent studies have identified new mechanisms and yielded insight into light-dependent differences. This review highlights the similarities and differences in light-dependent regulation of ethylene synthesis and response in seedlings grown at a range of light levels, focusing on recent publications establishing that the genetic redundancy in ethylene biosynthetic machinery, ethylene receptors, and transcriptional machinery may allow a complex suite of light-dependent developmental responses to this important hormone.

Basics of the Ethylene Signaling Pathway

The triple response of dark-grown seedlings was exploited in elegant genetic screens that identified mutants exhibiting either ethylene-insensitivity (*ein* or *etr* mutants) (Bleecker et al., 1988; Guzman and Ecker, 1990; Chang et al., 1993), enhanced ethylene signaling in the constitutive triple response (*ctr*) (Kieber et al., 1993; Huang et al., 2003), or synthesis in the ethylene overproducer (*eto*) mutants (Guzman and Ecker, 1990). The genes responsible for these phenotypes have been cloned and mapped to the ethylene signaling and biosynthetic pathways. The signaling pathway begins with ethylene binding to ER-localized receptor proteins (Kendrick and Chang, 2008), which act as negative regulators of the pathway (Hua and Meyerowitz, 1998). In Arabidopsis, these receptors are ETR1, ETR2, EIN4, ERS1, and ERS2 (Chang et al., 1993; Schaller and Bleecker, 1995; Hua and Meyerowitz, 1998; Sakai et al., 1998), which fall into two subfamilies based on sequence similarity of the ethylene binding domains and the presence of conserved histidine kinase domains (Kendrick and Chang, 2008; Stepanova and Alonso, 2009; Shakeel et al., 2013). When ethylene binds, the receptors are turned off, resulting in decreased activity of the inhibitory CTR1 protein kinase and increased EIN2 output (Kieber et al., 1993; Alonso et al., 1999; Huang et al., 2003; Qiao et al., 2009). C-terminal proteolytic cleavage of EIN2 promotes the nuclear localization of the EIN2 C-terminal proteolytic fragment (EIN2-CEND) (Ju et al., 2012; Qiao et al., 2012; Wen et al., 2012). EIN2-CEND-mediated targeting of *EBF1/2* mRNA to the processing body further enhances signaling output (Li et al., 2015; Merchante et al., 2015). Nuclear EIN2-CEND alters transcription *via* activation of the EIN3 and EIN3-LIKE (EIL1 and EIL2) transcription factors (TFs), which then turn on expression of genes encoding other TFs, such as *ERF1* and *EDF1-EDF4* (Chao et al., 1997; Solano et al., 1998; Alonso et al., 2003; Chang et al., 2013). These core TFs likely work with other TFs as part of a gene regulatory network leading to a diversity of transcriptional responses, which have been characterized in multiple genome-wide transcriptional studies (Stepanova et al., 2007; Chang et al., 2013; Feng et al., 2017; Harkey et al., 2018). Ethylene signaling is also modulated by EIN2-mediated translational regulation (Merchante et al., 2015), as well as F-box dependent proteolysis of EIN2 and EIN3 *via* ETP1/2 and EBF1/2, respectively (Guo and Ecker, 2003; Potuschak et al., 2003; Qiao et al., 2009). EBF1/2 are also destabilized by ethylene in an EIN2-dependent manner, allowing increased accumulation of EIN3 (An et al., 2010).

Ethylene signaling proteins have roles that extend beyond their functions in dark-grown Arabidopsis hypocotyls. Genes encoding these proteins have been found across the plant kingdom (Wang et al., 2015), and the proteins have been shown to function in a diversity of tissues and under a range of light conditions (Lanahan et al., 1994; Binder et al., 2006; Plett et al., 2009; Wilson et al., 2014a). Both CTR1 and EIN2 are required for normal ethylene responsiveness in all light conditions in Arabidopsis, indicating that each of these gene products plays a central and non-redundant role in ethylene signaling, regardless of light conditions. Mutants lacking *CTR1* show constitutive ethylene responses in roots and shoots grown in light or dark (Kieber et al., 1993). Mutations in *EIN2* confer insensitivity to added ethylene in dark-grown hypocotyls (Alonso et al., 1999), light-grown rosettes (Kieber et al., 1993), light-grown hypocotyls (Smalle et al., 1997), and roots of dark-grown (Stepanova et al., 2005) and light-grown seedlings (Negi et al., 2008; Harkey et al., 2018).

Ethylene receptors are members of a conserved multi-gene family (Shakeel et al., 2013). As these receptors function as negative regulators, dominant gain-of-function (GOF) mutations, such as *etr1-1* and *etr1-3* in Arabidopsis (Bleecker et al., 1988; Guzman and Ecker, 1990; Chang et al., 1993) and *Neverripe* in tomato (Wilkinson et al., 1995), yield ethylene-insensitive plants. In contrast, null or loss-of-function (LOF) alleles can confer constitutive ethylene response phenotypes (Hua and Meyerowitz, 1998; Shakeel et al., 2013). In Arabidopsis, the five ethylene receptors have been shown to have distinct roles that are tied to specific developmental responses (Shakeel et al., 2013), some of which can be studied only in older plants, which are necessarily grown in light. Similarly, the tomato *Neverripe* gene belongs to a seven-member ethylene receptor gene family

and the *Neverripe* mutant carries a GOF mutation that confers ethylene insensitivity in phenotypes observed in both light and dark conditions (e.g., fruit ripening, hypocotyl triple response, and root development) (Wilkinson et al., 1995; Negi et al., 2010; Klee and Giovannoni, 2011). Tomato plants with knockdown of mRNA encoding receptors have also revealed distinct functions for two tomato ethylene receptors (Kevany et al., 2007). In the sections below, we highlight studies that have revealed differences in ethylene responses that are influenced by light and developmental stage, and which require distinct ethylene signaling or synthesis machinery.

Basics of the Ethylene Biosynthesis Pathway

The enzymatic steps of the ethylene biosynthetic pathway were uncovered in fruit; subsequent work in fruit and in dark-grown Arabidopsis seedlings identified a conserved biosynthetic pathway and revealed important regulatory mechanisms that control pathway activity (Adams and Yang, 1979; Yang and Hoffman, 1984; Booker and DeLong, 2015; Yoon, 2015). The simple and highly conserved pathway has only two committed steps: conversion of S-adenosyl-l-methionine (SAM) to 1-aminocyclopropane-1-carboxylic acid (ACC) by ACC synthase (ACS), followed by conversion of ACC to ethylene by ACC oxidase (ACO) (Houben and Van de Poel, 2019). ACS has been a primary target for researchers interested in understanding regulation of ethylene biosynthesis, as this enzyme catalyzes the first biosynthetic step, which is frequently described as the rate-limiting step (Adams and Yang, 1979; Yang and Hoffman, 1984). *ACS* gene families in land plants encode isozymes belonging to three classes, type-1, type-2, and type-3 (El-Sharkawy et al., 2008; Lin et al., 2009; Booker and DeLong, 2015; Zhu et al., 2015; Lee et al., 2019). The evolution and regulation of ACO, including consideration of conditions under which ACO activity is limiting for ethylene production, have been recently reviewed (Houben and Van de Poel, 2019). There are both transcriptional and post-translational mechanisms that control which ACS and ACO isozymes are expressed and active, leading to distinct enzyme populations in tissue- and developmental stage-specific contexts (Booker and DeLong, 2015; Houben and Van de Poel, 2019). Positive feedback loops, largely driven by transcriptional controls of these biosynthetic enzymes, drive dramatic increases in ethylene production to accelerate fruit ripening (Klee and Giovannoni, 2011). This review will examine new insight into the molecular mechanisms by which ethylene synthesis is modulated by light levels at both transcriptional and post-translational levels.

LIGHT-DEPENDENT AND -INDEPENDENT ETHYLENE RESPONSES

Ethylene Effects in Hypocotyls Are Opposite in Light and Dark

The ethylene response in the hypocotyls of young seedlings is highly dependent on light level. The triple response of etiolated seedlings, including inhibited hypocotyl elongation, is the basis of much of the current molecular insight into ethylene signaling (Bleecker et al., 1988; Guzman and Ecker, 1990). Ethylene treatment under shade covering, rather than complete darkness, also leads to decreased hypocotyl growth (Das et al., 2016). The hypocotyl response to ethylene is coordinated with light-dependent hypocotyl elongation changes during photomorphogenesis (Yu and Huang, 2017). Light inhibits hypocotyl elongation, which is important as plants growing in soil transition to light (Montgomery, 2016). In opposition to the effect of ethylene in the dark, light-grown Arabidopsis seedlings show increased hypocotyl elongation in response to ethylene (Smalle et al., 1997; Le et al., 2005; Das et al., 2016; Seo and Yoon, 2019), as illustrated in **Figure 1**. In both light and dark, the ACC or ethylene response is tied to differences in cell expansion (Smalle et al., 1997; Seo and Yoon, 2019). These light-dependent differences have more frequently been reported in response to treatment with the ethylene precursor, ACC (Smalle et al., 1997; Le et al., 2005), but ethylene yields the same light-dependent increases in elongation (**Figure 1**), and ethylene-insensitive mutants are shorter than wild-type in the light (Le et al., 2005). Intriguingly, the nutrient content of the growth media affects the ethylene response in light-grown, but not dark-grown, seedlings (Smalle et al., 1997; Collett et al., 2000).

Another striking feature of the ethylene triple response in etiolated seedlings is the accentuation of the apical hook. As part of photomorphogenesis, the apical hook opens and cotyledons expand, so it is important to ask whether this ethylene response, like hypocotyl elongation, is also light dependent (Bleecker et al., 1988; Raz and Ecker, 1999; Mazzella et al., 2014; Van de Poel et al., 2015). The formation of apical hooks in etiolated seedlings protects the shoot apical meristem during growth through soil, and ethylene build-up in denser soil exaggerates this hook to assist in emergence (Zhong et al., 2014; Shi et al., 2016a). Ethylene insensitive mutants with receptor and signaling defects show impaired hook formation, while the *ctr1-1* null mutant has an exaggerated hook (Abbas et al., 2013). Localized accumulation of ACO across the hook may also contribute to hook maintenance in dark-grown seedlings (Peck et al., 1998; Raz and Ecker, 1999). Mutants with elevated ethylene synthesis show enhanced hook formation (Guzman and Ecker, 1990). A central feature of ethylene-accentuated hook formation is crosstalk with auxin. Asymmetries in auxin synthesis and auxin transport, which lead to accumulation of growth-inhibiting auxin levels on the inside of the hook, are enhanced by ethylene treatment (Vandenbussche et al., 2010; Zádníková et al., 2010). The process of hypocotyl hook opening in response to light is also ethylene regulated (Vandenbussche et al., 2010; Zádníková et al., 2010; Van de Poel et al., 2015). In dark-grown seedlings, the *ein3-1 eil1-1* double mutant has enhanced hook opening, while an EIN3 overexpression line has a tightly closed, exaggerated hook like *ctr1-1*, and shows delayed hook opening in the light (Zhang et al., 2018), consistent with ethylene negatively regulating hook opening in both light and dark.

Ethylene Modulates Light-Dependent and Light-Independent Root Development

In seedling roots, ethylene and ACC inhibit elongation in both light and dark conditions (Rahman et al., 2001; Ruzicka

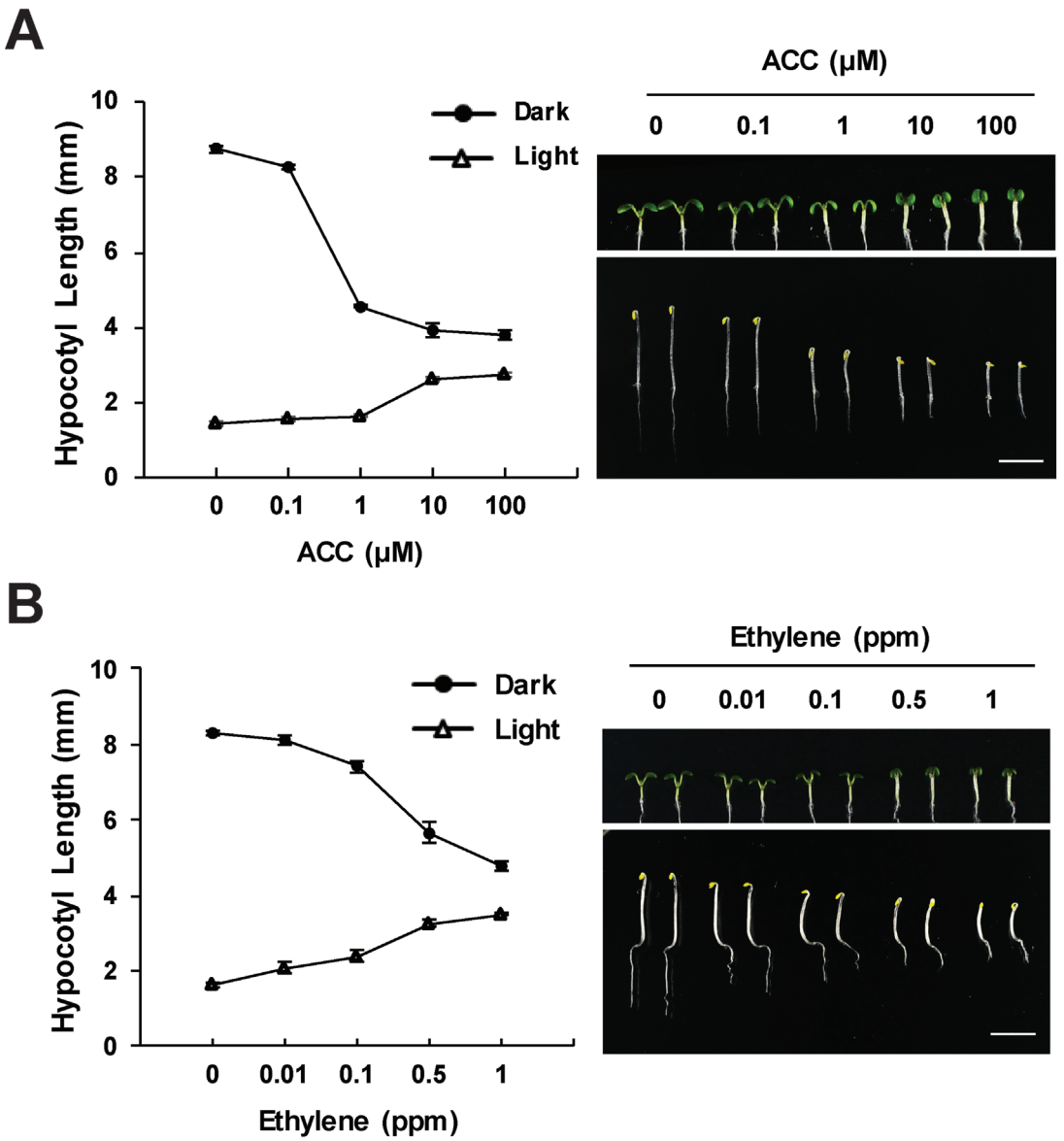

FIGURE 1 | Ethylene and ACC inhibit hypocotyl elongation in the dark and increase elongation in the light. Wild-type seedlings were grown on media containing the indicated concentrations of ACC or on control media and treated with ethylene gas for 3 days in the dark or 5 days in light. The effects of **(A)** ACC or **(B)** ethylene on hypocotyl growth in dark and light conditions. Images generated by the Yoon lab (Seo and Yoon, 2019), recapitulating previous findings (Bleecker et al., 1988; Guzman and Ecker, 1990; Smalle et al., 1997; Le et al., 2005; Liang et al., 2012). Values shown are the average and SD of three replicates, each containing at least 20 seedlings.

et al., 2007; Stepanova et al., 2007; Swarup et al., 2007; Negi et al., 2008; Negi et al., 2010; Strader et al., 2010) while enhancing root hair initiation (Cutter, 1978; Tanimoto et al., 1995; Pitts et al., 1998; Dolan, 2001; Rahman et al., 2002; Strader et al., 2010). In both light- and dark-grown seedlings, these root responses to ethylene are lost in ethylene-insensitive *etr1-3*, a dominant gain of function (GOF) receptor mutant, and in the *ein2-5* signaling mutant (Ruzicka et al., 2007; Swarup et al., 2007; Negi et al., 2008; Lewis et al., 2011a). These effects on root elongation are tied to auxin and ethylene cross-talk in a light-independent fashion. Ethylene enhances auxin synthesis, transport, and signaling to control root development (Stepanova et al., 2005; Ruzicka et al., 2007; Stepanova et al., 2007; Swarup et al., 2007; Negi et al., 2008; Stepanova et al., 2008; Lewis et al., 2011a; Muday et al., 2012).

In contrast, the inhibitory effect of ethylene and ACC on lateral root (LR) formation in Arabidopsis and tomato has been examined only in light-grown seedlings, as LRs do not form in roots of dark-grown seedlings (Ivanchenko et al., 2008; Negi et al., 2008; Negi et al., 2010; Lewis et al., 2011b; Lewis et al., 2011a). Ethylene and ACC block early stages of LR initiation (Ivanchenko et al., 2008). As with the inhibition of root elongation, ethylene inhibits LR formation by modulating

auxin synthesis, signaling, and transport, which control this process (Stepanova et al., 2007; Muday et al., 2012). Similarly, the effects of ethylene and ACC on root gravitropism and root waving, which have been assayed only in light-grown seedlings, also are blocked in the ethylene signaling mutants *ein2-5* and the GOF *etr1-3* receptor mutant (Buer et al., 2003; Buer et al., 2006). Overall, published data support a light-independent function of the EIN2 protein in ethylene signaling in roots (Ruzicka et al., 2007; Stepanova et al., 2007; Swarup et al., 2007; Negi et al., 2008; Lewis et al., 2011a). However, these data do not reveal which specific receptors function in the roots, because the use of GOF mutants (like *etr1-1* and *etr1-3*) can perturb the functions of the entire receptor family (Chang et al., 1993; Shakeel et al., 2013). Using LOF alleles in each receptor subtype is a powerful strategy to resolve the specific function of the family of ethylene receptors; this approach has been used to understand ethylene-regulated growth and development in a light-dependent context, as discussed below.

MECHANISTIC CONNECTIONS BETWEEN LIGHT RESPONSE AND ETHYLENE BIOSYNTHESIS

Changes in ethylene synthesis in response to changing light levels have been reported in many different species and under many different growth conditions, with dramatically varying results. The ability of light to modulate ethylene synthesis was reported half a century ago, when a single dose of red light was shown to decrease ethylene levels in etiolated pea seedlings in a far-red reversible manner, suggesting that phytochrome negatively controls ethylene biosynthesis (Goeschl et al., 1967). Conversely, high-intensity illumination of green seedlings induced an increase in ethylene synthesis, demonstrating a positive effect of light on ethylene production (Weckx and Van Poucke, 1989). Subsequent studies have confirmed that the effect of light on ethylene synthesis is complex and context-dependent (Foo et al., 2006; Khanna et al., 2007; Jeong et al., 2016; Song et al., 2018), and is also affected by crosstalk with other plant hormone response pathways (Vandenbussche et al., 2003; Arteca and Arteca, 2008; Muday et al., 2012; Lee et al., 2017). For instance, etiolated Arabidopsis seedlings show age- and light-dependent increases in ethylene biosynthesis with higher levels in the light; increased ethylene production is detectable as rapidly as 4 h after transfer to light, but becomes more dramatic with increasing time in light (Seo and Yoon, 2019). As discussed below, these effects are mediated at both the transcriptional and post-translational levels, and although much work has focused on regulation of ACS expression and activity, additional data reveal light-dependent effects on regulation of ACO function.

Light-Mediated Transcriptional Regulation of ACS and ACO

Regulation of ethylene synthesis *via* alteration of *ACS* and/or *ACO* gene expression is a primary mechanism through which differences in the quality, quantity, or periodicity of light modulate ethylene production and signaling outputs to coordinate plant growth and development (Yamagami et al., 2003; Tsuchisaka and Theologis, 2004; Wang et al., 2005). The combinatorial effects of light with phytohormones and biotic or abiotic stresses add further complexity to light-mediated control of ethylene biosynthesis. For example, IAA treatment induces expression of Arabidopsis *ACS* genes in seedlings grown in darkness or in constant light, but this induction is less dramatic in plants grown with a light/dark cycle (Rashotte et al., 2005). Furthermore, light differentially influences the transcript levels of various *ACS* genes, depending on the developmental stage and the length of light treatment (Seo and Yoon, 2019). The mRNA levels of a subset of type-1 and type-2 *ACSs* (*ACS6* and *ACS5*, *8,* and *9*, respectively) declined rapidly and steeply after etiolated seedlings were transferred to light, and these transcript levels remained low for 5 days. Meanwhile, *ACS2* (type-1) and *ACS4* (type-2) showed gradual increases in their transcript levels after light exposure (Seo and Yoon, 2019). Together, these data suggest distinct roles for ACS isozymes depending on the light conditions, with *ACS5*, *6*, *8*, and *9* playing the primary roles in dark-grown seedlings, while expression of *ACS2* and *ACS4* is implicated in controlling ethylene production in the light.

Analysis of light signaling mutants and transgenic lines expressing light signaling components has also provided insight into the light-mediated regulation of ethylene biosynthesis. Mutations in the phytochrome genes *PHYA* and *PHYB* increased ethylene biosynthesis in pea, consistent with a negative effect of light on ethylene synthesis, with a more profound effect observed in the *phyA* mutant (Foo et al., 2006). Intriguingly, in Arabidopsis and sorghum, *phyA* mutants show less profound increases in ethylene biosynthesis than do *phyB* mutants, indicating species-specific functions of these photoreceptors in controlling ethylene levels. Similarly, transgenic lines overexpressing Arabidopsis PHYTOCHROME-INTERACTING FACTOR5 (PIF5), a basic helix-loop-helix transcription factor that specifically interacts with the photoactivated form of PhyB, showed a marked increase in ethylene production in the dark that is correlated with increased abundance of *ACS4*, *ACS8*, and other *ACS* transcripts (Khanna et al., 2007). Although the *pif1 pif3 pif4 pif5* (*pifq*) mutant initially produced less ethylene than wild-type seedlings, consistent with the higher ethylene levels in *PIF5* overexpression lines, at later time-points the *pifq* mutant showed higher ethylene production (Jeong et al., 2016), indicating a developmental stage-dependent role of PIFs in controlling ethylene biosynthesis.

The regulation of *ACO* gene expression has received much less study than that of *ACS* (Houben and Van de Poel, 2019), yet the levels of *ACO* transcripts are also regulated by light and other factors that control pathway activity (Argueso et al., 2007; Rodrigues et al., 2014). In tomato fruits, *ACO1* is upregulated by pulses of white light (Scott et al., 2018). Classic work demonstrated that *ACO* expression is both a driver of ethylene production and a reporter for ethylene response in etiolated tissues (Peck and Kende, 1995; Kim et al., 1997), creating a positive feedback loop. *ACO* transcript increases have also been reported after ACC treatment of aerial tissues of light-grown seedlings (Zhong and Burns, 2003). The meta-analysis discussed below provides strong support for this feed-forward mechanism. Furthermore, when ACS activity is

elevated during climacteric ripening in tomato or banana fruits (and during flooding stress), ACO activity becomes rate limiting, and ACO expression is up-regulated (Ruduś et al., 2013; Xiao et al., 2013; Houben and Van de Poel, 2019). This suggests that one role of the feed-forward mechanism is to "clear" excess ACC when ACO activity limits ethylene production.

Light-Mediated Post-Translational Control of ACS and ACO Activity

An early study suggested that light regulates ethylene biosynthesis by altering stability/activity of ACS isozymes (Rohwer and Schierle, 1982). More recent work has confirmed that light modulates ethylene biosynthesis *via* post-translational mechanisms including reversible phosphorylation and protein turnover (Steed et al., 2004; Chae and Kieber, 2005; Yoon and Kieber, 2013b; Zdarska et al., 2015; Seo and Yoon, 2019). Post-translational regulation of ACS is largely dependent on the regulatory motifs located in the C-terminus of ACS proteins (Chae and Kieber, 2005). All three ACS types contain a well-conserved N-terminal catalytic domain, whereas the C-termini vary among ACS isoforms. Type-1 ACSs (ACS1, 2, and 6 in Arabidopsis) possess phosphorylation target sites for mitogen-activated protein kinases (MAPKs) and calcium-dependent protein kinases (CDPKs) (Tatsuki and Mori, 2001; Hernández Sebastià et al., 2004; Liu and Zhang, 2004). Type-2 ACSs (ACS4, 5, 8, 9, and 11 in Arabidopsis) contain a phosphorylation site for CDPKs and a unique regulatory motif called Target of ETO1 (TOE) in the C-terminus. The TOE motif is the binding site for ETHYLENE OVERPRODUCER1 (ETO1) and its two paralogs, ETO1-LIKE1 and 2 (EOL1 and EOL2). ETO1/EOL1/EOL2 are BTB/TRP-containing E3 ligases that control the degradation of type-2 ACS proteins *via* the 26S proteasome (Yoshida et al., 2005). In contrast to both type-1 and type-2 ACSs, the single type-3 ACSs does not contain known regulatory motifs in the C-terminus, but as discussed below, an N-terminal motif may control the stability of Arabidopsis ACS7 (Xiong et al., 2014), a sole type 3 isozyme in Arabidopsis.

The protein stability of all three ACS isozyme types is regulated by 14-3-3 proteins (Yoon and Kieber, 2013a). 14-3-3 proteins are an evolutionarily well-conserved family of regulatory proteins involved in numerous cellular processes such as cell cycle regulation, cell division, cell metabolism, proliferation, and protein oligomerization and localization (Dougherty and Morrison, 2004; Darling et al., 2005; Oecking and Jaspert, 2009; Freeman and Morrison, 2011). 14-3-3 activity influences ethylene biosynthesis by destabilizing ETO/EOL proteins and by stabilizing ACS proteins in an ETO/EOL-independent manner (Yoon and Kieber, 2013a). The range of light-dependent developmental phenotypes observed in 14-3-3 LOF mutants (Pnueli et al., 2001; Mayfield et al., 2007; Tseng et al., 2012; Adams et al., 2014) suggests interaction with multiple light signaling components. Although there is no direct evidence that light regulates interactions between 14-3-3 proteins, ACS isozymes, and ETO/EOLs, the 14-3-3s proteins are logical candidates to mediate crosstalk between light signaling and ethylene biosynthesis pathways.

Light-dependent post-translational control of ACS5 (and perhaps other type-2 ACSs) and the associated increase in ethylene production are critical for regulating hypocotyl elongation during the dark-to-light transition. Intriguingly, PIF3 may be involved in this process (Seo and Yoon, 2019). As described above, PIF3 is required for ethylene-induced stimulation of hypocotyl elongation in the light, and ethylene treatment specifically antagonizes light-induced degradation of PIF3 (Zhong et al., 2012). Light-induced stabilization of type-2 ACS enzymes should lead to increased ethylene production, which may play a role in PIF3 stabilization, thereby driving ethylene-induced hypocotyl elongation in the light (Seo and Yoon, 2019). PP2A is another regulatory component that contributes to post-translational regulation of ACS stability. Genetic analysis indicated that PP2A-mediated dephosphorylation negatively controls the protein stability of ACS6 in the dark, but has a much weaker effect on ethylene production in the light (Skottke et al., 2011). Paradoxically, the stability of ACS5, a type-2 isozyme, is positively regulated by PP2A; differential effects on the two isozyme types likely accounts for the lesser effect of PP2A inhibition in light-grown plants (Muday et al., 2006; Skottke et al., 2011).

Compared to type-1 and type-2 ACS isozymes, the sole Arabidopsis type-3 isozyme, ACS7, has unique protein stability characteristics; regulation of ACS7 turnover remains somewhat controversial (Lyzenga et al., 2012; Xiong et al., 2014; Lee et al., 2017). Because of the lack of C-terminal regulatory motifs in type-3 ACS, it was thought that these isozymes might be generally stable compared to other ACS isozymes. However, recent work showed that the stability of type-3 ACS is negatively regulated by ubiquitin-dependent turnover mediated by XBAT32, a RING-type E3 ligase (Lyzenga et al., 2012). Moreover, a putative N-terminal degron of ACS7 is active only in light-grown plants (Xiong et al., 2014) and is poorly conserved (Booker and DeLong, 2015). This light-dependent regulation of ACS7 stability may be similar to the turnover regulation of type-2 ACS, allowing the fine-tuning of ethylene production to impose transient growth control under changing conditions. Considering the regulatory role of the N-terminal domain in ACS7, it may be important to revisit the question of N-terminal motifs that could be involved in regulating the stability of other ACS proteins in response to various stimuli, including light.

The post-translational modifications of ACO have been examined in less detail than those that regulate ACS activity. However, recent work has identified several post-translational mechanisms for controlling ACO activity, including glutathionylation (Dixon et al., 2005) and sulfhydration of cysteine residues on ACO (Friso and van Wijk, 2015). While the effect of glutathionylation on ACO activity has not been reported, S-sulfhydration of LeACO1 and LeACO2 results in a decrease in ACO activity and ethylene production (Jia et al., 2018), establishing an *in vivo* role for post-translational control of ACO. Determining whether these modifications contribute to light-dependent regulation of ethylene production is an open question for future research.

MECHANISTIC CONNECTIONS BETWEEN LIGHT RESPONSE AND THE ETHYLENE SIGNALING PATHWAY

Ethylene Receptor Function Is Dependent on Light and Developmental Context

The five ethylene receptors in Arabidopsis are not functionally equivalent, with sub-functionalization observed for responses in different tissues and developmental stages (as reviewed by Shakeel et al., 2013). This subfunctionalization was revealed though detailed phenotypic analysis of LOF receptor mutants (Wang et al., 2003; Binder et al., 2004; Binder et al., 2006; Qu et al., 2007; Liu et al., 2010; McDaniel and Binder, 2012; Wilson et al., 2014b; Bakshi et al., 2015; Harkey et al., 2018). This sub-functionalization is likely due to diversity in receptor structure and signaling capabilities (O'Malley et al., 2005; Wang et al., 2006; Shakeel et al., 2013; Bakshi et al., 2015). Like the central signaling mutant *ein2-1*, a GOF *etr1-3* mutant was insensitive to ethylene or ACC in seedlings growth in light or dark (Guzman and Ecker, 1990; Roman et al., 1994; Negi et al., 2008). In an examination of nutation of etiolated hypocotyls, ethylene-dependent nutations were lost in the *etr1-7* LOF mutant no other single receptor LOF mutations affected this process (Binder et al., 2004; Binder et al., 2006). In contrast, the function of EIN4 was light-dependent. In dark-grown seedlings the *ein4-1* receptor GOF mutant showed no ethylene response (Roman et al., 1994). When grown in the light, however, *ein4-1* seedlings show a partial response to ACC (Smalle et al., 1997), suggesting differences in this receptor's role in dark vs. light.

The functional role of the five ethylene receptors has been explored in roots of light-grown Arabidopsis seedlings (Harkey et al., 2018). Transcripts encoding all five ethylene receptors are expressed in roots, and the abundance of transcripts encoding three receptors, *ETR2, ERS1*, and *ERS2*, is increased by treatments that elevated ethylene (Hua et al., 1998; Harkey et al., 2018). The GOF *ETR1* mutant (*etr1-3*) is insensitive to the effects of ethylene on root elongation, LR development, and root hair initiation (Negi et al., 2008; Lewis et al., 2011a). Using null mutants in each of the five receptors, the major role of ETR1 in controlling root responses to ACC was reported, with subtle changes in development in null mutants in any of the other receptors (Harkey et al., 2018). Using multiple LOF mutants in two or three receptor genes, minor and redundant roles for *ETR2* and *EIN4* were identified, especially in root hair formation. A triple mutant carrying *etr1-6, etr2-3*, and *ein4-4* LOF mutations has short roots, with no LRs and with extreme proliferation of root hairs. All three phenotypes are largely complemented with a genomic copy of ETR1 (Harkey et al., 2018). These results argue that the ETR1 receptor has a predominant role in controlling ethylene-inhibited LR formation, and ethylene-stimulated root hair initiation in light-grown roots, similar to the major role of this receptor in controlling nutations and responses to silver ions (Shakeel et al., 2013). Two specific receptors regulate the size of the root apical meristem, however (Street et al., 2015). In contrast with findings in LRs and root hairs, LOF *etr1-9* or *ers1-3* single mutants showed wild-type meristem size, but the LOF *etr1-9 ers1-3* double mutant exhibited a substantially reduced root apical meristem size, similar to that found in the *ctr1-2* mutant, consistent with multiple receptors controlling this aspect of root development (Street et al., 2015).

The role of specific ethylene receptors in root elongation in dark-grown seedlings has also been reported. Images of dominant GOF mutants in *ETR1*, *ERS1*, *ERS2*, and *EIN4* show roots that appear to be ethylene-insensitive (Hua et al., 1995; Hua et al., 1998). Responses to added ACC were quantified for several *etr1* and *ers1* mutant alleles, which showed reduced sensitivity (Hua et al., 1995). In comparison, the GOF *etr2-1* mutant appears to have an intermediate phenotype, with roots shorter in ethylene than in air, but not as short as wild-type roots in ethylene (Sakai et al., 1998). One study observed that subfamily 2 receptors (*ETR2*, *ERS2*, and *EIN4*) are not required for ethylene root response, as the *etr1-9 ers1-3* double mutant which carries strong LOF alleles has constitutive ethylene signaling, suggesting that the remaining receptors were not sufficient to repress ethylene signaling (Hall et al., 2012). Additionally, complementation with a wild-type copy of *ETR1* was adequate to restore ethylene sensitivity (Hall et al., 2012). Another group assayed phenotypes of receptor mutants in both light and dark (Adams and Turner, 2010), but in the absence of sucrose, which is also known to influence ethylene response (Zhou et al., 1998; Gibson et al., 2001; Yanagisawa et al., 2003; Haydon et al., 2017). Root length in the GOF *etr1-1* mutant was unchanged in response to ethylene under conditions of continuous darkness, but not continuous light. Some differences in the responses of other receptor LOF mutants were observed in dark- versus light-grown seedlings, but all receptors were at least partially required under both conditions (Adams and Turner, 2010). Together, these results demonstrate that ethylene receptors in Arabidopsis have distinct functions, dependent on tissue and light context.

The EIN3 and EBFs Mediate Light-Dependent Transcriptional Responses to Ethylene

The EIN3 TF is an essential mediator of ethylene response in hypocotyls of dark-grown seedlings, but its role is more complex in light-grown seedlings. The *ein3-1* mutant has ethylene-insensitive hypocotyl elongation in either light- or dark-grown hypocotyls (Chao et al., 1997; Smalle et al., 1997), suggesting that elongation responses to ethylene in the hypocotyl require EIN3 in a light-independent manner. EIN3 also regulates chlorophyll biosynthesis during the dark-to-light transition (Liu et al., 2017). However, the function of EIN3 in roots is light-dependent. In roots of dark-grown seedlings, double mutants between *ein3-1* and either *eil1-1* or *eil1-2* show no response to added ACC, while single mutants in *ein3* and *eil1* show partial response to this treatment (Alonso et al., 2003). In contrast, in roots of light-grown seedlings, *ein3-1*, *eil1-1*, and the double mutant all exhibit ACC-inhibition of root elongation and LR formation, and ACC stimulation of root hair formation (Harkey et al., 2018). A subset of ethylene-responsive transcripts from light-grown roots were identified as binding targets of EIN3 (Harkey et al., 2018) as reported by a DAP-Seq dataset (O'Malley et al., 2016), but many other transcripts were not direct EIN3 targets. These results are consistent with EIN3

and EIL1 controlling only a subset of ethylene responses in roots of light-grown seedlings. One example where there is light-dependent function of EIN3 is in regulation of *ACO2* transcript abundance. Upregulation of *ACO2* after ethylene treatment was lost in dark-grown *ein3-1* mutant seedlings (and EIN3 has been shown to bind to *ACO2 via* ChIP-Seq) (Chang et al., 2013). In contrast, in light-grown plants, that upregulation was present in the *ein3-1* single mutant, but was lost in both *ein3-1 eil1-1* and *ein3-1 eil1-2* double mutants (Lee et al., 2006), suggesting that EIL1 can compensate for EIN3 in regulating *ACO2* only in light-grown plants.

Recent results have suggested that differences in EIN3 function in the light and dark may be controlled at the level of turnover of this protein. Although *EIN3* transcript accumulation is not regulated by ethylene (Chao et al., 1997; Harkey et al., 2018), EIN3 and EIL1 protein accumulation is tightly controlled *via* ethylene-regulated turnover. In the absence of ethylene, EIN3 and EIL1 are ubiquitinated by EIN3-BINDING F-BOX PROTEIN1 and 2 (EBF1 and 2), two F-box proteins that act in SCF complexes, leading to EIN3 degradation. When ethylene levels rise, EBF1 and 2 are targeted for degradation in an EIN2-dependent manner, stabilizing EIN3 (Guo and Ecker, 2003; Gagne et al., 2004; Binder et al., 2007; An et al., 2010). EIN3 and EIL1 protein turnover is also regulated by crosstalk with light signaling *via* cryptochromes and HY5. The stimulation of hypocotyl elongation by ethylene in light-grown plants requires CRY1 or CRY2 (Vandenbussche et al., 2007), as well as HY5 (Yu et al., 2013). In darkness, CONSTITUTIVE PHOTOMORPHOGENESIS 1 (COP1), an integrator of light signaling, targets EBF1/2 and HY5 for ubiquitination and degradation, allowing EIN3 accumulation (Shi et al., 2016a), and preventing HY5-mediated inhibition of hypocotyl elongation. Movement of COP1 from the nucleus to the cytoplasm in light conditions allows HY5 to accumulate and inhibit growth. If ethylene signaling is activated in light conditions, EIN3 antagonizes HY5 and stimulates elongation by promoting nuclear localization of COP1, leading to HY5 degradation (Yu et al., 2013). The red light receptor PhyB also directly interacts with EIN3 and EBF1/2 after exposure to red light and enhances degradation of EIN3 (Shi et al., 2016b).

EIN3 regulation of *PIF3* and *ERF1*, which have antagonistic roles in regulating growth, constitutes one of the primary mechanisms driving the inverse hypocotyl responses to ethylene in light *versus* dark (Zhong et al., 2012). Both *PIF3* and *ERF1* are direct transcriptional targets of EIN3 (Chang et al., 2013). ERFs are stabilized by light, and they generally inhibit growth. EIN3 upregulates *ERF1* both in darkness and in light, but ERF1 effects on hypocotyl growth are only measurable under darkness, where other ERFs are absent. Conversely, *pif3* mutants are insensitive to ethylene-induced hypocotyl elongation in light, but not to hypocotyl inhibition in the dark (Zhong et al., 2012). PIFs generally promote elongation, and are destabilized in light, contributing to reduced elongation in light-grown seedlings. Transcriptional regulation of *PIF3* by ethylene *via* EIN3 is inconsequential in darkness, where many other PIFs are also active, but becomes significant under light, where other PIFs are degraded, and *PIF3* activation leads to increased hypocotyl growth. EBF1/2 also mediate red light-dependent degradation of PIF3 (Dong et al., 2017). EBFs can synergistically reduce PIF3 levels both directly, by promoting PIF3 degradation, and indirectly, by targeting EIN3 for degradation and thus reducing *PIF3* mRNA. This modulation of EIN3 and its targets by light enables complex responses to ethylene under different light contexts, such as opposite response in hypocotyl elongation. As discussed above light-dependent ethylene synthesis may also contribute to PIF3 stabilization and amplification of ethylene responses.

Downstream transcriptional effects of EIN3 and light signaling pathways cannot be completely disentangled. Recent work revealed that an *ein3 eil1* double mutant retains shade response, although ethylene-stimulated hypocotyl elongation is abolished (Das et al., 2016), suggesting that shade does not induce hypocotyl elongation by acting directly through the EIN3/EIL1 response pathway. The similar growth effects of ethylene and light are accompanied by many common transcriptional responses (Das et al., 2016). The COP1 effects on EIN3 targets are also complex. COP1 has been shown to increase EIN3 protein levels by targeting EBF1/2 for degradation in the dark (Shi et al., 2016a). In the light, ACC treatment and EIN3 overexpression lead to increased transcript levels of growth-promoting genes such as *YUCCA1* and *5*. This effect is lost in the dark but is restored in the *cop1-4* null mutant (Liang et al., 2012). This suggests that COP1 works by some mechanism downstream of EIN3 to fine tune expression of these particular genes so that they promote elongation in the light, but not in the dark. EIN3 and PIF1 transcriptionally regulate many of the same gene targets independently from one another, but mostly in the same direction (Jeong et al., 2016), and EIN3 and PIF1 pathways are each sufficient to maintain skotomorphogenesis (Shi et al., 2018). Overlapping transcriptional responses are also involved in EIN3/EIL1- and PIF3-mediated regulation of hypocotyl hook opening (Zhang et al., 2018). Downstream transcription factors, such as ERF72, may also have activity that is modulated by light to influence developmental responses (Liu et al., 2018). As described above, differential regulation of specific proteins, such as HY5, contributes to the opposing ethylene effects observed in light and dark (Smalle et al., 1997).

DOWNSTREAM ETHYLENE TRANSCRIPTIONAL EFFECTS ARE INFLUENCED BY LIGHT

A number of ethylene transcriptome studies have been performed with plants grown under a range of light conditions, revealing distinct transcriptional networks downstream of ethylene perception. We previously compared a dataset from dark-grown seedlings treated with ethylene (Chang et al., 2013) with another dataset from light-grown roots treated with ACC (Harkey et al., 2018). Both datasets used similar time points across a 24-h period after treatment, and we used the same statistical analysis of both datasets. However, we found limited overlap in differentially expressed (DE) genes (71 common genes out of 449 in the light-grown root dataset and out of 971 in the dark-grown seedling dataset). In principle, these changes could be explained by differences in light condition,

tissue type, and/or method of elevating ethylene levels (ACC treatment vs. ethylene gas). This last possibility seems unlikely because all ACC responses were lost in the ethylene-insensitive *etr1-3* and *ein2-5* mutants (Harkey et al., 2018). Comparing a larger number of transcriptomic data sets is essential for more complete understanding of the light-dependent effects of ethylene on transcript accumulation.

To identify transcriptional responses to ethylene that are light- and tissue-specific, we looked for datasets that were suitable for a meta-analysis that could resolve differences and similarities in ethylene-responsive transcriptomes in the light and dark. We searched the Gene Expression Omnibus (GEO) for the term "ethylene." Twenty-five datasets were identified in the original search based on treatment with ACC, ethylene, or with compounds that block ethylene synthesis (such as AVG), and/or mutations or transgenes that alter ethylene production or response. Many of these datasets were not usable because of dissimilar approaches or incomplete information. Five datasets were excluded due to insufficient information on experimental methods; another five used specific mutants or transgenic lines that were not found in any other dataset and did not include wild-type seedlings treated with ACC or ethylene. Although there were many datasets utilizing Col-0 and/or *ein2*, *ein3*, and *eil1* mutants in light and dark conditions, they used experimental methods, tissue types, or plants that were not developmentally matched. Seven additional datasets used 3- or 4-day-old whole dark-grown seedlings, while the remaining five datasets came from light-grown material using a variety of ages and tissue types. This highlights the need for future work that directly compares ethylene effects in light versus dark.

Ultimately, we identified three datasets with highly similar experimental methods and plant age in which transcript abundance was quantified after 4 h of ethylene or ACC treatment in roots (Stepanova et al., 2007; Feng et al., 2017; Harkey et al., 2018), and a fourth that provided an interesting comparison between ethylene treatment and shade treatment in hypocotyls or in cotyledons (Das et al., 2016). The most relevant differences between the three root datasets can be found in **Figure 3**, and further details on the process of identifying these datasets can be found in **Supplemental Datasheet 1**, along with a description of the experimental conditions used in each study. The fourth dataset was of particular interest because the authors compared the transcriptional effects of shade and ethylene in experimental conditions that were otherwise identical (Das et al., 2016). The authors noted that the effect of combined shade and ethylene on hypocotyl elongation was intermediate between the two individual treatments, consistent with ethylene and light signaling pathways sharing downstream signaling and/or effector components. However, samples treated with both ethylene and shade were not included in the transcriptomic analysis. Among genes that responded to ethylene and shade consistently and with the same direction of change, the authors found enrichments for annotations including hormone signaling, cell wall, and photomorphogenesis, among others, as well as two TFs, *AtHB28* and *IBL1*. Analysis of mutant and overexpression lines showed that *AtHB28* and *IBL1* are important for both shade and ethylene response (Das et al., 2016).

We developed a statistical pipeline to apply to all datasets used in our analysis to avoid discrepancies that might arise from differences in data analysis methods. We generated lists of DE genes that could more properly be compared to one another. (Note that this re-analysis results in DE lists that differ from those derived in the original publications.) For the three root datasets, we combined expression data from all three experiments into one master dataframe; both this dataframe and the Das et al. dataset were analyzed for differential expression using *limma* and other packages in R (Davis and Meltzer, 2007; R Core Team, 2014; Ritchie et al., 2015; Gu et al., 2016). Additional details of these analyses can be found in **Supplemental Datasheet 1**.

To identify the entire overlap between ethylene and shade transcriptional responses in the Das et al. (2016) dataset, we used this data analysis pipeline. First, we identified the complete set of ethylene-responsive genes, and then queried their expression responses in the shade dataset. Compared to cotyledons, hypocotyls showed a greater response to ethylene, which is expected given the changes in hypocotyl growth that occur in etiolated seedlings treated with ethylene, described above, so we focused on that tissue type. Not surprisingly, of the 7,248 hypocotyl transcripts that showed a significant response to ethylene, more than half of those genes also showed a shade response (4,239; **Figure 2A**). The majority of these gene expression changes occurred in the same direction and with similar kinetics. Full results for all ethylene-responsive transcripts can be found in **Supplemental Datasheet 2**.

To better illustrate the relationship between ethylene and shade response, we plotted the $\log_2$ fold-changes in transcripts in response to ethylene against the fold-change in response to transition to shade (using the 25.5-h time point, which showed the most striking changes from the control) using the previously published transcript abundance values from Das et al. (2016). This graph highlights the strong correlation between ethylene response and shade response (**Figure 2B**). The correlation between the magnitude of change in response to ethylene and shade is statistically significant both for genes with the same direction of response (Pearson's correlation, $r = 0.89$, $p < 0.001$) and in genes with the opposite direction of response (Pearson's correlation, $r = -0.87$, $p < 0.001$). Dark- or shade-grown plants exhibit a different transcriptional landscape than their light-grown counterparts. Our analysis illustrates that many transcripts show similar responses to ethylene and shade; thus, studies that use dark-grown tissues to examine ethylene response will likely miss changes that occur only in light-grown plants.

We performed a meta-analysis using the three root-specific ethylene-response datasets identified as sufficiently matched for comparison (Stepanova et al., 2007; Feng et al., 2017; Harkey et al., 2018) to screen for light-dependent and light-independent changes in ethylene-regulated transcript abundance. We used our new pipeline to reanalyze the root-specific transcriptomes to identify differences that are linked to the light environment of seedling growth. This analysis yielded interesting patterns of light-dependent and light-independent changes in transcript abundance that are summarized in a Venn Diagram in **Figure 3**. A list of all transcripts that showed significant responses to ethylene or ACC in at least one dataset and their magnitude of change

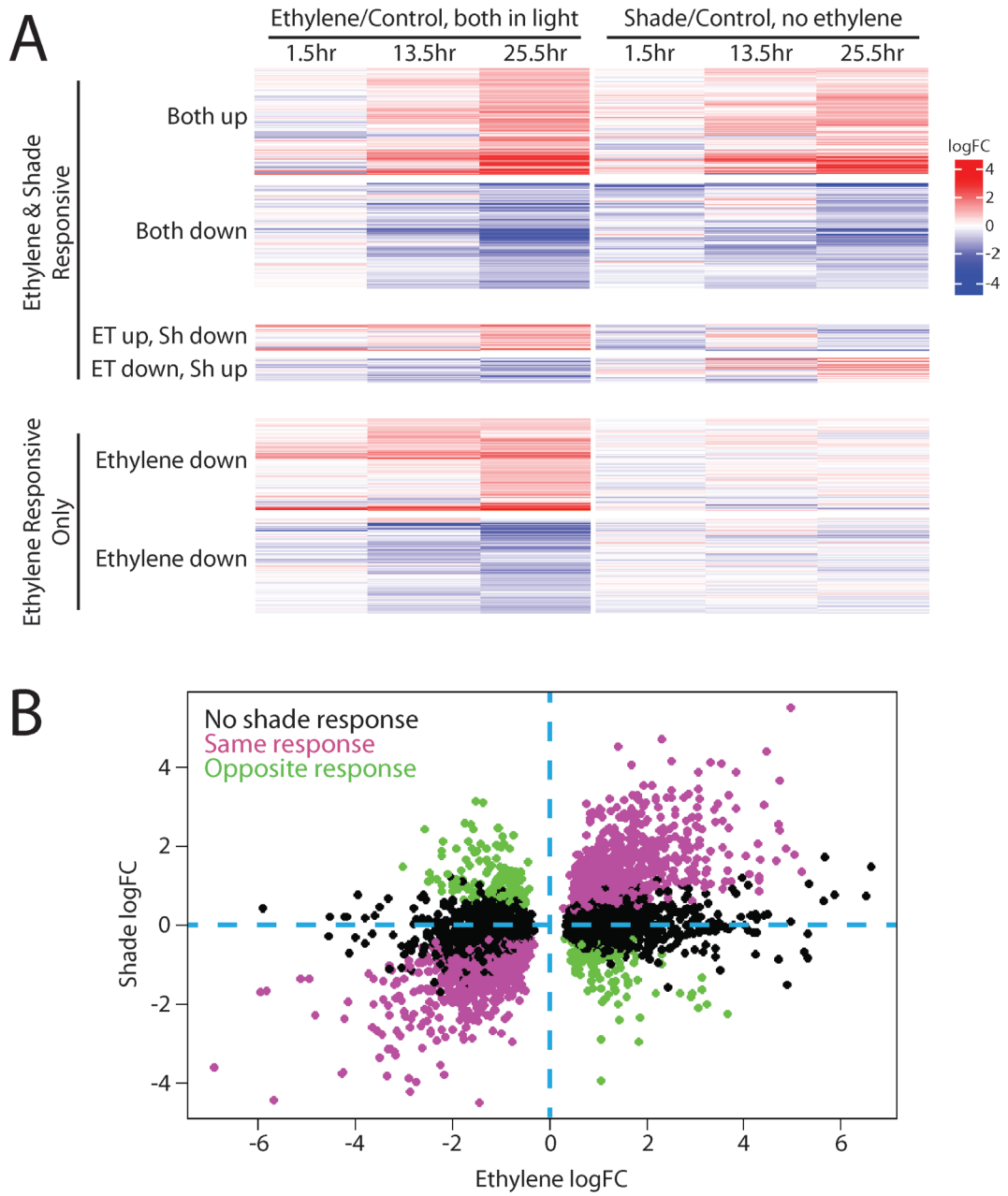

FIGURE 2 | Ethylene and shade regulate many of the same genes in Arabidopsis hypocotyls. A transcriptional dataset in which seedlings were grown in the light and then either treated with ethylene or moved to shade (Das et al., 2016) and were refiltered as described in **Supplemental Datasheet 1**, revealing that many transcripts share both ethylene and shade regulation. **(A)** A heat map, generated using the Complex Heatmaps package in R (Gu et al., 2016), shows transcripts that had statistically significant responses to ethylene in at least one time point and how those transcripts responded to shade treatment. Most genes regulated by ethylene were also regulated by shade, with the majority changing in the same direction and a smaller subset changing in opposite directions, and with a limited number of transcripts showing no response to shade. **(B)** To better define the relationship between magnitude change in response to ethylene and light, the transcripts that showed significant changes in abundance with ethylene treatment in the 25.5 h sample (which showed most dramatic ethylene-induced abundance changes) were plotted as a function of their change in response to shading. Genes that were also regulated by shade in this dataset showed strong statistical correlations between ethylene logFC and shade logFC (positive for genes with the same direction of regulation (Pearson's correlation, $r = 0.89$, $p < 0.001$), and negative for genes with the opposite direction of regulation (Pearson's correlation, $r = -0.87$, $p < 0.001$).

can be found in **Supplemental Datasheet 2**. As expected, many more DE genes were identified in the RNA-seq dataset (Feng et al., 2017) than in the microarray-based datasets (Stepanova et al., 2007; Harkey et al., 2018), because RNA-Seq has a greater dynamic range. Although only 3% of the DE genes identified responded to ethylene in all three datasets, nearly a third (32%) were DE in two datasets. A number of genes were DE in the two datasets from light-grown seedlings (Feng et al., 2017; Harkey et al., 2018), but

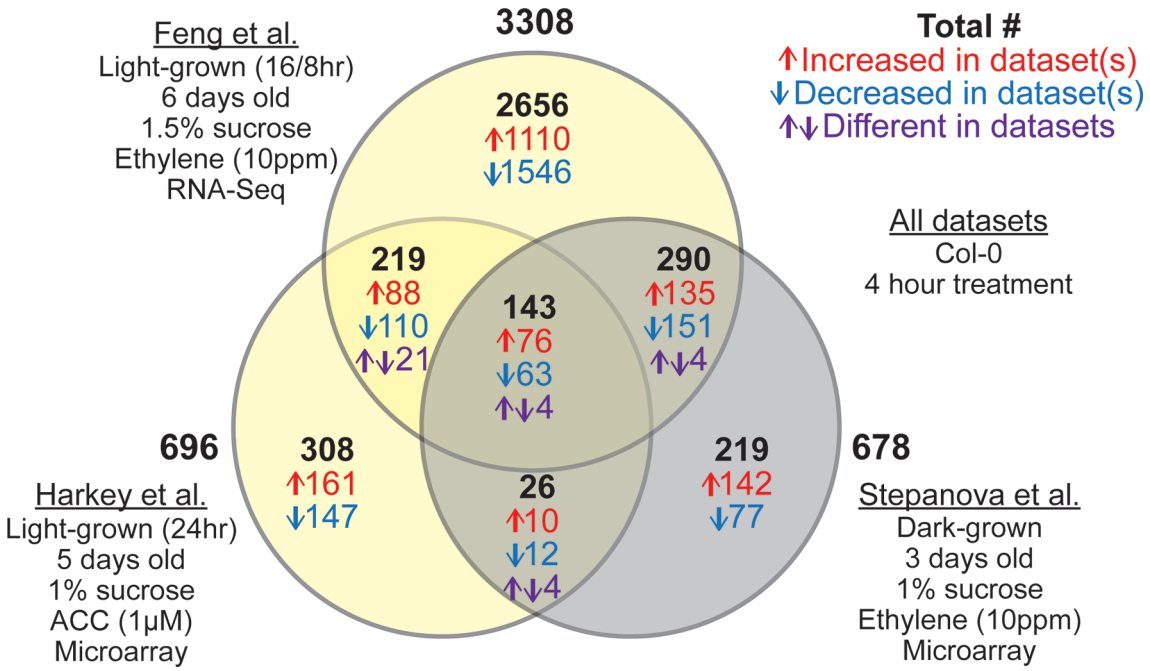

FIGURE 3 | Three root-specific ethylene response datasets show light-dependent and light-independent overlaps. Venn diagram represents number of overlapping and non-overlapping DE genes between three root-specific transcriptomic datasets: Stepanova et al. (2007), Harkey et al. (2018), and Feng et al. (2017). Differences in experimental conditions are summarized under each dataset name. Details of the analysis can be found in **Supplemental Datasheet 1**. Once DE lists were generated for individual datasets, we compared the lists to find overlapping and non-overlapping genes. In the Venn diagram, the two light-grown datasets are represented in yellow, and the dark-grown dataset is represented in gray. The number of transcripts within each overlap are color coded, with the total in black, the number increasing in both or all three in red, the number decreasing in blue, and purple indicating transcripts that changed in different directions between datasets.

not in the dark (Stepanova et al., 2007), suggesting light-dependent regulation by ethylene. There was also substantial overlap (433 transcripts) between the two datasets that used ethylene treatment but differed in the presence of light during growth. We identified 169 transcripts in the overlap between the dark-grown ethylene dataset (Stepanova et al., 2007) and light-grown ACC dataset (Harkey et al., 2018). This number is greater than in our previously reported comparison of these two datasets (80, transcripts; Harkey et al., 2018), due to the common filtering used for both datasets in this meta-analysis. A surprising number of genes, however, were specifically regulated in one dataset, and not in the other two, despite the similarity of experimental techniques. These differences may be related to other conditions such as plant age (3, 5, or 6 days), light cycle (continuous light vs. 16 h light 8 h dark), or differences in media (e.g., sucrose concentration, which is also known to influence ethylene response; Gibson et al., 2001; Haydon et al., 2017; Yanagisawa et al., 2003). These results demonstrate the need for direct comparisons of ethylene effects under experimental conditions that vary only by light level.

In addition to the light-specific transcripts described above, this analysis identified a core set of 143 transcripts that responded to ethylene or ACC in all three datasets, regardless of light. Of these transcripts, 139 (97%) changed in the same direction in all treatments (**Figure 3**). This set of 139 genes with consistent direction of change should be considered the "gold standard," for root ethylene response, much like a previously identified set of cytokinin-responsive genes from another meta-analysis (Bhargava et al., 2013). The full list of ethylene- or ACC-responsive genes from any dataset can be found in **Supplemental Datasheet 2** , with "gold standard" genes indicated.

A subset of the "gold standard" genes is summarized in **Table 1**. This group of 44 genes was chosen based on three criteria: the largest logFC values (in the positive or negative direction), known roles in ethylene synthesis or signaling (highlighted in red in Table 1), and/or known EIN3 targets based on DAP-Seq (O'Malley et al., 2016) and/or CHiP-Seq (Chang et al., 2013) analysis. Interestingly, most of the upregulated "gold" genes were identified as EIN3 targets by at least one method (72.4%), but very few downregulated "gold" genes were bound by EIN3 (6.3%). "Gold standard" genes also included a number of auxin-related genes (e.g., *SAUR76*, *SAUR8*, *IAA2*, and *IAA4/AUX2-11*), and genes involved in cell wall regulation (e.g., a pectin methylesterase inhibitor). Not surprisingly, the 139 transcripts were also enriched in gene annotations for cellular response to ethylene stimulus and negative regulation of the ethylene pathway.

Within this group of 139 transcripts, we identified 13 core genes in ethylene signaling or synthesis whose levels increased in all three datasets (and in Das et al., 2016). This core gene set includes genes encoding TFs that participate in ethylene signaling (for example, EDF1, EDF3, EDF4, and several ERFs), negative regulators of the signaling pathway CTR1, EBF2 and ARGOS, and the ethylene receptors ETR2, ERS1, and ERS2. Thus, a core output of the ethylene response is upregulation of its own signaling pathway

TABLE 1 | Selected gold standard transcripts regulated in all three datasets. The transcripts in red are all implicated in ethylene signaling or synthesis.

		logFC				EIN3 target?	
Gene ID	**Gene Description**	**Feng 2017**	**Harkey 2018**	**Stepan. 2007**	**Ave**	**DAP-Seq**	**ChIP-Seq**
AT5G19890	Peroxidase superfamily protein	6.20	3.55	6.49	5.41	YES	–
AT3G59900	ARGOS (Auxin-Regulated Gene Involved in Organ Size)	4.89	2.94	6.46	4.76	YES	YES
AT2G41230	ARGOS-LIKE2 (ARL2); (OSR1)	4.25	2.94	5.10	4.09	–	–
AT5G40590	Cysteine/Histidine-rich C1 domain family protein	3.86	4.05	4.36	4.09	–	YES
AT2G39980	HXXXD-type acyl-transferase family protein	4.63	2.96	4.25	3.95	–	YES
AT2G44080	ARGOS-LIKE (ARL)	4.37	2.43	3.90	3.57	YES	YES
AT5G53980	HOMEOBOX PROTEIN 52 (HB52)	4.15	1.97	3.34	3.15	–	YES
AT4G38410	Dehydrin family protein	2.99	2.77	3.68	3.14	–	–
AT5G02760	ARABIDOPSIS PP2C CLADE D 7 (APD7); (SSPP)	5.03	2.02	2.19	3.08	YES	YES
AT5G20820	SMALL AUXIN UPREGULATED RNA 76 (SAUR76)	3.61	2.61	2.75	2.99	–	YES
AT2G19590	ACC OXIDASE 1 (ACO1)	2.67	2.23	3.28	2.73	–	–
AT2G26070	REVERSION-TO-ETHYLENE SENSITIVITY1 (RTE1)	3.00	1.09	2.92	2.33	–	YES
AT3G23150	ETHYLENE RESPONSE 2 (ETR2)	2.21	1.80	2.79	2.27	YES	YES
AT3G25730	ETHYLENE RESPONSE DNA BINDING FACTOR3 (EDF3)	2.22	1.54	2.15	1.97	–	YES
AT1G04310	ETHYLENE RESPONSE SENSOR 2 (ERS2)	2.07	0.52	3.18	1.92	YES	YES
AT1G72360	ETHYLENE RESPONSE FACTOR 73 (ERF73); (HRE1)	1.66	2.14	1.68	1.83	–	–
AT5G25190	ETHYLENE AND SALT INDUCIBLE 3 (ESE3)	2.90	0.59	1.20	1.56	YES	YES
AT5G25350	EIN3-BINDING F BOX PROTEIN 2 (EBF2)	1.75	1.23	1.57	1.52	YES	YES
AT1G62380	ACC OXIDASE 2 (ACO2)	2.03	1.02	1.18	1.41	–	YES
AT2G40940	ETHYLENE RESPONSE SENSOR 1 (ERS1)	1.14	0.86	1.19	1.06	YES	YES
AT5G13330	RELATED TO AP2 6L (Rap2.6L)	1.36	0.84	0.79	1.00	YES	YES
AT5G03730	CONSTITUTIVE TRIPLE RESPONSE 1 (CTR1)	1.05	0.58	1.31	0.98	–	YES
AT5G04120	Cofactor-dependent phosphoglycerate mutase-like (dPGM) -	−5.49	−3.50	−3.52	−4.17	–	–
AT3G59370	Vacuolar calcium-binding protein-like protein	−4.33	−1.93	−2.91	−3.06	–	–
AT4G25250	PECTINMETHYLESTERASE INHIBITOR 4 (PMEI4)	−4.81	−1.81	−2.38	−3.00	–	–
AT2G20750	EXPANSIN B1 (EXPB1)	−3.57	−1.67	−3.29	−2.84	–	–
AT3G19320	Leucine-rich repeat (LRR) family protein	−4.19	−0.81	−3.42	−2.80	–	–
AT4G22460	Bifunctional inhibitor/lipid-transfer protein	−4.86	−1.52	−1.82	−2.73	–	–
AT2G18800	XYLOGLUCAN ENDOTRANSGLUCOSYLASE/ HYDROLASE 21 (XTH21)	−4.46	−1.43	−1.66	−2.52	–	–
AT5G42590	CYTOCHROME P450, (CYP71A16); (MRO)	−2.00	−2.16	−2.30	−2.15	–	–
AT5G42580	CYTOCHROME P450, (CYP705A12)	−2.14	−2.12	−1.91	−2.06	–	–
AT5G24100	Leucine-rich repeat protein kinase family protein	−3.48	−1.02	−1.68	−2.06	–	–
AT3G25655	INFLORESCENCE DEFICIENT IN ABSCISSION (IDA)-LIKE 1 (IDL1)	−2.29	−2.15	−1.26	−1.90	–	–
AT4G02290	GLYCOSYL HYDROLASE 9B13 (GH9B13)	−2.64	−0.91	−2.15	−1.90	–	–
AT2G18980	Peroxidase superfamily protein	−3.70	−0.97	−0.74	−1.80	–	–
AT5G64620	VACUOLAR INHIBITOR OF FRUCTOSIDASE 2 (C/VIF2)	−2.98	−0.70	−1.57	−1.75	–	–
AT4G15290	CELLULOSE SYNTHASE LIKE 5 (CSLB5)	−3.11	−1.09	−1.04	−1.75	–	–
AT5G02230	Haloacid dehalogenase-like hydrolase (HAD) superfamily	−1.61	−1.23	−1.88	−1.57	YES	YES
AT5G59220	SENESCENCE ASSOCIATED GENE(SAG113); (HAI1)	−1.80	−1.22	−1.31	−1.44	–	YES
AT4G12730	FASCICLIN-LIKE ARABINOGALACTAN 2 (FLA2)	−2.01	−0.54	−0.93	−1.16	–	YES
AT1G08500	EARLY NODULIN-LIKE PROTEIN 18 (ENODL18)	−1.18	−1.32	−0.62	−1.04	YES	YES
AT4G30400	RING/U-box superfamily protein	−0.66	−0.57	−0.64	−0.62	–	YES

components including both positive and negative regulators of ethylene responses. The core set also includes transcripts encoding ethylene biosynthetic proteins. There is consistent upregulation of transcripts encoding the ACO enzymes, with *ACO1* and *ACO2* upregulated in all three datasets and *ACO3*, *ACO4*, and *ACO5* upregulated in two of the three datasets. *ACO2* was also upregulated by ethylene, although down-regulated in shade in Das et al. (2016). Interestingly, *ACS* transcript levels show less consistent positive regulation, showing no changes for any *ACS* gene in two datasets (Stepanova et al., 2007; Harkey et al., 2018) and changes in only two to four *ACS* transcripts (out of 11 family members) in two other data sets (Das et al., 2016; Feng et al., 2017). These results indicate that a positive feedback loop drives ethylene synthesis *via* upregulation of *ACO* expression, while *ACS* mRNA levels appear to be subject to a more complex control network, as discussed above (see *Light-Mediated Transcriptional Regulation of ACS and ACO*).

Finally, included in this comparison is an annotation of genes that are regulated by ethylene in dark-grown whole seedlings as detected by RNA-Seq (Chang et al., 2013) (as found in a separate column in the **Supplemental Datasheet 2**). Of the 77 up-regulated genes in the gold-standard list, 40 were also found to be sites of EIN3 binding while only 2 of the 62 down-regulated genes showed ethylene-regulated expression. Therefore, one can further refine these genes into root-specific and tissue-independent transcripts, using the detailed annotations in **Supplemental Datasheet 2**. Together, this meta-analysis reveals many candidate genes for conserved ethylene responses that are also induced by the ethylene precursor, ACC, and transcripts whose responses depend on light

or tissue type. This information can allow formulation of a wealth of hypotheses that can be tested to further refine our understanding of ethylene signaling across plant development.

CONCLUSIONS

As seedlings germinate, elongate through soil, and then emerge into light, they undergo profound changes in development. The importance of ethylene levels in controlling development is best understood in the early dark phases, but new studies that examine the role of ethylene during developmental transitions from dark to light or in light-dependent development are providing new insight into the functions of ethylene during seedling development. Recent studies have revealed novel mechanisms that modulate ethylene biosynthesis, including important transcriptional and post-translational regulatory strategies that control production of this hormone. The pathways that control ethylene response include central signaling proteins that function in ethylene response under all conditions, but also receptors and transcription factors with light- and developmental stage-specific functions. Comparison of genome-wide transcriptional datasets allows identification of candidate genes that contribute to all ethylene responses and other genes that may contribute to developmental outputs that are specific to the light environment. Together, light regulation of ethylene biosynthesis, signaling, and developmental response have far-reaching effects on a plant's ability to adapt to the environment in early stages of development and throughout the life cycle. Understanding the mechanisms by which light and ethylene interact at the molecular and organismal levels is an important goal of future research.

AUTHOR CONTRIBUTIONS

AH performed the meta-analysis, drafted text, prepared figures, and edited the manuscript; GY drafted text, prepared figures, and edited the manuscript; DS prepared figures; AD and GM drafted text and edited the manuscript.

FUNDING

This work was supported by grants from the US National Science Foundation to GM (MCB-1716279) and GY (MCB-1817286).

ACKNOWLEDGMENTS

We appreciate the assistance of Joëlle Mühlemann with the meta-analysis and the helpful comments on the manuscript from Emily Martin.

SUPPLEMENTARY MATERIAL

The Supplementary Material for this article can be found online at: https://www.frontiersin.org/articles/10.3389/fpls.2019.01094/full#supplementary-material

SUPPLEMENTAL DATASHEET 1 | Extended methods for meta-analysis of ethylene-regulated transcripts and ethylene- and shade-regulated transcripts

SUPPLEMENTAL DATASHEET 2 | Summary of differentially expressed transcripts from roots in response to ethylene or ACC and overlap of shade-and ethylene-regulated transcriptomes

REFERENCES

Abbas, M., Alabadí, D., and Blázquez, M. A. (2013). Differential growth at the apical hook: all roads lead to auxin. *Front. Plant Sci.* 4, 441. doi: 10.3389/fpls.2013.00441

Adams, D. O., and Yang, S. F. (1979). Ethylene biosynthesis: identification of 1-aminocyclopropane-1-carboxylic acid as an intermediate in the conversion of methionine to ethylene. *Proc. Natl. Acad. Sci.* 76, 170–174. doi: 10.1073/pnas.76.1.170

Adams, E., Diaz, C., Hong, J.-P., and Shin, R. (2014). 14-3-3 proteins participate in light signaling through association with PHYTOCHROME INTERACTING FACTORs. *Int. J. Mol. Sci.* 15, 22801–22814. doi: 10.3390/ijms151222801

Adams, E., and Turner, J. (2010). COI1, a jasmonate receptor, is involved in ethylene-induced inhibition of Arabidopsis root growth in the light. *J. Exp. Bot.* 61, 4373–4386. doi: 10.1093/jxb/erq240

Alonso, J. M., Hirayama, T., Roman, G., Nourizadeh, S. D., and Ecker, J. R. (1999). EIN2, a bifunctional transducer of ethylene and stress responses in Arabidopsis. *Science* 284, 2148–2152. doi: 10.1126/science.284.5423.2148

Alonso, J. M., Stepanova, A. N., Solano, R., Wisman, E., Ferrari, S., Ausubel, F. M., et al. (2003). Five components of the ethylene-response pathway identified in a screen for weak ethylene-insensitive mutants in Arabidopsis. *Proc. Natl. Acad. Sci.* 100, 2992–2997. doi: 10.1073/pnas.0438070100

An, F., Zhao, Q., Ji, Y., Li, W., Jiang, Z., Yu, X., et al. (2010). Ethylene-induced stabilization of ETHYLENE INSENSITIVE3 and EIN3-LIKE1 is mediated by proteasomal degradation of EIN3 binding F-box 1 and 2 that requires EIN2 in Arabidopsis. *Plant Cell* 22, 2384–2401. doi: 10.1105/tpc.110.076588

Argueso, C. T., Hansen, M., and Kieber, J. J. (2007). Regulation of ethylene biosynthesis. *J. Plant Growth Regul.* 26, 92–105. doi: 10.1007/s00344-007-0013-5

Arteca, R. N., and Arteca, J. M. (2008). Effects of brassinosteroid, auxin, and cytokinin on ethylene production in *Arabidopsis thaliana* plants. *J. Exp. Bot.* 59, 3019–3026. doi: 10.1093/jxb/ern159

Bakshi, A., Wilson, R. L., Lacey, R. F., Kim, H., Wuppalapati, S. K., and Binder, B. M. (2015). Identification of regions in the receiver domain of the ETHYLENE RESPONSE1 ethylene receptor of Arabidopsis important for functional divergence. *Plant Physiol.* 169, 219–232. doi: 10.1104/pp.15.00626

Bhargava, A., Clabaugh, I., To, J. P., Maxwell, B. B., Chiang, Y.-H., Schaller, G. E., et al. (2013). Identification of cytokinin-responsive genes using microarray meta-analysis and RNA-Seq in Arabidopsis1[C][W][OA]. *Plant Physiol.* 162, 272–294. doi: 10.1104/pp.113.217026

Binder, B. M., Malley, R. C. O., Wang, W., Moore, J. M., Parks, B. M., Spalding, E. P., et al. (2004). Arabidopsis seedling growth response and recovery to ethylene. A Kinetic Analysis. *Plant Physiol.* 136, 2913–2920. doi: 10.1104/pp.104.050369

Binder, B. M., O'Malley, R. C., Wang, W., Zutz, T. C., and Bleecker, A. B. (2006). Ethylene stimulates nutations that are dependent on the ETR1 receptor. *Plant Physiol.* 142, 1690–1700. doi: 10.1104/pp.106.087858

Binder, B. M., Walker, J. M., Gagne, J. M., Emborg, T. J., Hemmann, G., Bleecker, A. B., et al. (2007). The Arabidopsis EIN3 binding F-box proteins EBF1 and EBF2 have distinct but overlapping roles in ethylene signaling. *Plant Cell Online* 19, 509–523. doi: 10.1105/tpc.106.048140

Bleecker, A. B., Estelle, M. A., Somerville, C., and Kende, H. (1988). Insensitivity to ethylene conferred by a dominant mutation in *Arabidopsis thaliana*. *Science* 241, 1086–1089. doi: 10.1126/science.241.4869.1086

Booker, M. A., and DeLong, A. (2015). Producing the ethylene signal: regulation and diversification of ethylene biosynthetic enzymes1. *Plant Physiol.* 169, 42–50. doi: 10.1104/pp.15.00672

Buer, C. S., Sukumar, P., and Muday, G. K. (2006). Ethylene modulates flavonoid accumulation and gravitropic responses in roots of Arabidopsis. *Plant Physiol.* 140, 1384–1396. doi: 10.1104/pp.105.075671

Buer, C. S., Wasteneys, G. O., and Masle, J. (2003). Ethylene modulates root-wave responses in Arabidopsis. *Plant Physiol.* 132, 1085–1096. doi: 10.1104/pp.102.019182

Chae, H. S., and Kieber, J. J. (2005). Eto Brute? Role of ACS turnover in regulating ethylene biosynthesis. *Trends Plant Sci.* 10, 291–296. doi: 10.1016/j.tplants.2005.04.006

Chang, C., Kwok, S., Bleecker, A. B., and Meyerowitz, E. M. (1993). Arabidopsis ethylene-response gene ETR1: similarity of product to two-component regulators. *Science* 262, 539–544. doi: 10.1126/science.8211181

Chang, K. N., Zhong, S., Weirauch, M. T., Hon, G., Pelizzola, M., Li, H., et al. (2013). Temporal transcriptional response to ethylene gas drives growth hormone cross-regulation in Arabidopsis. *eLife* 2, e00675. doi: 10.7554/eLife.00675

Chao, Q., Rothenberg, M., Solano, R., Roman, G., Terzaghi, W., and Ecker, J. R. (1997). Activation of the ethylene gas response pathway in Arabidopsis by the nuclear protein ETHYLENE-INSENSITIVE3 and related proteins. *Cell* 89, 1133–1144. doi: 10.1016/S0092-8674(00)80300-1

Collett, C. E., Harberd, N. P., and Leyser, O. (2000). Hormonal interactions in the control of Arabidopsis hypocotyl elongation. *Plant Physiol.* 124, 553–562. doi: 10.1104/pp.124.2.553

Cutter, E. (1978). "The epidermis," in *Plant Anatomy* (London: Clowes & Sons), 94–106.

Darling, D. L., Yingling, J., and Wynshaw-Boris, A. (2005). Role of 14–3–3 proteins in eukaryotic signaling and development. *Curr. Top. Dev. Biol.* 68, 281–315. doi: 10.1016/S0070-2153(05)68010-6

Das, D., Onge, K. R. S., Voesenek, L. A. C. J., Pierik, R., and Sasidharan, R. (2016). Ethylene- and shade-induced hypocotyl elongation share transcriptome patterns and functional regulators. *Plant Physiol.* 172, 718–733. doi: 10.1104/pp.16.00725

Davis, S., and Meltzer, P. S. (2007). GEOquery: a bridge between the Gene Expression Omnibus (GEO) and BioConductor. *Bioinforma. Oxf. Engl.* 23, 1846–1847. doi: 10.1093/bioinformatics/btm254

Dixon, D. P., Skipsey, M., Grundy, N. M., and Edwards, R. (2005). Stress-induced protein S-glutathionylation in Arabidopsis. *Plant Physiol.* 138, 2233–2244. doi: 10.1104/pp.104.058917

Dolan, L. (2001). The role of ethylene in root hair growth in Arabidopsis. *J. Plant Nutr. Soil Sci.* 164, 141–145. doi: 10.1002/1522-2624(200104)164:2<141::AID-JPLN141>3.0.CO;2-Z

Dong, J., Ni, W., Yu, R., Deng, X. W., Chen, H., and Wei, N. (2017). Light-dependent degradation of PIF3 by SCFEBF1/2 promotes a photomorphogenic response in Arabidopsis. *Curr. Biol.* 27, 2420+. doi: 10.1016/j.cub.2017.06.062

Dougherty, M. K., and Morrison, D. K. (2004). Unlocking the code of 14-3-3. *J. Cell Sci.* 117, 1875–1884. doi: 10.1242/jcs.01171

El-Sharkawy, I., Kim, W. S., Jayasankar, S., Svircev, A. M., and Brown, D. C. W. (2008). Differential regulation of four members of the ACC synthase gene family in plum. *J. Exp. Bot.* 59, 2009–2027. doi: 10.1093/jxb/ern056

Feng, Y., Xu, P., Li, B., Li, P., Wen, X., An, F., et al. (2017). Ethylene promotes root hair growth through coordinated EIN3/EIL1 and RHD6/RSL1 activity in Arabidopsis. *Proc. Natl. Acad. Sci.* 114, 13834–13839. doi: 10.1073/pnas.1711723115

Foo, E., Ross, J. J., Davies, N. W., Reid, J. B., and Weller, J. L. (2006). A role for ethylene in the phytochrome-mediated control of vegetative development. *Plant J.* 46, 911–921. doi: 10.1111/j.1365-313X.2006.02754.x

Freeman, A. K., and Morrison, D. K. (2011). 14-3-3 proteins: diverse functions in cell proliferation and cancer progression. *Semin. Cell Dev. Biol.* 22, 681–687. doi: 10.1016/j.semcdb.2011.08.009

Friso, G., and van Wijk, K. J. (2015). Posttranslational protein modifications in plant metabolism. *Plant Physiol.* 169, 1469–1487. doi: 10.1104/pp.15.01378

Gagne, J. M., Smalle, J., Gingerich, D. J., Walker, J. M., Yoo, S.-D., Yanagisawa, S., et al. (2004). Arabidopsis EIN3-binding F-box 1 and 2 form ubiquitin-protein ligases that repress ethylene action and promote growth by directing EIN3 degradation. *Proc. Natl. Acad. Sci. U.S.A.* 101, 6803–6808. doi: 10.1073/pnas.0401698101

Gibson, S. I., Laby, R. J., and Kim, D. (2001). The sugar-insensitive1 (sis1) mutant of Arabidopsis is allelic to ctr1. *Biochem. Biophys. Res. Commun.* 280, 196–203. doi: 10.1006/bbrc.2000.4062

Goeschl, J., Pratt, H., and Bonner, B. (1967). An effect of light on production of ethylene and growth of plumular portion of etiolated pea seedlings. *Plant Physiol.* 42, 1077–. doi: 10.1104/pp.42.8.1077

Gu, Z., Eils, R., and Schlesner, M. (2016). Complex heatmaps reveal patterns and correlations in multidimensional genomic data. *Bioinforma. Oxf. Engl.* 32, 2847–2849. doi: 10.1093/bioinformatics/btw313

Guo, H., and Ecker, J. R. (2003). Plant responses to ethylene gas are mediated by SCFEBF1/EBF2- dependent proteolysis of EIN3 transcription factor. *Cell* 115, 667–677. doi: 10.1016/S0092-8674(03)00969-3

Guzman, P., and Ecker, J. R. (1990). Exploiting the triple response of Arabidopsis to identify ethylene-related mutants. *Plant Cell* 2, 513–523. doi: 10.1105/tpc.2.6.513

Hall, B. P., Shakeel, S. N., Amir, M., Ul Haq, N., Qu, X., and Schaller, G. E. (2012). Histidine kinase activity of the ethylene receptor ETR1 facilitates the ethylene response in Arabidopsis. *Plant Physiol.* 159, 682–695. doi: 10.1104/pp.112.196790

Harkey, A. F., Watkins, J. M., Olex, A. L., DiNapoli, K. T., Lewis, D. R., Fetrow, J. S., et al. (2018). Identification of transcriptional and receptor networks that control root responses to ethylene. *Plant Physiol.* 176, 2095–2118. doi: 10.1104/pp.17.00907

Haydon, M. J., Mielczarek, O., Frank, A., Roman, A., and Webb, A. A. R. (2017). Sucrose and ethylene signaling interact to modulate the circadian clock. *Plant Physiol.* 175, 947–958. doi: 10.1104/pp.17.00592

Hernández Sebastià, C., Hardin, S. C., Clouse, S. D., Kieber, J. J., and Huber, S. C. (2004). Identification of a new motif for CDPK phosphorylation *in vitro* that suggests ACC synthase may be a CDPK substrate. *Arch. Biochem. Biophys.* 428, 81–91. doi: 10.1016/j.abb.2004.04.025

Houben, M., and Van de Poel, B. (2019). 1-Aminocyclopropane-1-carboxylic acid oxidase (ACO): the enzyme that makes the plant hormone ethylene. *Front. Plant Sci.* 10, 695. doi: 10.3389/fpls.2019.00695

Hua, J., Chang, C., Sun, Q., and Meyerowitz, E. M. (1995). Ethylene insensitivity conferred by Arabidopsis ERS gene. *Science* 269, 1712–1714. doi: 10.1126/science.7569898

Hua, J., and Meyerowitz, E. M. (1998). Ethylene responses are negatively regulated by a receptor gene family in *Arabidopsis thaliana*. *Cell* 94, 261–271. doi: 10.1016/S0092-8674(00)81425-7

Hua, J., Sakai, H., Nourizadeh, S., Chen, Q. G., Bleecker, A. B., Ecker, J. R., et al. (1998). EIN4 and ERS2 are members of the putative ethylene receptor gene family in Arabidopsis. *Plant Cell* 10, 1321–1332. doi: 10.1105/tpc.10.8.1321

Huang, Y., Li, H., Hutchison, C. E., Laskey, J., and Kieber, J. J. (2003). Biochemical and functional analysis of CTR1, a protein kinase that negatively regulates ethylene signaling in Arabidopsis. *Plant J.* 33, 221–233. doi: 10.1046/j.1365-313X.2003.01620.x

Ivanchenko, M. G., Muday, G. K., and Dubrovsky, J. G. (2008). Ethylene-auxin interactions regulate lateral root initiation and emergence in *Arabidopsis thaliana*. *Plant J. Cell Mol. Biol.* 55, 335–347. doi: 10.1111/j.1365-313X.2008.03528.x

Jeong, J., Kim, K., Kim, M. E., Kim, H. G., Heo, G. S., Parka, O. K., et al. (2016). Phytochrome and ethylene signaling integration in Arabidopsis occurs *via the* transcriptional regulation of genes co-targeted by PIFs and EIN3. *Front. Plant Sci.* 7, 1055. doi: 10.3389/fpls.2016.01055

Jia, H., Chen, S., Liu, D., Liesche, J., Shi, C., Wang, J., et al. (2018). Ethylene-induced hydrogen sulfide negatively regulates ethylene biosynthesis by persulfidation of ACO in tomato under osmotic stress. *Front. Plant Sci.* 9, 1517. doi: 10.3389/fpls.2018.01517

Ju, C., Mee, G., Marie, J., Lin, D. Y., Ying, Z. I., Chang, J. et al. (2012). CTR1 phosphorylates the central regulator EIN2 to control ethylene hormone signaling from the ER membrane to the nucleus in Arabidopsis, *PNAS* 109, 19486–19491. doi: 10.1073/pnas.1214848109

Kendrick, M. D., and Chang, C. (2008). Ethylene signaling: new levels of complexity and regulation. *Curr. Opin. Plant Biol.* 11, 479–485. doi: 10.1016/j.pbi.2008.06.011

Kevany, B. M., Tieman, D. M., Taylor, M. G., Cin, V. D., and Klee, H. J. (2007). Ethylene receptor degradation controls the timing of ripening in tomato fruit. *Plant J.* 51, 458–467. doi: 10.1111/j.1365-313X.2007.03170.x

Khanna, R., Shen, Y., Marion, C. M., Tsuchisaka, A., Theologis, A., Schäfer, E., et al. (2007). The basic helix-loop-helix transcription factor PIF5 acts on ethylene biosynthesis and phytochrome signaling by distinct mechanisms. *Plant Cell* 19, 3915–3929. doi: 10.1105/tpc.107.051508

Kieber, J. J., Rothenberg, M., Roman, G., Feldmann, K. A., Ecker, J. R., Kieber, J. J., et al. (1993). CTRI, a negative regulator of the ethylene pathway in arabidopsis,

encodes a member of the Raf family of protein kinases. *Cell* 72, 427–441. doi: 10.1016/0092-8674(93)90119-B

Kim, J. H., Kim, W. T., Kang, B. G., and Yang, S. F. (1997). Induction of 1-aminocyclopropane-1-carboxylate oxidase mRNA by ethylene in mung bean hypocotyls: involvement of both protein phosphorylation and dephosphorylation in ethylene signaling. *Plant J.* 11, 399–405. doi: 10.1046/j.1365-313X.1997.11030399.x

Klee, H. J., and Giovannoni, J. J. (2011). Genetics and control of tomato fruit ripening and quality attributes. *Annu. Rev. Genet.* 45, 41–59. doi: 10.1146/annurev-genet-110410-132507

Lanahan, M. B., Yen, H. C., Giovannoni, J. J., and Klee, H. J. (1994). The never ripe mutation blocks ethylene perception in tomato. *Plant Cell* 6, 521–530. doi: 10.1105/tpc.6.4.521

Le, J., Vandenbussche, F., De Cnodder, T., Van Der Straeten, D., and Verbelen, J.-P. (2005). Cell Elongation and Microtubule Behavior in the Arabidopsis Hypocotyl: responses to Ethylene and Auxin. *J. Plant Growth Regul.* 24, 166–178. doi: 10.1007/s00344-005-0044-8

Lee, H. Y., Chen, Y.-C., Kieber, J. J., and Yoon, G. M. (2017). Regulation of the turnover of ACC synthases by phytohormones and heterodimerization in Arabidopsis. *Plant J.* 91, 491–504. doi: 10.1111/tpj.13585

Lee, H. Y., Chen, Z., Zhang, C., and Yoon, G. M. (2019). Editing of the OsACS locus alters phosphate deficiency-induced adaptive responses in rice seedlings. *J. Exp. Bot.* 70, 1927–1940. doi: 10.1093/jxb/erz074

Lee, J.-H., Deng, X. W., and Kim, W. T. (2006). Possible role of light in the maintenance of EIN3/EIL1 stability in Arabidopsis seedlings. *Biochem. Biophys. Res. Commun.* 350, 484–491. doi: 10.1016/j.bbrc.2006.09.074

Lewis, D. R., Negi, S., Sukumar, P., and Muday, G. K. (2011a). Ethylene inhibits lateral root development, increases IAA transport and expression of PIN3 and PIN7 auxin efflux carriers. *Development* 138, 3485–3495. doi: 10.1242/dev.065102

Lewis, D. R., Ramirez, M. V., Miller, N. D., Vallabhaneni, P., Ray, W. K., Helm, R. F., et al. (2011b). Auxin and ethylene induce flavonol accumulation through distinct transcriptional networks. *Plant Physiol.* 156, 144–164. doi: 10.1104/pp.111.172502

Li, W., Ma, M., Feng, Y., Li, H., Wang, Y., Ma, Y., et al. (2015). EIN2-directed translational regulation of ethylene signaling in Arabidopsis. *Cell* 163, 670–683. doi: 10.1016/j.cell.2015.09.037

Liang, X., Wang, H., Mao, L., Hu, Y., Dong, T., Zhang, Y., et al. (2012). Involvement of COP1 in ethylene- and light-regulated hypocotyl elongation. *Planta* 236, 1791–1802. doi: 10.1007/s00425-012-1730-y

Lin, Z., Zhong, S., and Grierson, D. (2009). Recent advances in ethylene research. *J. Exp. Bot.* 60, 3311–3336. doi: 10.1093/jxb/erp204

Liu, K., Li, Y., Chen, X., Li, L., Liu, K., Zhao, H., et al. (2018). ERF72 interacts with ARF6 and BZR1 to regulate hypocotyl elongation in Arabidopsis. *J. Exp. Bot.* 69, 3933–3947. doi: 10.1093/jxb/ery220

Liu, Q., Xu, C., and Wen, C.-K. (2010). Genetic and transformation studies reveal negative regulation of ERS1 ethylene receptor signaling in Arabidopsis. *BMC Plant Biol.* 10, 60. doi: 10.1186/1471-2229-10-60

Liu, X., Liu, R., Li, Y., Shen, X., Zhong, S., and Shi, H. (2017). EIN3 and PIF3 form an interdependent module that represses chloroplast development in buried Seedlings. *Plant Cell* 29, 3051–3067. doi: 10.1105/tpc.17.00508

Liu, Y., and Zhang, S. (2004). Phosphorylation of 1-aminocyclopropane-1-carboxylic acid synthase by MPK6, a stress-responsive mitogen-activated protein kinase, induces ethylene biosynthesis in Arabidopsis. *Plant Cell* 16, 3386–3399. doi: 10.1105/tpc.104.026609

Lyzenga, W. J., Booth, J. K., and Stone, S. L. (2012). The Arabidopsis RING-type E3 ligase XBAT32 mediates the proteasomal degradation of the ethylene biosynthetic enzyme, 1-aminocyclopropane-1-carboxylate synthase 7. *Plant J.* 71, 23–34. doi: 10.1111/j.1365-313X.2012.04965.x

Mayfield, J. D., Folta, K. M., Paul, A.-L., and Ferl, R. J. (2007). The 14-3-3 proteins μ and υ influence transition to flowering and early phytochrome response. *Plant Physiol.* 145, 1692–1702. doi: 10.1104/pp.107.108654

Mazzella, M. A., Casal, J. J., Muschietti, J. P., and Fox, A. R. (2014). Hormonal networks involved in apical hook development in darkness and their response to light. *Front. Plant Sci.* 5, 52. doi: 10.3389/fpls.2014.00052

McDaniel, B. K., and Binder, B. M. (2012). Ethylene receptor 1 (ETR1) is sufficient and has the predominant role in mediating inhibition of ethylene responses by silver in *Arabidopsis thaliana*. *J. Biol. Chem.* 287, 26094–26103. doi: 10.1074/jbc.M112.383034

Merchante, C., Binder, B. M., and Heber, S. (2015). Gene-specific translation regulation mediated by the Hormone-signaling molecule EIN2 article gene-specific translation regulation mediated by the hormone-signaling molecule EIN2. *Cell* 163, 684–697. doi: 10.1016/j.cell.2015.09.036

Muday, G. K., Brady, S. R., Argueso, C., Deruere, J., Kieber, J. J., and DeLong, A. (2006). RCN1-regulated phosphatase activity and EIN2 modulate hypocotyl gravitropism by a mechanism that does not require ethylene signaling. *Plant Physiol.* 141, 1617–1629. doi: 10.1104/pp.106.083212

Muday, G. K., Rahman, A., and Binder, B. M. (2012). Auxin and ethylene: collaborators or competitors? *Trends Plant Sci.* 17, 181–195. doi: 10.1016/j.tplants.2012.02.001

Negi, S., Ivanchenko, M. G., and Muday, G. K. (2008). Ethylene regulates lateral root formation and auxin transport in *Arabidopsis thaliana*. *Plant J. Cell Mol. Biol.* 55, 175–187. doi: 10.1111/j.1365-313X.2008.03495.x

Negi, S., Sukumar, P., Liu, X., Cohen, J. D., and Muday, G. K. (2010). Genetic dissection of the role of ethylene in regulating auxin-dependent lateral and adventitious root formation in tomato. *Plant J.* 61, 3–15. doi: 10.1111/j.1365-313X.2009.04027.x

Oecking, C., and Jaspert, N. (2009). Plant 14-3-3 proteins catch up with their mammalian orthologs. *Curr. Opin. Plant Biol.* 12, 760–765. doi: 10.1016/j.pbi.2009.08.003

O'Malley, R. C., Huang, S. C., Song, L., Lewsey, M. G., Bartlett, A., Nery, J. R., et al. (2016). Cistrome and epicistrome features shape the regulatory DNA landscape. *Cell* 165, 1280–1292. doi: 10.1016/j.cell.2016.04.038

O'Malley, R. C., Rodriguez, F. I., Esch, J. J., Binder, B. M., O'Donnell, P., Klee, H. J., et al. (2005). Ethylene-binding activity, gene expression levels, and receptor system output for ethylene receptor family members from Arabidopsis and tomato. *Plant J.* 41, 651–659. doi: 10.1111/j.1365-313X.2004.02331.x

Peck, S. C., and Kende, H. (1995). Sequential induction of the ethylene biosynthetic enzymes by indole-3-acetic acid in etiolated peas. *Plant Mol. Biol.* 28, 293–301. doi: 10.1007/BF00020248

Peck, S. C., Pawlowski, K., and Kende, H. (1998). Asymmetric responsiveness to ethylene mediates cell elongation in the apical hook of peas. *Plant Cell* 10, 713–719. doi: 10.1105/tpc.10.5.713

Pitts, R. J., Cernac, A., and Estelle, M. (1998). Auxin and ethylene promote root hair elongation in Arabidopsis. *Plant J.* 16, 553–560. doi: 10.1046/j.1365-313x.1998.00321.x

Plett, J. M., Cvetkovska, M., Makenson, P., Xing, T., and Regan, S. (2009). *Arabidopsis* ethylene receptors have different roles in Fumonisin B1-induced cell death. *Physiol. Mol. Plant Pathol.* 74, 18–26. doi: 10.1016/j.pmpp.2009.08.004

Pnueli, L., Gutfinger, T., Hareven, D., Ben-Naim, O., Ron, N., Adir, N., et al. (2001). Tomato SP-interacting proteins define a conserved signaling system that regulates shoot architecture and flowering. *Plant Cell* 13, 2687–2702. doi: 10.1105/tpc.010293

Potuschak, T., Lechner, E., Parmentier, Y., Yanagisawa, S., Grava, S., Koncz, C., et al. (2003). EIN3-dependent regulation of plant ethylene hormone signaling by two arabidopsis F box proteins: EBF1 and EBF2. *Cell* 115, 679–689. doi: 10.1016/S0092-8674(03)00968-1

Qiao, H., Chang, K. N., Yazaki, J., and Ecker, J. R. (2009). Interplay between ethylene, ETP1/ETP2 F-box proteins, and degradation of EIN2 triggers ethylene responses in Arabidopsis. *Genes Dev.* 23, 512–521. doi: 10.1101/gad.1765709

Qiao, H., Shen, Z., Huang, S. C., Schmitz, R. J., Mark, A., Briggs, S. P., et al. (2012). Processing and subcellular trafficking of ER-tethered EIN2 control response to ethylene gas. *Science* 338, 390–393. doi: 10.1126/science.1225974

Qu, X., Hall, B. P., Gao, Z., and Schaller, G. E. (2007). A strong constitutive ethylene-response phenotype conferred on Arabidopsis plants containing null mutations in the ethylene receptors ETR1 and ERS1. *BMC Plant Biol.* 7, 3. doi: 10.1186/1471-2229-7-3

R Core Team (2014), *R: a language and environment for statistical computing*. Vienna, Austria: R Foundation for Statistical Computing. Available at: http://www.r-project.org/.

Rahman, A., Amakawa, T., Goto, N., and Tsurumi, S. (2001). Auxin is a positive regulator for ethylene-mediated response in the growth of arabidopsis roots. *Plant Cell Physiol.* 42, 301–307. doi: 10.1093/pcp/pce035

Rahman, A., Hosokawa, S., Oono, Y., Amakawa, T., Goto, N., and Tsurumi, S. (2002). Auxin and ethylene response interactions during Arabidopsis root hair development dissected by auxin influx modulators. *Plant Physiol.* 130, 1908–1917. doi: 10.1104/pp.010546

Rashotte, A. M., Chae, H. S., Maxwell, B. B., and Kieber, J. J. (2005). The interaction of cytokinin with other signals. *Physiol. Plant.* 123, 184–194. doi: 10.1111/j.1399-3054.2005.00445.x

Raz, V., and Ecker, J. R. (1999). Regulation of differential growth in the apical hook of Arabidopsis. *Dev. Camb. Engl.* 126, 3661–3668.

Ritchie, M. E., Phipson, B., Wu, D., Hu, Y., Law, C. W., Shi, W., et al. (2015). limma powers differential expression analyses for RNA-sequencing and microarray studies. *Nucleic Acids Res.* 43, e47. doi: 10.1093/nar/gkv007

Rodrigues, M. A., Bianchetti, R. E., and Freschi, L. (2014). Shedding light on ethylene metabolism in higher plants. *Front. Plant Sci.* 5, 665. doi: 10.3389/fpls.2014.00665

Rohwer, F., and Schierle, J. (1982). Effect of light on ethylene production: red light enhancement of 1-aminocyclopropane-1-carboxylic acid concentration in etiolated pea shoots. *Z. Pflanzenphysiol.* 107, 295–300. doi: 10.1016/S0044-328X(82)80195-5

Roman, G., Lubarsky, B., Kieber, J. J., Rothenberg, M., and Ecker, J. R. (1994). Genetic analysis of ethylene signal transduction in *arabidopsis thaliana*: five novel mutant loci integrated into a stress response pathway. *Genetics* 139, 1393–1409

Ruduś, I., Sasiak, M., and Kępczyński, J. (2013). Regulation of ethylene biosynthesis at the level of 1-aminocyclopropane-1-carboxylate oxidase (ACO) gene. *Acta Physiol. Plant.* 35, 295–307. doi: 10.1007/s11738-012-1096-6

Ruzicka, K., Ljung, K., Vanneste, S., Podhorska, R., Beeckman, T., Friml, J., et al. (2007). Ethylene regulates root growth through effects on auxin biosynthesis and transport-dependent auxin distribution. *Plant Cell* 19, 2197–2212. doi: 10.1105/tpc.107.052126

Sakai, H., Hua, J., Chen, Q. G., Chang, C., Medrano, L. J., Bleecker, A. B., et al. (1998). ETR2 is an ETR1-like gene involved in ethylene signaling in Arabidopsis. *Proc. Natl. Acad. Sci.* 95, 5812–5817. doi: 10.1073/pnas.95.10.5812

Schaller, G. E., and Bleecker, A. B. (1995). Ethylene-binding sites generated in yeast expressing the Arabidopsis ETR1 gene. *Science* 270, 1809–1811. doi: 10.1126/science.270.5243.1809

Scott, G., Dickinson, M., Shama, G., and Rupar, M. (2018). A comparison of the molecular mechanisms underpinning high-intensity, pulsed polychromatic light and low-intensity UV-C hormesis in tomato fruit. *Postharvest Biol. Technol.* 137, 46–55. doi: 10.1016/j.postharvbio.2017.10.017

Seo, D. H., and Yoon, G. M. (2019). Light-induced stabilization of ACS contributes to hypocotyl elongation during the dark-to-light transition in Arabidopsis seedlings. *Plant J. Cell Mol. Biol.* 98, 898–911 doi: 10.1111/tpj.14289

Shakeel, S. N., Wang, X., Binder, B. M., and Schaller, G. E. (2013). Mechanisms of signal transduction by ethylene: overlapping and non-overlapping signalling roles in a receptor family. *AoB Plants* 5, plt010–plt010. doi: 10.1093/aobpla/plt010

Shi, H., Liu, R., Xue, C., Shen, X., Wei, N., Deng, X. W., et al. (2016a). Seedlings transduce the depth and mechanical pressure of covering soil using COP1 and ethylene to regulate EBF1/EBF2 for soil emergence. *Curr. Biol.* 26, 139–149. doi: 10.1016/j.cub.2015.11.053

Shi, H., Lyu, M., Luo, Y., Liu, S., Li, Y., He, H., et al. (2018). Genome-wide regulation of light-controlled seedling morphogenesis by three families of transcription factors. *Proc. Natl. Acad. Sci.* 115, 6482–6487. doi: 10.1073/pnas.1803861115

Shi, H., Shen, X., liu, R., Xue, C., Wei, N., Deng, X. W., et al. (2016b). The red light receptor phytochrome B directly enhances substrate-E3 ligase interactions to attenuate ethylene responses. *Dev. Cell* 39, 597–610. doi: 10.1016/j.devcel.2016.10.020

Skottke, K. R., Yoon, G. M., Kieber, J. J., and DeLong, A. (2011). Protein phosphatase 2A controls ethylene biosynthesis by differentially regulating the turnover of ACC synthase isoforms. *PLoS Genet.* 7, e1001370. doi: 10.1371/journal.pgen.1001370

Smalle, J., Haegman, M., Kurepa, J., Van Montagu, M., and Straeten, D. V. D. (1997). Ethylene can stimulate Arabidopsis hypocotyl elongation in the light. *Proc. Natl. Acad. Sci.* 94, 2756–2761. doi: 10.1073/pnas.94.6.2756

Solano, R., Stepanova, A. N., Chao, Q., and Ecker, J. R. (1998). Nuclear events in ethylene signaling: a transcriptional cascade mediated by ETHYLENE-INSENSITIVE3 and ETHYLENE-RESPONSE-FACTOR1. *Genes Dev.* 12, 3703–3714. doi: 10.1101/gad.12.23.3703

Song, Q., Ando, A., Xu, D., Fang, L., Zhang, T., Huq, E., et al. (2018). Diurnal down-regulation of ethylene biosynthesis mediates biomass heterosis. *Proc. Natl. Acad. Sci.* 115, 5606–5611. doi: 10.1073/pnas.1722068115

Steed, C. L., Taylor, L. K., and Harrison, M. A. (2004). Red light regulation of ethylene biosynthesis and gravitropism in etiolated pea stems. *Plant Growth Regul.* 43, 117–125. doi: 10.1023/B:GROW.0000040116.10016.c3

Stepanova, A. N., and Alonso, J. M. (2009). Ethylene signaling and response: where different regulatory modules meet. *Curr. Opin. Plant Biol.* 12, 548–555. doi: 10.1016/j.pbi.2009.07.009

Stepanova, A. N., Hoyt, J. M., Hamilton, A. A., and Alonso, J. M. (2005). A link between ethylene and auxin uncovered by the characterization of two root-specific ethylene-insensitive mutants in Arabidopsis. *Plant Cell* 17, 2230–2242. doi: 10.1105/tpc.105.033365

Stepanova, A. N., Robertson-Hoyt, J., Yun, J., Benavente, L. M., Xie, D.-Y., Doležal, K., et al. (2008). TAA1-mediated auxin biosynthesis is essential for hormone crosstalk and plant development. *Cell* 133, 177–191. doi: 10.1016/j.cell.2008.01.047

Stepanova, A. N., Yun, J., Likhacheva, A. V., and Alonso, J. M. (2007). Multilevel interactions between ethylene and auxin in Arabidopsis roots. *Plant Cell* 19, 2169–2185. doi: 10.1105/tpc.107.052068

Strader, L. C., Chen, G. L., and Bartel, B. (2010). Ethylene directs auxin to control root cell expansion. *Plant J. Cell Mol. Biol.* 64, 874–884. doi: 10.1111/j.1365-313X.2010.04373.x

Street, I. H., Aman, S., Zubo, Y., Ramzan, A., Wang, X., Shakeel, S. N., et al. (2015). Ethylene inhibits cell proliferation of the Arabidopsis root meristem. *Plant Physiol.* 169, 338–350. doi: 10.1104/pp.15.00415

Swarup, R., Perry, P., Hagenbeek, D., Van Der Straeten, D., Beemster, G. T. S., Sandberg, G., et al. (2007). Ethylene upregulates auxin biosynthesis in Arabidopsis seedlings to enhance inhibition of root cell elongation. *Plant Cell* 19, 2186–2196. doi: 10.1105/tpc.107.052100

Tanimoto, M., Roberts, K., and Dolan, L. (1995). Ethylene is a positive regulator of root hair development in *Arabidopsis thaliana*. *Plant J. Cell Mol. Biol.* 8, 943–948. doi: 10.1046/j.1365-313X.1995.8060943.x

Tatsuki, M., and Mori, H. (2001). Phosphorylation of Tomato 1-aminocyclopropane-1-carboxylic Acid Synthase, LE-ACS2, at the C-terminal Region. *J. Biol. Chem.* 276, 28051–28057. doi: 10.1074/jbc.M101543200

Tseng, T.-S., Whippo, C., Hangarter, R. P., and Briggs, W. R. (2012). The role of a 14-3-3 protein in stomatal opening mediated by PHOT2 in Arabidopsis. *Plant Cell* 24, 1114–1126. doi: 10.1105/tpc.111.092130

Tsuchisaka, A., and Theologis, A. (2004). Unique and overlapping expression patterns among the Arabidopsis 1-amino-cyclopropane-1-carboxylate synthase gene family members. *Plant Physiol.* 136, 2982–3000. doi: 10.1104/pp.104.049999

Van de Poel, B., Smet, D., and Van Der Straeten, D. (2015). Ethylene and hormonal cross talk in vegetative growth and development1. *Plant Physiol.* 169, 61–72. doi: 10.1104/pp.15.00724

Vandenbussche, F., Petrásek, J., Zádníková, P., Hoyerová, K., Pesek, B., Raz, V., et al. (2010). The auxin influx carriers AUX1 and LAX3 are involved in auxin-ethylene interactions during apical hook development in *Arabidopsis thaliana* seedlings. *Dev. Camb. Engl.* 137, 597–606. doi: 10.1242/dev.040790

Vandenbussche, F., Vancompernolle, B., Rieu, I., Ahmad, M., Phillips, A., Moritz, T., et al. (2007). Ethylene-induced Arabidopsis hypocotyl elongation is dependent on but not mediated by gibberellins. *J. Exp. Bot.* 58, 4269–4281. doi: 10.1093/jxb/erm288

Vandenbussche, F., Vriezen, W. H., Smalle, J., Laarhoven, L. J. J., Harren, F. J. M., and Straeten, D. V. D. (2003). Ethylene and auxin control the Arabidopsis response to decreased light intensity. *Plant Physiol.* 133, 517–527. doi: 10.1104/pp.103.022665

Wang, C., Liu, Y., Li, S.-S., and Han, G.-Z. (2015). Insights into the origin and evolution of the plant hormone signaling machinery. *Plant Physiol.* 167, 872–886. doi: 10.1104/pp.114.247403

Wang, N. N., Shih, M.-C., and Li, N. (2005). The GUS reporter-aided analysis of the promoter activities of Arabidopsis ACC synthase genes AtACS4, AtACS5, and AtACS7 induced by hormones and stresses. *J. Exp. Bot.* 56, 909–920. doi: 10.1093/jxb/eri083

Wang, W., Esch, J. J., Shiu, S.-H., Agula, H., Binder, B. M., Chang, C., et al. (2006). Identification of important regions for ethylene binding and signaling in the transmembrane domain of the ETR1 ethylene receptor of Arabidopsis. *Plant Cell* 18, 3429–3442. doi: 10.1105/tpc.106.044537

Wang, W., Hall, A. E., O'Malley, R., and Bleecker, A. B. (2003). Canonical histidine kinase activity of the transmitter domain of the ETR1 ethylene receptor from Arabidopsis is not required for signal transmission. *Proc. Natl. Acad. Sci.* 100, 352–357. doi: 10.1073/pnas.0237085100

Weckx, J., and Van Poucke, M. (1989). "The effect of white light on the ethylene biosynthesis of intact green seedlings," in *Biochemical and Physiological Aspects*

of Ethylene Production in Lower and Higher Plants: proceedings of a Conference held at the Limburgs Universitair Centrum, Diepenbeek, Belgium, 22–27 August 1988 Advances in Agricultural Biotechnology. Eds. H. Clijsters, M. De Proft, R. Marcelle, and M. Van Poucke (Dordrecht: Springer Netherlands), 279–290. doi: 10.1007/978-94-009-1271-7_32

Wen, X., Zhang, C., Ji, Y., Zhao, Q., He, W., An, F., et al. (2012). Activation of ethylene signaling is mediated by nuclear translocation of the cleaved EIN2 carboxyl terminus. *Cell Res.* 22, 1613–1616. doi: 10.1038/cr.2012.145

Wilkinson, J. Q., Lanahan, M. B., Yen, H.-C., Giovannoni, J. J., and Klee, H. J. (1995). An ethylene-inducible component of signal transduction encoded by Never-ripe. *Science* 270, 1807–1809. doi: 10.1126/science.270.5243.1807

Wilson, R. L., Bakshi, A., and Binder, B. M. (2014a). Loss of the ETR1 ethylene receptor reduces the inhibitory effect of far-red light and darkness on seed germination of *Arabidopsis thaliana*. *Front. Plant Sci.* 5, 1–13. doi: 10.3389/fpls.2014.00433

Wilson, R. L., Kim, H., Bakshi, A., and Binder, B. M. (2014b). The ethylene receptors ETHYLENE RESPONSE1 and ETHYLENE RESPONSE2 have contrasting roles in seed germination of Arabidopsis during salt stress. *Plant Physiol.* 165, 1353–1366. doi: 10.1104/pp.114.241695

Xiao, Y., Chen, J., Kuang, J., Shan, W., Xie, H., Jiang, Y., et al. (2013). Banana ethylene response factors are involved in fruit ripening through their interactions with ethylene biosynthesis genes. *J. Exp. Bot.* 64, 2499–2510. doi: 10.1093/jxb/ert108

Xiong, L., Xiao, D., Xu, X., Guo, Z., and Wang, N. N. (2014). The non-catalytic N-terminal domain of ACS7 is involved in the post-translational regulation of this gene in Arabidopsis. *J. Exp. Bot.* 65, 4397–4408. doi: 10.1093/jxb/eru211

Yamagami, T., Tsuchisaka, A., Yamada, K., Haddon, W. F., Harden, L. A., and Theologis, A. (2003). Biochemical diversity among the 1-amino-cyclopropane-1-carboxylate synthase isozymes encoded by the Arabidopsis gene family. *J. Biol. Chem.* 278, 49102–49112. doi: 10.1074/jbc.M308297200

Yanagisawa, S., Yoo, S.-D., and Sheen, J. (2003). Differential regulation of EIN3 stability by glucose and ethylene signalling in plants. *Nature* 425, 521–525. doi: 10.1038/nature01984

Yang, S. F., and Hoffman, N. E. (1984). Ethylene biosynthesis and its regulation in higher plants. *Annu. Rev. Plant Physiol.* 35, 155–189. doi: 10.1146/annurev.pp.35.060184.001103

Yoon, G. M. (2015). New insights into the protein turnover regulation in ethylene biosynthesis. *Mol. Cells* 38, 597–603. doi: 10.14348/molcells.2015.0152

Yoon, G. M., and Kieber, J. J. (2013a). 14-3-3 Regulates 1-aminocyclopropane-1-carboxylate synthase protein turnover in Arabidopsis. *Plant Cell* 25, 1016–1028. doi: 10.1105/tpc.113.110106

Yoon, G. M., and Kieber, J. J. (2013b). ACC synthase and its cognate E3 ligase are inversely regulated by light. *Plant Signal. Behav.* 8, e26478. doi: 10.4161/psb.26478

Yoshida, H., Nagata, M., Saito, K., Wang, K. L., and Ecker, J. R. (2005). Arabidopsis ETO1 specifically interacts with and negatively regulates type 2 1-aminocyclopropane-1-carboxylate synthases. *BMC Plant Biol.* 5, 14. doi: 10.1186/1471-2229-5-14

Yu, Y., and Huang, R. (2017). Integration of ethylene and light signaling affects hypocotyl growth in Arabidopsis. *Front. Plant Sci.* 8, 57. doi: 10.3389/fpls.2017.00057

Yu, Y., Wang, J., Zhang, Z., Quan, R., Zhang, H., Deng, X. W., et al. (2013). Ethylene promotes hypocotyl growth and HY5 degradation by enhancing the movement of COP1 to the nucleus in the light. *PLOS Genet.* 9, e1004025. doi: 10.1371/journal.pgen.1004025

Zádníková, P., Petrásek, J., Marhavy, P., Raz, V., Vandenbussche, F., Ding, Z., et al. (2010). Role of PIN-mediated auxin efflux in apical hook development of *Arabidopsis thaliana*. *Dev. Camb. Engl.* 137, 607–617. doi: 10.1242/dev.041277

Zdarska, M., Dobisová, T., Gelová, Z., Pernisová, M., Dabravolski, S., and Hejátko, J. (2015). Illuminating light, cytokinin, and ethylene signalling crosstalk in plant development. *J. Exp. Bot.* 66, 4913–4931. doi: 10.1093/jxb/erv261

Zhang, X., Ji, Y., Xue, C., Ma, H., Xi, Y., Huang, P., et al. (2018). Integrated regulation of apical hook development by transcriptional coupling of EIN3/EIL1 and PIFs in Arabidopsis. *Plant Cell* 30, 1971–1988. doi: 10.1105/tpc.18.00018

Zhong, G. Y., and Burns, J. K. (2003). Profiling ethylene-regulated gene expression in *Arabidopsis thaliana* by microarray analysis. *Plant Mol. Biol.* 53, 117–131. doi: 10.1023/B:PLAN.0000009270.81977.ef

Zhong, S., Shi, H., Xue, C., Wang, L., Xi, Y., Li, J., et al. (2012). A molecular framework of light-controlled phytohormone action in Arabidopsis. *Curr. Biol.* 22, 1530–1535. doi: 10.1016/j.cub.2012.06.039

Zhong, S., Shi, H., Xue, C., Wei, N., Guo, H., and Deng, X. W. (2014). Ethylene-orchestrated circuitry coordinates a seedling's response to soil cover and etiolated growth. *Proc. Natl. Acad. Sci.* 111, 3913–3920. doi: 10.1073/pnas.1402491111

Zhou, L., Jang, J., Jones, T. L., and Sheen, J. (1998). Glucose and ethylene signal transduction crosstalk revealed by an Arabidopsis glucose-insensitive mutant. *Proc. Natl. Acad. Sci.* 95, 10294–10299. doi: 10.1073/pnas.95.17.10294

Zhu, J.-H., Xu, J., Chang, W.-J., and Zhang, Z.-L. (2015). Isolation and molecular characterization of 1-aminocyclopropane-1-carboxylic acid synthase genes in Hevea brasiliensis. *Int. J. Mol. Sci.* 16, 4136–4149. doi: 10.3390/ijms16024136

Conflict of Interest Statement: The authors declare that the research was conducted in the absence of any commercial or financial relationships that could be construed as a potential conflict of interest.

frontiers in Plant Science

ORIGINAL RESEARCH
published: 26 September 2019
doi: 10.3389/fpls.2019.01101

Ethylene Signaling Is Required for Fully Functional Tension Wood in Hybrid Aspen

*Carolin Seyfferth[1], Bernard A. Wessels[1], András Gorzsás[2], Jonathan W. Love[3], Markus Rüggeberg[4,5], Nicolas Delhomme[6], Thomas Vain[7], Kamil Antos[8], Hannele Tuominen[1], Björn Sundberg[6,9] and Judith Felten[6]**

[1] Umeå Plant Science Centre, Department of Plant Physiology, Umeå University, Umeå, Sweden, [2] Department of Chemistry, Umeå University, Umeå, Sweden, [3] Arevo AB, Umeå, Sweden, [4] Institute for Building Materials, Swiss Federal Institute of Technology Zurich (ETH Zurich), Zurich, Switzerland, [5] Laboratory of Wood Materials, Swiss Federal Laboratories of Materials Science and Technology, Dubendorf, Switzerland, [6] Umeå Plant Science Centre, Department of Forest Genetics and Plant Physiology, Swedish University of Agricultural Sciences, Umeå, Sweden, [7] DIADE, Univ Montpellier, IRD, Montpellier, France, [8] Department of Integrative Medical Biology, Umeå University, Umeå, Sweden, [9] Stora Enso AB, Nacka, Sweden

OPEN ACCESS

Edited by:
Dominique Van Der Straeten, Ghent University, Belgium

Reviewed by:
Deqiang Zhang, Beijing Forestry University, China
Antonio Ferrante, University of Milan, Italy

***Correspondence:**
Judith Felten
Judith.felten@slu.se

Specialty section:
This article was submitted to Plant Physiology, a section of the journal Frontiers in Plant Science

Received: *24 April 2019*
Accepted: *12 August 2019*
Published: *26 September 2019*

Citation:
Seyfferth C, Wessels BA, Gorzsás A, Love JW, Rüggeberg M, Delhomme N, Vain T, Antos K, Tuominen H, Sundberg B and Felten J (2019) Ethylene Signaling Is Required for Fully Functional Tension Wood in Hybrid Aspen. Front. Plant Sci. 10:1101. doi: 10.3389/fpls.2019.01101

Tension wood (TW) in hybrid aspen trees forms on the upper side of displaced stems to generate a strain that leads to uplifting of the stem. TW is characterized by increased cambial growth, reduced vessel frequency and diameter, and the presence of gelatinous, cellulose-rich (G-)fibers with its microfibrils oriented parallel to the fiber cell axis. Knowledge remains limited about the molecular regulators required for the development of this special xylem tissue with its characteristic morphological, anatomical, and chemical features. In this study, we use transgenic, ethylene-insensitive (ETI) hybrid aspen trees together with time-lapse imaging to show that functional ethylene signaling is required for full uplifting of inclined stems. X-ray diffraction and Raman microspectroscopy of TW in ETI trees indicate that, although G-fibers form, the cellulose microfibril angle in the G-fiber S-layer is decreased, and the chemical composition of S- and G-layers is altered than in wild-type TW. The characteristic asymmetric growth and reduction of vessel density is suppressed during TW formation in ETI trees. A genome-wide transcriptome profiling reveals ethylene-dependent genes in TW, related to cell division, cell wall composition, vessel differentiation, microtubule orientation, and hormone crosstalk. Our results demonstrate that ethylene regulates transcriptional responses related to the amount of G-fiber formation and their properties (chemistry and cellulose microfibril angle) during TW formation. The quantitative and qualitative changes in G-fibers are likely to contribute to uplifting of stems that are displaced from their original position.

Keywords: xylem, wood, ethylene, tension wood, lignin, microfibril angle, Raman microspectroscopy, transcriptomics

INTRODUCTION

When angiosperm tree stems are displaced from their original growing position, due to external factors including wind, snow load, and/or growth on uneven terrain, they form tension wood (TW) in order to reorient/uplift the stem towards its original growth position (Felten and Sundberg, 2013). TW formation is characterized by asymmetric xylem growth in the stem, originating from

enhanced activity of the secondary cambium at the upper (TW) side of the stem as compared with the lower [opposite wood (OW)] side (Timell, 1986). TW is characterized by an increased fiber-to-vessel ratio compared with OW (Esau, 1977). Another typical feature of TW is the presence of an altered cell wall layer structure in fiber cells. In many tree species, TW fibers [called gelatinous (G)-fibers] are characterized by the presence of a tertiary cell wall layer, mainly composed of a gelatinous, cellulose-rich layer (G-layer) with microfibrils having high crystallinity (Müller et al., 2006). Typically, a bimodal distribution of the cellulose microfibril angle (MFA) is observed in TW fibers using X-ray diffraction. The S2-layer exhibits an MFA of 20–40°, which is considerably larger than the values reported for the S2 of normal wood (NW) (5–15°), whereas the G-layer shows a very small MFA of 0–5° (Müller et al., 2006; Goswami et al., 2008; Rüggeberg et al., 2013). The highly porous structure of the G-layer (Norberg and Meier, 1966; Gierlinger and Schwanninger, 2006; Clair et al., 2008; Chang et al., 2009) allows for water incorporation resulting in a gelatinous aspect, from which the name gelatinous- or G-layer originates. The G-layer with its low MFA together with the S2 layer with its high MFA is thought of as a crucial factor to establish the tensile force that leads to the uplifting of the tree in response to the initial displacement (Goswami et al., 2008; Mellerowicz and Gorshkova, 2012). Even though the G-layer formation is a common phenomenon observed in the TW of many tree species, numerous tree species form TW without typical G-fibers, but rather with other cell wall layer modifications that all have small MFAs in common, which similarly exerts a tensile strain that leads to re-orientation of the stem (summarized in Ruelle, 2014).

In aspen, the plant hormone ethylene (ET) has been demonstrated to influence many of the features that characterize TW formation (Love et al., 2009; Felten et al., 2018). Indeed, after stem displacement, ET biosynthesis increases on the TW side in parallel with an asymmetric induction of 1-aminocyclopropane-1-carboxylate oxidase (ACO), which converts the ET precursor 1-aminocyclopropane-1-carboxylic acid (ACC) to ET (Andersson-Gunnerås et al., 2003). Furthermore, exogenous application of ET or ACC could mimic all typical TW characteristics such as enhanced cambial growth, increased fiber-to-vessel ratio and induction of the G-layer formation (Felten et al., 2018). Finally, the role of endogenous ET signaling in the unilateral growth response induced by leaning was investigated by constructing ET-insensitive (ETI) hybrid aspen trees. This study demonstrated an overall reduction in the TW/OW ratio in the ETI trees compared with wild-type trees (Love et al., 2009). Whether this reduced asymmetry affected the functionality of the TW was, however, not shown. Also, whether endogenous ET induced by leaning mediates the secondary wall modification in fibers observed in TW remains to be evaluated.

TW-forming tissues exhibit a strongly modified transcriptome (Paux et al., 2005; Andersson-Gunnerås et al., 2006; Chen et al., 2015; Zinkgraf et al., 2018), and it seems plausible that this is at least partly regulated through ET signaling. ET is perceived by the ET receptors localized at the endoplasmic reticulum (Bleecker et al., 1988; Cancel and Larsen, 2002). Ethylene binding derepresses the downstream ET signaling cascade (Merchante et al., 2013; Xu and Zhang, 2015). This leads to phosphorylation of the downstream component ETHYLENE-INSENSITIVE 2 (EIN2) and the cleavage of the EIN2 C-terminus (EIN2Cend) that translocates into the nucleus. The translocation triggers the expression of the ETHYLENE-INSENSITIVE 3 (EIN3)/EIN3-LIKE 1 (EIL1) transcription factors (TFs) and stabilizes EIN3/EIL1 proteins by preventing their proteasomal degradation (Qiao et al., 2009; Wen et al., 2012; Li et al., 2015; Merchante et al., 2015; Zhang et al., 2016). It has long been thought that EIN3/EIL1 activates the expression of ETHYLENE RESPONSE FACTORS (ERFs), which then trigger expression of their target genes through binding to GCC-boxes in the promoter region (Solano et al., 1998; Zhang et al., 2011; Shi et al., 2012). Recently, however, EIN3/EIL1 has been shown to directly bind to the promoter of many targets (beyond ERFs) and to modulate their expression (Chang et al., 2013). Furthermore, the ET downstream genes that were activated in hybrid aspen by exogenously applied ACC more frequently contained the EIN3/EIL1-binding motif (TEIL motif) in their promoter rather than the GCC-box (ERF-binding motif), and only a few ACC-activated ERFs contained the TEIL motif in their promoter (Felten et al., 2018). Therefore, it is likely that both ERFs and EIN3/EIL1 connect the ET signaling pathway to the molecular program of (tension) wood formation. In NW, we have identified *in silico* that ERFs and EIN3/EIL1 members act as hubs for regulating genes involved in wood formation (Seyfferth et al., 2018). Also, certain ERFs are transcriptionally induced in TW (Vahala et al., 2013).

We hypothesize here i) that ET signaling is required for all aspects of TW formation (cambial activity, vessel differentiation, G-layer formation, and MFA orientation) and that TW in ETI trees lacks these typical TW features and consequently the capacity to upright an inclined stem, and ii) that there is a molecular connection on transcriptional level between ET signaling and the molecular pathways regulating the typical developmental modifications in TW. To test these hypotheses, we conducted leaning experiments with wild-type and ETI hybrid aspen (*Populus tremula* L. × *Populus tremuloides* Michx) trees (Love et al., 2009), and we investigated how ET insensitivity affected TW formation, the uplifting response, and transcriptome changes in TW-forming tissues.

MATERIALS AND METHODS

Biological Material and Growth Conditions

The genetic background of the trees used in this study was hybrid aspen (*P. tremula* L. × *P. tremuloides* Michx.) clone T89. The strongest ETI genotype, according to previous experiments (Love et al., 2009; Felten et al., 2018), *pLMX5::etr1-1*, was chosen (line 6E) for all experiments. Transgenic and wild-type trees were transferred to soil after 4 weeks of *in vitro* propagation (Nilsson et al., 1992). For TW experiments (note: conditions specific for uplifting experiments are different and stated below), trees were propagated *in vitro* (for details see Felten et al., 2018) and at about 8- to 10-cm height transferred to the greenhouse and grown in a mixture of commercial soil–sand–fertilizer mixture (Yrkes Plantjord, Kronmull, Weibulls Horto, Sweden) under

18-h photoperiod at 20/15°C (light/dark). In total, 25 trees per genotype were grown in the greenhouse. Trees were fertilized with about 150 ml of 1% Rika-S (N/P/K 7:1:5, Weibulls Horto) once a week. Trees were grown to about 0.8- to 1-m height with weekly rotation to minimize positional effects before 10 trees per genotype were inclined to an angle of 45° against a table and bound to that table approximately 10 cm below the tip of the stem for TW formation or kept upright for NW controls. After 22 days of inclination, stems were harvested between 10 and 50 cm above soil level; split into three parts for RNA extraction and transcriptomics, MFA measurements, and Fourier transform infrared (FT-IR) and Raman microspectroscopy; frozen in liquid nitrogen; and stored at −80°C until processing.

Uplifting Experiments

After being outplanted into the greenhouse, wild-type and ETI trees were grown upright for 6 weeks. Then trees were either kept upright to continue forming NW, or the pots were horizontally inclined (90°) on the surface of a table to produce TW (see Supplementary Video S1). The uplifting response of the inclined trees was assayed over 4 weeks. All trees were grown in controlled greenhouse conditions with an 18/6-h photoperiod under light-emitting diode (LED lamps) (Fiona Lighting FL300 Sunlight), with an average day temperature ranging between 24°C and 25°C and average night temperature between 15°C and 17°C. Relative humidity ranged between 50% and 60%. Trees were fertilized once per week with Rika-S (Weibulls Horto, Hammenhög, Sweden), starting at the third week after planting and ending at the week before the experiments began in the case of the horizontally inclined trees, in order to reduce the additive effects on TW formation due to high nitrogen fertilization (Pitre et al., 2010). Measurements of height and diameter (twice, perpendicular at 10 cm above soil level) were taken weekly for upright grown trees, but only before inclination and after the end of the uplifting phase for the horizontally inclined trees. The stem spanning 5–12 cm above soil level was sampled in two parts. The lower half was frozen in liquid nitrogen and stored at −80°C, and the upper half was used directly for sectioning. Experiments were carried out on six biological replicates for each treatment and genotype. Time-lapse movies of the uplifting response were produced from photographs taken using a custom Raspberry Pi (Rpi) setup. Three cameras were connected to each Rpi, forming one unit. Units were clamped to the sides of opposing tables, and each camera was positioned to photograph two plants undergoing the gravibending response on the opposite tables. Using this setup, we captured 12 plants placed horizontally in each experiment. The Rpi was programmed to take photographs every 10 min the first day and thereafter once per hour for the remainder of the experiment. Quantification of stem lift and curvature was analyzed as described in Gerttula et al. (2015). In brief, we marked the point of primary bending with pink elastics (see in **Supplementary Video S1**). This point is defined as "the basal point of tropism of the primary, herbaceous portion of the stem" (Gerttula et al., 2015) and is clearly visible after a few hours of inclination. Thereafter, using the first picture taken each day (n = 28), we traced the stem from the base to the marked position (see in **Supplementary Video S1**). These stem traces were digitized in the form of *XY* coordinates in ImageJ (ImageJ, version 1.51j8 USA) and used to quantify the uplifting response. Normalized degree of lift was determined as the difference in height between the primary bending point and the base of the stem (in terms of their "*Y*" positions), divided by the respective length of the entire stem for each day [($Y_{apex} - Y_{base}$)/(Total Stem Length)]. We calculated the curvature (the summed differences in angle between subsequent pairs of *XY* coordinates or vectors), which indicates the deviation from a straight line in degrees. Scripts used in this experiment are available under https://github.com/UPSCb/UPSCb/tree/master/manuscripts/Seyfferth2019

Histology, Microscopy, and Vessel Quantification

For both the upright and horizontally inclined trees, the stem at 10 cm above soil level was used to prepare fresh 70-µm-thick sections (vibrating blade microtome Leica VT1000S, Wetzlar, Germany) stained with Safranin : Alcian Blue (1:2) for 30 s, washed and mounted in 50% glycerol, and imaged with a Zeiss Axioplan2 microscope, AxioCam HRc camera, and AxioVision V 4.8.2 software (Carl Zeiss Light Microscopy, Göttingen, Germany). For TW : OW ratio determination, stereomicroscope images were obtained with a Canon PowerShot G7 digital camera. The distance from the center of the pith to the cambium of both the upper (TW) and lower (OW) sides was used to calculate the TW/OW ratio. Images for vessel quantification were taken with 10× magnification on a Zeiss Axioplan2 microscope. Images just inwards of the cambium, taken for NW, OW, and TW, were analyzed using ImageJ (version 1.51j8 USA).

Vibrational Microspectroscopy and Data Analysis

FT-IR microspectroscopy with a single-element detector was performed using existing protocols (Gorzsás and Sundberg, 2014). Transverse sections with thickness of 20 µm were prepared from frozen stem samples using a Microm cryotome HM505E and dried in a desiccator between two polished rectangular BaF_2 windows (38.5 mm × 19.5 mm × 4 mm, International Crystal Laboratories, Garfield, NJ, USA) for at least 48 h. One section from each of five biological replicates per genotype and treatment was analyzed. Single-element detector images were recorded over four positions, approximately 90° from one another around the entire cross section. A single spectrum was recorded from each position covering an area of approximately 430 × 430 µm, using a Bruker Equinox 55 spectrometer equipped with a Hyperion 3,000 microscopy accessory (Bruker Optics GmbH, Ettlingen, Germany). Spectra were recorded in transmission mode over the range of 700–3,800 cm^{-1}, with a spectral resolution of 4 cm^{-1}. Six hundred interferograms were co-added to improve signal-to-noise ratio, and a zero-filling factor of 2 was employed. Spectra were converted to data point tables using OPUS (v7.0.122, Bruker Optik GmbH, Ettlingen, Germany), baseline corrected (2-point linear baseline at 812 and 1,809 cm^{-1}), and total sum (area-) normalized in the region of 812–1,809 cm^{-1}, using in-house

scripts (https://www.umu.se/en/research/infrastructure/visp/downloads/) written in Matlab (version 7.0, MathWorks, Natick, MA, USA, http://www.mathworks.com). Spectra were extracted, and the area measuring 816–1,803 cm^{-1} was used in subsequent multivariate analyses. Principal component analysis (PCA) and orthogonal projections to latent structures discriminant analysis (OPLS-DA) (Trygg and Wold, 2002) were performed using SIMCA-P+ (versions 12-14, Umetrics AB, Umeå, Sweden).

For Raman microspectroscopic analysis, 20-µm-thick transverse sections were prepared from frozen stem material (ca. 30 cm above soil level) using a Microm cryotome HM505E and kept between a standard glass microscope slide and cover slip in deuterated water (D_2O). Spectral maps were recorded using a Renishaw inVia Raman spectrometer and microscope with a 100× oil immersion lens and a 514-nm Ar^+ laser. Spectral maps comprising of 60–80 voxels with step sizes of 1 µm in the *X* and *Y* directions were recorded on two positions from each one to two cross sections of TW and NW, of each of three wild-type and three *pLMX5::etr1-1* trees that were grown upright or had been leaned at 45° and fixed in this position for 22 days. The maps were recorded in radial orientation over three fiber cells from lumen of cell 1 to lumen of cell 3. The following settings were used for spectral recording: static scans centered at 1,190 cm^{-1} (resulting in a spectral range of ca. 510 to 1,802 and ca. 1 cm^{-1} resolution with a 2,400 lines grating), standard confocality, laser power set at 100% in the software, and exposure time of 30 s per spectrum. Spectra were noise filtered and cleaned from cosmic rays using the chemometrics package of WiRE (version 3.4, Renishaw Plc, Wotton-under-Edge, UK). Data pre-processing was carried out in Matlab (version 2018a, MathWorks Inc., Natick, Massachusetts, USA), using an open source graphical user interface adapted from Felten et al. (2015) (https://www.umu.se/en/research/infrastructure/visp/downloads/) with the following parameters: spectra were cut to a range of 510 to 1,800 cm^{-1}, asymmetric least squares baseline corrected (λ = 5,000, pVal = 0.001, Eilers, 2004), total area normalized, and smoothed with Savitzky–Golay filtering (first-order polynomial, with a frame size of 3). Multivariate curve resolution-alternating least squares (MCR-ALS) analysis was first conducted on TW samples. Based on singular value decomposition, the data were fitted using four components and only non-negativity constraints for both spectral and concentration directions. Two of the resolved components showed spectral features corresponding to bands previously assigned to cellulose and lignin. The third resolved spectral profile showed features characteristic of aromatic extractives, while the fourth had residual, unidentified contributions (**Supplementary Figure S1A**). These resolved spectral profiles were used as initial estimates in the MCR-ALS modeling of NW spectra (**Supplementary Figure S1B**). The resolved components were used to classify voxels into chemically distinct categories, using hard *k*-means clustering. Three clusters were used, corresponding to distinct zones: lumen (in all samples), G-layer and S-layer (in TW and NW samples, respectively), and S-layer plus middle lamella (in all samples) (**Figure 3**, **Supplementary Figure S2**). Spectral maps where no zones could be distinguished were removed from further analyses. Spectra originating from the distinct chemical zones of interest (cell wall layers) of the respective genotypes/conditions were used for PCA and, when appropriate, for OPLS-DA analysis (Trygg and Wold, 2002) in SIMCA-P+ (version 14.0, Umetrics AB, Umeå, Sweden) to reveal chemical changes in cell wall layers between the genotypes and conditions.

Microfibril Angle Measurements

Radial-longitudinal stem sections of 100-µm thickness and 0.5- to 2-mm width were generated from six stems per genotype and condition (ca. 35 cm above soil level) using a Microm cryotome HM505E and dried between two microscopy glass slides. Xylem strips were transferred to metal holders for X-ray diffraction analysis. The X-ray diffraction experiments were carried out at the µ-spot beamline at the synchrotron facility BESSY II, Berlin, Germany. The radiation energy was set to 15 keV, corresponding to a wavelength of 0.8265 A. The (200)-Bragg peaks of cellulose, which were taken for orientation analysis, occurred at a scattering angle 2θ of 11.8. The samples were measured in ambient air, with the long axis of the fiber cells being perpendicular to the incident X-ray beam. The sample-detector distance was set to 245 mm, and the exposure time to 60 s. The beam diameter was set to 100 µm, so several measurements could be performed on one sample. Azimuthal intensity profiles (azimuthal angle φ vs. intensity) of the diffraction patterns were obtained by radially integrating the intensity of the (200)-peaks within 2θ ± 0.2° with an azimuthal step size of 1°. Microfibril orientation distributions and mean MFA were calculated by the simulation and fitting routine as described in detail previously (Rüggeberg et al., 2013).

Transcriptomics and Data Analysis

From greenhouse grown upright or inclined trees (22 days fixed at 45°) a 10- to 30-cm stem piece above soil level was harvested and frozen in liquid N2. We chose to analyze transcriptomes at a late stage of TW formation (22 days after inclination) since at this stage all processes that lead to uprighting are active, which is suggested by reduced performance in stem correction of ETI trees compared with WT (**Figure 1**, **Supplementary Video S1**). From trees forming TW, the bark was peeled off from the TW side of the stem, and developing wood and phloem/cambium (inner surface of the bark) were scraped with a scalpel into liquid nitrogen (Gray-Mitsumune et al., 2004). For NW, phloem/cambium and developing wood were scraped all around the stem after peeling off the bark. Scrapings from three trees per genotype and condition were pooled equally by weight and ground to a fine powder using a mortar and pestle in liquid nitrogen. One hundred milligram of powder was used to extract RNA using the cetyl trimethylammonium bromide (CTAB) method (Chang et al., 1993). DNA removal was carried out using DNA-free™ DNase (Ambion). After DNA removal, RNA was cleaned with the Qiagen MinElute kit. RNA concentration was measured with a Nanodrop ND-1000 (Nano-Drop Technologies, Delaware, USA), and its quality was assessed using an Agilent 2100 Bioanalyzer with Agilent RNA 6000 Nano Chips according to manufacturer's instructions. Sequencing library generation and sequencing using Illumina HiSeq 2000 were carried out at SciLifeLab (Science for Life Laboratory, Stockholm, Sweden). Data sequences are available from the European Nucleotide Archive under the accession number PRJEB32252. Quality assessment and pre-processing of the obtained RNA-Seq reads were done

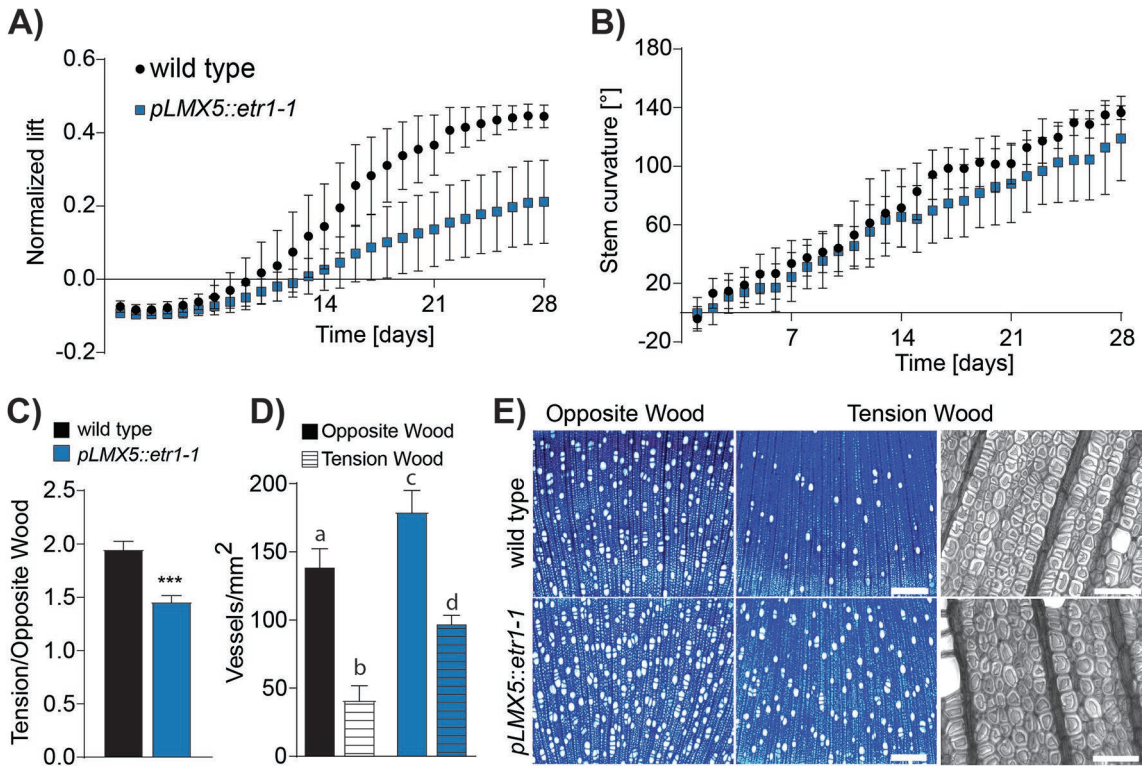

FIGURE 1 | Quantification of the gravibending response in ETI hybrid aspen trees. **(A)** Normalized lift of six wild-type and six ETI trees (*pLMX5::etr1-1*). **(B)** Stem curvature of these trees. One time-lapse image per day was digitized to *XY* coordinates in ImageJ by tracing stems from the base to the point where primary bending occurs in the stem. Normalized degree of lift is the difference in height between the primary bending point and the base of the stem divided by the respective length of the entire stem for each day. Stem curvature is the summed differences in angle between each subsequent pair of *XY*. Error bars indicate ± SD. **(C)** TW : OW ratio of the ethylene-insensitive trees ($n = 6$). Asterisks indicate statistical significant differences from wild type according to Student *T*-test with Welch correction [pVal < 0.001 (***)]. **(D)** Vessel density in OW and TW of wild-type and ETI trees ($n = 6$). Error bars indicate ± SD. Letters indicate statistical significant differences between both genotypes and both tissues (OW/TW) calculated using a two-way analysis of variance (ANOVA) and a Tukey test (using a pVal cutoff = 0.05). **(E)** Representative 10× magnified images of OW and TW in inclined hybrid aspen wild-type or ETI stems. Insets show higher magnification of a TW area that visualizes the presence of G-layers in both genotypes. 10× magnified images were used for vessel density determination in **(C)**. Scale = 50 µm. ETI, ethylene insensitive; OW, opposite wood; TW, tension wood.

following the guidelines described in Delhomme et al. (2014). Briefly, FastQC (v0.11.5; Andrews, 2010) was used to assess the quality of the raw data. Then, ribosomal RNAs and sequencing adapters were removed using SortMeRNA (Kopylova et al., 2012) and Trimmomatic (Bolger et al., 2014), respectively. Read quality was assessed using FastQC after both these steps and reads that passed the quality assessment were aligned to the *P. tremula* genome (v1; available at http://plantgenie.org/, Sundell et al., 2015). HTSeq was used for summarizing read counts (Anders et al., 2015). Read counts were normalized in R (v3.5.3, R Core Team, 2019) using DESeq2 (v1.30.0, Love et al., 2014) and used for PCA and differential gene expression analysis. Gene expression was normalized considering the effect from the genotype (wild type or *pLMX5::etr1-1*) and tissue (TW or NW) using the following model: gene counts ~ genotype + tissue. Variance-stabilizing transformation was applied using the DESeq2 package. A PCA was conducted (using the plotPCA command in DESEq2) to show general differences between all analyzed samples. Differentially regulated genes (DRGs) were selected using an absolute log2 fold change (log2FC) larger or equal to 0.5 (pAdj < 0.05) as cutoff (suggested in Schurch et al., 2016). The script used for the transcriptome analysis is available under https://github.com/UPSCb/UPSCb/tree/master/manuscripts/Seyfferth2019. Gene ontology (GO) enrichment analysis was performed with the GO and PFAM enrichment tool at www.aspwood.org (Sundell et al., 2015). Visualization of comparative expression analyses was performed using the drawing tool available at http://bioinformatics.psb.ugent.be/webtools/Venn and gplots (v3.1.0). Promoter sequences of *Populus trichocarpa* of up to 2,000 bp in length were obtained and screened for the presence of the TEIL (tobaccoEIN3like) motif (AYGWAYCT; Kosugi and Ohashi, 2000), the GCC-box (AGCCGCC; Ohme-Takagi and Shinshi, 1995), and the ET-responsive element (ERE) (ATTTCAAA; Itzhaki et al., 1994). For precise promoter and cis-element prediction, we chose the *P. trichocarpa* genome (v3) as reference for this analysis, because it has a higher coverage in non-coding genome regions than does the available *P. tremula* genome sequence (v1). The "best hit" (*P. trichocarpa* sequence with the highest sequence similarity to *P. tremula* sequence) was defined as *P. trichocarpa* homolog, and the respective promoter sequences were obtained

using the "Sequence Search" webtool from Popgenie (http://popgenie.org/sequence_search). Sequence match analyses are described in Felten et al. (2018).

Quantitative Polymerase Chain Reaction (qPCR)

Total RNA extraction for qPCR analysis was carried out from 100-mg wood powder with Qiagen RNeasy Plant Mini kit according to the manufacturer's instructions (using RLT buffer for lysis). Each of the three biological replicate samples per condition and genotype was a pool of xylem scrapings from three individual trees similar as described for material used for RNA-Seq experiments. An on-column DNA removal was carried out using Qiagen RNase-Free DNAse. Samples were subjected to a second DNA-removal step using the Invitrogen DNA-free kit according to the manufacturer's manual. RNA quality was assessed by gel electrophoresis and quantitated by a Qubit 2.0 fluorometer using the Invitrogen Qubit RNA BR Assay. cDNA was synthesized using Biorad iScript from 300-ng RNA per sample according to the manual. qPCR was carried out on a Biorad CFX96 real-time PCR machine with a C1000 Touch Thermal Cycler in duplicate reactions measuring 15 µl consisting of 7.5 µl 2× Roche LightCycler 480 SYBR Green I Master solution, 0.3 µM of each primer, and 2 µl of cDNA. For evaluating primer efficiency, equal aliquots of every cDNA sample were taken, mixed, and diluted five times with a dilution factor of 5. For expression analysis, a 1/10 dilution of cDNA was used. The primer list is found in **Supplementary Table S8**. The qPCR program consisted of an initial denaturation step (95°C, 5 min); followed by 40 cycles of denaturation (95°C, 10 s), annealing (55–58°C, 10 s), and elongation (72°C, 20 s); and followed by a melting curve (65–95°C with a 0.5°C interval for fluorescence reading). Biorad CFX maestro software was used to determine the most stable reference genes among the five tested ones and yielded ideal values (M = 0.339 and stability Ln(1/Avg$M$ = 1.082) for two genes, *UBC21* (*Potri.006G240900*) and *DAT* (*Potri.002G127700*), which were hence used for normalization of target gene expression data. Experimentally assessed primer efficiencies were taken into account for delta Cq calculations.

Statistical Analysis

Statistical analysis of OW/TW ratios (**Figure 1C**) between wild-type and ETI trees was calculated using a Student T-test with Welch correction. Differences were significant with pVal <0.05 (*), pVal < 0.01 (**), and pVal < 0.001 (***). Statistical differences between the number of vessels in TW and OW (**Figure 1D**) in wild-type and ETI trees were calculated by a two-way analysis of variance (ANOVA), and a post-ANOVA Tukey test was used for pairwise comparisons (pVal < 0.05). An ANOVA and a Tukey test were also used to assigned statistical differences in MFAs obtained in the G- or S2-layer and in gene expression of ET-dependent genes in wild-type and ETI trees (**Figure 2**). Details about PCA and OPLS-DA (Trygg and Wold, 2002) models generated in SIMCA-P+ (version 14.0, Umetrics AB, Umeå, Sweden) on spectroscopic data are given in the respective figure legends (**Figures 3** and **4**), and the choice of these methods is described in detail in Felten et al. (2018). Statistical analysis for differential gene expression analysis (**Figure 5**) was performed using pre-set statistical settings in the DESeq2 package (Love et al., 2014). Briefly, pValues were calculated using the Wald test, and multiple testing correction was performed using the Benjamini–Hochberg approach. Statistical tests for GO term enrichment were performed on the basis of Fisher's exact test and included multiple testing (for detailed description, see Sjödin et al., 2009). Hypergeometric distribution was used to determine statistical significant enrichment of cis-elements (Felten et al., 2018; **Figure 5**).

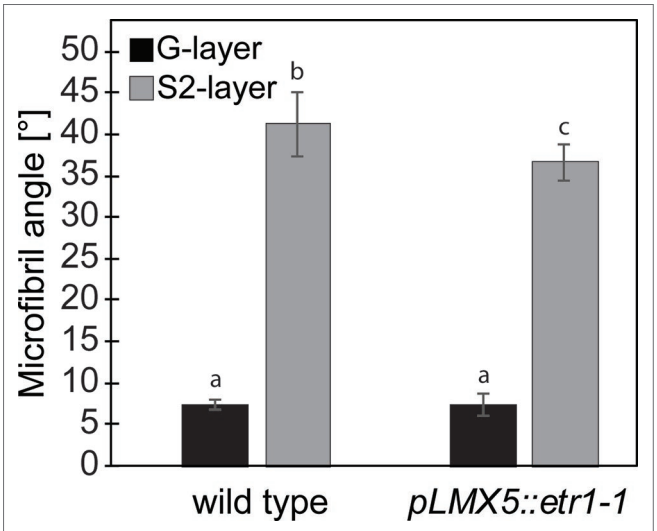

FIGURE 2 | Cellulose microfibril angles in TW of hybrid aspen wild-type and ETI hybrid aspen trees (*pLMX5::etr1-1*). Bars represent average ± SD obtained from six individual trees per genotype. Letters indicate statistical significant differences between angles obtained in both genotypes and the G- or S2-layer calculated using a two-way analysis of variance (ANOVA) and a Tukey test (using a pVal cutoff = 0.05). ETI, ethylene insensitive; TW, tension wood.

RESULTS

Ethylene Signaling Is Required for Fully Functional Tension Wood

We compared the uplifting response of wild-type and ETI hybrid aspen after horizontal inclination through time-lapse photography over a period of 28 days. The ETI trees overexpress the dominant negative *Atetr1-1* receptor under the control of the wood-specific *pLMX5* promoter. We have previously shown that transformation of hybrid aspen trees with the *pLMX5::etr1-1* construct conveys strong ET insensitivity to woody tissues (Love et al., 2009; Felten et al., 2018). Representative videos tracking the response of one out of the six tested wild-type trees and one out of the six ETI trees over the first 21 days of leaning were compiled using the same number of pictures per day and per genotype, enabling direct comparison (**Supplementary Video S1**). The videos illustrate qualitatively a delayed bending and reduced

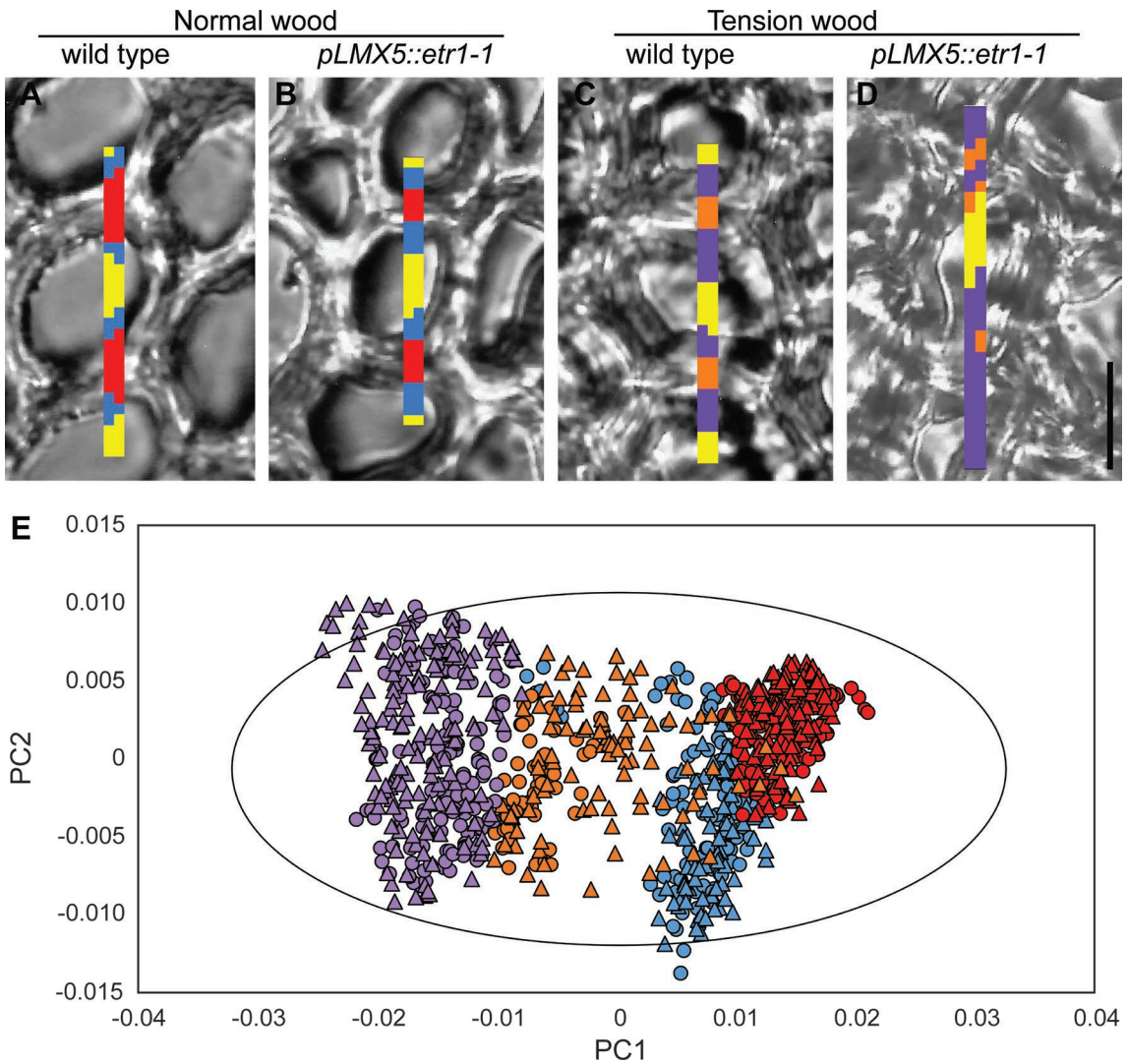

FIGURE 3 | Identification and chemical comparison of cell wall layers in NW and TW of wild-type and ETI (*pLMX5::etr1-1*) hybrid aspen trees. **(A)** Overlay of white light images on one representative section out of six scanned sections per genotype and scanned maps after *k*-means clustering based on four MCR-ALS resolved components and three clusters. The sizes of the spectral maps are as follows: **(A)** 2 × 29 spectra, **(B)** 2 × 25 spectra, **(C)** 2 × 30 spectra, and **(D)** 2 × 34 spectra. Lateral step size is 1 μm^2, and scale bar in **(D)** is 10 μm. Clusters in NW correspond to lumen (yellow), middle lamella + S-layer (red), and S-layer (blue); in TW, clusters correspond to lumen (yellow), middle lamella + S-layer (orange), and G-layer (violet). **(E)** Score plots (PC1 and PC2) of a PCA of spectra from all cluster maps shown in **Supplementary Figure S2**. Colors correspond to cell wall layers as described above. Triangles represent wild type, and circles *pLMX5::etr1-1*. Model details: autofitted (70 components, 893 observations), PC1 explained 79% of variation, PC2 explained 10% of variation. R2X(cum) = 0.996, Q2(cum) = 0.99. The ellipse in **(E)** indicates a 95% confidence interval (Hotelling's T^2). ETI, ethylene insensitive; MCR-ALS, multivariate curve resolution-alternating least squares; NW, normal wood; PCA, principal component analysis; TW, tension wood.

uplifting of the ETI trees as compared with the wild-type tree. To quantify this response, we selected the first time-lapse image of each day over the entire experimental period (n = 28) and calculated both the normalized lift and the curvature from stem traces captured in ImageJ (**Figures 1A, B**). While these two traits are interdependent, they also reveal slightly different aspects of the TW response since the same normalized lift may be supported by different curvatures. The curvature also gives an indication of the shape of the stem (e.g., 180° is a perfect half circle or "C" shape). The ETI trees showed a delayed bending response with a dramatic 52% reduction in lift relative to wild type on the final day of the experiment (**Figure 1A**). Stem curvature was also negatively affected in ETI trees, but to a lesser extent (**Figure 1B**). This illustrated that functional ethylene signaling is required in xylem tissues for the uplifting response.

Asymmetric Growth and Vessel Reduction, but Not G-Fiber Formation, Require Functional Ethylene Signaling

To assess potential anatomical causes of the reduced uplifting response in ETI trees, we inspected the xylem anatomy

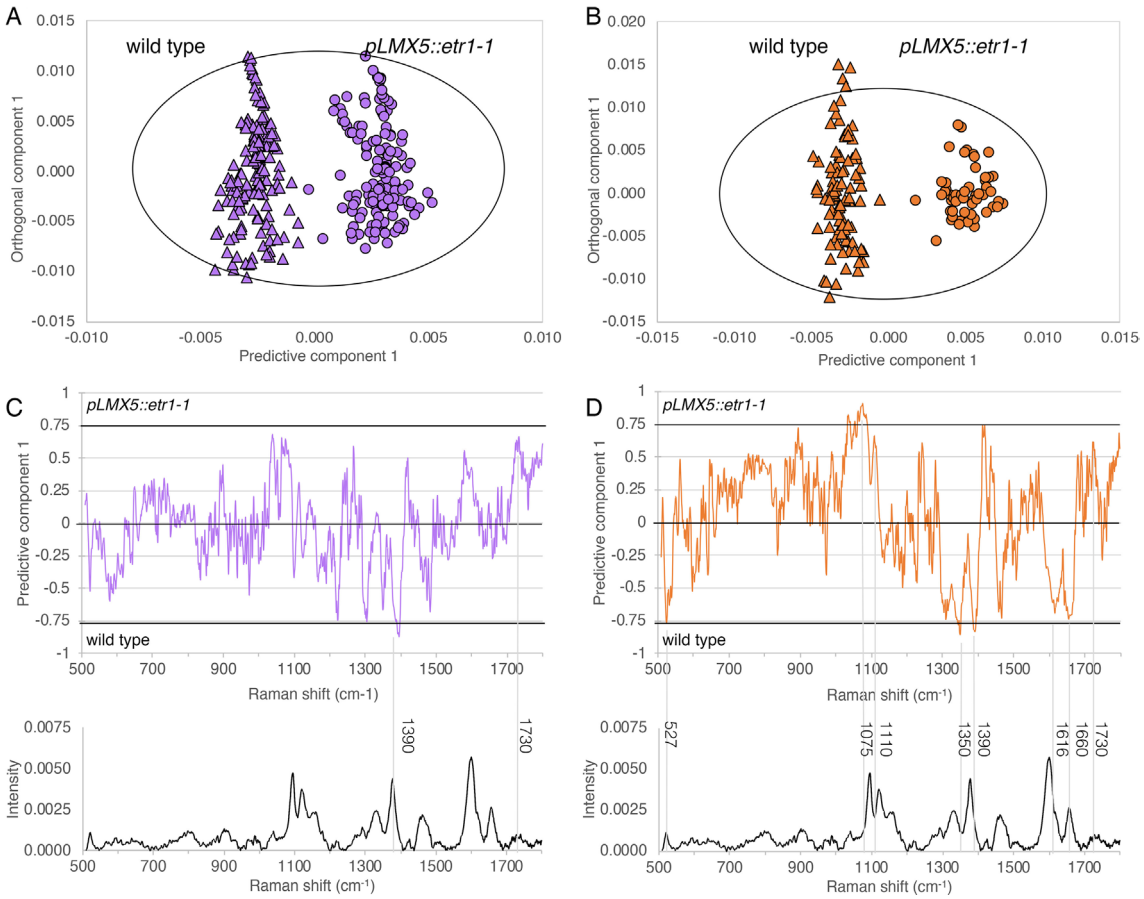

FIGURE 4 | Chemical differences among G-layer **(A** and **C)** and S-layer **(B** and **D)** in TW of wild-type and ETI (*pLMX5::etr1-1*) hybrid aspen revealed by Raman microspectroscopy. **(A** and **B)** OPLS-DA score plots of 1 + 2 (predictive + orthogonal) component models based on the respective cluster extracted from all cluster maps shown in **Supplementary Figure S2**. Specification for the models: **(A)** 296 observations, R2X(cum) = 0.723, R2Y(cum) = 0.924, and Q2(cum) = 0.921; **(B)** 149 observations, R2X(cum) = 0.804, R2Y(cum) = 0.946, and Q2(cum) = 0.941. The ellipses in **(A)** and **(B)** correspond to 95% confidence intervals (Hotelling's T^2). **(C)** and **(D)** The corresponding correlation-scaled loadings plots with a randomly selected spectrum underneath each representing the spectra used in the models. Wavenumbers with high correlation to separation are labeled. Noticeably, these do not always correspond to distinct peaks in **(D)** but can indicate shoulders (1,616 cm^{-1}) or shifts towards different energy levels (lower, e.g., 1,075 cm^{-1}; higher e.g., 1,390 cm^{-1}), the latter being indicative of structural rather than proportional changes (qualitative rather than quantitative differences). ETI, ethylene insensitive; OPLS-DA, orthogonal projections to latent structures discriminant analysis; TW, tension wood.

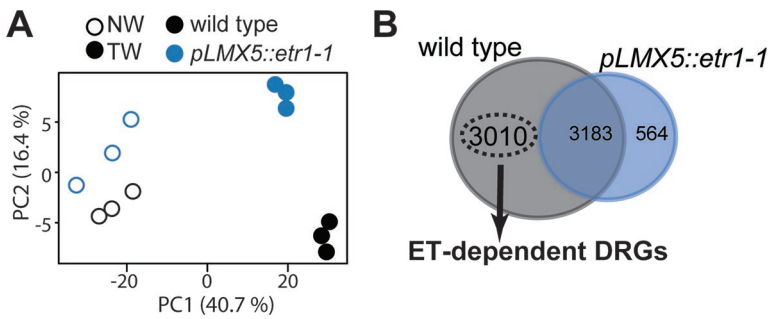

FIGURE 5 | Continued

in cross sections of leaned trees. The TW : OW ratio was significantly reduced in ETI trees (**Figure 1C**), confirming previous observations of reduced asymmetric growth in this genotype (Love et al., 2009). Horizontally inclined wild-type trees displayed a dramatic and expected decrease in vessel density on the TW side compared with the OW side after 4 weeks (**Figure 1E**). Compared with wild-type trees, the ETI trees had a higher vessel density in both TW (increase of

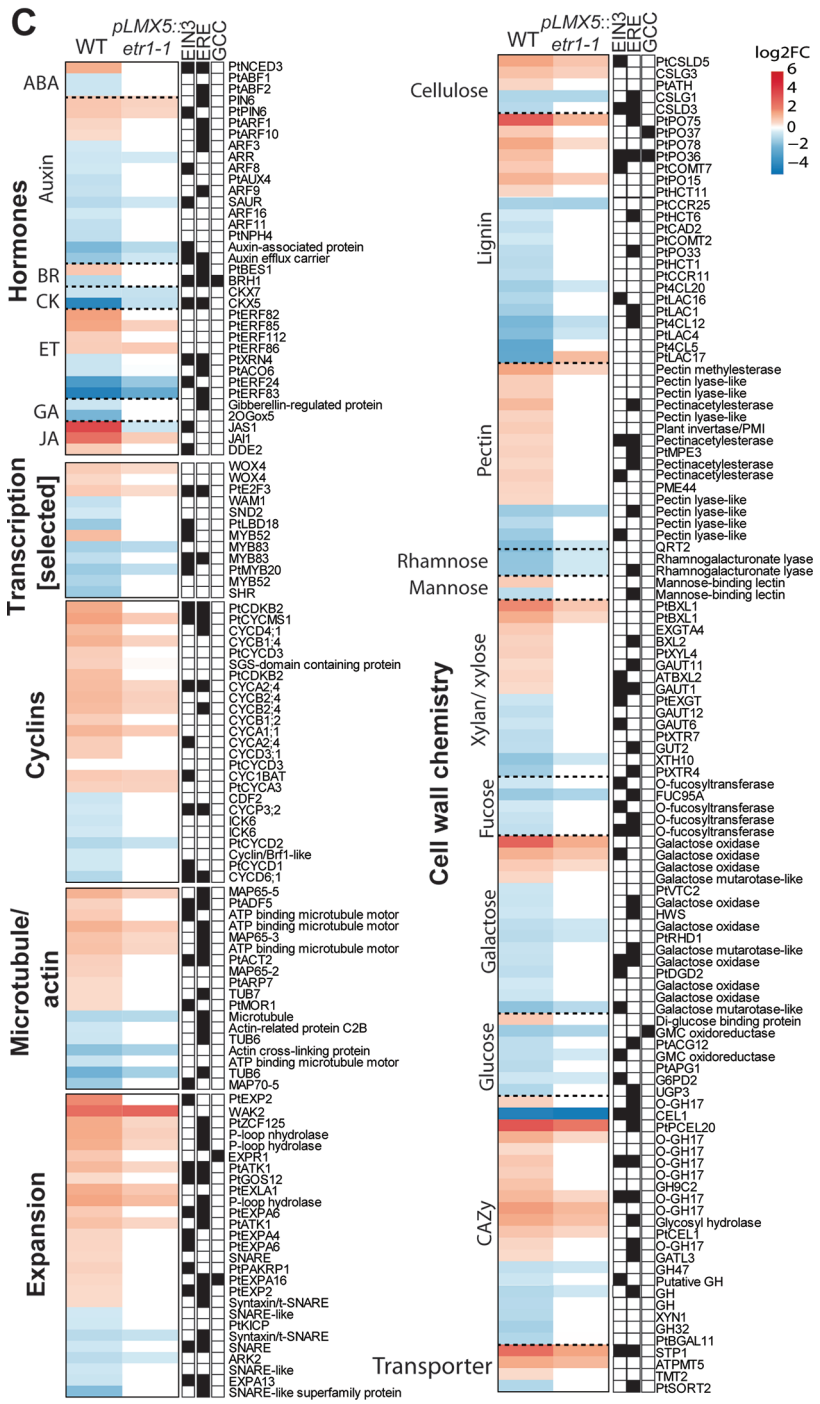

FIGURE 5 | Transcriptome analysis between wild-type (WT) and ETI (*pLMX5::etr1-1*) hybrid aspen trees identifies ethylene-downstream genes with potential roles in TW formation. **(A)** PCA of transcriptome data. PC1 explains 41% of the variation and refers to the difference in NW and TW data. PC2 (16%) separates the TW transcriptomes of the WT and *pLMX5::etr1-1*. Each of the three replicate samples per genotype and condition originates from a pool of xylem/phloem scrapings from three trees. ERE, ethylene-responsive element; ETI, ethylene insensitive; NW, normal wood; PCA, principal component analysis; TW, tension wood. **(B)** Venn diagram highlighting the number of differentially regulated genes (DRGs; $|\log2FC| \geq 0.5$ and pAdj <0.05) in NW-to-TW comparisons. DRGs that only showed a significant change in expression in WT, but not in *pLMX5::etr1-1*, are further called "ET-dependent" (**Supplementary Tables S1–S3**). **(C)** Heat map showing expression changes (log2FC) of ET-dependent DRGs in TW compared with NW (**Supplementary Table S5**). Red indicates induction and blue suppression of gene expression in TW as compared with NW. White indicates absence of significant change in gene expression between TW and NW. Genes depicted in the heat map function in transcriptional regulation of cell division, xylem differentiation, and secondary cell wall biosynthesis; phytohormone signaling; microtubule and actin organization; and cell expansion and cell wall chemistry. Black boxes next to each gene indicate the presence of the ERE, TEIL-motif, and/or the GCC-box in its promoter region (**Supplementary Table S7**). ABA, abscisic acid; BR, brassinosteroid; CK, cytokinin; ET, ethylene; GA, gibberellins; JA, jasmonic acid.

133%) and OW (increase of 30%) but not in NW (**Figures 1D, E**, **Supplementary Figure S3**). Strikingly, ETI trees presented G-fibers with no obvious anatomical difference compared with wild-type G-fibers, despite their reduced capacity to lift and the commonly held view of G-fiber involvement in generating the mechanical strain needed to uplift the stem (Mellerowicz and Gorshkova, 2012). Taken together, ETI trees showed decreased asymmetric growth, higher vessel density in both TW and OW, and a reduced uplifting response after inclination than did wild type, indicating that ET signaling is required for many characteristic features of the TW response, but not necessarily G-fiber formation.

S-Layers in G-Fibers of Ethylene-Insensitive Trees Have an Altered Cellulose Microfibril Angle and Chemical Composition

With the aim to reveal potential causes of the attenuated uplifting response despite the presence of G-fibers in ETI TW, we inspected the cellulose MFA and chemical composition of the secondary cell wall more closely. When measuring MFA in TW of six wild-type and ETI trees that were each inclined to 45° and fixed in this position for 22 days, we observed in both genotypes the bimodal MFA distribution typical for TW and originating from small (0–5°) G-layer MFAs and larger (20–40°) S-layer MFAs (Müller et al., 2006; Goswami et al., 2008; Rüggeberg et al., 2013). This was expected as both genotypes formed S2- and G-layers (**Figure 1E**). There was no significant difference in average G-layer MFAs between the genotypes (**Figure 2**). However, the average S2-layer MFAs in ETI trees were significantly lower than those in wild-type trees (36.7 ± 2.2° for ETI trees and 41.2 ± 4° for wild-type trees).

We furthermore assessed whether G-fiber-rich TW areas were chemically altered, in cross sections of ETI and wild-type trees using FT-IR microspectroscopy with a single-element detector. PCA performed on these spectra did not show clear grouping (**Supplementary Figure S4**), indicating that the overall chemical composition of the sampled areas is not altered. As unaltered cells/cell wall layers can mask subtle changes confined to small zones/specific layers, we used Raman microspectroscopy with high lateral resolution to specifically focus on the chemical information from G- and S-layers in wild-type and ETI trees. While analyzing data from spectral maps scanned over three adjacent fiber cells with 1-µm step size in TW and NW of both genotypes, four chemically different zones were assigned based on spectral information that overlapped with cell layers visible in the sections: (1) cellulose rich G-layer, (2) cellulose- and lignin-containing S-layer, (3) lignin-rich zone including both the S-layer and the middle lamella (hereafter called S + ML), and (4) lumen (**Figures 3A–D**, **Supplementary Figures S1, S2**). Comparison of NW S-layer spectra between wild-type and ETI trees or NW S + ML layer spectra between wild-type and ETI trees by PCA did not reveal any clear grouping and thereby ruled out any genotype-related chemical differences at the start of the leaning experiment (**Supplementary Figure S5**). PCA of non-lumen spectra from TW and NW from both genotypes revealed clear groupings of TW and NW samples (**Figure 3E**) as well as between the respective cell wall layers. This suggests that TW is chemically different from NW not only by the addition of the G-layer to fibers but also by a chemical alteration of the S-layer itself. The respective OPLS-DA models for TW G-layer and TW S-layer spectra of both genotypes indicated a chemical difference in both layers between wild-type and ETI trees (**Figures 4A, B**). The corresponding correlation-scaled loadings revealed a limited number of distinct bands that contribute to the difference in the G-layer (**Figure 4C**), a higher proportion of –C═O double-bond vibrations in the ETI G-layer (1,730 cm^{-1}, not related to cellulose), together with a lower proportion of –C–H vibrations (1,376 cm^{-1}, typically assigned to cellulose based on Gierlinger and Schwanninger, 2006). The correlation-scaled loadings for S-layers in G-fibers revealed more variables contributing to the differences between wild-type and ETI trees (**Figure 4D**). The S-layer spectra in ETI G-fibers had, in addition to bands already marked in the G-layer loadings in **Figure 4C**, a lower proportion of lignin-associated vibrations (1,616 and 1,660 cm^{-1}) and a higher contribution of bands associated with polysaccharidic compounds (carbohydrate ring-associated vibrations around 1,100 cm^{-1}). Taken together, Raman microspectroscopy was able to identify chemical differences among S- and G-layers of wild-type compared with ETI TW, with a clearer difference in the S-layers of G-fibers, as compared with their G-layers. This is in line with results from X-ray diffraction that also revealed a stronger effect on the S-layer ultrastructure of the G-fibers as compared with the G-layers themselves in ETI trees.

Ethylene Signaling Suppresses Lignin Biosynthesis Genes and Induces Expression of Microtubule and Actin-Related Genes in Tension Wood

To understand the impact of ET signaling on transcriptional reprogramming during TW formation, we compared transcriptomes from TW (trees inclined to and fixed at 45° for 22 days) and NW (upright trees) forming tissues in wild-type and ETI trees (**Figure 5**). PCA suggested that the predominant difference between the obtained transcriptomes (describing 41% of variation in the data set) is explained by the tissue type (NW or TW) (**Figure 5A**). The second component (describing approximately 16% of the overall variation in the data set) separated transcriptomes based on the genotypic background. The separation between wild-type and ETI trees was seen for both TW and NW transcriptomes. We next selected genes with significantly changed expression (DRGs, $|\log2FC| \geq 0.5$ and $pAdj < 0.05$) in TW compared with NW in both the wild-type and ETI trees (**Supplementary Tables S1, S2**). We detected 6,193 DRGs in wild type, while only 3,747 DRGs were identified in ETI trees (**Figure 5B**). We observed an almost equal distribution of induced and repressed genes in both genotypes (**Supplementary Figure S6A**). Expression of 3,010 DRGs, with close to equal numbers of induced and repressed ones, was significantly changed only in TW of wild-type trees (**Figure 5B**, **Supplementary Table S3**). Loss of transcriptional regulation

of these genes in the ETI trees implicates that their expression requires functional ethylene signaling. We therefore defined these genes as "ET-dependent genes." GO term analysis of the ET-dependent genes revealed an enrichment of genes related to ribosomes and translation (**Supplementary Table S4**). Functional characterization of the ET-dependent genes identified several TFs with known functions in xylem differentiation and gene networks related to hormone pathways, cell expansion, cytoskeleton organization, and cell wall chemistry (**Figure 5C**, **Supplementary Table S5**). To investigate a potential direct transcriptional regulation of these ET-dependent genes by TF families that function downstream of the ET receptors, we screened promoter regions of ET-dependent genes (2,000-bp upstream of the start codon) for the presence of the ERE, EIN3 (TEIL)- and ERF (GCC-box)-binding motifs (**Figure 5C**, **Supplementary Table S6**). The vast majority of the selected ET-dependent genes with a function in wood development, anatomy, or chemistry contained the ERE motif (90 genes), the TEIL motif (66 genes), and/or a GCC-box (six genes) in their promoter region. Approximately 37% (101 genes) of the 234 ET-dependent genes that were selected based on their association with hormone pathways, cell expansion, cytoskeleton organization, cell wall chemistry, or transcriptional regulation during wood formation did not contain any motif.

We detected 35 hormone-related genes among the ET-dependent DRGs, with the largest group of them (15 genes) being related to auxin transport and signaling (**Figure 5C**). The ET-dependent genes suggested that ET signaling stimulates induction of abscisic acid (e.g., *9-CIS-EPOXYCAROTENOID DIOXYGENASE* (*PtNCED*)) and jasmonic acid (e.g., *DELAYED DEHISCENCE 2* (*DDE2*) biosynthesizes genes and suppresses genes involved in ET biosynthesis (e.g., *PtACO6*) and degradation of cytokinins (e.g., *CYTOKININ OXIDASE*s (*CKX*s)). We also identified genes involved in signaling of auxin (e.g., *AUXIN RESPONSE FACTOR*s (*ARF*s)), brassinosteroids (e.g., *BRI1-EMS-SUPPRESSOR 1* (*BES1*)), and gibberellins (GAs) (e.g., *A-STIMULATED IN ARABIDOPSIS 14* (*GASA14*)). We evaluated the effect of overexpression of *Atetr1-1* on the expression of genes related to the ET pathway (**Supplementary Figure S6B**). Whereas TW formation resulted in differential expression of ET biosynthesis genes (*PtSAM*s, *PtACO*s, and *PtACS*) regardless of ET insensitivity, differential expression of many ET downstream genes (mainly TFs like *PtEIN3* and various *PtERF*s) was absent or attenuated in ETI trees during TW formation. We further found that wild type, but not ETI trees, showed induced expression of genes involved in cell division (*WOX4* (*WUSCHEL RELATED HOMEOBOX 4*), *E2F3* (*E2F TRANSCRIPTION FACTOR 3*), and *CYCLIN*s), actin and microtubule organization (e.g., *MICROTUBULE-ASSOCIATED PROTEINS* (*MAP*s)), and cell expansion (e.g., *EXPANSIN*s) in TW (**Figure 5C**; **Supplementary Figure S6D**). The ET-dependent genes also included two key TFs for xylem fiber differentiation and vascular patterning, *SND2* (*SECONDARY WALL-ASSOCIATED NAC DOMAIN PROTEIN 2*) and *SHR* (*SHORT ROOT*). These TFs were suppressed in TW of wild-type trees, while no change in expression was observed in ETI trees. In line with the observed lower amount of vessels in TW of wild-type trees (**Figure 1D**), we observed during TW formation in wild-type trees a slight repression of two *Populus* homologs (*PtVND7.1* and *PtVND7.2*) of the master regulator of vessel formation *VASCULAR-RELATED NAC-domain 7* (*VND7*) (although statistically not significant, **Supplementary Figure S6C**). During TW formation in ETI trees, no transcript change was observed for *PtVND7.2* but a slight, but not statistically significant, induction of *PtVND7.1*. Statistically significant ET-mediated suppression of genes involved also genes in the lignin pathway (e.g., *MY52*, *MYB83*, *CAFFEATE O-METHYLTRANSFERASE2* (*PtCOMT2*), and *CINNAMYL ALCOHOL DEHYDROGENASE* (*PtCAD2*)) (**Figure 5C**), whereas no phenylalanine ammonia lyase (PAL)-encoding genes that act upstream during lignin biosynthesis were among our target genes. qPCR results validated that ETI trees lost regulation of genes involved in lignin biosynthesis such as *PtCOMT2* during TW formation (**Supplementary Figure S6D**). The ET-dependent genes also comprised genes encoding cellulose synthases (e.g., *PtCSLD5*), pectin lyases/acetyltransferase/methylesterases (e.g., *PME44*), CAZymes (e.g., *CELLULASE1*), and sugar transporters (e.g., *SUGAR TRANSPORTER1* (*STP1*)). Despite the large impact of ET on gene regulation in TW, only two G-layer-associated fasciclin-like arabinogalactan (*FLA*) genes (Lafarguette et al., 2004; Kaku et al., 2009) were found among the ET-dependent genes (*FLA1* and *AGP14*, **Supplementary Table S3**), which is in line with the presence of a G-layer even in ETI trees (**Figure 1E**).

This analysis of ET-dependent genes suggests that ET signaling triggers expression of genes underlying cell division and expansion and suppresses genes involved in vessel differentiation and biosynthesis and polymerization of lignin. A part of these genes may be directly regulated by TFs of the ET signaling cascade as indicated by the presence of GCC-box, TEIL, or ERE motifs in the promoters of these genes.

DISCUSSION

Understanding the mechanisms by which trees sense displacement and react to correct their stem position through TW formation is a long-standing question. A role for phytohormones, such as GAs, auxin, and ET, has been discussed in this context (Andersson-Gunnerås et al., 2003; Love et al., 2009; Nugroho et al., 2012; Gerttula et al., 2015), but the significance of ET signaling remains unclear. In this study, we report on the importance of signaling by the phytohormone ET for both TW formation and functionality. ET signaling is often induced in response to environmental stimuli such as abiotic and biotic stresses (Dubois et al., 2018). In the absence of any stress signals, such as during upright growth in greenhouse conditions, ETI trees are similar to wild-type trees and do not show any obvious growth defects (Love et al., 2009). Therefore, these trees are ideally suited to study the role of ET signaling during an induced stress like displacement. Our data indicate that loss of ET signaling in ETI trees restricts the lifting response of inclined stems (**Figure 1**) and interferes with most developmental responses that are characteristic for TW, but not the formation of G-layers. Stem eccentricity observed in TW is the result of enhanced cambial growth at the upper side of the leaning stem (Ruelle et al., 2006; Ruelle, 2014).

Stimulation of xylem growth on the TW side was attenuated in ETI trees during tilting resulting in a lower TW : OW ratio than in wild-type trees. The concept that the reduced TW : OW ratio results from reduced cambial cell division in ETI TW (**Figure 1C**) is supported on a molecular level by the attenuated reprogramming of cell cycle regulators, such as *CYCD3* and *E2F3* in ETI trees during TW formation (Kosugi and Ohashi, 2002), as well as regulators of cambial cell division activity like *WOX4* (Hirakawa et al., 2010; Ji et al., 2010; Suer et al., 2011; Kucukoglu et al., 2017; Shi et al., 2019; **Figure 5C**). *WOX4* expression is controlled by auxin signaling. Auxin forms a gradient over the cambium in the stem and is known to function as a positional signal and to positively influence cambial growth (Tuominen et al., 1997; Uggla et al., 1998; Smetana et al., 2019). Conversely, inhibiting auxin signaling in stems of transgenic trees negatively impacts (in addition to primary also) secondary growth (Nilsson et al., 1992). We identified several genes related to auxin transport and signaling (e.g., *PIN6* and *ARF*s) among the ET-dependent DRGs in our study (**Figure 5C**), which is in line with previous reports that showed that ET influences both auxin biosynthesis and transport (Swarup et al., 2007; Muday et al., 2012; Vaseva et al., 2018). Based on these results, it is possible that the reduced stimulation of cambial growth observed in ETI TW is explained through ET–auxin crosstalk. ETI TW showed a reduced amount of G-fibers than did wild-type TW, due to the mentioned reduced cambial stimulation and as a result of lower fiber-to-vessel ratio because of reduced suppression of vessel formation (**Figure 1C**; Love et al., 2009). Reduced vessel frequency is observed in many other species during TW formation (Yoshizawa et al., 2000; Jourez et al., 2001; Ruelle et al., 2006; Sultana et al., 2010). Results from yeast one-hybrid assays identified the cell-cycle regulator E2Fc as a regulator of transcriptional gene networks for secondary cell wall formation in *Arabidopsis*. E2Fc can directly bind to promoter regions of NAC TFs involved in vessel differentiation, namely, *VND6* and *VND7* (Taylor-Teeples et al., 2015). Only TW of wild-type trees showed induction of a *Populus E2F* homolog (*E2F3*) and a slight, yet not statistically significant, suppression of *PtVND7.1* and *PtVND7.2*, while such expression changes were not observed in ETI trees (**Figure 5C**, **Supplementary Figure S6C**, **Supplementary Tables S3, S7**). Furthermore, *PtLBD18* (*LATERAL ORGAN BOUNDARIES DOMAIN 18*), a homolog of *AtLBD18*, which has been shown to regulate expression of *AtVND7* (Soyano et al., 2008), was among the ET-dependent genes. The EIN3-binding motif is present in promoters of *Populus E2F3*, *LBD18*, and *VND7*, suggesting that expression of these genes might be under the direct control of EIN3 during TW formation (**Figure 6**). Furthermore, ET–auxin interaction might also contribute to the changes in vessel formation. Auxin, when exogenously applied, suppresses expression of *NAC*s involved in fiber differentiation and stimulates expression of *NAC*s involved in vessel formation in hybrid aspen stems (Johnsson et al., 2018). Expression of several genes involved in auxin signaling was regulated by ET in TW (**Figure 5C**), some of them harboring TEIL or ERE motifs in their promoters (e.g., *PtPIN6*, *PtARF1*, and *PtARF10*). Therefore, in addition to a direct effect of ET on *NAC* expression and vessel density, a potential regulation of vessel differentiation through *NAC* regulation *via* ET–auxin crosstalk is also plausible. The absence of repression of *E2F3* and *VND7* in ETI TW could also contribute to the reduced suppression of vessel development during TW formation in ETI trees. The reduction of vessel elements in TW of wild-type trees as compared with NW likely causes an absolute decrease of lignin levels on tissue level, because lignin content in vessel cell walls is generally higher as compared with the one in fiber S2 walls (Saka and Goring, 2009; Xu et al., 2005). As less of the highly lignified vessels are formed in wild-type TW compared with NW, the lignin biosynthesis machinery is expected to be downregulated. During formation of TW in ETI trees, the absence of vessel suppression goes in line with an absence of downregulation of genes involved in lignin biosynthesis as observed in our data (**Figure 5C**). An effect of ET signaling and regulation of lignification has previously been demonstrated in experiments where lignification of tracheary elements (TEs) in cell culture was blocked by inhibiting ET signaling (Pesquet et al., 2013). For a few of the ET-dependent lignin biosynthesis genes from our data set, we identified the EIN3, GCC-box, or ERE-motif in their promoters, suggesting a direct regulation of their expression by TFs in the ET pathway (**Figures 5C** and **6**).

We previously reported that exogenously enhancing ET signaling was sufficient to induce the G-layer formation in hybrid aspen in an ET signaling-dependent manner (Felten et al., 2018). Unexpectedly, in the present study, we observed that G-fibers with G-layers could form during TW formation in ETI trees (**Figure 1E**), despite inhibited ET signaling, with no altered ultrastructure in the G-layer (**Figure 2**) and no dramatic changes in gene expression typically associated with G-layer presence, such as induction of *FLA*s (**Supplementary Table S2**). This is, to a large extent, similar to what has been found with GAs. Although it remains to be shown that GA biosynthesis is altered during tilting, exogenously applied GAs can induce G-fiber formation and xylem growth (Jiang et al., 1998; Jiang et al., 2008; Nugroho et al., 2012). Conversely, inhibition of GA signaling counteracts stem bending and lifting and lowers eccentric growth in displaced stems, despite G-fibers being formed (Jiang et al., 1998; Jiang et al., 2008; Nugroho et al., 2012). This suggests that both GA and ET signaling can induce G-fiber formation but that inhibiting one of these pathways does not abolish G-fiber formation. We found very few GA-associated genes among the ET-dependent DRGs, suggesting that GA signaling is not impacted in ETI trees. It will be interesting to investigate whether a combination of both ET and GA signaling inhibition can fully inhibit the G-layer formation during stem tilting and whether these phytohormone pathways can compensate for each other's absence. The present study also confirms what was observed with exogenous ACC/ET application experiments (Felten et al., 2018), that the effect of ET signaling on vessel and the G-layer formation is uncoupled and must therefore occur as independent routes downstream of ET signaling.

Even though G-fiber formation as such was not inhibited during TW formation in ETI trees, we observed ultrastructural and chemical alteration of G-fiber S-layers in ETI TW

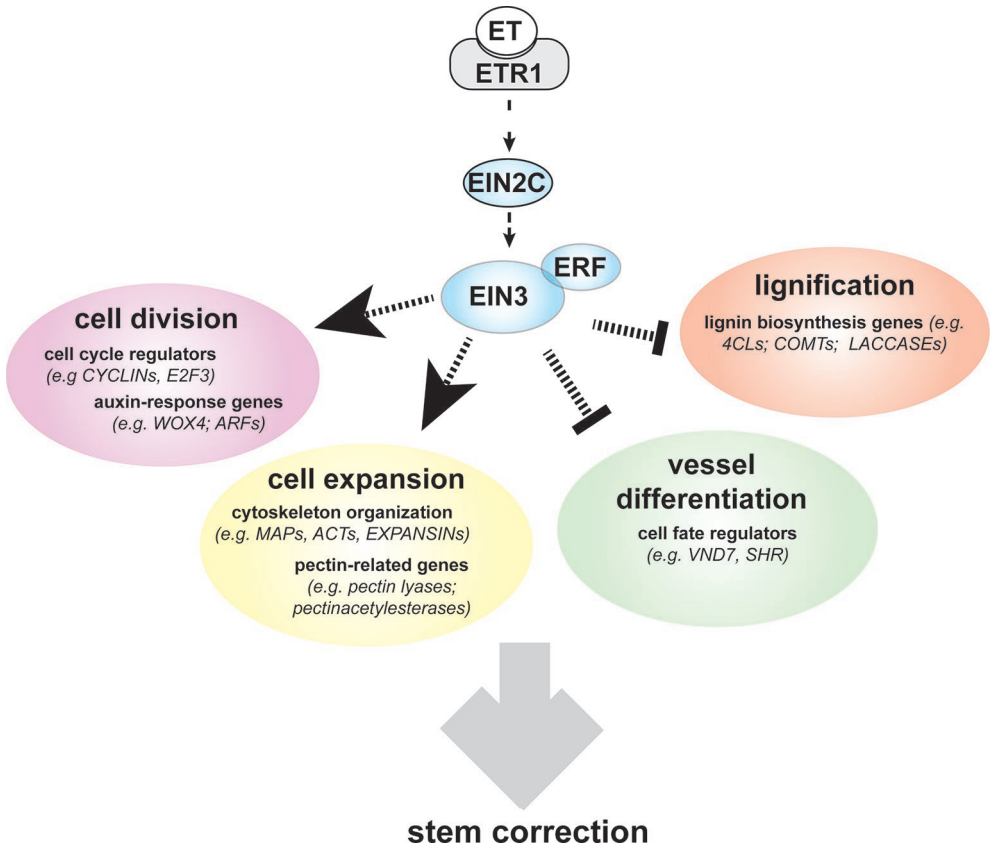

FIGURE 6 | Model showing ethylene-regulated pathways that potentially induce anatomical, ultrastructural, and chemical modifications of xylem cells during TW formation. Ethylene stimulates cell division during TW formation possibly by EIN3 binding to the promoter of *PtE2F3*, by induction of *PtWOX4* through ethylene–auxin interaction and by direct or indirect induction of *PtCYCLIN*s. Ethylene suppresses vessel formation and lignification (likely because of the decreased amounts of highly lignified vessels) during TW formation. Vessel suppression might be mediated by *PtVND7* repression, through PtE2F3, and repression of *SHR*, potentially through ethylene–auxin interaction. Suppression of lignin biosynthesis is likely a result of a combination of a direct gene regulation of lignin genes with ERE, TEIL, and GCC-boxes in their promoter, as well as a secondary effect resulting from suppression of vessel differentiation. During TW formation, ethylene alters gene expression related to cell wall expansion, such as expansins *PtEXP*s, *PtMAP*s, and pectin-related genes. Expansin induction goes in line with enhanced primary wall formation due to enhanced cambial activity and cell proliferation during TW formation. *PtMAP*s could influence the cytoskeleton and subsequently cellulose microfibril angles. Direct regulation through EIN3 and ERFs can be assumed for *EXPANSIN*s harboring TEIL and GCC-boxes in their promoter as well as indirect effects through ethylene–auxin interaction. TW, tension wood.

(**Figures 2**–**4**). The significantly lower MFA of the S2 layer in ETI TW suggests a role of ET in modification of secondary cell wall MFA in TW. G-layers had, however, no alternated MFA in ETI TW. Using Raman microspectroscopy, we observed chemical alterations in both the G- and S-layers of G-fibers as a result of ET insensitivity (**Figure 4**). Our spectroscopic data suggest differences both in the relative proportions of major cell wall polymers and in the structure of the polymers such as changes in cellulose crystallinity or a difference in cross-linking of polymers. It is possible that the chemical differences identified originate either from the layers itself or from a shift in clustering related to the composition of layer boundaries (e.g., the boundary of S- and G-layers). Gradients across the G-layer in both the polymer composition and the cellulose ultrastructure have been observed (Prodhan et al., 1995; Joseleau et al., 2004; Gierlinger and Schwanninger, 2006; Arend, 2008; Sandquist et al., 2010; Ruelle, 2014). At the S-G-layer interface, an accumulation of xyloglucan and rhamnogalacturonan has been detected (Sandquist et al., 2010) and linked to the mechanisms required for stress generation in G-fibers (Nishikubo et al., 2007; Mellerowicz and Gorshkova, 2012). As such boundaries and gradients are narrower than what can be resolved in a separate class by the Raman microspectroscopy, their chemical composition will influence the cluster that they are included in by *k*-means clustering. If the composition of this boundary was altered in ETI TW, the pixels comprising them may chemically become more similar to another neighboring layer (S instead of G) and therefore be included in that latter cluster. In conclusion, the chemical differences detected in the ETI G-fiber S-layer (lower lignin and higher polysaccharide contribution) could result either from a chemical alteration within the layer or from a higher proportion of S–G-boundary pixels, low in lignin and high in hemicellulose, included in the cluster of this layer. This is, to our knowledge, the first report that shows that ET can interfere with both the cellulose ultrastructure and the chemical composition of the secondary cell wall.

In summary, we have detected both ET-dependent quantitative (G-fiber number) and qualitative (G-fiber properties) aspects that could contribute to the observed attenuated uplifting in ETI plants. The G-layer itself does not seem to be a prerequisite for high tensile stress generation in TW, since other cell wall layer arrangements leading to a low cellulose MFA in the main cell wall layer can also induce the tensile stress required for stem lifting (Okuyama et al., 1994; Yoshizawa et al., 2000; Ruelle et al., 2007a; Ruelle et al., 2007b). However, in species containing a G-layer, there is a relationship between its thickness, its cellulose MFA, and the potential growth strain exerted (Fang et al., 2008; Goswami et al., 2008). Typically, in TW of *Populus*, the MFA in the S-layer is much larger than in NW, while the G-layer inherits an MFA close to 0° (Timell, 1986; Lautner et al., 2012). It has been hypothesized that the interplay between the G-layer and the S2-layer with its high MFA facilitates generation of the tensile stress upon swelling, required to correct the stem position through uplifting (Goswami et al., 2008). G-layer swelling leads to a pressure on the surrounding cell walls that is translated into axial stress. According to a model by Goswami et al. (2008), this stress enhancement factor depends on the orientation of the MFAs in the S2 layer. The MFA alteration observed in our study for the S2-layer of ETI TW is within the range of stress enhancement factors leading to a sufficient axial stress for uplifting and lies in a range of MFAs also observed in TW of other wild-type trees with G-fibers. Taken together, as the G-layer MFA is not altered in ETI TW and the S-layer MFA is not altered to an extent that would limit the uplifting response according to the model proposed by Goswami et al. (2008), the origin of inhibited lifting observed in ETI trees (**Figure 1**) can not only be attributed to altered MFA angles. Other authors have observed a correlation between the stem bending response and the amount of G-fibers formed (Nugroho et al., 2012). This indicates that there is both qualitative and quantitative effects of G-layers/G-fibers on the potential of stem reorientation. Given the rather low changes in qualitative G-fiber properties in ETI TW in comparison with the large effect on G-fiber quantity, we propose that it is rather the latter that is decisive for the reduced uplifting response, even though we cannot exclude that G-fiber amounts and S-layer chemistry and ultrastructure in ETI G-fibers have additive effects.

Taken together, the results presented here demonstrate the importance of ET signaling to define TW characteristics and to correct stem position after tilting. We also revealed key genes that potentially can coordinate these responses downstream of ET signaling during TW formation (**Figure 6**).

DATA AVAILABILITY

The raw sequencing data for this study can be found in the European Nucleotide Archive (ENA) under accession PRJEB32252.

AUTHOR CONTRIBUTIONS

CS performed transcriptomic analysis. BW performed and analyzed uplifting experiments. AG performed FT-IR and Raman microspectroscopic measurements and data analysis. JL supplied biological material for FT-IR measurements. MR carried out cellulose MFA measurements. ND gave support for transcriptomics analysis. TV and BW performed vessel density quantification. KA developed software for data analysis of uplifting experiments. BS and JF conceived the study. JF, BS, and HT supervised the experiments. JF generated biological material for the experiments. CS and JF wrote the manuscript with contribution of all authors.

FUNDING

The experiments as well as BW, JWL, and JF were funded by the Swedish Research Council Formas (grant nos. 213-2011-1148 and 239-2011-1915) and the Swedish Foundation for Strategic Research (grant no. RBP14-0011). CS was funded by The Kempe Foundation (SMK-1649 and SMK-1533) and the Lily och Sven Lawskis fund. Experimentation was financially supported also by the Swedish Governmental Agency for Innovation Systems Vinnova (grant no. 2016-00504) and the Knut and Alice Wallenberg Foundations (grant no. 2016-0341).

ACKNOWLEDGMENTS

We thank the students of the Design Build Test course 2016 at Umeå University (Carolina Eriksson, Karolina Eriksson, Oskar Hallberg, Alexander Lindström, and Johan Lundberg) for developing the imaging tools to record and measure tree uplifting. The support of the Chemical Biological Centre and the Department of Chemistry, Umeå University, Sweden, for the Vibrational Spectroscopy Core Facility is gratefully acknowledged. We would also like to acknowledge support from Science for Life Laboratory, the National Genomics Infrastructure funded by the Swedish Research Council, and Uppsala Multidisciplinary Center for Advanced Computational Science for assistance with massively parallel sequencing and access to the UPPMAX computational infrastructure. MR would like to thank Stephan Siegel and Chenghao Li for the support with the X-ray powder diffraction (XRD) measurements at BESSY II.

SUPPLEMENTARY MATERIAL

The Supplementary Material for this article can be found online at: https://www.frontiersin.org/articles/10.3389/fpls.2019.01101/full#supplementary-material

SUPPLEMENTARY VIDEO S1 | Time-lapse video of the uplifting response of one representative pLMX5::etr1-1 and one representative wild type hybrid aspen tree imaged over the first 21 days of the experiment.

REFERENCES

Anders, S., Pyl, P. T., and Huber, W. (2015). HTSeq—a Python framework to work with high-throughput sequencing data. *Bioinformatics* 31, 166–169. doi: 10.1093/bioinformatics/btu638

Andersson-Gunnerås, S., Hellgren, J. M., Björklund, S., Regan, S., Moritz, T., and Sundberg, B. (2003). Asymmetric expression of a poplar ACC oxidase controls ethylene production during gravitational induction of tension wood. *Plant J.* 34, 339–349. doi: 10.1046/j.1365-313X.2003.01727.x

Andersson-Gunnerås, S., Mellerowicz, E. J., Love, J., Segerman, B., Ohmiya, Y., Coutinho, P. M., et al. (2006). Biosynthesis of cellulose-enriched tension wood in Populus: global analysis of transcripts and metabolites identifies biochemical and developmental regulators in secondary wall biosynthesis. *Plant J.* 45, 144–165. doi: 10.1111/j.1365-313X.2005.02584.x

Andrews, S. (2010). FastQC: a quality control tool for high throughput sequence data [Preprint]. Available online at: http://www.bioinformatics.babraham.ac.uk/projects/fastqc (Accessed August 26, 2019).

Arend, M. (2008). Immunolocalization of (1,4)-β-galactan in tension wood fibers of poplar. *Tree Physiol.* 28, 1263–1267. doi: 10.1093/treephys/28.8.1263

Bleecker, A. B., Estelle, M. A., Somerville, C., and Kende, H. (1988). Insensitivity to ethylene conferred by a dominant mutation in Arabidopsis thaliana. *Science* 241, 1086–1089. doi: 10.1126/science.241.4869.1086

Bolger, A. M., Lohse, M., and Usadel, B. (2014). Trimmomatic: a flexible trimmer for Illumina sequence data. *Bioinformatics* 30, 2114–2120. doi: 10.1093/bioinformatics/btu170

Cancel, J. D., and Larsen, P. B. (2002). Loss-of-function mutations in the ethylene receptor ETR1 cause enhanced sensitivity and exaggerated response to ethylene in Arabidopsis. *Plant Physiol.* 129, 1557–1567. doi: 10.1104/pp.003780

Chang, S., Puryear, J., and Cairney, J. (1993). A simple and efficient method for isolating RNA from pine trees. *Plant Mol. Biol. Rep.* 11, 113–116. doi: 10.1007/BF02670468

Chang, S. S., Clair, B., Ruelle, J., Beauchene, J., Di Renzo, F., Quignard, F., et al. (2009). Mesoporosity as a new parameter for understanding tension stress generation in trees. *J. Exp. Bot.* 60, 3023–3030. doi: 10.1093/jxb/erp133

Chang, K. N., Zhong, S., Weirauch, M. T., Hon, G., Pelizzola, M., Li, H., et al. (2013). Temporal transcriptional response to ethylene gas drives growth hormone cross-regulation in Arabidopsis. *eLife* 2, e00675. doi: 10.7554/eLife.00675

Chen, J., Chen, B., and Zhang, D. (2015). Transcript profiling of Populus tomentosa genes in normal, tension, and opposite wood by RNA-seq. *BMC Genomics* 16, 164. doi: 10.1186/s12864-015-1390-y

Clair, B., Gril, J., Di Renzo, F., Yamamoto, H., and Quignard, F. (2008). Characterization of a gel in the cell wall to elucidate the paradoxical shrinkage of tension wood. *Biomacromolecules* 9, 494–498. doi: 10.1021/bm700987q

Delhomme, N., Mähler, N., Schiffthaler, B., Sundell, D., Hvidsten, T. R., and Street, N. R. (2014). Guidelines for RNA-Seq data analysis 24 [Preprint]. Available at: https://www.epigenesys.eu/en/protocols/bio-informatics/1283-guidelines-for-rna-seq-data-analysis (Accessed August 26, 2019).

Dubois, M., Van den Broeck, L., and Inzé, D. (2018). The pivotal role of ethylene in plant growth. *Trends Plant Sci.* 23, 311–323. doi: 10.1016/j.tplants.2018.01.003

Esau, K. (1977). *Anatomy of seed plants*. New York: Wiley.

Eilers, P. H. C. (2004). Parametric time warping. *Anal. Chem.* 76, 404–411. doi: 10.1021/ac034800e

Fang, C.-H., Clair, B., Gril, J., and Liu, S.-Q. (2008). Growth stresses are highly controlled by the amount of G-layer in poplar tension wood. *IAWA J.* 29 , 237–246. doi: 10.1163/22941932-90000183

Felten, J., and Sundberg, B. (2013). "Biology, chemistry and structure of tension wood," in *Cellular aspects of wood formation plant cell monographs*. Ed. J. Fromm (Berlin, Heidelberg: Springer Berlin Heidelberg), 203–224. doi: 10.1007/978-3-642-36491-4_8

Felten, J., Hall, H., Jaumot, J., Tauler, R., de Juan, A., and Gorzsás, X. X. X. A. (2015). Vibrational spectroscopic image analysis of biological material using multivariate curve resolution-alternating least squares (MCR-ALS). *Nat. Protoc.* 10 (2), 217–240. doi: 10.1038/nprot.2015.008

Felten, J., Vahala, J., Love, J., Gorzsás, A., Rüggeberg, M., Delhomme, N., et al. (2018). Ethylene signaling induces gelatinous layers with typical features of tension wood in hybrid aspen. *New Phytol.* 218, 999–1014. doi: 10.1111/nph.15078

Gerttula, S., Zinkgraf, M., Muday, G. K., Lewis, D. R., Ibatullin, F. M., Brumer, H., et al. (2015). Transcriptional and hormonal regulation of gravitropism of woody stems in Populus. *Plant Cell* 27, 2800–2813. doi: 10.1105/tpc.15.00531

Gierlinger, N., and Schwanninger, M. (2006). Chemical imaging of poplar wood cell walls by confocal Raman microscopy. *Plant Physiol.* 140, 1246–1254. doi: 10.1104/pp.105.066993

Gorzsás, A., and Sundberg, B. (2014). Chemical fingerprinting of Arabidopsis using Fourier transform infrared (FT-IR) spectroscopic approaches. *Methods Mol. Biol.* 1062, 317–352. doi: 10.1007/978-1-62703-580-4_18

Goswami, L., Dunlop, J. W. C., Jungnikl, K., Eder, M., Gierlinger, N., Coutand, C., et al. (2008). Stress generation in the tension wood of poplar is based on the lateral swelling power of the G-layer. *Plant J.* 56, 531–538. doi: 10.1111/j.1365-313X.2008.03617.x

Gray-Mitsumune, M., Mellerowicz, E. J., Abe, H., Schrader, J., Winzéll, A., Sterky, F., et al. (2004). Expansins abundant in secondary xylem belong to subgroup A of the alpha-expansin gene family. *Plant Physiol.* 135, 1552–1564. doi: 10.1104/pp.104.039321

Hirakawa, Y., Kondo, Y., and Fukuda, H. (2010). TDIF peptide signaling regulates vascular stem cell proliferation via the WOX4 homeobox gene in Arabidopsis. *Plant Cell* 22, 2618–2629. doi: 10.1105/tpc.110.076083

Itzhaki, H., Maxson, J. M., and Woodson, W. R. (1994). An ethylene-responsive enhancer element is involved in the senescence-related expression of the carnation glutathione-S-transferase (GST1) gene. *Proc. Natl. Acad. Sci. U.S.A.* 91, 8925–8929. doi: 10.1073/pnas.91.19.8925

Ji, J., Strable, J., Shimizu, R., Koenig, D., Sinha, N., and Scanlon, M. J. (2010). WOX4 promotes procambial development. *Plant Physiol.* 152, 1346–1356. doi: 10.1104/pp.109.149641

Jiang, S., Furukawa, I., Honma, T., Mori, M., Nakamura, T., and Yamamoto, F. (1998). Effects of applied gibberellins and uniconazole-P on gravitropism and xylem formation in horizontally positioned Fraxinus mandshurica seedlings. *J. Wood Sci.* 44, 385–391. doi: 10.1007/BF01130452

Jiang, S., Xu, K., Wang, Y.-Z., Ren, Y.-P., and Gu, S. (2008). Role of GA3, GA4 and uniconazole-P in controlling gravitropism and tension wood formation in Fraxinus mandshurica Rupr. var. japonica Maxim. seedlings. *J. Integr. Plant Biol.* 50, 19–28. doi: 10.1111/j.1744-7909.2007.00552.x

Johnsson, C., Jin, X., Xue, W., Dubreuil, C., Lezhneva, L., and Fischer, U. (2018). The plant hormone auxin directs timing of xylem development by inhibition of secondary cell wall deposition through repression of secondary wall NAC-domain transcription factors. *Physiol. Plant.* 165, 673–689. doi: 10.1111/ppl.12766

Joseleau, J.-P., Imai, T., Kuroda, K., and Ruel, K. (2004). Detection in situ and characterization of lignin in the G-layer of tension wood fibres of Populus deltoids. *Planta* 219, 338–345. doi: 10.1007/s00425-004-1226-5

Jourez, B., Riboux, A., and Leclercq, A. (2001). Anatomical characteristics of tension wood and opposite wood in young inclined stems of poplar (Populus euramericana cv 'ghoy'). *IAWA J.* 22, 133–157. doi: 10.1163/22941932-90000274

Kaku, T., Serada, S., Baba, K., Tanaka, F., and Hayashi, T. (2009). Proteomic analysis of the G-layer in poplar tension wood. *J. Wood Sci.* 55, 250–257. doi: 10.1007/s10086-009-1032-6

Kopylova, E., Noé, L., and Touzet, H. (2012). SortMeRNA: fast and accurate filtering of ribosomal RNAs in metatranscriptomic data. *Bioinformatics* 28, 3211–3217. doi: 10.1093/bioinformatics/bts611

Kosugi, S., and Ohashi, Y. (2000). Cloning and DNA-binding properties of a tobacco Ethylene-Insensitive3 (EIN3) homolog. *Nucleic Acids Res.* 28, 960–967. doi: 10.1093/nar/28.4.960

Kosugi, S., and Ohashi, Y. (2002). E2F sites that can interact with E2F proteins cloned from rice are required for meristematic tissue-specific expression of rice and tobacco proliferating cell nuclear antigen promoters. *Plant J.* 29, 45–59. doi: 10.1046/j.1365-313x.2002.01196.x

Kucukoglu, M., Nilsson, J., Zheng, B., Chaabouni, S., and Nilsson, O. (2017). WUSCHEL-RELATED HOMEOBOX4 (WOX4)-like genes regulate cambial cell division activity and secondary growth in Populus trees. *New Phytol.* 215, 642–657. doi: 10.1111/nph.14631

Lafarguette, F., Leplé, J.-C., Déjardin, A., Laurans, F., Costa, G., Lesage-Descauses, M.-C., et al. (2004). Poplar genes encoding fasciclin-like arabinogalactan proteins are highly expressed in tension wood. *New Phytol.* 164, 107–121. doi: 10.1111/j.1469-8137.2004.01175.x

Lautner, S., Zollfrank, C., and Fromm, J. (2012). Microfibril angle distribution of poplar tension wood. *IAWA J.* 33, 431–439. doi: 10.1163/22941932-90000105

Li, W., Ma, M., Feng, Y., Li, H., Wang, Y., Ma, Y., et al. (2015). EIN2-directed translational regulation of ethylene signaling in Arabidopsis. *Cell* 163, 670–683. doi: 10.1016/j.cell.2015.09.037

Love, J., Björklund, S., Vahala, J., Hertzberg, M., Kangasjärvi, J., and Sundberg, B. (2009). Ethylene is an endogenous stimulator of cell division in the cambial meristem of Populus. *Proc. Natl. Acad. Sci. U.S.A.* 106, 5984–5989. doi: 10.1073/pnas.0811660106

Love, M. I., Huber, W., and Anders, S. (2014). Moderated estimation of fold change and dispersion for RNA-seq data with DESeq2. *Genome Biol.* 15, 550. doi: 10.1186/s13059-014-0550-8

Mellerowicz, E. J., and Gorshkova, T. A. (2012). Tensional stress generation in gelatinous fibres: a review and possible mechanism based on cell-wall structure and composition. *J. Exp. Bot.* 63, 551–565. doi: 10.1093/jxb/err339

Merchante, C., Alonso, J. M., and Stepanova, A. N. (2013). Ethylene signaling: simple ligand, complex regulation. *Curr. Opin. Plant Biol.* 16, 554–560. doi: 10.1016/j.pbi.2013.08.001

Merchante, C., Brumos, J., Yun, J., Hu, Q., Spencer, K. R., Enríquez, P., et al. (2015). Gene-specific translation regulation mediated by the hormone-signaling molecule EIN2. *Cell* 163, 684–697. doi: 10.1016/j.cell.2015.09.036

Muday, G. K., Rahman, A., and Binder, B. M. (2012). Auxin and ethylene: collaborators or competitors? *Trends Plant Sci.* 17, 181–195. doi: 10.1016/j.tplants.2012.02.001

Müller, M., Burghammer, M., and Sugiyama, J. (2006). Direct investigation of the structural properties of tension wood cellulose microfibrils using microbeam X-ray fibre diffraction. *Holzforschung* 60, 474–479. doi: 10.1515/HF.2006.078

Nilsson, O., Aldén, T., Sitbon, F., Anthony Little, C. H., Chalupa, V., Sandberg, G., et al. (1992). Spatial pattern of cauliflower mosaic virus 35S promoter-luciferase expression in transgenic hybrid aspen trees monitored by enzymatic assay and non-destructive imaging. *Transgenic Res.* 1, 209–220. doi: 10.1007/BF02524751

Nishikubo, N., Awano, T., Banasiak, A., Bourquin, V., Ibatullin, F., Funada, R., et al. (2007). Xyloglucan endo-transglycosylase (XET) functions in gelatinous layers of tension wood fibers in poplar—a glimpse into the mechanism of the balancing act of trees. *Plant Cell Physiol.* 48, 843–855. doi: 10.1093/pcp/pcm055

Norberg, P. H., and Meier, H. (1966). Physical and chemical properties of gelatinous layer in tension wood fibres of aspen (*Populus tremula L*). *Holzforschung* 20, 174–178. doi: 10.1515/hfsg.1966.20.6.174

Nugroho, W. D., Yamagishi, Y., Nakaba, S., Fukuhara, S., Begum, S., Marsoem, S. N., et al. (2012). Gibberellin is required for the formation of tension wood and stem gravitropism in Acacia mangium seedlings. *Ann Bot* 110, 887–895. doi: 10.1093/aob/mcs148

Ohme-Takagi, M., and Shinshi, H. (1995). Ethylene-inducible DNA binding proteins that interact with an ethylene-responsive element. *Plant Cell* 7, 173–182. doi: 10.1105/tpc.7.2.173

Okuyama, T., Yamamoto, H., Yoshida, M., Hattori, Y., and Archer, R. R. (1994). Growth stresses in tension wood: role of microfibrils and lignification. *Ann. For. Sci.* 51, 291–300. doi: 10.1051/forest:19940308

Paux, E., Carocha, V., Marques, C., Sousa, A. M., Borralho, N., Sivadon, P., et al. (2005). Transcript profiling of Eucalyptus xylem genes during tension wood formation. *New Phytol.* 167, 89–100. doi: 10.1111/j.1469-8137.2005.01396.x

Pesquet, E., Zhang, B., Gorzsás, A., Puhakainen, T., Serk, H., Escamez, S., et al. (2013). Non-cell-autonomous postmortem lignification of tracheary elements in Zinnia elegans. *Plant Cell* 25, 1314–1328. doi: 10.1105/tpc.113.110593

Pitre, F. E., Lafarguette, F., Boyle, B., Pavy, N., Caron, S., Dallaire, N., et al. (2010). High nitrogen fertilization and stem leaning have overlapping effects on wood formation in poplar but invoke largely distinct molecular pathways. *Tree Physiol.* 30, 1273–1289. doi: 10.1093/treephys/tpq073

Prodhan, A. K. M. A., Funada, R., Ohtani, J., Abe, H., and Fukazawa, K. (1995). Orientation of microfibrils and microtubules in developing tension-wood fibres of Japanese ash (Fraxinus mandshurica var. japonica). *Planta* 196, 577–585. doi: 10.1007/BF00203659

Qiao, H., Chang, K. N., Yazaki, J., and Ecker, J. R. (2009). Interplay between ethylene, ETP1/ETP2 F-box proteins, and degradation of EIN2 triggers ethylene responses in Arabidopsis. *Genes Dev.* 23, 512–521. doi: 10.1101/gad.1765709

R Core Team (2019). *R: a language and environment for statistical computing*. Vienna, Austria: R Foundation for Statistical. Computing. URL https://www.R-project.org/

Ruelle, J., Clair, B., Beauchêne, J., Prévost, M. F., and Fournier, M. (2006). Tension wood and opposite wood in 21 tropical rain forest species. *IAWA J.* 27, 341–376. doi: 10.1163/22941932-90000159

Ruelle, J., Yamamoto, H., and Thibaut, B. (2007a). Growth stresses and cellulose structural parameters in tension and normal wood from three tropical rainforest angiosperm species. *BioResources* 2, 235-251. doi: 10.15376/biores.2.2.235-251

Ruelle, J., Yoshida, M., Clair, B., and Thibaut, B. (2007b). Peculiar tension wood structure in Laetia procera (Poepp.) Eichl. (Flacourtiaceae). *Trees* 21, 345–355. doi: 10.1007/s00468-007-0128-0

Ruelle, J. (2014). "Morphology, anatomy and ultrastructure of reaction wood," in *The biology of reaction wood*. Eds. B. Gardiner, J. Barnett, P. Saranpää, and J. Gril (Berlin, Heidelberg: Springer-Verlag), 13–35. doi: 10.1007/978-3-642-10814-3_2

Rüggeberg, M., Saxe, F., Metzger, T. H., Sundberg, B., Fratzl, P., and Burgert, I. (2013). Enhanced cellulose orientation analysis in complex model plant tissues. *J. Struct. Biol.* 183, 419–428. doi: 10.1016/j.jsb.2013.07.001

Saka, S., and Goring, D. A. I. (2009). The distribution of lignin in white birch wood as determined by bromination with TEM-EDXA. *Holzforschung* 42, 149–153. doi: 10.1515/hfsg.1988.42.3.149

Sandquist, D., Filonova, L., Schantz, L., Ohlin, M., and Daniel, G. (2010). Microdistribution of xyloglucan in differentiating poplar cells. *BioResources* 5, 796-807–807.

Schurch, N. J., Schofield, P., Gierliński, M., Cole, C., Sherstnev, A., Singh, V., et al. (2016). How many biological replicates are needed in an RNA-seq experiment and which differential expression tool should you use? *RNA* 22, 839–851. doi: 10.1261/rna.053959.115

Seyfferth, C., Wessels, B., Jokipii-Lukkari, S., Sundberg, B., Delhomme, N., Felten, J., et al. (2018). Ethylene-related gene expression networks in wood formation. *Front. Plant Sci.* 9, 272. doi: 10.3389/fpls.2018.00272

Shi, Y., Tian, S., Hou, L., Huang, X., Zhang, X., Guo, H., et al. (2012). Ethylene signaling negatively regulates freezing tolerance by repressing expression of CBF and type-A ARR genes in Arabidopsis. *Plant Cell* 24, 2578–2595. doi: 10.1105/tpc.112.098640

Shi, D., Lebovka, I., López-Salmerón, V., Sanchez, P., and Greb, T. (2019). Bifacial cambium stem cells generate xylem and phloem during radial plant growth. *Development* 146, dev171355. doi: 10.1242/dev.171355

Sjödin, A., Street, N. R., Sandberg, G., Gustafsson, P., and Jansson, S. (2009). The Populus Genome Integrative Explorer (PopGenIE): a new resource for exploring the Populus genome. *New Phytol.* 182, 1013–1025. doi: 10.1111/j.1469-8137.2009.02807.x

Smetana, O., Mäkilä, R., Lyu, M., Amiryousefi, A., Rodríguez, F. S., Wu, M.-F., et al. (2019). High levels of auxin signalling define the stem-cell organizer of the vascular cambium. *Nature* 565, 485. doi: 10.1038/s41586-018-0837-0

Solano, R., Stepanova, A., Chao, Q., and Ecker, J. R. (1998). Nuclear events in ethylene signaling: a transcriptional cascade mediated by ETHYLENE-INSENSITIVE3 and ETHYLENE-RESPONSE-FACTOR1. *Genes Dev.* 12, 3703–3714. doi: 10.1101/gad.12.23.3703

Soyano, T., Thitamadee, S., Machida, Y., and Chua, N.-H. (2008). ASYMMETRIC LEAVES2-LIKE19/LATERAL ORGAN BOUNDARIES DOMAIN30 and ASL20/LBD18 regulate tracheary element differentiation in Arabidopsis. *Plant Cell* 20, 3359–3373. doi: 10.1105/tpc.108.061796

Suer, S., Agusti, J., Sanchez, P., Schwarz, M., and Greb, T. (2011). WOX4 imparts auxin responsiveness to cambium cells in Arabidopsis. *Plant Cell* 23, 3247–3259. doi: 10.1105/tpc.111.087874

Sultana, R. S., Ishiguri, F., Yokota, S., Iizuka, K., Hiraiwa, T., and Yoshizawa, N. (2010). Wood Anatomy of nine Japanese Hardwood species forming reaction wood without gelatinous fibers. *IAWA Journal* 31, 191–202. doi: 10.1163/22941932-90000016

Sundell, D., Mannapperuma, C., Netotea, S., Delhomme, N., Lin, Y.-C., Sjödin, A., et al. (2015). The plant genome integrative explorer resource: PlantGenIE.org. *New Phytol.* 208, 1149–1156. doi: 10.1111/nph.13557

Swarup, R., Perry, P., Hagenbeek, D., Van Der Straeten, D., Beemster, G. T. S., Sandberg, G., et al. (2007). Ethylene upregulates auxin biosynthesis in Arabidopsis Seedlings to enhance inhibition of root cell elongation. *Plant Cell* 19, 2186–2196. doi: 10.1105/tpc.107.052100

Taylor-Teeples, M., Lin, L., de Lucas, M., Turco, G., Toal, T. W., Gaudinier, A., et al. (2015). An Arabidopsis gene regulatory network for secondary cell wall synthesis. *Nature* 517, 571–575. doi: 10.1038/nature14099

Timell, T. E. (1986). *Compression wood in gymnosperms*. Heidelberg: Springer-Verlag. doi: 10.1007/978-3-642-61616-7

Trygg, J., and Wold, S. (2002). Orthogonal projections to latent structures (O-PLS). *J. Chemom.* 16, 119–128. doi: 10.1002/cem.695

Tuominen, H., Puech, L., Fink, S., and Sundberg, B. (1997). A radial concentration gradient of indole-3-acetic acid is related to secondary xylem development in hybrid aspen. *Plant Physiol.* 115, 577–585. doi: 10.1104/pp.115.2.577

Uggla, C., Mellerowicz, E. J., and Sundberg, B. (1998). Indole-3-acetic acid controls cambial growth in scots pine by positional signaling. *Plant Physiol.* 117, 113–121. doi: 10.1104/pp.117.1.113

Vahala, J., Felten, J., Love, J., Gorzsás, A., Gerber, L., Lamminmäki, A., et al. (2013). A genome-wide screen for ethylene-induced ethylene response factors (ERFs) in hybrid aspen stem identifies ERF genes that modify stem growth and wood properties. *New Phytol.* 200, 511–522. doi: 10.1111/nph.12386

Vaseva, I. I., Qudeimat, E., Potuschak, T., Du, Y., Genschik, P., Vandenbussche, F., et al. (2018). The plant hormone ethylene restricts Arabidopsis growth via the epidermis. *Proc. Natl. Acad. Sci. U.S.A.* 115, E4130–E4139. doi: 10.1073/pnas.1717649115

Wen, X., Zhang, C., Ji, Y., Zhao, Q., He, W., An, F., et al. (2012). Activation of ethylene signaling is mediated by nuclear translocation of the cleaved EIN2 carboxyl terminus. *Cell Res.* 22, 1613–1616. doi: 10.1038/cr.2012.145

Xu, F., Sun, R.-C., Lu, Q., and Jones, G. L. (2005). Comparative study of anatomy and lignin distribution in normal and tension wood of Salix gordejecii. *Wood Sci. Technol.* 40, 358. doi: 10.1007/s00226-005-0049-2

Xu, J., and Zhang, S. (2015). "Ethylene biosynthesis and regulation in plants," in *Ethylene in plants*. Ed. C.-K. Wen (Springer Netherlands: Dordrecht), 1–25. doi: 10.1007/978-94-017-9484-8_1

Yoshizawa, N., Inami, A., Miyake, S., Ishiguri, F., and Yokota, S. (2000). Anatomy and lignin distribution of reaction wood in two Magnolia species. *Wood Sci. Technol.* 34, 183–196. doi: 10.1007/s002260000046

Zhang, L., Li, Z., Quan, R., Li, G., Wang, R., and Huang, R. (2011). An AP2 domain-containing gene, ESE1, targeted by the ethylene signaling component EIN3 is important for the salt response in Arabidopsis. *Plant Physiol.* 157, 854–865. doi: 10.1104/pp.111.179028

Zhang, F., Qi, B., Wang, L., Zhao, B., Rode, S., Riggan, N. D., et al. (2016). EIN2-dependent regulation of acetylation of histone H3K14 and non-canonical histone H3K23 in ethylene signalling. *Nat. Commun.* 7, 13018. doi: 10.1038/ncomms13018

Zinkgraf, M., Gerttula, S., Zhao, S., Filkov, V., and Groover, A. (2018). Transcriptional and temporal response of Populus stems to gravi-stimulation. *J. Integr. Plant Biol.* 60, 578–590. doi: 10.1111/jipb.12645

Conflict of Interest Statement: Björn Sundberg is employed by Stora Enso AB, Sweden. The remaining authors declare that the research was conducted in the absence of any commercial or financial relationships that could be construed as a potential conflict of interest.

frontiers in Plant Science

ORIGINAL RESEARCH
published: 07 October 2019
doi: 10.3389/fpls.2019.01204

Super-*Agrobacterium* ver. 4: Improving the Transformation Frequencies and Genetic Engineering Possibilities for Crop Plants

Satoko Nonaka[1,2], Tatsuhiko Someya[2], Yasuhiro Kadota[3], Kouji Nakamura[2] and Hiroshi Ezura[1,2]**

[1] Tsukuba Plant Innovation Research Center, Gene Research Center, University of Tsukuba, Tsukuba, Japan, [2] Faculty of Life and Environmental Sciences, University of Tsukuba, Tsukuba, Japan, [3] RIKEN Center for Sustainable Resource Science, Plant Immunity Group, Yokohama, Japan

OPEN ACCESS

Edited by:
Dominique Van Der Straeten,
Ghent University,
Belgium

Reviewed by:
Benoit Lacroix,
Stony Brook University,
United States
Kan Wang,
Iowa State University,
United States

***Correspondence:**
Satoko Nonaka
nonaka.satoko.gt@u.tsukuba.ac.jp
Hiroshi Ezura
ezura.hiroshi.fa@u.tsukuba.ac.jp

Specialty section:
This article was submitted to Plant Physiology, a section of the journal Frontiers in Plant Science

Received: 24 April 2019
Accepted: 02 September 2019
Published: 07 October 2019

Citation:
Nonaka S, Someya T, Kadota Y, Nakamura K and Ezura H (2019) Super-Agrobacterium ver. 4: Improving the Transformation Frequencies and Genetic Engineering Possibilities for Crop Plants. Front. Plant Sci. 10:1204. doi: 10.3389/fpls.2019.01204

Agrobacterium tumefaciens has been utilized for both transient and stable transformations of plants. These transformation methods have been used in fields such as breeding GM crops, protein production in plant cells, and the functional analysis of genes. However, some plants have significantly lower transient gene transfer and stable transformation rates, creating a technical barrier that needs to be resolved. In this study, Super-*Agrobacterium* was updated to ver. 4 by introducing both the ACC deaminase (*acdS*) and GABA transaminase (*gabT*) genes, whose resultant enzymes degrade ACC, the ethylene precursor, and GABA, respectively. *A. tumefaciens* strain GV2260, which is similar to other major strains (EHA105, GV3101, LBA4404, and MP90), was used in this study. The abilities of the Super-*Agrobacterium* ver. 4 were evaluated in *Erianthus ravennae*, *Solanum lycopersicum* "Micro-Tom," *Nicotiana benthamiana*, and *S. torvum*. Super-*Agrobacterium* ver. 4 showed the highest T-DNA transfer (transient transformation) frequencies in *E. ravennae* and *S. lycopersicum*, but not in *N. benthamiana* and *S. torvum*. In tomato, Super-*Agrobacterium* ver. 4 increased the stable transformation rate by 3.6-fold compared to the original GV2260 strain. Super-*Agrobacterium* ver. 4 enables reduction of the amount of time and labor required for transformations by approximately 72%, and is therefore a more effective and powerful tool for plant genetic engineering and functional analysis, than the previously developed strains. As our system has a plasmid containing the *acdS* and *gabT* genes, it could be used in combination with other major strains such as EHA105, EHA101, LBA4404, MP90, and AGL1. Super-*Agrobacterium* ver. 4, could thus possibly be a breakthrough application for improving basic plant science research methods.

Keywords: *Agrobacterium tumefaciens*, Super-*Agrobacterium*, genetic engineering, plant transformation, gamma-aminobutyric acid, ethylene, GABA transaminase, ACC deaminase

INTRODUCTION

Agrobacterium tumefaciens is an α-proteobacteria that causes crown gall disease in many agriculturally and economically important species, such as those from the families *Rosaceae* (rose, apple, cherry, and pear), *Vitaceae* (grape), and the genus Juglans (walnut) (Kado, 2014). *A. tumefaciens* has the ability to transfer T-DNA from bacterial cells to plant cells (T-DNA transfer). Transferred T-DNA is integrated into the plant genome *via* complicated plant cell systems (Guo et al., 2019), and results in crown gall disease. To utilize this unique ability of *A. tumefaciens* for research purposes, there has been a great deal of effort to remove its oncogenesis characteristics, and to develop a binary vector system (Zambryski et al., 1983; Hoekema et al., 1983; Bevan, 1984; Komari et al., 2006). There has been further effort to increase the T-DNA transfer frequency of *A. tumefaciens*; one effective strategy was to upregulate its *vir* gene expression levels. The application of *vir* gene inducers (Stachel et al., 1985; Stachel et al., 1986; Cangelosi et al., 1990; He et al., 2009; Hu et al., 2013), using ternary system (van der Fits et al., 2000), utilization of Super-binary vectors (Komari, 1990; Hiei et al., 1994; Ishida et al., 1996), and a modification of the Ori of the binary vector (Ye et al., 2011; Vaghchhipawala et al., 2018), have subsequently improved its transformation frequencies.

Another strategy to increase T-DNA transfer frequencies was the removal of the negative factors of the *Agrobacterium*-plant interactions, such as ethylene, the gaseous phytohormone. Applications, such as aminoethoxyvinylglycine (AVG), an ethylene biosynthesis inhibitor, and $AgNO_3$ or silver thiosulfate (STS), ethylene perception inhibitors, were effective at improving the T-DNA transfer frequencies in tomato, melon, and bottle gourd (Davis et al., 1992; Ezura et al., 2000; Han et al., 2005; Nonaka and Ezura, 2014). An alternative strategy was the utilization of ACC deaminase (AcdS) activity, which cleaves ACC, the ethylene precursor, to ammonia and α keto-butyrate. This enzyme was found in some plant growth promoting bacteria (PGPBs), such as *Pseudomonas* sp., which were found on the plant surface (Sheehy et al., 1991), and these bacteria utilize ACC as a nitrogen source. However, *A. tumefaciens* C58 strain, which was the original strain for *Agrobacterium*-mediated transformation, does not have the *acdS* gene or its activities (Wood et al., 2001; Nonaka et al., 2008a). Therefore, the utilization AcdS activity seemed to be reasonable. Indeed, *A. tumefaciens* GV2260 that had AcdS activity introduced into it, was efficacious in the suppression of ethylene evolution from plant tissues during co-cultivation and increasing T-DNA transfer [Nonaka et al., 2008a (Super-*Agrobacterium* ver.1); Ntui et al., 2010; Hao et al., 2010]. Moreover, Super-*Agrobacterium* ver.1 showed stronger inhibition of ethylene evolution and higher T-DNA transfer frequencies than chemical treatments in melon and wild water melon (Nonaka et al., 2008a; Malambane et al., 2018). For the further improvement of Super-*Agrobacterium* ver.1, a stronger promoter was used to drive *acdS*. In Super-*Agrobacterium* ver.1, the expression of *acdS* gene was under the control of the *lac* promoter, which shows constitutive expression in *A. tumefaciens*. Instead of the *lac* promoter, the *virD* promoter was cloned from *A. tumefaciens* and was used in Super-*Agrobacterium* ver. 2 (Someya et al., 2013). *virD* genes are induced by acetosyringone at pH 5.2, which is the co-cultivation condition. This promoter showed higher gene expression levels than the *lac* promoter during co-cultivation (Someya et al., 2013), resulting in higher T-DNA transfer frequencies in Super-*Agrobacterium* ver. 2 than in ver.1 (Someya et al., 2013).

Gamma-aminobutyric acid (GABA), an amino acid, was determined to be another negative factor in *Agrobacterium*-plant interactions (Chevrot et al., 2006; Haudecoeur et al., 2009; Nonaka et al., 2017). GABA is taken up into *A. tumefaciens* and triggers the degradation of the quorum-sensing (QS) signal, resulting in the reduced horizontal gene transfer of the Ti plasmid and the aggressiveness of the plant host (Chevrot et al., 2006; Haudecoeur et al., 2009). GABA is a biologically active agent in animals, plants, and bacteria. In animals, GABA is particularly well known as an effector, lowering blood pressure (Elliott and Hobbiger, 1959; Takahashi et al., 1961; Takahashi et al., 1995), and its mechanism of action has been well studied. It was found that some chemical compounds control GABA effect in animals. While contrarily, in plants, GABA was know as modulator cell elongation, abiotic stress and pathogen attack (Park et al., 2010; Renault et al., 2011; Shelp et al., 2012; Forlani et al., 2014), but the action mechanisms of GABA in-plants are still to be clarified, and the chemical compounds related with GABA perception or signal transduction in plants have not been identified. Some bacteria are known to harbor GABA transaminase (*gabT*), a GABA degradation enzyme. Utilization of GabT activities increased the transient and stable transformation frequencies in tomato and grass plants [Nonaka et al., 2017 (Super-*Agrobacterium* ver.3)]. Super-*Agrobacterium* ver. 3 was also effective in the agro-infiltration method (Hoshikawa et al., 2019; Knoch et al., 2019).

Stable transformation techniques are important as they are used for breeding GM crops. Transient transformations are also widely used in plant science; for example, protein production by excessive gene overexpression and gene function analysis by the virus-induced gene silencing (VIGS) system (Velásquez et al., 2009), are based on transient gene transfers. However, some plants have significantly lower transient gene transfer rates, creating a limitation in plant science research that should be resolved by increasing the transient transformation (T-DNA transfer) frequency in a wide variety of plant hosts. Therefore, the host range of *A. tumefaciens* must be enlarged, and its transformation efficiency increased. In this study, to further increase the transient and/or stable transformation frequencies, Super-*Agrobacterium* was updated to ver. 4 by introducing both AcdS and GabT activity to the GV2260 strain, which has similar abilities, compared with other strains such as EHA105, EHA101, LBA4404, and MP90 (Sun et al., 2006 and Chetty et al., 2013). The abilities of the Super-*Agrobacterium* ver. 4 were evaluated in *Erianthus ravennae*, *Solanum lycopersicum* "Micro-Tom," *Nicotiana benthamiana*, and *S. torvum* for both transient and stable transformations.

MATERIALS AND METHODS

Bacterial Strains, Vectors, and Culture Conditions

All bacterial strains and vectors, which were used in this study, were listed up in **Table 1**. The vector maps were described in

TABLE 1 | List of *A. tumefaciens* strains and plasmids that are used in this study.

	Description	Reference
Strain name		
GV2260	Non-oncogenic *A. tumefaciens* strain	Deblaere et al. (1985)
C	*A. tumefaciens* GV2260 (pBBR1MCS-5)	Nonaka et al. (2008a)
V1	*A. tumefaciens* GV2260 (pBBRacdS) (Super-*Agrobacterium* ver. 1)	Nonaka et al. (2008a)
V3	*A. tumefaciens* GV2260 (pBBRgabT) (Super-*Agrobacterium* ver. 3)	Nonaka et al. (2017)
V4	*A. tumefaciens* GV2260 (pBBRacdSgabT) (Super-*Agrobacterium* ver. 4)	This study.
C-E	*A. tumefaciens* GV2260 (pBBR1MCS-5, $pEKH_2$)	Nonaka et al. (2008a)
V1-E	*A. tumefaciens* GV2260 (pBBRacdS, $pEKH_2$) (Super-*Agrobacterium* ver. 1)	Nonaka et al. (2008a)
V3-E	*A. tumefaciens* GV2260 (pBBRgabT, $pEKH_2$) (Super-*Agrobacterium* ver. 3)	Nonaka et al. (2017)
V4-E	*A. tumefaciens* GV2260 (pBBRacdSgabT, $pEKH_2$) (Super-*Agrobacterium* ver. 4)	This study.
C-G	*A. tumefaciens* GV2260 (pBBR1MCS-5, pIG121-Hm)	Nonaka et al. (2008a)
V1-G	*A. tumefaciens* GV2260 (pBBRacdS, pIG121-Hm) (Super-*Agrobacterium* ver. 1)	Nonaka et al. (2008a)
V3-G	*A. tumefaciens* GV2260 (pBBRgabT, pIG121-Hm) (Super-*Agrobacterium* ver. 3)	Nonaka et al. (2017)
V4-G	*A. tumefaciens* GV2260 (pBBRacdSgabT, pIG121-Hm) (Super-*Agrobacterium* ver. 4).	This study.
C-Q	*A. tumefaciens* GV2260 (pBBR1MCS-5, pEAQ-GFP-HT)	Nonaka et al. (2008a)
V1-Q	*A. tumefaciens* GV2260 (pBBRacdS, pEAQ-GFP-HT) (Super-*Agrobacterium* ver. 1)	Nonaka et al. (2008a)
V3-Q	*A. tumefaciens* GV2260 (pBBRgabT, pEAQ-GFP-HT) (Super-*Agrobacterium* ver. 3),	Nonaka et al. (2017)
V4-Q	*A. tumefaciens* GV2260 (pBBRacdSgabT, pEAQ-GFP-HT) (Super-*Agrobacterium* ver. 4),	This study.
Plasmid		
pBBR1MCS-5	Broad-host-range shuttle vector; Gen^R	Kovach et al. (1995)
pBBRacdS	Overexpression vector for ACC deaminase under the control of the lac promoter; Gm^R	Nonaka et al. (2008a)
pBBRgabT	Overexpression vector for GABA under the control of the lac promoter; Gm^R	Nonaka et al. (2017)
pBBRacdSgabT	Overexpression vector for ACC deaminase and GABA transaminase under the control of the lac promoter; Gm^R	This study.
$pEKH_2$	pEKH2-nosPNPTII-ubiPGUS-35SPHPT, bBinary vector plasmid carrying the b-glucuronidase gene (*uidA*) between the T-borders; Sp^R	Hoshikawa et al. (2012)
pIG121-Hm	Binary vector plasmid carrying the b-glucuronidase gene (*uidA*) between the T-borders; Km^R	Ohta et al. (1990)
pEAQ-GFP-HT	Binary vector plasmid carrying the Green Fluorescent Protein gene (*GFP*) between the T-borders; Km^R	Sainsbury et al. (2009)

Supplemental Figure 1. *A. tumefaciens* strains were grown at 28°C in Luria Broth (LB) medium (1% bacto-tryptone, 0.5% yeast extract, and 0.5% NaCl). Antibiotics were added at the following final concentrations: ampicillin at 100 μg/ml, gentamicin at 50 μg/ml, spectinomycin at 50 μg/ml, and kanamycin at 50 μg/ml. *A. tumefaciens* strains were then cultured on solid LB medium at 28°C for 2 days. A single colony was picked and cultured in 2 ml of LB medium at 28°C and 200 rpm for 2 days until the pre-culture reached the stationary phase. From this, 15 μl of culture was harvested and added to 15 ml of LB medium and cultured at 28°C and 200 rpm. When the $O.D._{600}$ of the culture reached 0.7 to 0.9, the cells were then centrifuged, collected, and checked for enzymatic activity. For transformations, the pelleted bacterial cells were resuspended in liquid Murashige and Skoog (1962) (MS) containing 30 g/l glucose, and 500 μM acetosyringone at pH 5.2. The cell density was then adjusted to 0.4–0.5 at $O.D._{600}$.

Construction of *acdS* and *gabT* Expression Plasmids

The *gabT* gene was cloned from pBBRgabT in a previous study (Nonaka et al., 2017) by polymerase chain reaction (PCR) with the primers acdSF (5′- TCTGCGCGTAATCT GCTGCTTGAGCGCAACGCAATTAATG -3′) and gabTR (5′- CGATTCTGGACTACTGCTTCGCCTCATCAAAAC-3′). The transcription terminal sequence of the ampicillin resistance gene was cloned from the pUC18 vector using PCR with the primer's amp_ter-for2 (5′-GCTAGAATTCCTGTCAGACCA AGTTTACTC-3′) and amp_ter-rev2 (5′-CATTAATTG CGTTGCGCTCAAGCAGCAGATTACGCGCAGA-3′). Then, the two fragments were combined by fusion-PCR with the primer's amp_ter-for2 and gabTR. The ligated fragment was inserted into pBBRacdS (Nonaka et al., 2008a) and digested with *Eco*RI and *Xba*I (New England Biolabs, Hirchin, UK). The expression of both genes was under the control of the *lacZ* gene promoters (pBBRacdSgabT, **Figure 1A**). pBBR1MCS5, pBBRacdS, pBBRgabT, and pBBRacdSgabT were introduced into *A. tumefaciens* GV2260 ($pEKH_2$-nosPNPTII-ubiPGUS-35SPHPT; $pEKH_2$), *A. tumefaciens* GV2260 (pIG121-Hm), or *A. tumefaciens* GV2260 (pEAQ-GFP-HT) *via* electroporation.

ACC Deaminase Activity Assay

Cells were collected and washed twice with 100 mM Tris–HCl (pH 8.5) and resuspended in 1.5 ml of lysate buffer. The cells were lysed on ice by sonication and centrifuged at 5,000 × *g* at 4°C for 15 min. The AcdS activity was measured according to a modified protocol based on that of Honma and Shimomura (1978). The AcdS activity was measured spectrophotometrically at 340 nm. The protein content of the extracts was determined using the Bradford method (Bradford, 1976).

GABA Transaminase Activity in *A. tumefaciens*

The pellet of *A. tumefaciens* was re-suspended in 100 μl of BugBuster Master mix (Novagen, MA, USA) for lysate

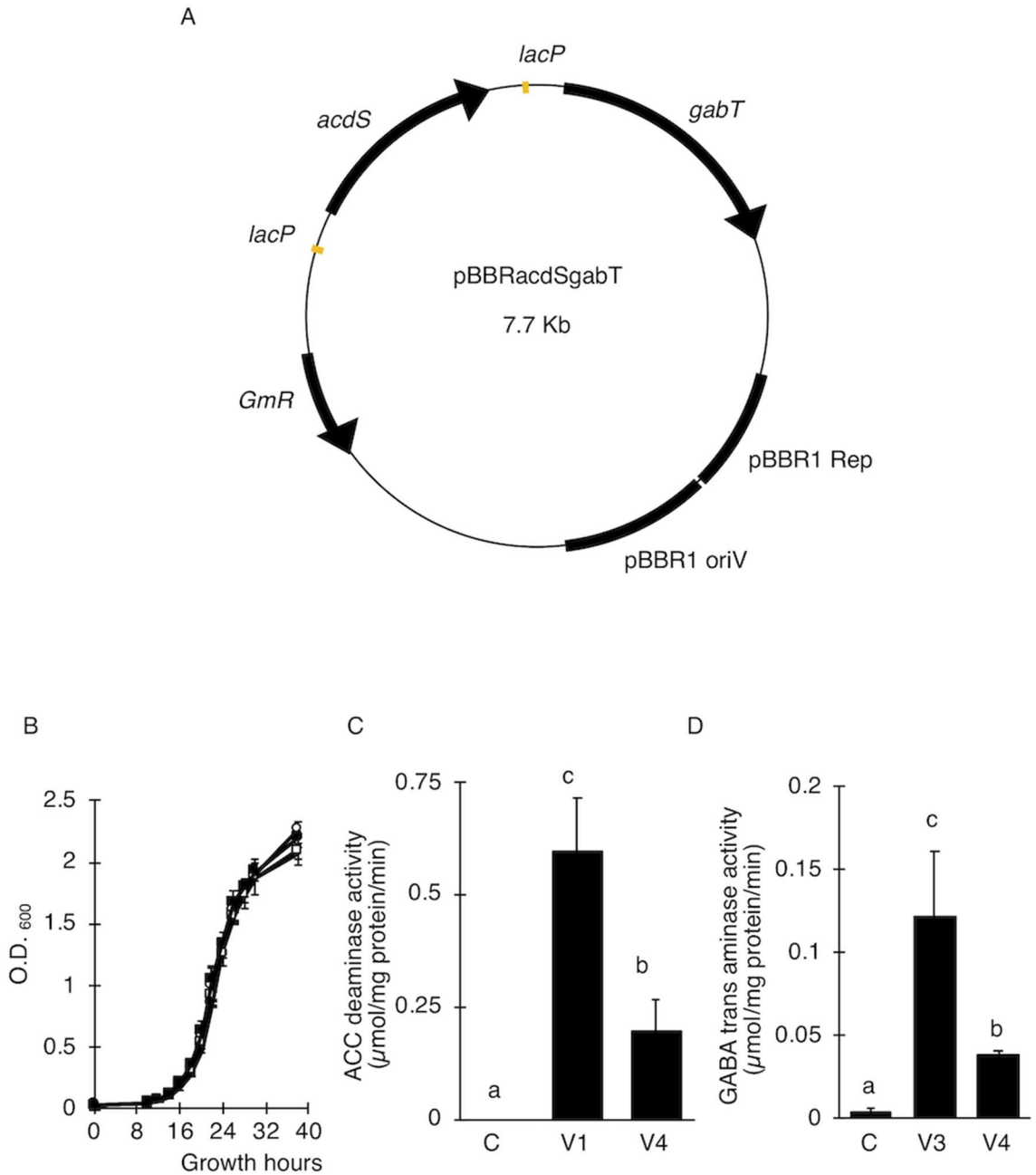

FIGURE 1 | Effect of ACC deaminase and GABA transaminase activity on the transfer of T-DNA. **(A)** Map of a plasmid for the expression of ACC deaminase (*acdS*) and GABA transaminase (*gabT*) in *A. tumefaciens*. *lacP*, lac gene promoter from *E. coli; acdS*, ACC deaminase gene from *Psedomonas* sp (Sheehy et al., 1991, Accession No. M73488); *gabT*, GABA transaminase gene from *E. coli* (Accession No. CP040667); pBBR1 Rep, replication protein for the broad-host-range plasmid pBBR1 from *Bordetella bronchiseptica*; pBBR1 oriV, replication origin of the broad-host-range plasmid pBBR1 from *B. bronchiseptica*; pBBR1 Rep, protein for replication required by pBBR1 oriV, *GmR*, Gentamicin resistance gene. **(B)** Growth curve of *A. tumefaciens*. Open and solid circles represent *A. tumefaciens* C and V1, respectively. Open and solid squares represent V3 and V4, respectively. **(C)** ACC deaminase activity in *A. tumefaciens*. **(D)** Detection of GABA transaminase activity in *A. tumefaciens*. C, GV2260 (pBBRMCS1-5); V1, *A. tumefaciens* GV2260 (pBBRacdS); V3, *A. tumefaciens* GV2260 (pBBRgabT); V4, *A. tumefaciens* GV2260 (pBBRacdSgabT). Bars represent the standard deviation (n = 3). Different characters indicate values that were statistically different in the one-way ANOVA and Tukey-Kramer method, multiple comparison method ($P < 0.01$).

preparation. The protein concentration of the lysate was measured with a BCA Protein Assay Kit (Novagen, MA, USA). The amount of protein was adjusted to 100 μg *per* reaction mixture. The reaction mixture contained 0.1 M bicine–NaOH, 0.1 M pyridoxal phosphate, 10 mM 2-ketoglutarate, 10 mM GABA, and a proteinase inhibitor cocktail. The reaction mixture was incubated at 37°C. GabT metabolizes GABA to glutamate; therefore, to estimate the GabT activity, we detected the glutamate

concentration in the reaction mixture using a Yamaki glutamate assay kit (Yamaki, Tokyo, Japan) (Akihiro et al., 2008).

T-DNA Transfer Assay in *E. ravennae* and *S. lycopersicum*

Calli of *E. ravennae* were kindly provided by Prof. Masahiro Mii from Chiba University, Japan. The calli were induced directly from the seeds on MS medium, containing 1 g/l casamino acids, 2 mg/l 2,4-dichlorophenoxyacetic acid (2,4-D), 0.2 mg/l 6-benzylaminopurine (BAP), 30 g/l 4-O-α-D-glycopyranosyl-D-glycopyranose (maltose H) (Wako, Tokyo, Japan), and 3% Gelrite (Wako, Tokyo, Japan), were subcultured for 2 weeks before inoculation. After co-cultivation, the β-glucuronidase (GUS) activity of the *E. ravennae* calli were assayed histochemical with X-Gluc buffer containing 100 mM phosphate buffer, 10 mM EDTA, 2.5 mM potassium ferricyanide, 2.5 mM potassium ferrocyanide, 0.1% Triton X-100, and 0.5 mg/l X-glucuronide. The GUS-stained calli were observed using a stereoscopic microscope (Leica: MX FLIII, DFC300 FX, Application Suite, Leica, Germany), the number of GUS-stained spots per 1 g of calli calculated, and the T-DNA transfer efficiency was estimated, based on the relative number of GUS spots.

Tomato seeds were washed with 70% ethanol for 10 s, sterilized with 5% hypochlorous acid containing 10% Triton X-100 for 45 min, and washed three times with sterilized water. After the third wash, the seeds were kept in water for 2 days. The sterilized tomato seeds were sown on MS medium, containing 15 g/L sucrose (Wako, Tokyo, Japan) and 0.3% Gelrite (Wako, Tokyo, Japan). Cotyledons from 7-day-old tomato seedlings were cut into four pieces and used to generate two locations for inoculations with *A. tumefaciens*. Thirty explants were subjected to each treatment. The inoculated explants were cultured on co-cultivation medium (pH 5.2) containing MS salts, 30 g/L glucose, 500 μM acetosyringone, and 0.3% Gelrite (Wako, Tokyo, Japan) at 25°C, for 3 days in the dark. After 3 days of co-cultivation, the tomato explants were assayed histochemically for GUS activity with X-Gluc buffer, described above. GUS stained tomato cotyledon explants were observed and images were taken using a stereoscopic microscope system (Leica: MX FLIII, DFC300 FX, Application Suite, Leica, Wetzlar, Germany). The GUS stained areas were converted into numerical values by Image J (National Institutes of Health: http://rsbweb.nih.gov/ij/) and the percentage of GUS stained area for each explant was calculated. According to the results, GUS stained tomato explants were categorized into 4 classes: (Class 1) less than 5%, (Class 2) 5–10%, (Class 3) 10–20%, and (Class 4) more than 20%. To estimate the T-DNA transfer, the frequency of more than 20% was calculated.

Tomato Stable Transformation

Tomato transformations followed the protocol by Sun et al. (2006). In brief, after 3 days of co-cultivation, tomato cotyledon segments were placed on a callus-induction medium [MS medium containing 0.3% Gelrite (Wako, Tokyo, Japan), 1.5 mg/l zeatin, 100 mg/l kanamycin, and 375 mg/l Augmentin (GlaxoSmithKline, London, UK)] for 4 weeks. Calli that formed segments were cultured on shoot-induction medium [MS medium containing 0.3% Gelrite (Wako, Tokyo, Japan), 1.0 mg/l zeatin, 100 mg/l kanamycin, and 375 mg/l Augmentin (GlaxoSmithKline, London, UK)] for 4 weeks. The shoots were then placed on rooting medium, which consisted of half-strength MS medium, 0.3% Gelrite (Wako, Tokyo, Japan), 100 mg/L kanamycin, and 375 mg/l Augmentin, for 2 weeks. Tissues were each subcultured for 10–14 days.

Agro Infiltration Method

A. tumefaciens GV2260 carrying pEAQ-GFP-HT (Sainsbury et al., 2009) was grown in LB media, resuspended in 10 mM $MgCl_2$, 10 mM MES, pH 5.6, 150 μM acetosyringone, and incubated for 3 h at room temperature. The leaves were then syringe infiltrated with the *A. tumefaciens*. Concentrations of *A. tumefaciens* were 0.3 at $O.D._{600}$ for *N. benthamiana* and 1 at $O.D._{600}$ for *S. torvum*. GFP fluorescence was detected 3 and 5 days after infiltration for *N. benthamiana* and *S. torvum*, respectively. Each experiment was repeated three times.

Ploidy Analysis

The ploidy of the rooting shoots was checked with flow cytometry. One square centimeter of leaf was cut from the rooting shoots, chopped, and added to 250 μl of nucleus-extraction solution (CyStain UV Precise P, Sysmex, Hyogo, Japan). To purify the nucleus-extraction solution, 1 mm^2 mesh was used. After purification, 1 ml of staining solution (CyStain UV Precise P, Sysmex, Hyogo, Japan) was added and incubated for 1 min. This solution was applied to an Attune focusing analyzer (ABI, CA, USA), and 2n plants were selected. The 2n plants were then planted on solid medium and acclimatized.

Southern Blot Analysis

Genomic DNA was extracted from young tomato leaves using Maxwell 16 System DNA Purification kits (Promega, WI, USA). The purified DNA was digested with *Hin*dIII, electrophoretically separated in 0.8% agarose gel, and transferred onto Gene Screen Plus nylon membranes (Roche Diagnostics, Basel, Swiss) with 20× saline–sodium citrate (SSC) buffer. After ultraviolet (UV) cross-linking, the membranes were hybridized in a solution containing 7% sodium dodecyl sulfate (SDS), 50% deionized formamide, 50 mM sodium phosphate (pH 7.0), 2% blocking solution, 0.1% N-lauroylsarcosine, 0.75 M NaCl, and 75 mM sodium citrate at 42°C overnight. For hybridization, a digoxigenin (DIG)-labeled DNA probe, specific for *nptII* (0.8 Kb), was used. A DIG-labeled probe was generated by DIG-High Prime, and the DIG signal was detected according to the manufacturer's protocol (Roche Diagnostics, Basel, Swiss).

Statistical Analysis

The average values were obtained from three biological replicates. One-way analysis of variance (ANOVA) and Tukey Kramer's multiple range test, with $P < 0.01$ or $P < 0.05$, were carried out

to determine the significant differences. Statistical analyses were carried out using the SAS statistics program (version 8.0, SAS Institute Cary, NC, USA).

RESULTS

Introduction of AcdS and GabT Activity Did Not Affect Bacterial Growth

Since ethylene and GABA suppress the transfer of T-DNA in different ways, we predicted that the introduction of AcdS and GabT activity into *A. tumefaciens* would be effective at increasing the T-DNA transfer. These two genes were introduced by pBBR1MCS-5, the broad host range plasmid (Kovach et al., 1995) (**Figure 1A**, pBBRacdSgabT), and expressed under the control of the *lac* promoter (Nonaka et al., 2008a; Nonaka et al., 2017). To estimate whether these two genes affect bacterial growth or not, growth curves were compared for the four strains [(C), (V1), (V3), and (V4)]. In all strains, the accelerated growth period began 10 h after culturing, and after 18 to 26 h, the logarithmic growth phases were observed (**Figure 1B**). These results indicate that introducing the *acdS* and *gabT* at the same time in *A. tumefaciens* did not affect its bacterial growth. To measure the AcdS and GabT activity, cells were collected by centrifugation, and the lysate was prepared. Then, the AcdS and GabT activity were measured, as described in previous studies (Nonaka et al., 2008a; Nonaka et al., 2017). Both activities were detected in the V4 strain, but the AcdS and GabT activities in V4 were one-third of the V1 and V3, respectively (**Figures 1C**, **D**).

Evaluation of the Super-*Agrobacterium* for T-DNA Transfer in Plants

To examine whether the AcdS and GabT activities were enough to increase the transfer of T-DNA, the T-DNA transfers in *E. ravennae* and *S. lycopersicum* "Micro-Tom" were observed. *E. ravennae* is known for its high bio-mass production and is relevant for practical agriculture. After 3 days of co-cultivation, the number of blue spots were counted to evaluate the T-DNA transfer in *E. ravennae*. Four strains, (C-E), (V1-E), (V3-E), and (V4-E) were used for the transformation. The V1-E, V3-E, and V4-E showed higher T-DNA transfer frequencies than the control, C-E. The inoculation of V4-E increased the T-DNA transfer frequency by 7.2, 2.4, and 1.7 times, compared to the C-E, V1-E, and V3-E, respectively (**Figure 2A**). Next, we evaluated the abilities of Super-*Agrobacterium* V4 using *S. lycopersicum* "Micro-Tom." Almost 100 explants of "Micro-Tom" were inoculated for each bacterial strain [(C-G), (V1-G), (V3-G), and (V4-G)]. The *uidA* gene was used as an indicator of T-DNA transfer, and the blue area indicated transformed cells (**Figure 2B**). The GUS-stained area was determined in each of the explants with Image J, as described in the *Materials and Methods* section (in "2.5 T-DNA transfer assay in *E. ravennae* and *S. lycopersicum*"). The degree of staining was categorized into 4 classes (**Figure 2B**). To evaluate the ability of the T-DNA transfer in C-G, V1-G, V3-G, and V4-G, the frequency of class 4 was compared. V4-G showed the highest frequency of class 4; the frequencies were 3.9, 1.4, and 1.5 times higher than the C-G, V1-G, and V3-G, respectively. V1-G

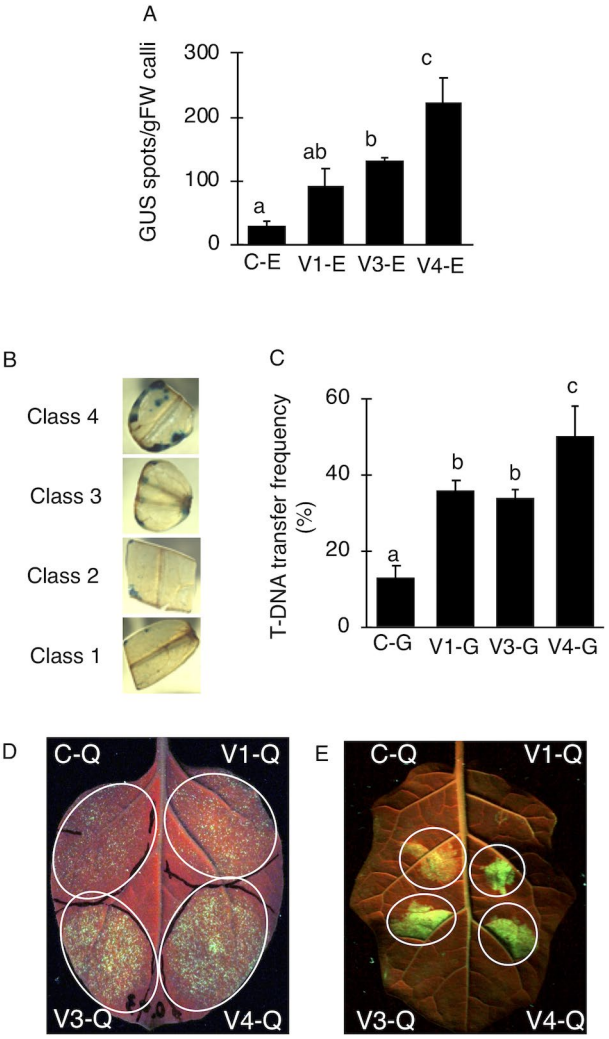

FIGURE 2 | Transient transformations in tomato *via* tissue culture and co-cultivation method. **(A)** Occurrence of T-DNA transformations in *E. ravennae*. The number of GUS-stained spots *per* 1 g of *E. ravennae* calli were counted for each treatment. The bars indicate the standard deviation (n = 3). Different characters indicate values that were significantly different according to the one-way analysis of variance, multiple comparison method ($P < 0.01$). C-E: *A. tumefaciens* GV2260 (pBBR1MCS-5, pEKH$_2$), V1-E: *A. tumefaciens* GV2260 (pBBRacdS. pEKH$_2$), V3-E: *A. tumefaciens* GV2260 (pBBRgabT, pEKH$_2$), V4-E: *A. tumefaciens* GV2260 (pBBRacdSgabT, pEKH$_2$). **(B)** GUS stained explants of *S. lycopersicum* "Micro-Tom." Explants were prepared from 7 days old seedlings. After 3 days of co-cultivation, explants were stained. Classification of GUS-stained cotyledon explants. GUS stained tomato cotyledons were categorized depending on the stained area. Categorized into 4 classes: (Class 1) less than 5%, (Class 2) 5–10%, (Class 3) 10–20%, and (Class 4) more than 20%. **(C)** Appearance ratio Class 4 in tomato cotyledons. C-G: *A. tumefaciens* GV2260 (pBBRMCS1-5, pIG121-Hm); V1-G: *A. tumefaciens* GV2260 (pBBRacdS, pIG121-Hm); V3-G: *A. tumefaciens* GV2260 (pBBRgabT, pIG121-Hm); V4-G: *A. tumefaciens* GV2260 (pBBRacdSgabT, pIG121-Hm). Bars represent the standard deviation (n = 3). Different characters indicate values that were statistically different in a one-way ANOVA and the Tukey-Kramer method, multiple comparison method ($P < 0.01$). **(D)** Transient transformation *via* agroinfiltration methods on *N. benthamiana*. **(E)** Transient transformation *via* Agroinfiltration methods on *S. torvum*. GFP signals were used as indicators of transformation. C-Q: *A. tumefaciens* GV2260 (pBBRMCS1-5, pEAQ-GFP-HT); V1-Q: *A. tumefaciens* GV2260 (pBBRacdS, pEAQ-GFP-HT); V3-Q: *A. tumefaciens* GV2260 (pBBRgabT, pEAQ-GFP-HT); V4-Q: *A. tumefaciens* GV2260 (pBBRacdSgabT, pEAQ-GFP-HT).

and V3-G showed almost the same levels (**Figure 2C**). Therefore, the activities of AcdS and GabT in V4-E and V4-G, were enough to increase the T-DNA transfer frequencies in *E. ravennae* and *S. lycopersicum* "Micro-Tom." Additionally, we evaluated the ability of T-DNA transformation with V4 in the Agroinfiltration method. Plasmid pEAQ-GFP-HT was used as a binary vector in Agroinfiltration method. *N. benthamiana* and *S. torvum* were inoculated with four strains [(C-Q), (V1-Q), (V3-Q), and (V4-Q)]. The strength of the GFP signal was used as an indicator of the frequency of the T-DNA transfer. In *N. benthamiana*, V4-Q induced higher GFP expression than the C-Q strain and V1-Q (**Figure 2D**), but it was the same level as the V3-Q. In *S. torvum,* the success of the V4-Q strain with the Agroinfiltration treatment was greater than that of the C-Q strain, but the same as that of the V1-Q and V3-Q strains (**Figure 2E**).

A. tumefaciens With Both AcdS and GabT Activities Resulted in the Enhanced Stable Transformation of Tomato

V4 was effective at the T-DNA transfer in *E. ravennae* and *S. lycopersicum* "Micro-Tom" (**Figures 2A**, **C**), however this is one step of the stable transformation process. The entire process for *Agrobacterium*-mediated stable transformation is divided into four steps: i) T-DNA transfer and integration into the plant genome, ii) calli induction, iii) the regeneration of the shoots, and iv) rooting. It was not clear if the V4 affected these other steps. To ascertain this information, the frequency of each process was observed in *S. lycopersicum* "Micro-Tom," which has a well-established regeneration system for processes (ii) to (iv) (Sun et al., 2006). To characterize each strain, C-G, V1-G, V3-G, and V4-G were used. One-month after inoculation, the calli inductions were observed. All Super-*Agrobacterium* strains increased the callus inductions compared with the C-G (**Figures 3A–D**). V1-G and V4-G showed slightly higher calli induction ratios (calli number / segments number) than the V3-G. The C-G, V1-G, V3-G, and V4-G showed calli induction frequencies of 51.5 ± 0.6, 85.2 ± 8.8, 73.8 ± 2.03, and 91.8 ± 3.7%, respectively (**Figure 3E**, **Table 2**). Shoot regeneration ratios (shooting number / calli number) were increased with the inoculation of the V3-G and V4-G. V1-G was slightly higher than that of the C-G. The frequency of the shoot regeneration ratios with the inoculations of C-G, V1-G, V3-G, and V4-G were 49.7 ± 10.9, 80.4 ± 29.2, 181.8 ± 23.4, and 176.3 ± 58.9%, respectively (**Figure 3F**, **Table 2**). The frequencies for rooting from the shoots (rooting number/ shoots number) were similar for all strains (**Figure 3G**, **Table 2**). These results suggest that V1-G had positive effects on step (ii) calli induction, V3-G increased step (iii) shooting, and V4-G accelerated both steps (ii) and (iii) in the *Agrobacterium*-mediated stable transformation process. After regenerated diploid shoots (2n) were selected, the exogenous T-DNA was detected by PCR (data not shown) and Southern hybridization analysis (**Supplemental Figure 2**). The stable transformation frequencies were evaluated with single-copy-number plants, and identification by Southern hybridization analysis. These results imply that all of the lines we obtained were independent and did not contain a cloned plant. The C-G, V1-G, V3-G, and V4-G showed the stable transformation efficiencies of 4.3 ± 1.9, 9.7 ± 0.4, 9.8 ± 1.6, and 15.2 ± 1.1%, respectively (mean ± SD of three repetitions) (**Figure 3H** and **Table 2**). Thus, V4 exhibited approximately 3.6, 1.6, and 1.6 times the stable transformation frequency of C-G, V1-G, and V3-G, respectively. The frequency of regenerated rooting shoot with single copy was same level in all *A. tumefaciens* strains (**Figure 3I**).

DISCUSSION

A. tumefaciens with AcdS and GabT was expected to cause reduced ethylene and GABA content in plants. Indeed, the ethylene levels in the plant tissues during the transformation were reduced by the *A. tumefaciens* with AcdS activity (Nonaka et al., 2008a; Malambane et al., 2018). On the other hand, significant differences in GABA content during the co-cultivation were not observed between *A. tumefaciens* with GabT activity and the control (data not shown). As *A. tumefaciens* takes the GABA from the plant into the bacterial cell through a kind of ABC transporter (Planamente et al., 2010; Planamente et al., 2013), if the GabT activity introduced *A. tumefaciens*, GABA taken into bacterial cell would be degraded. The degradation of GABA occurred only in bacterial cells, and at very localized areas. Therefore, it was difficult to detect the differences of GABA content. ACC deaminase activity and GabT activity in *A. tumefaciens* were effective at increasing the T-DNA transfer frequency (Nonaka et al., 2008a; Nonaka et al., 2017; Ntui et al., 2010; Hao et al., 2010), but it was not clear which was more effective in *Agrobacterium*-plant interactions. To ascertain this, the T-DNA transfer abilities of Super-*Agrobacterium* ver. 1 and ver. 3 were compared in *E. ravennae* and tomato with the tissue culture and co-cultivation methods. No differences were observed between the strains in *E. ravennae* and *S. lycopersicum* "Micro-Tom" (**Figures 2A**, **C**). With the Agroinfiltration method, the same tendency was observed in *S. torvum* (**Figure 2E**). These results mean that ethylene and GABA influence the T-DNA transfer frequencies at almost the same level in these plant species. On the other hand, in *N. benthamiana*, Super-*Agrobacterium* ver. 3 and ver. 4 showed higher level of T-DNA transfer than GV2260 and Super-*Agrobacterium* ver. 1, but the level of T-DNA transfer was same in ver. 3 and ver. 4. This showed that in the *N. benthaminana*, AcdS activity did not improve the T-DNA transfer, but GabT activity was effective at increasing the T-DNA transfer. Therefore, in *N. benthamiana*, GABA is a stronger negative factor than ethylene. From these results, the effect of the Super-*Agrobacterium* was found to be different, dependent on the plant species, thus the selection of the most suitable strain is important for the successful application of the technology.

Even under conditions where the *vir* gene is sufficiently expressed, our Super-*Agrobacterium* strains could further improve T-DNA transfer. In this study, with the tissue culture and co-cultivation methods, 500 μM of acetosyringone, which was enough to induce *vir* gene expression (Nonaka et al., 2008b), was used during co-cultivation. Super-*Agrobacterium* ver. 1, ver. 3, and ver. 4 further increased the T-DNA transfer frequency, despite the existence of enough *vir* gene inducers (**Figures 2A**, **C**). The additional effects of AcdS and GabT under the acetosyringone indicate that in the T-DNA transfer, the ethylene and GABA affect

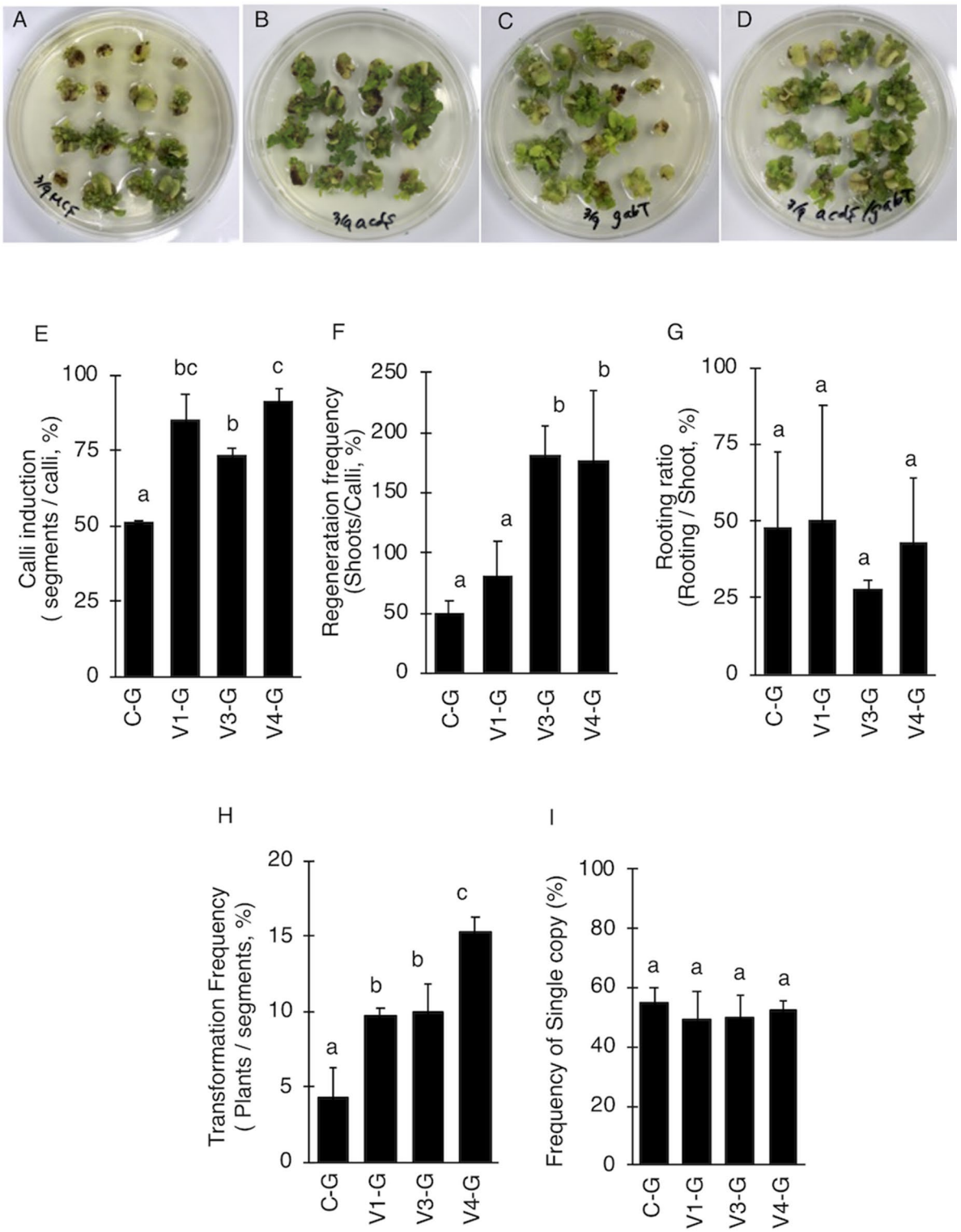

FIGURE 3 | Effect of AcdS and GabT activity on regeneration and stable transformation. Regenerated shoots from "Micro-Tom" calli inoculated with **(A)** C-G, **(B)** V1-G, **(C)** V3-G, and **(D)** V4-G. **(E)** Appearance of calli, **(F)** Frequency of regeneration, **(G)** Rooting ratio, **(H)** Frequency of calli regeneration. **(I)** Frequency of appearence for transgenic tomato plants which have single copy of T-DNA. C-G: *A. tumefaciens* GV2260 (pBBRMCS1-5, pIG121-Hm); V1-G: *A. tumefaciens* GV2260 (pBBRacdS, pIG121-Hm); V3-G: *A. tumefaciens* GV2260 (pBBRgabT, pIG121-Hm); V4-G: *A. tumefaciens* GV2260 (pBBRacdSgabT, pIG121-Hm). Bars represent the standard deviation (n = 3). Different characters indicate statistical differences in a one-way ANOVA and the Tukey-Kramer method, multiple comparison method ($P < 0.01$).

TABLE 2 | Effect of the Super-Agrobacterium ver.1, ver.3, and ver.4 on plant regeneration and transformation of the 'Micro-Tom' cotyledons.

Experiment repetition	Agrobacterium strain	Numbers of						Transformation frequency
		Segments	Calli	Shoots	Rooting	Diploid	Single copy	Inoculated Segments /Single copy (%)
1st	C-G	110	56	26	7	5	3	2.7
	V1-G	125	94	52	47	19	12	9.6
	V3-G	92	80	152	39	14	8	8.7
	V4-G	96	84	163	59	29	14	14.6
2nd	C-G	94	49	20	15	11	6	6.4
	V1-G	88	78	88	15	23	9	10.2
	V3-G	95	72	144	40	22	11	11.6
	V4-G	75	70	157	41	20	11	14. 7
3rd	C-G	82	42	26	11	6	3	3.7
	V1-G	85	78	57	25	16	8	9.4
	V3-G	88	65	101	31	16	8	9.1
	V4-G	91	86	95	63	28	15	16.5

Each column "Segments," "Calli," "Shoots," "Rooting," "Diploid," and "Single copy" indicated the number of occurrences. "Segments" means the number of segments used for inoculation of A. tumefaciens. "Calli," "Shoots," and "Rooting" showed the number of regenerate calli, shoot, and rooting. "Diploid" was the number rooting shoots that were diploid, detected by the ploidy analyzer. "Single copy" means the number of diploid rooting shoots with single copy of T-DNA, identified by Southern blot analysis. Transformation frequency was calculated as follows: the total number of transgenic plants with diploid and single copy was divided by the number of explants inoculated and then multiplied by 100. Only one plant regenerated per cotyledon explant was considered to calculate transformation efficiency. Three replications were done for this experiment.

different from the level of *vir* gene inducer. Previous studies have demonstrated that GABA was independent of *vir* gene expression (Chevrot et al., 2006; Haudecoeur et al., 2009). Thus, the inhibition of GABA further increased the transformation. On the other hand, research has shown that the ethylene target points are involved with *vir* gene expression, and the ethylene perceiving plant would reduce *vir* gene inducers or release antagonists of the *vir* gene inducers (Nonaka et al., 2008b). If the target point of the ethylene was the reduction of the *vir* gene inducer, the effect of the Super-*Agrobacterium* ver. 1 would be masked by acetosyringone. In fact, our results showed that the Super-*Agrobacterium* ver. 1 increased the transformation frequency up to 3.2 and 2.8 times in *E. ravennae* and *S. lycopersicum*, respectively, even with the application of the *vir* gene inducers. Therefore, these results suggest that the target point of ethylene is not the reduction of *vir* gene inducers, but the suppression of the antagonists.

In Super-*Agrobacterium* ver. 4, the enzymatic activity was one third of the Super-*Agrobacterium* ver. 1 and ver. 3, but it was effective in *E. ravennae* and *S. lycopersicum* "Micro-Tom" (**Figures 2A**, **C**). The amount of AcdS protein in the Super-*Agrobacterium* ver. 4 was one third of that found in Super-*Agrobacterium* ver. 1 (**Supplemental Figure 3**). Expressing multiple genes using the same promoter may reduce the expression levels of each gene. In this study, we used the lac promoter to drive both the *acdS* and *gabT* genes. If stronger promoters were used, the expression levels would be increased. Previous research compared the *vir* gene promoters (*virB*, *virC,* and *virD*) with the *lac* promoter activities; the *vir* gene promoters were found to show higher promoter activities than the *lac* promoter (Someya et al., 2013). Therefore, using these promoters would be effective to increase *acdS* and *gabT* expression in the Super-*Agrobacterium* ver. 4. Indeed, replacement of the promoter increased the *acdS* gene expression and the activity in *A. tumefaciens*, resulting in increased T-DNA transformation frequencies (Super-*Agrobacterium* ver. 2) (Someya et al., 2013). Therefore, replacing promoters would increase the transient transformations in *S. torvum via* the agroinfiltration method.

In this study, the stable transformation frequency was 15.2 ± 1.1%. This value was calculated as the ratio between independently transformed plants with diploid and single copy number in soil (checked by a ploidy analyzer and Southern blot analysis) and the total number of explants infected with *A. tumefaciens*. Previous studies have reported transformation frequencies that differ from ours (Sun et al., 2006; Khoudi et al., 2009; Khuong et al., 2013; Chetty et al., 2013). The transformation frequency might depend on the bacterial strain, binary vector and the selection method. In our study, the transformation frequency was calculated using regenerated rooting shoot with diploid and a single copy *per* inoculated segment. In contrast, most previous studies calculated this frequency from the PCR-positive tomatoes (Sun et al., 2006; Khoudi et al., 2009; Khuong et al., 2013; Chetty et al., 2013). Therefore, it would be difficult to compare between our and previous results. To create a transgenic plant, it is important to avoid somaclonal variation and multiple copies, which our method did.

The process of *Agrobacterium*-mediated stable transformation contains four steps: i) the T-DNA transfer into plant cells and integration into the host genome, ii) callus induction, iii) the regeneration of shoots, and iv) rooting. The activity of AcdS and GabT increased step (i) (**Figures 2A**, **C**). In the rooting step, there were no significant differences detected between them. Other steps showed different responses to AcdS and/or GabT activity (**Figure 3** and **Table 2**). The AcdS activity showed higher callus induction frequencies than the GabT activity, whereas the GabT activity induced higher shoot regeneration ratios than the AcdS. The browning callus appearance was suppressed by *A. tumefaciens* with AcdS (**Figures 3A**–**D**), as the ethylene induced hypersensitive responses and programmed cell death

(Wang et al., 2017); infection of *A. tumefaciens* with AcdS (Super-*Agrobacterium* ver. 1 or ver. 4) with the ability to remove ethylene, suppressed the browning phenomena. Although the function of GABA in plants needs to be clarified, there have been several studies regarding the functions of GABA as a signaling compound in plant growth and development. The increased endogenous concentrations of GABA seem to be the reason for impaired cell elongation in the *Arabidopsis thaliana* mutants, *pop2,* and *her1*, and the corresponding phenotypes (Renault et al., 2011). Infection of *A. tumefaciens* with GabT activity locally decreased GABA content in the plant calli and maintained higher shoot regeneration frequencies. Since both activities have different effective points in the transformation process, Super-*Agrobacterium* ver. 4. with AcdS and GabT activity at the same time, enhanced the stable transformation frequency approximately 3.6 times, compared with that of the original GV2260 strain.

We succeeded in producing an *A. tumefaciens* strain with improved potential for transformation by imbuing it with the ability to remove ethylene and GABA, which are negative factors in the *Agrobacterium*-plant interactions. *A. tumefaciens* with AcdS and GabT increased the T-DNA tranfer and stable transformation frequency. Especially in tomato, this newly bred bacterium (Super-*Agrobacterium* ver. 4) enables us to decrease the number of cotyledons used for transformation and allows us to reduce 72% of the time and labor required for transformation. Moreover, because our system was the plasmid with *acdS* and *gabT* gene, it is used in combination with other strains, such as the EHA105, EHA101, LBA4404, MP90, and AGL1. Based on this, we conclude that this new system is a useful tool for plant genetic engineering. On the other hand, the frequency is still not enough depending on the plant species and cultivars (**Figures 3E**, **F**). Therefore, the additional effort should have been required to adapt *Agrobacterium*-mediated transformation for a wide variety of plants. Other negative factors in *Agrobacterium*-plant interactions, aside from ethylene and GABA, have been reported by previous studies (Liu and Nester, 2006; Yuan et al., 2007; Yuan et al., 2008; Anand et al., 2008). Therefore, to expand plant spices and cultivars adapting *Agrobacterium*-mediated transformation, multiply suppress of these negative factors would be also effective.

DATA AVAILABILITY STATEMENT

All datasets GENERATED for this study are included in the manuscript/**Supplementary Files**.

AUTHOR CONTRIBUTIONS

SN designed the experiments, analyzed the data, and wrote the manuscript. TS constructed the plasmid pBBRacdSgabT and did the western blot analysis. YK performed the experiments about Agroinfiltration. HE and KN critically revised and approved the manuscript for publication.

FUNDING

This research was supported by grants from the New Energy and Industrial Technology Development Organization (NEDO) to HE and from JSPS KAKENHI (Grant Numbers JP24780001 and JP19K05964) to SN. Cooperative Research Grant from Plant Transgenic Design Initiative (PTraD), Gene Research Center in Tsukuba Innovation Plant Research Center (T-PIRC), University of Tsukuba, Japan supported this research.

ACKNOWLEDGMENTS

We appreciate the help of Prof. Mii (Chiba University, Japan) for kindly providing the *E. ravennae* calli. We also thank Prof. Nakamura (Chiba University, Japan) and Prof. Mitsui (Tohoku University, Japan) for the gift of the $pEKH_2$ plasmid and pBBR1MCS-5, respectively. We would like to thank Editage (www.editage.jp) for English language editing.

SUPPLEMENTARY MATERIAL

The Supplementary Material for this article can be found online at: https://www.frontiersin.org/articles/10.3389/fpls.2019.01204/full#supplementary-material

SUPPLEMENTAL FIGURE 1 | Map of binary vectors. **(A)** Map of $pEKH_2$-nosPNPTII-ubiPGUS-35SPHPT. NosP; Nopalin synthesis gene promoter, UbiP; ubiquitin gene promoter from rice, NosT; Nopalin synthesis gene terminator, *nptII*; neomycin phosphotransferase gene, *uidA*; beta-glucuronidase gene, *hptII*; hygromycin phosphotransferase gene, OriV; replication origin V (IncPα, plasmid RK2 from *E. coli*, GeneBank accession #J01780), *KanR*; Kanamycin resistance gene. RB; Right border sequence, LB; Left border sequence. **(B)** Map of pIG121-Hm. NosP; Nopalin synthesis gene promoter, CaMV 35S P; Cauliflower mosaic virus 35S promoter, NosT; Nopalin synthesis gene terminator, *nptII*; neomycin phosphotransferase gene, *uidA*; beta-glucuronidase gene, *hptII*; hygromycin phosphotransferase gene, OriV; replication origin V (IncPα, plasmid RK2 from *E. coli*, GeneBank accession #J01780), *KanR*; Kanamycin resistance gene, RB; Right border sequence, LB; Left border sequence. **(C)** Map of pEAQ-GFP-HT. CaMV 35S P; Cauliflower mosaic virus 35S promoter, NosT; Nopalin synthesis gene terminator, GFP; green fluorescence gene, RB; Right border sequence, LB; Left border sequence.

SUPPLEMENTAL FIGURE 2 | Map of the pIG121-Hm vector and the southern blot analysis of the T_0 generation. **(A)** Present the maps of the T-DNA region in the pIG121-Hm expression vectors used for the stable transformation. Red bars represent the position of probes used in the southern blot analysis. *Hin*dIII indicates the restriction enzyme sites that were used in the southern hybridization. NPTII probes were used in. **(B)** Southern blot analysis of the T_0 generation. Red numbers indicate the transgenic lines with single copy. C-G: *A. tumefaciens* GV2260 (pBBRMCS1-5, pIG121-Hm); V1-G: *A. tumefaciens* GV2260 (pBBRacdS, pIG121-Hm); V3-G: *A. tumefaciens* GV2260 (pBBRgabT, pIG121-Hm); V4-G: *A. tumefaciens* GV2260 (pBBRacdSgabT, pIG121-Hm).

SUPPLEMENTAL FIGURE 3 | Western blot analysis of ACC deaminase expression in *A. tumefaciens* strains using the cell lysate at the 'Early stage' ($O.D._{600}$ 0.7). ACC deaminase was probed with an anti-ACC deaminase antibody. Coomassie Brilliant Blue staining (bottom panel) is shown as an internal control. C-G: *A. tumefaciens* GV2260 (pBBRMCS1-5, pIG121-Hm); V1-G: *A. tumefaciens* GV2260 (pBBRacdS, pIG121-Hm); V3-G: *A. tumefaciens* GV2260 (pBBRgabT, pIG121-Hm); V4-G: *A. tumefaciens* GV2260 (pBBRacdSgabT, pIG121-Hm).

REFERENCES

Akihiro, T., Koike, S., Tani, R., Tominaga, T., Watanabe, S., Iijima, Y., et al. (2008). Biochemical mechanism on GABA accumulation during fruit development in tomato. *Plant Cell Physiol.* 49 (9), 1378–1389. doi: 10.1093/pcp/pcn113

Anand, A., Uppalapati, S. R., Ryu, C. M., Allen, S. N., Kang, L., Tang, Y., et al. (2008). Salicylic acid and systemic acquired resistance play a role in attenuating crown gall disease caused by *Agrobacterium tumefaciens*. *Plant Physiol.* 146 (2), 703–175. doi: 10.1104/pp.107.111302

Bevan, M. (1984). Binary *Agrobacterium* vectors for plant transformation. *Nucleic Acids Res.* 12 (22), 8711–8721. doi: 10.1093/nar/12.22.8711

Bradford, M. M. (1976). A rapid and sensitive method for the quantitation of microgram quantities of protein utilizing the principle of protein-dye binding. *Anal. Biochem.* 72, 248–254. doi: 10.1016/0003-2697(76)90527-3

Cangelosi, G. A., Ankenbauer, R. G., and Nester, E. W. (1990). Sugars induce the *Agrobacterium* virulence genes through a periplasmic binding protein and a transmembrane signal protein. *Proc. Natl. Acad. Sci. U. S. A.* 87 (17), 6708–6712. doi: 10.1073/pnas.87.17.6708

Chetty, V. J., Ceballos, N., Garcia, D., Narváez-Vásquez, J., Lopez, W., and Orozco-Cárdenas, M. L. (2013). Evaluation of four Agrobacterium tumefaciens strains for the genetic transformation of tomato (Solanum lycopersicum L.) cultivar Micro-Tom. *Plant Cell Rep.* 32 (2), 239–247. doi: 10.1007/s00299-012-1358-1

Chevrot, R., Rosen, R., Haudecoeur, E., Cirou, A., Shelp, B. J., Ron, E., et al. (2006). GABA controls the level of quorum-sensing signal in *Agrobacterium tumefaciens*. *Proc. Natl. Acad. Sci. U. S. A.* 103 (19), 7460–7464. doi: 10.1073/pnas.0600313103

Davis, M. E., Miller, A. R., and Lineberger, R. D. (1992). Studies on the effects of ethylene on transformation of tomato cotyledons (*Lycopersicon esculentum* Mill.) by *Agrobacterium tumefaciens*. *J. Plant Physiol.* 139 (3), 309–312. doi: 10.1016/S0176-1617(11)80343-3

Deblaere, R., Bytebier, B., De Greve, H., Deboeck, F., Schell, J., Van Montagu, M., et al. (1985). Efficient octopine Ti plasmid-derived vectors for *Agrobacterium*-mediated gene transfer to plants. *Nucleic Acids Res.* 13 (13), 4777–4788. doi: 10.1093/nar/13.13.4777

Elliott, K. A. C., and Hobbiger, F. (1959). Gamma aminobutyric acid: circulatory and respiratory effects in different species; re-investigation of the anti-strychnine action in mice. *J. Physiol.* 146, 70–84. doi: 10.1113/jphysiol.1959.sp006178

Ezura, H., Yuhashi, K. I., Yasuta, T., and Minamisawa, K. (2000). Effect of ethylene on *Agrobacterium tumefaciens*-mediated gene transfer to melon. *Plant Breed.* 119 (1), 75–79. doi: 10.1046/j.1439-0523.2000.00438.x

Forlani, G., Bertazzini, M., and Giberti, S. (2014). Differential accumulation of γ-aminobutyric acid in elicited cells of two rice cultivars showing contrasting sensitivity to the blast pathogen. *Plant Biol.* 16 (6), 1127–1132. doi: 10.1111/plb.12165

Guo, M., Ye, J., Gao, D., Xu, N., and Yang, J. (2019). Agrobacterium-mediated horizontal gene transfer: Mechanism, biotechnological application, potential risk and forestalling strategy. *Biotechnol Adv.* 37 (1), 259–270. doi: 10.1016/j.biotechadv.2018.12.008

Han, J. S., Kim, C. K., Park, S. H., Hirschi, K. D., and Mok, I. (2005). *Agrobacterium*-mediated transformation of bottle gourd (*Lagenaria siceraria* Standl.). *Plant Cell Rep.* 23 (10–11), 692–698. doi: 10.1007/s00299-004-0874-z

Hao, Y., Charles, T. C., and Glick, B. R. (2010). ACC deaminase increases the *Agrobacterium tumefaciens*-mediated transformation frequency of commercial canola cultivars. *FEMS Microbiol. Lett.* 307 (2), 185–190. doi: 10.1111/j.1574-6968.2010.01977.x

Haudecoeur, E., Planamente, S., Cirou, A., Tannières, M., Shelp, B. J., Moréra, S., et al. (2009). Proline antagonizes GABA-induced quenching of quorum-sensing in *Agrobacterium tumefaciens*. *Proc. Natl. Acad. Sci. U. S. A.* 106 (34), 14587–14592. doi: 10.1073/pnas.0808005106

He, F., Nair, G. R., Soto, C. S., Chang, Y., Hsu, L., Ronzone, E., et al. (2009). Molecular basis of ChvE function in sugar binding, sugar utilization, and virulence in *Agrobacterium tumefaciens*. *J. Bacteriol.* 191 (18), 5802–5813. doi: 10.1128/JB.00451-09

Hiei, Y., Ohta, S., Komari, T., and Kumashiro, T. (1994). Efficient transformation of rice (*Oryza sativa* L.) mediated by *Agrobacterium* and sequence analysis of the boundaries of the T-DNA. *Plant J.* 6 (2), 271–282. doi: 10.1046/j.1365-313X.1994.6020271.x

Hoekema, A., Hirsch, P. R., Hooykaas, P. J. J., and Schilperoort, R. A. (1983). A binary plant vector strategy based on separation of *vir*- and T-region of the *Agrobacterium tumefaciens* Ti-plasmid. *Nature* 303 (5913), 179–180. doi: 10.1038/303179a0

Honma, S., and Shimomura, T. (1978). Metabolism of 1-aminocyclopropane-1-carboxylic acid. *Agric. Biol. Chem.* 42 (10), 1825–1831. doi: 10.1080/00021369.1978.10863261

Hoshikawa, K., Fujita, S., Renhu, N., Ezura, K., Yamamoto, T., Nonaka, S., et al. (2019). Efficient transient protein expression in tomato cultivars and wild species using agroinfiltration-mediated high expression system. *Plant Cell Rep.* 38 (1), 75–84. doi: 10.1007/s00299-018-2350-1

Hoshikawa, K., Ishihara, G., Takahashi, H., and Nakamura, I. (2012). Enhanced resistance to gray mold (*Botrytis cinerea*) in transgenic potato plants expressing thionin genes isolated from *Brassicaceae* species. *Plant Biotechnol.* 29, 87–93. doi: 10.5511/plantbiotechnology.12.0125a

Hu, X., Zhao, J., DeGrado, W. F., and Binns, A. N. (2013). *Agrobacterium tumefaciens* recognizes its host environment using *ChvE* to bind diverse plant sugars as virulence signals. *Proc. Natl. Acad. Sci. U. S. A.* 110 (2), 678–683. doi: 10.1073/pnas.1215033110

Ishida, Y., Saito, H., Ohta, S., Hiei, Y., Komari, T., and Kumashiro, T. (1996). High efficiency transformation of maize (*Zea mays* L.) mediated by *Agrobacterium tumefaciens*. *Nat. Biotechnol.* 14 (6), 745–750. doi: 10.1038/nbt0696-745

Kado, C. I. (2014). Historical account on gaining insights on the mechanism of crown gall tumorigenesis induced by *Agrobacterium tumefaciens*. *Front Microbiol.* 5, 340. doi: 10.3389/fmicb.2014.00340

Khoudi, H., Nouri-Khemakhem, A., Gouiaa, S., and Masmoudi, K. (2009). Optimization of regeneration and transformation parameters in tomato and improvement of its salinity and drought tolerance. *Afr. J. Biotechnol.* 8, 6068–6076. doi: 10.5897/AJB09.057

Khuong, T. T., Crété, P., Robaglia, C., and Caffarri, S. (2013). Optimisation of tomato Micro-tom regeneration and selection on glufosinate/Basta and dependency of gene silencing on transgene copy number. *Plant Cell Rep.* 32 (9), 1441–1454. doi: 10.1007/s00299-013-1456-8

Knoch, E., Sugawara, S., Mori, T., Poulsen, C., Fukushima, A., Harholt, J., et al. (2019). Third DWF1 paralog in Solanaceae, sterol Δ24-isomerase, branches withanolide biosynthesis from the general phytosterol pathway. *Proc. Natl. Acad. Sci. U. S. A.* 115 (34), E8096–E8103. doi: 10.1073/pnas.1807482115

Komari, T. (1990). Transformation of cultured cells of Chenopodium quinoa by binary vectors that carry a fragment of DNA from the virulence region of pTiBo542. *Plant Cell Rep.* 9 (6), 303–306. doi: 10.1007/BF00232856

Komari, T., Takakura, Y., Ueki, J., Kato, N., Ishida, Y., and Hiei, Y. (2006). Binary vectors and super-binary vectors. *Methods Mol. Biol.* 343, 15–41. doi: 10.1385/1-59745-130-4:15

Kovach, M. E., Elzer, P. H., Hill, D. S., Robertson, G. T., Farris, M. A., Roop, R. M., 2nd, et al. (1995). Four new derivatives of the broad-host-range cloning vector pBBR1MCS, carrying different antibiotic-resistance cassettes. *Gene.* 166 (1), 175–176. doi: 10.1016/0378-1119(95)00584-1

Liu, P., and Nester, E. W. (2006). Indoleacetic acid, a product of transferred DNA, inhibits *vir* gene expression and growth of *Agrobacterium tumefaciens* C58. *Proc. Natl. Acad. Sci. U. S. A.* 103 (12), 4658–4662. doi: 10.1073/pnas.0600366103

Malambane, G., Nonaka, S., Shiba, H., Ezura, H., Tsujimoto, H., and Akashi, K. (2018). Comparative effects of ethylene inhibitors on *Agrobacterium*-mediated transformation of drought-tolerant wild watermelon. *Biosci Biotechnol Biochem.* 82 (3), 433–441. doi: 10.1080/09168451.2018.1431516

Murashige, T., and Skoog, F. (1962). A revised medium for rapid growth and bio assays with tobacco tissue cultures. *Physiol. Plant.* 15, 473–497. doi: 10.1111/j.1399-3054.1962.tb08052.x

Nonaka, S., and Ezura, H. (2014). Plant-*Agrobacterium* interaction mediated by ethylene and super-*Agrobacterium* conferring efficient gene transfer. *Front. Plant Sci.* 5, 681. doi: 10.3389/fpls.2014.00681

Nonaka, S., Someya, T., Zhou, S., Takayama, M., Nakamura, K., and Ezura, H. (2017). An *Agrobacterium* tumefaciens strain with gamma-aminobutyric acid transaminase activity shows an enhanced genetic transformation ability in plants. *Sci. Rep.* 7, 42649. doi: 10.1038/srep42649

Nonaka, S., Sugawara, M., Minamisawa, K., Yuhashi, K., and Ezura, H. (2008a). 1-Aminocyclopropane-1-carboxylate deaminase enhances *Agrobacterium tumefaciens*-mediated gene transfer into plant cells. *Appl. Environ. Microbiol.* 74 (8), 2526–2528. doi: 10.1128/AEM.02253-07

Nonaka, S., Yuhashi, K., Takada, K., Sugaware, M., Minamisawa, K., and Ezura, H. (2008b). Ethylene production in plants during transformation suppresses *vir* gene expression in *Agrobacterium tumefaciens*. *New Phytol.* 178 (3), 647–656. doi: 10.1111/j.1469-8137.2008.02400.x

Ntui, V. O., Khan, R. S., Chin, D. P., Nakamura, I., and Mii, M. (2010). An efficient *Agrobacterium tumefaciens*-mediated genetic transformation of "Egusi" melon (*Colocynthis citrullus* L.). *Plant Cell Tiss. Organ. Cult.* 103, 15–22. doi: 10.1007/s11240-010-9748-y

Ohta, S., Mita, S., Hattori, T., and Nakamura, K. (1990). Construction and expression in tobacco of a β-glucuronidase (GUS) reporter gene containing an intron within the coding sequence. *Plant Cell Physiol.* 31, 805–813. doi: 10.1093/oxfordjournals.pcp.a077982

Park, D. H., Mirabella, R., Bronstein, P. A., Preston, G. M., Haring, M. A., Lim, C. K., et al. (2010). Mutations in γ-aminobutyric acid (GABA) transaminase genes in plants or Pseudomonas syringae reduce bacterial virulence. *Plant J.* 64 (2), 318–330. doi: 10.1111/j.1365-313X.2010.04327.x

Planamente, S., Moréra, S., and Faure, D. (2013). In planta fitness-cost of the Atu4232-regulon encoding for a selective GABA-binding sensor in Agrobacterium. *Commun Integr Biol.* 6 (3), e23692. doi: 10.4161/cib.23692

Planamente, S., Vigouroux, A., Mondy, S., Nicaise, M., Faure, D., and Moréra, S. (2010). A conserved mechanism of GABA binding and antagonism is revealed by structure-function analysis of the periplasmic binding protein Atu2422 in *Agrobacterium tumefaciens*. *J Biol Chem.* 285 (39), 30294–30303. doi: 10.1074/jbc.M110.140715

Renault, H., El Amrani, A., Palanivelu, R., Updegraff, E. P., Yu, A., Renou, J. P., et al., et al. (2011). GABA accumulation causes cell elongation defects and a decrease in expression of genes encoding secreted and cell wall-related proteins in *Arabidopsis thaliana*. *Plant Cell Physiol.* 52 (5), 894–908. doi: 10.1093/pcp/pcr041

Sainsbury, F., Thuenemann, E. C., and Lomonossoff, G. P. (2009). pEAQ: versatile expression vectors for easy and quick transient expression of heterologous proteins in plants. *Plant Biotechnol. J.* 7 (7), 682–693. doi: 10.1111/j.1467-7652.2009.00434.x

Sheehy, R. E., Honma, M., Yamada, M., Sasaki, T., Martineau, B., and Hiatt, W. R. (1991). Isolation, sequence, and expression in *Escherichia coli* of the *Pseudomonas* sp. strain ACP gene encoding 1-aminocyclopropane-1-carboxylate deaminase. *J Bacteriol.* 173 (17), 5260–5265. doi: 10.1128/jb.173.17.5260-5265.1991

Shelp, B. J., Bozzo, G. G., Trobacher, C. P., Zarei, A., Deyman, K. L., and Brikis, C. J. (2012). Hypothesis/review: contribution of putrescine to 4-aminobutyrate (GABA) production in response to abiotic stress. *Plant Sci.* 193–194, 130–135. doi: 10.1016/j.plantsci.2012.06.001

Someya, T., Nonaka, S., Nakamura, K., and Ezura, H. (2013). Increased 1-aminocyclopropane-1-carboxylate deaminase activity enhances *Agrobacterium tumefaciens*-mediated gene delivery into plant cells. *Microbiol. Open.* 2 (5), 873–880. doi: 10.1002/mbo3.123

Stachel, S. E., Messens, E., Van Montagu, M., and Zambryski, P. (1985). Identification of the signal molecules produced by wounded plant cells that activate T-DNA transfer in *Agrobacterium tumefaciens*. *Nature* 318 (6047), 624–629. doi: 10.1038/318624a0

Stachel, S. E., Nester, E. W., and Zambryski, P. C. (1986). A plant cell factor induces *Agrobacterium tumefaciens vir* gene expression. *Proc. Natl. Acad. Sci. U. S. A.* 83 (2), 379–383. doi: 10.1073/pnas.83.2.379

Sun, H. J., Uchii, S., Watanabe, S., and Ezura, H. (2006). A highly efficient transformation protocol for Micro-Tom, a model cultivar for tomato functional genomics. *Plant Cell Physiol.* 47 (3), 426–431. doi: 10.1093/pcp/pci251

Takahashi, H., Sumi, M., and Koshino, F. (1961). Effect of gamma-aminobutyric acid (GABA) on normotensive or hypertensive rats and men. *Jpn. J. Physiol.* 11, 89–95. doi: 10.2170/jjphysiol.11.89

Takahashi, H., Tiba, M., Iino, M., and Takayasu, T. (1995). The effect of γ-aminobutyric acid on blood pressure. *Jpn. J. Physiol.* 5, 334–341. doi: 10.2170/jjphysiol.5.334

Vaghchhipawala, Z., Radke, S., Nagy, E., Russell, M. L., Johnson, S., Gelvin, S. B., et al. (2018). RepB C-terminus mutation of a pRi-repABC binary vector affects plasmid copy number in Agrobacterium and transgene copy number in plants. *PLoS One.* 13 (11), e0200972. doi: 10.1371/journal.pone.0200972.

van der Fits, L., Deakin, E. A., Hoge, J. H. C., and Memelink, J. (2000). The ternary transformation system: constitutive virG on a compatible plasmid dramatically increases *Agrobacterium*-mediated plant transformation. *Plant Mol. Biol.* 43 (4), 495–502. doi: 10.1023/A:1006440221718

Velásquez, A. C., Chakravarthy, S., and Martin, G. B. (2009). Virus-induced gene silencing (VIGS) in Nicotiana benthamiana and tomato. *J Vis Exp.* 10, 1292. doi: 10.3791/1292

Wang, H., Lin, J., Chang, Y., and Jiang, C. Z. (2017). Comparative transcriptomic analysis reveals that ethylene/H2O2-mediated hypersensitive response and programmed cell death determine the compatible interaction of sand pear and *Alternaria alternata*. *Front. Plant Sci.* 8, 195. doi: 10.3389/fpls.2017.00195

Wood, D. W., Setubal, J. C., Kaul, R., Monks, D. E., Kitajima, J. P., Okura, V. K., et al. (2001). The genome of the natural genetic engineer *Agrobacterium tumefaciens* C58. *Science.* 294 (5550), 2317–2323. doi: 10.1126/science.1066804

Ye, X., Williams, E. J., Shen, J., Johnson, S., Lowe, B., Radke, S., et al. (2011). Enhanced production of single copy backbone-free transgenic plants in multiple crop species using binary vectors with a pRi replication origin in *Agrobacterium tumefaciens*. *Transgenic Res.* 20 (4), 773–786. doi: 10.1007/s11248-010-9458-6

Yuan, Z. C., Edlind, M. P., Liu, P., Saenkham, P., Banta, L. M., Wise, A. A., et al. (2007). The plant signal salicylic acid shuts down expression of the vir regulon and activates quormone-quenching genes in Agrobacterium. *Proc. Natl. Acad. Sci. U. S. A.* 104 (28), 11790–11795.

Yuan, Z. C., Haudecoeur, E., Faure, D., Kerr, K. F., and Nester, E. W. (2008). Comparative transcriptome analysis of *Agrobacterium tumefaciens* in response to plant signal salicylic acid, indole-3-acetic acid and gamma-amino butyric acid reveals signalling cross-talk and *Agrobacterium*-plant co-evolution. *Cell Microbiol.* 10 (11), 2339–2354. doi: 10.1111/j.1462-5822.2008.01215.x

Zambryski, P., Joos, H., Genetello, C., Leemans, J., Van Montagu, M., and Schell, J. (1983). Ti plasmid vector for the introduction of DNA into plant cells without alteration of their normal regeneration capacity. *EMBO J.* 2 (12), 2143–2150. doi: 10.1002/j.1460-2075.1983.tb01715.x

Conflict of Interest: The authors declare that the research was conducted in the absence of any commercial or financial relationships that could be construed as a potential conflict of interest.

frontiers in Plant Science

ORIGINAL RESEARCH
published: 09 October 2019
doi: 10.3389/fpls.2019.01248

Red to Brown: An Elevated Anthocyanic Response in Apple Drives Ethylene to Advance Maturity and Fruit Flesh Browning

*Richard V. Espley[1], Davin Leif[1], Blue Plunkett[1], Tony McGhie[2], Rebecca Henry-Kirk[1], Miriam Hall[1], Jason W. Johnston[3], Matthew P. Punter[3], Helen Boldingh[4], Simona Nardozza[1], Richard K. Volz[3], Samuel O'Donnell[1] and Andrew C. Allan[1,5]**

[1] Plant & Food Research, Auckland, New Zealand, [2] Plant & Food Research, Palmerston North, New Zealand, [3] Hawke's Bay Research Centre, Plant & Food Research, Havelock North, New Zealand, [4] Plant & Food Research, Hamilton, New Zealand, [5] School of Biological Sciences, University of Auckland, Auckland, New Zealand

OPEN ACCESS

Edited by:
Autar Krishen Mattoo, Agricultural Research Service (USDA), United States

Reviewed by:
Prabodh Kumar Trivedi, National Botanical Research Institute (CSIR), India
Ai-Sheng Xiong, Nanjing Agricultural University, China

***Correspondence:**
Andrew C. Allan
andrew.allan@plantandfood.co.nz

Specialty section:
This article was submitted to Plant Physiology, a section of the journal Frontiers in Plant Science

Received: *16 May 2019*
Accepted: *06 September 2019*
Published: *09 October 2019*

Citation:
Espley RV, Leif D, Plunkett B, McGhie T, Henry-Kirk R, Hall M, Johnston JW, Punter MP, Boldingh H, Nardozza S, Volz RK, O'Donnell S and Allan AC (2019) Red to Brown: An Elevated Anthocyanic Response in Apple Drives Ethylene to Advance Maturity and Fruit Flesh Browning. Front. Plant Sci. 10:1248. doi: 10.3389/fpls.2019.01248

The elevation of anthocyanin contents in fruits and vegetables is a breeding target for many crops. In some fruit, such as tomato, higher anthocyanin concentrations enhance storage and shelf life. In contrast, highly anthocyanic red-fleshed apples (*Malus* x *domestica*) have an increased incidence of internal browning flesh disorder (IBFD). To determine the mechanisms underlying this, 'Royal Gala' cultivar apples over-expressing the anthocyanin-related transcription factor (TF) MYB10 (35S:MYB10), which produces fruit with highly pigmented flesh, were compared with standard 'Royal Gala' Wild Type (WT) grown under the same conditions. We saw no incidence of IBFD in WT 'Royal Gala' but the over-expression of MYB10 in the same genetic background resulted in a high rate of IBDF. We assessed concentrations of potential substrates for IBDF and a comparison of metabolites in these apples showed that anthocyanins, chlorogenic acid, pro-cyanidins, flavon-3-ols, and quercetin were all higher in the MYB10 lines. For the flavol-3-ols sub-group, epicatechin rather than catechin was elevated in MYB10 lines compared with the control fruit. Internal ethylene concentrations were measured throughout fruit development and were significantly higher in 35S:MYB10 lines, and ethylene was detected at an earlier developmental stage pre-harvest. Expression analysis of key genes associated with ethylene biosynthesis (aminocyclopropane-1-carboxylic acid synthase and oxidase; *ACS* and *ACO*) and polyphenol oxidase (*PPO*) showed the potential for increased ethylene production and the mechanism for enhanced PPO-mediated browning. The expression of a transcription factor of the ethylene response factor (ERF) class, *ERF106*, was elevated in red flesh. Analysis of transcriptional activation by MYB10 showed that this transcription factor could activate the expression of apple *ACS*, *ACO,* and *ERF106* genes. Our data show a link between the elevation of anthocyanin-related transcription factors and an undesirable fruit disorder. The accelerated advancement of maturity *via* premature ethylene induction has implications for the breeding and storage of these more highly pigmented plant products.

Keywords: apple, anthocyanin, flavonoids, ethylene, peroxidase, transcription factors, enzymatic browning, ripening

INTRODUCTION

Apples have a long history of association with human civilisation and over 8,000 years of domestication. The current domesticated apple (*Malus* x *domestica*) has become a fruit with high economic value with over 83 million tonnes harvested worldwide (FAO, 2018). Novel cultivars continue to be bred, such as red-fleshed apples created by crossing wild-red fleshed apples with domesticated varieties (Espley et al., 2007; Volz et al., 2009). While large red-fleshed apples are now available, they suffer from a variety of fruit quality issues. Most notably, red-fleshed apples suffer from an increased incidence in enzymatic browning (Volz et al., 2013).

In fruit development, ripening represents the final stage. During this period, important structural, biochemical, and physiological changes such as net starch degradation, softening of the flesh, changes in aroma and flavour profiles occur (Giovannoni et al., 2017). Additionally, two types of fruit ripening behaviour are present amongst plants, climacteric and non-climacteric (Lelievre et al., 1997). Climacteric fruits usually undergo a large burst of ethylene just before, during, or after a respiratory peak also known as a climacteric rise (Wills et al., 2001). Apples fall under this category. Non-climacteric fruits do not exhibit the large burst of ethylene nor any changes in respiration. Fruits that fall under this category include citrus (Alonso et al., 1995), grape, and strawberry (Giovannoni, 2004).

Apple fruit, such as 'Royal Gala', reach the stage of commercial harvest maturity at around 130 days after full bloom (Janssen et al., 2008), although maturity ranges from around 100 to 190 days after full bloom (DAFB), depending on cultivar and climate. In this phase, cell wall modifying enzymes are produced, causing changes in texture which makes the fruit palatable (Schaffer et al., 2013). This causes cell wall polysaccharides, including pectin and cellulose, to be broken down by cell wall degrading enzymes such as polygalacturonase. Changes in flavour are mainly due to a change in sugar-acid balance, a breakdown of bitter compounds (tannins and flavonoids) and an increase in production of volatiles such as methyl esters (ocimene and myrcene) to a total of at least 34 esters upon ripening in 'Royal Gala' (Young et al., 2004; Defilippi et al., 2009). Apple also undergoes a colour change as a result of the reduced production of chlorophyll and its degradation causing the unmasking of pigments that were already previously formed and synthesis of new pigments (carotenoids or anthocyanins) (Ferrer et al., 2005).

Browning (enzymatic browning) is a reaction that often occurs in fruit at the end of ripening and the beginning of over-ripening (Murata et al., 1995). Apple fruit, because of their high phenolic content, are highly susceptible to browning (Holderbaum et al., 2010). Internal browning can be triggered when the fruit is wounded (Queiroz et al., 2008). Browning is also related to abiotic stress in storage, such as low temperature, low oxygen, and/or high carbon dioxide (Mellidou et al., 2014). Browning occurs when phenolic compounds are oxidised by the enzyme polyphenol oxidase (PPO) which causes brown pigments to be generated (Queiroz et al., 2008). PPOs belong to a large gene family and of these, ten PPO genes have been mapped to the 'Golden Delicious' apple genome (Di Guardo et al., 2013). Polyphenol compounds are stored in vacuoles whilst PPOs are found in plastids (Holderbaum et al., 2010). Wounding, such as cutting or dropping the fruit, can weaken the cells, which allows both PPO and phenolic compounds to interact, causing polyphenols to revert to their corresponding quinones when oxidised by PPO. These then polymerise with other quinones or phenols to form brown pigments (Murata et al., 1995). Similarly, ripening also causes weakening effects in cells because enzymes, such as polygalacturonases, break down cell walls (Kramer and Redenbaugh, 1994). In apple cultivars, such as 'Aori27' and 'Mellow', chlorogenic acid is the major phenolic compound that is oxidised. In 'Fuji', chlorogenic acid and epicatechin are the major phenolic compounds, whilst in 'Elstar', epicatechin and procyanidin predominate (Holderbaum et al., 2010). The activity of PPO has also been shown to decrease as the apple ripens. This is due to a denaturing of the protein and not reduced PPO production (Murata et al., 1995). The ability to control enzymatic browning is important because it negatively impacts on colour, taste, flavour, and nutritional value in many fruits and vegetables (Holderbaum et al., 2010). Recently one apple has been engineered to reduce enzymatic browning. Named the 'Artic' apple, it possesses a non-browning trait conferred to it by silencing the PPO through RNA interference (RNAi), therefore reducing its expression (Waltz, 2015). This results in an apple which retains its colour, taste, flavour, and nutritional value even when damaged or cut.

Anthocyanins are a class of flavonoids commonly found in fruits and vegetables responsible for the vivid red, blue, and purple colours commonly found in nature (He and Giusti, 2010). In apple, the anthocyanins are primarily composed of cyanidin-3-galactoside with cyanidin-3-arabinoside, cyanidin-7-arabinoside, and cyanidin-3-xyloside usually in minor amounts (Vrhovsek et al., 2004; Meng et al., 2016). Overall, anthocyanins compose around 1–3% of total polyphenols in apples (Vrhovsek et al., 2004).

Anthocyanins are generated by enzymes of the phenylpropanoid pathway, including chalcone synthase (CHS) and chalcone isomerase (CHI), flavanone 3-hydroxylase (F3H), flavonoid 3'-hydroxylase (F3'H), flavonoid 3',5'-hydroxylase (F3'5'H) dihydroflavonol reductase (DFR), anthocyanidin synthase (ANS), and leucoanthocyanidin dioxygenase (LDOX) flavonoid-3-O-glycosyltransferase (UFGT/UF3GT) (Holton and Cornish, 1995; Winkel-Shirley, 2001; Tanaka et al., 2008). These enzymes are regulated at the transcriptional level by a well-studied complex termed the MBW complex (proteins of the transcription factor [TF] classes MYB, basic helix-loop-helix bHLH and a WD40 repeat protein). In apple, MYB10, which is allelic to MYB1/MYBA, regulates anthocyanin biosynthesis, having 58% overall protein identity to PRODUCTION OF ANTHOCYANIN PIGMENT 1 (PAP1/MYB75) in Arabidopsis. The apple bHLHs MdbHLH3 and MdbHLH33 are both members of the IIIf subfamily (Heim et al., 2003) and interact with MdMYB10. Both share high homology with TT8 in Arabidopsis and Delila in snapdragon (Espley et al., 2007).

In addition to the MBW complex, other TFs affect anthocyanin biosynthesis *via* protein-protein interaction with the MBW complex, or regulation of expression levels of genes

encoding the MBW. A SQUAMOSA MADS-box gene regulates anthocyanin accumulation in bilberry (Jaakola et al., 2010). More recently, ethylene response factors (ERFs) have been shown to affect fruit colour at this level. In apple, MdERF1B has been shown to bind to the promoters of anthocyanin and proanthocyanidin regulating MYBs to alter anthocyanin and proanthocyanidin concentration (Zhang et al., 2018). In pear, PyERF3 interacts with PyMYB114 and its partner PybHLH3 to co-regulate anthocyanin biosynthesis (Yao et al., 2017) while in apple MYB1/10 was shown to activate expression of apple ERF3 (a close homologue to pear ERF3) and this increase in ERF expression increases ethylene emission from apple callus (An et al., 2018). Furthermore, it was shown that EIL1 directly bound to the promoter of MYB1 to induce anthocyanin production, while MYB1 was able to interact with ERF3, providing a positive feedback loop for ethylene biosynthesis. The apple bHLH3, a known partner to MYB1/10 in the MBW complex, has also been implicated in activating ACO and ACS1 and ACS5 genes to drive ethylene production (Hu et al., 2019). In a recent study of the transcriptome of red-fleshed apple (Wang et al., 2018), WRKY11 and ERF106 were identified as being differentially regulated and both were more expressed in red flesh.

Here, we use isogenic lines of 'Royal Gala' that differ genetically by only the over-expression of *MYB10* (Espley et al., 2007). These lines show that MYB10 can activate the expression of apple *ACS* and *ACO* genes, possibly *via* up-regulation of *ERF* genes. This activation links anthocyanin concentrations and ethylene, as well as enhanced amounts of PPO and substrates for the browning reaction. This linkage has implications for the quality of highly pigmented apples.

MATERIALS AND METHODS

Plant Materials

To generate highly anthocyanic apple fruit, the *Malus* x *domestica* 'Royal Gala' apple cultivar was transformed with an over-expression construct containing *MYB10* cDNA under the control of the CaMV35S promoter as previously described (Espley et al., 2007). Fruit from multiple trees for three independent transgenic lines (A1, A3, and A4) over two seasons (2013–2014 and 2014–2015) were used in this study and compared with non-transformed wild type (WT) 'Royal Gala' fruit grown under the same conditions in a containment glasshouse. Samples from each season were collected at seven different time points: T1 = 35 Days After Full Bloom (DAFB); T2 = 65DAFB; T3 = 85 DAFB; T4 = 110 DAFB = T5, 120 DAFB; T6 = 130 DAFB (WT 'Royal Gala' commercial maturity); T7, 140 DAFB, using fruit from two or three transgenic lines (A1, A3, A4; dependent on fruit number) and WT control fruit. For gene expression analysis T2 to T6 were assayed, to capture the most relevant developmental stages.

Fruit Maturity and Ripening Assessments

Ethylene concentrations were determined both during fruit development and at harvest on three transgenic lines (A1, A3, and A4) and 'Royal Gala' WT fruit. For fruit *on planta*, a needle was inserted into the core cavity and the insertion site was sealed with wax to prevent wounding-related damage or gaseous loss; this remained in place during fruit development. Internal ethylene concentration was determined by extracting a 1 ml core cavity gas sample, using a compatible syringe to the inserted needle, and injecting it into a gas chromatograph (Hewlett Packard, 5890 series II) as previously described (Johnston et al., 2009). For harvested fruit, ethylene samples were extracted at one of the developmental time points using the same analysis method with five biological replicates. Fruit firmness was assessed by Texture Analyser TAXT plus (Stable Microsystems, United Kingdom) fitted with a 7.9-mm Effegi penetrometer probe (Johnston et al., 2009). Soluble solids content (SSC) was assessed by hand-held refractometer. Fruit were also maintained in industry-standard storage conditions for ten weeks after harvest at 0.5°C and assessed for extent of internal browning.

Peroxidase Enzyme Assay

Enzyme activity was assessed spectrophotometrically at 25°C. All assays were performed on a SpectroMax plus 384 UV-vis spectrophotometer and analysed using the SoftMax Pro v5.4.5 software. Peroxidase (POX) was extracted and assayed based on a modified version previously described (Lester et al., 2004). Apple cortical tissue was frozen and ground into a fine powder in liquid nitrogen; 250 mg of tissue was then homogenised in 1 ml of 100 mM phosphate buffer pH 7.0 containing 0.5 mM cysteine and 4% w/v polyvinylpolypyrrolidone (PVPP). POX activity was determined by adding 25 µL of the extract to 225µL of assay reagent (50 mM potassium phosphate, pH 7.0, 10 mM guaiacol, and 10 mM H_2O_2) in a 96-well plate. The reaction was initiated by adding 10 mM guaiacol, and the activity determined by the rate of formation of tetraguaiacol at 470 nM. Assays were performed in triplicate for each of the biological replicates. Results are presented as the maximum rate of change per mg of protein.

Non-Structural Carbohydrates and Anthocyanin Analysis

Fruit flesh tissue was ground under liquid nitrogen using an IKA (IKA, Staufen, Germany) grinder and stored at -80°C. Soluble sugars were extracted from 200 mg aliquots of ground flesh in 80% ethanol. The soluble sugars (glucose, fructose, sucrose, and sorbitol) were analysed by ion chromatography as described in Nardozza et al. (2013). Starch was analysed by a colorimetric method following enzymatic digestion of the pellet obtained from the sugar extraction, as previously described by Smith et al. (1992). Anthocyanin and flavonoids were extracted in methanol (75% in water) and quantified by High Performance Liquid Chromatography (HPLC), using a method previously described (Espley et al., 2013). Starch accumulation rate/degradation was calculated using the Relative Growth Rate (RGR) where the primary data were logarithmically transformed to homogenise variability (Opara, 2000).

Gene Expression Analysis

RNA from apple flesh was isolated using the Spectrum™ Plant Total RNA kit (Sigma) and cDNA was synthesised using the

Qantitect® Reverse Transcription kit (Qiagen), both according to the manufacturer's recommendations. Primers used for qPCR analysis was designed using Geneious 8.1.9 (Kearse et al., 2012) and synthesised by Macrogen (Republic of Korea). Primers are listed in **Table S1**. qPCR analysis was performed using the LightCycler® 480 using LightCycler FastStart SYBR Green Mix (Roche Diagnostics), according to the manufacturer's guideline. Reactions contained 2.5 µl Master Mix, 0.25 µl of each primer (10 mM), 1.25 ml diluted cDNA (1:25), and nuclease-free water (Roche Diagnostics) to a total volume of 5 µl, using reaction conditions previously reported (Espley et al., 2007). Expression was normalised against *Malus* x *domestica Elongation factor 1* (*MdEF1α*), a 'housekeeping' gene known for its consistent transcript level in apple fruits and leaves (Chagné et al., 2013).

Isolation and Cloning of Apple Gene Promoter Sequences

For the cloning of apple promoters used in the Dual Luciferase assays, nested primers were designed to the target sequence. The inner primers for use in promoter isolation were designed to isolate approximately 2 kb upstream of the transcription start site of each gene. PCR fragments were cloned using Platinum® Taq DNA Polymerase High Fidelity (Thermofisher Scientific) as per manufacturer's protocols. For all candidate gene promoters, outer PCR amplification was first performed and checked on agarose gels. The PCR product was diluted 100 x and 1.5 µl of this was used as the template for the inner PCR amplification. Fragments were cleaned using DNA Clean and Concentrator™ (Zymo Research) as per manufacturer's protocol and cloned into the pGreenII 0800-Luc using the In-Fusion® HD Cloning Kit. Promoter fragments were verified by sequencing. Analysis of putative binding TF sites in the MdERF106 promoter was carried out using PlantPAN 2.0 (Chien et al., 2015). The MYB TF over-expression constructs used in the luciferase assays were as previously described (Lin-Wang et al., 2011; Brendolise et al., 2017).

Dual Luciferase Assays

Glasshouse-grown *Nicotiana benthamiana* plants were used for the dual luciferase assays to determine transcription factor activation of promoter sequences, as previously described (Hellens et al., 2005).

Phylogenic and Statistical Analysis

Arabidopsis and other plant protein sequences were obtained from NCBI. Full-length sequences were aligned using MEGA 6.06 (Tamura et al., 2013) MUSCLE (open = -2.9, gap = 0) (Edgar, 2004). Phylogenetic analysis of the proteins were performed using MEGA 6.06 using a maximum likelihood method based on the JTT matrix-based model (Jones et al., 1992) and 1,000 bootstrap replicates. Analysis of the ERF genes was performed using MEGA 6.06 (6140226) *via* the Neighbour-Joining method (Saitou and Nei, 1987) with evolutionary distances calculated using the JTT matrix-based model and 1,000 bootstrap replicates.

The effects of the transgenic modification and fruit developmental stage (factors) on secondary metabolites, ethylene, peroxidase enzyme activity, and non-structural carbohydrates were analysed by ANOVA (type 3 sums of squares Kenward-Roger's method) using a linear mixed effects model in R (version 3.5.1). The effect of transcription factors (which is the factor in the analysis) on activating a selected promoter was analysed with the same method. The biological replicates were treated as random effects. The means were separated on the base of all pairwise comparisons of least-squares means (letters assigned).

RESULTS

Elevated Anthocyanin Content Causes a Higher Incidence of Internal Browning Flesh Disorder (IBFD)

'Royal Gala' is a cultivar with little reported incidence of IBFD. There are reports of flesh browning but these tend to be after prolonged storage (Lee et al., 2016). We used three independent transgenic lines with high concentrations of flesh anthocyanin to test any link with flesh browning (**Figure 1A**). At harvest (T7), some of the transgenic fruit showed high incidence of IBDF (**Figure 1B**). In WT 'Royal Gala' and two of the transgenic lines (A1, A3) there was no IBFD at harvest. However, in the line with the highest anthocyanin content in the flesh, A4, IBDF was apparent in 16% of fruit at harvest (**Figure 1B**). After 10 weeks in standard storage conditions at 0.5°C, the incidence of IBFD was 67, 23, and 60% for the transgenic lines A1, A3, and A4, respectively. No IBFD was detected in any of the 'Royal Gala' fruit assessed. All the fruit tested at harvest, including WT, were relatively small compared with field-grown fruit and line A4, in particular, appears smaller than WT (**Table 1**). Both A1 and A3 showed lower fruit firmness than WT. Line A4 also showed a difference in SSC (P <0.001).

Metabolic Comparison of MYB10 Fruit During Development

Previously it has been shown that the most dramatic effect of over-expression of MYB10 is a greater than a 20-fold increase in total anthocyanins in whole fruit (Espley et al., 2013). This is particularly evident in the fruit flesh, which goes from non-detectable amounts of anthocyanin in 'Royal Gala' to more than 700 µg/gFW in the transgenic lines. However, there are also significant changes in other polyphenols and these, together with the anthocyanin, may contribute to a substrate pool. We analysed this in the highly anthocyanic lines under-going IBFD (**Figure 1C**). This confirmed a trend to have higher concentrations of epi-catechin, chlorogenic acid (CGA), and quercetin (**Figures 1D–G**). In contrast, by maturity catechin was not significantly different between control and MYB10 lines (**Figure 1D**). As has been commonly reported, many of the major polyphenols in apple are highly abundant at the earlier stages in fruit development (Henry-Kirk et al., 2012) but the concentrations reduce as the fruit expands and matures. While there is some evidence for this in the anthocyanic transgenic lines, the reduction in these key metabolites is at a lower rate than in 'Royal Gala' and relatively high concentrations of epicatechin, CGA and quercetin are maintained in the ripe fruit. Since these polyphenols are a potential source

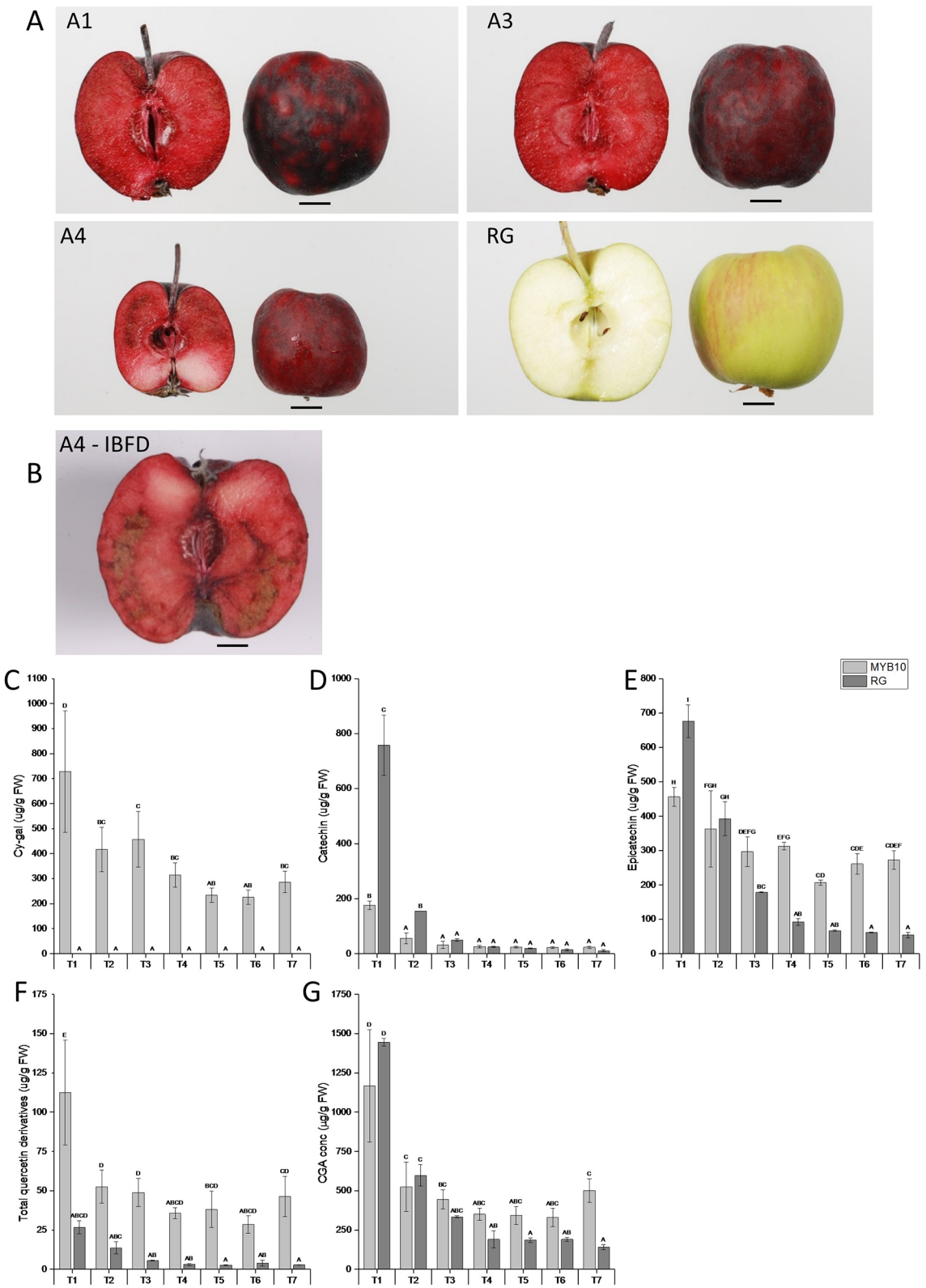

FIGURE 1 | Representative images of **(A)** harvested apple fruit from three independent transgenic lines (A1, A3, and A4) and Wild Type (WT) and **(B)** incidence of IBFD in line A4. Chemical analysis *via* HPLC of metabolites in pooled transgenic lines (MYB10) and WT 'Royal Gala' (RG) of **(C)** cyanidin galactoside (Cy-gal) **(D)** catechin **(E)** epicatechin **(F)** total quercetin derivatives and **(G)** chlorogenic acid (CGA). Mean of three biological replicates. T1, 35 Days After Full Bloom (DAFB); T2, 65DAFB; T3, 85 DAFB; T4, 110 DAFB; T5, 120 DAFB; T6, 130 DAFB; and T7, 140 DAFB. Error bars show ± SEM, different letters indicate statistical difference with $P < 0.05$.

TABLE 1 | Fruit assessment for average weight, firmness and soluble solids content (SSC) of WT and three independent transgenic lines of 'Royal Gala' at harvest and after 10 weeks in storage. Incidence of browning by percentage of flesh showing symptoms by visual observation.

Line	Weight (g)	Firmness (kgf)	SSC (°Brix)	IBFD (%) at harvest	IBFD (%) after 10 wks
WT	88.9 ± 9.5	10.5 ± 0.5	11.7 ± 0.4	0	0
A1	68.6 ± 7.7	9.0 ± 0.5	12.2 ± 0.2	0	67
A3	53.9 ± 6.1	9.1 ± 0.5	14.1 ± 0.4	0	23
A4	49.8 ± 5.3	13.1 ± 0.3	11.5 ± 0.3	16	60

Values are averages ± SEM.

of enzymatic oxidation substrate, we measured the peroxidative potential of fruit throughout the development series.

Enzymatic browning in fruit can occur when phenolic compounds are oxidised, so we measured total peroxidase activity using the rate of conversion of guaiacol to tetraguaiacol. Total peroxidative activity in control 'Royal Gala' fruit flesh steadily declined during fruit development to very low rates by maturity (**Figure S1**). In contrast, peroxidative activity was seen to increase in the MYB10 lines.

Ethylene Induction in MYB10 Lines

Internal ethylene concentration (IEC) measurements were performed on attached fruit through fruit development using an *in planta* method. A sample of apple fruit core cavity gas was extracted while fruit remained on the tree, by insertion of a needle into the core cavity space. These measurements, made on three individual apples from the three independent lines of MYB10 'Royal Gala', and four individual control 'Royal Gala' fruit, were carried out over a 90-day period. Ethylene production for the transgenic lines increased at a much earlier point in fruit development (**Figure 2A**). Low rates of ethylene production occurred in these lines before T4, after which ethylene increased. By T5, IEC in two of the transgenic lines had reached greater than 2 ml/L while in WT it was less than 0.5 ml/L. As expected, ethylene was detected in the WT control fruit commensurate with the onset of on-tree ripening between T5 and T6.

IEC was also assessed destructively with off-tree fruit measurement at six developmental time points equivalent to 65, 85, 95, 100, and 108 DAFB on three separate biological replicates for each line and controls (**Figure 2B**). These standard assays confirmed results for the on-tree assessments with an early ethylene production detected in all transgenic lines compared with the control fruit.

Effects on Starch Concentration

Flesh starch concentration in transgenic MYB10 apple fruit was significantly lower than in WT 'Royal Gala' fruit (ANOVA main effect of wild type over transgenic lines; $P < 0.0001$) (**Figure S2**). Differences were evident from developmental stage T2 and were maintained throughout fruit growth. Starch degradation is an indicator of apple fruit maturity (Brookfield et al., 1997). Minimal starch concentrations at T6 and T7 indicated that fruit maturation was near completion in transgenic fruit at T6, whilst in 'Royal Gala' WT fruit starch degradation was still occurring by T7 stage. Furthermore, the rate of starch degradation was faster in transgenic MYB10 apple fruit compared to the WT (**Figure S3A**). Flesh sorbitol concentration in transgenic MYB10 apple fruit was significantly higher than in WT 'Royal Gala' fruit (ANOVA main effect of transgenic lines over wild type; $P < 0.001$) (**Figure S2B**). Fructose concentration was higher in WT 'Royal Gala' fruit than that in the transgenic fruit (ANOVA main effect of wild type over transgenic lines; $P < 0.001$) (**Figure S3B**). Fruit sucrose concentration was significantly higher in WT 'Royal Gala' than the transgenic lines at T7 ($P < 0.05$; **Figure S3C**). Glucose concentration was overall higher in transgenic lines, although the differences were not statistically significant (**Figure S3D**).

Expression Analysis of PPO and Ethylene-Related Genes

We tested a number of PPO genes (PPOa, PPOb, PPOc, and PPOd) for transcript abundance in both red and white apple flesh tissue. There were high rates of expression in both transgenic lines (A1 and A4) compared with WT control for all tested genes (no transcript was detected for PPOc) (**Figure 3**). This expression was evident at early time points in fruit development, T2 for PPOb and PPOd and T3 for PPOa in the transgenic lines. In WT 'Royal Gala' there was no detectable expression in PPOa and PPOb and a gradual increase in expression of PPOd, albeit at a lower rate than the red-fleshed lines. In most cases line A4, the most highly pigmented and prone to IBFD, showed the highest expression for all the genes tested.

With evidence for an early peak in ethylene production in the anthocyanic fruit, the key genes in the ethylene biosynthesis pathway, ACO and ACS, were tested for transcript abundance in the fruit flesh of two transgenic lines (A1 and A4) and WT (**Figure 3**). For ACO1, transcript was detectable in both A1 and A4 at T4, while in 'Royal Gala' WT transcript was not detected until T5. The highest ACO transcript abundance was detected in the A1 and A4 transgenic lines at the final time point, T6. For ACS1, transcript was at low levels with an anomalous peak of expression for RG at T5. For the previous year tested, an early peak of ACS1 expression was evident for both transgenic lines tested at T4 but at the final time point the highest expression was seen in control tissue (**Figure S4**). For ACS3, the most abundant ASC gene, transcript was detected at an even earlier stage (T3) for A1 and A4 but was evident in all samples, including WT control, at T4. By the final time point (T6), expression was higher in the transgenic lines. ACS5 was never detected in control samples but there was low expression in A1 and greater expression, albeit at a low level, in A4.

Based on data from a previous study using RNA-sequencing on red and white fleshed apples (Wang et al., 2018), we selected ERF106 as a possible candidate gene for involvement in the regulation of anthocyanin-related early ethylene production. We found low levels of transcript abundance throughout fruit development in 'Royal Gala' but consistently higher abundance in both of the transgenic lines tested. MdERF106 is similar to Arabidopsis AtDEWAX and AtDEWAX2 (AtERF107/ERF106) (**Figure 4**, **Figure S5**) which negatively regulate cuticular wax biosynthesis (Go et al., 2014; Kim et al., 2018), and other ERFs such as AtERF5 and AtERF6 involved in biotic and abiotic stress response (Moffat et al., 2012;

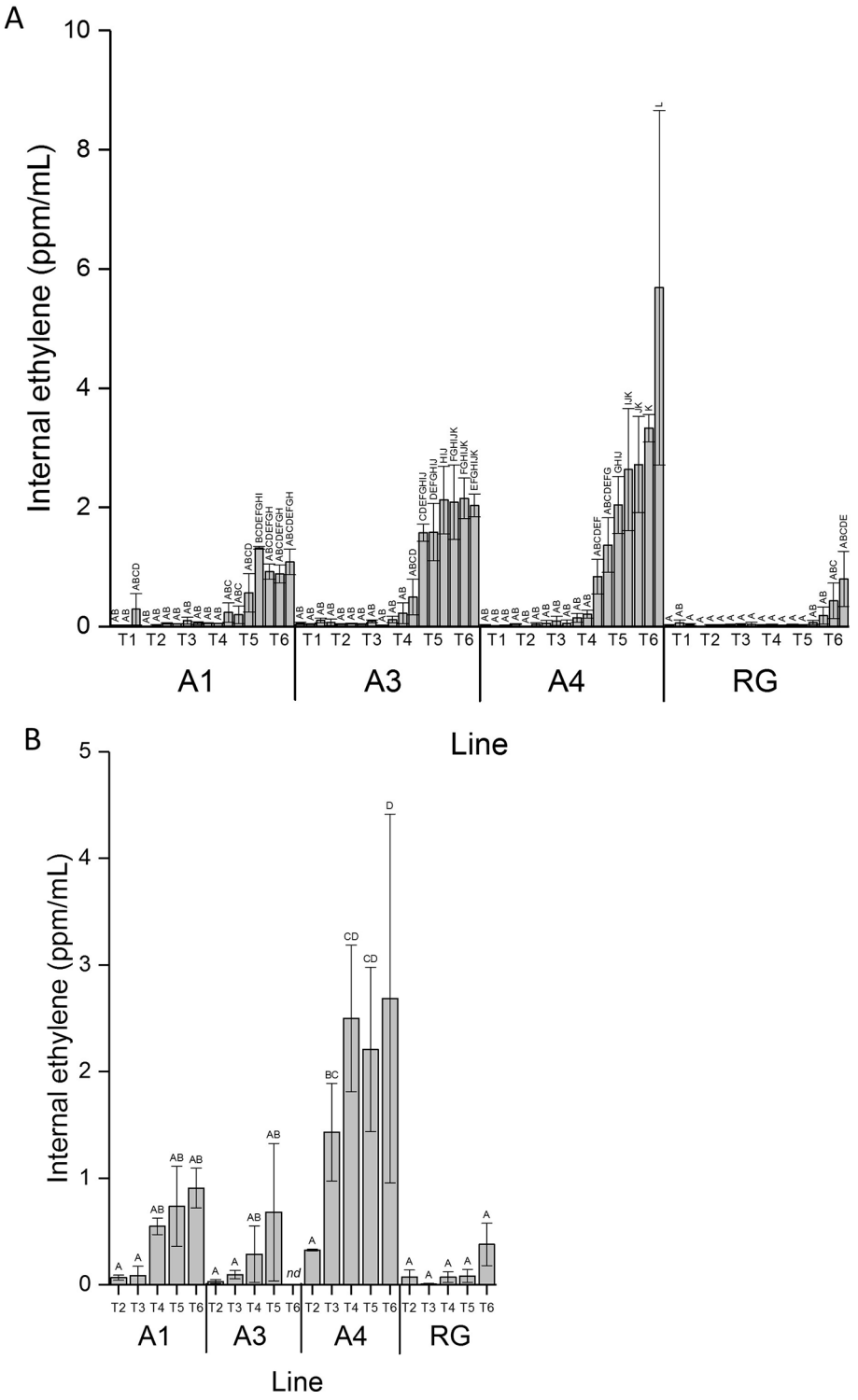

FIGURE 2 | Ethylene induction was earlier in anthocyanic fruit. **(A)** Internal ethylene concentration taken from the same fruit on the tree over fruit development for lines A1, A3, and A4 and WT control (RG). **(B)** Internal ethylene concentration taken from fruit harvested from the tree from time points T2 to T6. Mean of five biological replicates. T1, 35 DAFB; T2, 65DAFB; T3, 85 DAFB; T4, 110 DAFB; T5, 120 DAFB; T6, 130 DAFB. Error bars show ± SEM, different letters indicate statistical difference with $P < 0.05$.

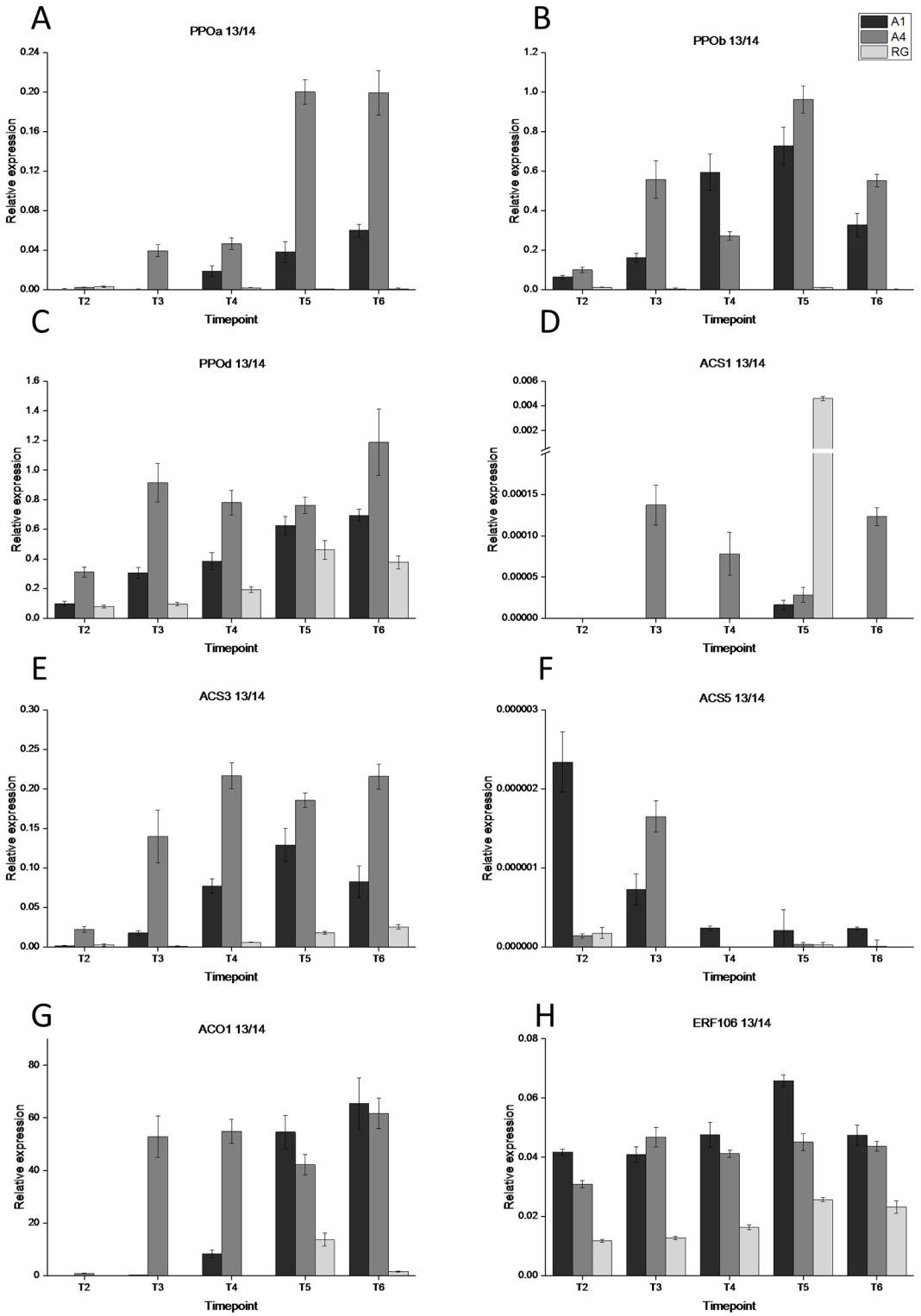

FIGURE 3 | Gene expression analysis of eight maturity and browning associated genes at five time points during fruit development during 2013-2014. **(A)** PPOa, **(B)** PPOb, **(C)** PPOd, **(D)** ACS1, **(E)** ACS3, **(F)** ACS5, **(G)** ACO1, and **(H)** ERF106. T1, 35 DAFB; T2, 65DAFB; T3, 85 DAFB; T4, 110 DAFB; T5, 120 DAFB; T6, 130 DAFB. Expression was normalised to EF1a and error bars are SE of four technical replicates of at least 5 pooled fruit per time point. Expression is shown for three lines; dark grey—A1, medium grey—A4, and light grey—RG.

Dubois et al., 2013). Previously it has been shown that MYB1/10 activates expression of apple ERF3 (a close homologue to pear ERF3) to increase ethylene emission from apple callus (An et al., 2018), while MdERF1B has been shown to alter anthocyanin and proanthocyanidin concentration (Zhang et al., 2018). In pear PyERF3 interacts with PyMYB114 to co-regulate anthocyanin biosynthesis (Yao et al., 2017). These ERFs are less similar to MdERF106.

Activation of Non-Anthocyanin Related Genes by MYB10

To test for the possibility of direct activation of ethylene-related gene by MYB10, we cloned the promoters of ACO, ACS1, ACS3, ACS5, and ERF106, which were fused with the luciferase reporter gene sequence. These were then tested for MYB10 activation using the dual luciferase assay. Since MYB10 is known to partner with bHLH3 in the MBW complex and is required for full activation of the anthocyanin structural genes, the apple bHLH3 TF was also included. A non-anthocyanin related MYB, MYB8, was used as a control MYB to test for specificity of MYB10. The promoter fragment of apple DFR was used as a positive control for MYB10 activation. As expected, MYB8 had little activation potential on DFR, while MYB10 did induce promoter activity and luciferase production (**Figure 5A**). This was further enhanced by the co-infiltration of bHLH3.

For the ACS3 and ACS5 promoters there was no apparent activation by MYB10, with or without bHLH3, or for the control MYB8. However, both MYB8 and MYB10 appeared to activate ACS1, suggesting a non-specific MYB activation. This was somewhat reduced for MYB10 when co-infiltrated with bHLH3. For ACO1, there was also activation by MYB8 and MYB10, with higher activation for the latter that was then somewhat diminished by the inclusion of bHLH3.

We tested the MYBs for activity on the ERF106 promoter fragment. Here we found no detectable activation by the control MYB8 but a strong activation by MYB10. Again, this was reduced with the co-infiltration of bHLH3.

To further test the specificity of MYB10 on the ERF106 promoter, a number of known apple flavonoid activating and repressing MYB TFs were assayed against the ERF106 promoter. The strongest activation was seen with the anthocyanin-related activators MYB10 and MYB110 (**Figure 5B**). A lower level of activation was seen with infiltration of the flavonoid-related MYB12, while the anthocyanin repressors showed mixed results, with no activation by MYBs 15 and 16 but some activation by both MYB27 and MYB111.

DISCUSSION

Of the widely cultivated varieties of apple, 'Royal Gala' does not normally exhibit IBFD. However, the MYB10-induced ectopic accumulation of anthocyanin in fruit flesh leads to a severe browning phenotype, suggestive of a link between flesh colour and browning. Alternatively, an increase in other polyphenols may be the cause, providing increased substrate for downstream oxidation. The concentration of polyphenols in apple fruit usually reduces over development but in MYB10 lines a relatively high concentration of epi-catechin, CGA, and quercetin is still present at maturity, in addition to the high concentration of cyanidin-galactoside. The incidence of IBFD in these highly anthocyanic transgenic lines is resonant with data from a traditionally bred red-fleshed apple population (Volz et al., 2013). In the red-fleshed breeding populations tested, quantitative trait loci (QTL) for IBFD were detected at two genetic locations on Linkage Group (LG) 9 and LG6, consistent with a QTL for red flesh, and suggesting a strong genetic link between MYB10 and IBFD.

Adding to these possibilities, there is also an increase in the ripening-related gaseous hormone, ethylene. Since the developmental accumulation of anthocyanin colour in apple is part of the ripening process, it is likely that these processes are connected. Here we show that MYB10 may play a role in ethylene biosynthesis, *via* ethylene-related transcription factors and that this premature ethylene production is closely associated with a reduction in fruit quality, ultimately leading to IBDF. A previous study in a F_1 population of red and white fleshed apples showed a higher concentration in flavonoid content as well as anthocyanin in red fleshed apples (Wang et al., 2015). In this study a comparative transcriptome showed a higher incidence of abiotic and biotic stress-related genes in red flesh, and that this was associated with an increased production of flavonoids. Whether these stress-related genes are up-regulated in direct response to flavonoid production or the potential detrimental effects of an increase in flavonoids leading to premature ripening is yet to be fully determined. This study was conducted on ripe fruit although some ethylene-related genes such as ACO (gene ID 103404960, equivalent to MDP0000195885) showed greater transcript abundance in red flesh compared to white.

Anthocyanin Is Associated With Major Changes in Fruit Physiology

The ectopic accumulation of anthocyanin does not necessarily lead to reduced fruit quality. This is convincingly demonstrated in tomato where elevation of anthocyanin in transgenic purple tomato fruit leads to an extended shelf life and a reduction in susceptibility to grey mould (Zhang et al., 2013). In this study, it appears that the increased anthocyanin boosts antioxidant capacity in the fruit which is likely to slow the over-ripening process. This is in direct contrast to results presented here for apple. We have previously shown an elevated antioxidant capacity for these highly anthocyanic apples (Espley et al., 2014) despite a reduction in ascorbic acid, suggesting that the increase in anthocyanins and flavonoids are the reason for this increase. However, this increased capacity did not improve shelf life and the red-flesh apples over-ripened more quickly than the white-fleshed controls. Like apple, tomato is a climacteric fruit and so reliant on ethylene for ripening. In the purple tomatoes, ethylene production was 2-fold greater than control fruit, although this was just after the breaker stage. This differs for apple, where we see an ethylene burst earlier in fruit development.

There are reports of flesh browning (flesh breakdown) in 'Royal Gala' but these tend to be after prolonged storage of more than three months and may be more prevalent in larger fruit (Lee et al., 2013; Lee et al., 2016). In these transgenic lines, a high incidence of IBFD is visible at (and even before) harvest (Line

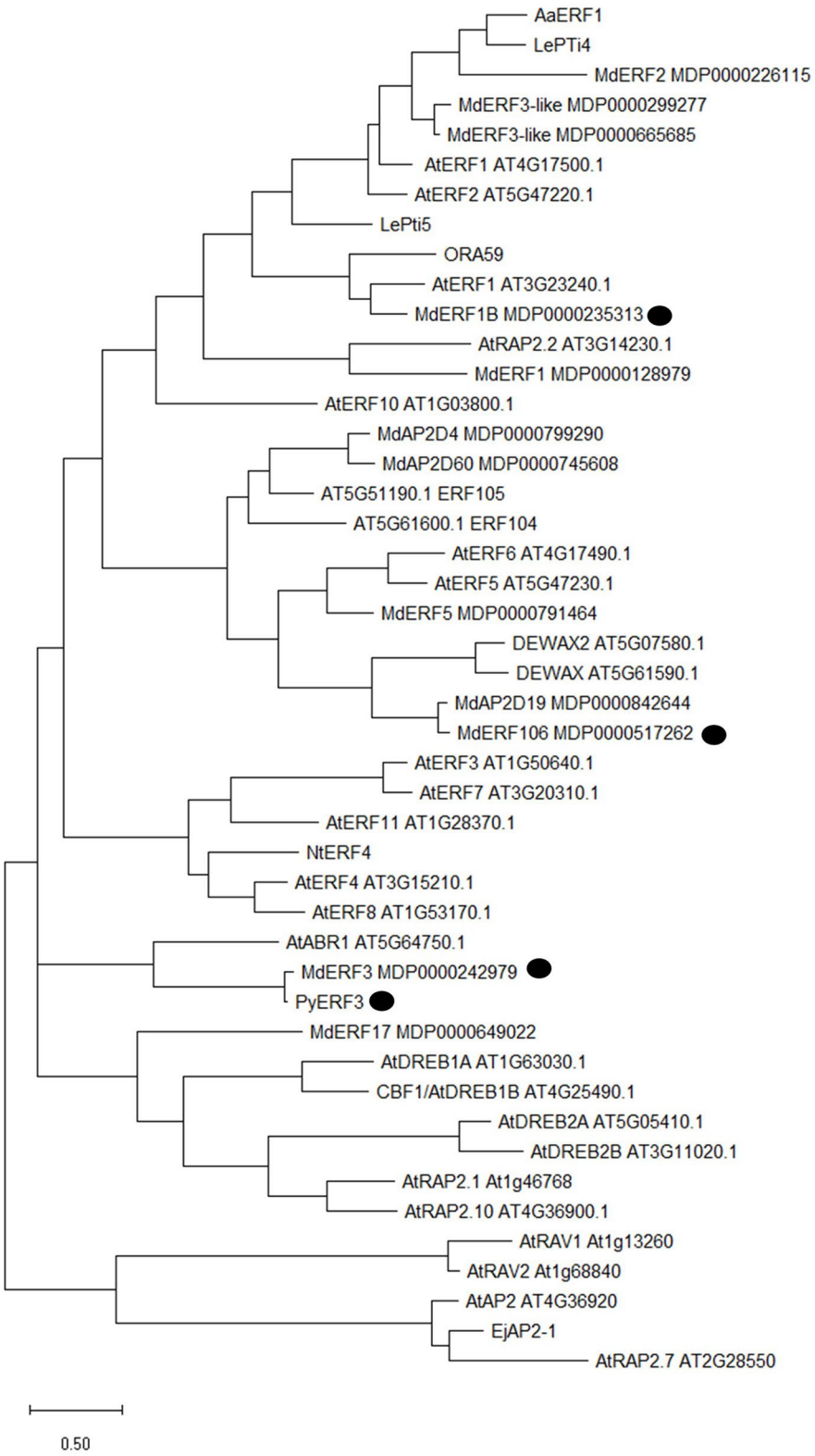

FIGURE 4 | Phylogenetic tree analysis of MdERF106 protein and other related AP2/ERF TFs from different species. Published Rosaceous proteins implicated in ethylene responses are indicated by a black circle. Protein identifiers are either published MDP numbers for *Malus*, TAIR for *Arabidopsis,* or NCBI accession numbers for other species as follows: LePti4 (NM_001347076.1), LePti5 (U89256.1), ORA59 (NM_100497.3), AaERF1 (JN162091.1), PyERF3 (MF489220), NtERF4 (NM_001325253.1), and EjAP2-1 (KM506584.1).

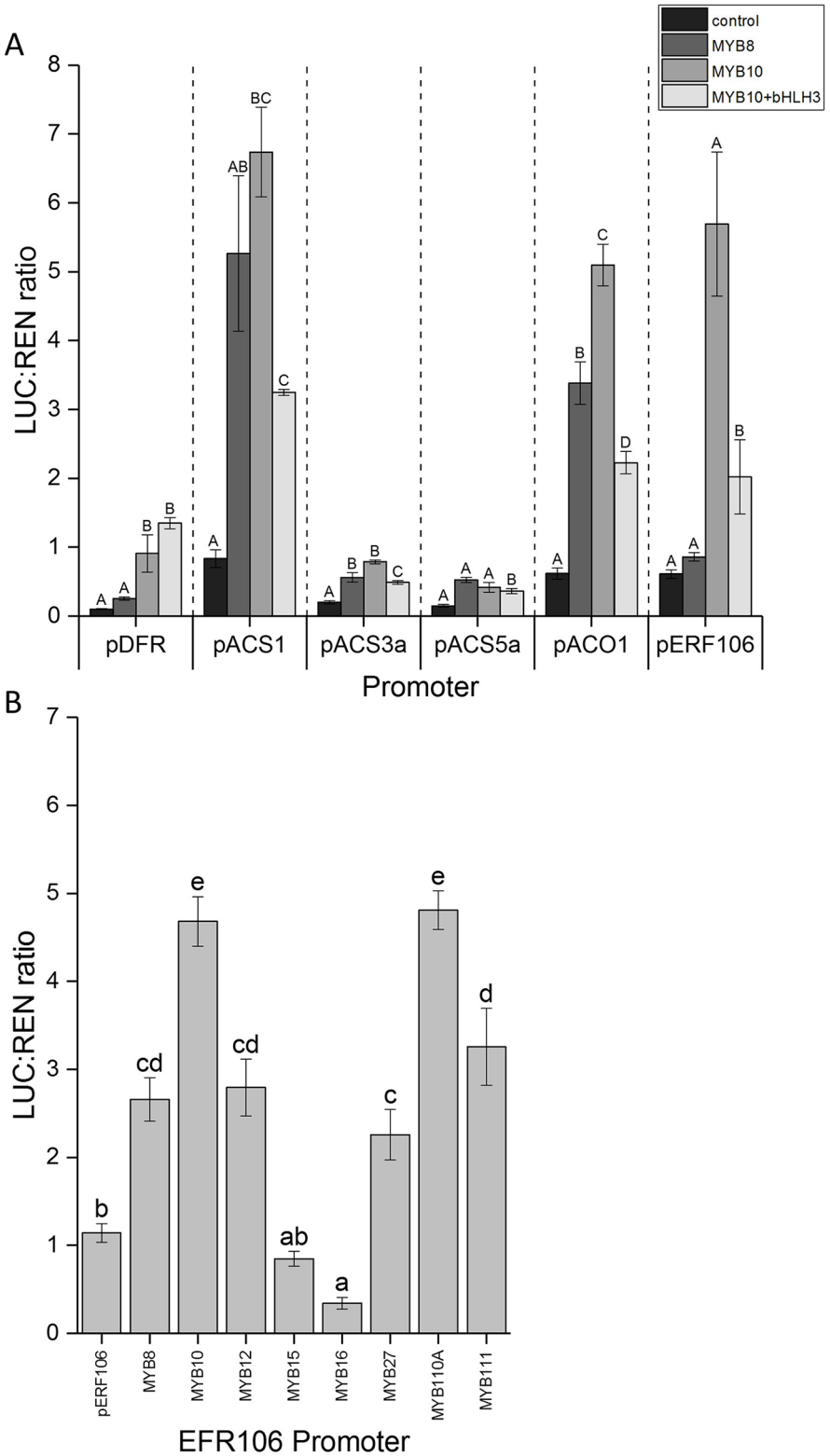

FIGURE 5 | (A) MYB10 activates the promoters of ethylene-associated genes. The promoter sequences from ACS1, ACS3, ACS5, ACO1, and ERF106 were isolated and cloned into the dual luciferase reporter construct and infiltrated into *N. benthamiania* leaves in combination with MYB10 with and without bHLH3. MYB8 was included as a control. **(B)** Anthocyanin activating MYBs activate the promoter of ERF106. The promoter sequence from ERF106 was isolated and cloned into the dual luciferase reporter construct and infiltrated into *N. benthamiania* leaves either on its own or in combination with activating or repressing MYB TFs. Different letters indicate statistical difference with $P < 0.05$ (7A refers to each promoter independently). Mean of four biological replicates. Error bars show ± SEM.

A4) and is severe by 10 weeks in storage, while WT 'Royal Gala' showed no visible symptoms.

Apple has an unusual carbohydrate metabolism compared to the more commonly studied model plants (e.g. Arabidopsis) as sucrose is not the major carbohydrate metabolite. Indeed sorbitol is the major photosynthetic product in apple leaves (60–80% of sugars), and it is translocated in the phloem to sink tissues where it is quickly converted into fructose by sorbitol dehydrogenase (Loescher, 1987; Klages et al., 2001; Wu et al., 2015), so that sorbitol concentrations in fruit are usually low (Yamaki and Ishikawa, 1986). Apple fruit are mainly fructose accumulators, although early in development they store both fructose and transitory starch in similar amounts (Li et al., 2018). Fruit sorbitol dehydrogenase genes respond to variable levels of source sorbitol, decreasing in expression when leaf sorbitol levels decrease. In sorbitol dehydrogenase antisense lines, translocated sorbitol is reduced, lowering the levels of sorbitol in fruit (Teo et al., 2006; Li et al., 2018). In our experiment, transgenic MYB10 lines had fruit with higher a concentration of sorbitol in the fruit flesh than the wild type 'Royal Gala'. This phenotype could be due to the up-regulation of leaf sorbitol metabolism in transgenic MYB10 lines or by a down-regulation of the sorbitol dehydrogenase genes in the fruit so that sorbitol is converted more slowly into fructose. However, it could be also linked to the maturation stage the fruit have reached. Onset of net transitory starch degradation in apple occurs whilst fruit are still on the tree (Zhang et al., 2017), and it is an indication of fruit maturation (Brookfield et al., 1997). In apple, starch degradation is a process with low dependency but high sensitivity to ethylene (Johnston et al., 2009) which means an earlier onset of endogenous production of the hormone (from T3 rather than T5 in WT) could trigger faster starch degradation in the fruit, as observed in this study with the transgenic MYB10 lines. Sorbitol is likely to be linked to the ripening stage (Aprea et al., 2017). The accumulation of sorbitol in the MYB10 lines could be a result of the fruit switching to a ripening stage at T4–T5, and sorbitol translocated to the fruit is converted to fructose more slowly.

In the highly anthocyanic MYB10 fruit, there is an increase in a number of polyphenols as previously shown (Espley et al., 2013). These polyphenols could provide added substrate to fruit flesh for enzymatic browning to occur. The peroxidative activity is also higher in all the MYB10 lines, therefore, both the potential substrates for browning and the peroxidative enzymes are at greater concentration in red-fleshed lines than in WT control. This is further shown in the PPO expression analysis, where an increase in transcript in both transgenic lines tested was evident for PPOa, PPOb, and PPOd. Results from the published transcriptomic analysis of red versus white apple flesh at harvest (Wang et al., 2015), shows that PPOa, and particularly PPOb, are more highly expressed in the red flesh while PPOc and PPOd are more highly expressed in the white fleshed fruit. It would appear that the key finding presented in our data is the demonstration of very early PPO expression.

Early Production of Ethylene *via* the Up-Regulation of Ethylene Genes in Red-Fleshed Fruit

The rate of ethylene production can vary widely between apple cultivars (Harada et al., 2000). It has also been previously shown that mature red-fleshed apples start to produce more ethylene than those with white flesh just two days after harvest (An et al., 2018). In our study, apples from the same genetic background were used, so from a genetic level it might be expected that ethylene production would be similar. However, we detected a very different ethylene production profile for all three transgenic lines compared with WT. Production was at levels normally consistent with the onset of the ripening-related ethylene burst but at four to six weeks earlier than expected. The collection of ethylene samples while fruit were still attached to the tree was chosen as the most representative method of assessing the actual increase in ethylene production in developing fruit. As this is method is novel, we also used a standard practice for ethylene assessment for harvested fruit and found very similar patterns.

Studies have shown that the biosynthesis of ethylene is transcriptionally regulated (Schaffer et al., 2013). ACC synthase (ACS) converts *S*-adenosyl-L-methionine to 1-aminocyclopropane-1-carboxylate (ACC) and is thought to be the rate limiting step

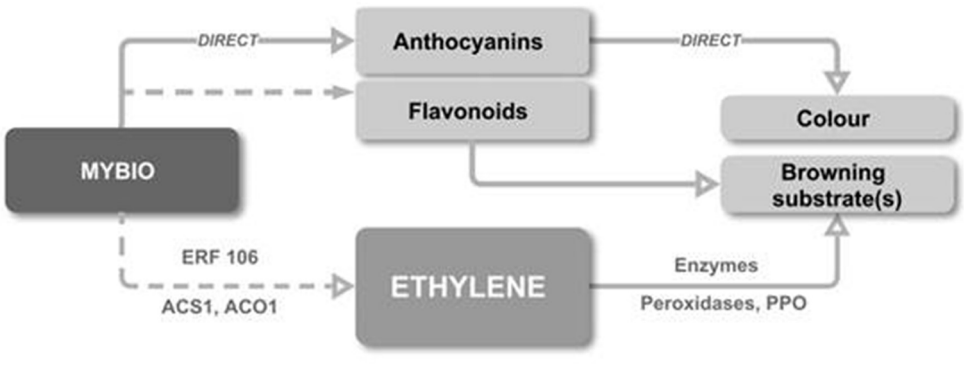

FIGURE 6 | A proposed model for the link between elevated flesh anthocyanin and IBFD. The up-regulation of MYB10 directly increases anthocyanin concentration and indirectly causes increased production of flavonoid. MYB10 is also associated the early onset of ethylene production, possibly *via* interaction with ERF106. Ethylene production advances fruit maturity and an increase in transcription and enzyme activity of PPO. These events lead to early ripening, the production of peroxidise enzymes and a pool of additional substrate which culminate in IBFD.

(Yang and Hoffman, 1984). We tested the transcript abundance of three versions of ACS: ACS1, ACS3, and ACS5. For all three versions we found an increase in transcription at a considerably advanced stage in the anthocyanic fruit compared to WT 'Royal Gala'. ACS1 is associated with the ripening-specific climacteric burst (Harada et al., 2000), while ACS3 is transcriptionally active before ACS1 and is likely to be involved in the transition from system-1 to system-2 ethylene biosynthesis (Wang et al., 2009). ACS3 transcript was just detectable in the transgenic lines at T3, and clearly detectable at T4, as was ACS1. However, there did not appear to be negative feedback for ACS3, as previously reported (Wang et al., 2009) and transcription increased as fruit developed. ACS5 is possibly more associated with wounding rather than ethylene-related ripening (Costa et al., 2005). The transcript abundance of ACS5 was detectable at low levels in the MYB10 lines, particularly A4, but was at very low rates.

The oxidation step performed by ACC oxidase (ACO) to form ethylene follows the ACS-mediated conversion to ACC. ACO transcript abundance was measured and the first major peak in expression was seen at T4 but only in the transgenic lines A1 and A4. At T5 transcript was also detected in control fruit. There are other ACO gene family members (not tested here) that may also contribute to the rise in ethylene and ACO has been linked to internal browning in white-fleshed fruit (Mellidou et al., 2014). The pattern for the highly anthocyanic fruit shows that the presence of ACS3 transcript at T3 precedes both ACS1 and ACO transcript at T4 while the later expression of ACS3 in control fruit at T4 ACO precedes ACO1 at T5 and ACS1 at T6. Since ACS1 has been shown to be responsible for system-2 type autocatalytic ethylene production (Tan et al., 2013) the results here are entirely consistent with premature ripening in MYB10 fruit.

A Proposed Model for the Association Between Anthocyanin and IBFD

The Ethylene Signalling Cascade Ends With the ERFs and These Can Either Activate or Repress Ethylene production as well as regulating the expression of ripening-related genes (Liu et al., 2015). In apple, the ERF2 TF has been shown to negatively regulate ethylene biosynthesis by suppressing the transcription of ACS1 (Li et al., 2016). Previous data has shown that one ethylene-related TF, ERF106, was differentially expressed in red compared with white apple flesh (Wang et al., 2018).

A study by Zhang et al. (2018) showed that ERF1B was capable of interacting with the promotors of anthocyanin and proanthocyanidin MYB TFs. This interaction leads to increases in the related metabolites and suggests that ethylene regulation and anthocyanin regulation might be linked in either direction.

It appears that both MYB apple flesh anthocyanin regulators, the Type 1 MYB10 and Type 2 MYB110 (Chagné et al., 2013) were capable of activating the promoter of ERF106. Some of the other MYBs tested did demonstrate some level of activation, but to a lesser extent. The MYB binding sites may confer some non-specific binding and hence, activation. Interestingly, two known apple anthocyanin repressors, MYBs 15 and 16 (Lin-Wang et al., 2011), showed no activation with reporter levels below that of the control. Further work is required to test if these MYB repressors can compete with activators or repress promoter activity.

We propose a model (**Figure 6**) whereby the up-regulation of MYB10 directly increases anthocyanin concentration by regulating the anthocyanin biosynthetic pathway and indirectly causes the increased production of flavonoids by enhanced pathway flux. MYB10 is also associated with an increase in early ethylene production, possibly *via* interaction with ERF106. This ethylene production advances mechanisms that drive fruit maturity, including the elevation of PPO. These direct and indirect events produce a scenario where early ripening is triggered and where the production of peroxidise enzymes and large pool of additional substrate come together to culminate in IBFD.

Summary

The data presented here describes a mechanism for elevated IBFD in anthocyanin tissue in apple fruit. This has implications for the breeding of high quality novel red-fleshed cultivars. The genetic background may be key to IBDF evasion, such as the use of low ethylene producing parents in a breeding population. Alternative strategies to avoid IBDF could include genetic manipulation such as demonstrated by knocking out PPO in Arctic® apple (Waltz, 2015) which could also be achieved using CRISPR/Cas9 gene editing approach.

DATA AVAILABILITY STATEMENT

All datasets for this study are included in the manuscript/ **Supplementary Files**.

AUTHOR CONTRIBUTIONS

RE, DL, BP, RH-K, MH, and SO'D contributed to the harvest and postharvest assessments, qPCR, transactivation experiments. MP and BP conducted peroxidase assays. HB and SN performed carbohydrate assessment. TM performed chemical analysis. RE, AA, RV, and JJ developed the experimental design. RE, AA, SN, and BP wrote the manuscript and all authors contributed to editing.

ACKNOWLEDGMENTS

This work was funded by the New Zealand Government, Ministry of Business, Innovation and Employment. We thank Robert Schaffer and Adam Friend for helpful advice on the manuscript.

SUPPLEMENTARY MATERIAL

The Supplementary Material for this article can be found online at: https://www.frontiersin.org/articles/10.3389/fpls.2019.01248/full#supplementary-material

REFERENCES

Alonso, J. M., Chamarro, J., and Granell, A. (1995). Evidence for the involvement of ethylene in the expression of specific RNAs during maturation of the orange, a non-climacteric fruit. *Plant Mol. Biol.* 29, 385–390. doi: 10.1007/BF00043661

An, J.-P., Wang, X.-F., Li, Y.-Y., Song, L.-Q., Zhao, L.-L., You, C.-X., et al. (2018). EIN3-LIKE1, MYB1, and ETHYLENE RESPONSE FACTOR3 act in a regulatory loop that synergistically modulates ethylene biosynthesis and anthocyanin accumulation. *Plant Physiol.* 178, 808–823. doi: 10.1104/pp.18.00068

Aprea, E., Charles, M., Endrizzi, I., Laura Corollaro, M., Betta, E., Biasioli, F., et al. (2017). Sweet taste in apple: the role of sorbitol, individual sugars, organic acids and volatile compounds. *Sci. Rep.* 7, 44950. doi: 10.1038/srep44950

Brendolise, C., Espley, R. V., Lin-Wang, K., Laing, W., Peng, Y., Mcghie, T., et al. (2017). Multiple copies of a simple MYB-binding site confers trans-regulation by specific flavonoid-related R2R3 MYBs in diverse species. *Front. Plant Sci.* 8, 1864. doi: 10.3389/fpls.2017.01864

Brookfield, P., Murphy, P., Harker, R., and Macrae, E. (1997). Starch degradation and starch pattern indices; Interpretation and relationship to maturity. *Postharvest Biol. Technol.* 11, 23–30. doi: 10.1016/S0925-5214(97)01416-6

Chagné, D., Lin-Wang, K., Espley, R. V., Volz, R. K., How, N. M., Rouse, S., et al. (2013). An ancient duplication of apple MYB transcription factors is responsible for novel red fruit-flesh phenotypes. *Plant Physiol.* 161, 225. doi: 10.1104/pp.112.206771

Chien, C.-H., Chow, C.-N., Zheng, H.-Q., Wu, N.-Y., Yang, T.-Y., Chiang-Hsieh, Y.-F., et al. (2015). PlantPAN 2.0: an update of plant promoter analysis navigator for reconstructing transcriptional regulatory networks in plants. *Nucleic Acids Res.* 44, D1154–D1160. doi: 10.1093/nar/gkv1035

Costa, F., Stella, S., Van De Weg, W. E., Guerra, W., Cecchinel, M., Dallavia, J., et al. (2005). Role of the genes Md-ACO1 and Md-ACS1 in ethylene production and shelf life of apple (Malus domestica Borkh). *Euphytica* 141, 181–190. doi: 10.1007/s10681-005-6805-4

Defilippi, B. G., Manríquez, D., Luengwilai, K., and González-Agüero, M. (2009). "Chapter 1 aroma volatiles: biosynthesis and mechanisms of modulation during fruit ripening," in *Advances in Botanical Research*, 1–37. doi: 10.1016/S0065-2296(08)00801-X

Di Guardo, M., Tadiello, A., Farneti, B., Lorenz, G., Masuero, D., Vrhovsek, U., et al. (2013). A multidisciplinary approach providing new insight into fruit flesh browning physiology in apple (Malus x domestica Borkh.). *Plos One* 8, 15. doi: 10.1371/journal.pone.0078004

Dubois, M., Skirycz, A., Claeys, H., Maleux, K., Dhondt, S., De Bodt, S., et al. (2013). ETHYLENE RESPONSE FACTOR6 acts as a central regulator of leaf growth under water-limiting conditions in arabidopsis. *Plant Physiol.* 162, 319–332. doi: 10.1104/pp.113.216341

Edgar, R. C. (2004). MUSCLE: multiple sequence alignment with high accuracy and high throughput. *Nucleic Acids Res.* 32, 1792–1797. doi: 10.1093/nar/gkh340

Espley, R. V., Bovy, A., Bava, C., Jaeger, S. R., Tomes, S., Norling, C., et al. (2013). Analysis of genetically modified red-fleshed apples reveals effects on growth and consumer attributes. *Plant Biotechnol. J.* 11, 408–419. doi: 10.1111/pbi.12017

Espley, R. V., Butts, C. A., Laing, W. A., Martell, S., Smith, H., Mcghie, T. K., et al. (2014). Dietary flavonoids from modified apple reduce inflammation markers and modulate gut microbiota in mice. *J. Nutr.* 144, 146–154. doi: 10.3945/jn.113.182659

Espley, R. V., Hellens, R. P., Putterill, J., Stevenson, D. E., Kutty-Amma, S., and Allan, A. C. (2007). Red colouration in apple fruit is due to the activity of the MYB transcription factor, MdMYB10. *Plant J.* 49, 414–427. doi: 10.1111/j.1365-313X.2006.02964.x

FAO (2018). *Food and Agriculture Organization of the United Nations* [Online]. http://www.fao.org/statistics. Available: http://www.fao.org/statistics [Accessed 2018].

Ferrer, A., Remón, S., Negueruela, A. I., and Oria, R. (2005). Changes during the ripening of the very late season Spanish peach cultivar Calanda: feasibility of using CIELAB coordinates as maturity indices. *Sci. Hortic.* 105, 435–446. doi: 10.1016/j.scienta.2005.02.002

Giovannoni, J., Nguyen, C., Ampofo, B., Zhong, S. L., and Fei, Z. J. (2017). The epigenome and transcriptional dynamics of fruit ripening. *Annu. Rev. Plant Biol.* 68, 61–84. ed. S.S. Merchant. (Palo Alto: Annual Reviews). doi: 10.1146/annurev-arplant-042916-040906

Giovannoni, J. J. (2004). Genetic regulation of fruit development and ripening. *Plant Cell* 16, S170. doi: 10.1105/tpc.019158

Go, Y. S., Kim, H., Kim, H. J., and Suh, M. C. (2014). *Arabidopsis* cuticular wax biosynthesis is negatively regulated by the *DEWAX* gene encoding an AP2/ERF-type transcription factor. *Plant Cell* 26, 1666–1680. doi: 10.1105/tpc.114.123307

Harada, T., Sunako, T., Wakasa, Y., Soejima, J., Satoh, T., and Niizeki, M. (2000). An allele of the 1-aminocyclopropane-1-carboxylate synthase gene (Md-ACS1) accounts for the low level of ethylene production in climacteric fruits of some apple cultivars. *Theor. Appl. Genet.* 101, 742–746. doi: 10.1007/s001220051539

He, J., and Giusti, M. M. (2010). Anthocyanins: natural colorants with health-promoting properties. *Annu. Rev. Food Sci. Tech.* 1, 163–187. doi: 10.1146/annurev.food.080708.100754

Heim, M. A., Jakoby, M., Werber, M., Martin, C., Weisshaar, B., and Bailey, P. C. (2003). The basic helix–loop–helix transcription factor family in plants: a genome-wide study of protein structure and functional diversity. *Mol. Biol. Evol.* 20, 735–747. doi: 10.1093/molbev/msg088

Hellens, R. P., Allan, A. C., Friel, E. N., Bolitho, K., Grafton, K., Templeton, M. D., et al. (2005). Transient expression vectors for functional genomics, quantification of promoter activity and RNA silencing in plants. *Plant Methods* 1, 13. doi: 10.1186/1746-4811-1-13

Henry-Kirk, R. A., Mcghie, T. K., Andre, C. M., Hellens, R. P., and Allan, A. C. (2012). Transcriptional analysis of apple fruit proanthocyanidin biosynthesis. *J. Exp. Bot.* 63, 5437–5450. doi: 10.1093/jxb/ers193

Holderbaum, D. F., Kon, T., Kudo, T., and Guerra, M. P. (2010). Enzymatic browning, polyphenol oxidase activity, and polyphenols in four apple cultivars: dynamics during fruit development. *HortScience* 45, 1150. doi: 10.21273/HORTSCI.45.8.1150

Holton, T. A., and Cornish, E. C. (1995). Genetics and biochemistry of anthocyanin biosynthesis. *Plant Cell* 7, 1071–1083. doi: 10.2307/3870058

Hu, D. G., Yu, J. Q., Han, P. L., Xie, X. B., Sun, C. H., Zhang, Q. Y., et al. (2019). The regulatory module MdPUB29-MdbHLH3 connects ethylene biosynthesis with fruit quality in apple. *New Phytol.* 221, 1966–1982. doi: 10.1111/nph.15511

Jaakola, L., Poole, M., Jones, M. O., Kämäräinen-Karppinen, T., Koskimäki, J. J., Hohtola, A., et al. (2010). A SQUAMOSA MADS box gene involved in the regulation of anthocyanin accumulation in bilberry fruits. *Plant Physiol.* 153, 1619. doi: 10.1104/pp.110.158279

Janssen, B. J., Thodey, K., Schaffer, R. J., Alba, R., Balakrishnan, L., Bishop, R., et al. (2008). Global gene expression analysis of apple fruit development from the floral bud to ripe fruit. *BMC Plant Biol.* 8, 16. doi: 10.1186/1471-2229-8-16

Johnston, J. W., Gunaseelan, K., Pidakala, P., Wang, M., and Schaffer, R. J. (2009). Co-ordination of early and late ripening events in apples is regulated through differential sensitivities to ethylene. *J. Exp. Bot.* 60, 2689–2699. doi: 10.1093/jxb/erp122

Jones, D. T., Taylor, W. R., and Thornton, J. M. (1992). The rapid generation of mutation data matrices from protein sequences. *Bioinformatics* 8, 275–282. doi: 10.1093/bioinformatics/8.3.275

Kearse, M., Moir, R., Wilson, A., Stones-Havas, S., Cheung, M., Sturrock, S., et al. (2012). Geneious basic: an integrated and extendable desktop software platform for the organization and analysis of sequence data. *Bioinformatics* 28, 1647–1649. doi: 10.1093/bioinformatics/bts199

Kim, H., Go, Y. S., and Suh, M. C. (2018). DEWAX2 transcription factor negatively regulates cuticular wax biosynthesis in arabidopsis leaves. *Plant Cell Physiol.* 59, 966–977. doi: 10.1093/pcp/pcy033

Klages, K., Donnison, H., Wünsche, J., and Boldingh, H. (2001). Diurnal changes in non-structural carbohydrates in leaves, phloem exudate and fruit in Braeburn apple. *Funct. Plant Biol.* 28, 131–139. doi: 10.1071/PP00077

Kramer, M. G., and Redenbaugh, K. (1994). Commercialization of a tomato with an antisense polygalacturonase gene: the FLAVR SAVR™ tomato story. *Euphytica* 79, 293–297. doi: 10.1007/BF00022530

Lee, J., Mattheis, J. P., and Rudell, D. R. (2013). Fruit size affects physiological attributes and storage disorders in cold-stored 'royal gala' apples. *HortScience* 48, 1518. doi: 10.21273/HORTSCI.48.12.1518

Lee, J., Mattheis, J. P., and Rudell, D. R. (2016). Storage temperature and 1-methylcyclopropene treatment affect storage disorders and physiological attributes of 'royal gala' apples. *HortScience* 51, 84. doi: 10.21273/HORTSCI.51.1.84

Lelievre, J. M., Latche, A., Jones, B., Bouzayen, M., and Pech, J. C. (1997). Ethylene and fruit ripening. *Physiol. Plant.* 101, 727–739. doi: 10.1111/j.1399-3054.1997.tb01057.x

Lester, G. E., Hodges, D. M., Meyer, R. D., and Munro, K. D. (2004). Pre-extraction preparation (fresh, frozen, freeze-dried, or acetone powdered) and long-term storage of fruit and vegetable tissues: effects on antioxidant enzyme activity. *J. Agric. Food Chem.* 52, 2167–2173. doi: 10.1021/jf030713b

Li, M. J., Li, P. M., Ma, F. W., Dandekar, A. M., and Cheng, L. L. (2018). Sugar metabolism and accumulation in the fruit of transgenic apple trees with decreased sorbitol synthesis. *Hortic Res-Engl.* 5, 60. doi: 10.1038/s41438-018-0064-8

Li, T., Jiang, Z., Zhang, L., Tan, D., Wei, Y., Yuan, H., et al. (2016). Apple (Malus domestica) MdERF2 negatively affects ethylene biosynthesis during fruit ripening by suppressing MdACS1 transcription. *Plant J.* 88, 735–748. doi: 10.1111/tpj.13289

Lin-Wang, K. U. I., Micheletti, D., Palmer, J., Volz, R., Lozano, L., Espley, R., et al. (2011). High temperature reduces apple fruit colour *via* modulation of the anthocyanin regulatory complex. *Plant Cell Environ.* 34, 1176–1190. doi: 10.1111/j.1365-3040.2011.02316.x

Liu, M., Pirrello, J., Chervin, C., Roustan, J.-P., and Bouzayen, M. (2015). Ethylene control of fruit ripening: revisiting the complex network of transcriptional regulation. *Plant Physiol.* 169, 2380. doi: 10.1104/pp.15.01361

Loescher, W. H. (1987). Physiology and metabolism of sugar alcohols in higher plants. *Physiol. Plant.* 70, 553–557. doi: 10.1111/j.1399-3054.1987.tb02857.x

Mellidou, I., Buts, K., Hatoum, D., Ho, Q. T., Johnston, J. W., Watkins, C. B., et al. (2014). Transcriptomic events associated with internal browning of apple during postharvest storage. *BMC Plant Biol.* 14, 328. doi: 10.1186/s12870-014-0328-x

Meng, R., Zhang, J., An, L., Zhang, B., Jiang, X., Yang, Y., et al. (2016). Expression profiling of several gene families involved in anthocyanin biosynthesis in apple (Malus domestica Borkh.) skin during fruit development. *J. Plant Growth Regul.* 35, 449–464. doi: 10.1007/s00344-015-9552-3

Moffat, C. S., Ingle, R. A., Wathugala, D. L., Saunders, N. J., Knight, H., and Knight, M. R. (2012). ERF5 and ERF6 play redundant roles as positive regulators of JA/Et-mediated defense against botrytis cinerea in arabidopsis. *PloS One* 7, e35995. doi: 10.1371/journal.pone.0035995

Murata, M., Tsurutani, M., Tomita, M., Homma, S., and Kaneko, K. (1995). Relationship between apple ripening and browning: changes in polyphenol content and polyphenol oxidase. *J. Agric. Food Chem.* 43, 1115–1121. doi: 10.1021/jf00053a001

Nardozza, S., Boldingh, H. L., Osorio, S., Hohne, M., Wohlers, M., Gleave, A. P., et al. (2013). Metabolic analysis of kiwifruit (*Actinidia deliciosa*) berries from extreme genotypes reveals hallmarks for fruit starch metabolism. *J. Exp. Bot.* 64, 5049–5063. doi: 10.1093/jxb/ert293

Opara, L. U. (2000). Fruit growth measurement and analysis. *Hortic. Rev.* 24, 373–431. doi: 10.1002/9780470650776.ch8

Queiroz, C., Mendes Lopes, M. L., Fialho, E., and Valente-Mesquita, V. L. (2008). Polyphenol oxidase: characteristics and mechanisms of browning control. *Food Rev. Int.* 24, 361–375. doi: 10.1080/87559120802089332

Saitou, N., and Nei, M. (1987). The neighbor-joining method: a new method for reconstructing phylogenetic trees. *Mol. Biol. Evol.* 4, 406–425. doi: 10.1093/oxfordjournals.molbev.a040454

Schaffer, R. J., Ireland, H. S., Ross, J. J., Ling, T. J., and David, K.M. (2013). SEPALLATA1/2-suppressed mature apples have low ethylene, high auxin and reduced transcription of ripening-related genes. *AoB Plants* 5, pls047. doi: 10.1093/aobpla/pls047

Smith, G. S., Clark, C. J., and Boldingh, H. L. (1992). Seasonal accumulation of starch by components of the kiwifruit vine. *Annals Bot.* 70, 19–25. doi: 10.1093/oxfordjournals.aob.a088434

Tamura, K., Filipski, A., Peterson, D., Stecher, G., and Kumar, S. (2013). MEGA6: Molecular evolutionary genetics analysis version 6.0. *Mol. Biol. Evol.* 30, 2725–2729. doi: 10.1093/molbev/mst197

Tan, D., Li, T., and Wang, A. (2013). Apple 1-Aminocyclopropane-1-Carboxylic Acid Synthase genes, MdACS1 and MdACS3a, are expressed in different systems of ethylene biosynthesis. *Plant Mol. Biol. Rep.* 31, 204–209. doi: 10.1007/s11105-012-0490-y

Tanaka, Y., Sasaki, N., and Ohmiya, A. (2008). Biosynthesis of plant pigments: anthocyanins, betalains and carotenoids. *Plant J.* 54, 733–749. doi: 10.1111/j.1365-313X.2008.03447.x

Teo, G., Suzuki, Y., Uratsu, S. L., Lampinen, B., Ormonde, N., Hu, W. K., et al. (2006). Silencing leaf sorbitol synthesis alters long-distance partitioning and apple fruit quality. *Proc. Natl. Acad. Sci. U. S. A.* 103, 18842–18847. doi: 10.1073/pnas.0605873103

Volz, R., Oraguzie, N., Whitworth, C., How, N., Chagné, D., Carlisle, C., et al. (2009). Red flesh breeding in apple—progress and challenges. *Acta Hortic.* 814, 337–342. doi: 10.17660/ActaHortic.2009.814.54

Volz, R. K., Kumar, S., Chagné, D., Espley, R., Mcghie, T. K., and Allan, A. C. (2013). Genetic relationships between red flesh and fruit quality traits in apple. *Acta Hortic.* 976, 363–368. doi: 10.17660/ActaHortic.2013.976.49

Vrhovsek, U., Rigo, A., Tonon, D., and Mattivi, F. (2004). Quantitation of polyphenols in different apple varieties. *J. Agric. Food Chem.* 52, 6532–6538. doi: 10.1021/jf049317z

Waltz, E. (2015). Nonbrowning GM apple cleared for market. *Nat. Biotechnol.* 33, 326. doi: 10.1038/nbt0415-326c

Wang, A., Yamakake, J., Kudo, H., Wakasa, Y., Hatsuyama, Y., Igarashi, M., et al. (2009). Null mutation of the MdACS3 gene, coding for a ripening-specific 1-aminocyclopropane-1-carboxylate synthase, leads to long shelf life in apple fruit. *Plant Physiol.* 151, 391. doi: 10.1104/pp.109.135822

Wang, N., Liu, W., Zhang, T., Jiang, S., Xu, H., Wang, Y., et al. (2018). Transcriptomic analysis of red-fleshed apples reveals the novel role of MdWRKY11 in flavonoid and anthocyanin biosynthesis. *J. Agric. Food Chem.* 66, 7076–7086. doi: 10.1021/acs.jafc.8b01273

Wang, N., Zheng, Y., Duan, N., Zhang, Z., Ji, X., Jiang, S., et al. (2015). Comparative transcriptomes analysis of red- and white-fleshed apples in an F1 population of Malus sieversii f. niedzwetzkyana crossed with M. domestica 'Fuji'. *PloS One* 10, e0133468–e0133468. doi: 10.1371/journal.pone.0133468

Wills, R. B. H., Warton, M. A., Mussa, D. M. D. N., and Chew, L. P. (2001). Ripening of climacteric fruits initiated at low ethylene levels. *Aust. J. Exp. Agric.* 41, 89–92. doi: 10.1071/EA00206

Winkel-Shirley, B. (2001). Flavonoid biosynthesis. A colorful model for genetics, biochemistry, cell biology, and biotechnology. *Plant Physiol.* 126, 485–493. doi: 10.1104/pp.126.2.485

Wu, T., Wang, Y., Zheng, Y., Fei, Z. J., Dandekar, A. M., Xu, K. N., et al. (2015). Suppressing sorbitol synthesis substantially alters the global expression profile of stress response genes in apple (*Malus domestica*) leaves. *Plant Cell Physiol.* 56, 1748–1761. doi: 10.1093/pcp/pcv092

Yamaki, S., and Ishikawa, K. (1986). Role of four sorbitol related enzymes and invertase in the seasonal alteration of sugar metabolism in apple tissue. *J. Am. Soc. Hortic. Sci.* 111, 134–137.

Yang, S. F., and Hoffman, N. E. (1984). Ethylene biosynthesis and its regulation in higher plants. *Annu. Rev. Plant Physiol.* 35, 155–189. doi: 10.1146/annurev.pp.35.060184.001103

Yao, G., Ming, M., Allan, A. C., Gu, C., Li, L., Wu, X., et al. (2017). Map-based cloning of the pear gene MYB114 identifies an interaction with other transcription factors to coordinately regulate fruit anthocyanin biosynthesis. *Plant J.* 92, 437–451. doi: 10.1111/tpj.13666

Young, J. C., Chu, C. L. G., Lu, X., and Zhu, H. (2004). Ester variability in apple varieties as determined by solid-phase microextraction and gas chromatography–mass spectrometry. *J. Agric. Food Chem.* 52, 8086–8093. doi: 10.1021/jf049364r

Zhang, J., Xu, H., Wang, N., Jiang, S., Fang, H., Zhang, Z., et al. (2018). The ethylene response factor MdERF1B regulates anthocyanin and proanthocyanidin biosynthesis in apple. *Plant Mol. Biol.* 98, 205–218. doi: 10.1007/s11103-018-0770-5

Zhang, W., Lunn, J. E., Feil, R., Wang, Y. F., Zhao, J. J., Tao, H. X., et al. (2017). Trehalose 6-phosphate signal is closely related to sorbitol in apple (*Malus domestica* Borkh. cv. Gala). *Biol. Open* 6, 260–268. doi: 10.1242/bio.022301

Zhang, Y., Butelli, E., De Stefano, R., Schoonbeek, H. J., Magusin, A., Pagliarani, C., et al. (2013). Anthocyanins double the shelf life of tomatoes by delaying overripening and reducing susceptibility to gray mold. *Curr. Biol.* 23, 1094–1100. doi: 10.1016/j.cub.2013.04.072

Conflict of Interest: The authors declare that the research was conducted in the absence of any commercial or financial relationships that could be construed as a potential conflict of interest.

frontiers in Plant Science

ORIGINAL RESEARCH
published: 06 December 2019
doi: 10.3389/fpls.2019.01591

The Ethylene Precursor ACC Affects Early Vegetative Development Independently of Ethylene Signaling

*Lisa Vanderstraeten†, Thomas Depaepe†, Sophie Bertrand and Dominique Van Der Straeten**

Laboratory of Functional Plant Biology, Department of Biology, Ghent University, Ghent, Belgium

The plant hormone ethylene plays a pivotal role in virtually every aspect of plant development, including vegetative growth, fruit ripening, senescence, and abscission. Moreover, it acts as a primary defense signal during plant stress. Being a volatile, its immediate biosynthetic precursor, 1-aminocyclopropane-1-carboxylic acid, ACC, is generally employed as a tool to provoke ethylene responses. However, several reports propose a role for ACC in parallel or independently of ethylene signaling. In this study, pharmacological experiments with ethylene biosynthesis and signaling inhibitors, 2-aminoisobutyric acid and 1-methylcyclopropene, as well as mutant analyses demonstrate ACC-specific but ethylene-independent growth responses in both dark- and light-grown *Arabidopsis* seedlings. Detection of ethylene emanation in ethylene-deficient seedlings by means of laser-based photoacoustic spectroscopy further supports a signaling role for ACC. In view of these results, future studies employing ACC as a proxy for ethylene should consider ethylene-independent effects as well. The use of multiple knockout lines of ethylene biosynthesis genes will aid in the elucidation of the physiological roles of ACC as a signaling molecule in addition to its function as an ethylene precursor.

Keywords: 1-aminocyclopropane-1-carboxylic acid, ethylene signaling, root growth, rosette growth, triple response, vegetative growth

OPEN ACCESS

Edited by:
Gerrit T. S. Beemster, University of Antwerp, Belgium

Reviewed by:
Jie Le, Institute of Botany (CAS), China
Chi-Kuang Wen, Shanghai Institutes for Biological Sciences (CAS), China

***Correspondence:**
Dominique Van Der Straeten
Dominique.VanDerStraeten@UGent.be

†These authors have contributed equally to this work and are named in reverse alphabetical order

Specialty section:
This article was submitted to Plant Physiology, a section of the journal Frontiers in Plant Science

Received: *17 July 2019*
Accepted: *13 November 2019*
Published: *06 December 2019*

Citation:
Vanderstraeten L, Depaepe T, Bertrand S and Van Der Straeten D (2019) The Ethylene Precursor ACC Affects Early Vegetative Development Independently of Ethylene Signaling. Front. Plant Sci. 10:1591. doi: 10.3389/fpls.2019.01591

INTRODUCTION

The gaseous plant hormone ethylene has been shown to regulate a myriad of physiological and developmental processes including germination, root growth and root hair formation, leaf expansion, leaf and flower senescence, abscission, fruit ripening, nodulation, and the response to numerous stresses (Burg and Burg, 1962; Abeles et al., 1992; Vandenbussche et al., 2012). Ethylene is formed from the amino acid methionine in three subsequent steps with S-adenosylmethionine (SAM) and 1-aminocyclopropane-1-carboxylic acid (ACC) as intermediates. The rate-limiting step in the biosynthesis of ethylene is the conversion of SAM to ACC, catalyzed by the enzyme ACC synthase (ACS) (Boller et al., 1979; Yang and Hoffman, 1984). In *Arabidopsis*, ACS proteins are encoded by a multigene family, eight of which are functional ACC synthases. The transcription of *ACS* genes is highly regulated during plant development and in response to a wide variety of developmental, hormonal, and environmental stimuli (Liang et al., 1992; Van Der Straeten et al., 1992; Tsuchisaka and Theologis, 2004). The final step of ethylene biosynthesis, the oxidation of ACC to ethylene, is catalyzed by the enzyme ACC oxidase (ACO) (Ververidis and John, 1991). In *Arabidopsis*, the *ACO* gene family consists of five members that are also differentially regulated (Barry et al., 1996; Nakatsuka et al., 1998). Although ACS is the major rate-limiting enzyme in

ethylene biosynthesis, under certain conditions, for example, during fruit ripening, ACO can also become rate-limiting (Barry et al., 1996; Van De Poel et al., 2012). Moreover, the levels of ACC are not only regulated at the level of ACS and ACO activity, but are also dependent on conjugation and deamination of ACC (Amrhein et al., 1981; Martin et al., 1995; Glick et al., 1998; Mcdonnell et al., 2009).

As the immediate and water-soluble precursor of ethylene, the main role of ACC is to act as a mobile signal for short- and long-distance communication within the plant. Transport of ACC throughout the plant has been observed in numerous cases (Bradford and Yang, 1980; Lurssen, 1981; Zarembinski and Theologis, 1993; Morris and Larcombe, 1995; Jackson, 2002; Almeida et al., 2003; Jackson, 2008; Vanderstraeten and Van Der Straeten, 2017). Recently, the amino acid transporter LYSINE HISTIDINE TRANSPORTER1 (LHT1) has been demonstrated to transport ACC in etiolated *Arabidopsis* seedlings (Shin et al., 2015). While it is clear that a major role of ACC is to act as the precursor of ethylene, several studies suggest that ACC itself can act as a signal independent of its oxidation to ethylene. Exogenous ACC is widely applied as a tool to study ethylene responses in plants. Both the triple response phenotype in etiolated seedlings and the reduced rosette size in light-grown plantlets, typical ethylene-related phenotypes, are triggered by ACC as well (Guzman and Ecker, 1990; Van Der Straeten et al., 1993; Roman et al., 1995; Smalle et al., 1997). The comparison of null mutations in key ethylene signaling components and the octuple *ACS* (*acs8x*) ethylene biosynthesis mutant revealed that not ethylene but ACC is crucial for viability, since only the latter resulted in embryo lethality (Tsuchisaka et al., 2009). Moreover, Xu et al. (2008) suggest that ACC might act as a signaling molecule to regulate cell expansion in the FEI/SOS5 pathway. Investigating the *fei1fei2* mutant they found that the cell expansion phenotypes in roots could be reversed by blocking ethylene biosynthesis [using AOA (2-aminooxyacetic acid, an ACS inhibitor) or AIB (2-aminoisobutyric acid, an ACO inhibitor)] but could not be reversed by chemical [using 1-MCP (1-methylcyclopropene) or silver thiosulfate] or genetic (using *etr1* or *ein2* ethylene insensitive mutants) disruption of ethylene perception. A couple of years later, Tsang et al. (2011) observed that the short-term response to cell wall damage or PAMPs resulting in rapid reduction of primary root elongation depends on the biosynthesis of ACC but is independent of the perception of ethylene. They were able to show that AIB is capable of fully restoring the LEH (length of the first epidermal cell with a visible root hair bulge) in isoxaben-treated (inhibitor of cellulose biosynthesis) roots but did not affect the ACC response. Recently, a signaling role for ACC in stomatal development has been demonstrated (Yin et al., 2019). The symmetric division of the guard mother cell (GMC) into two guard cells represents the last step in stomatal development, a process depending on ACC. Pharmacological manipulation of ACC levels showed that ACC acts as a positive regulator in GMC division. Reduced levels of ACC, in the multiple *acs* knockout lines increased the occurrence of single guard cells (SGC). This phenotype could be rescued by addition of ACC but not by treating SGCs with the ethylene-releasing chemical ethephon. Altogether, these reports demand for a reassessment of the physiological role of ACC as a signaling molecule. In this study, the ethylene-independent signaling role of ACC has been investigated during early vegetative growth. Specifically, ACC negatively affected both rosette development and hypocotyl growth, and inhibited primary root elongation independently of ethylene perception. However, similar to ethylene dose-dependent growth inhibitory effects, roots were more sensitive to ACC compared to shoots.

MATERIALS AND METHODS

Plant Material and Growth Conditions

Arabidopsis thaliana (L.) Heynh. Columbia (Col-0) was used as wild-type (WT) in this study. Col-0, *ein2-1* (Roman et al., 1995) and *acs1-1acs2-1acs4-1acs5-2acs6-1acs7-1acs9-1acs11* (*acs8x*; Tsuchisaka et al., 2009), both in Col-0 background, were obtained from the Nottingham Arabidopsis Stock Center (NASC; arabidopsis.info/). Seeds were surface-sterilized for 12 min in a bleach solution containing 5% NaOCl and subsequently washed at least 3 times with sterile distilled water. Seeds were plated on half-strength Murashige and Skoog (1/2 × MS) medium containing 0% (**Figure S1**) or 1% sucrose (all other assays) and 0.8% agar and supplemented with the indicated chemicals. 1-aminocyclopropane-1-carboxylic acid (ACC) and 2-aminoisobutyric acid (AIB) were purchased from Sigma-Aldrich and stock solutions were prepared in distilled water. After a stratification of 3 days at 4°C, plates were transferred to a tissue culture chamber (21°C; 16/8-h photoperiod; 70 μmol s^{-1} m^{-2}) for the desired time. For assays with dark-grown seedlings, seeds were exposed to light for 6 h after stratification to induce germination and were subsequently grown for 4 days in complete darkness (21°C).

Gas Treatments

1-MCP

At the start of the experiment, plates were transferred to a dedicated gassing chamber (Van Cleven, Belgium) containing both a treatment and a control cell. Plants were treated with 1-methylcyclopropene (1-MCP) in the treatment cell for 20 h, followed by 4 h of flushing with 1-MCP-free air. The required amount of 1-MCP (EthylBloc) was dissolved in a buffer containing 0.9% KOH and 0.9% NaOH in a 200-ml beaker, which was immediately transferred to the chamber, to give a final concentration of 50, 100, or 250 ppm inside the treatment cell. In parallel, control plants were placed in the control cell and flushed continuously with 1-MCP-free air. The treatment was repeated on a daily basis until the end of the experiment.

Ethylene

Ethylene treatment on 2-week-old plants (**Figure S3**) was carried out in the gassing chambers described above. For combined treatments, plants were first treated with ethylene (Air Liquide, Belgium) for 4 h at a final concentration of 100 ppm, and subsequently treated with 1-MCP for 20 h. Both treatments were repeated on a daily basis until the end of the experiment.

Phenotypic Analysis

Plants were photographed with a Canon EOS 550D camera (Canon, Tokyo, Japan)) after 14 days of growth on horizontally standing plates. To evaluate effects on shoot growth, rosette area was measured with Rosette Tracker (De Vylder et al., 2012), an open-source plug-in in ImageJ (National Institutes of Health). In addition, root length was measured in ImageJ. The triple response assay was carried out, as described previously (Hu et al., 2017), to evaluate the growth of etiolated seedlings. The length of 4-day-old hypocotyls and roots were measured in ImageJ. Average values were obtained from three independent replicates.

Measurement of Ethylene Emanation

Ethylene emanation was monitored essentially as described in Van de Poel and Van Der Straeten (2017). For the detection of ethylene levels emitted by etiolated seedlings, approximately 30 seeds were sown in 10-ml chromatography vials (Chromacol, VWR) containing 5 ml ½ × MS medium (four independent biological repeats), transferred to a sterile box and grown in darkness at 21°C. Average values were obtained from four independent replicates. For the detection of ethylene levels in 14-day-old plants, three seeds were sown in 10-ml vials, containing 8 ml ½ × MS medium, and grown in a tissue culture chamber (21°C; 16/8-h photoperiod; 70 μmol s^{-1} m^{-2}). Average values were obtained from eight independent replicates 24 h before the start of the measurement, vials were sealed off with a rubber septum and a snap-cap (Chromacol, VWR) to allow ethylene accumulation. Ethylene levels were analyzed by means of laser-based photoacoustic spectroscopy (ETD-300, Sensor Sense, The Netherlands).

Ethylene Complementation Assay

To monitor residual ethylene biosynthesis in the presence of ACC and the ACO blocker AIB, ethylene emission was examined, as described above, in etiolated Col-0 seedlings on a daily basis. The effect of this concentration of ethylene was assessed as follows. Col-0 seeds were sown in 10-ml chromatography vials on media containing 0, 10, or 50 μM ACC in the absence or presence of 2 mM AIB. After germination, ethylene was injected with a gas-tight syringe (Hamilton) to a final concentration equivalent to the levels measured, over a 24-h period from day 3 to day 4, upon treating with 10 [= ETH(10)] or 50 μM ACC [= ETH(50)] in the presence of 2 mM AIB. The final concentrations were 116 and 585 ppb, respectively. Seedlings were allowed to grow for 3 days in complete darkness, after which the phenotypic effects were evaluated at the level of hypocotyl and root growth. Seedlings were grown in the same vials on media containing ACC and/or AIB with ethylene-free air as a control. Average values were obtained from four independent replicates.

Statistical Analysis

All statistical analyses were carried out in the free software environment for statistical computing and graphics R 3.2.3 (R Foundation for Statistical Computing, Vienna, Austria, www.R-project.org). Data are presented as means, error bars are standard deviations. Statistical analysis comparing two means was performed using the Wilcoxon rank sum test/T-test ($P < 0.01$). Statistical analysis comparing multiple means was performed using One-Way ANOVA/Kruskal-Wallis (one independent variable) or Scheirer-Ray-Hare (two independent variables) tests ($P < 0.01$) followed by *post hoc* Tukey's HSD/Dunn tests ($P < 0.01$) with Benjamini and Hochberg correction for multiple pairwise comparisons. In addition, effect sizes for multifactorial analyses are presented and interpreted with partial η^2 according to Richardson (2011). Small, medium, and large effects correspond with effect sizes of 0.01, 0.06, and 0.15, respectively. Partial η^2 is calculated as the sum of squares (SS) divided by the sum of SS and SS of the residuals. Effect size for comparisons between two groups is presented as r (Rosenthal, 1994). R was calculated as $Z / \sqrt{N}$ (Wilcoxon rank sum tests, Tukey's HSD and Dunn tests) or as √(t^2/(t^2+df)) (T-tests). Small, medium, and large effects correspond with effect sizes of 0.1, 0.3, and >0.5, respectively. Relevant output of effect sizes can be found in **Table S1**.

RESULTS

Dose-Dependent Effects of ACC on Shoot and Root Development Upon Ethylene Insensitivity

To explore the role of ACC in rosette development, possibly independent of ethylene, dose-response assays were conducted in 2-week-old WT Col-0 and in ethylene insensitive *ein2-1* plants (**Figures 1A**, **B**). In parallel, 1-methylcyclopropene (1-MCP) gas treatments, specifically blocking ethylene from binding to its receptor, were carried out to further investigate ACC-specific effects on rosette growth (**Figures 1C**, **D**). In WT Col-0, ACC reduced overall shoot growth in a dose-dependent manner, reflected by a decrease in rosette area (**Figures 1A**, **B**). Compared to the mock treatment, 10 μM ACC already reduced rosette area severely. A saturated response was visible as of 100 μM ACC. As expected, the phenotype of the rosettes was reminiscent of that of plants treated with exogenous ethylene or *ctr1* mutants, namely severe dwarfism caused by smaller leaf blades and petioles, as a result of inhibited cell expansion (Kieber et al., 1993; Rodrigues-Pousada et al., 1993). With a defective ethylene signaling pathway in *ein2-1*, rosettes responded differently to ACC compared to Col-0 (**Figures 1A**, **B**). At 10 μM ACC, *ein2-1* rosette size was slightly larger compared to a treatment with 0 μM ACC. Contrarily, at 100 μM ACC, the mean rosette area was decreased, as seen in Col-0 plants. The observation that ACC inhibited rosette development at higher doses regardless of the genotype, is indicative for an ethylene-independent effect of ACC. In addition, a small-scale experiment was carried out to determine whether the inhibitory effect of ACC on rosette growth is influenced by the presence of sucrose (**Figure S1**). In general, the omission of sucrose supplementation in the growth medium resulted in a decrease in rosette area in both Col-0 and *ein2-1* plants and irrespective of ACC concentration (**Figure S1B**). In the absence of ACC, a lack of sucrose resulted in a small inhibitory effect on rosette area in Col-0 and large decrease in *ein2-1*. However, at high concentrations of ACC (e.g., 100 μM) rosette area of Col-0 and *ein2-1* was reduced severely, irrespective of the presence of sucrose. However, the magnitude of the effect was

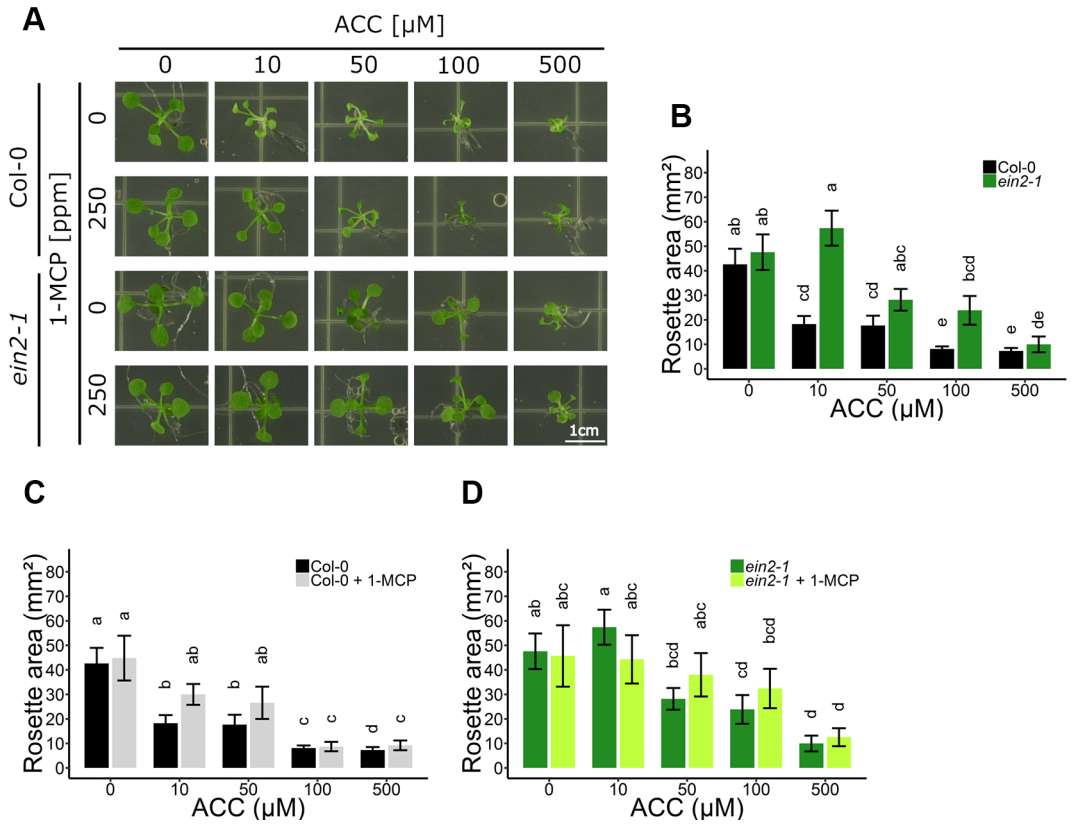

FIGURE 1 | Rosette development of *Arabidopsis* wild-type Col-0 and ethylene insensitive *ein2-1* on increasing concentrations of ACC with and without 1-MCP treatment. *Arabidopsis* wild-type Col-0 and ethylene insensitive mutant *ein2-1* were sown on 0, 10, 50, 100, and 500 µM ACC with or without treatment with 250 ppm 1-MCP. **(A)** Pictures of representative 2-week-old plants under long-day conditions (16-h light/8-h dark) at light intensity of 70 µmol m^{-2} s^{-1} at 21°C. **(B)** Rosette area of 2-week-old Col-0 and *ein2-1* plants without 1-MCP treatment. **(C)** Rosette area of 2-week-old Col-0 plants. **(D)** Rosette area of 2-week-old *ein2-1* plants. Data from a representative experiment are shown; further corroborated by a minimum of three independent experiments. Different letters indicate statistically significant differences between the different groups (Kruskal-Wallis, Dunn's Multiple Comparison Test, $P < 0.01$; $9 \leq n \leq 30$). Error bars are SD. Effect sizes are presented in **Table S1**.

larger upon sucrose supplementation. For instance, in *ein2-1*, 100 µM ACC decreased rosette area with 5.88 mm^2 and 12.30 mm^2 in the absence or presence of sucrose, respectively. Hence, although sucrose affects rosette growth in both WT and ethylene-insensitive plants, ACC is capable of inhibiting growth independently of ethylene and sucrose signaling.

When ethylene perception was blocked with 250 ppm 1-MCP, Col-0 rosettes were slightly larger compared to mock-treated rosettes, though this increase was negligible (**Figure 1C**). Furthermore, in the presence of 1-MCP, ACC was still able to reduce growth in a dose-dependent manner, indicating that ACC can affect shoot growth independently of ethylene perception. On 10 µM ACC, MCP-treated rosettes reached 30.01 mm^2 compared to 0 µM ACC, while 100 µM ACC further decreased rosette area to 8.72 mm^2 (**Figure 1C**). Nevertheless, in the presence of 1-MCP Col-0 exhibited a reduced sensitivity to ACC as compared to the absence of 1-MCP, consistent with the ACC dose-response in *ein2-1* (**Figures 1B, C**). Furthermore, 1-MCP did not substantially change the response of *ein2-1* to increasing concentrations of ACC (**Figures 1A, D**). An additional experiment using 50 ppm 1-MCP was conducted to verify that the observed inhibitory effects were not due to an excess of 1-MCP (**Figure S2**). The effects of ACC on rosette area were comparable to those in the presence of 250 ppm 1-MCP.

ACC can also negatively affect root growth independently of ethylene signaling (**Figure 2A**). Col-0 seedlings were grown on increasing concentrations of ACC in the absence or presence of 250 ppm 1-MCP. Both ACC and 1-MCP dramatically altered root growth. In the absence of 1-MCP, a reduction in root length was already apparent at 10 µM ACC (**Figure 2B**), consistent with previously reported effects of ethylene on root growth inhibition (Le et al., 2001). In contrast, at the same concentration of ACC in the presence of 1-MCP, a much smaller inhibition was observed (**Figure 2B**). A five-fold higher dose was required for an effective inhibition of root elongation in Col-0 plants subjected to 1-MCP treatment (**Figures 2A, B**). It is conceivable that the observed effects of ACC on both rosette and root growth, in the presence of 1-MCP, are due to an ethylene signal remaining present under an insufficient dose of 1-MCP. However, the binding affinity of 1-MCP to the ethylene receptors was demonstrated to be at least 10 times greater compared to ethylene (Hall et al., 2000; Binder et al., 2004). Additionally, previous reports demonstrated that 500

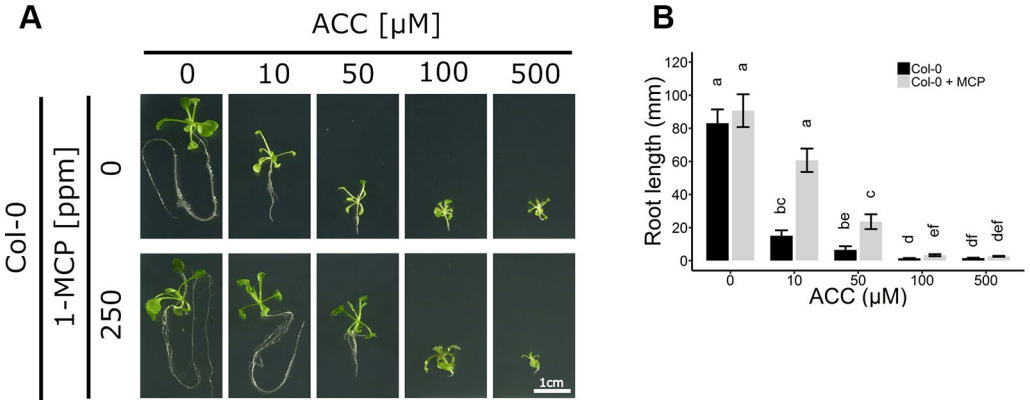

FIGURE 2 | Root development of *Arabidopsis* wild-type Col-0 on increasing concentrations of ACC with and without 1-MCP treatment. *Arabidopsis* wild-type Col-0 was sown on 0, 10, 50, 100, and 500 µM ACC with or without treatment with 250 ppm 1-MCP. **(A)** Pictures of representative 2-week-old plants under long-day conditions (16-h light/8-h dark) at light intensity of 70 µmol m^{-2} s^{-1} at 21°C. **(B)** Root length of 2-week-old Col-0 plants. Data from a representative experiment are shown; further corroborated by a minimum of three independent experiments. Different letters indicate statistically significant differences between the different groups (Kruskal-Wallis, Dunn's Multiple Comparison Test, $P < 0.01$; $28 \leq n \leq 44$). Error bars are SD. Effect sizes are presented in **Table S1**.

ppb of ethylene is sufficient to mimic the phenotypic effects of 50 µM ACC at the level of rosette growth inhibition (Vaseva et al., 2018). Moreover, a treatment of etiolated seedlings with 1 mM ACC was shown to give rise to ethylene levels ranging from 1 to 10 ppm (Woeste et al., 1999). Altogether, these findings support the interpretation that 250 ppm of 1-MCP is more than sufficient to block the effects of 500 µM ACC. To further corroborate this assumption, plants were treated for 2 weeks with ethylene in the presence of 1-MCP to assess ethylene insensitivity (**Figure S3**). A dose of 100 ppm ethylene was chosen to effectively supersede the effects of 500 µM ACC. WT plants supplemented with ethylene displayed a typical dwarfed phenotype and reduced root growth, in the absence of 1-MCP (**Figure S3**). However, these phenotypic effects disappeared when ethylene perception was blocked with 100 ppm 1-MCP, or similarly in *ein2-1*, which has a defective ethylene signaling pathway and is fully unresponsive to ethylene. Thus, ACC, at the concentrations tested, is capable of reducing overall growth during early plant development, independently of ethylene.

Effects of ACC on Vegetative Growth in the Presence of ACO Inhibitor AIB

To further investigate the role of ACC in vegetative development, experiments using the ACO inhibitor AIB were conducted. Ethylene emanation was measured in 2-week-old plants grown on increasing doses of ACC in the absence and presence of 2 mM AIB (**Figure 3A** and **Table S2**). A dose-dependent increase in ethylene levels was observed when plants were grown on ACC-containing media. In addition, AIB effectively blocked ACO-mediated conversion of ACC to ethylene, though a small increase in ethylene levels, could be observed at higher concentrations (50 µM ACC; **Table S2**). Nevertheless, the ethylene levels in plants treated with 50 µM ACC + AIB were more than two-fold lower than those in plants treated with 1 µM ACC alone (**Figure 3A** and **Table S2**). Concentrations of ACC exceeding 50 µM were henceforth omitted, since in such conditions 2 mM AIB was unable to outcompete ACC for binding to the catalytic site of ACO, resulting in notable ethylene emanation. Moreover, if the phenotypic effect upon treatment with 50 µM ACC + AIB was stronger compared to that of 1 µM ACC alone, it was considered a *bona fide* ACC effect.

In subsequent experiments, the phenotypic responses upon AIB with increasing doses of ACC were investigated both at the level of rosette and root growth (**Figure 3B**). Fifty micromolar of ACC was capable of reducing rosette expansion of 2-week-old WT Col-0 plants treated with 1-MCP (**Figures 1A**, **B**). The addition of 2 mM AIB resulted in a slight decrease in rosette area upon 50 µM ACC, compared to 0 µM ACC (**Figures 3B**, **C**). In *ein2-1* plantlets, 50 µM ACC decreased rosette size substantially in the absence of AIB. However, in the presence of 2 mM AIB, rosette area reduced only slightly upon treatment with 50 µM ACC (**Figures 3B–D**). Contrarily, when roots were evaluated after 2 weeks of growth on vertically standing plates, a dose-dependent reduction in root length was discovered in Col-0 and *ein2-1* even in the presence of 2 mM AIB (**Figures 4A–C**). In Col-0, 50 µM ACC decreased the average root length from 39.17 mm to 5.57 mm in the absence of AIB. In the presence of AIB, root length was decreased from 22.37 mm to 5.35 mm (**Figure 4B**). Likewise, 50 µM ACC reduced root elongation substantially in *ein2-1* both without and with AIB supplementation (**Figure 4C**). Since the application of 50 µM ACC + AIB led to ethylene levels lower than those observed upon 1 µM ACC alone (**Figure 3A**), and the inhibitory effect of the latter dose was relatively small for both rosettes and roots, the stronger inhibitory effect observed on 50 µM ACC + AIB is assumed to be a true ACC effect (**Figures 3B**, **C** and **4B**, **C**). In conclusion, AIB hinders the growth-inhibiting effect of ACC in light-grown plantlets, in an organ-dependent manner.

ACC Effects During Skotomorphogenic Development

As ACC/ethylene affect skotomorphogenic development as well, an ethylene-independent role for ACC was investigated

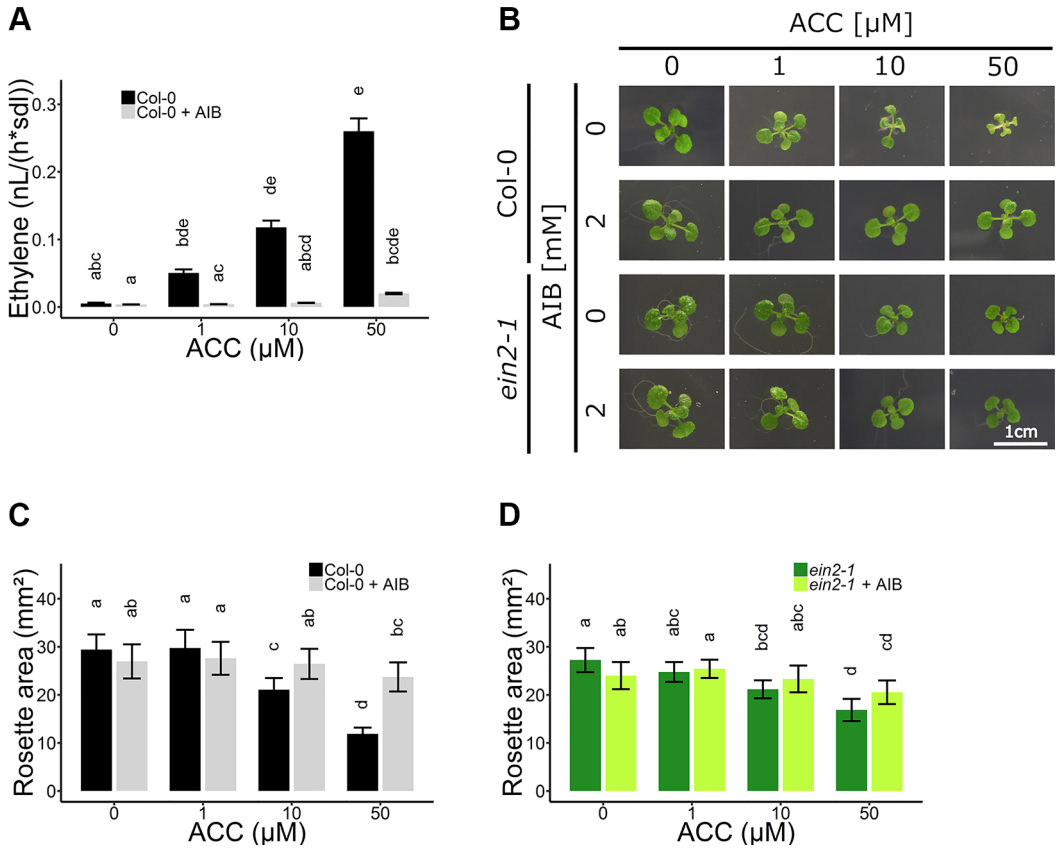

FIGURE 3 | Rosette development of *Arabidopsis* wild-type Col-0 and ethylene insensitive *ein2-1* on increasing concentrations of ACC with and without AIB treatment. *Arabidopsis* wild-type Col-0 and ethylene insensitive mutant *ein2-1* were sown on 0, 10, and 50 µM ACC with or without treatment with 2 mM AIB. **(A)** Ethylene production rates of 2-week-old Col-0 plants (n = 3; 8 independent replicates). **(B)** Pictures of representative 2-week-old plants under long-day conditions (16-h light/8-h dark) at light intensity of 70 µmol m^{-2} s^{-1} at 21°C. **(C)** Rosette area of 2-week-old Col-0 plants (10 ≤ n ≤ 24; 3 independent replicates). **(D)** Rosette area of 2-week-old *ein2-1* plants (8 ≤ n ≤ 15; 3 independent replicates). Different letters indicate statistically significant differences between the different groups (Kruskal-Wallis, Dunn's Multiple Comparison Test, P < 0.01). Error bars are SD. Effect sizes are presented in **Table S1**.

in etiolated seedlings (**Figure 5**). First, ethylene emanation by seedlings treated with ACC, AIB or a combination of both, was measured using laser-based photoacoustic spectroscopy (**Figure 5A**). AIB was able to effectively reduce ethylene synthesis to negligible levels up to doses of 10 µM ACC. At 10 µM ACC, AIB-treated seedlings emitted ethylene levels (µ = 1.29 pl seedling^{-1} h^{-1}) comparable to seedlings subjected to 0.1 µM ACC without AIB (µ = 1.00 pl seedling^{-1} h^{-1}) (**Table S3** and **Figure 5A**). A significant rise in ethylene levels could be observed at 50 µM ACC + AIB (µ = 6.50 pl seedling^{-1} h^{-1}), which was similar to ethylene levels released upon treatment with 0.75 µM ACC alone (µ = 5.96 pl seedling^{-1} h^{-1}) (**Table S3** and **Figure 5A**). Therefore, differences in phenotypic effects between the aforementioned treatments are indicative for true ACC effects.

Next, an AIB dose-response assay employing Col-0 and *ein2-1* was carried out on 4-day-old etiolated seedlings (**Figures 5B–F**). In Col-0, a dose-dependent inhibition of hypocotyl (**Figure 5C**; **Figure S4A**) and root (**Figures 5D** and **S4B**) elongation was observed, with roots being slightly more responsive to ACC at lower concentrations (as of 0.1 µM). Upon the addition of the ACO inhibitor AIB, hypocotyls demonstrated significant resistance to lower concentrations of ACC (0.5–10 µM), while reacting comparable to the wild type upon larger doses (>50 µM) (**Figure 5C**). For instance, 1 µM ACC reduced the average hypocotyl length from 10.88 mm to 4.08 mm, while in the presence of AIB, it only decreased from 9.81 mm to 8.11 mm (**Figure 5C**). In contrast, 50 µM ACC strongly inhibited hypocotyl length, irrespective of AIB treatment. A similar response was observed in AIB-treated roots (**Figure 5D**). In the ethylene-insensitive mutant *ein2-1*, ACC was able to significantly reduce hypocotyl and root growth as well, though to a much smaller extent than in Col-0 treated with AIB (**Figures 5B**, **E–F** and **S4C, D**). At 50 µM ACC and in the absence of AIB, hypocotyl length was merely reduced from 11.46 mm to 8.57 mm (**Figure 5E**).

Given that in Col-0, 10 and 50 µM ACC in the presence of AIB resulted in stronger inhibitory effects compared to 0.1 and 0.75 µM ACC, respectively, in the absence of AIB (**Figures 5B**, **C**), we hypothesized that these represent *bona fide* ACC responses. An ethylene complementation assay was conducted to rule out the possibility that residual ethylene biosynthesis upon AIB treatment is the cause of the observed phenotype in dark-grown seedlings (**Figure S5**). Specifically, the phenotypic effects

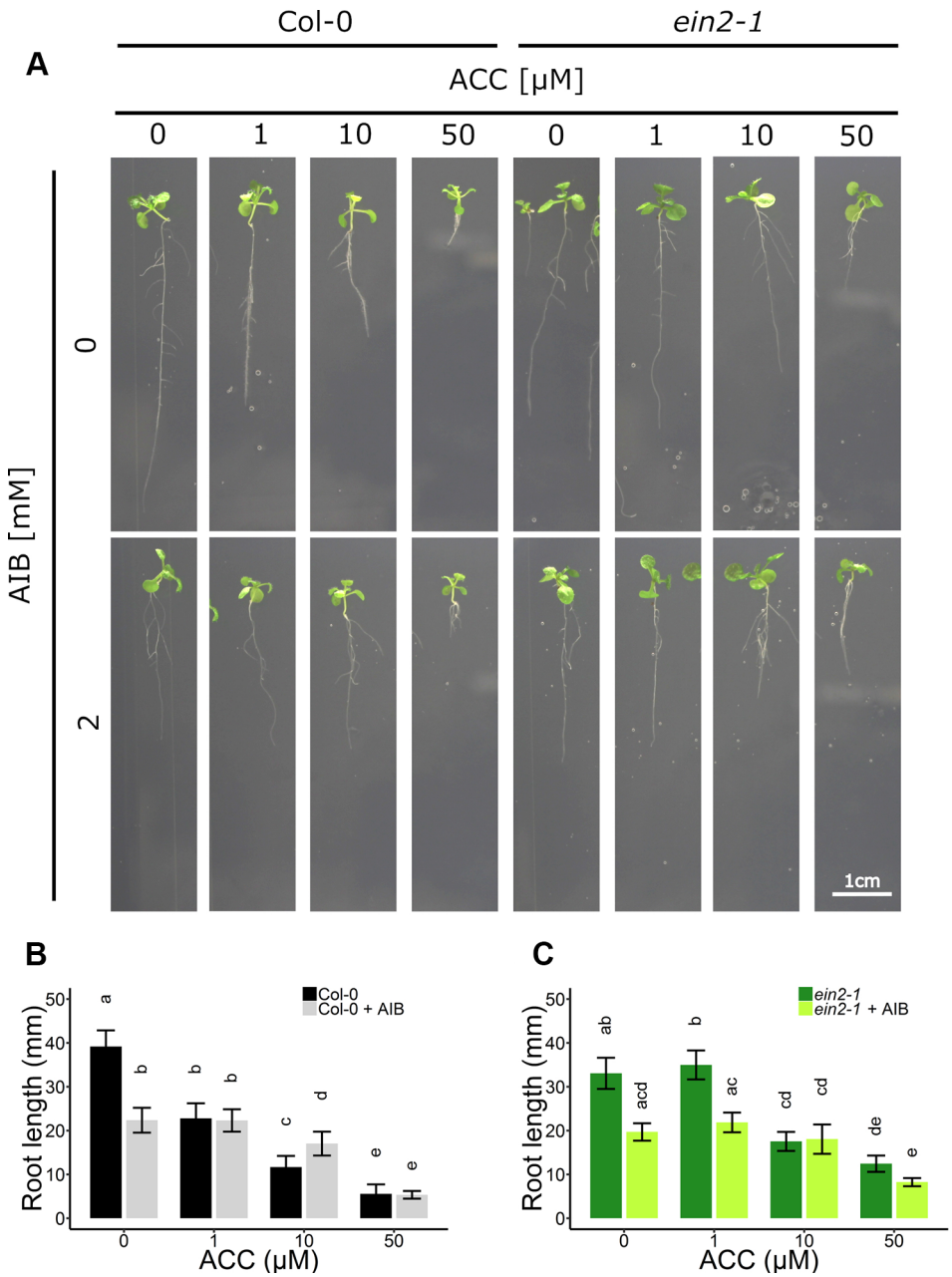

FIGURE 4 | Root development of *Arabidopsis* wild-type Col-0 and ethylene insensitive *ein2-1* on increasing concentrations of ACC with and without AIB treatment. *Arabidopsis* wild-type Col-0 and ethylene insensitive mutant *ein2-1* were sown on 0, 1, 10, and 50 µM ACC with or without AIB treatment (2 mM). **(A)** Pictures of representative 2-week-old plants under long-day conditions (16-h light/8-h dark) at light intensity of 70 µmol m^{-2} s^{-1} at 21°C. **(B)** Root length of 2-week-old Col-0 plants ($10 \leq n \leq 24$; 3 independent replicates). **(C)** Root length of 2-week-old *ein2-1* plants ($4 \leq n \leq 13$; 3 independent replicates). Different letters indicate statistically significant differences between the different groups **(B)** One-way ANOVA, Tukey HSD; **(C)** Kruskal-Wallis, Dunn's Multiple Comparison Test, $P < 0.01$). Error bars are SD. Effect sizes are presented in **Table S1**.

of the residual levels of ethylene emanated by seedlings treated with either 10 µM ACC + AIB [designated ETH (10); 116 ppb] and 50 µM ACC + AIB [designated ETH (50); 585 ppb] were investigated (**Table S3**). When seedlings were treated with ETH (10), hypocotyls and roots were almost indistinguishable from the mock treatment (**Figures S5A–C**). In the presence of 2 mM AIB, the effect of ETH (10) was slightly larger in both organs. However, the effect of 10 µM ACC + AIB on hypocotyl and root elongation was stronger than that of ETH (10) [**Figures S5A–C**; compare ETH (10) with 10 µM ACC; gray bars]. Similarly, the effect of ETH (50) was less pronounced compared to 50 µM ACC + AIB [**Figures S5A–C**; compare ETH (50) with 50 µM ACC; gray bars]. Nevertheless, it is clear that the inhibitory effect on elongation of ETH (50) is stronger than that of ETH (10).

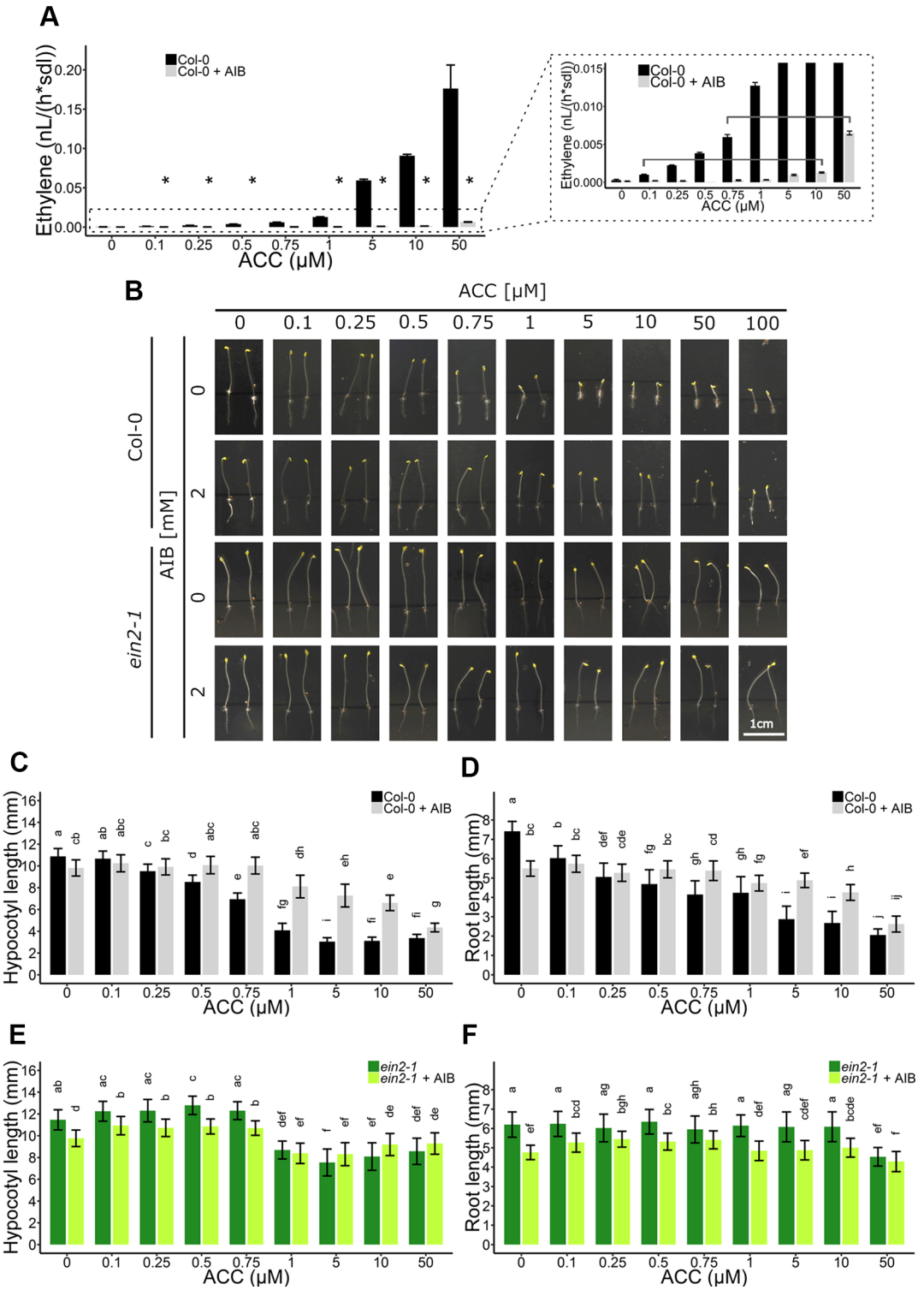

FIGURE 5 | Triple response development of *Arabidopsis* wild-type Col-0 and ethylene insensitive *ein2-1* on increasing concentrations of ACC with and without AIB treatment. *Arabidopsis* wild-type Col-0 and ethylene insensitive mutant *ein2-1* were sown in darkness on 0, 0.1, 0.25, 0.5, 0.75, 1, 5, 10, and 50 µM ACC with or without treatment with 2 mM AIB. **(A)** Ethylene production rates of 4-day-old etiolated Col-0 seedlings (n = 30; 4 independent replicates). **(B)** Pictures of representative 4-day-old etiolated Col-0 and *ein2-1* seedlings. **(C)** Hypocotyl length and **(D)** root length of Col-0 seedlings (38 ≤ n ≤ 55; 3 independent replicates). **(E)** Hypocotyl length and **(F)** root length of *ein2-1* seedlings (22 ≤ n ≤ 42; 3 independent replicates). Different letters indicate statistically significant differences between the different groups (Kruskal-Wallis, Dunn's Multiple Comparison Test, $P < 0.01$). Error bars are SD. The relative values of panels **(B–E)** are depicted in **Figure S4**. Effect sizes are presented in **Table S1**. $P < 0.01$ is indicated with *.

Interestingly, AIB reduced root length in both Col-0 and *ein2-1*, even in the absence of exogenous ACC or in the presence of ethylene (**Figures 4B**, **C**, **5D**, **F**, and **S5C**). In darkness, Col-0 and *ein2-1* roots were approximately 25% shorter when treated with 2 mM AIB (**Figures 5D**, **F**). To assess whether this inhibitory effect is caused by an accumulation of endogenous ACC or is due to a side effect of AIB, we investigated the response of the *acs8x* mutant, which is almost completely devoid of endogenous ACC, to AIB treatment (**Figure 6**). Etiolated *acs8x* seedlings exhibited significantly longer hypocotyls and shorter roots compared to the WT (**Figures 6A–C**), consistent with previous reports (Tsuchisaka et al., 2009). Upon addition of 2 mM AIB, both WT and *acs8x* roots were 30% shorter compared to roots in absence of AIB (**Figures 6C**, **E**). Furthermore, *acs8x* hypocotyls were slightly more sensitive to AIB compared to the WT (**Figures 6B**, **D**). These results strongly indicate that the response of seedlings to AIB is not related to an accumulation of ACC, as *acs8x* seedlings were not resistant to the treatment.

Altogether, these data corroborate an ethylene-independent role for ACC during skotomorphogenic shoot and root development (**Figure 5**), in addition to its negative effect on rosette and root development in light conditions (**Figures 1** and **4**). Furthermore, ACC evokes distinct responses in ethylene-sensitive compared to -insensitive backgrounds.

DISCUSSION

Since the discovery of ACC as a biosynthetic precursor of the plant hormone ethylene about 4 decades ago (Adams and Yang, 1979), most studies were focused on identifying the mechanisms controlling ethylene synthesis and its subsequent *in vivo* responses. Few studies, however, investigated whether ACC has a non-canonical function, independent of ethylene signaling or bypassing ethylene perception. Here, we provide evidence for a role of ACC in the regulation of early vegetative development in *Arabidopsis thaliana*. Using chemical inhibitors of ethylene biosynthesis and perception, in WT and in the ethylene-insensitive mutant background *ein2-1*, our study demonstrates that ACC can act as a negative regulator of rosette development (**Figures 1**, **3** and **S1**, **S2**), hypocotyl elongation in darkness (**Figures 5** and **S4**), and root growth in both light (**Figures 2** and **4**) and etiolated conditions (**Figure 5**), in parallel of ethylene perception. Based on these findings, we propose to revisit the current model on ACC/ethylene biosynthesis and signaling, including ACC-specific responses (**Figure 7**).

In roots, ACC or ethylene treatment is known to cause growth inhibition through a reduction in LEH, in a concentration- and time-dependent manner (Le et al., 2001). Specifically, ethylene perception in the epidermal layer of the transition zone is

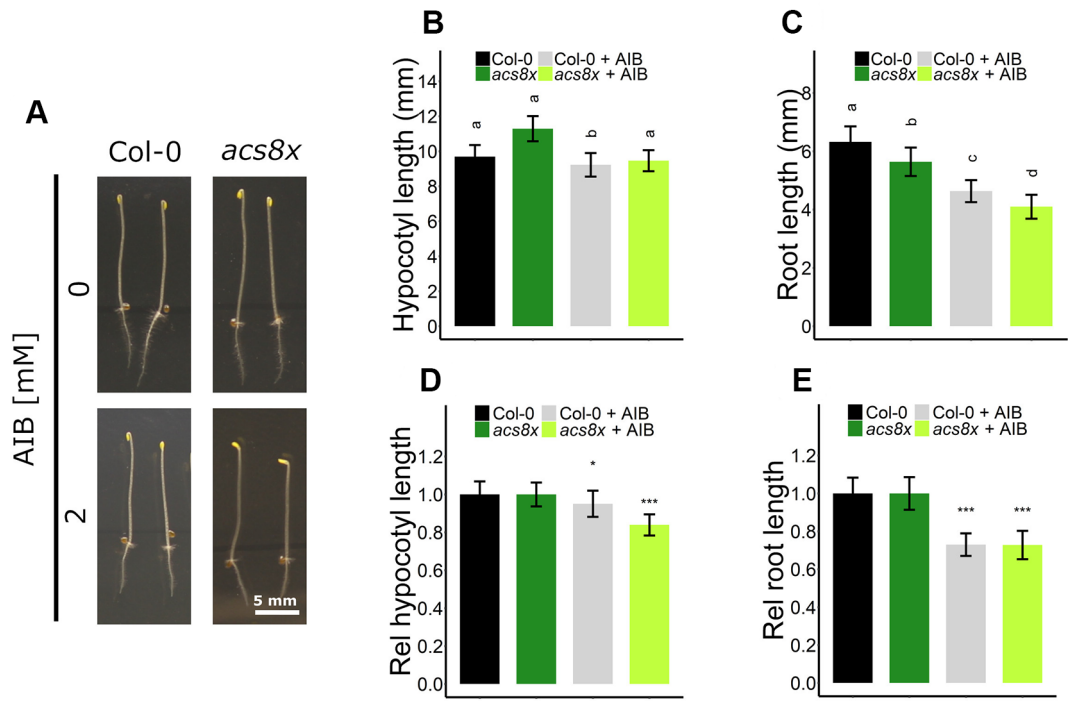

FIGURE 6 | Triple response of *Arabidopsis* wild-type Col-0 and ethylene biosynthesis octuple mutant *acs8x* with and without AIB treatment. *Arabidopsis* wild-type Col-0 and ethylene biosynthesis octuple mutant acs8x were sown with or without AIB treatment (2 mM). **(A)** Pictures of representative 4-day-old etiolated Col-0 and *acs8x* seedlings. **(B)** Hypocotyl length and **(C)** root length of Col-0 and *acs8x* seedlings ($13 \leq n \leq 26$; 3 independent replicates). **(D)** Relative hypocotyl length and **(E)** relative root length of *acs8x* seedlings. In panels **(D)** and **(E)**, lengths are expressed relative to the corresponding genotype on medium without AIB. In panels **(B)** and **(C)**, different letters indicate statistically significant differences between the different groups (Kruskal-Wallis, Dunn's Multiple Comparison Test, $P < 0.01$). T-tests were carried out in panels **(D)** and **(E)** to compare differences within a genotype ($P < 0.01$ is indicated with *; $P < 0.0001$ is indicated with ***). Error bars are SD. Effect sizes are presented in **Table S1**.

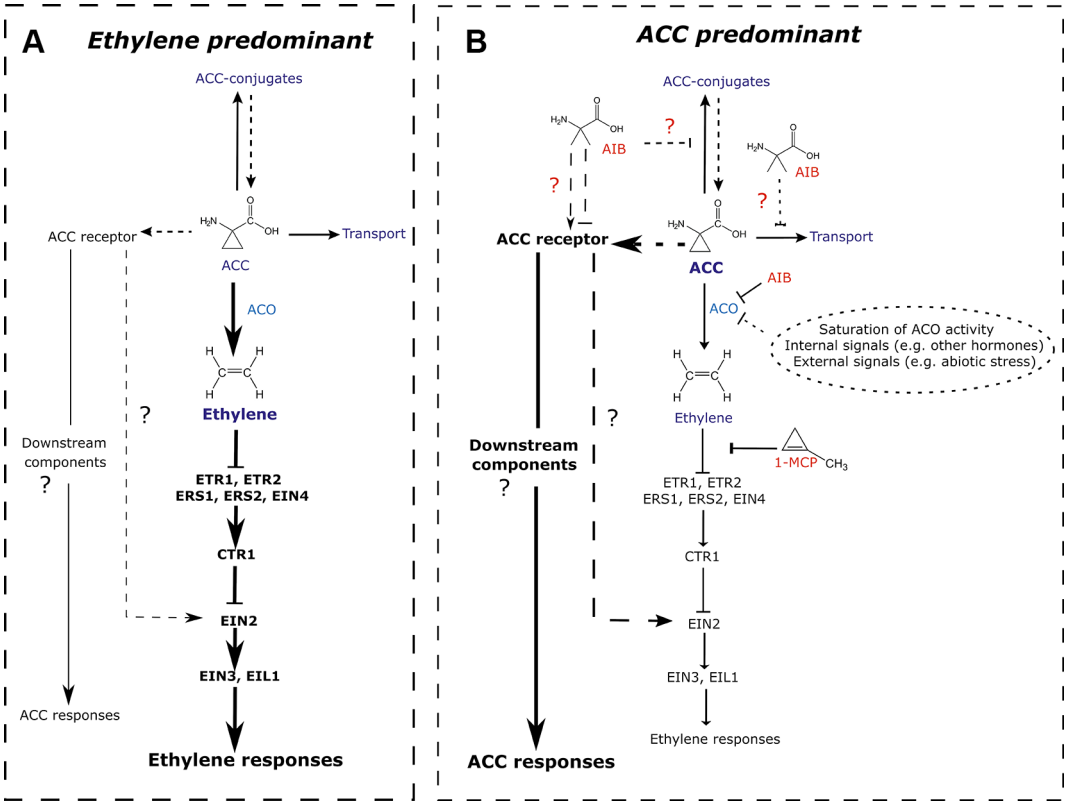

FIGURE 7 | Revisited model for ACC/ethylene biosynthesis and signaling. **(A)** ACC/ethylene signaling pathway in normal conditions, where the responses are mainly mediated by ethylene. A major portion of ACC is converted to ethylene by ACO. The signal is then transferred *via* key signaling components ultimately leading to ethylene responses. The remaining ACC is transported to other tissues, conjugated to storage forms or perceived by (a) putative ACC receptor(s). Subsequent ACC responses are assumed to be minimal. **(B)** ACC/ethylene signaling pathway in conditions where ACC accumulates and leads to ACC-specific responses. ACC accumulation can result from an inhibition of ACO by inhibitors (e.g., AIB; shown in red), saturation of ACO activity (leading to overflow), or any other inhibition of ACO caused by internal or external signals. Elevated levels of ACC bind to its receptor(s), activating unidentified downstream components, ultimately leading to ACC-specific responses. Alternatively, ACC could, upon interaction with its receptor(s) act *via* EIN2, activating ethylene-mediated gene expression, while bypassing the need for ethylene perception. Additionally, the ACO inhibitor AIB potentially affects other ACC binding proteins such as putative receptors, transporters or conjugating enzymes. Arrow-headed lines represent stimulatory interactions. Bar-headed lines represent inhibitory interactions. Thick lines depict the predominantly active pathway. Dashed lines indicated relations that have not been demonstrated experimentally. 1-MCP, 1-methylcyclopropene; ACC, 1-aminocyclopropane-1-carboxylic acid; ACO, ACC oxidase; ACS, ACC synthase; AIB, 2-aminoisobutyric acid; CTR, constitutive triple response; ETR, ethylene response; ERS, ethylene response sensor; EIN, ethylene insensitive; EIL, EIN3-like.

sufficient to inhibit root growth (Vaseva et al., 2018). Moreover, this response is mediated by changes in intracellular auxin levels concomitant with an apoplastic alkalinization, which in turn regulates the activity of cell-wall loosening agents and peroxidases (Staal et al., 2011; Barbez et al., 2017; Vaseva et al., 2018). Though ACC and ethylene root responses are certainly overlapping, our data demonstrate that ACC can affect primary root growth independently of ethylene perception and/or signaling (**Figures 2**, **4**, and **5**). We propose that this role might be either specific to ACC or related to a feedback regulatory mechanism involving auxin, mimicking ethylene-mediated root inhibition (Vaseva et al., 2018). An ethylene-independent role for ACC as a signal driving root growth has been proposed previously (Xu et al., 2008; Tsang et al., 2011). They suggest that ACC is involved in the sensing of cell wall integrity, a feature crucial in the control of root elongation. It is conceivable that crosstalk between ACC and ethylene exists, since the latter also acts on factors related to cell wall integrity. Until now, no role for ACC in the regulation of hypocotyl or shoot growth has been thoroughly characterized. Higher order mutants of *ACS* genes, however, do exhibit reduced branching, a phenotype clearly distinct from single ethylene signaling mutants (Tsuchisaka et al., 2009). In addition, embryo lethality in a homozygous octuple *acs* mutant points to a primary role of ACC in early vegetative growth (Tsuchisaka et al., 2009). Contrarily, a non-canonical ethylene pathway, such as the controversial CTR1-MKK9–MPK3/MPK6-EIN3 signaling cascade, could regulate embryo development as well (Yoo et al., 2008). Analysis of an *ACO* null mutant or a heptuple *etr1ers1etr2ers2ein4ctr1ein2* will shed light on this issue. Our work supports a role for ACC as a regulator of hypocotyl and shoot growth, independently of ethylene (**Figures 1**, **3**, and **5C**). Ethylene is known to regulate hypocotyl elongation and leaf expansion *via* changes in cell wall integrity and microtubule orientation (Collett et al., 2000; Le et al., 2005; Pierik et al., 2007). In addition, downstream effects on auxin and gibberellin homeostasis are linked to ethylene-mediated shoot

growth as well (Vriezen et al., 2004; Stepanova et al., 2007). It is unclear how ACC controls expansion in shoot tissues, but it could involve ACC-specific effects or depend on crosstalk with the abovementioned growth hormones too.

Sensitivity of plants to ACC or ethylene, as for other hormones (e.g., auxin) depends on the concentration, tissue, organ, developmental stage, species, and growth conditions (Abeles et al., 1992; Le et al., 2001; Vandenbussche et al., 2012; Vaseva et al., 2018). *Arabidopsis* roots are generally more sensitive to ACC/ethylene [> 0.1 μM in darkness (**Figure 5D**); > 1 μM in light (**Figure 4B**)] compared to hypocotyls (> 0.25 μM; **Figure 5C**) or rosettes (> 10 μM; **Figure 3C**). When ethylene effects were excluded using pharmacological or genetic approaches, a lower sensitivity to ACC could be observed in all tissues studied (**Figures 1–5**). The need for the application of relatively high doses of exogenous ACC is consistent with an "overflow model". Low doses of ACC are converted to ethylene by ACO (**Figure 7A**), whereas increasing concentrations of ACC are supposed to accumulate intracellularly due to ACO limitation, ultimately leading to ACC-specific responses (**Figure 7B**). Nevertheless, the possibility that phenotypic changes are due to toxicity rather than *bona fide* ACC effects when applied at higher doses cannot be excluded. However, this notion holds true for all pharmacological experiments with compounds that are not 100% pure. In addition, the activity of ACC most likely depends on the tissue, developmental stage, and environmental conditions. During flooding, for instance, ethylene evolution in tissues subjected to hypoxia is limited due to the lack of oxygen, a key factor for ACO activity (**Figure 7B**; Adams and Yang, 1979; Vanderstraeten and Van Der Straeten, 2017). On the one hand, ACC can act as a mobile signal, which is transported from root-to-shoot, where it can be converted to ethylene and induce the appropriate phenotypic response to stress (e.g., hyponasty, petiole and shoot elongation, etc.), if oxygen is present. On the other hand, upon complete submergence, ACC itself might act as a growth-limiting factor in roots and shoots, contributing to a quiescence strategy, eventually leading to enhanced survival. The precise role of ACC in these conditions should be further evaluated.

Whether ACC acts as a signal completely independent of ethylene signaling or whether it can interact with ethylene signaling components downstream of perception remains a key question to be resolved in future studies (**Figure 7B**). Given that a depletion of ACC confers embryo lethality and reduces branching, in contrast to ethylene insensitivity, distinct roles for ACC are probable (Tsuchisaka et al., 2009). Moreover, the stimulation of GMC division by ACC does not require the major ethylene signaling components, further hinting at an ethylene-independent ACC pathway (Yin et al., 2019). Tsang et al. (2011) have postulated the second option. ACC could act as a shortcut, bypassing the need for ethylene perception. In the latter scenario, ACC would have the capacity to elicit certain responses before the required threshold levels of ethylene are reached or when the synthesis of ethylene is hampered (e.g., upon hypoxia). Our results support the latter hypothesis, since—at least with respect to skotomorphogenic development—*ein2-1* is less sensitive to ACC compared to the WT supplemented with AIB (**Figures 5C–F**). Contrarily, a negative effect of ACC on rosette development or primary root development (in light conditions) appears to occur independently of ethylene (**Figures 1–4**), downstream or in parallel with EIN2. A thorough analysis employing different ethylene signaling mutants in combination with pharmacological treatments will shed light on the events occurring downstream of ACC. On the other hand, the differences in root growth inhibition by ACC could be stage- or light-dependent. For instance, a recent report demonstrated that root growth defects upon phosphate deficiency are related to blue light illumination, and are suppressed by growing roots in darkness, as usually the case in nature (Zhang et al., 2019). Furthermore, though we observe the same effect in the absence of sucrose, we cannot rule out the possibility that ACC effects are modulated by sucrose. Sucrose is known to affect various vegetative growth processes (Gibson, 2005). It was shown that 1% sucrose decreased hypocotyl length and enhanced root length in etiolated seedlings (Lu and Wen, 2019). Therefore, the degree of ethylene response diminished in hypocotyls, while being enhanced in roots. In addition, increasing concentrations of sugar reduces the stability of EIN3, the major transcription factor of the ethylene signaling pathway (Yanagisawa et al., 2003). Less is known about the effects of sucrose—and its interaction with ethylene—on rosette development. High levels of sucrose or glucose are inhibitory for growth (Zhou et al., 1995). Here, we demonstrated that 1% sucrose increased rosette size, though this effect disappeared upon increasing doses of ACC, irrespective of the genetic background (**Figure S1**). Hence, the growth inhibitory properties of ACC are not dependent on the presence of sucrose.

Interestingly, differences in ACC responsiveness could be observed between AIB and 1-MCP application. While hypocotyl or root growth was equally inhibited by ACC in the presence of AIB or 1-MCP (**Figures 2**, **4**, and **5**), rosettes were less responsive to ACC upon combination with AIB (**Figures 1** and **3**). These differences did not arise due to ethylene-related effects, as the concentrations used were considered sufficiently effective. Two millimolar of AIB effectively blocked ACO-mediated conversion of ACC to ethylene in plants treated with 50 μM ACC (**Figure 3B**). Furthermore, residual ethylene emanation was even lower compared to a treatment with 1 μM ACC without AIB (**Table S2**). For 1-MCP treatments, a dose of 100 ppm completely blocked the phenotypic effects induced by 100 ppm ethylene (**Figure S3A**). Therefore, notwithstanding the fact that a strict comparison remains difficult, the observed discrepancy is most likely caused by another factor. To further corroborate the results obtained with AIB, parallel analyses including higher order *aco* mutants as well as their crosses with *ein2-1* will be instrumental. Blocking the conversion of ACC to ethylene in a pentuple *aco* mutant would also lead to an excess of endogenous ACC similar to a treatment with AIB. However, such a mutant has not been constructed to date, and it remains to be seen whether it is even viable.

AIB was discovered as an ACO inhibitor, based on its structural similarities with ACC (Satoh and Esashi, 1982; Pirrung et al., 1998). Hence, it is plausible that AIB also has the capacity to interact with other ACC binding proteins, be it (a) putative ACC receptor(s),

conjugating enzymes or ACC transporters (**Figure 7B**). The decrease in ACC sensitivity at the level of rosette expansion when AIB is present (**Figure 3**), hints at possible competition for binding to the putative ACC receptor. On the other hand, in the presence of AIB, one might expect an increase in endogenous ACC levels resulting from a feedback effect at the level of ACS, leading to ACC effects at lower concentrations of exogenous ACC. However, this is not supported by our analysis. Moreover, AIB still inhibited root growth in the *acs8x* mutant, suggesting that AIB exhibits side effects unrelated to the accumulation of ACC (**Figure 5**). No additive effects were observed upon a combined application of AIB and low concentrations of ACC (**Figure 5D**), indicative for the absence of a genuine side effect. Therefore, it is more conceivable that AIB and ACC act on the same target, such as a putative ACC receptor. Different ACC receptors could have different sensitivities to ACC or structural analogues (e.g., AIB) and can be expressed in a tissue-specific manner or are developmentally regulated, explaining the variation in AIB sensitivity among tissues and conditions. Furthermore, our data do not determine whether AIB exhibits agonist or antagonist properties for the putative ACC receptor(s). Lastly, it remains to be clarified whether ACC itself, a derivative or a downstream element is the *bona fide* signal. The function of all three ACC conjugates is largely unknown (Amrhein et al. 1981; Kionka and Amrhein 1984; Martin et al. 1995). They are proposed to act as storage forms, depleting the pool of free ACC, but could also have signaling functions.

With this work, we demonstrated that ACC could function as a regulator of growth during early vegetative development, apart from its role as an ethylene precursor. Hence, researchers employing ACC as an ethylene precursor should be mindful of putative ACC effects confounding ethylene responses. The exact mechanism underlying the ACC response, however, remains to be identified. The discovery of a putative receptor will shed light on the molecular players involved in the ACC response, either directly or downstream. Additionally, phenotypic, genetic and transcriptomic analyses of higher order *aco* mutants and the identification of ACC transporters and conjugating enzymes *in vivo*, are merely few of the studies required to elucidate ACC metabolism and signaling. Though ACC research is still relatively uncharted territory, novel findings related to the non-canonical role of ACC and the related molecular mechanisms will open up exciting new avenues in plant hormone physiology, shedding light on the complex signaling networks shaping plant growth and development.

DATA AVAILABILITY STATEMENT

All datasets generated for this study are included in the article/ **Supplementary Material**.

AUTHOR CONTRIBUTIONS

All authors conceived and designed the research. LV, TD, and SB conducted the experiments. LV, TD, and DS analyzed the data. LV, TD, and DS wrote the first draft of the manuscript. All authors read and commented on the manuscript. DS coordinated the project.

FUNDING

DS gratefully acknowledges financial support from the Research Foundation Flanders (project G032717N) and Ghent University (Bijzonder Onderzoeksfonds, BOF-BAS 2018). LV is indebted to the Research Foundation Flanders for an SB-PhD fellowship (1S17917N).

ACKNOWLEDGMENTS

The authors thank Mira Haegman, Els Fostier, and Piet Vankeirsbilck for technical assistance with the ethylene and 1-MCP treatments.

SUPPLEMENTARY MATERIAL

The Supplementary Material for this article can be found online at: https://www.frontiersin.org/articles/10.3389/fpls.2019.01591/full#supplementary-material

REFERENCES

Abeles, F. B. M., Page, W., and Saltveit, M. E. (1992). *Ethylene in plant biology* (San Diego, CA: Academic Press).

Adams, D. O., and Yang, S. F. (1979). Ethylene biosynthesis - Identification of 1-aminocyclopropane-1-carboxylic acid as an intermediate in the conversion of methionine to ethylene. *Proc. Natl. Acad. Sci. U. S. A.* 76, 170–174. doi: 10.1073/pnas.76.1.170

Almeida, A. M., Vriezen, W. H., and Van Der Straeten, D. (2003). Molecular and physiological mechanisms of flooding avoidance and tolerance in rice. *Russ. J. Plant Physiol.* 50, 743–751. doi: 10.1023/B:RUPP.0000003272.65496.04

Amrhein, N., Schneebeck, D., Skorupka, H., Tophof, S., and Stockigt, J. (1981). Identification of a major metabolite of the ethylene precursor 1-aminocyclopropane-1-carboxylic acid in higher-plants. *Naturwissenschaften* 68, 619–620. doi: 10.1007/BF00398617

Barbez, E., Dunser, K., Gaidora, A., Lendl, T., and Bush, W. (2017). Auxin steers root cell expansion *via* apoplastic pH regulation in *Arabidopsis thaliana*. *Proc. Natl. Acad. Sci. U.S.A.* 114, 4884–4893. doi: 10.1073/pnas.1613499114

Barry, C. S., Blume, B., Bouzayen, M., Cooper, W., Hamilton, A. J., and Grierson, D. (1996). Differential expression of the 1-aminocyclopropane-1-carboxylate oxidase gene family of tomato. *Plant J.* 9, 525–535. doi: 10.1046/j.1365-313X.1996.09040525

Binder, B. M., Mortimore, L. A., Stepanova, A. N., Ecker, J. R., and Bleecker, A. B. (2004). Short-term growth responses to ethylene in Arabidopsis seedlings are EIN3/EIL1 independent. *Plant Physiol.* 136, 2921–2927. doi: 10.1104/pp.104.050393

Boller, T., Herner, R. C., and Kende, H. (1979). Assay for and enzymatic formation of an ethylene precursor, 1-aminocyclopropane-1-carboxylic acid. *Planta* 145, 293–303. doi: 10.1007/BF00454455

Bradford, K. J., and Yang, S. F. (1980). Xylem transport of 1-aminocyclopropane-1-carboxylic acid, an ethylene precursor, in waterlogged tomato plants. *Plant Physiol.* 65, 322–326. doi: 10.1104/pp.65.2.322

Burg, S. P., and Burg, E. A. (1962). Role of ethylene in fruit ripening. *Plant Physiol.* 37, 179–189. doi: 10.1104/pp/37.2.179

Collett, C. E., Harberd, N. P., and Leyser, O. (2000). Hormonal interactions in the control of Arabidopsis hypocotyl elongation. *Plant Physiol.* 124, 553–561. doi: 10.1104/pp.124.2.553

De Vylder, J., Vandenbussche, F., Hu, Y., Philips, W., and Van Der Straeten, D. (2012). Rosette tracker: an open-source image analysis tool for automatic quantification of genotype effects. *Plant Physiol.* 160, 1149–1159. doi: 10.1104/pp.112.202762

Gibson, S. I. (2005). Control of plant development and gene expression by sugar signaling. *Curr. Opin. Plant Biol.* 8, 93–102. doi: 10.1016/j.pbi.2004.11.003

Glick, B. R., Penrose, D. M., and Li, J. P. (1998). A model for the lowering of plant ethylene concentrations by plant growth-promoting bacteria. *J. Theor. Biol.* 190, 63–68. doi: 10.1006/jtbi.1997.0532

Guzman, P., and Ecker, J. R. (1990). Exploiting the triple response of Arabidopsis to identify ethylene-related mutants. *Plant Cell* 2, 513–523. doi: 10.1105/tpc.2.6.513

Hall, A. E., Findell, J. L., Schaller, E., Sisler, E. C., and Bleecker, A. B. (2000). Ethylene perception by the ERS1 protein in Arabidopsis. *Plant Physiol.* 123, 1449–1458. doi: 10.1104/pp.123.4.1449

Hu, Y., Depaepe, T., Smet D., Hoyerova, K., Klima, P., Cuypers, A., et al. (2017). ACCERBATIN, a small molecule at the intersection of auxin and reactive oxygen species homeostasis with herbicidal properties. *J. Exp. Bot.* 68, 4185–4203. doi: 10.1093/jxb/erx242

Jackson, M. B. (2002). Long-distance signalling from roots to shoots assessed: the flooding story. *J. Exp. Bot.* 53, 175–181. doi: 10.1093/jexbot/53.367.175

Jackson, M. B. (2008). Ethylene-promoted elongation: an adaptation to submergence stress. *Ann. Bot.* 101, 229–248. doi: 10.1093/aob/mcm237

Kieber, J. J., Rothenberg, M., Roman, G., Feldmann, K. A., and Ecker, J. R. (1993). Ctr1, a negative regulator of the ethylene response pathway in Arabidopsis, encodes a member of the Raf family of protein-kinases. *Cell* 72, 427–441. doi: 10.1016/0092-8674(93)90119-B

Kionka, C., and Amrhein, N. (1984). The enzymatic malonylation of 1-aminocyclopropane-1-carboxylic acid in homogenates of mung-bean hypocotyls. *Planta* 162, 226–235. doi: 10.1007/BF00397444

Le, J., Vandenbussche, F., Van Der Straeten, D., and Verbelen, J. P. (2001). In the early response of Arabidopsis roots to ethylene, cell elongation is up and down regulated and uncoupled from differentiation. *Plant Physiol.* 125, 519–522. doi: 10.1104/pp.125.2.519

Le, J., Vandenbussche, F., De Cnodder, T., Van Der Straeten, D., and Verbelen, J. P. (2005). Cell elongation and microtubule behavior in the Arabidopsis hypocotyl: responses to ethylene and auxin. *J. Plant Growth Regul.* 24, 166–178. doi: 10.1007/d00344-005-0044-8

Liang, X. W., Abel, S., Keller, J. A., Shen, N. F., and Theologis, A. (1992). The 1-aminocyclopropane-1-carboxylate synthase gene family of Arabidopsis-Thaliana. *Proc. Natl. Acad. Sci. U. S. A.* 89, 11046–11050. doi: 10.1073/pnas.89.22.11046

Lu, J., and Wen, C.-K. (2019). Settings, quantification, and statistical analyses beyond *p*-values for Arabidopsis ethylene responses. *Small Methods* 1900386. doi: 10.1002/smtd.201900386

Lurssen, K. (1981). Interference of amino-acids with the uptake of 1-aminocyclopropane-1-carboxylic acid in soybean leaf-disks. *Plant Sci. Lett.* 20, 365–370. doi: 10.1016/0304-4211(81)90252-2

Martin, M. N., Cohen, J. D., and Saftner, R. A. (1995). A new 1-aminocyclopropane-1-carboxylic acid-conjugating activity in tomato fruit. *Plant Phys.* 109, 917–926. doi: 10.1104/pp.109.3.917

Mcdonnell, L., Plett, J. M., Andersson-Gunneras, S., Kozela, C., Dugardeyn, J., Van Der Straeten, D., et al. (2009). Ethylene levels are regulated by a plant encoded 1-aminocyclopropane-1-carboxylic acid deaminase. *Physiol. Plant* 136, 94–109. doi: 10.1111/j.1399-3054.2009.01208.x

Morris, D. A., and Larcombe, N. J. (1995). Phloem transport and conjugation of foliar-applied 1-aminocyclopropane-1-carboxylic acid in cotton (Gossypium-Hirsutum L). *J. Plant Physiol.* 146, 429–436. doi: 10.1016/S0176-1617(11)82004-3

Nakatsuka, A., Murachi, S., Okunishi, H., Shiomi, S., Nakano, R., Kubo, Y., et al. (1998). Differential expression and internal feedback regulation of 1-aminocyclopropane-1-carboxylate synthase, 1-aminocyclopropane-1-carboxylate oxidase, and ethylene receptor genes in tomato fruit during development and ripening. *Plant Physiol.* 118, 1295–1305. doi: 10.1104/pp.118.4.1295

Pierik, R., Sasidharan, R., and Voesenek, L. A. C. J. (2007). Growth control by ethylene: adjusting phenotypes to the environment. *J. Plant Growth Regul.* 26, 188–200. doi: 10.1007/s00344-006-0124-4

Pirrung, M. C., Cao, J., and Chen, J. L. (1998). Ethylene biosynthesis, processing of a substrate analog supports a radical mechanism for the ethylene-forming enzyme. *Chem. Biol.* 5, 49–57. doi: 10.1016/S1074-5521(98)90086-2

Richardson, J. T. E. (2011). Eta squared and partial eta squared as measures of effect size in educational research. *Educ. Res. Rev.* 6, 135–147. doi: 10.1016/j.edurev.2010.12.001

Rodrigues-Pousada, R. A., De Rycke, R., Dedonder, A., Van Caeneghem, W., Engler, G., Van Montagu, M., et al. (1993). The Arabidopsis 1 aminocyclopropane 1 carboxylate synthase gene-1 is expressed during early development. *Plant Cell* 5, 897–911. doi: 10.1105/tpc.5.8.897

Roman, G., Lubarsky, B., Kieber, J. J., Rothenberg, M., and Ecker, J. R. (1995). Genetic-analysis of ethylene signal-transduction in Arabidopsis-thaliana - 5 novel mutant loci integrated into a stress-response pathway. *Genetics* 139, 1393–1409.

Rosenthal, R. (1994). "Parametric measures of effect size," in *The handbook of research synthesis*. Eds. H. Cooper, and L. V. Hedges (New York: Russell Sage Foundation), 231–244.

Satoh, S., and Esashi, Y. (1982). Effects of alpha-aminoisobutyric-acid and D-amino and L-amino-acids on ethylene production and content of 1-aminocyclopropane-1-carboxylic acid in cotyledonary segments of cocklebur seeds. *Physiol. Plant* 54, 147–152. doi: 10.1111/J.1399-3054.1982.tb06318.x

Shin, K., Lee, S., Song, W. Y., Lee, R. A., Lee, I., Ha, K., et al. (2015). Genetic identification of ACC-RESISTANT2 reveals involvement of LYSINE HISTIDINE TRANSPORTER1 in the uptake of 1-aminocyclopropane-1-carboxylic acid in Arabidopsis thaliana. *Plant Cell Physiol.* 56, 572–582. doi: 10.1093/pcp/pcu201

Smalle, J., Kurepa, J., Haegman, M., Van Montagu, M., and Van Der Straeten, D. (1997). "Biology and Biotechnology of the plant hormone ethylene," in *Ethylene and Arabidopsis Rosette Development*. Eds. A. K. Kanellis, C. Chang, H. Kende, and D. Grierson (Dordrecht: Springer).

Staal, M., De Cnodder, T., Simon, D., Vandenbussche, F., Van Der Straeten, D., Verbelen, J. P., et al. (2011). Apoplastic alkalinization is instrumental for the inhibition of cell elongation in the Arabidopsis root by the ethylene precursor 1-aminocyclopropane-1-carboxylic acid. *Plant Physiol.* 155, 2049–2055. doi: 10.1104/pp.110.168476

Stepanova, A. N., Yun, J., Likhacheva, A. V., and Alonso, J. M. (2007). Multilevel interactions between ethylene and auxin in Arabidopsis roots. *Plant Cell* 19, 2169–2185. doi: 10./1105/tpc.107.052068

Tsang, D. L., Edmond, C., Harrington, J. L., and Nuhse, T. S. (2011). Cell wall integrity controls root elongation *via a* general 1-aminocyclopropane-1-carboxylic acid-dependent, ethylene-independent pathway. *Plant Physiol.* 156, 596–604. doi: 10.1104/pp.111.175372

Tsuchisaka, A., and Theologis, A. (2004). Unique and overlapping expression patterns among the Arabidopsis 1-amino-cyclopropane-1-carboxylate synthase gene family members. *Plant Physiol.* 136, 2982–3000. doi: 10.1104/pp.104.049999

Tsuchisaka, A., Yu, G., Jin, H., Alonso, J. M., Ecker, J. R., Zhang, X., et al. (2009). A combinatorial interplay among the 1-aminocyclopropane-1-carboxylate isoforms regulates ethylene biosynthesis in Arabidopsis thaliana. *Genetics* 183, 979–1003. doi: 10.1534/genetics.109.107102

Van de Poel, B., and Van Der Straeten, D. (2017). "Plant ethylene detection using laser-based photo-acoustic spectroscopy," in *Ethylene signaling. Methods in molecular biology*. Eds. B. Binder, and G. Schaller (New York: Humana Press), 11–26.

Van De Poel, B., Bulens, I., Markoula, A., Hertog, M. L. A. T. M., Dreesen, R., Wirtz, M., et al. (2012). Targeted systems biology profiling of tomato fruit reveals coordination of the Yang cycle and a distinct regulation of ethylene biosynthesis during postclimacteric ripening. *Plant Physiol.* 160, 1498–1514. doi: 10.1104/pp.112.206086

Van Der Straeten, D., Rodrigues-Pousada, R. A., Villarroel, R., Hanley, S., Goodman, H. M., and Van Montagu, M. (1992). Cloning, genetic-mapping, and expression analysis of an Arabidopsis-thaliana gene that encodes 1-aminocyclopropane-1-carboxylate synthase. *Proc. Natl. Acad. Sci. U. S.A.* 89, 9969–9973. doi: 10.1073/pnas.89.20.9969

Van Der Straeten, D., Djudzman, A., Van Caeneghem, W., Smalle, J., and Van Montagu, M. (1993). Genetic and physiological analysis of a new locus in Arabidopsis that confers resistance to 1-aminocyclopropane-1-carboxylic acid and ethylene and specifically affects the ethylene signal-transduction pathway. *Plant Physiol.* 102, 401–408. doi: 10.1104/pp.102.2.401

Vandenbussche, F., Vaseva, I., Vissenberg, K., and Van Der Straeten, D. (2012). Ethylene in vegetative development, a tale with a riddle. *New Phytol.* 194, 895–909. doi: 10.1111/j.1469-8137.2012.04100.x

Vanderstraeten, L., and Van Der Straeten, D. (2017). Accumulation and transport of 1-aminocyclopropane-1-carboxylic acid in plants: current status, considerations for future research and agronomic applications. *Front. Plant Sci.* 8, 38. doi: 10.3389/fpls.2017.00038

Vaseva, I., Qudeimat, E., Potuschak, T., Du, Y., Genschik, P., Vandenbussche, F., et al. (2018). The plant hormone ethylene restricts Arabidopsis growth *via the* epidermis. *Proc. Natl. Acad. Sci. U. S. A.* 115, E4130–E4139. doi: 10.1073/pnas.1717649115

Ververidis, P., and John, P. (1991). Complete recovery *in vitro* of ethylene-forming enzyme-activity. *Phytochemistry* 30, 725–727. doi: 10.1016/0031-9422(91)85241-Q

Vriezen, W. H., Achard, P., Harberd, N. P., and Van Der Straeten, D. (2004). Ethylene-mediated enhancement of apical hook formation in etiolated Arabidopsis thaliana seedlings is giberellin-dependent. *Plant J.* 34, 505–516. doi: 10.1046/j.1365-313X.2003.01975.x

Woeste, K., Ye, C., and Kieber, J. (1999). Two Arabidopsis mutants that overproduce ethylene are affected in the posttranscriptional regulation of 1-aminocyclopropane-1-carboxylic acid synthase. *Plant Physiol.* 119, 521–529. doi: 10.1104/pp.119.2.521

Xu, S. L., Rahman, A., Baskin, T. I., and Kieber, J. J. (2008). Two leucine-rich repeat receptor kinases mediate signaling, linking cell wall biosynthesis and ACC synthase in Arabidopsis. *Plant Cell* 20, 3065–3079. doi: 10.1105/tpc.108.063354

Yanagisawa, S., Yoo, S. D., and Sheen, J. (2003). Differential regulation of EIN3 stability by glucose and ethylene signalling in plants. *Nature* 425, 521–525. doi: 10.1038/nature01984

Yang, S. F., and Hoffman, N. E. (1984). Ethylene biosynthesis and its regulation in higher-plants. *Ann. Rev. Plant Physiol.* 35, 155–189. doi: 10.1146/annurev.pp.35.060184.001103

Yin, J., Zhang, X., Zhang, G., Wen, Y., Liang, G., and Chen, X. (2019). Aminocyclopropane-1-carboxylic acid is a key regulator of guard mother cell terminal division in *Arabidopsis thaliana*. *J. Exp. Bot.* 70, 897–908. doi: 10.1093/jxb/ery413

Yoo, S. D., Cho, Y. H., Tena, G., Xiong, Y., and Sheen, J. (2008). Dual control of nuclear EIN3 by bifurcate MAPK cascades in C_2H_4 signalling. *Nature* 451, 789–795. doi: 10.1038/nature06543

Zarembinski, T. I., and Theologis, A. (1993). Anaerobiosis and plant-growth hormones induce 2 genes encoding 1-aminocyclopropane-1-carboxylate synthase in rice (Oryza-Sativa L). *Mol. Biol. Cell* 4, 363–373. doi: 10.1091/mbc.4.4.363

Zhang, Z., Wang, Z., Wang, X., and Liu, D. (2019). Blue light triggered-chemical reactions underlie phosphate deficiency-induced inhibition of root elongation of Arabidopsis seedlings grown in petri dishes. *Mol. Plant*. 12, 1515–1523. doi: 10.1016/j.molp.2019.08.001

Zhou, L., Jang, J.-C., Jones, T. L., and Sheen, J. (1995). Glucose and ethylene signal transduction crosstalk revealed by an Arabidopsis glucose-insensitive mutant. *Proc. Natl. Acad. Sci.* 95, 10294–10299. doi: 10.1073*pnas.95.17.10294

Conflict of Interest: The authors declare that the research was conducted in the absence of any commercial or financial relationships that could be construed as a potential conflict of interest.

Advantages of publishing in Frontiers

OPEN ACCESS
Articles are free to read for greatest visibility and readership

FAST PUBLICATION
Around 90 days from submission to decision

HIGH QUALITY PEER-REVIEW
Rigorous, collaborative, and constructive peer-review

TRANSPARENT PEER-REVIEW
Editors and reviewers acknowledged by name on published articles

Frontiers
Avenue du Tribunal-Fédéral 34
1005 Lausanne | Switzerland

Visit us: www.frontiersin.org
Contact us: info@frontiersin.org | +41 21 510 17 00

REPRODUCIBILITY OF RESEARCH
Support open data and methods to enhance research reproducibility

DIGITAL PUBLISHING
Articles designed for optimal readership across devices

FOLLOW US
@frontiersin

IMPACT METRICS
Advanced article metrics track visibility across digital media

EXTENSIVE PROMOTION
Marketing and promotion of impactful research

LOOP RESEARCH NETWORK
Our network increases your article's readership